

Analysis Note for Paper: Measurement of elliptic flow of light nuclei at $\sqrt{s_{NN}} = 200, 62.4,$ $39, 27, 19.6, 11.5$ and 7.7 GeV at RHIC

PAs: Md. Rihan Haque, Bedangadas Mohanty
Version 2.0

Abstract

We present the measurement of 2^{nd} order azimuthal anisotropy (v_2) at mid-rapidity ($|y| < 1.0$) for deuteron (d), anti-deuteron (\bar{d}), triton (t) and 3He ($^3\bar{He}$) in Au+Au collisions at $\sqrt{s_{NN}} = 200, 62.4, 39, 27, 19.6, 11.5$ and 7.7 GeV. These data were taken by the STAR experiment in the year 2010 (at $\sqrt{s_{NN}} = 7.7, 11.5, 39, 62.4, 200$ GeV) and in 2011 (at $\sqrt{s_{NN}} = 19.6, 27$ GeV). We have used the TPC and TOF detector of the STAR experiment. Elliptic flow v_2 of nuclei has been studied as a function of transverse momentum p_T as well as for centrality bins. The v_2 for minimum bias (0-80%) is found to increase monotonically with increasing p_T and exhibit mass ordering at low p_T . The v_2 of deuteron and anti-deuterons are of similar magnitude and they also show centrality dependence. The AMPT+coalescence model result is found to reproduce the measured v_2 of light nuclei from experiment.

1 Dataset

1.1 Event Selection

The results presented here are from the Au+Au data taken by STAR in year 2010 (at $\sqrt{s_{NN}} = 7.7, 11.5, 39, 62.4$ GeV) and in 2011 (at $\sqrt{s_{NN}} = 19.6, 27$ GeV). We have used minimum bias (0-80%) events for our analysis. We have removed bad events run by run for each energy and also applied proper Vertex cut to ensure good quality events. The cuts on primary vertex position along the longitudinal beam direction (V_z) is 40 cm for 39 and 62.4 GeV data set, 50 cm for 11.5 GeV data set and 70 cm for 7.7, 19.6 GeV and 27 GeV data set. The number of events for each center of mass energy, its trigger and event cuts are shown in Table 3:

Table 1: Event cuts and number of minimum bias events

DATA	Trigger ID (minimum bias)	Vertex _z	Vertex _r	no. of events
7.7 GeV	290001, 290003, 290004	$ V_z < 70$ cm	$ V_r < 2.0$ cm	4 M
11.5 GeV	310003, 310004, 310013, 310014	$ V_z < 50$ cm	$ V_r < 2.0$ cm	11 M
19.6 GeV	340001, 340002, 340011, 340012, 340021, 340022	$ V_z < 70$ cm	$ V_r < 2.0$ cm	33 M
27 GeV	360001, 360002	$ V_z < 70$ cm	$ V_r < 2.0$ cm	60 M
39 GeV	280001, 280002	$ V_z < 40$ cm	$ V_r < 2.0$ cm	119 M
62.4 GeV	270001, 270005, 270011, 270021	$ V_z < 40$ cm	$ V_r < 2.0$ cm	62 M
200 GeV	260001, 260021,	$ V_z < 30$ cm	$ V_r < 2.0$ cm	241 M

1.2 Event QA

Good quality events for each dataset have been used to do this analysis. The vertex cuts were studied and optimized during the data taking using the online vertex reconstruction performed by the high-level trigger (HLT) and basic quality assurance performance plots. The distributions of Z-positions of vertex are shown in Fig.1

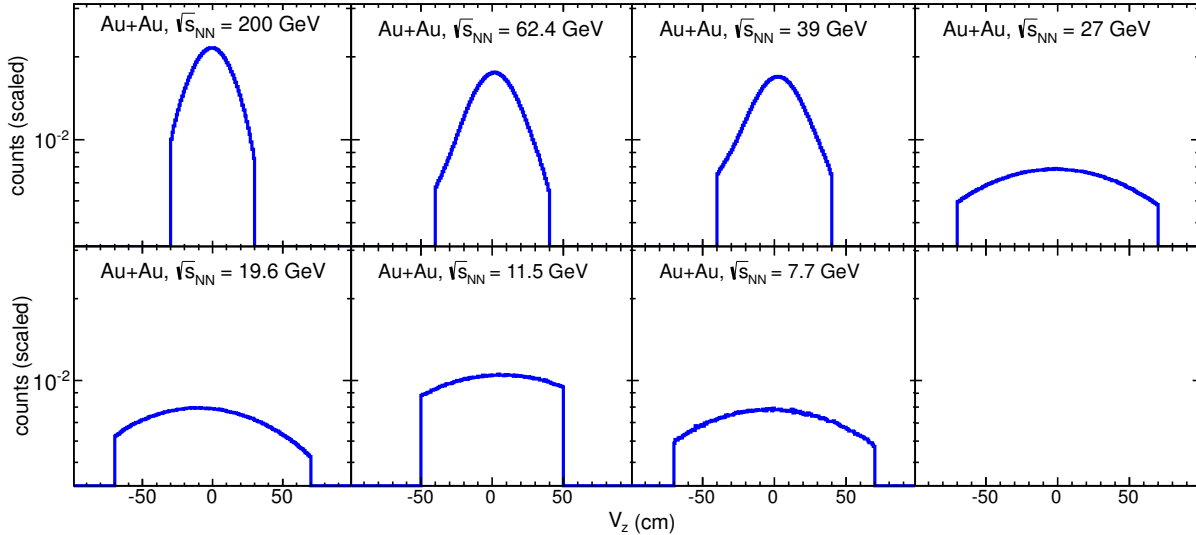


Figure 1: Distribution of Z-component of event vertex for different centre-of-mass energies.

In order to reject events which involves beam pipe interactions, the event vertex radius (defined as $V_r = \sqrt{V_x^2 + V_y^2}$, where V_x and V_y are the vertex positions along the x and y directions) is required to be less than 2 cm. To remove pileup events, it was required that at least two tracks from the primary vertex were matched to the cells of the TOF detector.

1.3 Centrality selection

To calculate centrality, we have used StRefMultCorr class developed for STAR data sets taken in the year and after 2010. A documentation of this class can be found at <http://www.star.bnl.gov/protected/common/common2010/centrality/index.html>

The collision centrality is determined by comparing the measured raw charged hadron multiplicity uncorrected for efficiency and acceptance effects (named as RefMult or N_{raw}) from the TPC within a pseudo-rapidity window $|\eta| \leq 0.5$ with Glauber Monte Carlo simulations. A two-component model [1] is used to calculate the simulated multiplicity distribution given by

$$\frac{dN_{ch}}{d\eta} = n_{pp}[(1-x)\frac{N_{part}}{2} + xN_{coll}]$$

where N_{part} is the number of participant nucleons and N_{coll} is the number of binary nucleon-nucleon collisions in the Glauber Monte-Carlo simulations. The fitting parameter n_{pp} is the average multiplicity per unit of pseudorapidity in minimum-bias $p + p$ collisions and x is the fraction of production of charged particles from the hard component. The x value is fixed at 0.12 ± 0.02 based on the linear interpolation of the PHOBOS results at $\sqrt{s_{NN}} = 19.6$ and 200 GeV [2]. The detailed procedures to obtain the simulated multiplicity are similar to that described in Ref.[3]. The uncorrected charged multiplicity (RefMult) distribution for minimum-bias events is shown in Fig.2. All the values of N_{raw} or RefMult for different centralities and different energies are listed in the Appendix section.

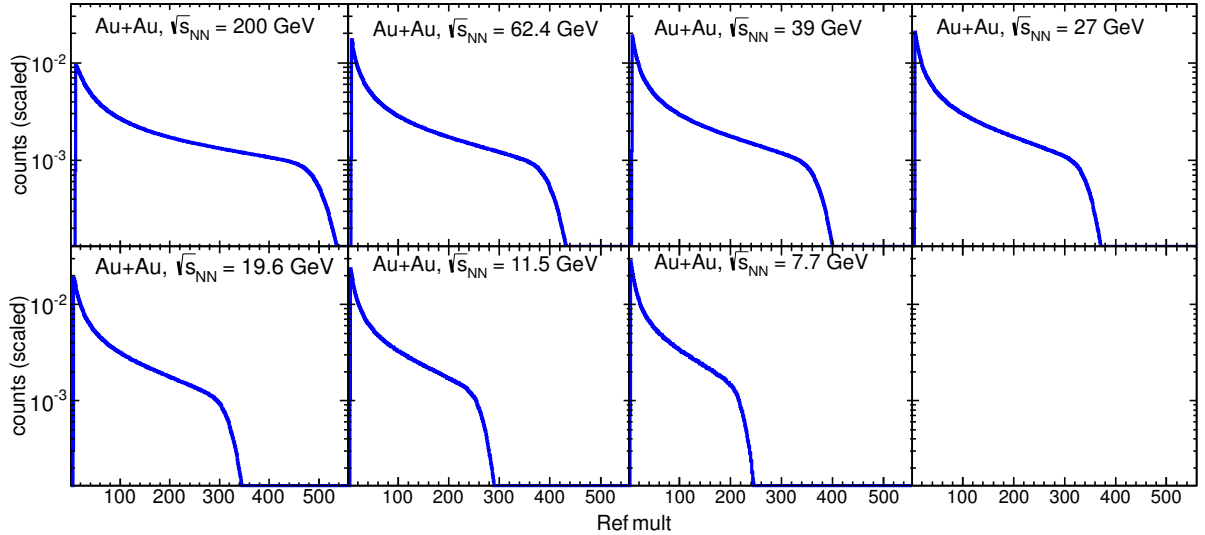


Figure 2: The uncorrected multiplicity distribution of reconstructed charged particles per unit pseudo-rapidity interval at mid-rapidity for the six different centre-of-mass energies.

1.4 Particle Identification

1.4.1 Using TPC

The TPC is the main tracking detector of the STAR experiment and is capable of measuring charged particles within $|\eta| < 1.8$ and within full azimuthal coverage [4]. TPC operates within a constant magnetic field and hence it can measure the momentum of the charged tracks following their curvature. TPC also measures the specific ionisation energy loss of the charged particles while they move inside the gas volume. A characteristic plot of TPC is shown in the Fig.3. In this figure, the theoretical predictions of energy loss for the charged particles are also shown in solid lines. The theoretical values of specific energy loss are obtained from Bichsel functions [5]. The basic cuts for selection of nuclei using TPC and ToF are listed in the Table2. In order to ensure good track momentum reconstruction, short tracks were eliminated from the analysis by requiring all tracks to have $p_T > 0.2 \text{ GeV}/c$ and a minimum number of 25 fit points (nHitsFit) in TPC for each track. The effect of track-splitting due to the tracking algorithm is minimized by further requiring that the number of fit points is more than half of the number of total possible hit points for a track i.e. $\text{nHitsFit}/\text{Max.nHitsFit} \geq 0.52$. A cut was applied on the no. of points (nHitsdEdx) used to calculate specific ionisation energy loss. Tracks with $\text{nHitsdEdx} > 15$ were used for this analysis. In addition, all tracks with distance of closest approach (DCA) from primary vertex greater than 1.0 cm were removed to reject the tracks coming from sources other than primary vertex. Finally tracks with $\eta < 1.0$, where the acceptance of TPC is uniform, has been used in the analysis.

1.4.2 Using TOF

The time-of-flight (TOF) detector measures the flight time (τ) of the tracks in full azimuthal coverage and in pseudorapidity window $|\eta| < 0.9$ [6]. The flight time is the time taken by a track to traverse the distance (L) from the primary vertex to the ToF detector. Using the time of flight information we can calculate its velocity (β) as,

$$\beta = \frac{L}{c\tau}$$

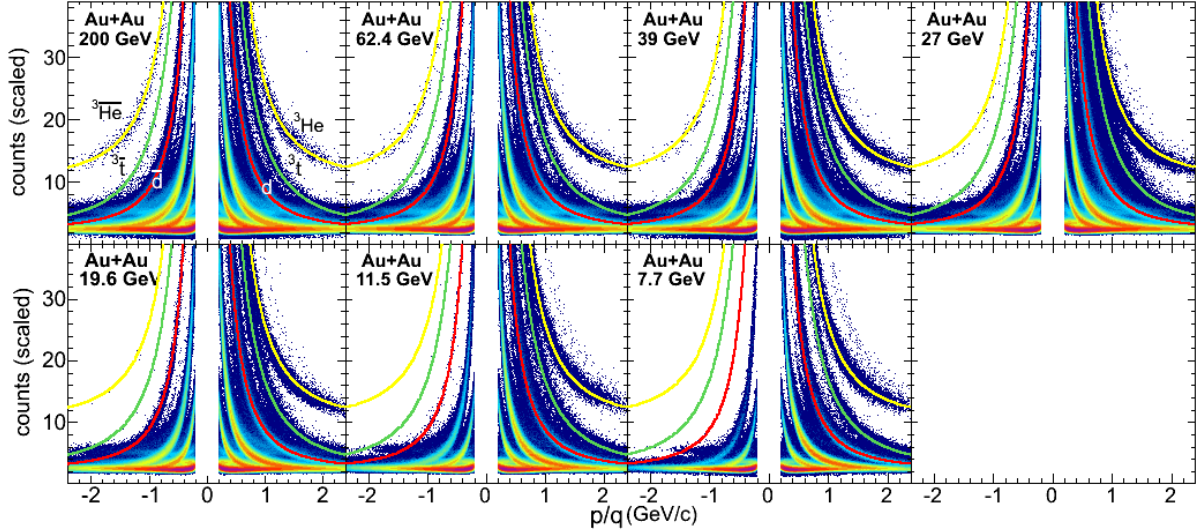


Figure 3: Energy loss as a function of rigidity for different beam energies. Solid lines corresponds to the theoreticaly predicted values for different nuclei.

Using this velocity information obtained from TOF and corresponding momentum information from TPC, we can calculate the mass (m) of the charged track using the relation:

$$m^2 = p^2(\frac{1}{\beta^2} - 1)$$

Therefore with the TOF information, we can apply cut on m^2 to enhance the signal contribution. The m^2 cut which were applied for this analysis are shown in Table2.

Table 2: Track selection cuts for analysis

Track parameter	minimum/maximum value
Transverse momentum (p_T)	$0.2 < p_T < 10.0$ (GeV/c)
Pseudorapidity (η)	$ \eta < 1.0$
no. of points for dE/dx (nHitsdEdx)	> 15
no. of fit points (nHitsFit)	> 25
nHitsFit/maximum nHitsFit (possible)	> 0.52
DCA (cm)	< 1.0
m^2 (GeV 2 /c 4)	$2.8 < m^2 < 4.2$ (for d) $6.3 < m^2 < 9.5$ (for t)

A characteristic plot of TOF, m^2 as a function of momentum (p), is shown in Fig.4 . Here different dotted line corresponds to the cuts applied for different nuclei. From Fig.4 we can see that TOF detector enhances the identification of the nuclei and allow us to extend the p_T reach to beyond 1 GeV/ c .

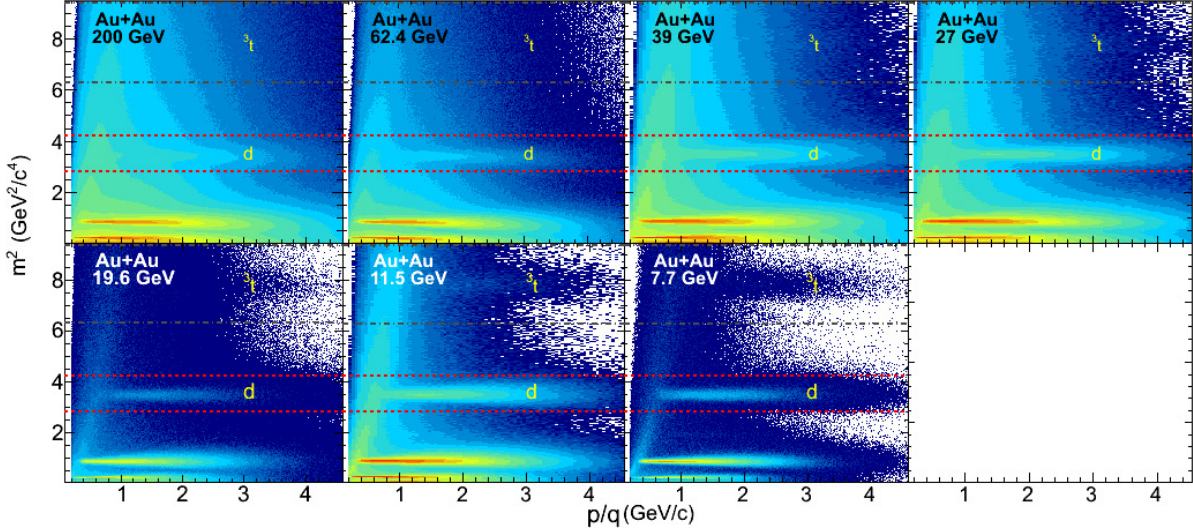


Figure 4: m^2 as a function of rigidity for different beam energies. Solid lines corresponds to the track selection cut applied for different nuclei.

2 Analysis Method

2.1 Elliptic flow

The azimuthal distribution of produced particles with respect to reaction plane angle (Ψ_r) can be decomposed in a Fourier series:

$$\frac{dN}{d\phi} \propto 1 + 2v_1 \cos(\phi - \Psi_r) + 2v_2 \cos(2(\phi - \Psi_r)) + \dots$$

where ϕ is the azimuthal angle of the produced particle. For a given rapidity window the second Fourier coefficient, i.e., v_2 can be defined as,

$$v_2 = \langle \cos(2(\phi - \Psi_r)) \rangle$$

Here $\langle \rangle$ denote average over all particles in all events. In order to measure the elliptic flow we have to calculate the reaction plane angle. Reaction plane is the plane which contains both beam (Z) axis and impact parameter (perpendicular distance between two centre of colliding nuclei). The angle between X-axis and reaction plane is called reaction plane angle. Since in experiment we can not measure the impact parameter between two colliding nuclei therefore the reaction plane angle is unknown. We used the method to estimate the reaction plane by using the anisotropic flow itself [7]. The estimated reaction plane is known as event plane. The first step is to calculate event flow vector \vec{Q}_n which is defined as

$$Q_n \cos(n\Psi_n) = Q_x = \sum_{i=1}^N w_i \cos(2\phi_i)$$

$$Q_n \sin(n\Psi_n) = Q_y = \sum_{i=1}^N w_i \sin(2\phi_i)$$

where w_i is the weight and N is the total number of particles in a event used for flow vector calculation. The n^{th} harmonic event plane angle can be calculated by

$$\Psi_n = \frac{1}{n} \tan^{-1} \frac{Q_y}{Q_x}$$

The choice of weights is to make the event plane resolution the best by maximizing the flow contributions to the flow vector. In this analysis weight $w_i = p_T i$ (for $p_T < 2 \text{ GeV}/c$) has been taken for event plane reconstruction. The p_T of tracks were used as a weight to get good event plane resolution, since the v_2 increases with p_T .

2.2 Event plane reconstruction

The anisotropic distribution of the produced particles is used to calculate the second order event plane angle (Ψ_2). The components of the event plane vector \vec{Q}_2 are estimated separately for both of these subevents as,

$$Q_{2,x} = \sum_i w_i \cos(2\phi_i), Q_{2,y} = \sum_i w_i \sin(2\phi_i),$$

where ϕ_i is the azimuthal angle of the particle in lab frame and w_i are weights, used to make the reaction plane resolution the best that is possible. In this analysis the weight is taken as transverse momentum p_T of the corresponding track (for $p_T < 2.0 \text{ GeV}/c$). The event plane (Ψ_2) then can be given as [7],

$$\Psi_2 = \frac{1}{2} \tan^{-1} \frac{Q_{2,y}}{Q_{2,x}}$$

Good quality primary tracks have been used to reconstruct event plane for this analysis. The minimum track cuts which is applied to reconstruct the η -sub event planes are shown in Table-2.

Table 3: Track selection cuts for event plane reconstruction

Track parameter	minimum/maximum value
Transverse momentum (p_T)	$0.2 < p_T < 2.0 \text{ (GeV}/c)$
Pseudorapidity (η)	$ \eta < 1.0$
no. of fit points (nHitsFit)	> 15
nHitsFit/maximum nHitsFit (possible)	> 0.52
DCA	$< 2.0 \text{ cm}$

2.2.1 η -sub Event plane

The η -sub event plane method helps to remove the effect of self-correlation and non-flow effects (mainly short range correlations) by correlating particles separated in pseudorapidity. In this method [7].., each single event is divided into two sub events in two separate η -windows, namely $\eta-$ ($-1.0 < \eta < -0.05$) and $\eta+$ ($0.05 < \eta < 1.0$). The the flow coefficient v_2 was calculated for each particle based on their measurement in the opposite hemisphere in pseudo-rapidity:

$$v_2(\eta_{\pm}) = \frac{\langle \cos(2(\phi_{\pm} - \Psi_{2\mp})) \rangle}{\sqrt{\langle \cos(\Psi_{2\eta+} - \Psi_{2\eta-}) \rangle}}$$

Here $\Psi_{2\eta+}$ and $\Psi_{2\eta-}$ are the second harmonic event plane angle defined respectively for particles with positive and negative pseudo-rapidity. An η gap of $|\eta| < 0.05$ between positive and negative pseudo-rapidity sub-events has been introduced to suppress non-flow effects. In the above equation, non-flow effects (correlations) are reduced in both the observed flow (numerator) and the event plane resolution (denominator) . Depending on the nature of the remaining non-flow effects, v_2

measured this way may have values that are either lower or higher than those obtained with the standard plane method [8]. But this method is not sufficient to reduce non-flow effects due to long-range correlations. The results presented in this thesis has been calculated using the $|\eta|$ -sub event plane method.

2.3 Detector acceptance correction

The event plane angle should be random in the laboratory frame and therefore its distribution should be flat for a perfect detector. However, in the experiments, the detectors may have a finite acceptance or non-uniform acceptance which may lead to anisotropic particle distributions in the lab frame. This anisotropy is not related to the true anisotropic flow arising due to pressure gradients developed in the colliding system which we want to measure. Therefore, it is necessary that event plane angle distribution should be uniform in the laboratory frame. Several methods have been theorised to correct the event plane angle distribution[7]. The most commonly used methods, is to use the distribution of the particles themselves as a measure of the correction for the acceptance effect. This is known as weight method. In this method, one can accumulates the laboratory frame azimuthal distribution of the particles for all events and uses the inverse of this as weights in the calculation of the event planes. But this method will not work if the azimuthal distribution of the particles is zero or very low in some part of the phase-space. Another disadvantage of this method is that, it does not take into account the multiplicity fluctuations around the mean value. The second method, known as re-centering, is to recenter the distribution of flow vectors (Q_x, Q_y) by subtracting the averaged flow vectors over all events, i.e.,

$$Q_x = Q_x - \langle Q_x \rangle$$

$$Q_y = Q_y - \langle Q_y \rangle$$

This method has been used for 2nd order event plane correction presented in this analysis. The main limitation of this method is that it does not eliminate the higher harmonics from the distribution of Ψ_2 . To eliminate the higher harmonics the event plane has been further corrected by the shift method. In this method one has to fit the unweighted event plane distribution in the s laboratory frame, summed over all events, to a Fourier expansion and devises an event-by-event shifting of the planes needed to make the final distribution isotropic. The equation for shift correction for n^{th} harmonic event plane is,

$$\Delta\Psi_n = \frac{1}{n} \sum_i^{i_{max}} \frac{2}{i} [-\langle \sin(in\Psi_n) \rangle \cos(in\Psi_n) + \langle \cos(in\Psi_n) \rangle \sin(in\Psi_n)]$$

The minimum value of $i_{max} = 4/n$ where n is the harmonic number of interest. The final corrected event plane is,

$$\Psi'_n = \Psi_n + \Delta\Psi_n$$

The 2nd order event plane (Ψ_2) distributions corrected by re-centering and shift method are shown in Fig.5 and Fig.6.

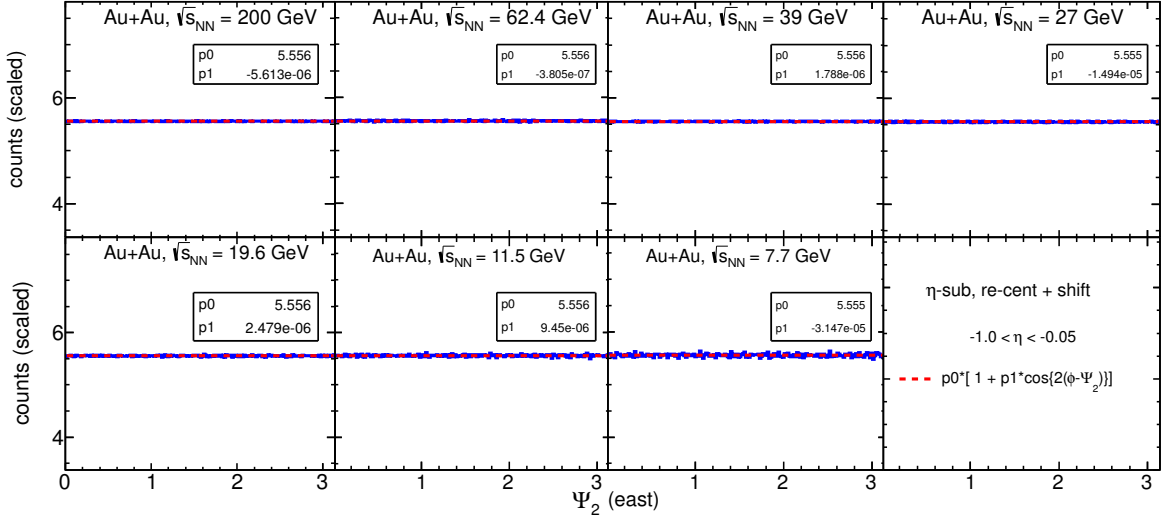


Figure 5: Event plane distribution for $-1.0 < \eta < -0.05$. Dotted line corresponds to the fit to the data. Fit function and fit parameters are shown in the legend.

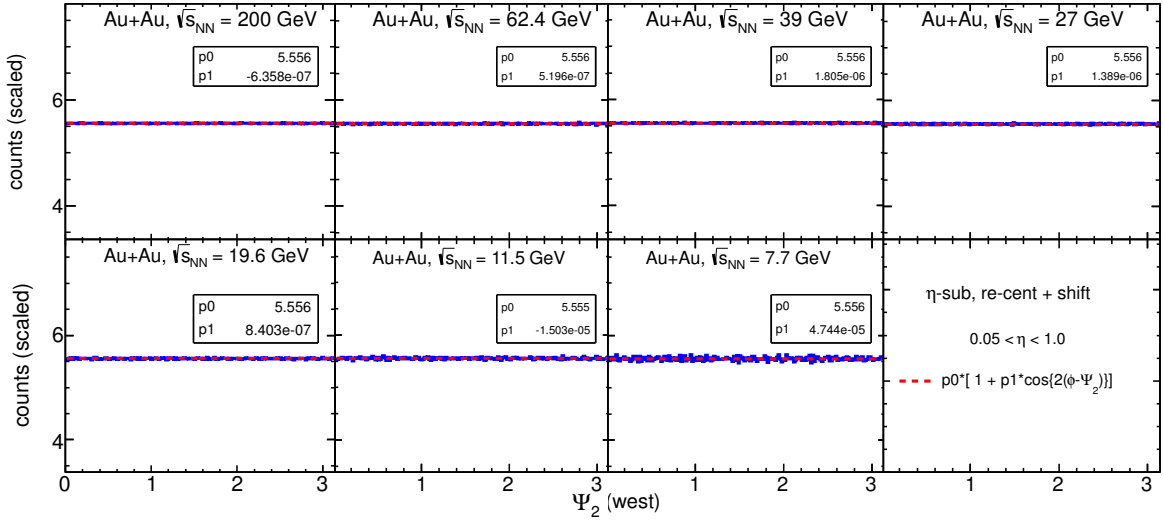


Figure 6: Event plane distribution for $0.05 < \eta < 1.0$. Dotted line corresponds to the fit to the data. Fit function and fit parameters are shown in the legend.

2.4 Resolution correction

Due to finite multiplicity of events, the event plane angle Ψ_2 may not coincide with the reaction plane angle Ψ_r , which is defined as the plane containing the beam axis and impact parameter of the collision. Hence a resolution correction need to be performed to obtain the correct measurement of flow coefficient. The resolution factor R is defined as,

$$R = \langle \cos(\Psi_2 - \Psi_r) \rangle$$

where $\langle \rangle$ denotes average over all events. Since Ψ_r is unknown, the event plane resolution is estimated by the correlation of the events planes of two sub-events A and B and is given by,

$$R = \langle \cos(\Psi_2 - \Psi_r) \rangle = K \sqrt{\langle \cos(\Psi_{2A} - \Psi_{2B}) \rangle}$$

where K is a constant calculated from the known multiplicity dependence of the resolution [7] and Ψ_{2A} and Ψ_{2B} are event plane angles for independent subset A and B. In this analysis, the subsets are in two different η -windows as shown in Fig5 and Fig.6.

For this analysis, the sub-events were constructed by dividing TPC acceptance into two η -sub group so that the multiplicity of each sub-event A and B are approximately the same and hence their respective resolutions should be equal. Fig.7 shows resolution for each sub event plane as function of centrality for different beam energies in Au+Au collisions. The event plane resolution has been calculated for nine different centrality individually (0–5%, 5–10%, 10–20%, 20–30%, 30–40%, 40–50%, 50–60%, 60–70% and 70–80%) As the event plane resolution depends on number of particles used for event plane reconstruction, therefore it should increase from peripheral to central collisions. On the other hand, since the event plane is calculated using the anisotropic flow of the event itself, it should degrades with more central collisions where flow values are small. Because of this two competing effects the final resolution first increases from peripheral to mid-central collision and then decreases.

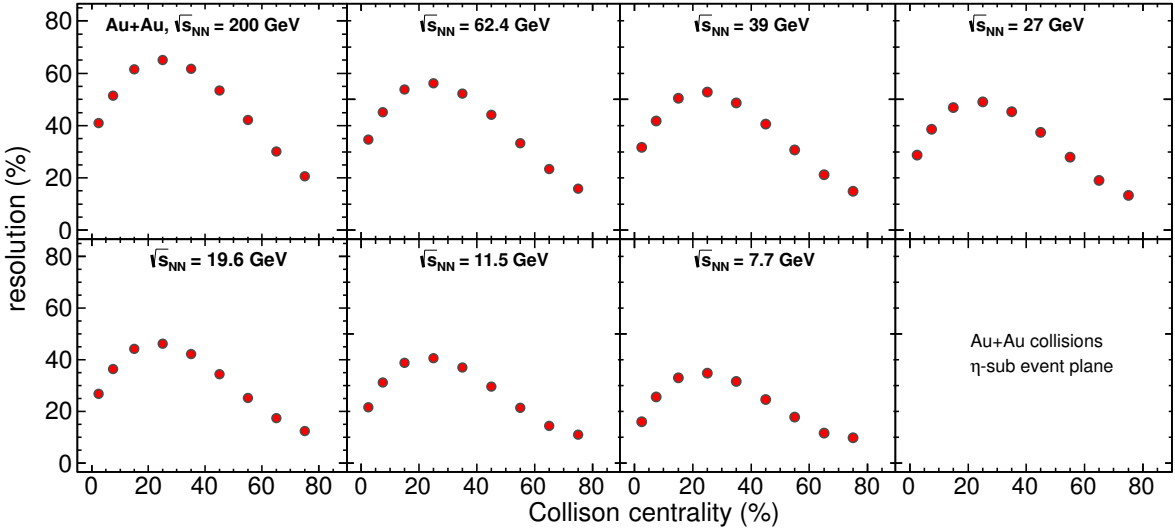


Figure 7: Resolution as a function of centrality for different beam energy. Two overlapping circles idicates the position of central and preriferal events along the X-axis. Centrality binnings are mentioned in section 2.3

Most commonly used method for resolution correction for an average v_2 over a centrality range is

$$\langle v_2 \rangle = \frac{\langle v_2^{obs} \rangle}{\langle R \rangle}$$

Here $\langle R \rangle$ is the mean resolution in that wide centrality bin and can be calculated as

$$\langle R \rangle = \frac{\sum N_i \langle R_i \rangle}{\sum N_i}$$

where N_i and $\langle R_i \rangle$ is the multiplicity and resolution of the i th narrow centrality bin, respectively. This procedure works well for narrow centrality bins, but fails for wider centrality bins like for example 0 – 80%. There is another approach, known as event by event resolution correction, for event plane resolution correction for wide centrality bin [?]. In this method resolution correction for wide centrality bin has been done by dividing the flow coefficient ($\cos(2(\phi - \Psi_2))$) of each track by the event plane resolution $\langle R \rangle$ for the corresponding centrality for each event. The results in this two methods are not same since,

$$\frac{\langle v_2 \rangle}{\langle R \rangle} \neq \langle \frac{v_2}{R} \rangle$$

2.5 Extraction of nuclei v_2

Good quality primary tracks have been used to study elliptic flow coefficient of nuclei. The minimum track cuts which are applied for this analysis are shown in Table 2. To select a track, we define a Z-variable such as

$$Z = \log\left(\frac{\frac{dE}{dx}|_{expt.}}{\frac{dE}{dx}|_{theory}}\right)$$

where, $\frac{dE}{dx}|_{expt.}$ is the experimentally measured specific energy loss and $\frac{dE}{dx}|_{theory}$ is corresponding the theoretical value. We calculate this Z-variable for different p_T and $\phi - \Psi_2$ bins. Then we, fit this Z-distributions to get the Yield of desired nucleie. A representative plot for Z-distributions is shown inf Fig.8

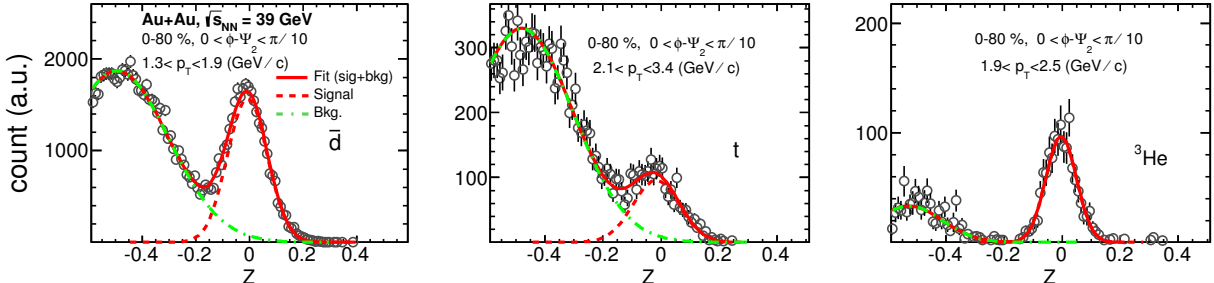


Figure 8: Distrribution of $Z = \log\left(\frac{\frac{dE}{dx}|_{expt.}}{\frac{dE}{dx}|_{theory}}\right)$ of reconstructed track for $|\eta| < 1$. The red solid line is fit to the Z-distribution with two Gaussian function (signal+background). The dotted red line corresponds to signal (for \bar{d} , t and 3He respectively) and dot-dashed green line corresponds to the background.

After calculating the Yield of nuclei in $\phi - \Psi_2$ bins, we fit the $\phi - \Psi_2$ distribution with a Fourier function to get the raw value of the 2nd order flow co-efficient, i.e., elliptic flow (v_2^{obs}). A representative plot for $\phi - \Psi_2$ distribution is shown in Fig.9. The raw 2nd order flow coefficient (v_2^{obs}) is then multiplied with weighted average of the inverse resolution ($\langle \frac{1}{R} \rangle$) to get the corrected flow coefficient (v_2), i.e.,

$$v_2 = v_{2obs} \langle \frac{1}{R} \rangle$$

The yield of nucleon in each centrality bin is used as weight to calculate average $\langle \frac{1}{R} \rangle$ for wide centrality bins.

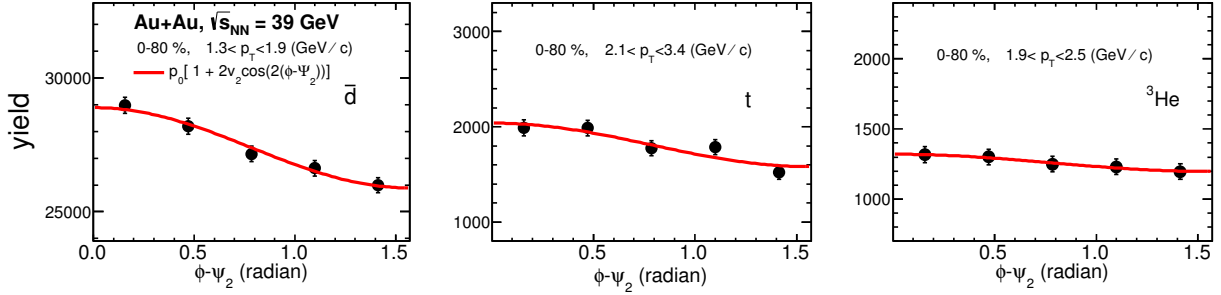


Figure 9: Extraction of raw value of flow coefficient (v_{2obs}) from $\phi - \Psi_2$ distributions of \bar{d} , t and ${}^3\text{He}$. The red solid line is fit to the $\phi - \Psi_2$ distribution with a Fourier function (shown in the legend with red solid line). The fit parameter p_1 is the magnitude of 2^{nd} order flow coefficient (v_{2obs}).

2.6 Systematic uncertainties

The systematic uncertainties were evaluated by varying the methods and parameters used to determine the particle yields. Uncertainties in the track momentum, track identification, fitting range variation etc. has been studied. Table 4 lists all the track cuts that were applied for systematics study. The systematics error is calculated as the root mean square deviation from the default values (Table 2).

Table 4: Track cuts for systematics study

Fixed cuts	varied cuts	combination
nHistdEdx > 15, dca < 1.0cm,	nHitsFit > 20, nHitsFit > 22, nHitsFit > 24, nHitsFit > 26	4
nHitsFit > 25, dca < 1.0cm,	nHitsdEdx > 12, nHitsdEdx > 14, nHitsdEdx > 16, nHitsdEdx > 18	4
nHistdEdx > 15, nHitsFit > 25,	dca > 20, dca > 22, dca > 24, dca > 26	4
nHistdEdx > 10, nHitsFit > 25,	dca > 20, dca > 22, dca > 24, dca > 26	4
nHistdEdx > 15, nHitsFit > 25,	$m^2 \pm 15\%$, $m^2 \pm 18\%$, $m^2 \pm 22\%$, $m^2 \pm 25\%$	4
nHistdEdx > 15, nHitsFit > 25,	$ Z < 0.16$, $ Z < 0.18$, $ Z < 0.22$, $ Z < 0.24$,	4

Systematic error is then calculated as the square root of the variance (i.e., σ), where the variance is calculated with the v_2 values obtained from the default analysis cut (listed in Table 2) as mean. The systematic error (σ) from various track cuts lies in between 1-10% for different nuclei species and for different p_T bins.

3 Result and Discussion

In this section the transverse momentum p_T , centrality and energy dependence of nuclei will be discussed. No. of constituent quark and mass scaling has been observed and has been discussed in the following sub-sections. Finally we have compared the nuclei v_2 with a model result in order to understand the mechanism of nuclei production in heavy ion collision. As mentioned previously that all the results are from η -sub event plane method and v_2 value are obtained from fitting the $\phi - \Psi_2$ distribution.

3.1 Differential v_2

The results for measurements of the nuclei v_2 as a function of p_T are presented in the Fig. 10. v_2 of all nuclei species show monotonic increasing trend with increasing p_T . d and \bar{d} , for all center of mass energies, show similar magnitude of v_2 . All nuclei v_2 show mass ordering at low p_T ($< 2.0 \text{ GeV}/c$). Triton (t) and Helium (${}^3\text{He}$) are also exhibit similar order of v_2 within the statistical error.

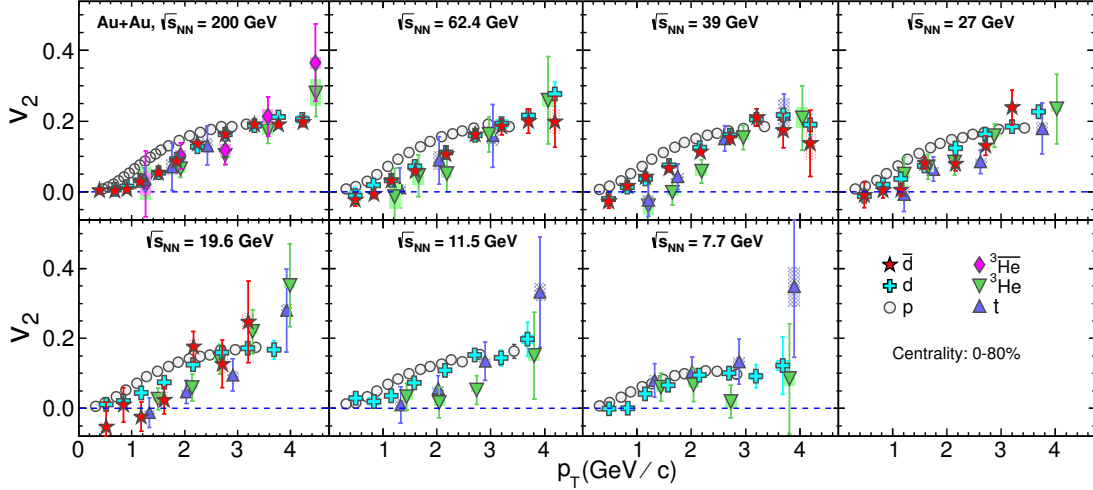


Figure 10: Elliptic flow v_2 of d , \bar{d} , t and ${}^3\text{He}$ as a function of transverse momentum p_T for 0-80% central events in Au+Au system for various beam energies. Bands corresponds to systematic errors which are smaller than the statistical errors

3.2 Mass ordering of nuclei v_2

Fig. 11 shows mass ordering of v_2 of d for all beam energies. v_2 of d has been compared with v_2 of π^+ , K_s^0 and p . From this figure we observe that nuclei v_2 mass ordering at low p_T/A ($< 2.0 \text{ GeV}/c$) similar to other hadron.

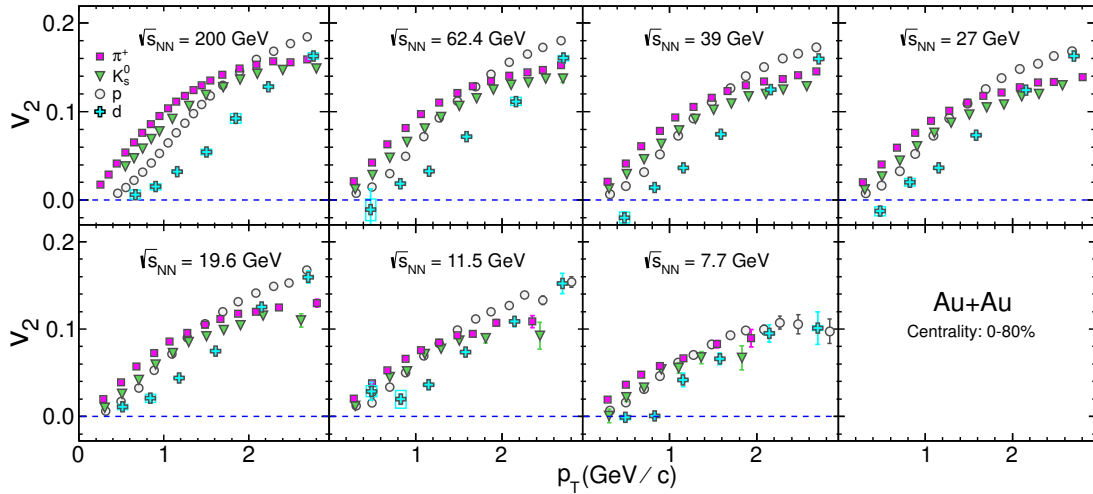


Figure 11: (Upper panel) Elliptic flow v_2 of triton (t) and ${}^3\text{He}$ as a function of transverse momentum p_T for 0-80% central events in Au+Au system for all beam energies. Bands corresponds to systematic errors which are smaller than the statistical errors

3.3 Nuclei and anti-nuclei v_2

While comparing v_2 of nuclei with corresponding anti-nuclei, it was found that they are of similar magnitude for beam energies $\sqrt{s_{NN}} = 200, 62.4, 39, 27$ and 19.6 GeV. The difference of v_2 of d with \bar{d} as a function of p_T is shown in Fig. 12. For comparison with hadrons, difference of v_2 of p and \bar{p} is also shown in open circles. For beam energies below 19.6 GeV, we lack statistics in anti-nuclei to carry out this analysis.

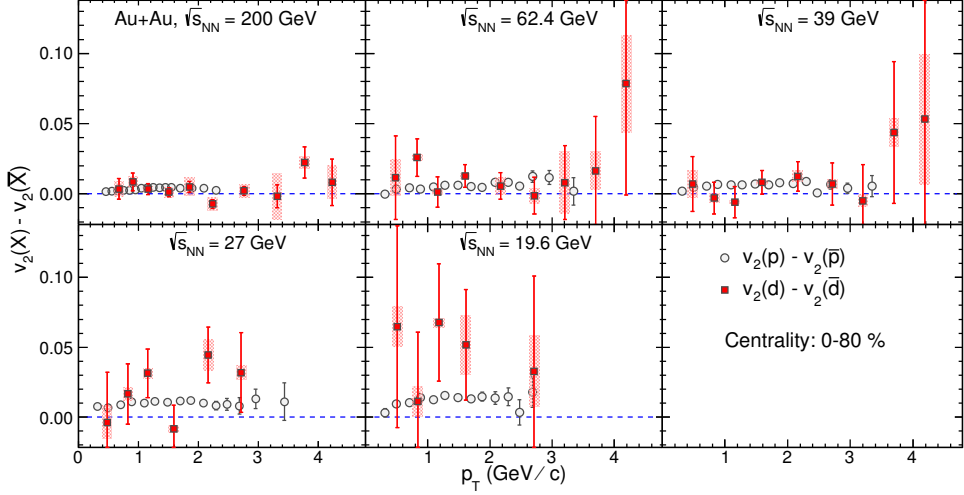


Figure 12: (Upper panel) Difference of v_2 of d, \bar{d} and p, \bar{p} as a function of transverse momentum p_T for 0-80% central events in Au+Au for $\sqrt{s_{NN}} = 200, 62.4, 39, 27$ and 19.6 GeV. Bands corresponds to systematic errors which are smaller than the statistical errors (lines)

3.4 Triton and ^3He v_2

Fig 13 shows comparison of triton (t) and ^3He v_2 for all beam energy. Within the statistical errors, we find the magnitude of t and ^3He v_2 are same.

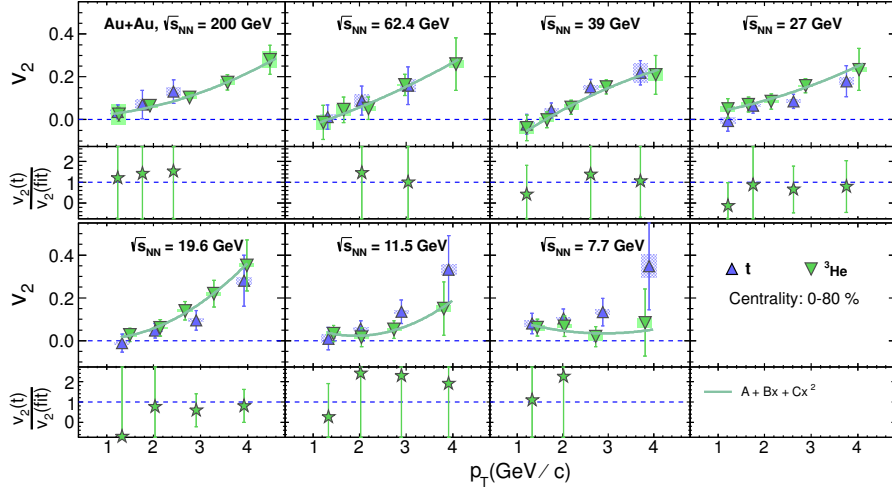


Figure 13: (Upper panel) Elliptic flow v_2 of triton (t) and ^3He as a function of transverse momentum p_T for 0-80% central events in Au+Au system for all beam energies. Bands corresponds to systematic errors which are smaller than the statistical errors

3.5 Centrality dependence of v_2

With sufficient statistics, centrality dependence of v_2 of d was carried out for two different centrality bins for $\sqrt{s_{NN}} = 62.4, 39, 27, 19.6, 11.5$ and 7.7 GeV. However, centrality dependence of v_2 of \bar{d} is observable for $\sqrt{s_{NN}} > 19.6$ GeV. For $\sqrt{s_{NN}} = 200$ GeV, centrality dependence of v_2 of d and \bar{d} is shown for three different centrality bins. Fig. 14 shows the centrality dependence.

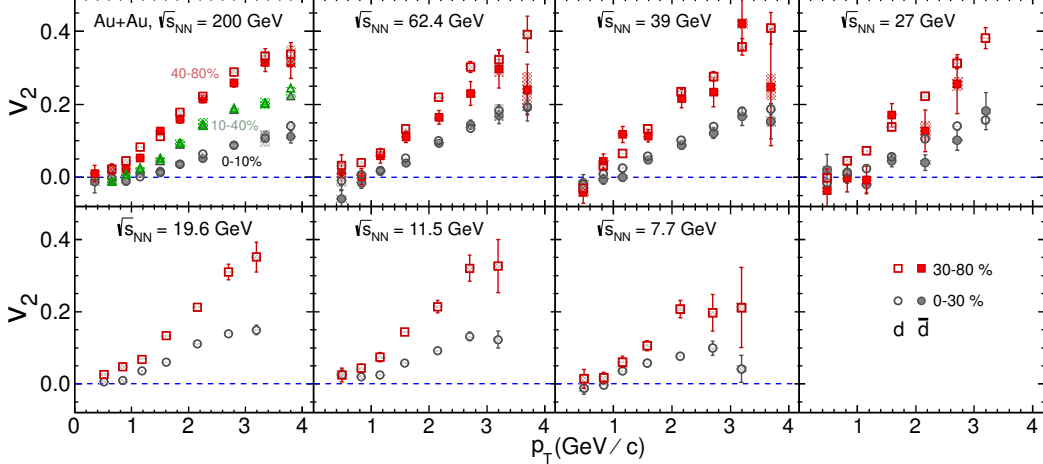


Figure 14: Centrality dependence of v_2 of d and \bar{d} . Bands corresponds to systematic errors which are smaller than the statistical errors

3.6 Mass scaling of nuclei v_2

Fig. 15 shows Atomic mass (A) number scaling of nuclei v_2 for all beam energies. The mass scaled nuclei v_2 results have been compared with corresponding v_2 of p (\bar{p}) results. From this figure we observe that v_2 of nuclei scales with its constituents v_2 for p_T/A up to 1.5 GeV/ c .

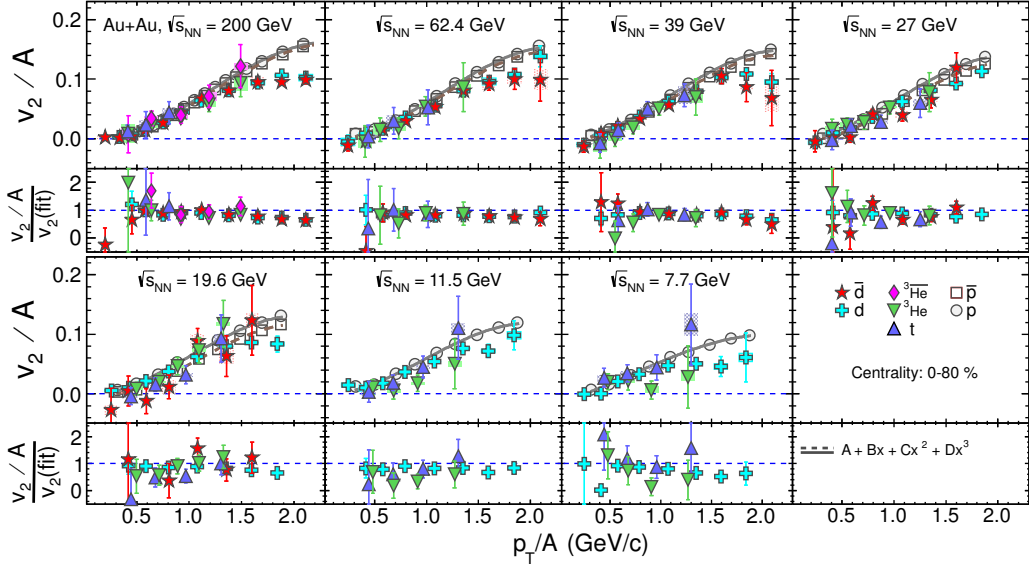


Figure 15: Atomic mass scaling of nuclei v_2 of for Au+Au collisions at $\sqrt{s_{NN}} = 200, 62.4, 39, 27, 19.6, 11.5$ and 7.7 GeV. Bands corresponds to systematic errors which are smaller than the statistical errors (lines)

3.7 Comparison with model

The nuclei v_2 from data has also been compared to coalescence model results and comparison is shown in Fig. 16. The phase space distributions of constituent nucleons (proton and neutron) from A Multi Phase Transport, (namely AMPT) model [11] has been used for this study. In the dynamical coalescence model, which has been used extensively at both intermediate [12] and high energies [13], the probability for producing a cluster is determined by the overlap of its Wigner phase-space density and the nucleon phase-space distribution at freeze-out. For light nuclei, the Wigner phase-space densities are obtained from their internal wave functions, which are taken to be those of a spherical harmonic oscillator [14].

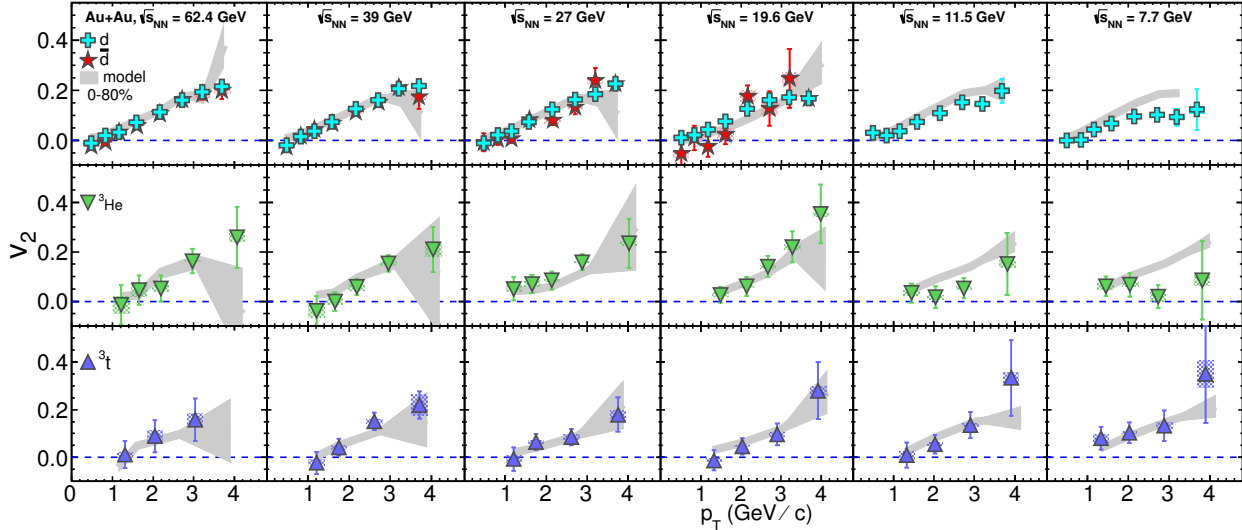


Figure 16: Model v_2 results (grey band) for different nuclei species and different energies compared with experimental results. String melting version of A Multi Phase Transport (AMPT) model has been used for this model study.

References

- [1] D. Kharzeev and M. Nardi, *Phys. Lett. B* 507, 121 (2001).
- [2] B. B. Back *et al.*, (PHOBOS Collaboration), *Phys. Rev. C* 70, 021902(R) (2004)
- [3] H. Masui and A. Schmah, *arXiv:* 1212.3650v1 [nucl-ex].
- [4] M. Anderson *et al.*, *Nucl. Inst. and Meth. A* 499, 659 (2003).
- [5] H. Bichsel, *Nucl. Instrum. Meth. A* 562 154 (2006).
- [6] B. Bonner *et al.*, *Nucl. Inst. and Meth. A* 508, 181 (2003).
- [7] A. M. Poskanzer and S. A. Voloshin, *Phys. Rev. C*, 58, 1671–1678 (1998).
- [8] B. I. Abelev *et al.*, (STAR Collaboration), *Phys. Rev. C* 77, 054901 (2008).
- [9] F. Retiere and M. Lisa, *Phys. Rev. C* 70, 044907 (2004).
- [10] L. Adamczyk *et al.*, *arXiv:* 1403.4972v1 [nucl-ex]

- [11] Z. Lin *et al.*, *Phys. Rev. C* **72**, 064901 (2005);
- [12] M. Gyulassy, K. Frankel, E. A. Relmer, *Nucl. Phys. A* **402**, 596 (1983); J. Aichelin *et al.*, *Phys. Rev. Lett.* **58**, 1926 (1987); V. Koch *et al.*, *Phys. Lett. B* **241**, 174 (1990); L. W. Chen, C.M. Ko, B. A. Li, *Phys. Rev. C* **68**, 017601 (2003).
- [13] J. L. Nagle *et al.*, *Phys. Rev. C* **53**, 367 (1996); R. Mattiello *et al.*, *Phys. Rev. C* **55**, 1443 (1997); L. W. Chen and C. M. Ko, *Phys. Rev. C* **73**, 044903 (2006).
- [14] R. Scheibl and U. Heinz, *Phys. Rev. C* **59**, 1585 (1999); A. T. M. Aerts and C. B. Dover, *Phys. Rev. D* **28**, 450 (1983).

Appendix

4 Removing beam pipe contamination from d yield

The region of beam pipe running through the TPC detector is made of low Z material (Berilium). The particles coming from the primary vertex can hit the beam pipe material and generate large numbers of secondary particles with low Z, including deuterons. The low momentum deuterons from collision vertex have a significant contamination from these background deuterons knocked out from the beam pipe. These background deuterons cannot be easily distinguished by the TPC as their ionization energy loss characteristics are similar to the primary deuterons from the primary vertex. The background deuteron tracks is not generated in the actual event and hence they are not related to the primary vertex. The characteristic quantity which defines how close the track is from the primary vertex is the distance of closest approach (DCA). For this analysis primary tracks which have $DCA < 1.0$ cm has been used as shown in Table 2. The DCA of primary deuterons is small, while the DCA of background deuterons could be either large or small. \bar{d} is not knocked out from the beam pipe, and it is expected that the DCA distributions of primary d tracks should have equivalent shapes as the DCA distributions of \bar{d} . Fig.17 shows the DCA distributions of d and \bar{d} in two different transverse momentum range.

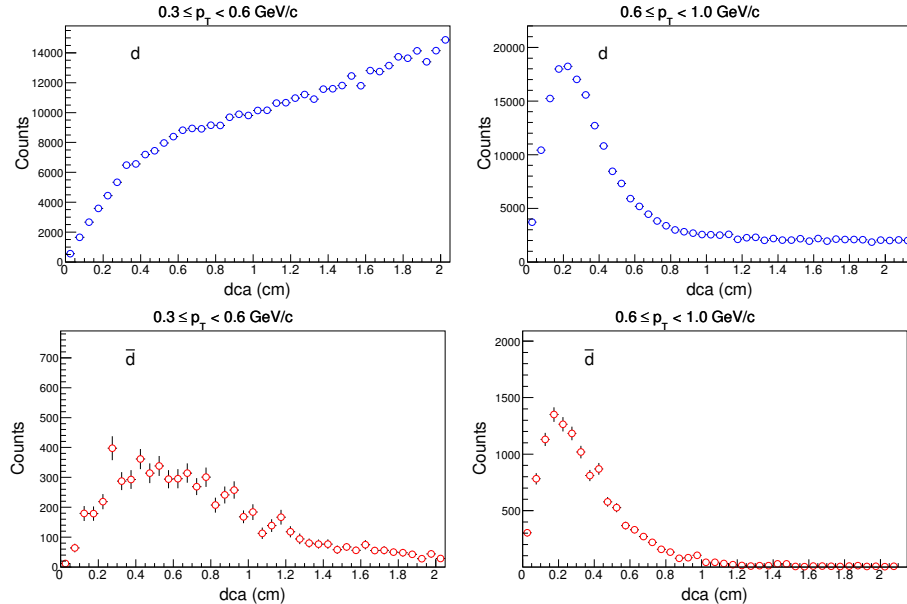


Figure 17: DCA ditribution of d (upper panel) and \bar{d} (lower panel) for $0 < (\phi - \Psi_2) < \frac{\pi}{10}$ and for 0-80% central events in Au+Au at $\sqrt{s_{NN}} = 39$ GeV.

From the Fig.17, it is obvious that DCA distributions of d is not similar to that of \bar{d} due to added contribution of knocked out deuterons from beam pipe. Therefore, this secondary deuterons has been removed from our analysis. We fit the DCA distribution of d in each p_T range by a function:

$$dca(d) = dca(\bar{d}) + A[1 - \exp(-\frac{dca}{dca_0})]^c$$

Where, $dca(\bar{d})$ is the scaled DCA distribution of \bar{d} and A , dca_0 and c are fit parameters. Hence, we obtained the beam pipe conribution of deuteron as given by the second part of the above equation. Therefore, we remove the beam pipe contamination in deuteron and then it

becomes identical to the DCA distribution of \bar{d} as shown in Fig.18.

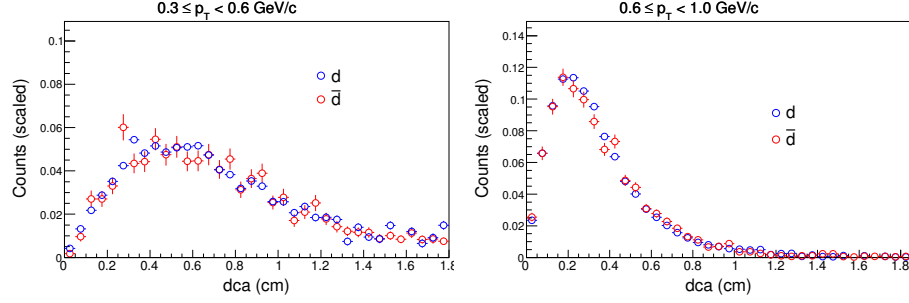


Figure 18: DCA ditribution of d (after removing beam pipe contamination) and \bar{d} for $0 < (\phi - \Psi_2) < \frac{\pi}{10}$ and 0-80% central events in Au+Au at $\sqrt{s_{NN}} = 39$ GeV.

Therefore, correct yield of d can be given as:

$$Yield(d) = \text{Integral of } dca(d) - \text{Integral of } A[1 - \exp(\frac{dca}{dca_0})]^c$$

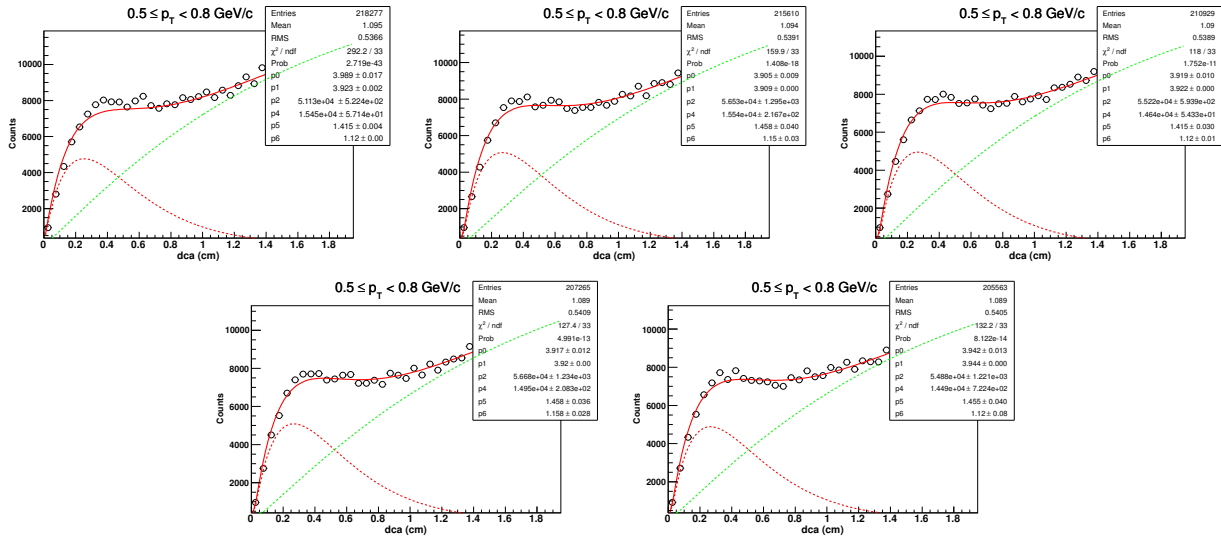
where, values of A , dca_0 and c are obtained by fitting the DCA distribution of deuteron as mentioned above. In this analysis, d yield has been calculated for $p_T < 1.0$ GeV/c following the method mentioned above. For $p_T > 1.0$ GeV/c, the usual Z-distribution method has been followed to calculate yield of d , t and 3He . To get \bar{d} yield Z-distribution method has been followed for all p_T range.

5 DCA and Z-distributions for Au+Au at $\sqrt{s_{NN}} = 200$ GeV

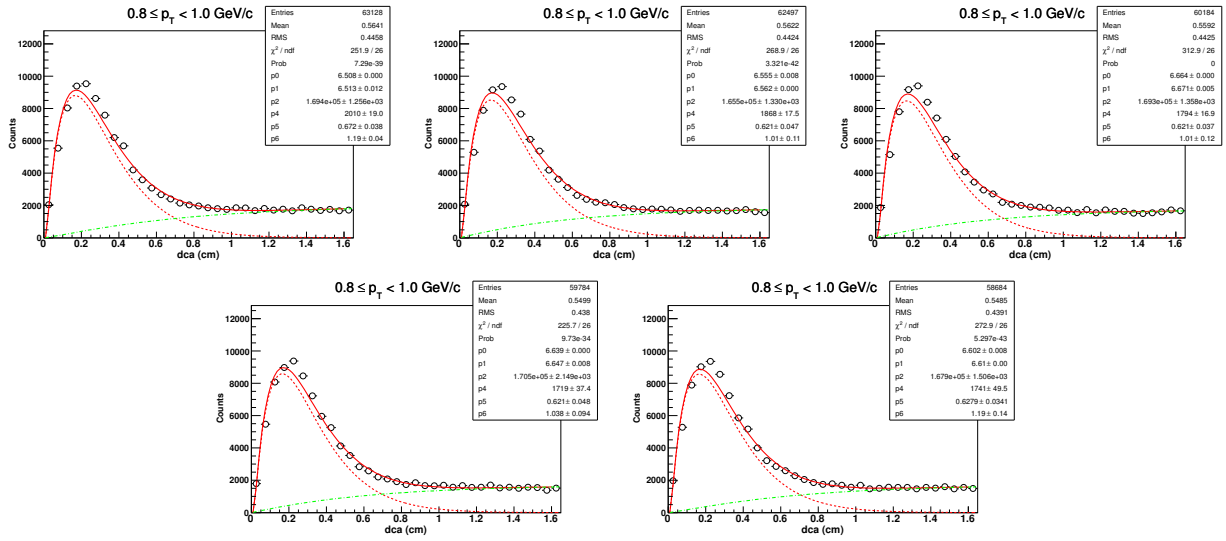
In this section we show the DCA and Z-distribution of deuteron and anti-deuteron for five different $(\phi - \Psi_2)$ bins namely, $0 - \frac{\pi}{10}$, $\frac{\pi}{10} - \frac{2\pi}{10}$, $\frac{2\pi}{10} - \frac{3\pi}{10}$, $\frac{3\pi}{10} - \frac{4\pi}{10}$ and $\frac{4\pi}{10} - \frac{5\pi}{10}$. DCA and Z-distribution of d for all centrality and all p_T bins are shown in the later sub-sections.

5.1 Centrality: 0-80%

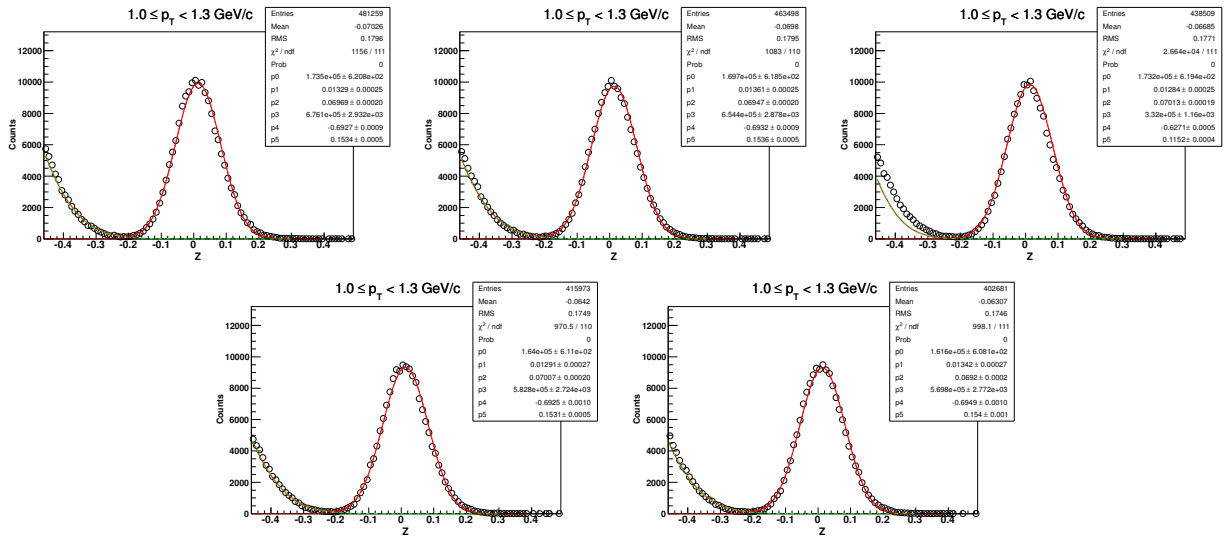
5.1.1 DCA-distribution of d for $0.5 < p_T < 0.8$ GeV/c



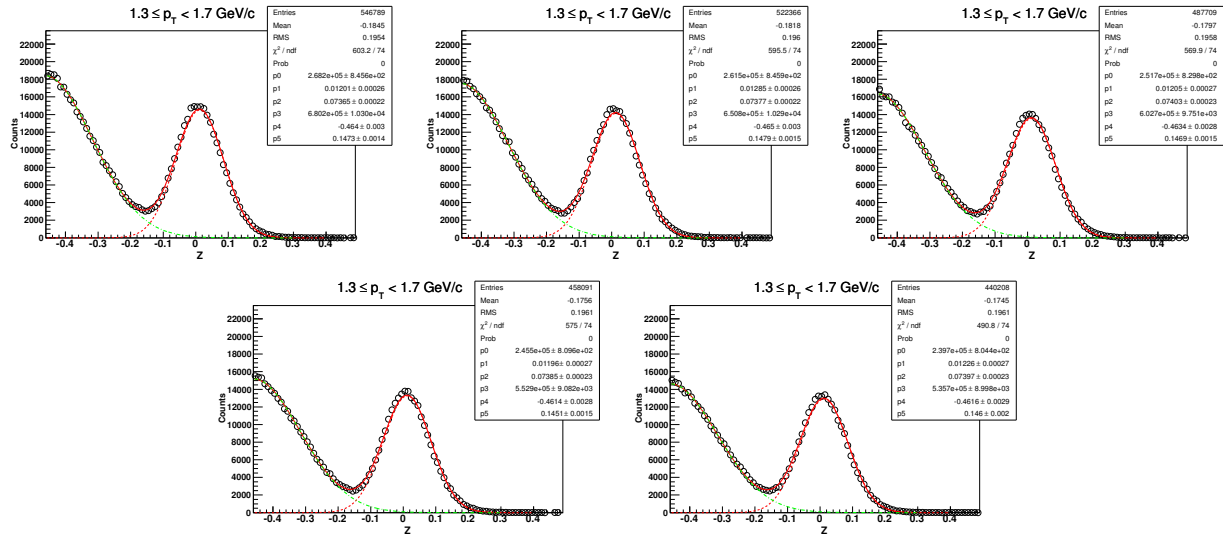
5.1.2 DCA-distribution of d for $0.8 < p_T < 1.0 \text{ GeV}/c$ ($\sqrt{s_{NN}} = 200 \text{ GeV}$, 0-80%)



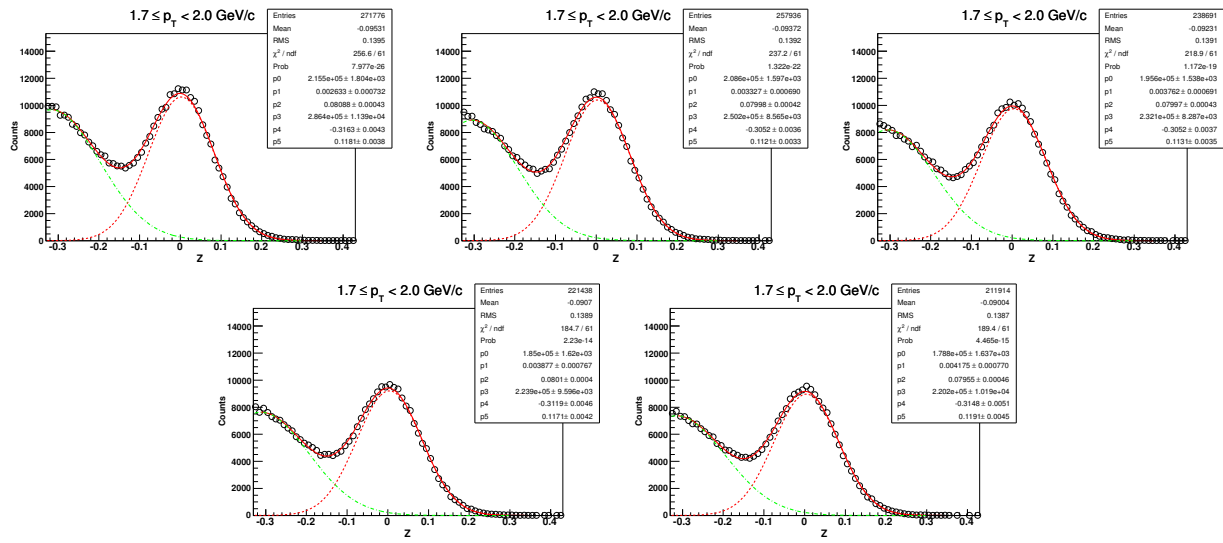
5.1.3 Z-distribution of d for $1.0 < p_T < 1.3 \text{ GeV}/c$ ($\sqrt{s_{NN}} = 200 \text{ GeV}$, 0-80%)



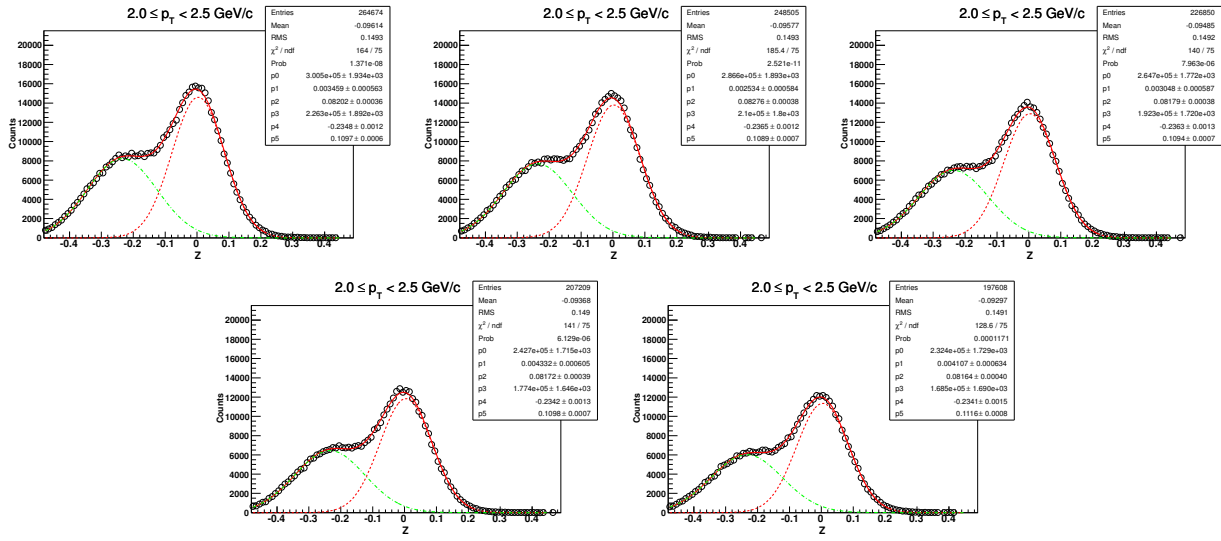
5.1.4 Z-distribution of d for $1.3 < p_T < 1.7 \text{ GeV}/c$ ($\sqrt{s_{NN}} = 200 \text{ GeV}$, 0-80%)



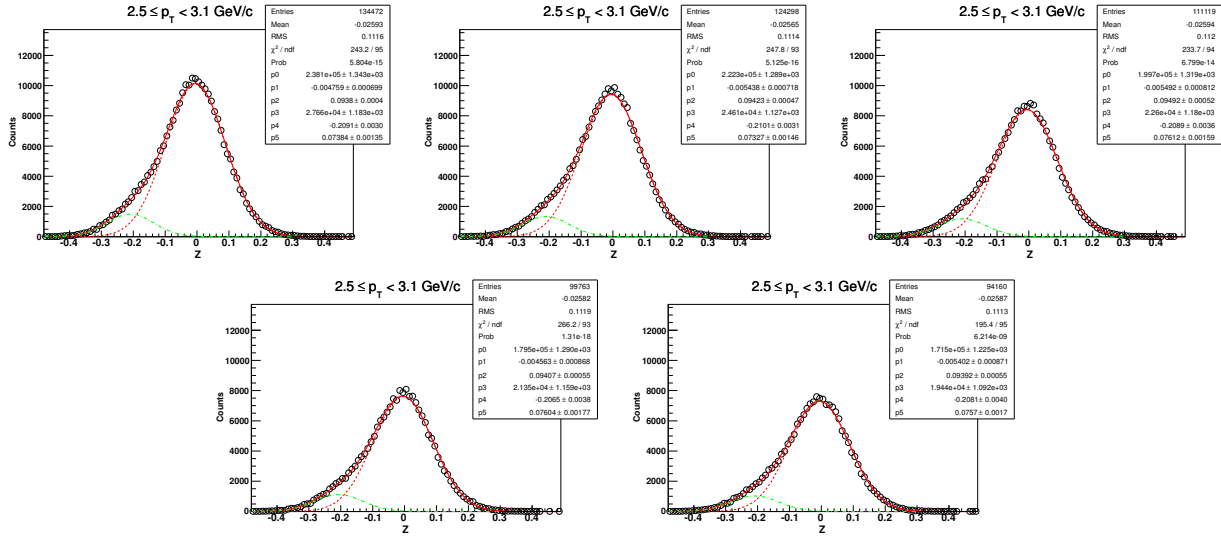
5.1.5 Z-distribution of d for $1.7 < p_T < 2.0 \text{ GeV}/c$ ($\sqrt{s_{NN}} = 200 \text{ GeV}$, 0-80%)



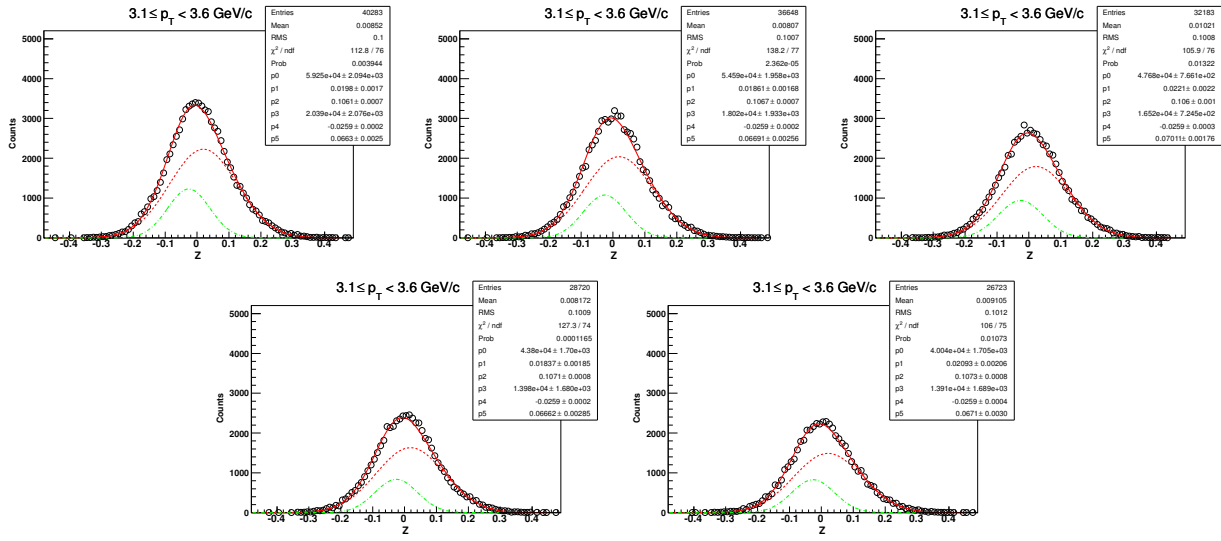
5.1.6 Z-distribution of d for $2.0 < p_T < 2.5 \text{ GeV}/c$ ($\sqrt{s_{NN}} = 200 \text{ GeV}$, 0-80%)



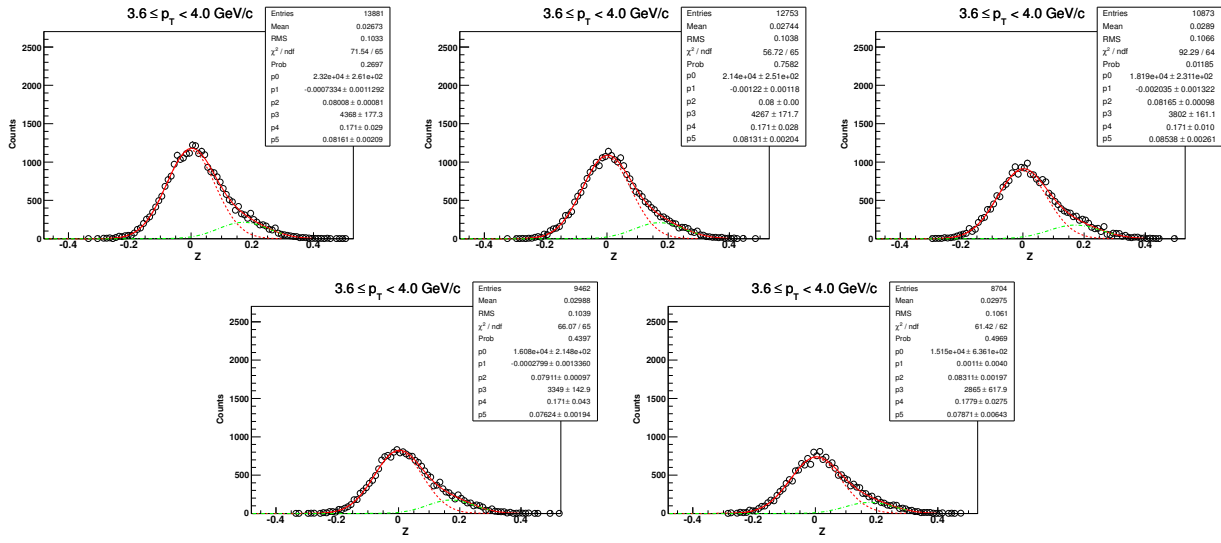
5.1.7 Z-distribution of d for $2.5 < p_T < 3.1 \text{ GeV}/c$ ($\sqrt{s_{NN}} = 200 \text{ GeV}$, 0-80%)



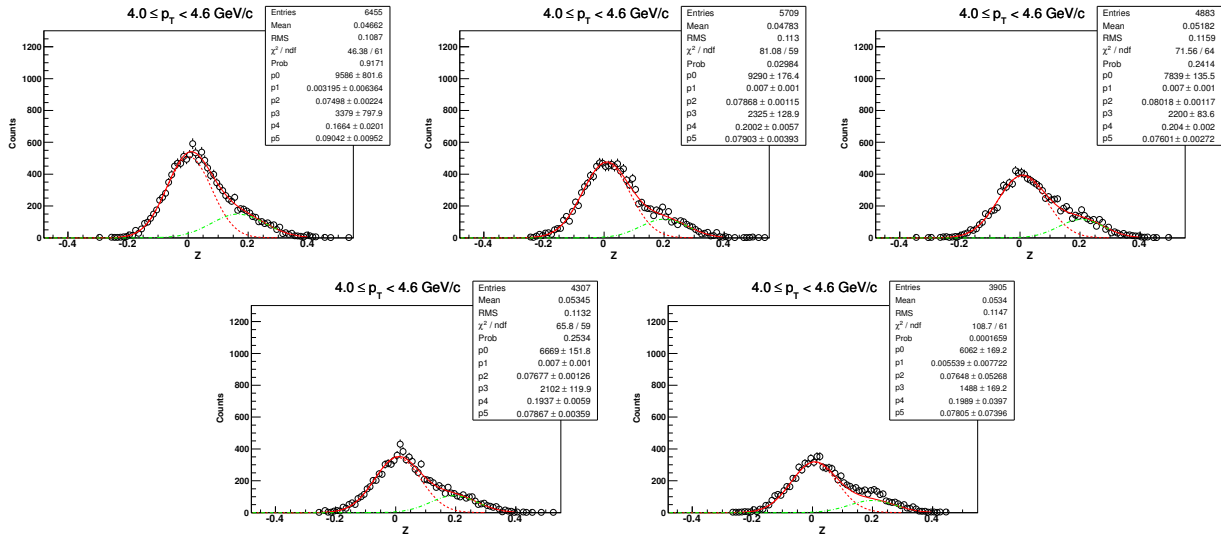
5.1.8 Z-distribution of d for $3.1 < p_T < 3.6 \text{ GeV}/c$ ($\sqrt{s_{NN}} = 200 \text{ GeV}$, 0-80%)



5.1.9 Z-distribution of d for $3.6 < p_T < 4.0 \text{ GeV}/c$ ($\sqrt{s_{NN}} = 200 \text{ GeV}$, 0-80%)

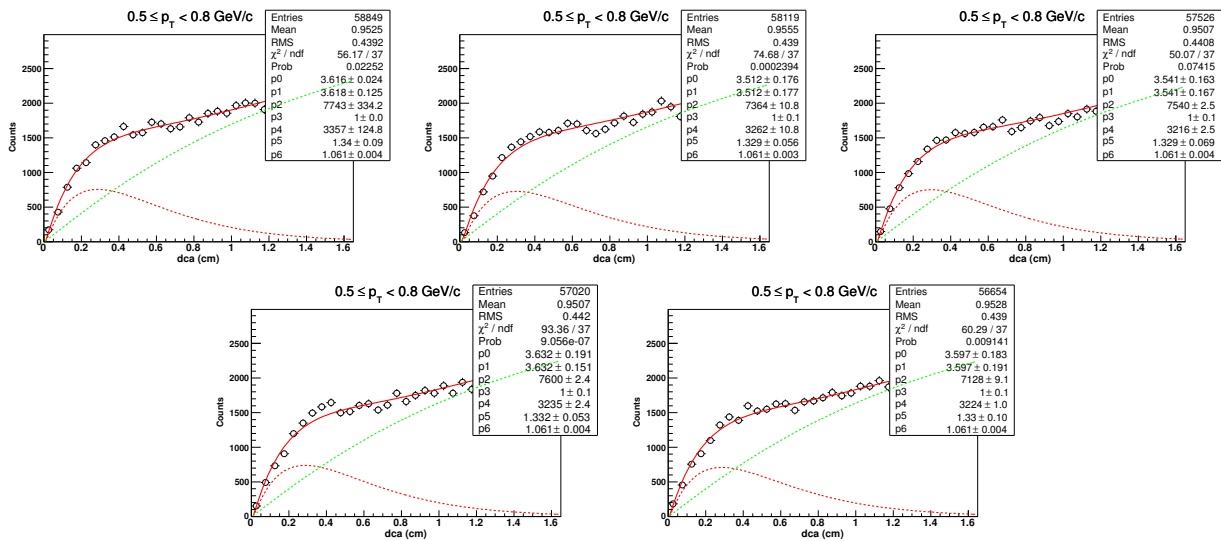


5.1.10 Z-distribution of d for $4.0 < p_T < 4.6 \text{ GeV}/c$ ($\sqrt{s_{NN}} = 200 \text{ GeV}$, 0-80%)

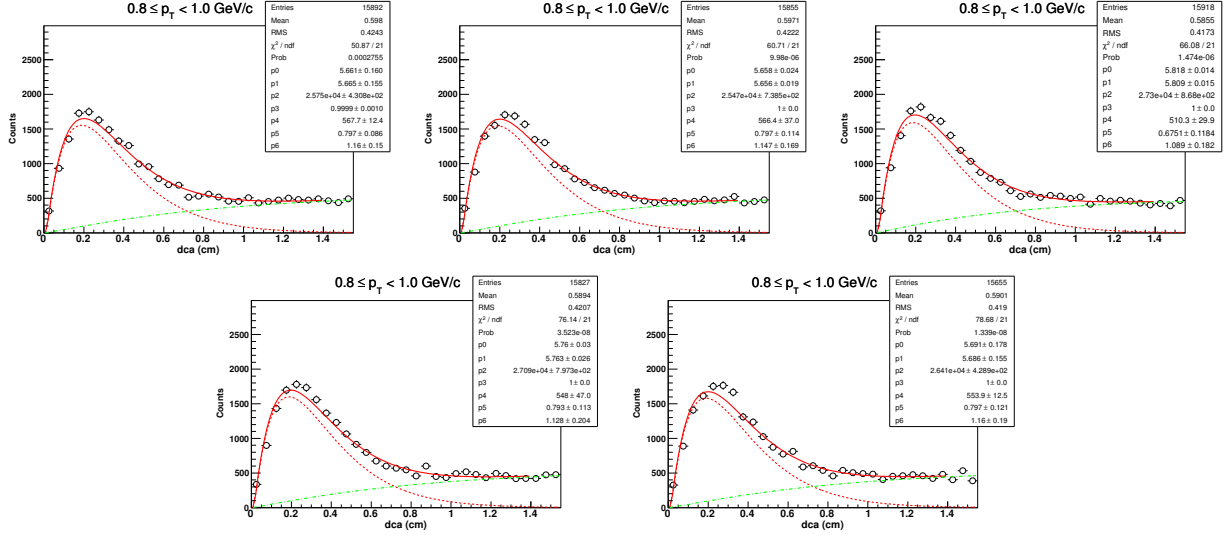


5.2 Centrality: 0-10% (Au+Au at $\sqrt{s_{NN}} = 200 \text{ GeV}$)

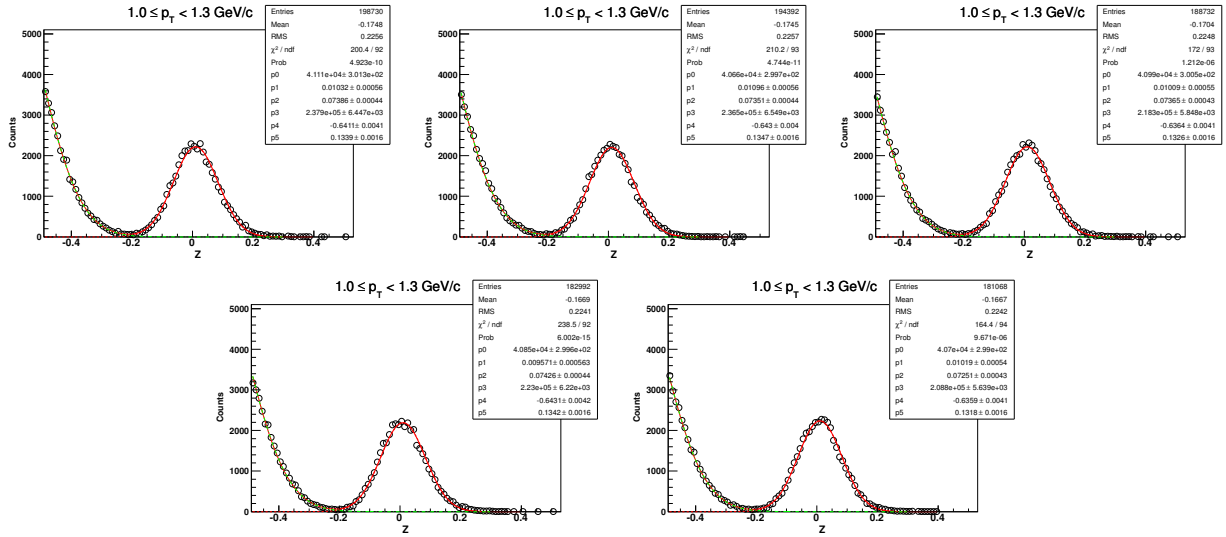
5.2.1 DCA-distribution of d for $0.5 < p_T < 0.8 \text{ GeV}/c$



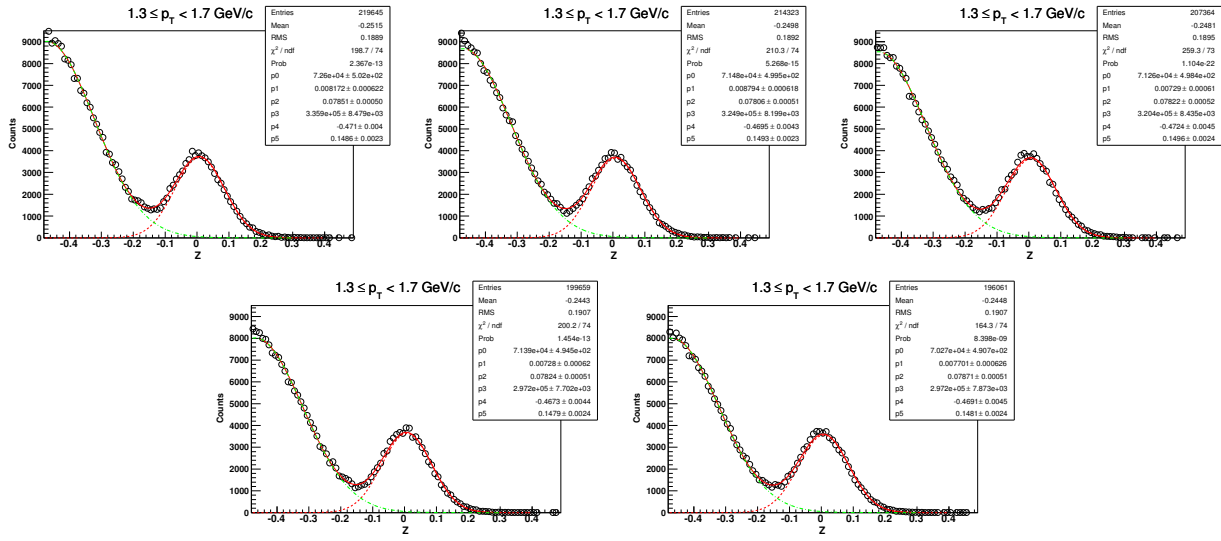
5.2.2 DCA-distribution of d for $0.8 < p_T < 1.0 \text{ GeV}/c$ ($\sqrt{s_{NN}} = 200 \text{ GeV}$, 0-10%)



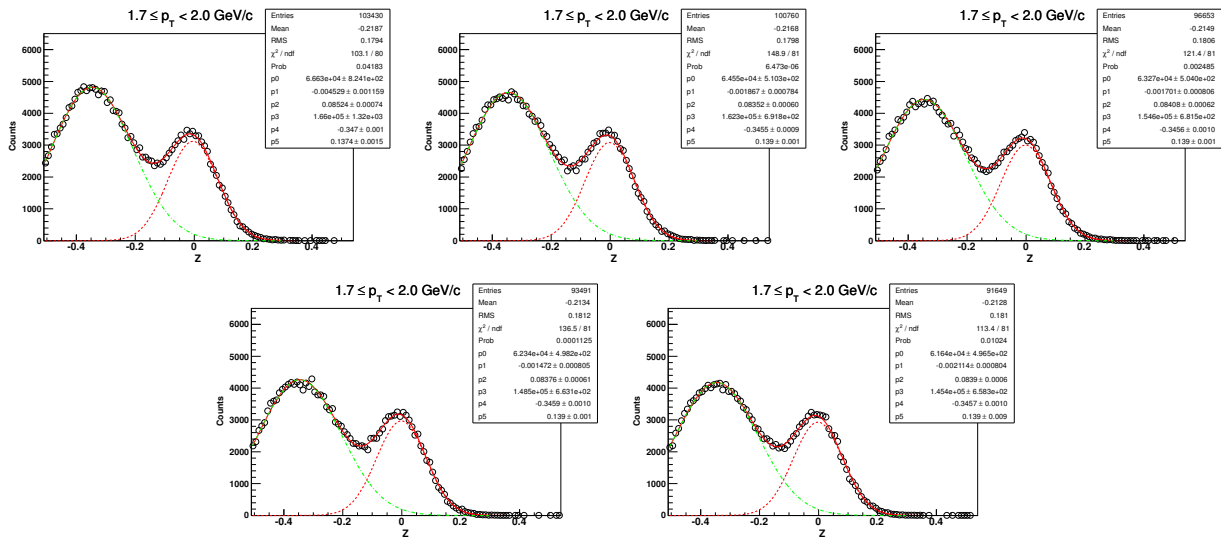
5.2.3 Z-distribution of d for $1.0 < p_T < 1.3 \text{ GeV}/c$ ($\sqrt{s_{NN}} = 200 \text{ GeV}$, 0-10%)



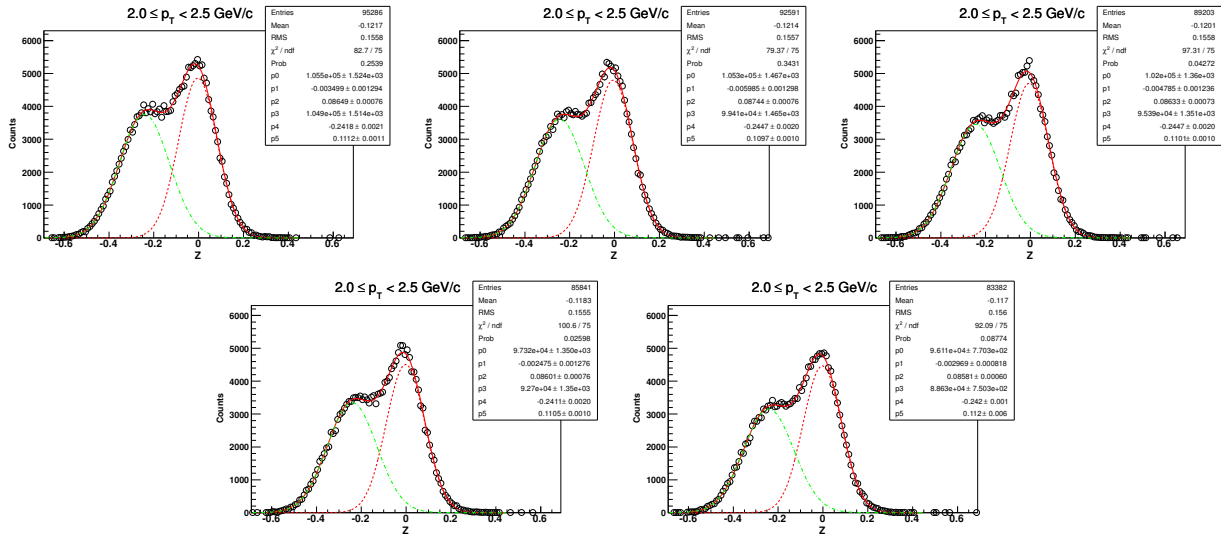
5.2.4 Z-distribution of d for $1.3 < p_T < 1.7 \text{ GeV}/c$ ($\sqrt{s_{NN}} = 200 \text{ GeV}$, 0-10%)



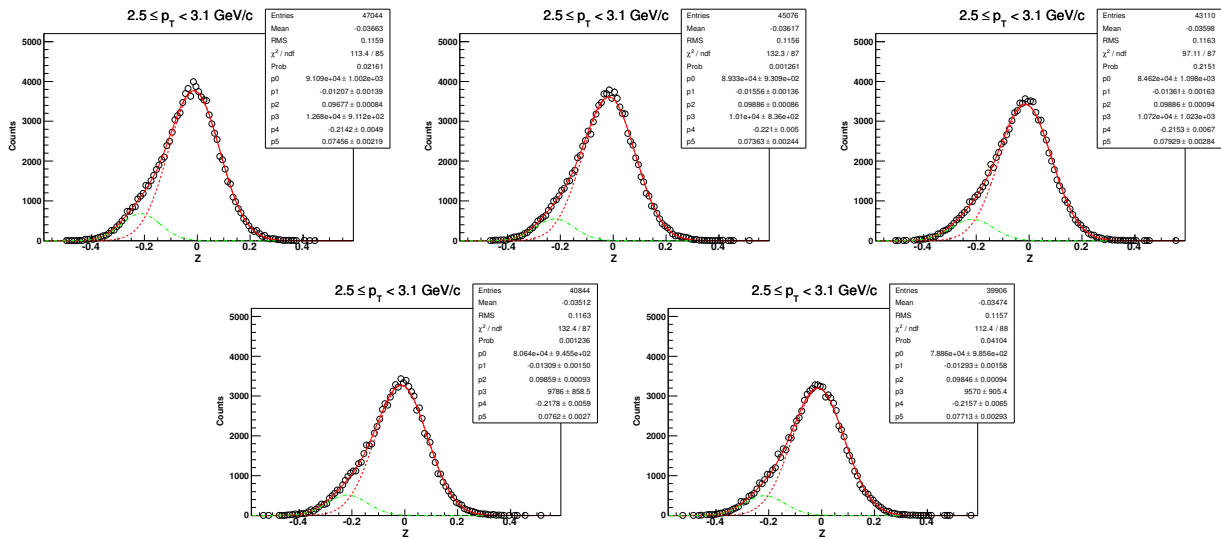
5.2.5 Z-distribution of d for $1.7 < p_T < 2.0 \text{ GeV}/c$ ($\sqrt{s_{NN}} = 200 \text{ GeV}$, 0-10%)



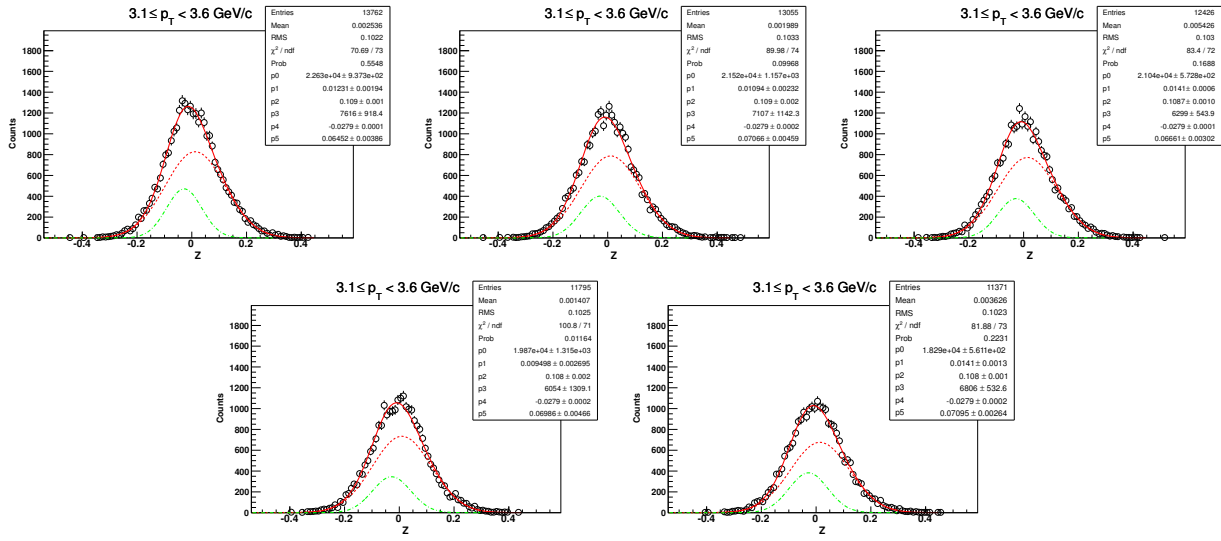
5.2.6 Z-distribution of d for $2.0 < p_T < 2.5 \text{ GeV}/c$ ($\sqrt{s_{NN}} = 200 \text{ GeV}$, 0-10%)



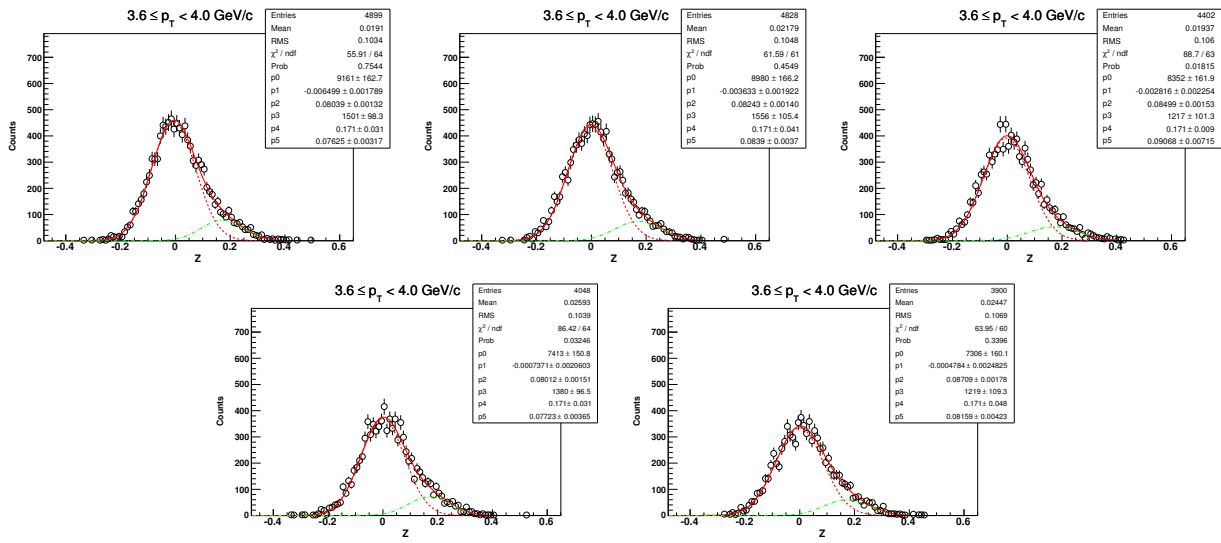
5.2.7 Z-distribution of d for $2.5 < p_T < 3.1 \text{ GeV}/c$ ($\sqrt{s_{NN}} = 200 \text{ GeV}$, 0-10%)



5.2.8 Z-distribution of d for $3.1 < p_T < 3.6 \text{ GeV}/c$ ($\sqrt{s_{NN}} = 200 \text{ GeV}$, 0-10%)

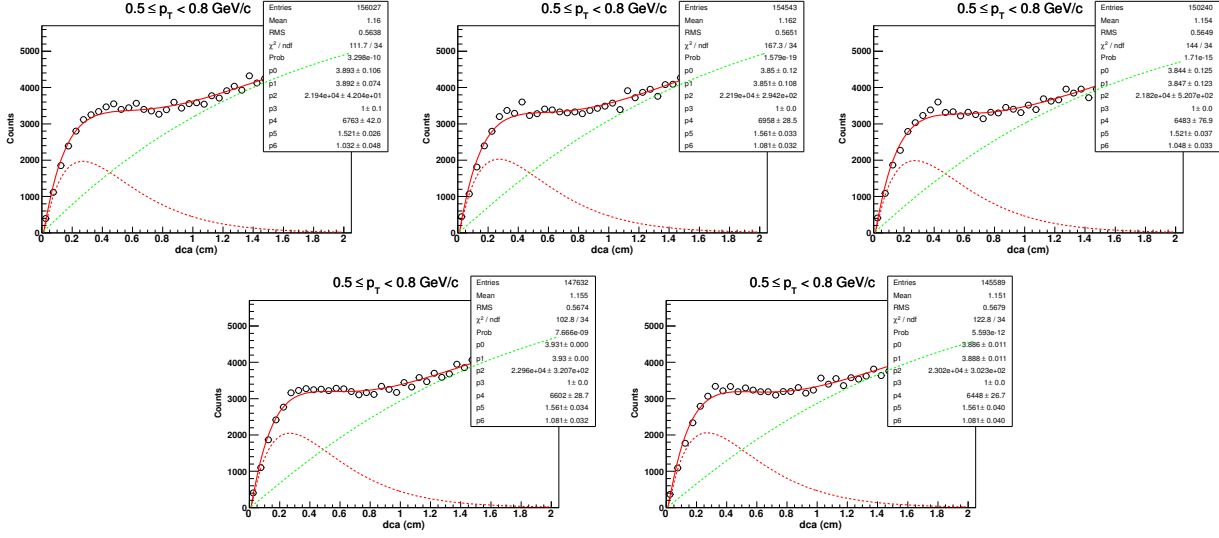


5.2.9 Z-distribution of d for $3.6 < p_T < 4.0 \text{ GeV}/c$ ($\sqrt{s_{NN}} = 200 \text{ GeV}$, 0-10%)

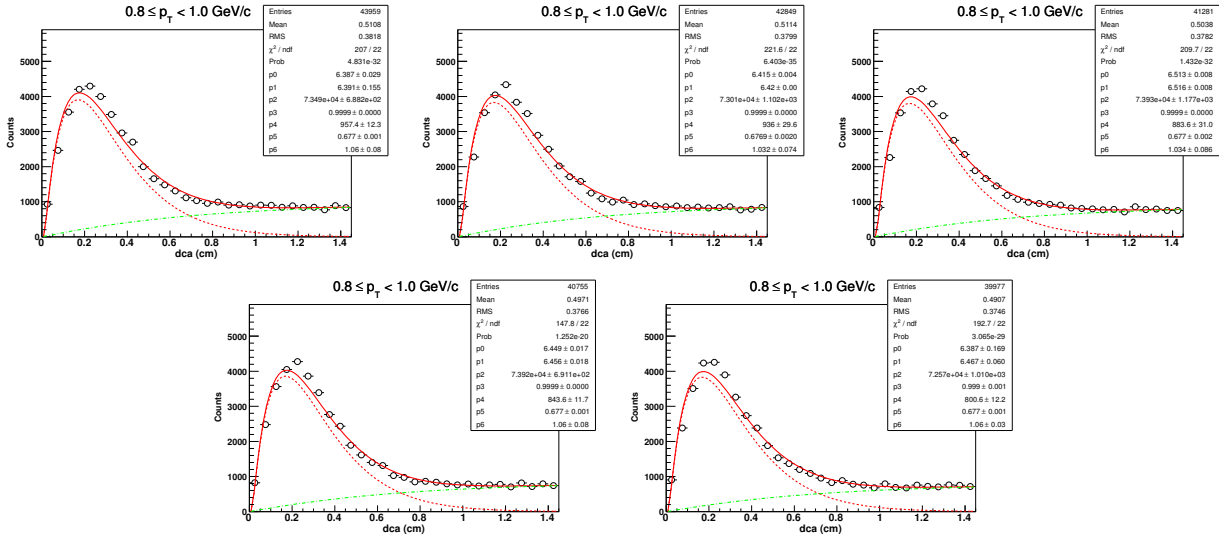


5.3 Centrality: 10-40% (Au+Au at $\sqrt{s_{NN}} = 200$ GeV)

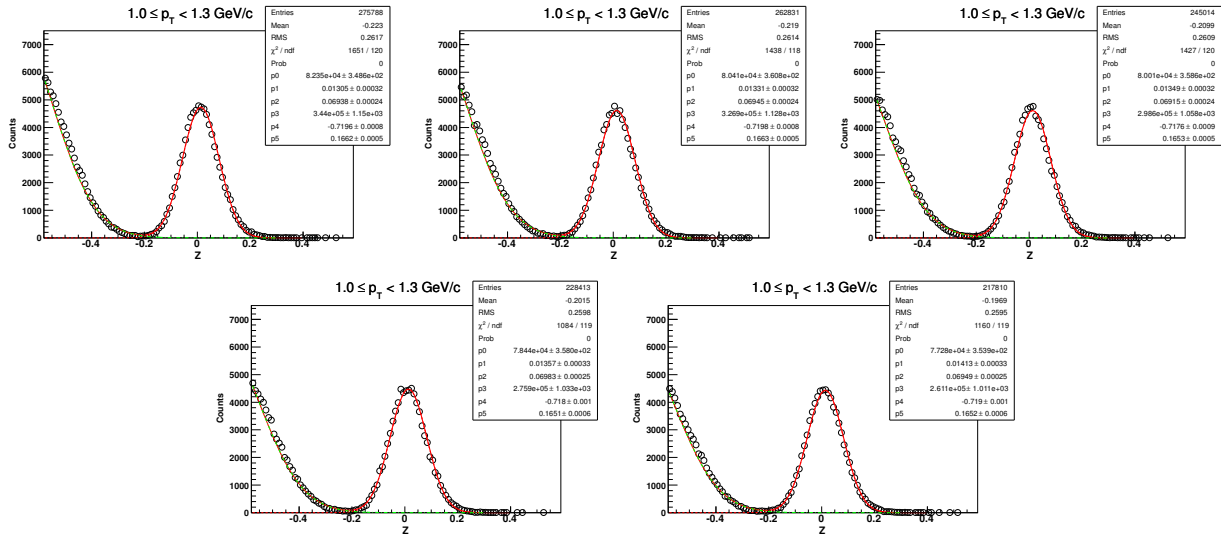
5.3.1 DCA-distribution of d for $0.5 < p_T < 0.8$ GeV/c



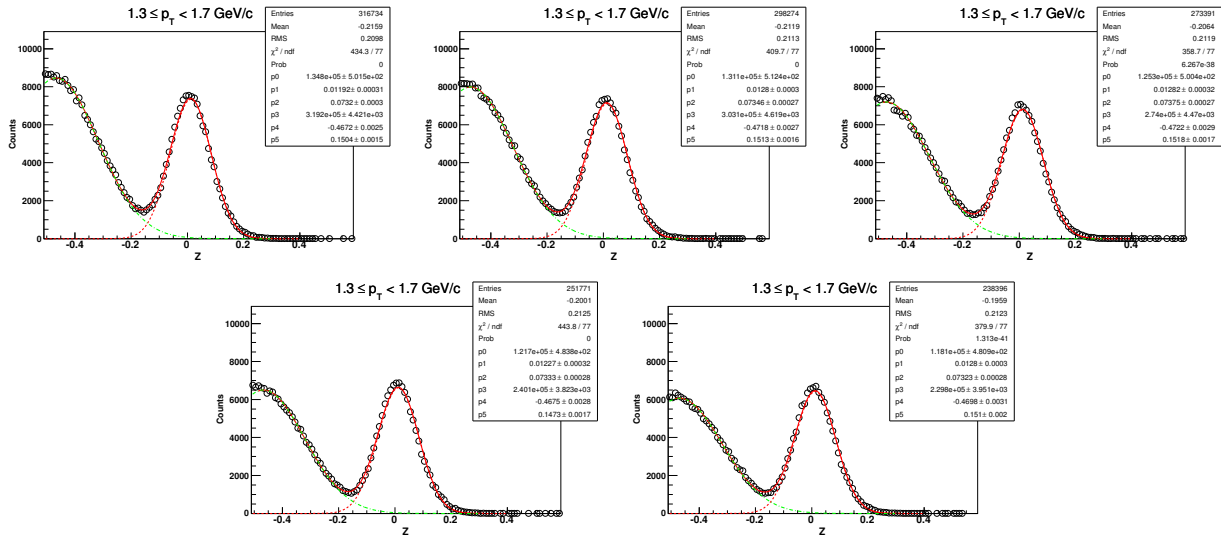
5.3.2 DCA-distribution of d for $0.8 < p_T < 1.0$ GeV/c ($\sqrt{s_{NN}} = 200$ GeV, 10-40%)



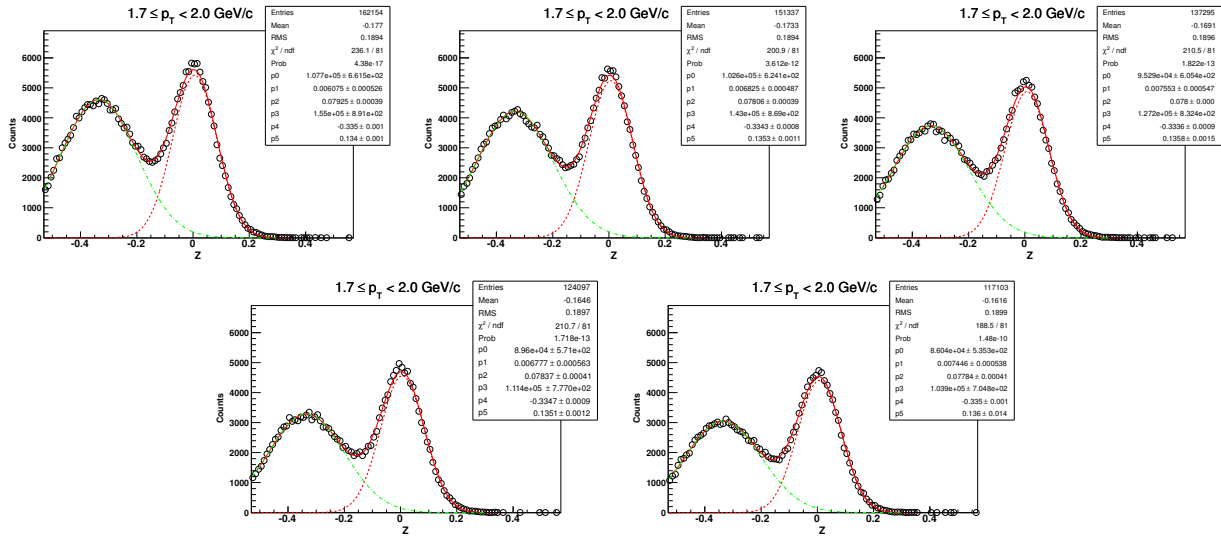
5.3.3 Z-distribution of d for $1.0 < p_T < 1.3 \text{ GeV}/c$ ($\sqrt{s_{NN}} = 200 \text{ GeV}$, 10-40%)



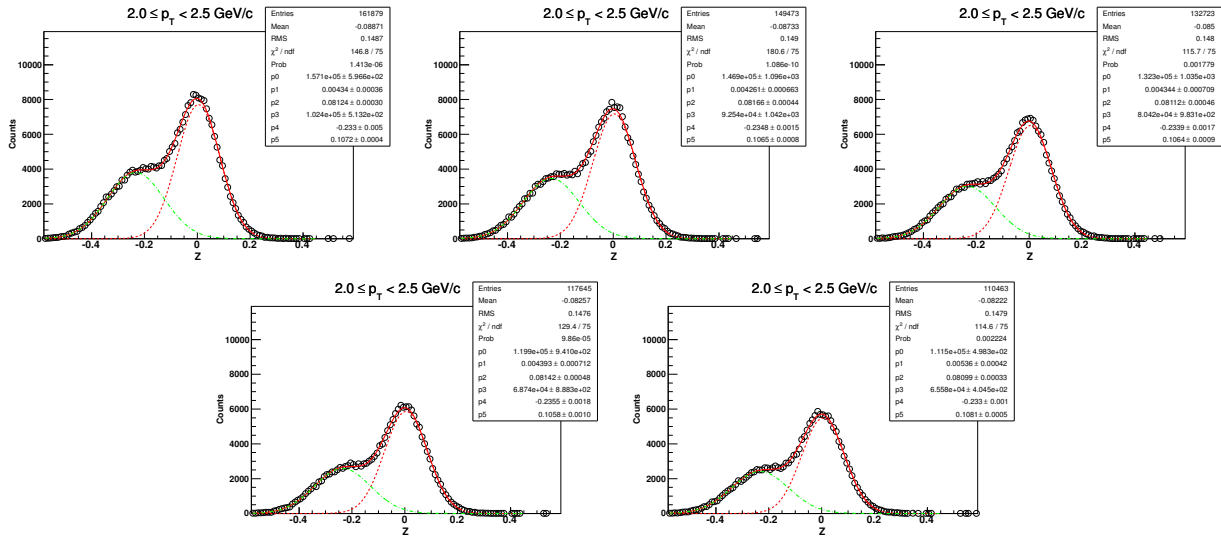
5.3.4 Z-distribution of d for $1.3 < p_T < 1.7 \text{ GeV}/c$ ($\sqrt{s_{NN}} = 200 \text{ GeV}$, 10-40%)



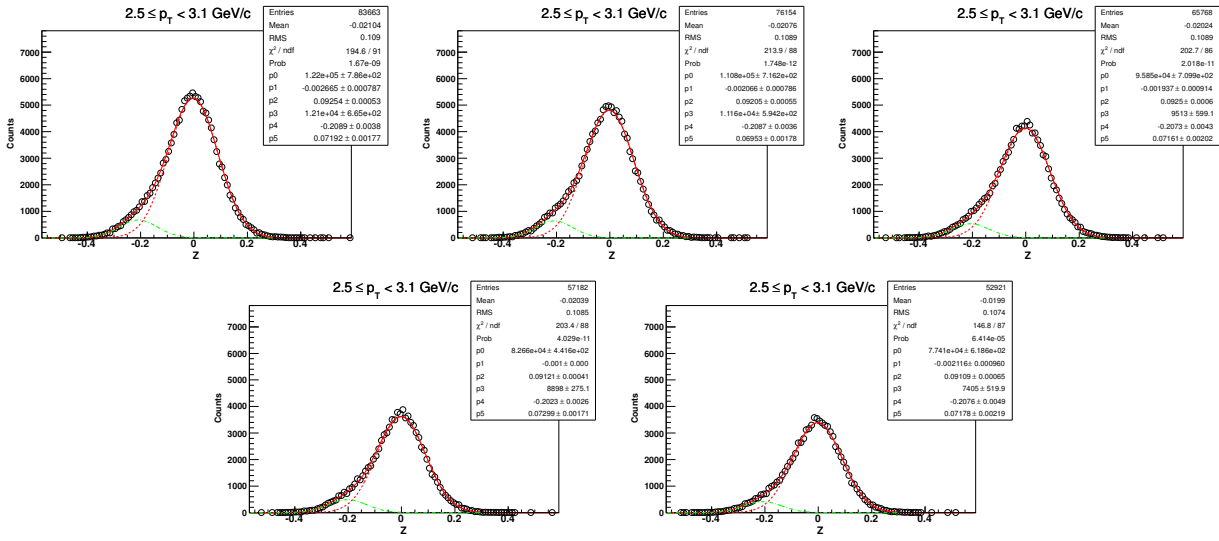
5.3.5 Z-distribution of d for $1.7 < p_T < 2.0 \text{ GeV}/c$ ($\sqrt{s_{NN}} = 200 \text{ GeV}$, 10-40%)



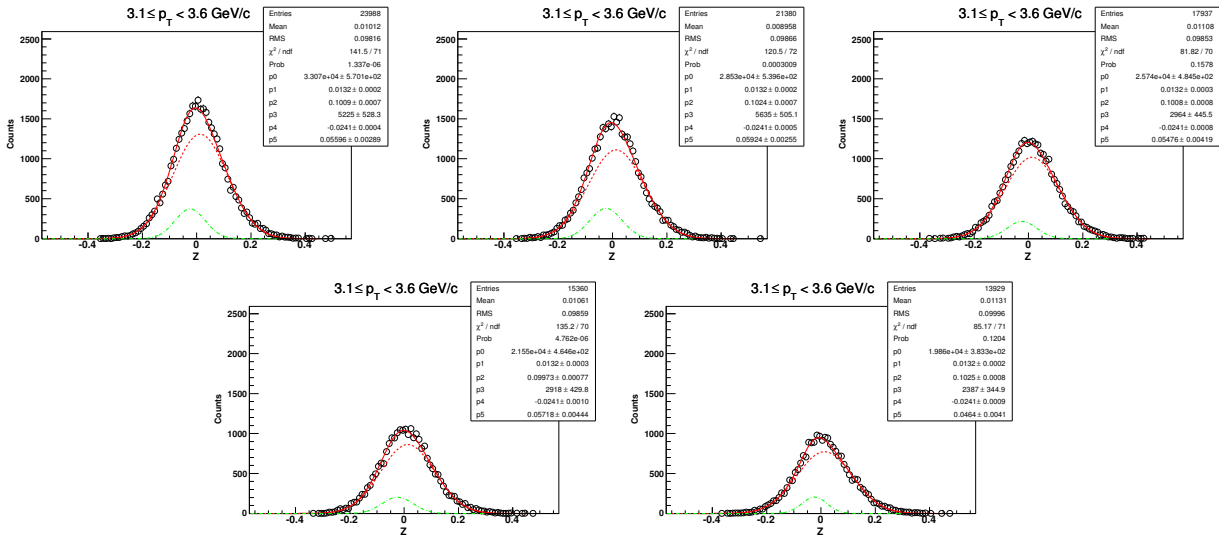
5.3.6 Z-distribution of d for $2.0 < p_T < 2.5 \text{ GeV}/c$ ($\sqrt{s_{NN}} = 200 \text{ GeV}$, 10-40%)



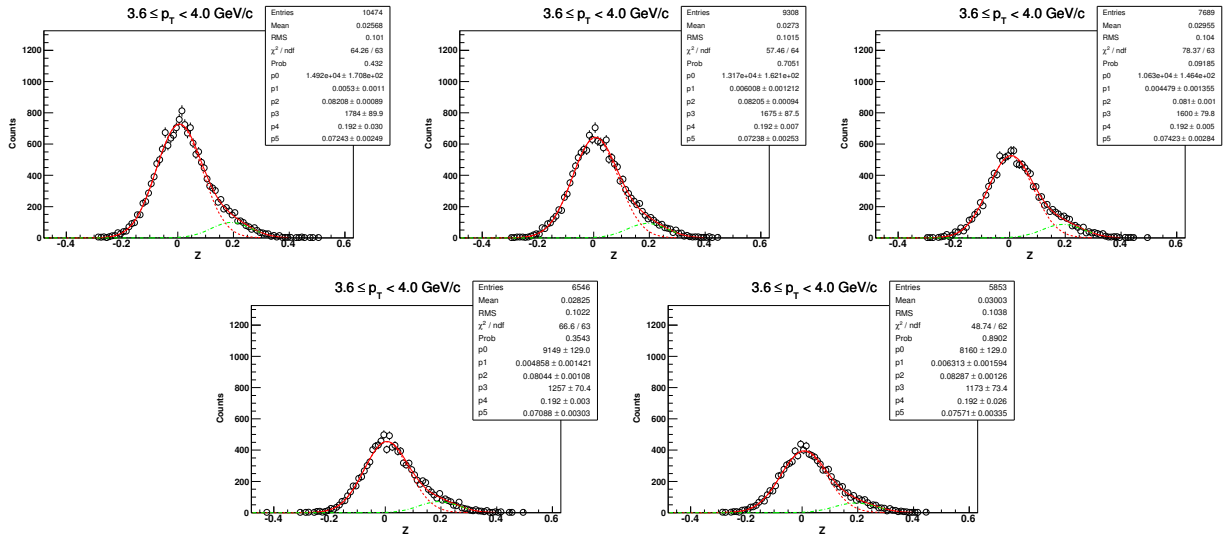
5.3.7 Z-distribution of d for $2.5 < p_T < 3.1 \text{ GeV}/c$ ($\sqrt{s_{NN}} = 200 \text{ GeV}$, 10-40%)



5.3.8 Z-distribution of d for $3.1 < p_T < 3.6 \text{ GeV}/c$ ($\sqrt{s_{NN}} = 200 \text{ GeV}$, 10-40%)

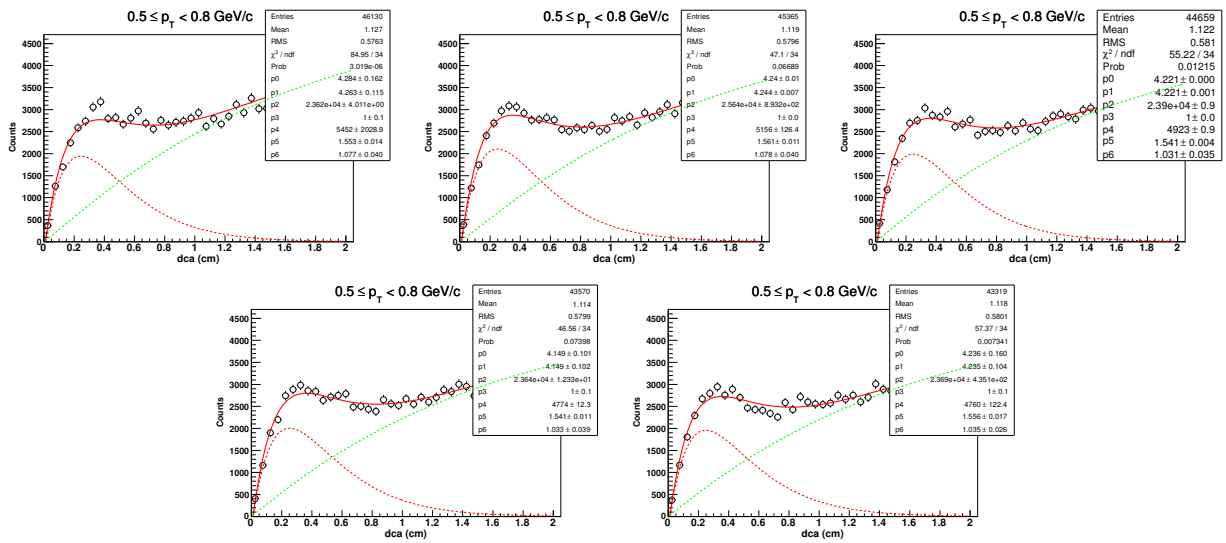


5.3.9 Z-distribution of d for $3.6 < p_T < 4.0 \text{ GeV}/c$ ($\sqrt{s_{NN}} = 200 \text{ GeV}$, 10-40%)

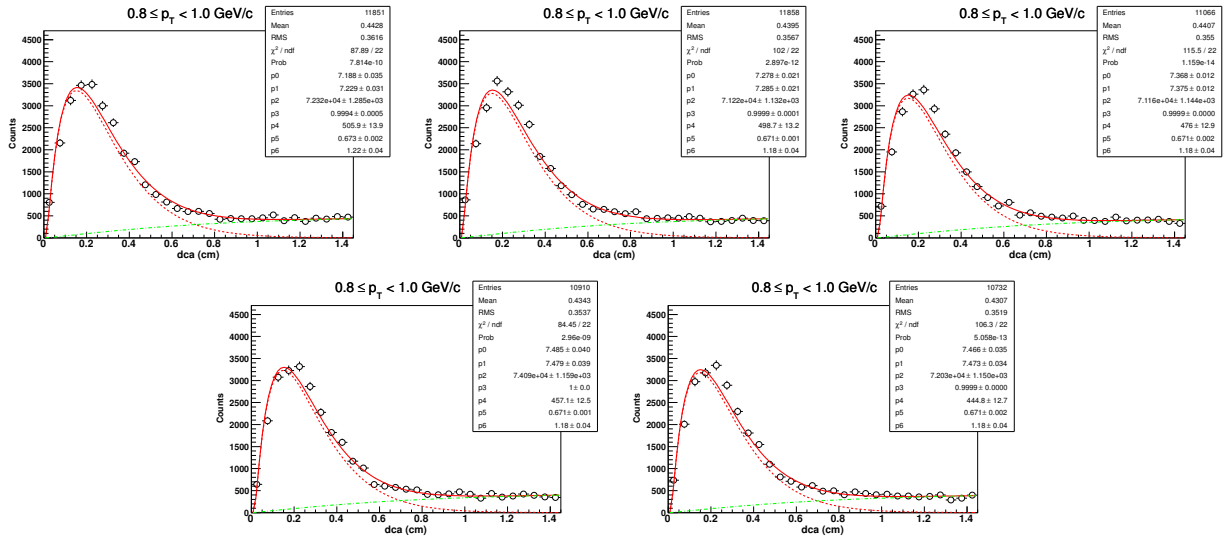


5.4 Centrality: 40-80% (Au+Au at $\sqrt{s_{NN}} = 200 \text{ GeV}$)

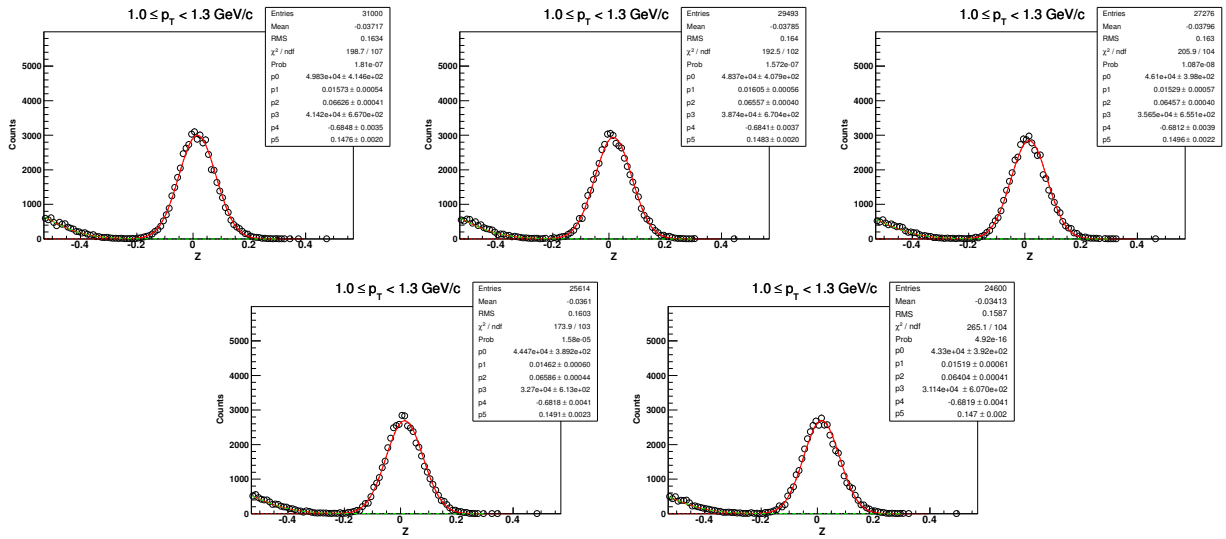
5.4.1 DCA-distribution of d for $0.5 < p_T < 0.8 \text{ GeV}/c$



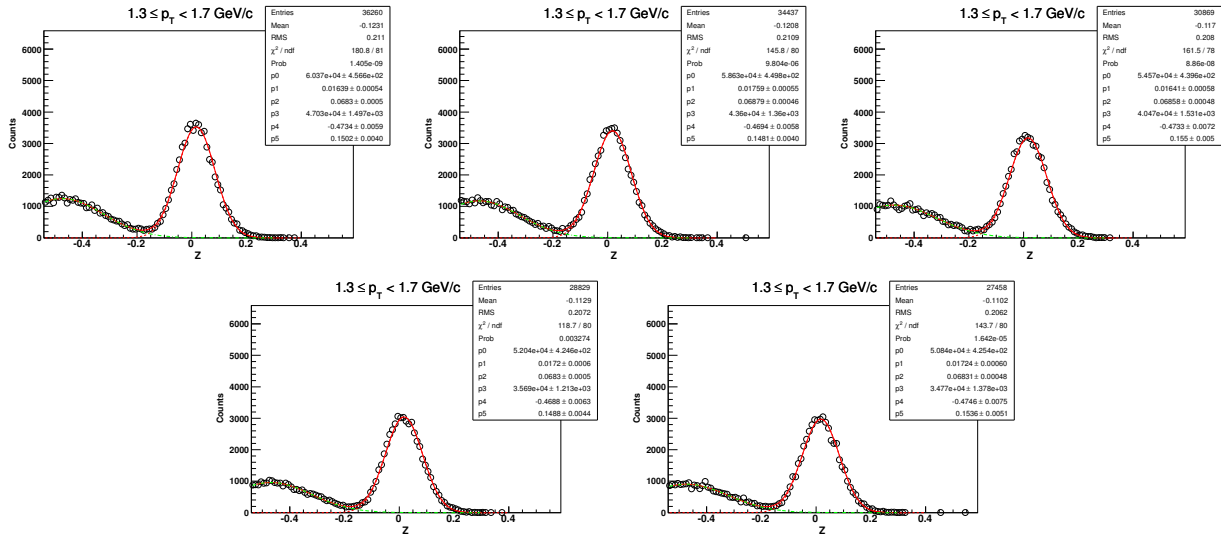
5.4.2 DCA-distribution of d for $0.8 < p_T < 1.0 \text{ GeV}/c$ ($\sqrt{s_{NN}} = 200 \text{ GeV}$, 40-80%)



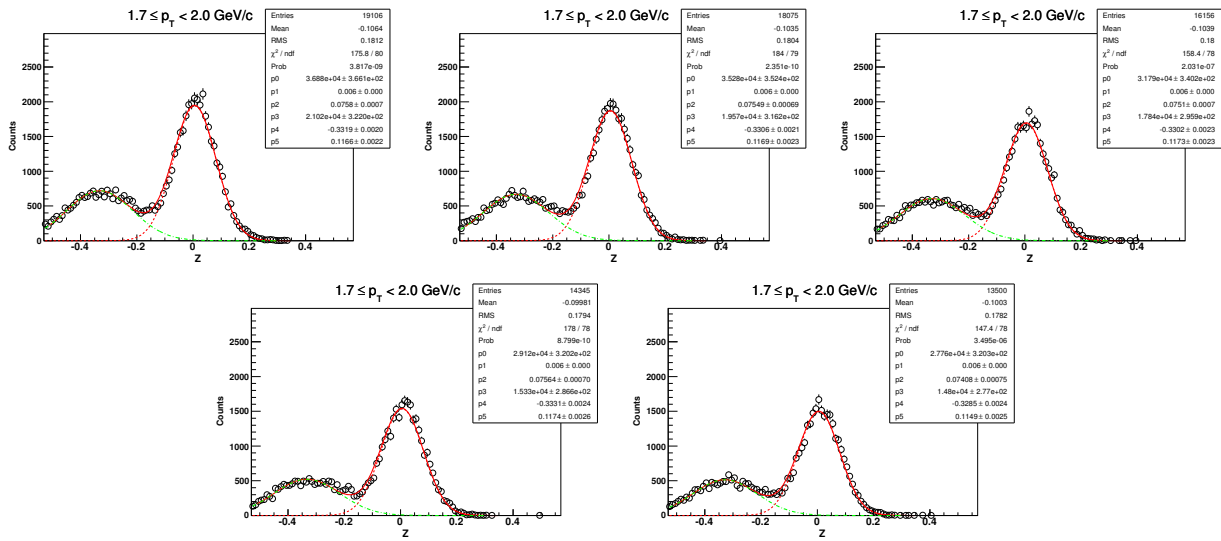
5.4.3 Z-distribution of d for $1.0 < p_T < 1.3 \text{ GeV}/c$ ($\sqrt{s_{NN}} = 200 \text{ GeV}$, 40-80%)



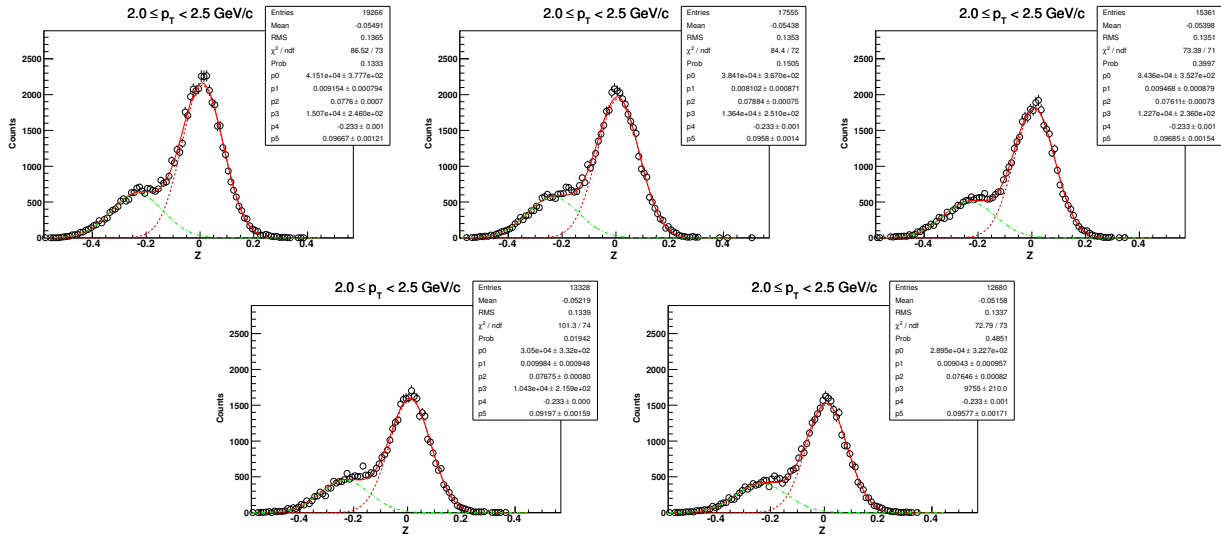
5.4.4 Z-distribution of d for $1.3 < p_T < 1.7 \text{ GeV}/c$ ($\sqrt{s_{NN}} = 200 \text{ GeV}$, 40-80%)



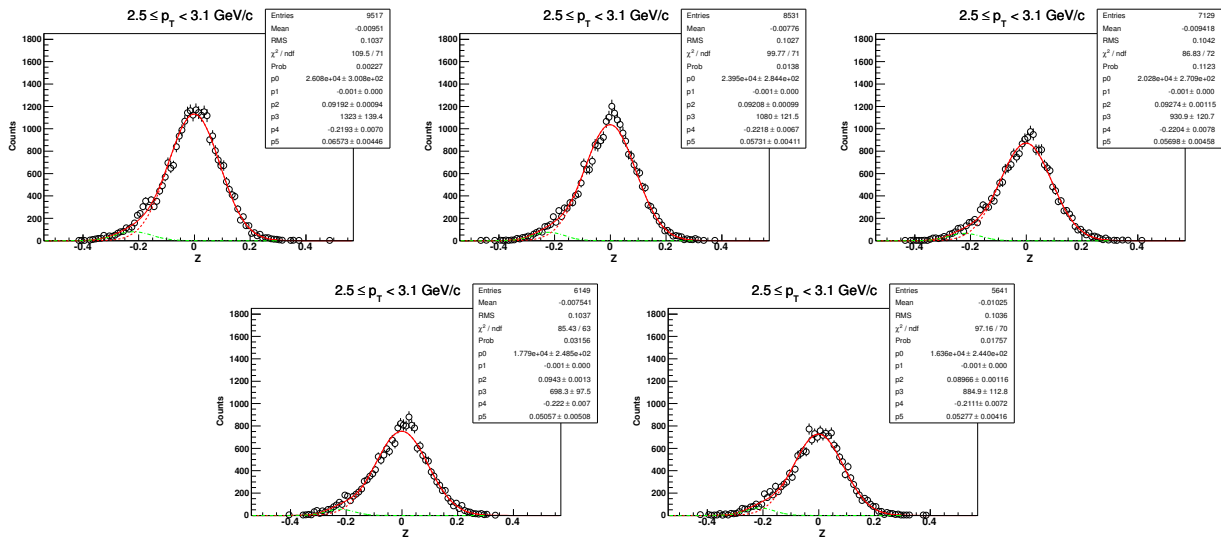
5.4.5 Z-distribution of d for $1.7 < p_T < 2.0 \text{ GeV}/c$ ($\sqrt{s_{NN}} = 200 \text{ GeV}$, 40-80%)



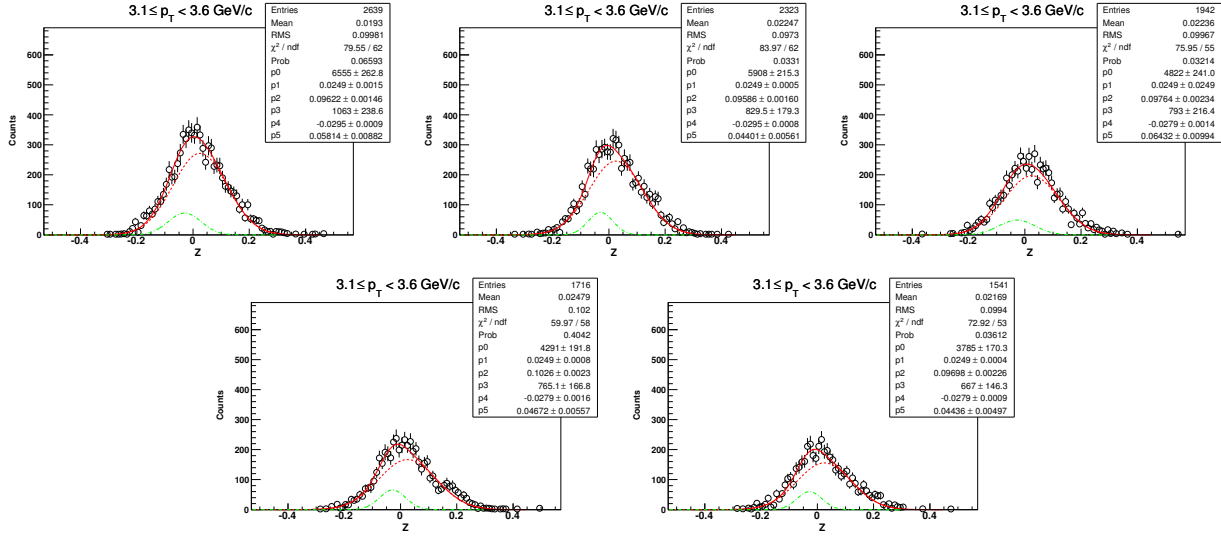
5.4.6 Z-distribution of d for $2.0 < p_T < 2.5 \text{ GeV}/c$ ($\sqrt{s_{NN}} = 200 \text{ GeV}$, 40-80%)



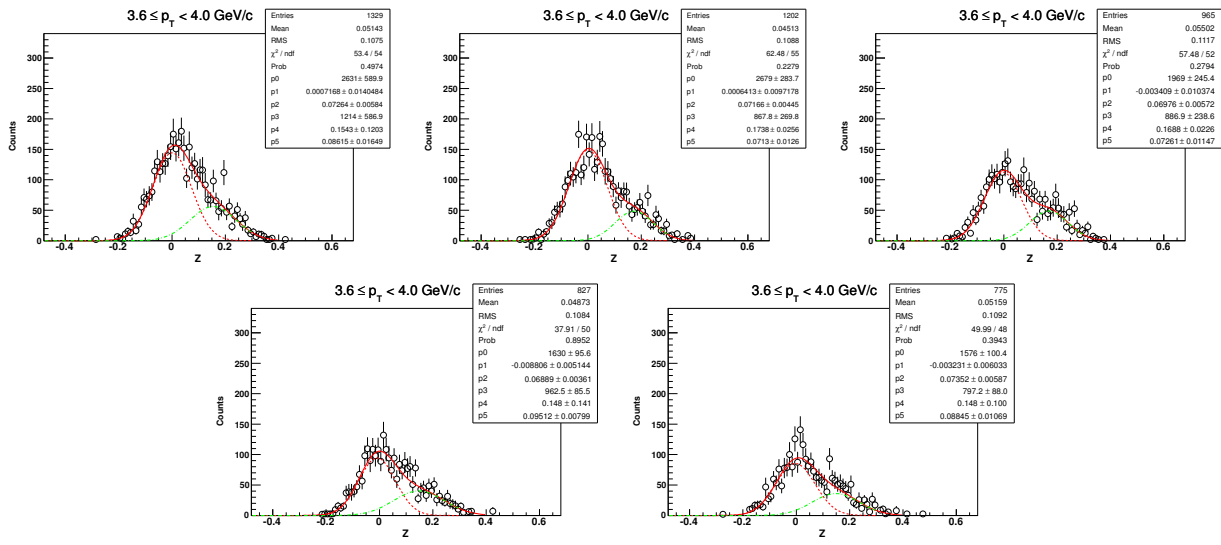
5.4.7 Z-distribution of d for $2.5 < p_T < 3.1 \text{ GeV}/c$ ($\sqrt{s_{NN}} = 200 \text{ GeV}$, 40-80%)



5.4.8 Z-distribution of d for $3.1 < p_T < 3.6 \text{ GeV}/c$ ($\sqrt{s_{NN}} = 200 \text{ GeV}$, 40-80%)

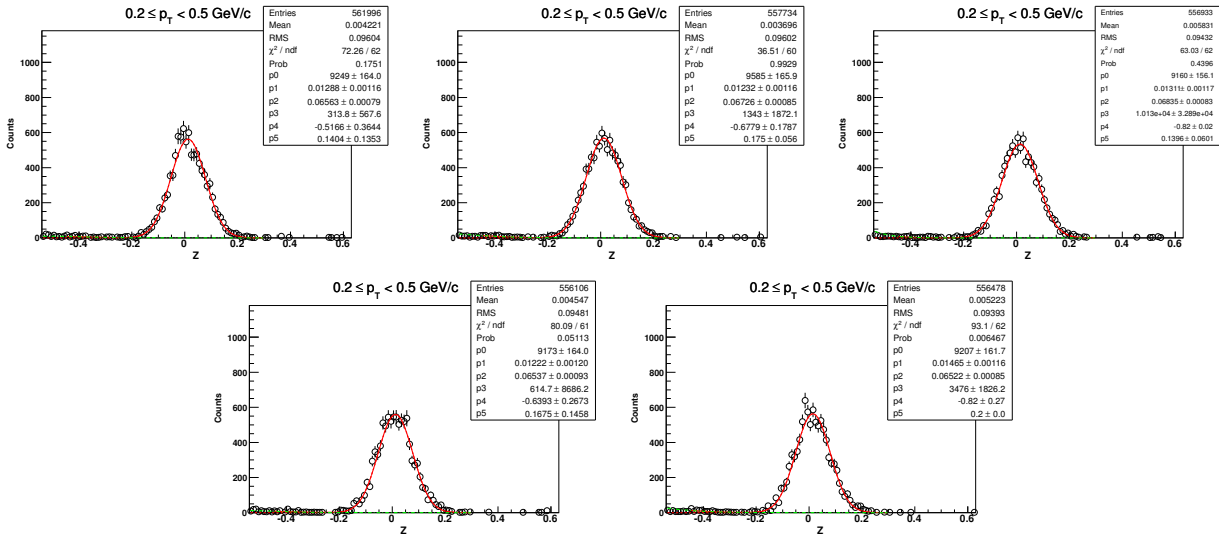


5.4.9 Z-distribution of d for $3.6 < p_T < 4.0 \text{ GeV}/c$ ($\sqrt{s_{NN}} = 200 \text{ GeV}$, 40-80%)

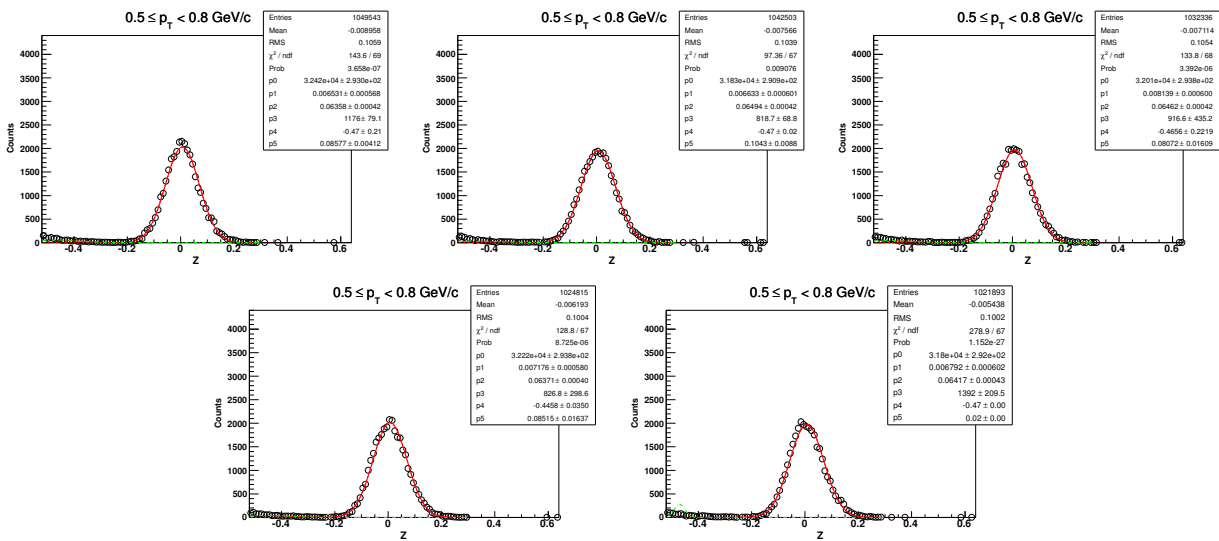


5.5 \bar{d} in $\sqrt{s_{NN}} = 200$ GeV for centrality: 0-80%

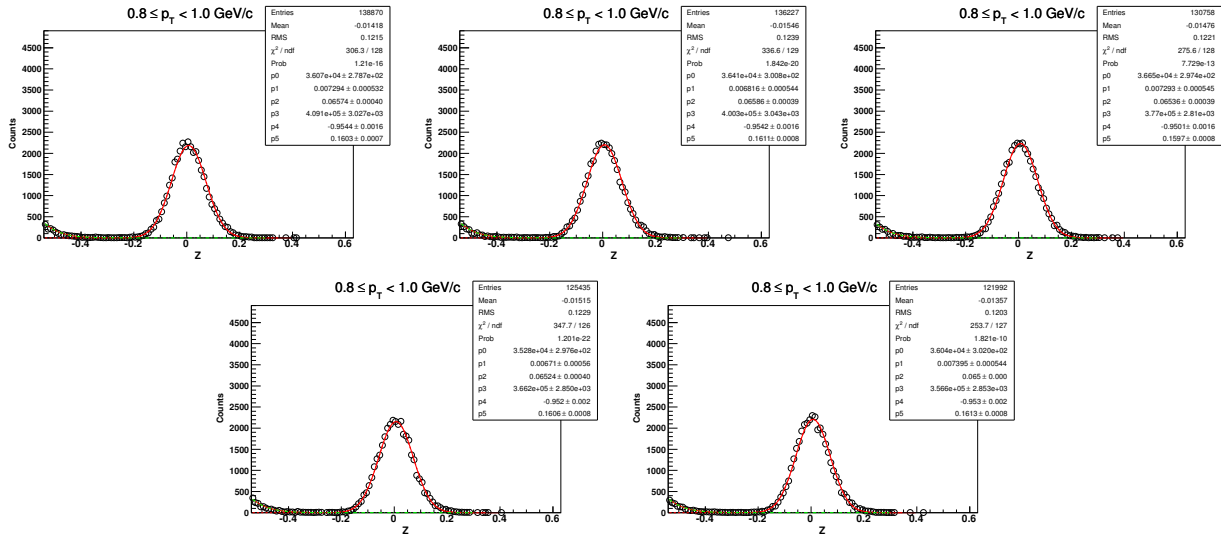
5.5.1 Z-distribution of \bar{d} for $0.2 < p_T < 0.5$ GeV/c



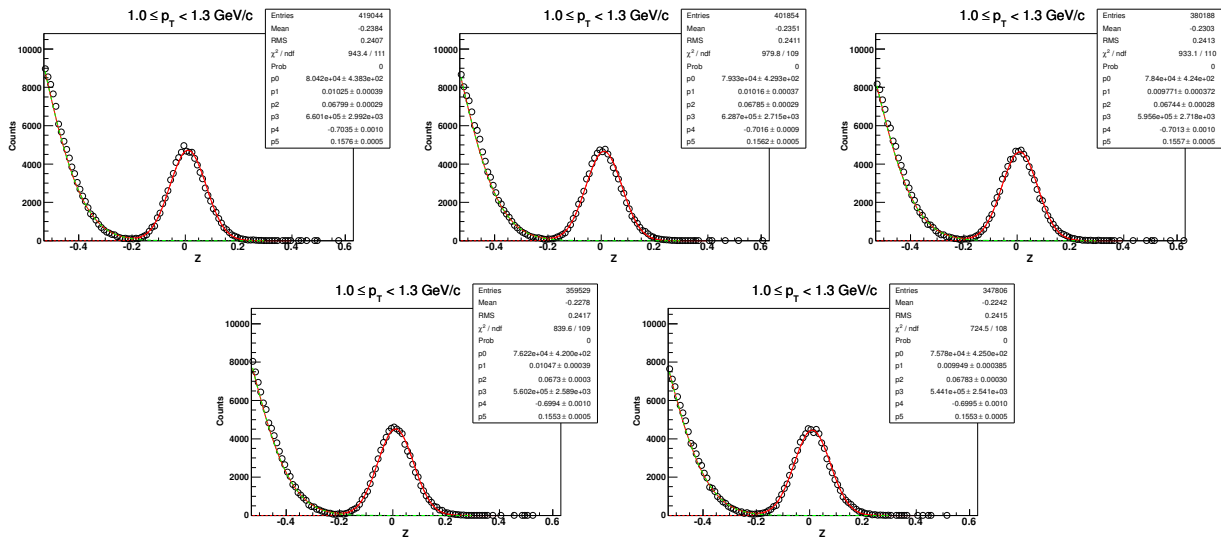
5.5.2 Z-distribution of \bar{d} for $0.5 < p_T < 0.8$ GeV/c ($\sqrt{s_{NN}} = 200$ GeV, 0-80%)



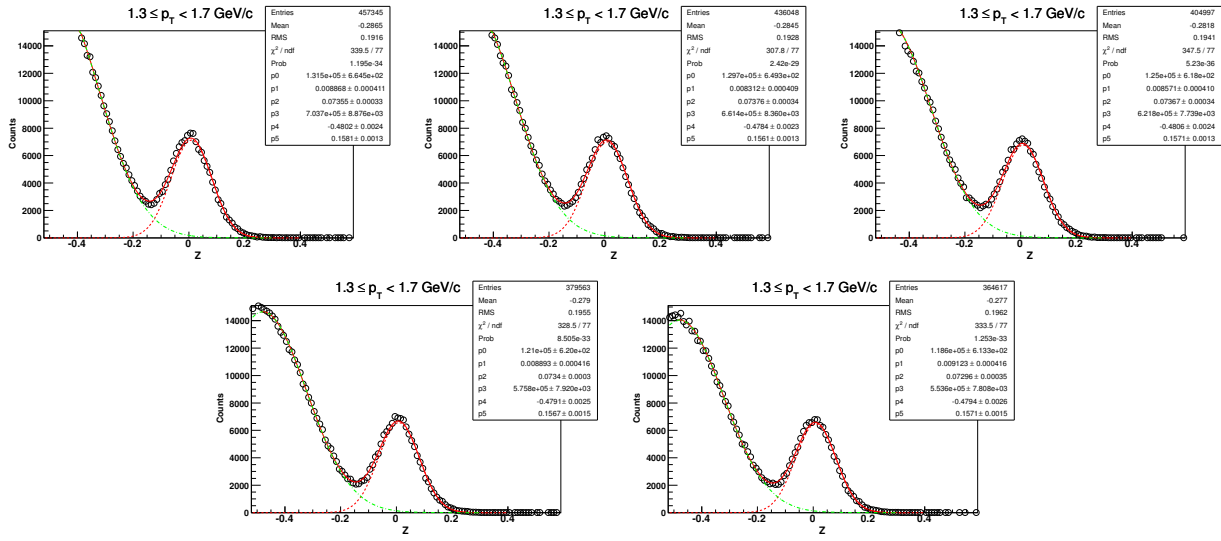
5.5.3 Z-distribution of \bar{d} for $0.8 < p_T < 1.0 \text{ GeV}/c$ ($\sqrt{s_{NN}} = 200 \text{ GeV}$, 0-80%)



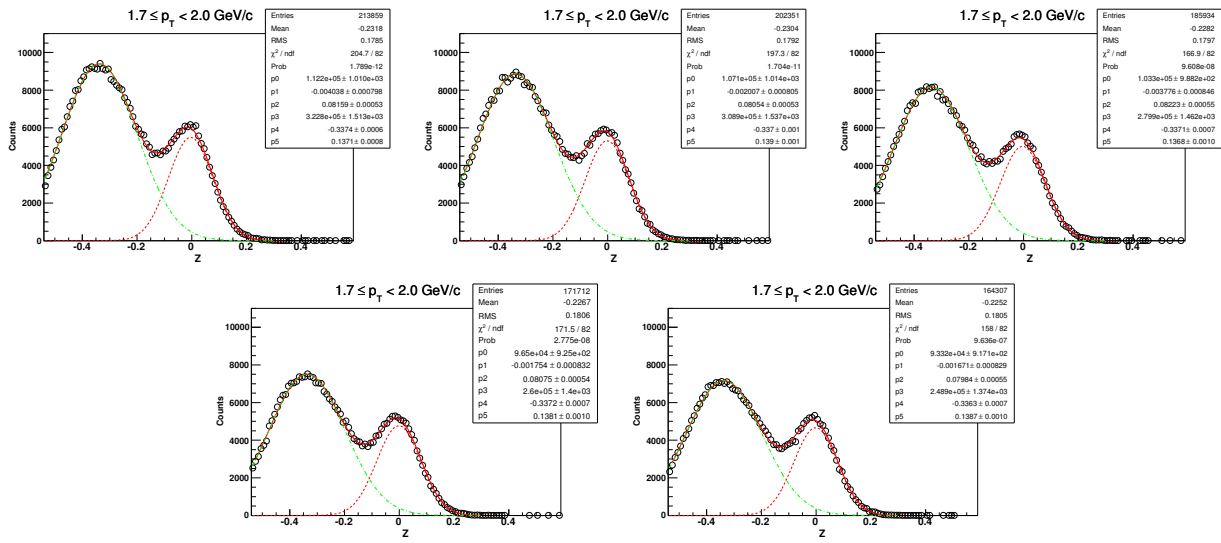
5.5.4 Z-distribution of \bar{d} for $1.0 < p_T < 1.3 \text{ GeV}/c$ ($\sqrt{s_{NN}} = 200 \text{ GeV}$, 0-80%)



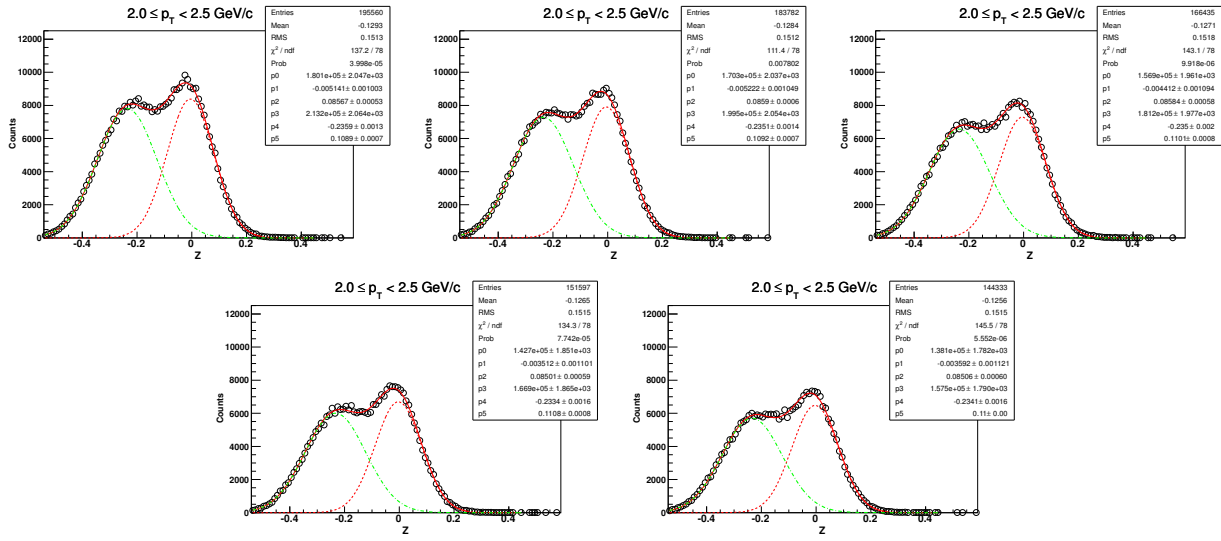
5.5.5 Z-distribution of \bar{d} for $1.3 < p_T < 1.7 \text{ GeV}/c$ ($\sqrt{s_{NN}} = 200 \text{ GeV}$, 0-80%)



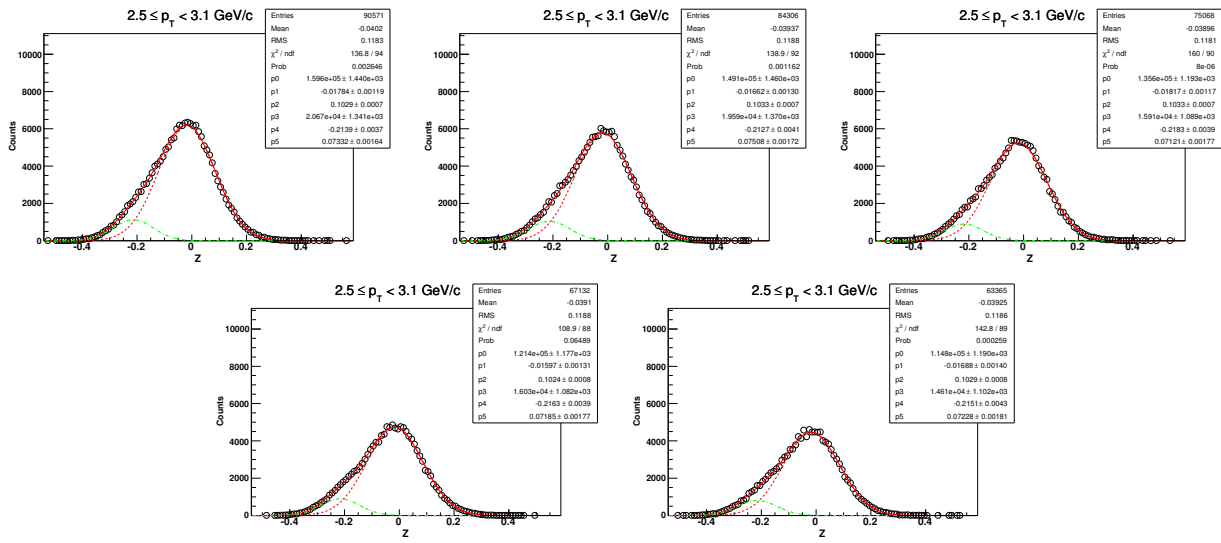
5.5.6 Z-distribution of \bar{d} for $1.7 < p_T < 2.0 \text{ GeV}/c$ ($\sqrt{s_{NN}} = 200 \text{ GeV}$, 0-80%)



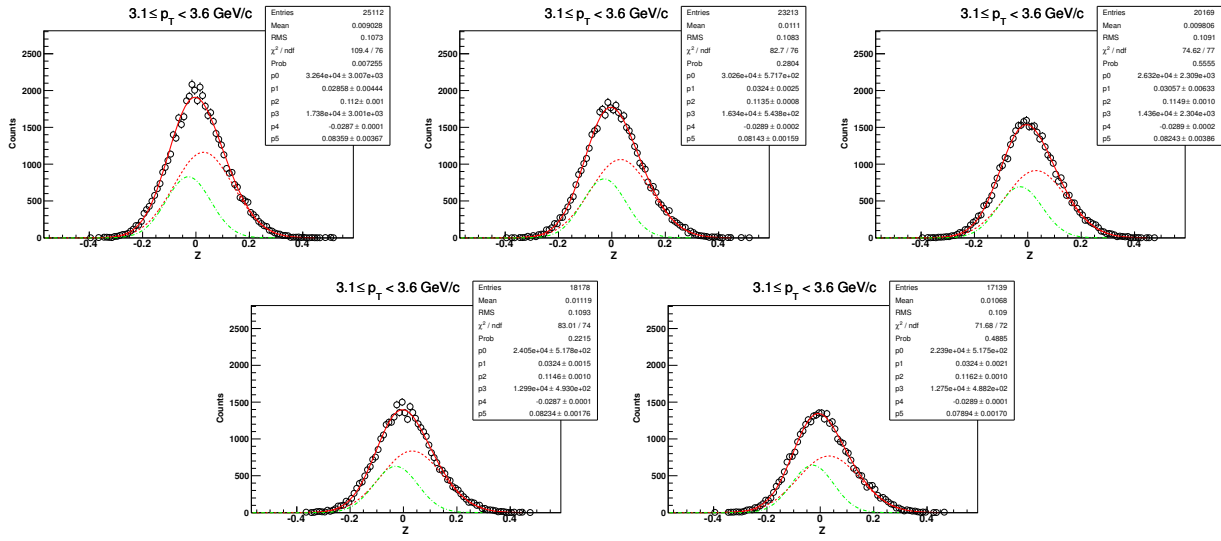
5.5.7 Z-distribution of \bar{d} for $2.0 < p_T < 2.5 \text{ GeV}/c$ ($\sqrt{s_{NN}} = 200 \text{ GeV}$, 0-80%)



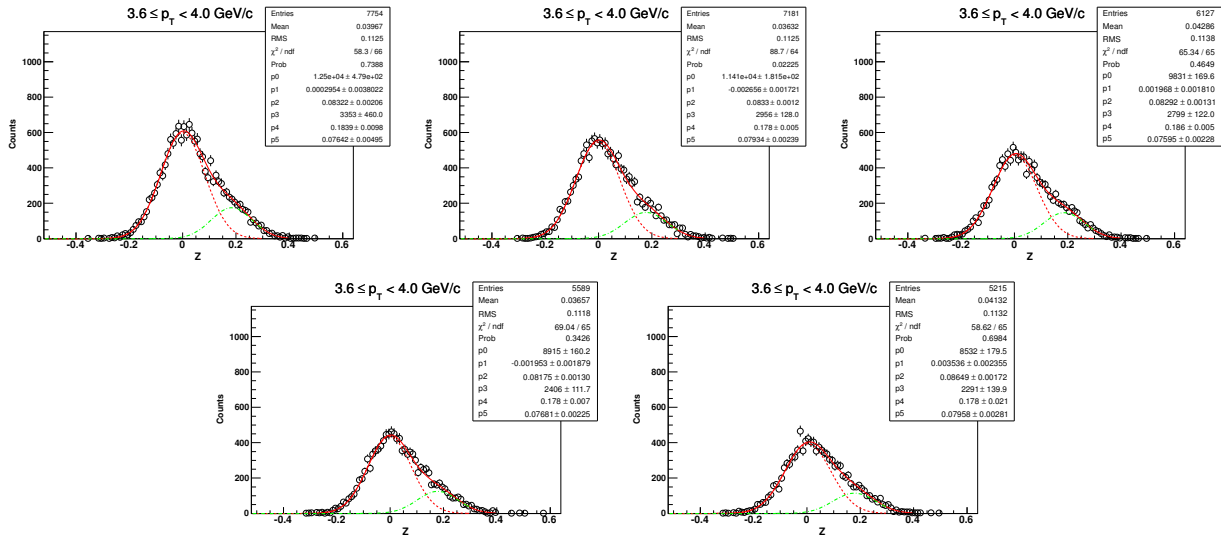
5.5.8 Z-distribution of \bar{d} for $2.5 < p_T < 3.1 \text{ GeV}/c$ ($\sqrt{s_{NN}} = 200 \text{ GeV}$, 0-80%)



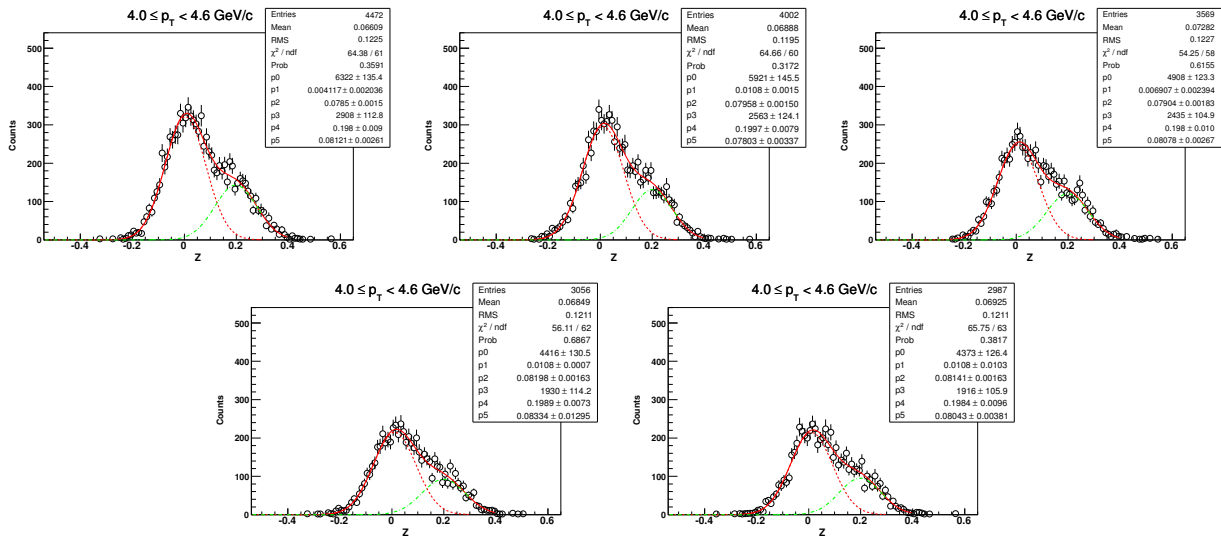
5.5.9 Z-distribution of \bar{d} for $3.1 < p_T < 3.6 \text{ GeV}/c$ ($\sqrt{s_{NN}} = 200 \text{ GeV}$, 0-80%)



5.5.10 Z-distribution of \bar{d} for $3.6 < p_T < 4.0 \text{ GeV}/c$ ($\sqrt{s_{NN}} = 200 \text{ GeV}$, 0-80%)

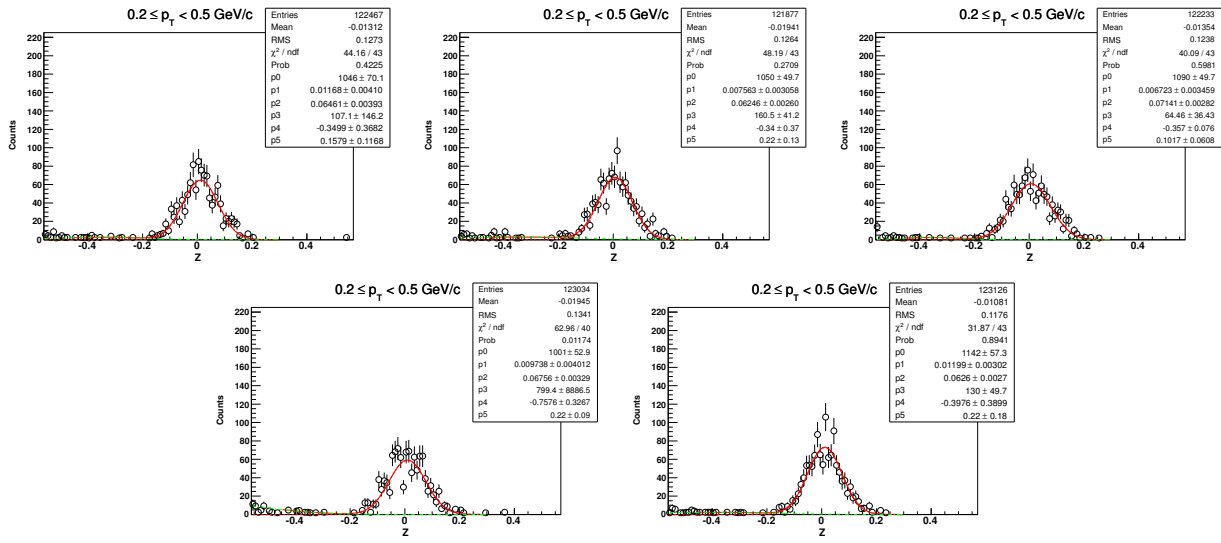


5.5.11 Z-distribution of \bar{d} for $4.0 < p_T < 4.6 \text{ GeV}/c$ ($\sqrt{s_{NN}} = 200 \text{ GeV}$, 0-80%)

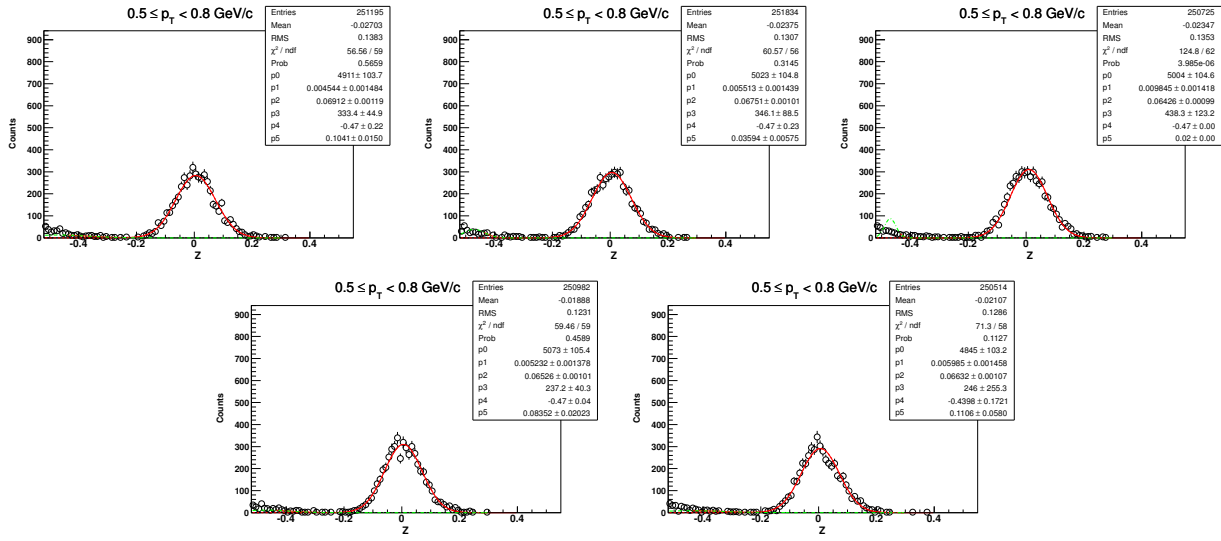


5.6 \bar{d} in $\sqrt{s_{NN}} = 200 \text{ GeV}$ for centrality: 0-10%

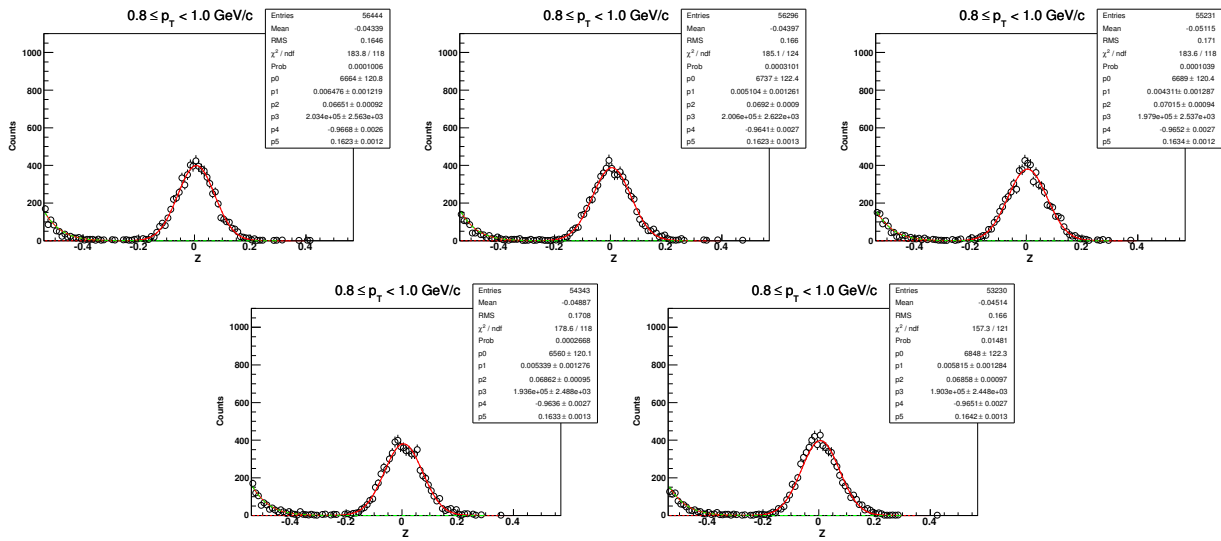
5.6.1 Z-distribution of \bar{d} for $0.2 < p_T < 0.5 \text{ GeV}/c$



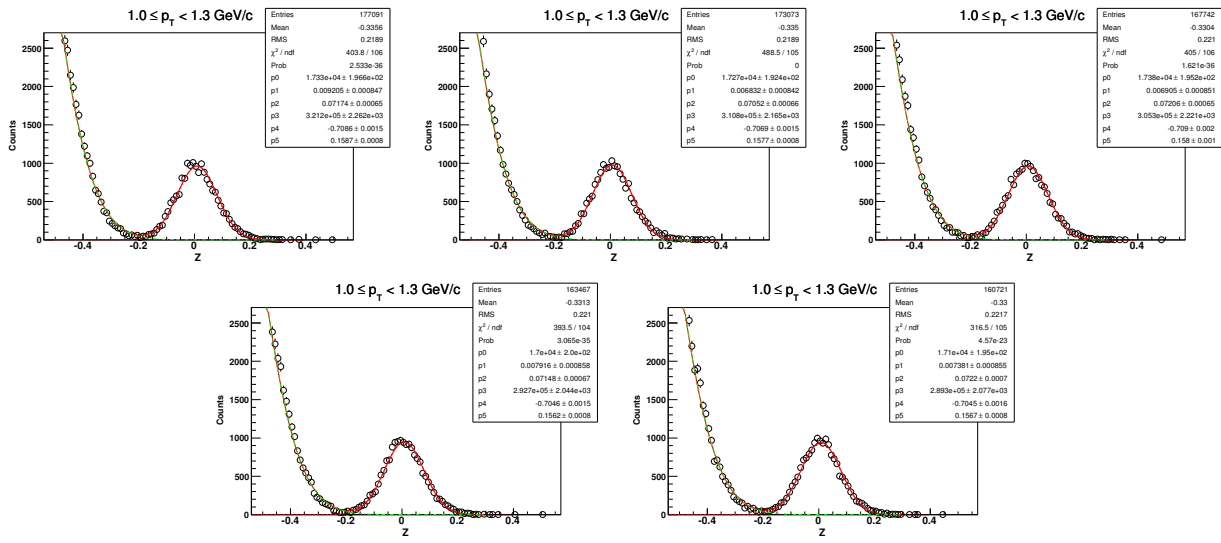
5.6.2 Z-distribution of \bar{d} for $0.5 < p_T < 0.8 \text{ GeV}/c$ ($\sqrt{s_{NN}} = 200 \text{ GeV}$, 0-10%)



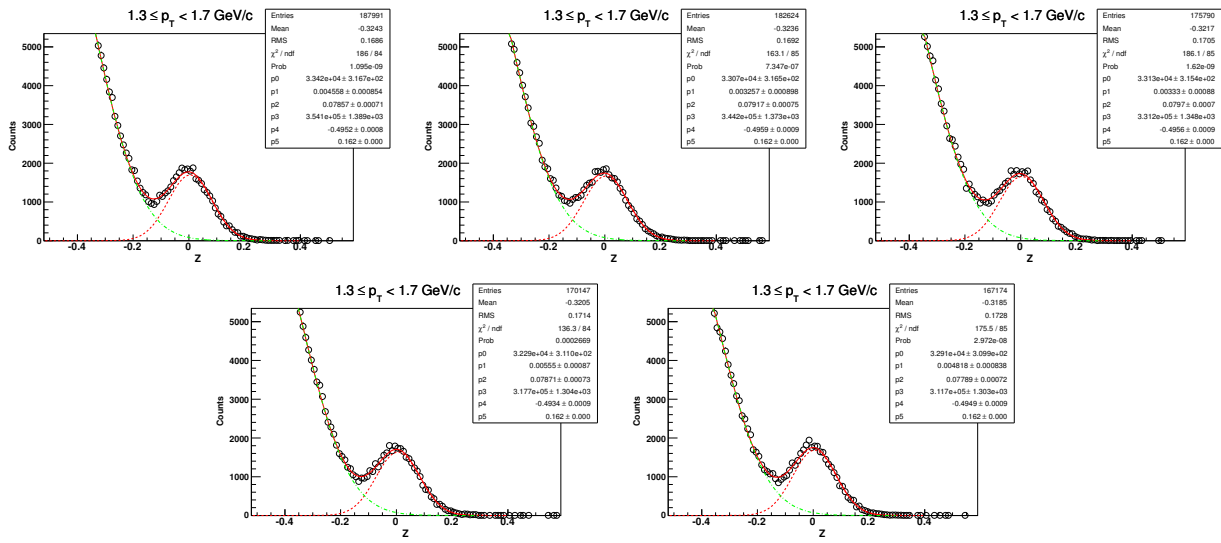
5.6.3 Z-distribution of \bar{d} for $0.8 < p_T < 1.0 \text{ GeV}/c$ ($\sqrt{s_{NN}} = 200 \text{ GeV}$, 0-10%)



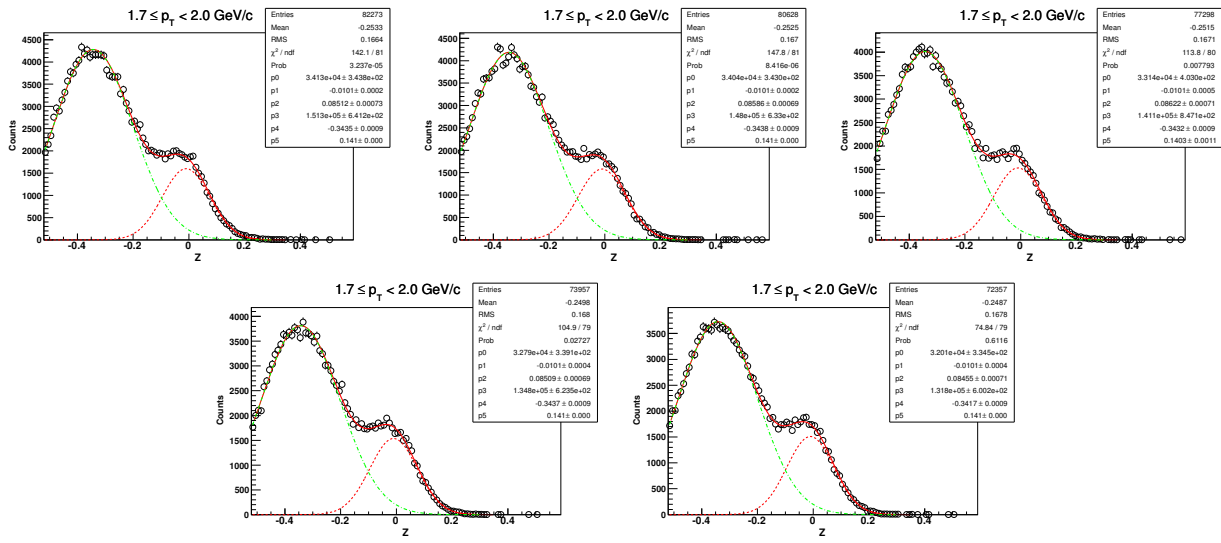
5.6.4 Z-distribution of \bar{d} for $1.0 < p_T < 1.3 \text{ GeV}/c$ ($\sqrt{s_{NN}} = 200 \text{ GeV}$, 0-10%)



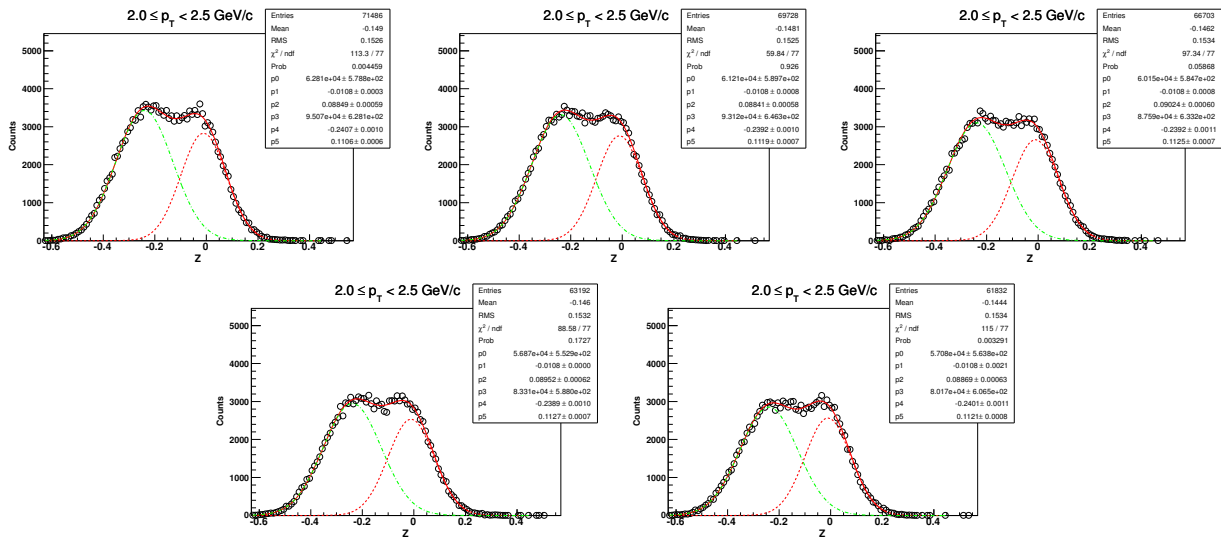
5.6.5 Z-distribution of \bar{d} for $1.3 < p_T < 1.7 \text{ GeV}/c$ ($\sqrt{s_{NN}} = 200 \text{ GeV}$, 0-10%)



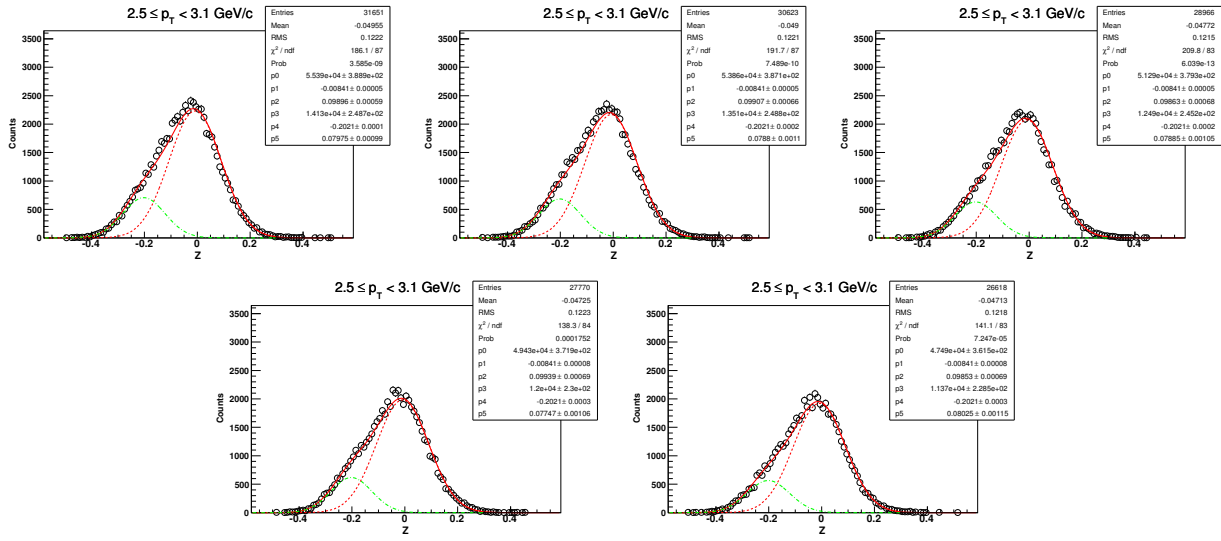
5.6.6 Z-distribution of \bar{d} for $1.7 < p_T < 2.0$ GeV/c ($\sqrt{s_{NN}} = 200$ GeV, 0-10%)



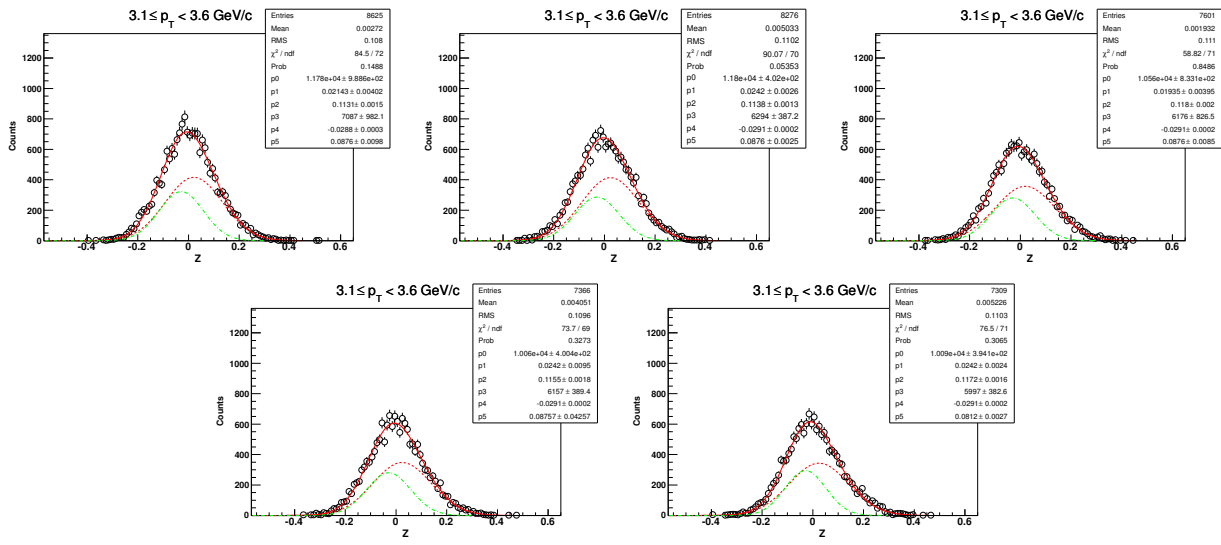
5.6.7 Z-distribution of \bar{d} for $2.0 < p_T < 2.5$ GeV/c ($\sqrt{s_{NN}} = 200$ GeV, 0-10%)



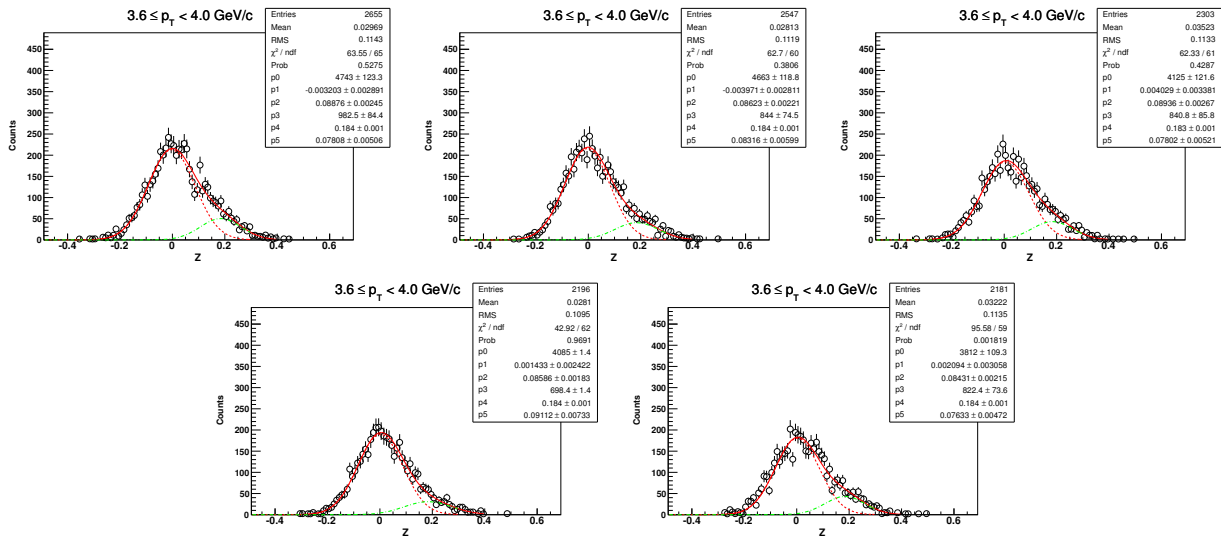
5.6.8 Z-distribution of \bar{d} for $2.5 < p_T < 3.1 \text{ GeV}/c$ ($\sqrt{s_{NN}} = 200 \text{ GeV}$, 0-10%)



5.6.9 Z-distribution of \bar{d} for $3.1 < p_T < 3.6 \text{ GeV}/c$ ($\sqrt{s_{NN}} = 200 \text{ GeV}$, 0-10%)

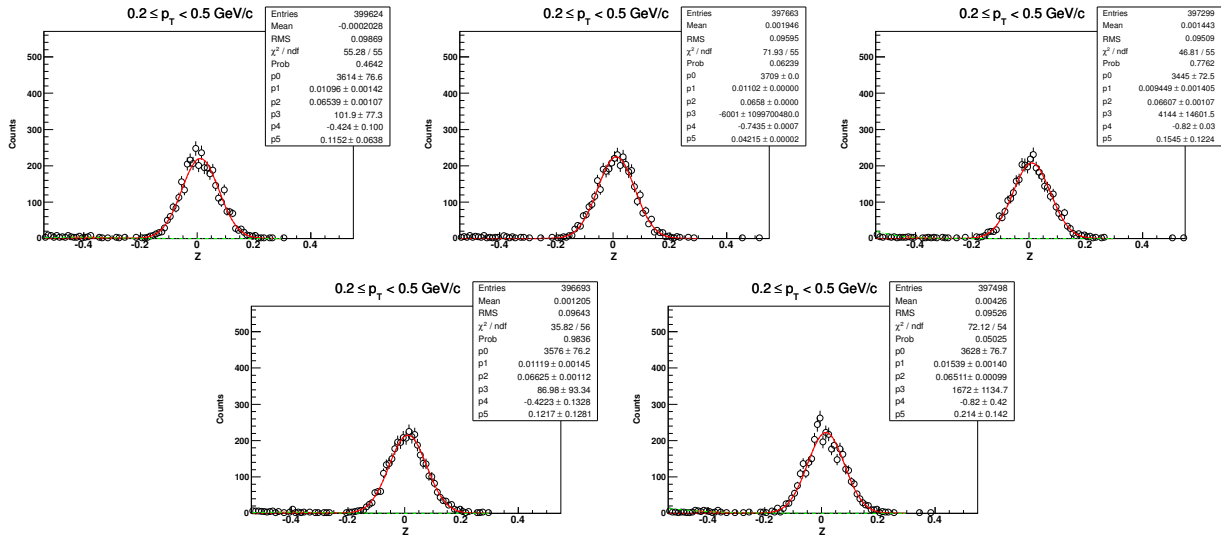


5.6.10 Z-distribution of \bar{d} for $3.6 < p_T < 4.0 \text{ GeV}/c$ ($\sqrt{s_{NN}} = 200 \text{ GeV}$, 0-10%)

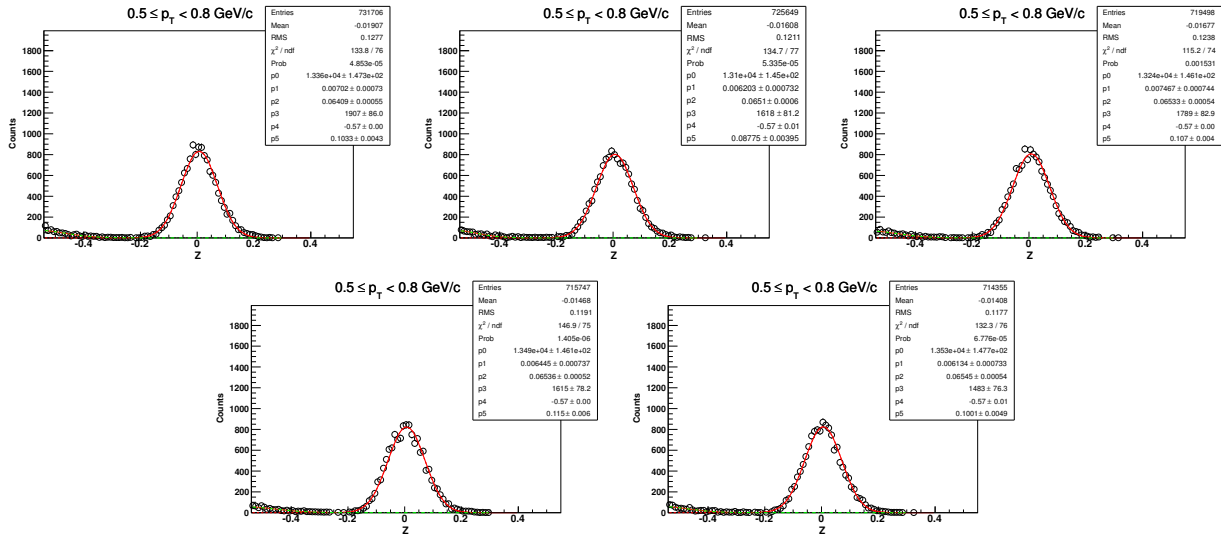


5.7 \bar{d} in $\sqrt{s_{NN}} = 200 \text{ GeV}$ for centrality: 10-40%

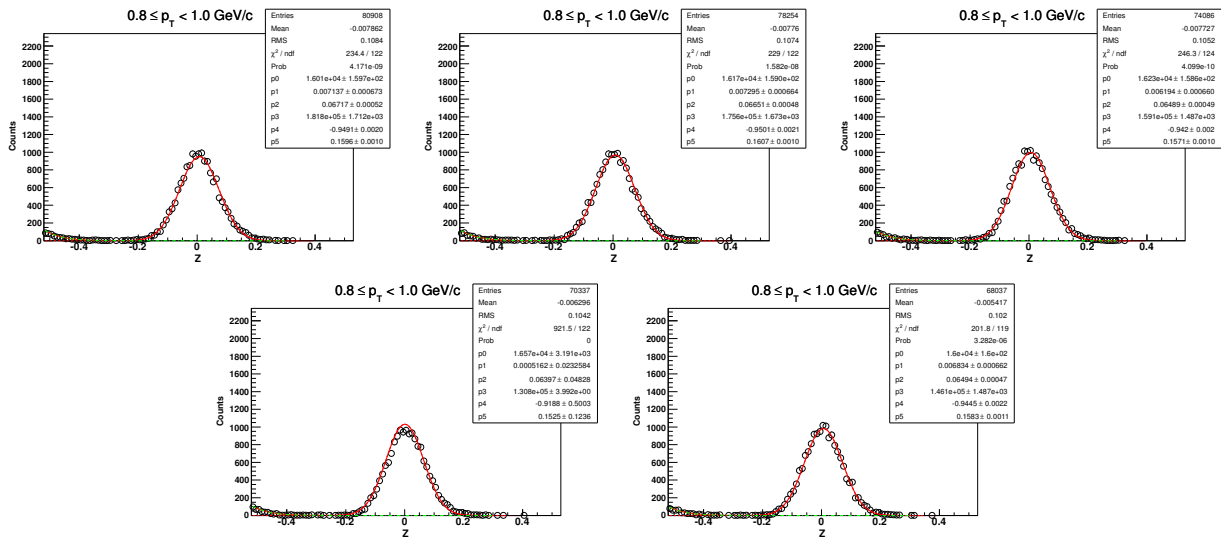
5.7.1 Z-distribution of \bar{d} for $0.2 < p_T < 0.5 \text{ GeV}/c$



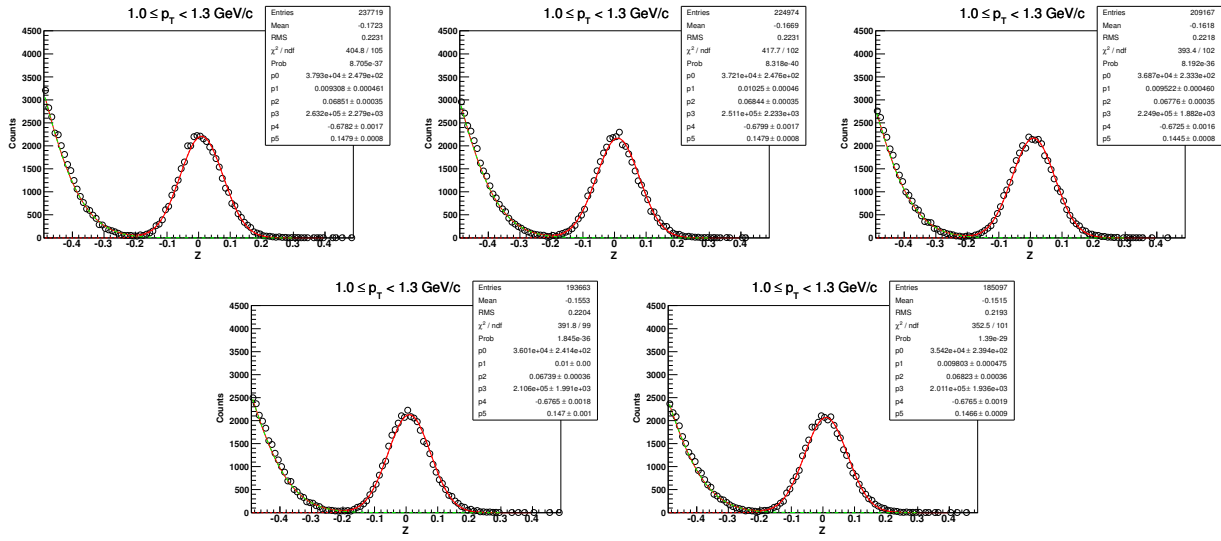
5.7.2 Z-distribution of \bar{d} for $0.5 < p_T < 0.8 \text{ GeV}/c$ ($\sqrt{s_{NN}} = 200 \text{ GeV}$, 10-40%)



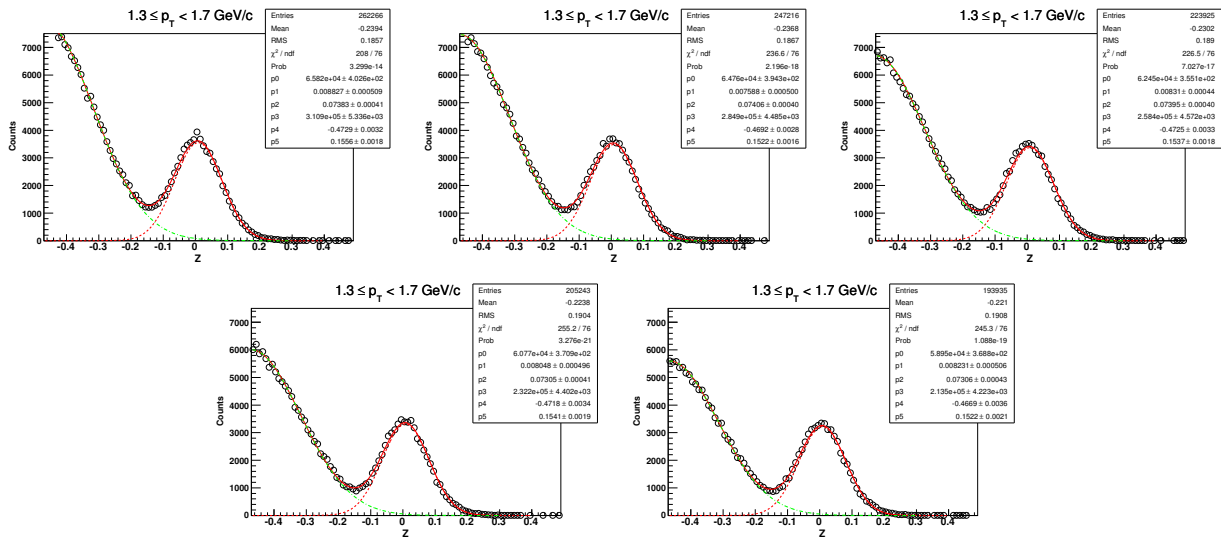
5.7.3 Z-distribution of \bar{d} for $0.8 < p_T < 1.0 \text{ GeV}/c$ ($\sqrt{s_{NN}} = 200 \text{ GeV}$, 10-40%)



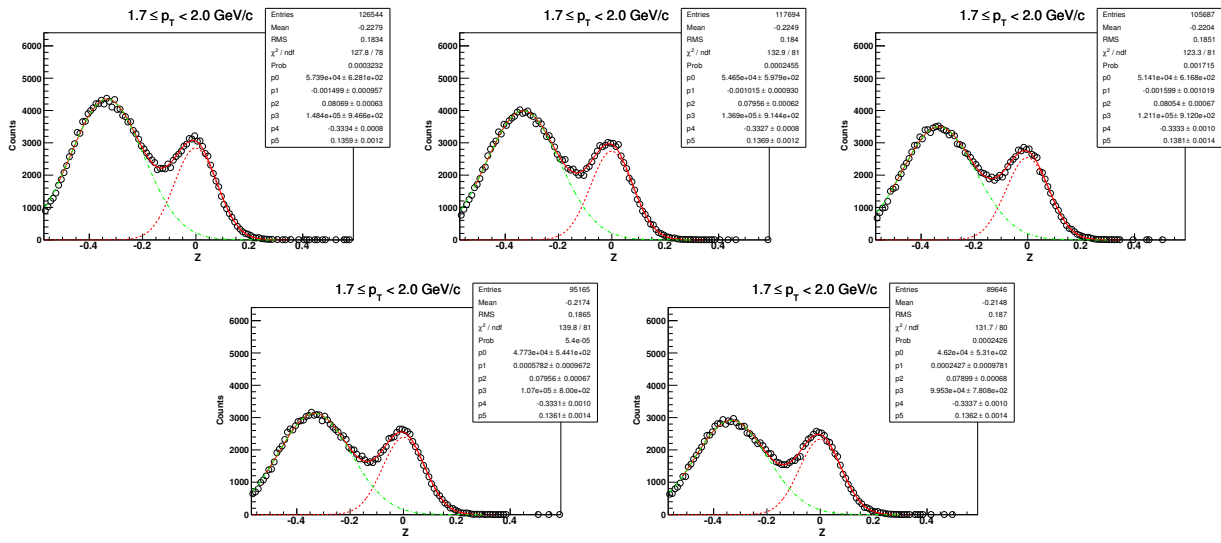
5.7.4 Z-distribution of \bar{d} for $1.0 < p_T < 1.3 \text{ GeV}/c$ ($\sqrt{s_{NN}} = 200 \text{ GeV}$, 10-40%)



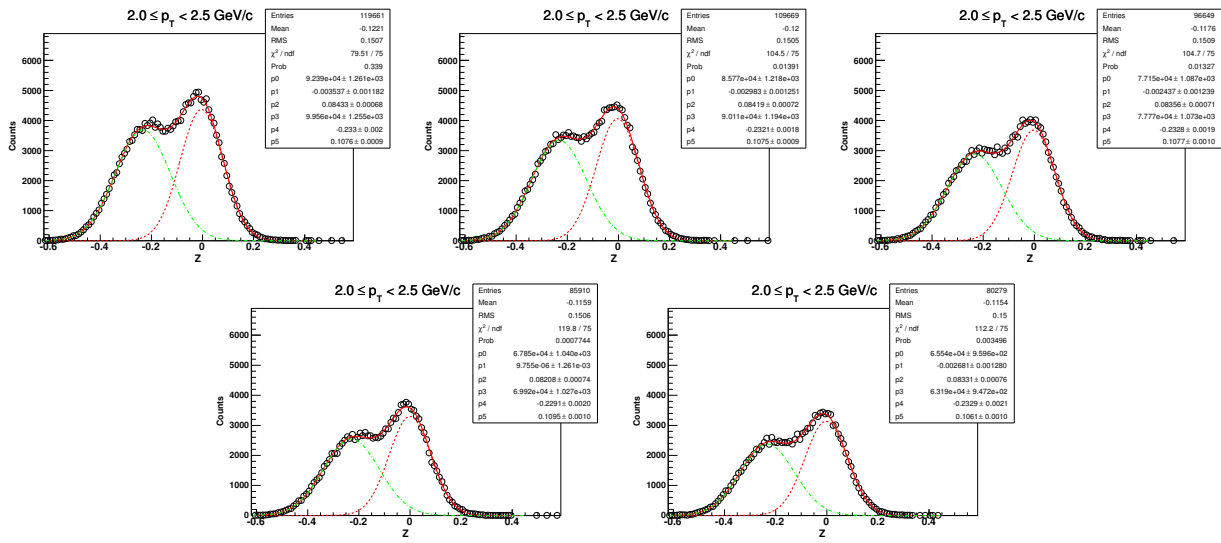
5.7.5 Z-distribution of \bar{d} for $1.3 < p_T < 1.7 \text{ GeV}/c$ ($\sqrt{s_{NN}} = 200 \text{ GeV}$, 10-40%)



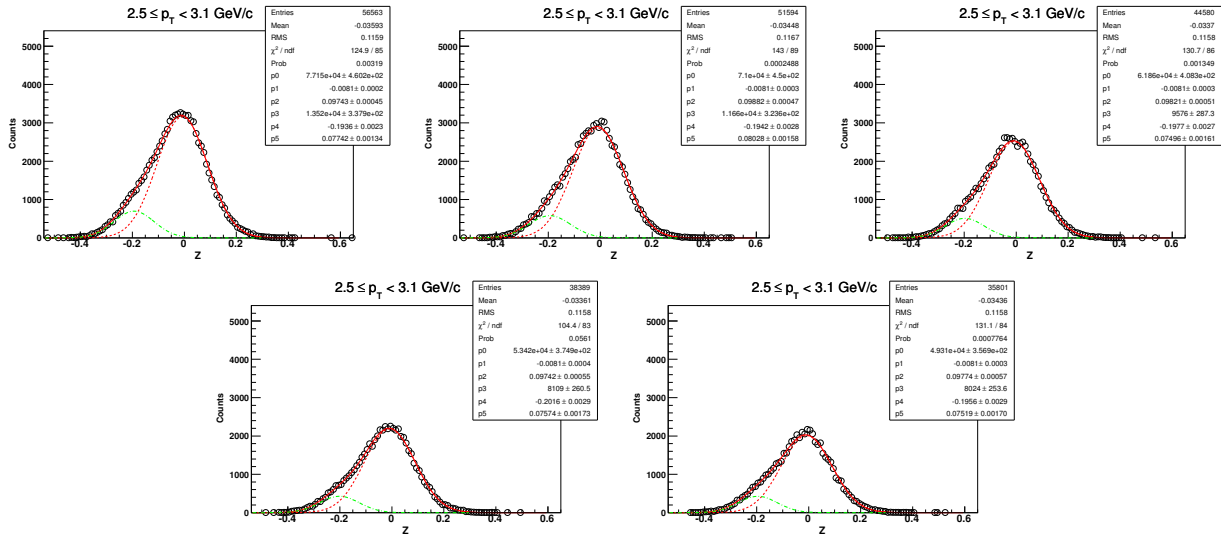
5.7.6 Z-distribution of \bar{d} for $1.7 < p_T < 2.0 \text{ GeV}/c$ ($\sqrt{s_{NN}} = 200 \text{ GeV}$, 10-40%)



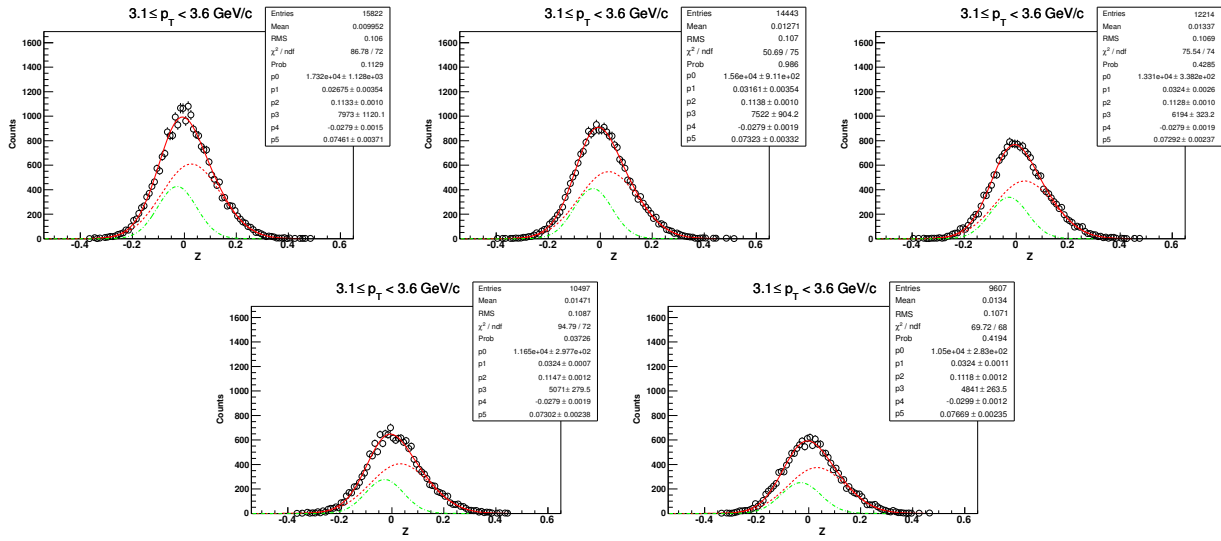
5.7.7 Z-distribution of \bar{d} for $2.0 < p_T < 2.5 \text{ GeV}/c$ ($\sqrt{s_{NN}} = 200 \text{ GeV}$, 10-40%)



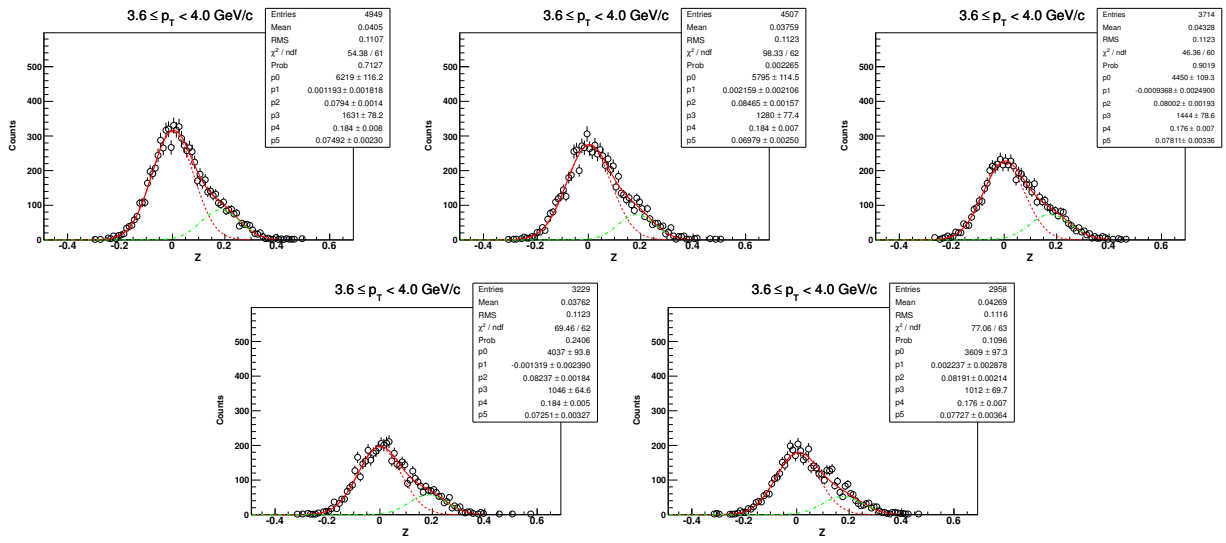
5.7.8 Z-distribution of \bar{d} for $2.5 < p_T < 3.1 \text{ GeV}/c$ ($\sqrt{s_{NN}} = 200 \text{ GeV}$, 10-40%)



5.7.9 Z-distribution of \bar{d} for $3.1 < p_T < 3.6 \text{ GeV}/c$ ($\sqrt{s_{NN}} = 200 \text{ GeV}$, 10-40%)

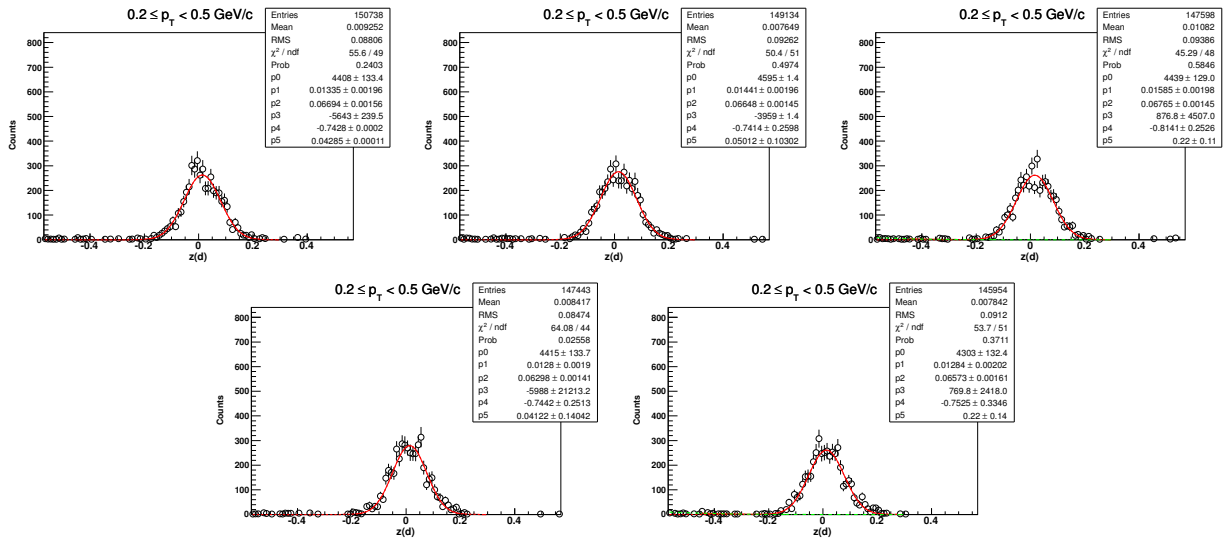


5.7.10 Z-distribution of \bar{d} for $3.6 < p_T < 4.0 \text{ GeV}/c$ ($\sqrt{s_{NN}} = 200 \text{ GeV}$, 10-40%)

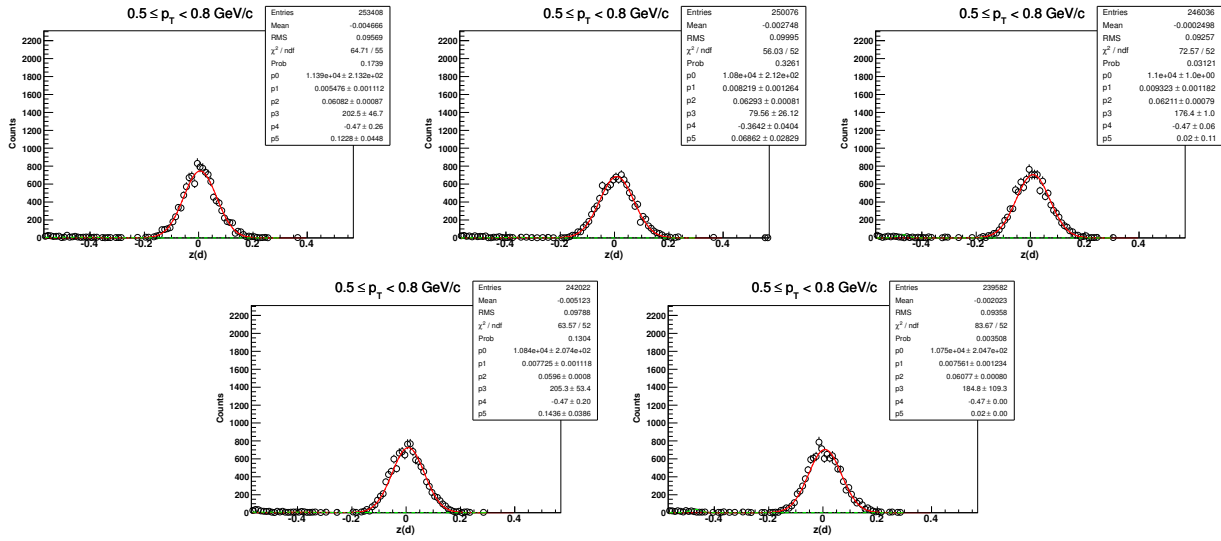


5.8 \bar{d} in $\sqrt{s_{NN}} = 200 \text{ GeV}$ for centrality: 40-80%

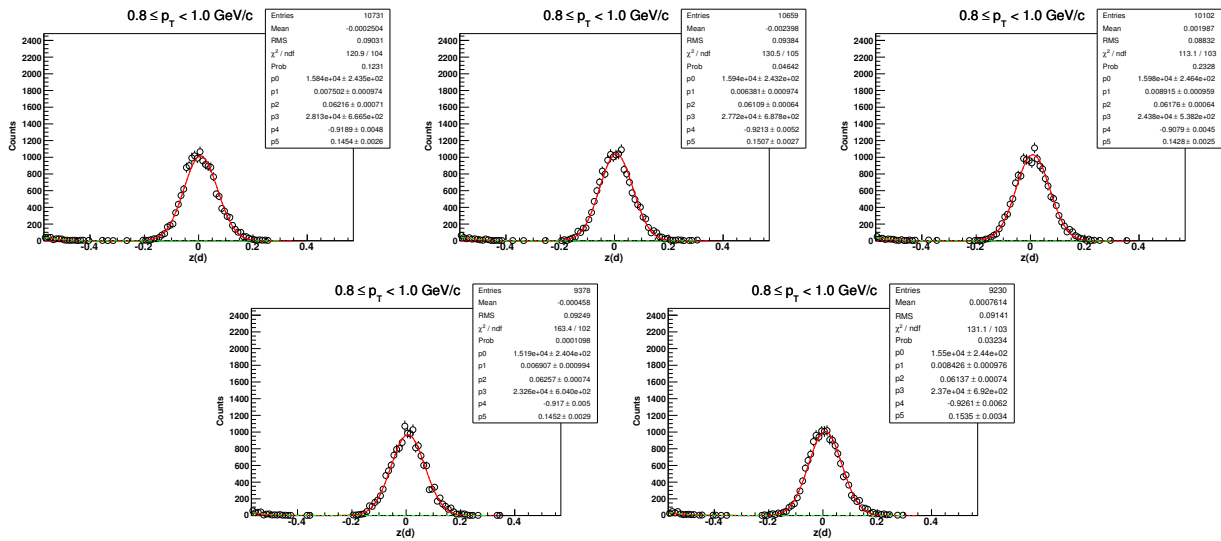
5.8.1 Z-distribution of \bar{d} for $0.2 < p_T < 0.5 \text{ GeV}/c$



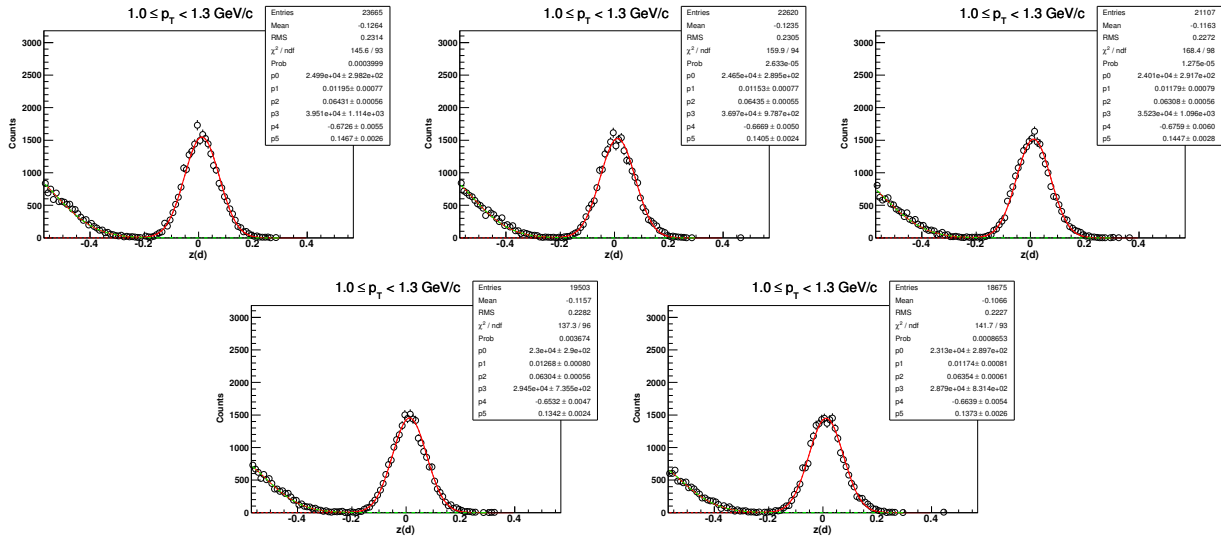
5.8.2 Z-distribution of \bar{d} for $0.5 < p_T < 0.8 \text{ GeV}/c$ ($\sqrt{s_{NN}} = 200 \text{ GeV}$, 40-80%)



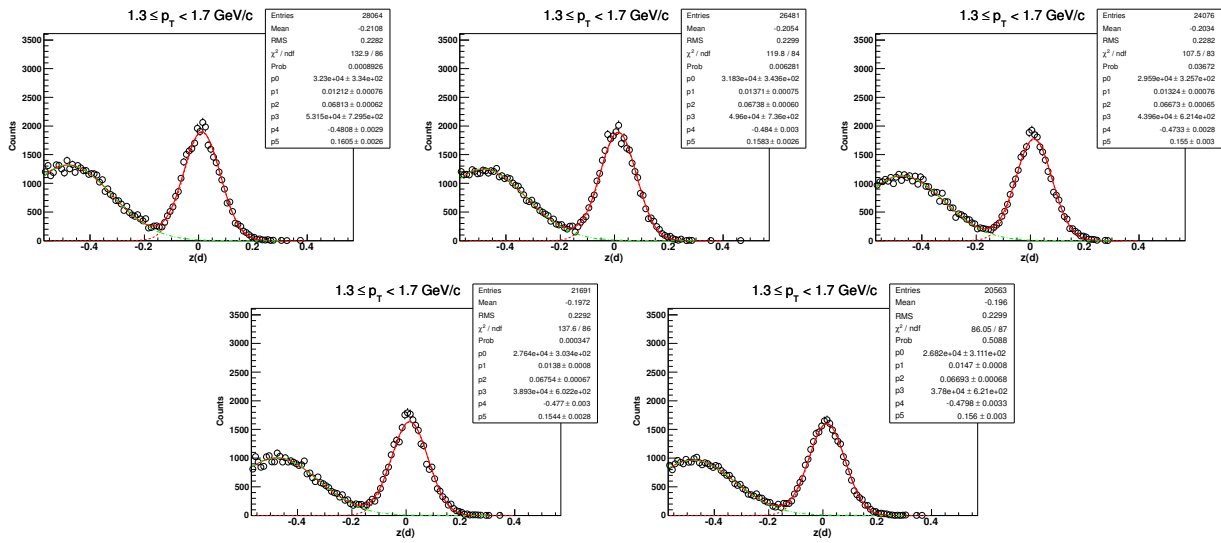
5.8.3 Z-distribution of \bar{d} for $0.8 < p_T < 1.0 \text{ GeV}/c$ ($\sqrt{s_{NN}} = 200 \text{ GeV}$, 40-80%)



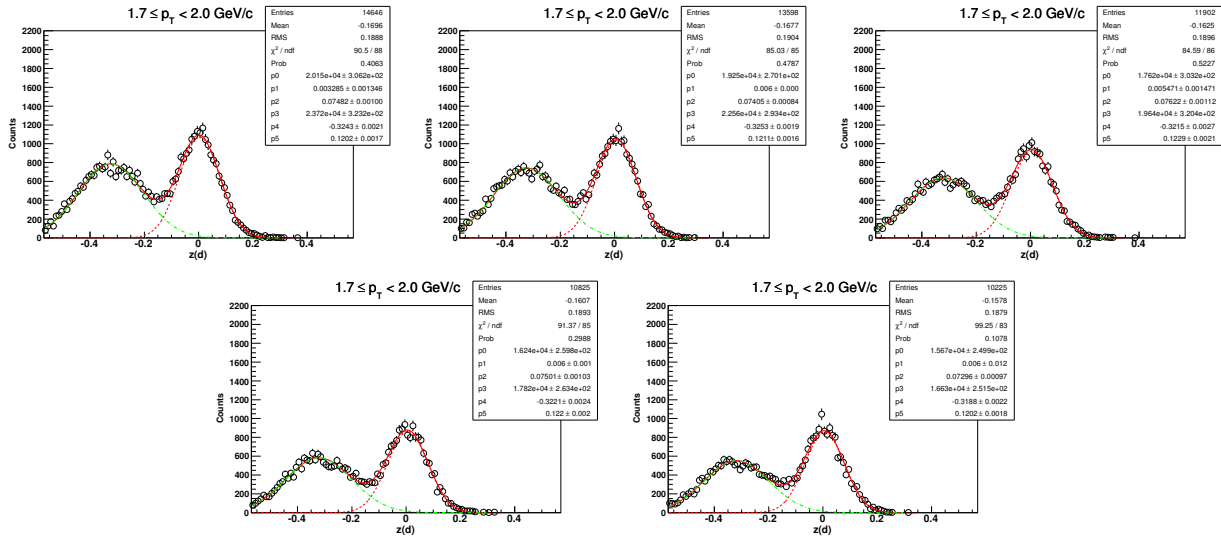
5.8.4 Z-distribution of \bar{d} for $1.0 < p_T < 1.3 \text{ GeV}/c$ ($\sqrt{s_{NN}} = 200 \text{ GeV}$, 40-80%)



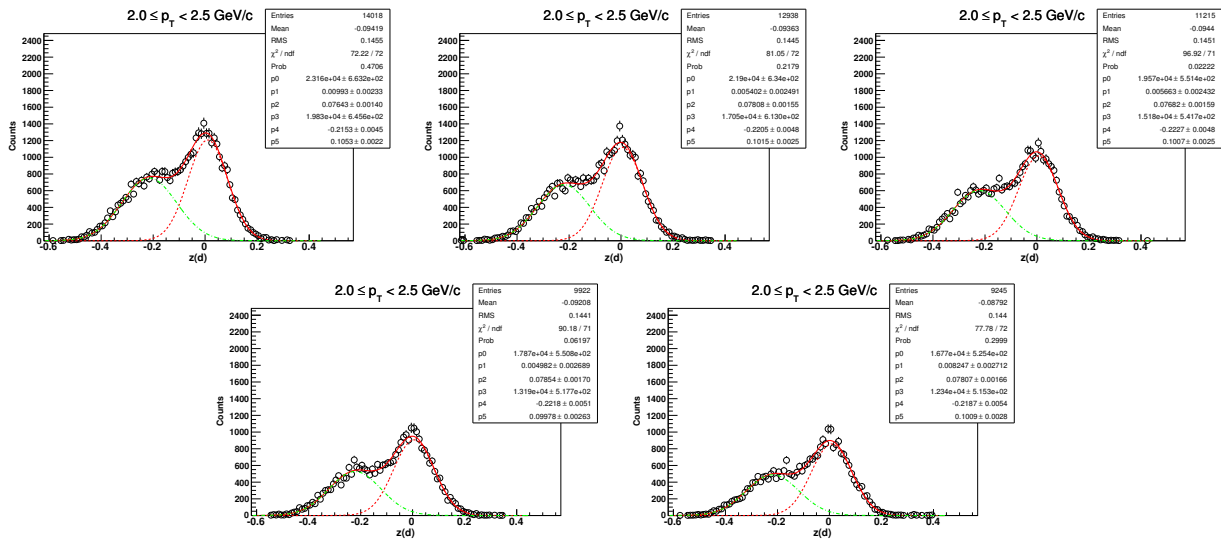
5.8.5 Z-distribution of \bar{d} for $1.3 < p_T < 1.7 \text{ GeV}/c$ ($\sqrt{s_{NN}} = 200 \text{ GeV}$, 40-80%)



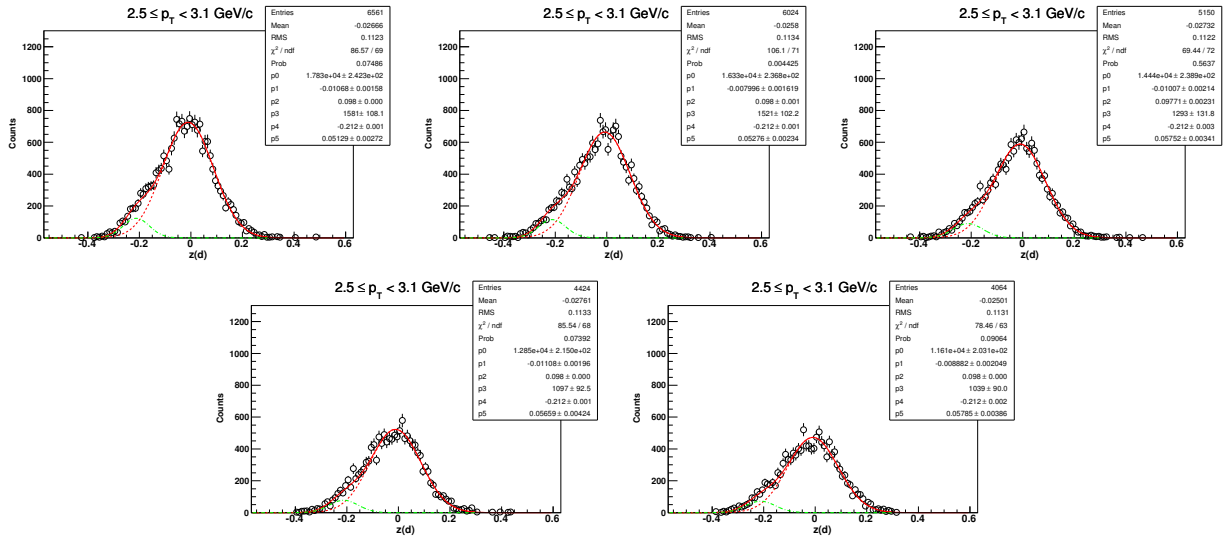
5.8.6 Z-distribution of \bar{d} for $1.7 < p_T < 2.0 \text{ GeV}/c$ ($\sqrt{s_{NN}} = 200 \text{ GeV}$, 40-80%)



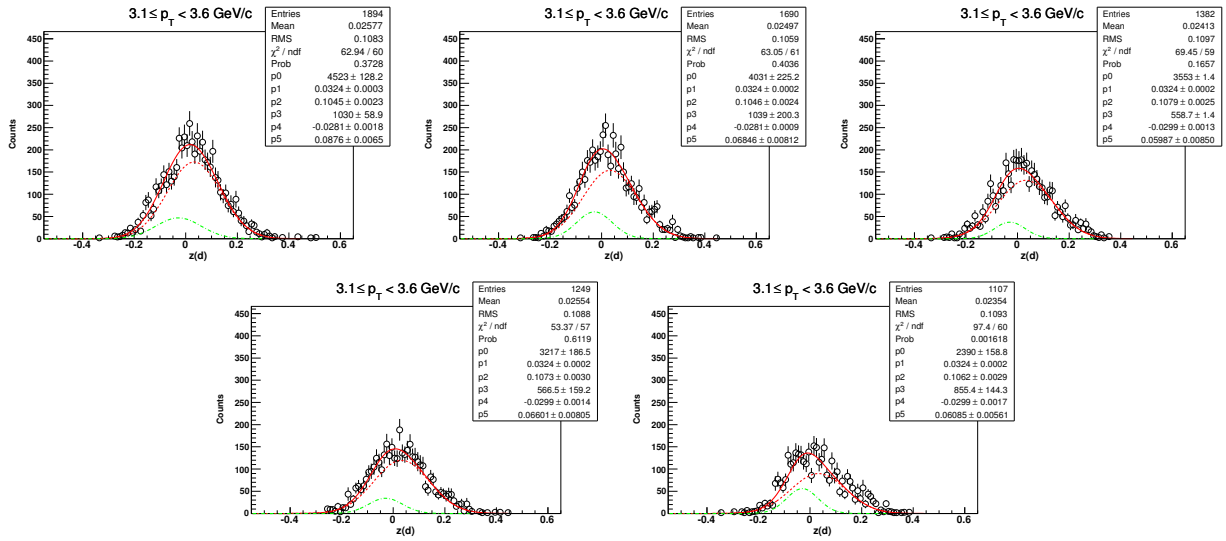
5.8.7 Z-distribution of \bar{d} for $2.0 < p_T < 2.5 \text{ GeV}/c$ ($\sqrt{s_{NN}} = 200 \text{ GeV}$, 40-80%)



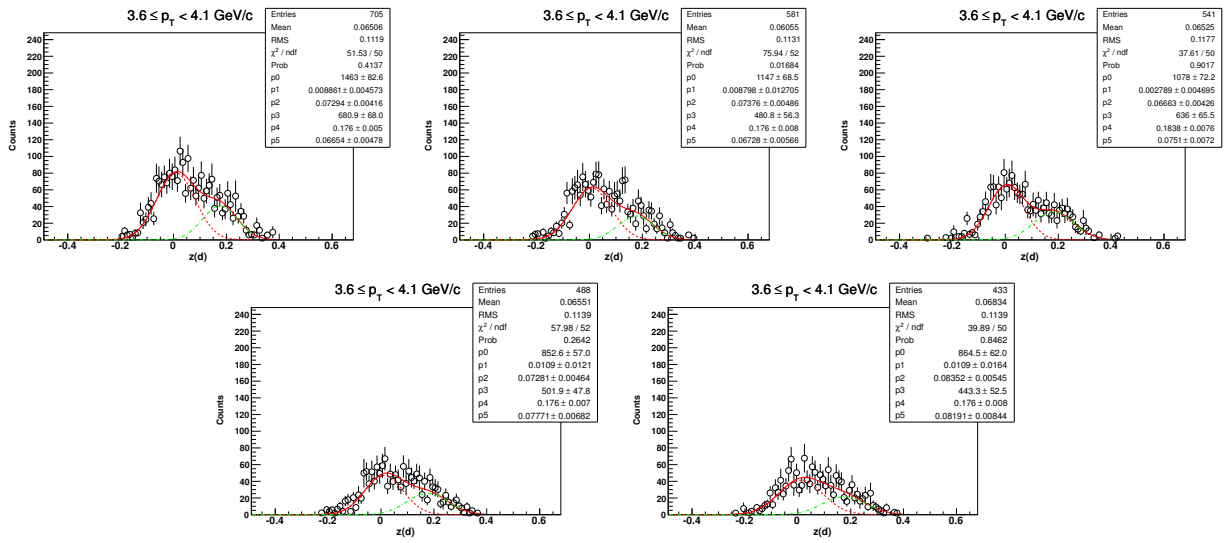
5.8.8 Z-distribution of \bar{d} for $2.5 < p_T < 3.1 \text{ GeV}/c$ ($\sqrt{s_{NN}} = 200 \text{ GeV}$, 40-80%)



5.8.9 Z-distribution of \bar{d} for $3.1 < p_T < 3.6 \text{ GeV}/c$ ($\sqrt{s_{NN}} = 200 \text{ GeV}$, 40-80%)

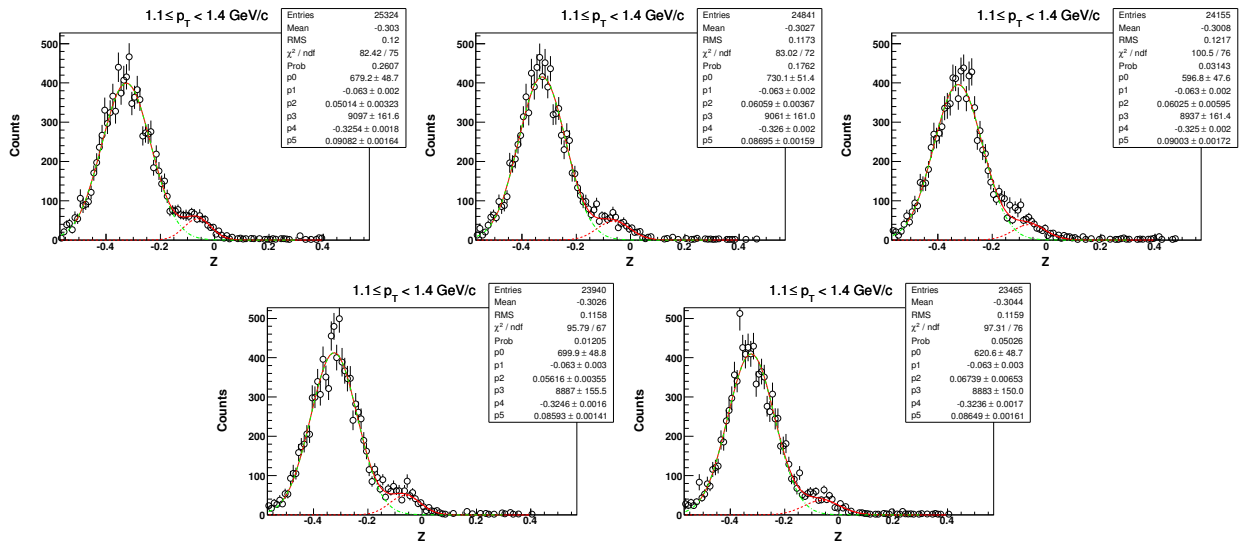


5.8.10 Z-distribution of \bar{d} for $3.6 < p_T < 4.0 \text{ GeV}/c$ ($\sqrt{s_{NN}} = 200 \text{ GeV}$, 40-80%)

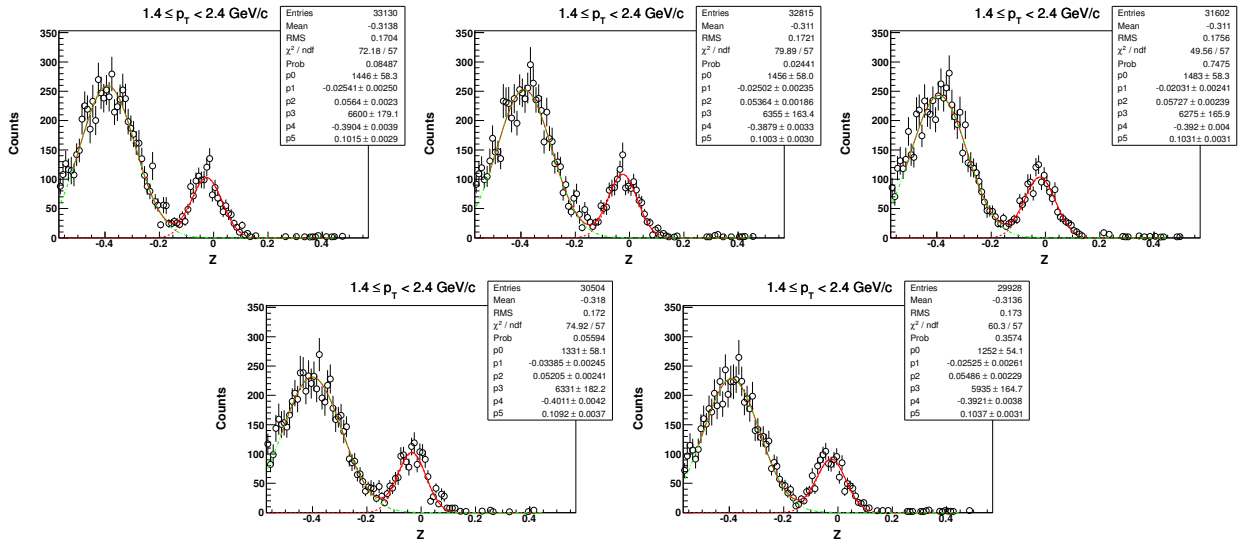


5.9 Z distribution of ${}^3\text{He}$ in $\sqrt{s_{NN}} = 200 \text{ GeV}$ (centrality: 0-80%)

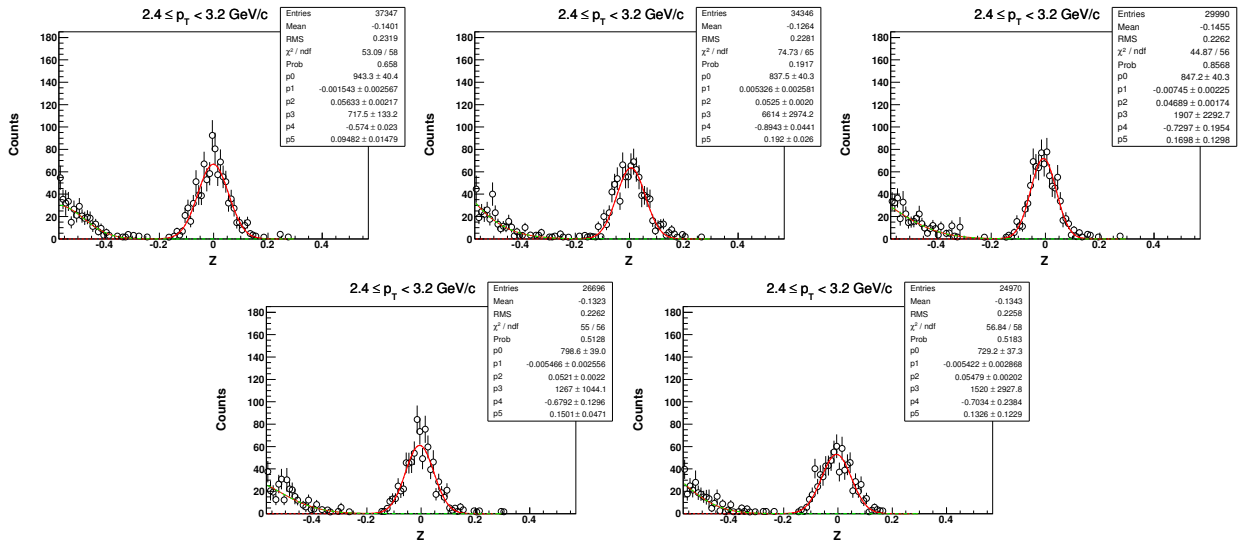
5.9.1 Z-distribution of ${}^3\text{He}$ for $1.1 < p_T < 1.4 \text{ GeV}/c$



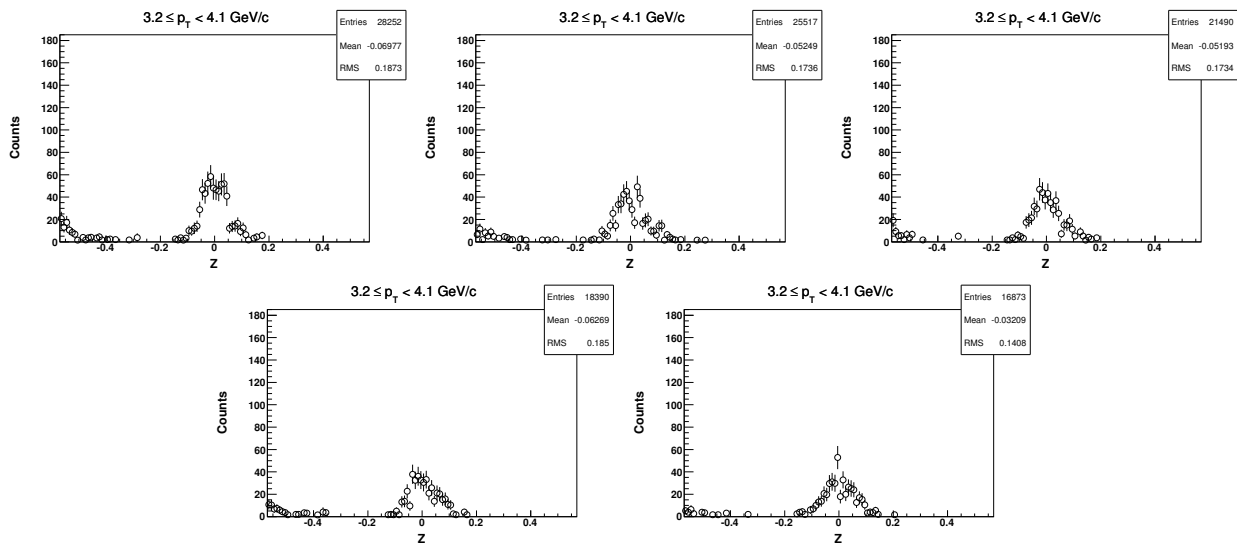
5.9.2 Z-distribution of 3He for $1.4 < p_T < 2.4 \text{ GeV}/c$ ($\sqrt{s_{NN}} = 200 \text{ GeV}$, 0-80%)



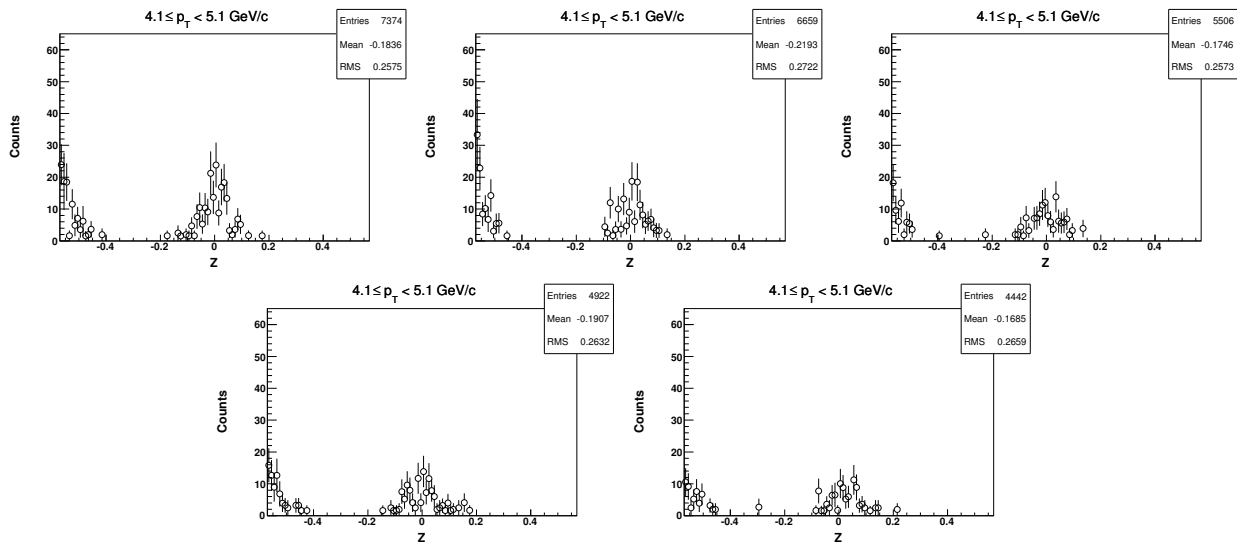
5.9.3 Z-distribution of 3He for $2.4 < p_T < 3.2 \text{ GeV}/c$ ($\sqrt{s_{NN}} = 200 \text{ GeV}$, 0-80%)



5.9.4 Z-distribution of ^3He for $3.2 < p_T < 4.1 \text{ GeV}/c$ ($\sqrt{s_{NN}} = 200 \text{ GeV}$, 0-80%)

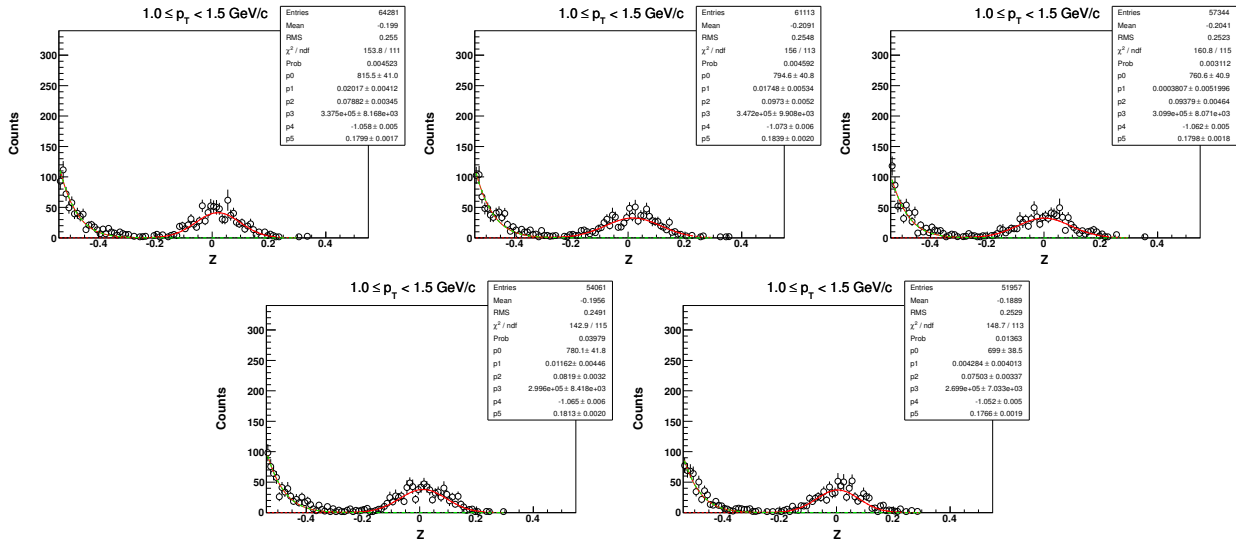


5.9.5 Z-distribution of ^3He for $4.1 < p_T < 5.1 \text{ GeV}/c$ ($\sqrt{s_{NN}} = 200 \text{ GeV}$, 0-80%)

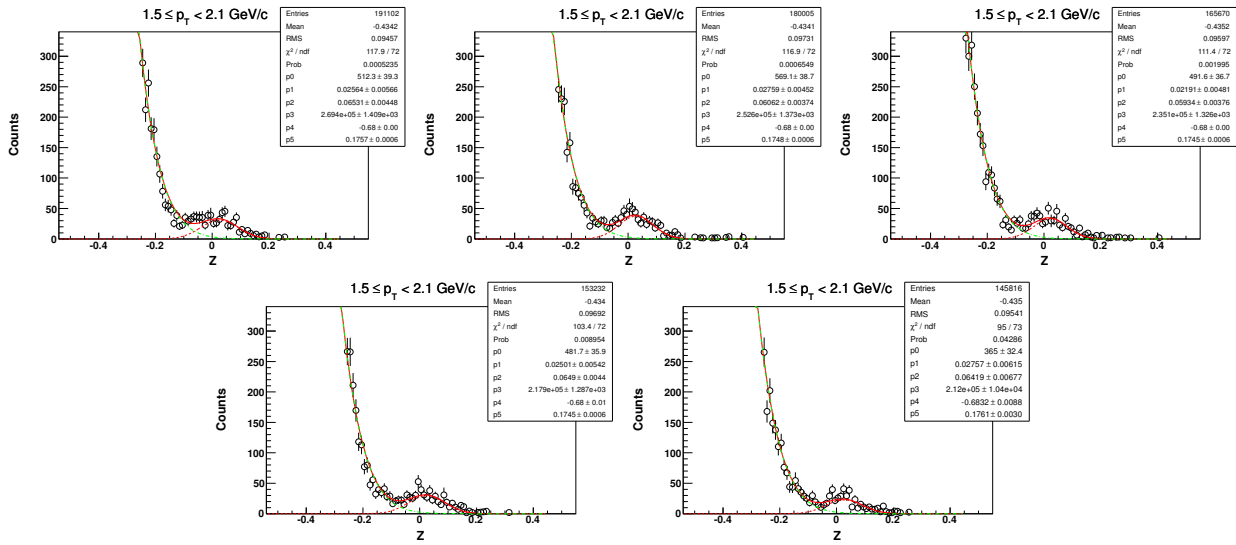


5.10 Z distribution of t in $\sqrt{s_{NN}} = 200$ GeV (centrality: 0-80%)

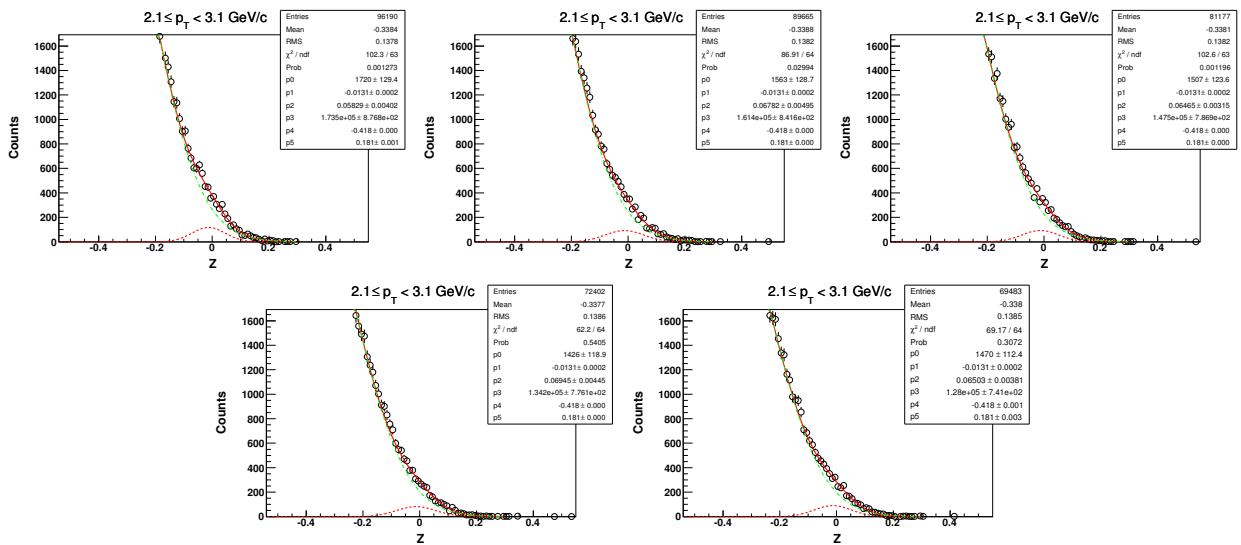
5.10.1 Z-distribution of t for $1.1 < p_T < 1.5$ GeV/c



5.10.2 Z-distribution of t for $1.5 < p_T < 2.1$ GeV/c ($\sqrt{s_{NN}} = 200$ GeV, 0-80%)

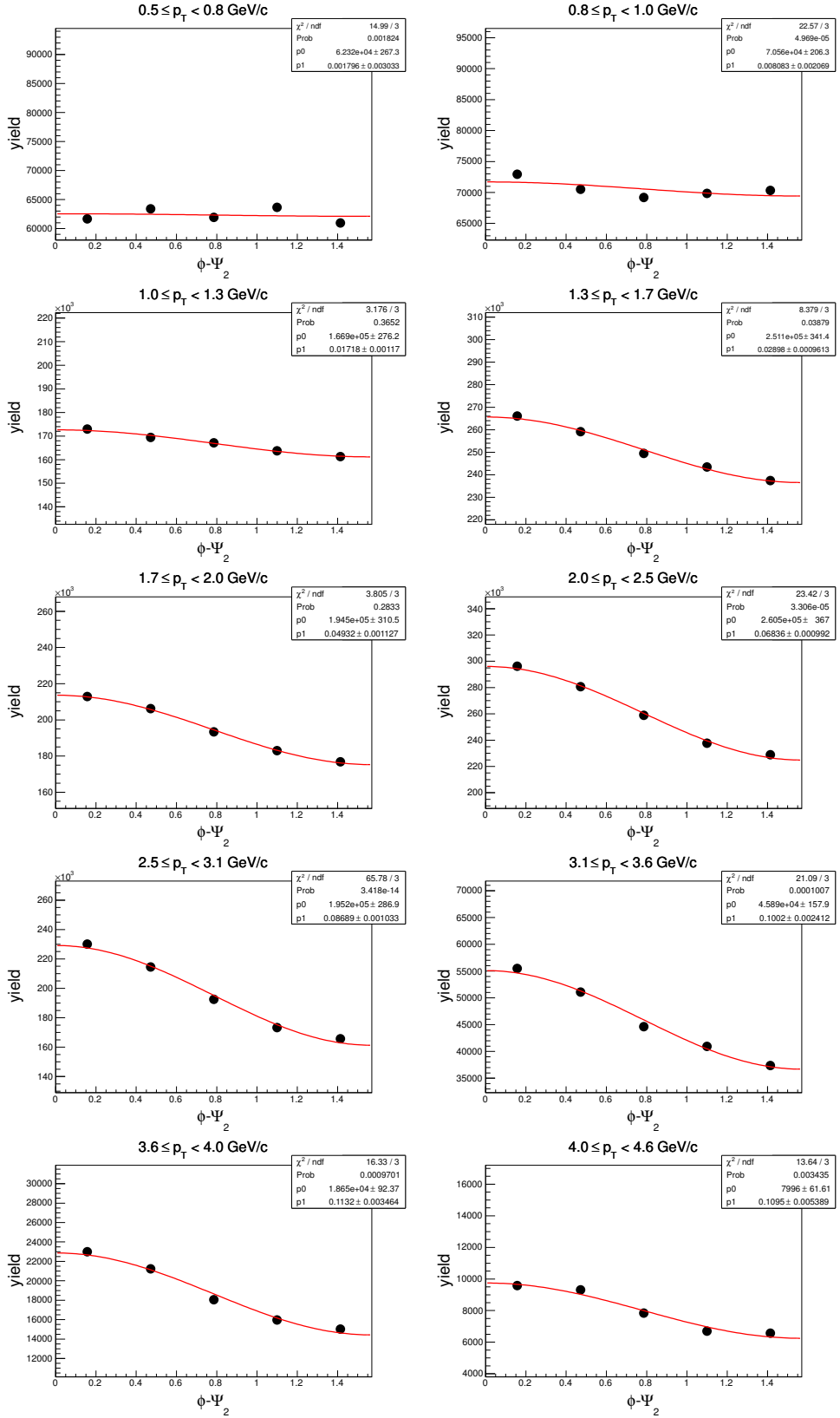


5.10.3 Z-distribution of t for $2.1 < p_T < 3.1 \text{ GeV}/c$ ($\sqrt{s_{NN}} = 200 \text{ GeV}$, 0-80%)

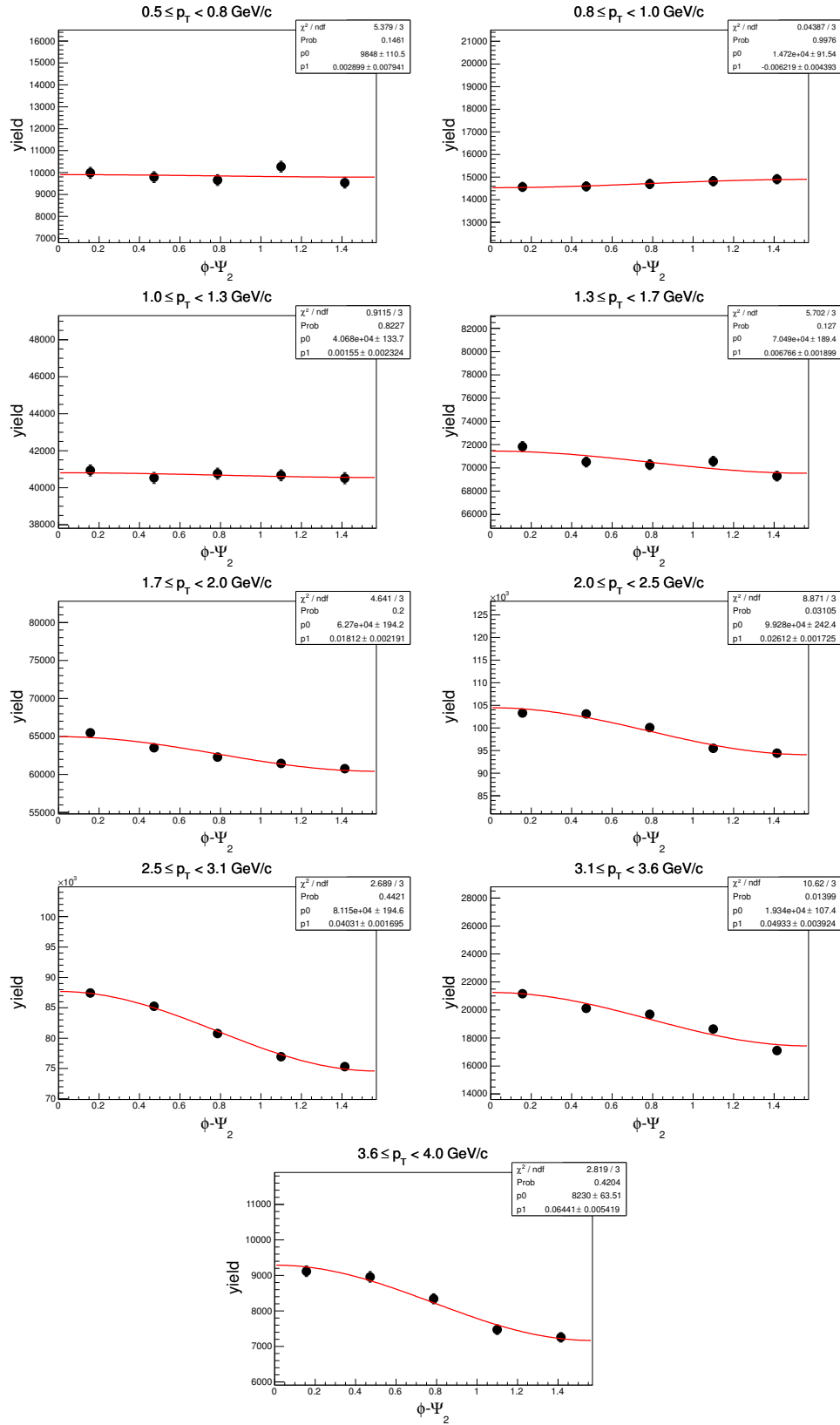


5.11 $\phi - \Psi_2$ distributions in Au+Au at $\sqrt{s_{NN}} = 200$ GeV

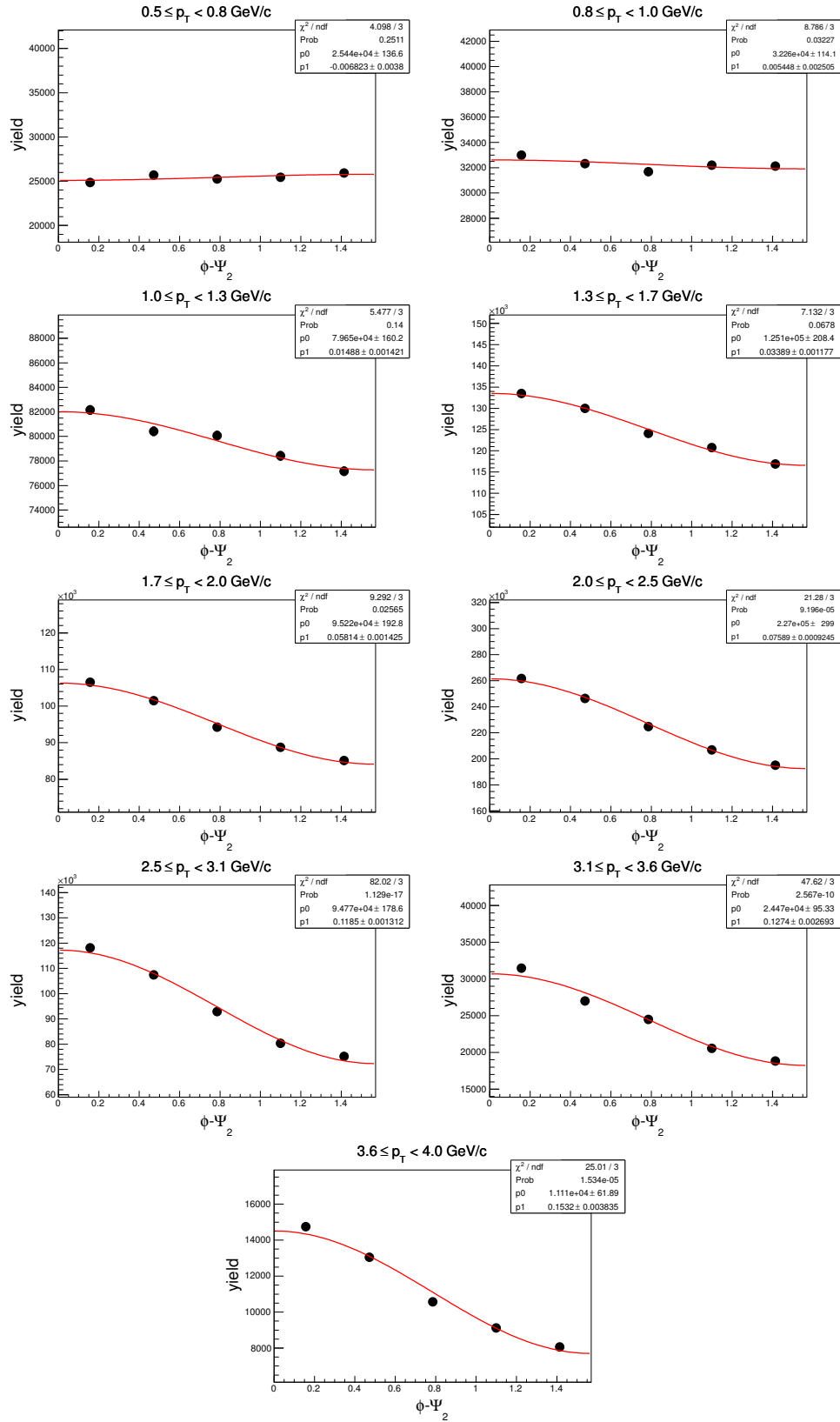
5.11.1 $\phi - \Psi_2$ of d in centrality: 0-80%



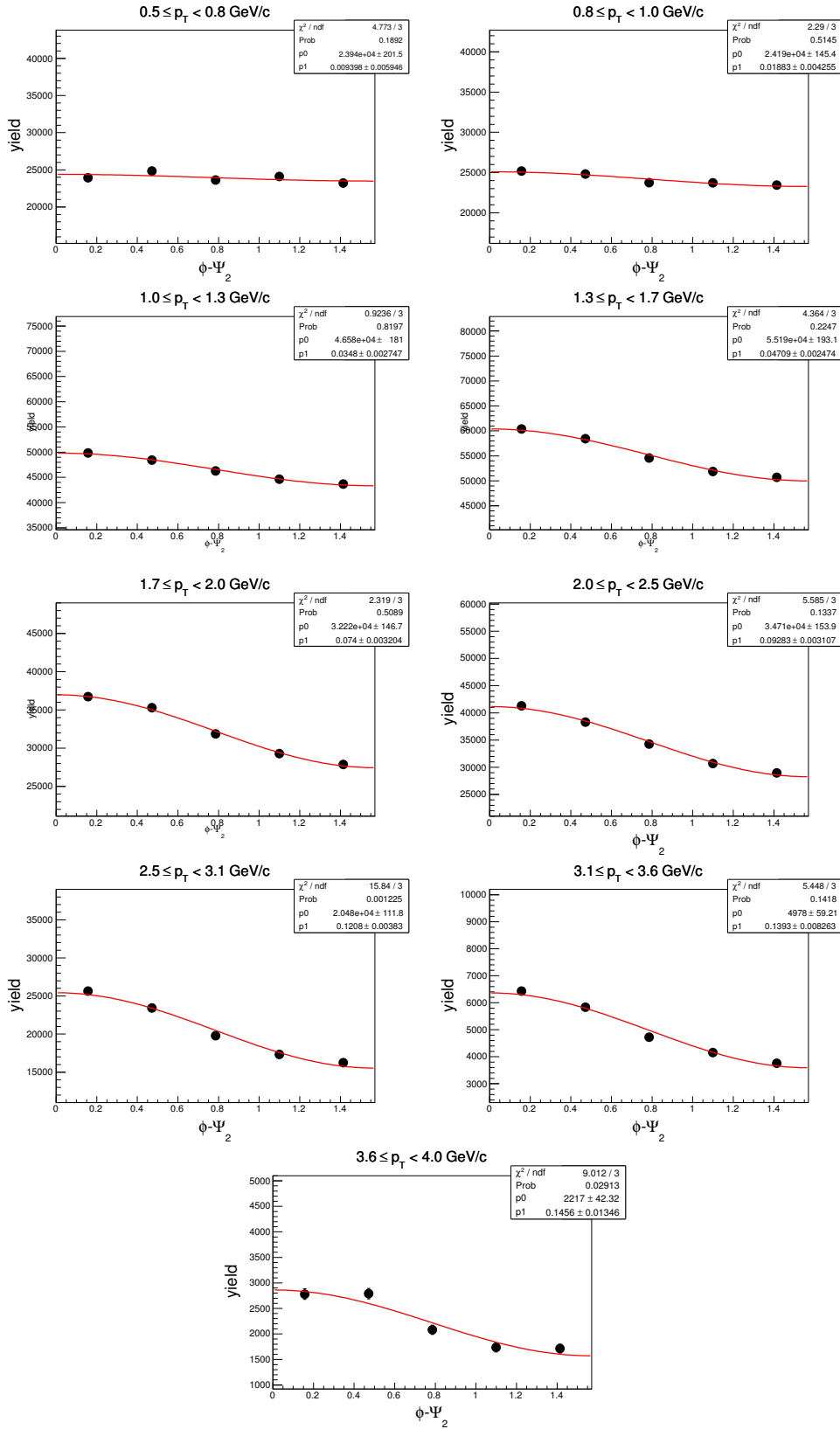
5.11.2 $\phi - \Psi_2$ of d in centrality: 0-10% ($\sqrt{s_{NN}} = 200$ GeV)



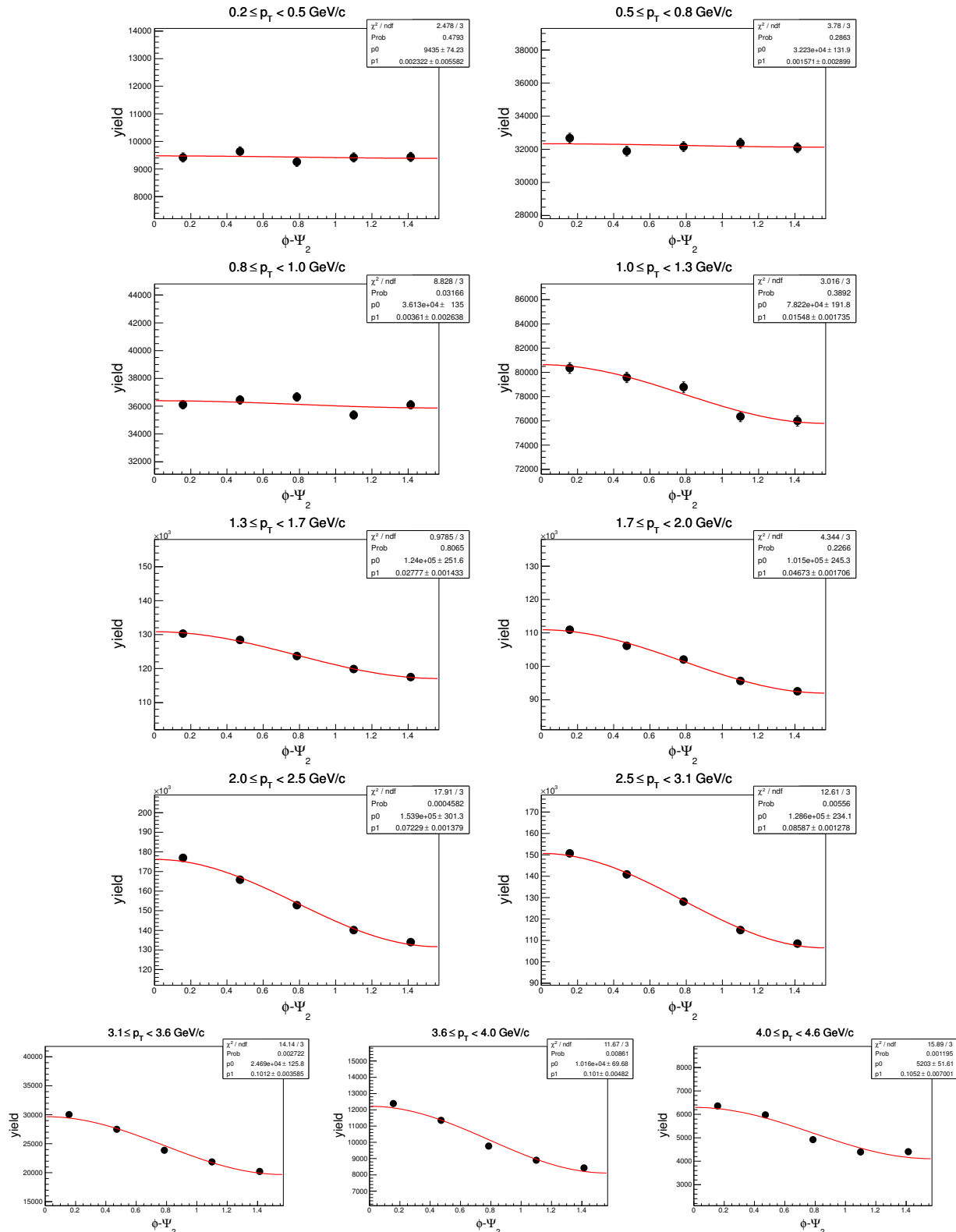
5.11.3 $\phi - \Psi_2$ of d in centrality: 10-40% ($\sqrt{s_{NN}} = 200$ GeV)



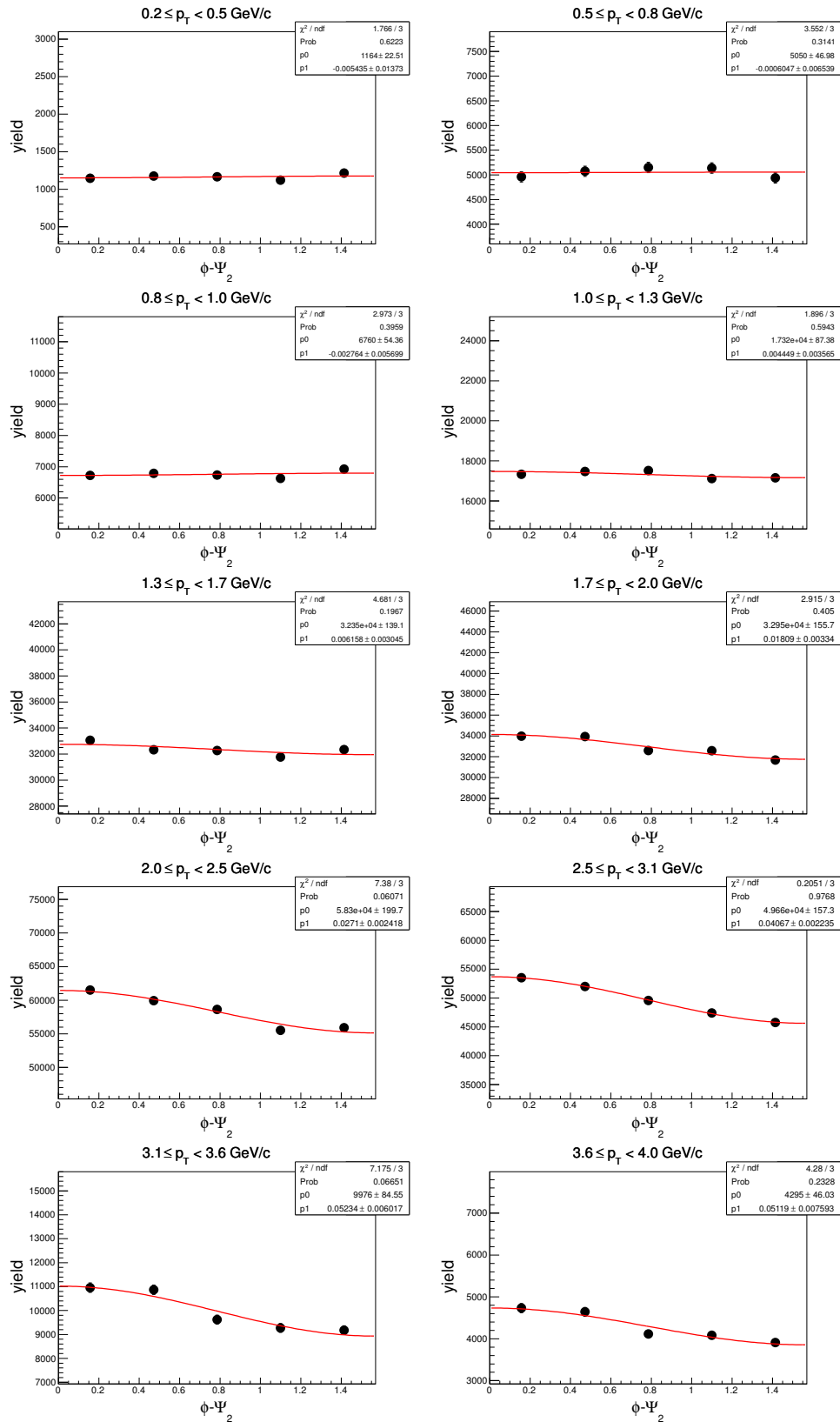
5.11.4 $\phi - \Psi_2$ of d in centrality: 40-80% ($\sqrt{s_{NN}} = 200$ GeV)



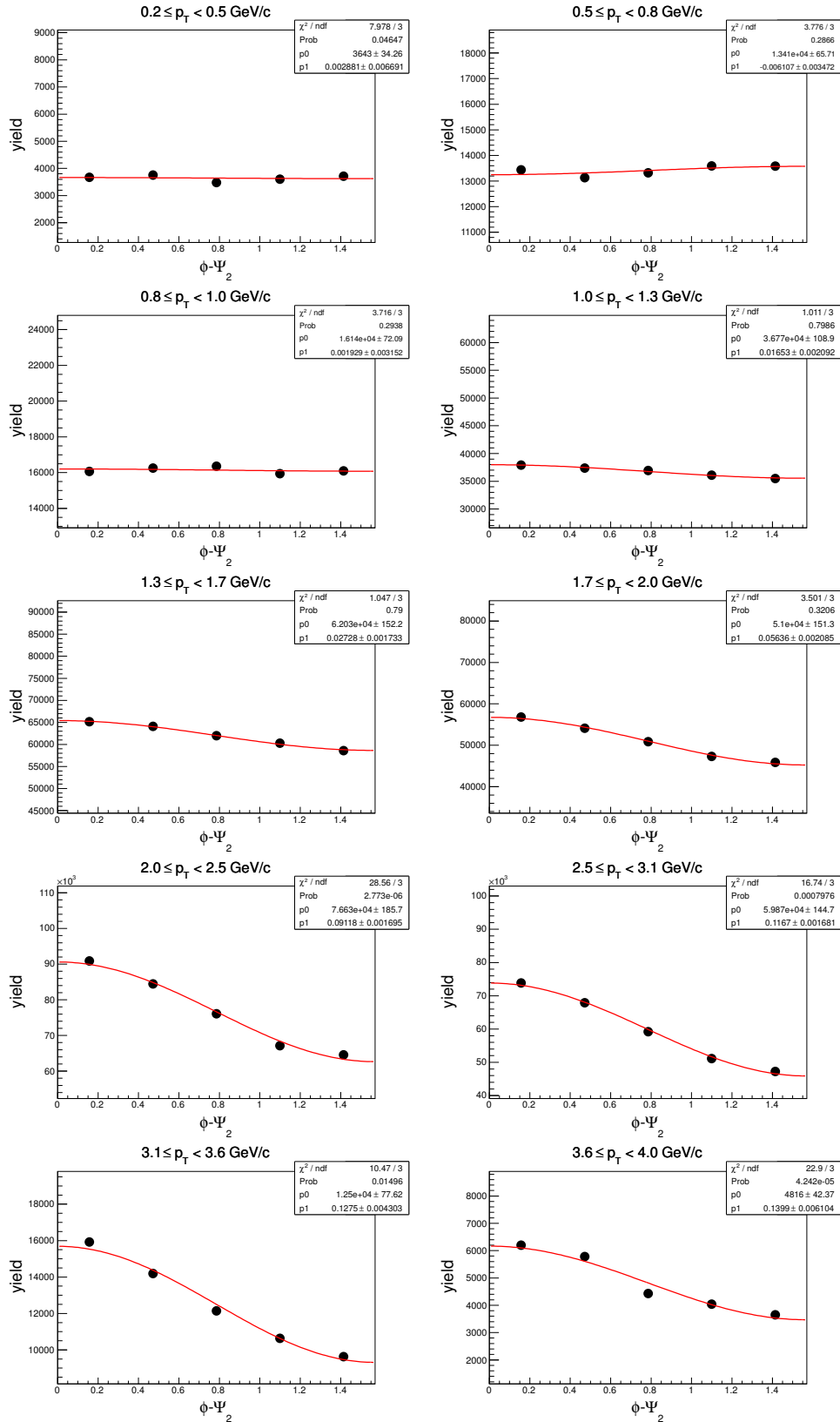
5.11.5 $\phi - \Psi_2$ of \bar{d} in centrality: 0-80% ($\sqrt{s_{NN}} = 200$ GeV)



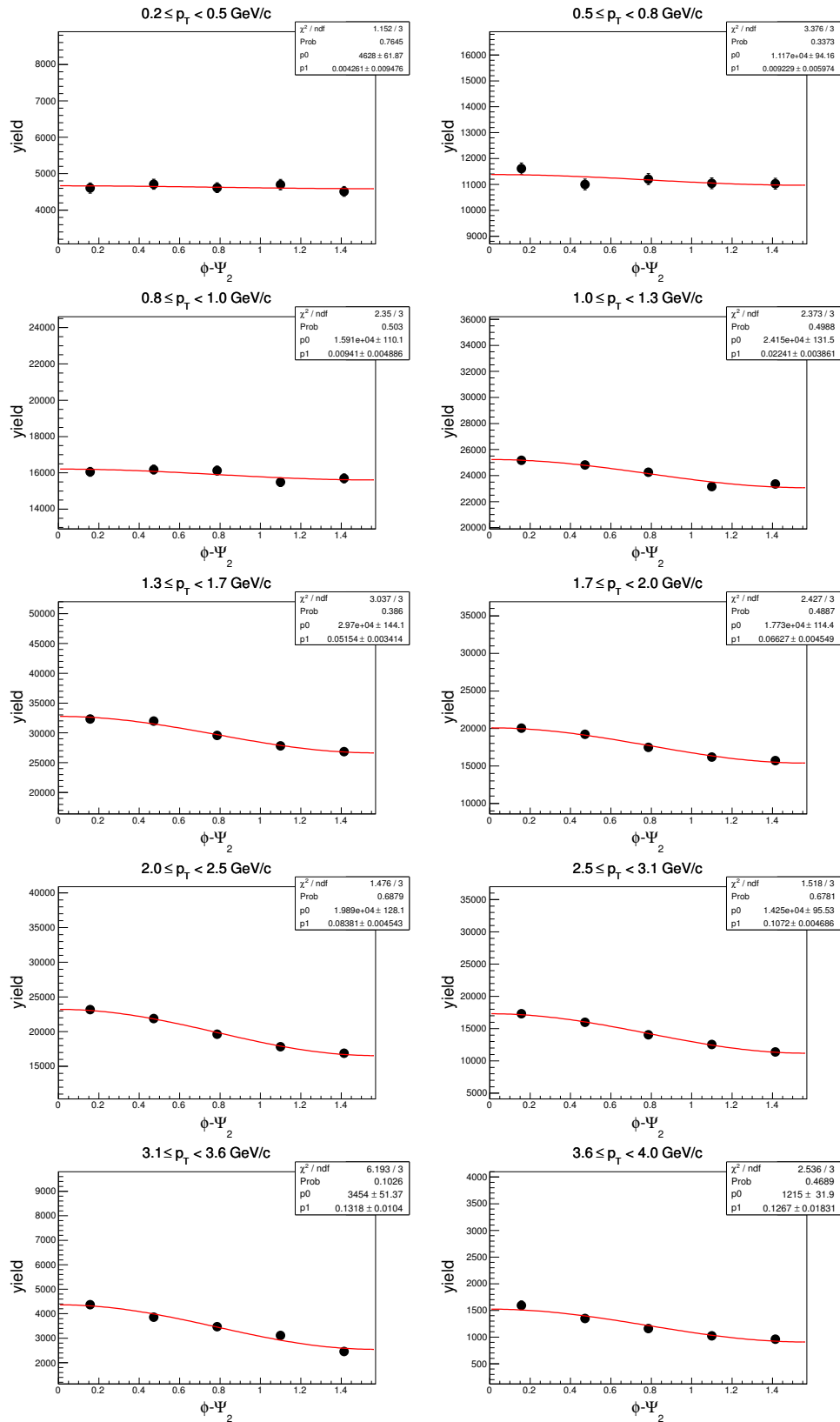
5.11.6 $\phi - \Psi_2$ of \bar{d} in centrality: 0-10% ($\sqrt{s_{NN}} = 200$ GeV)



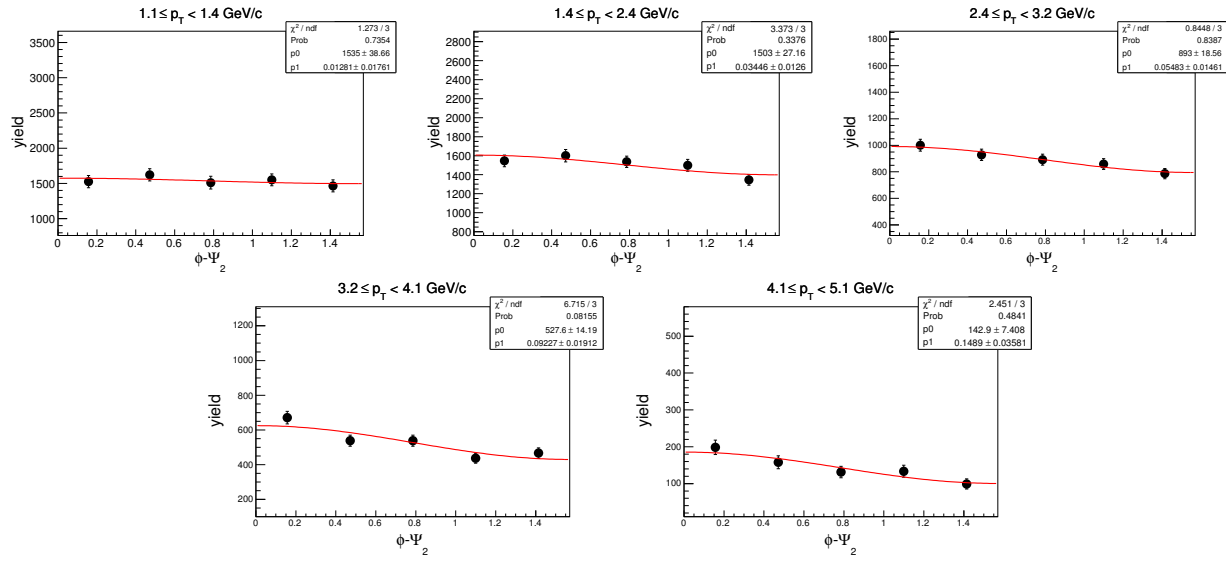
5.11.7 $\phi - \Psi_2$ of \bar{d} in centrality: 10-40% ($\sqrt{s_{NN}} = 200$ GeV)



5.11.8 $\phi - \Psi_2$ of \bar{d} in centrality: 40-80% ($\sqrt{s_{NN}} = 200$ GeV)



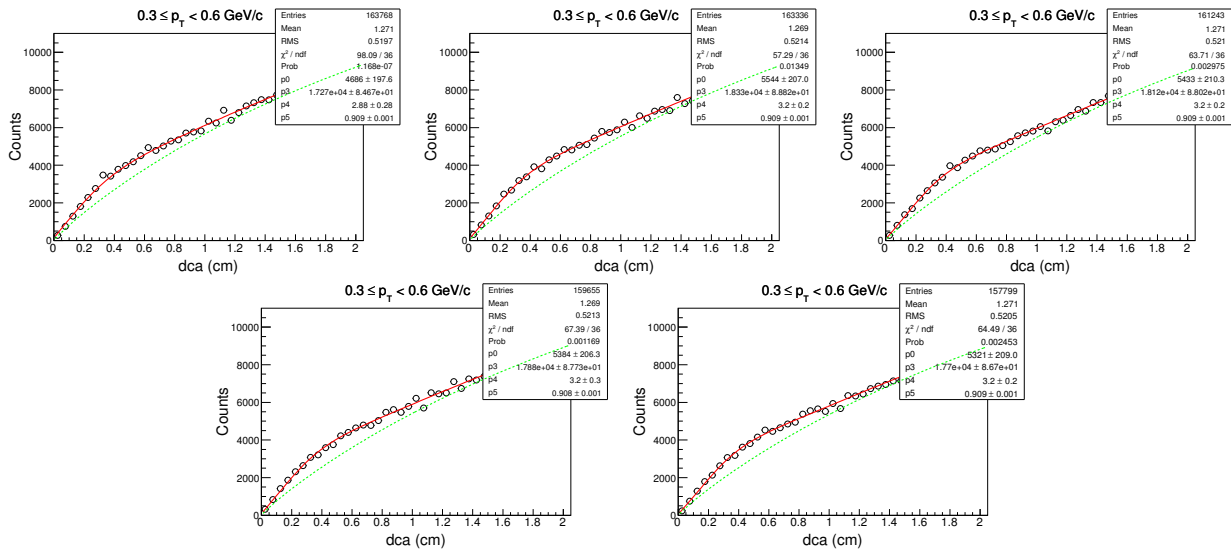
5.11.9 $\phi - \Psi_2$ of ${}^3\text{He}$ in centrality: 0-80% ($\sqrt{s_{NN}} = 200$ GeV)



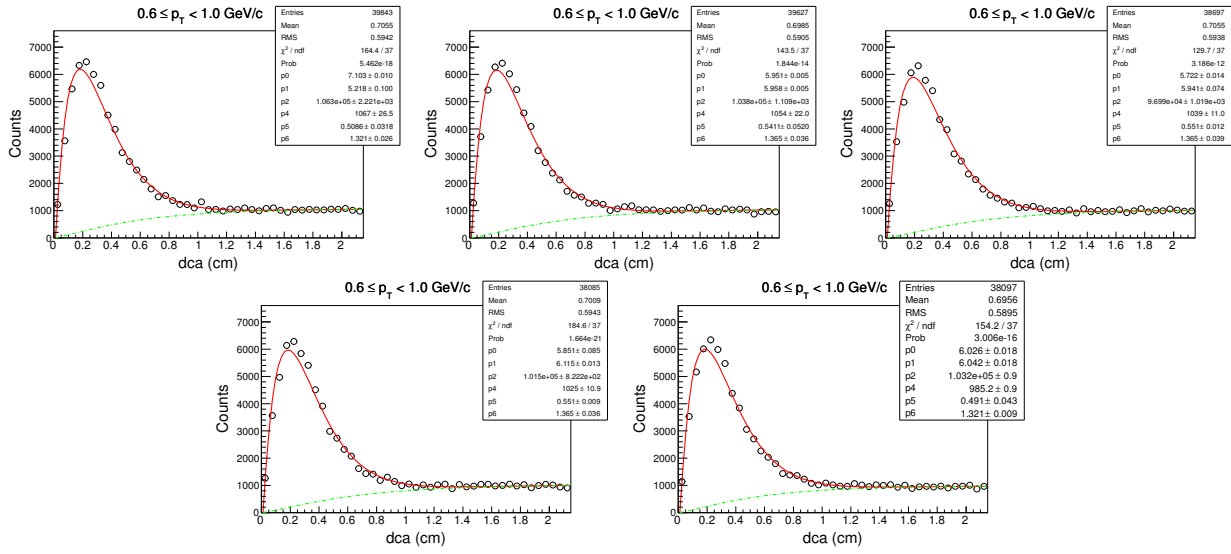
6 DCA and Z-distributions for Au+Au at $\sqrt{s_{NN}} = 62.4$ GeV

6.1 Centrality: 0-80%

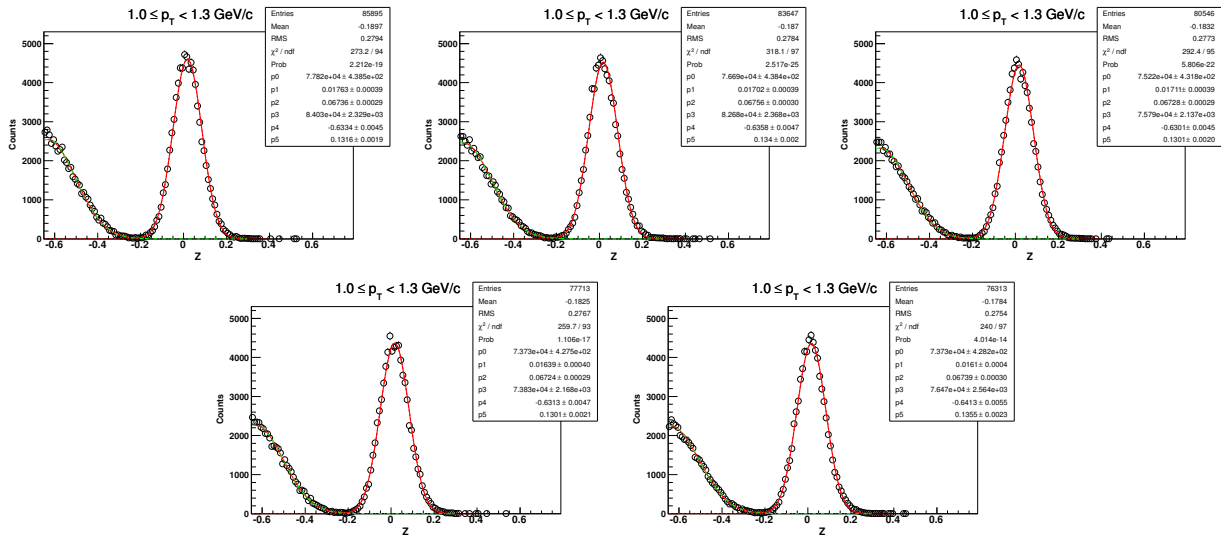
6.1.1 DCA-distribution of d for $0.3 < p_T < 0.6 \text{ GeV}/c$



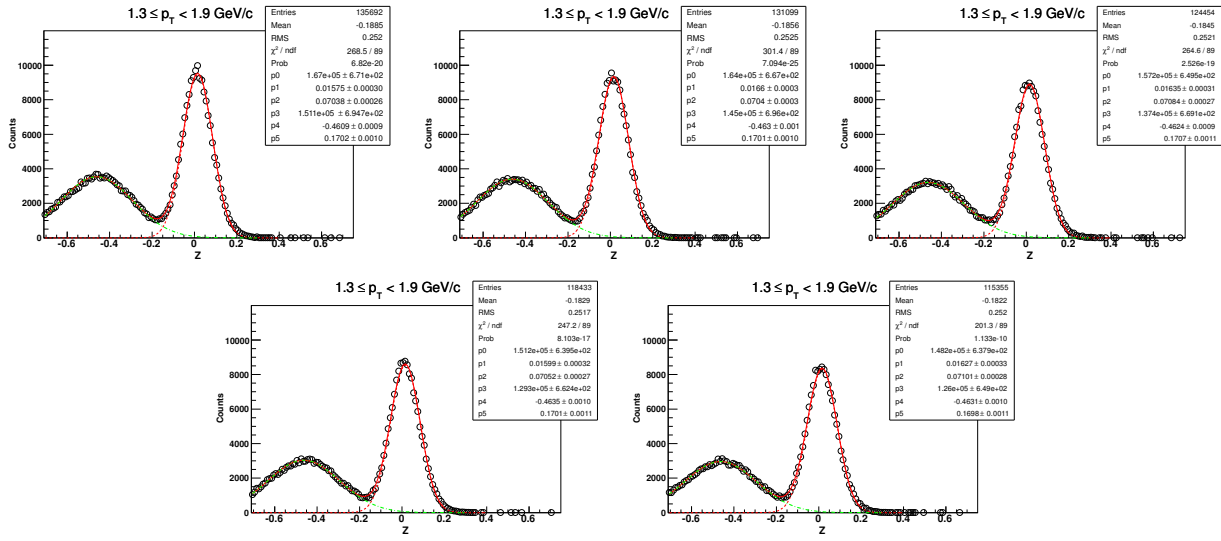
6.1.2 DCA-distribution of d for $0.6 < p_T < 1.0 \text{ GeV}/c$ ($\sqrt{s_{NN}} = 62.4 \text{ GeV}$, 0-80%)



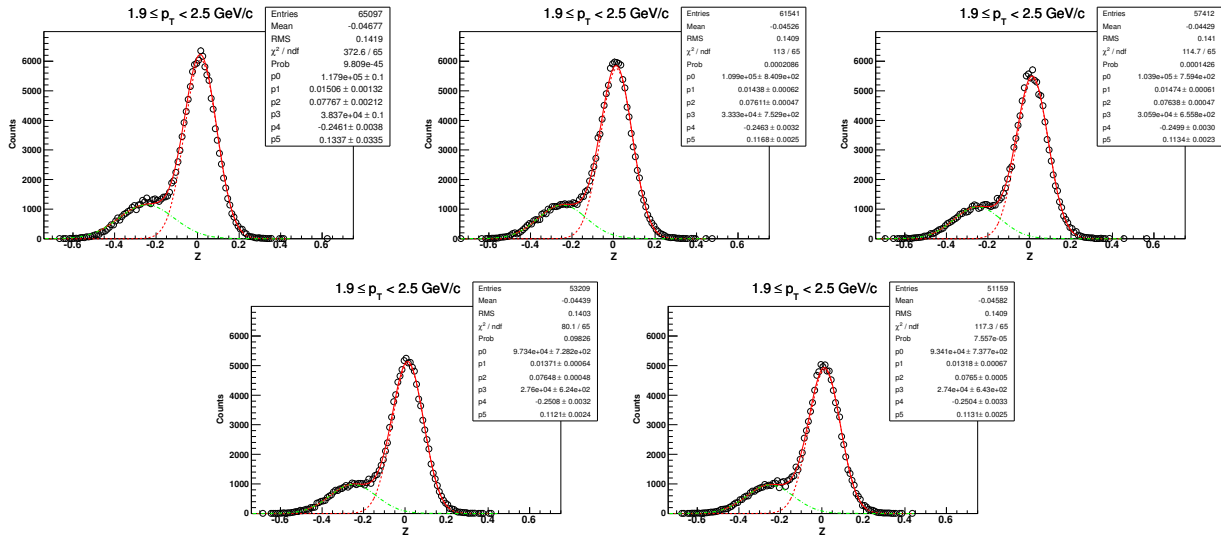
6.1.3 Z-distribution of d for $1.0 < p_T < 1.3 \text{ GeV}/c$ ($\sqrt{s_{NN}} = 62.4 \text{ GeV}$, 0-80%)



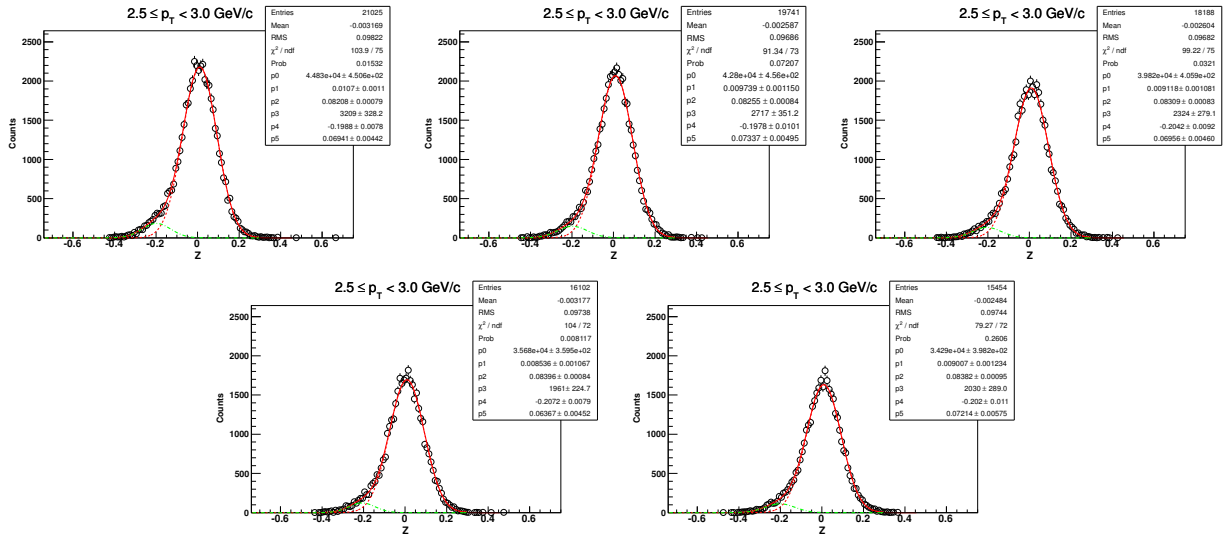
6.1.4 Z-distribution of d for $1.3 < p_T < 1.9 \text{ GeV}/c$ ($\sqrt{s_{NN}} = 62.4 \text{ GeV}$, 0-80%)



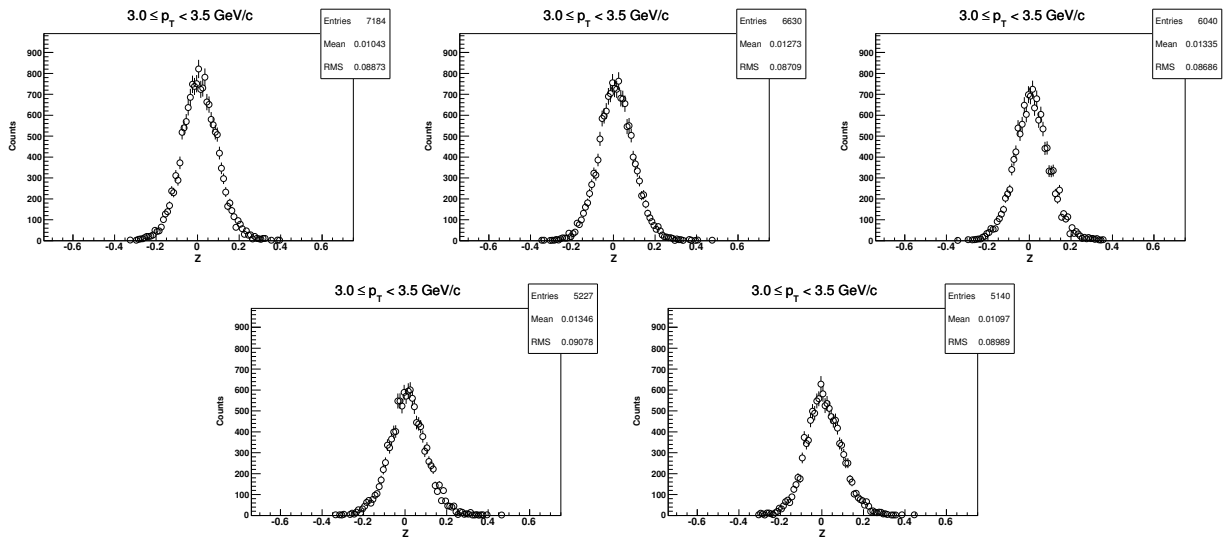
6.1.5 Z-distribution of d for $1.9 < p_T < 2.5 \text{ GeV}/c$ ($\sqrt{s_{NN}} = 62.4 \text{ GeV}$, 0-80%)



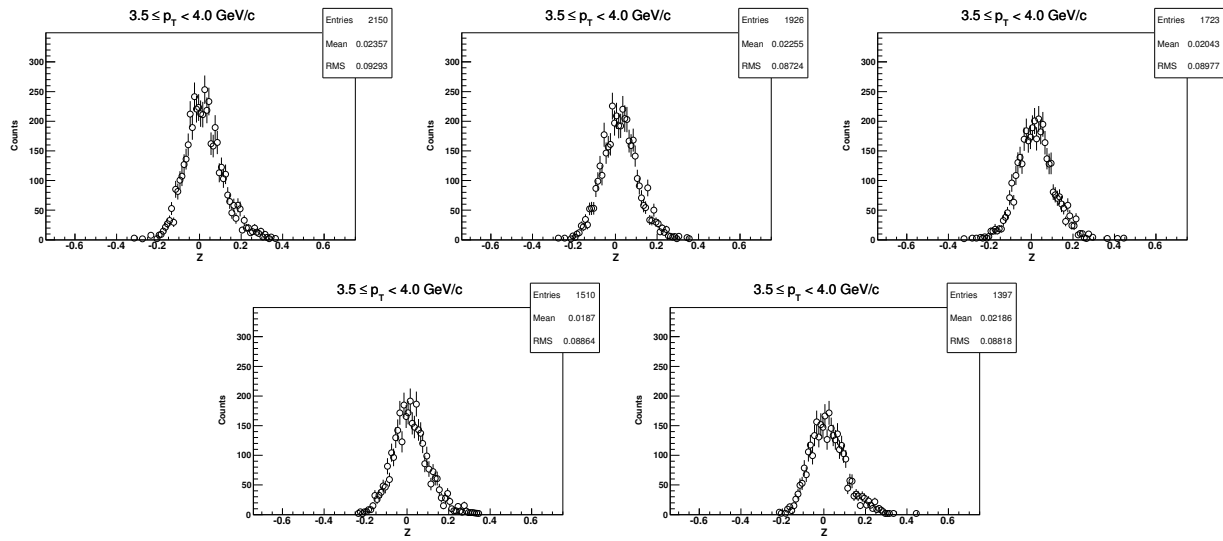
6.1.6 Z-distribution of d for $2.5 < p_T < 3.0 \text{ GeV}/c$ ($\sqrt{s_{NN}} = 62.4 \text{ GeV}$, 0-80%)



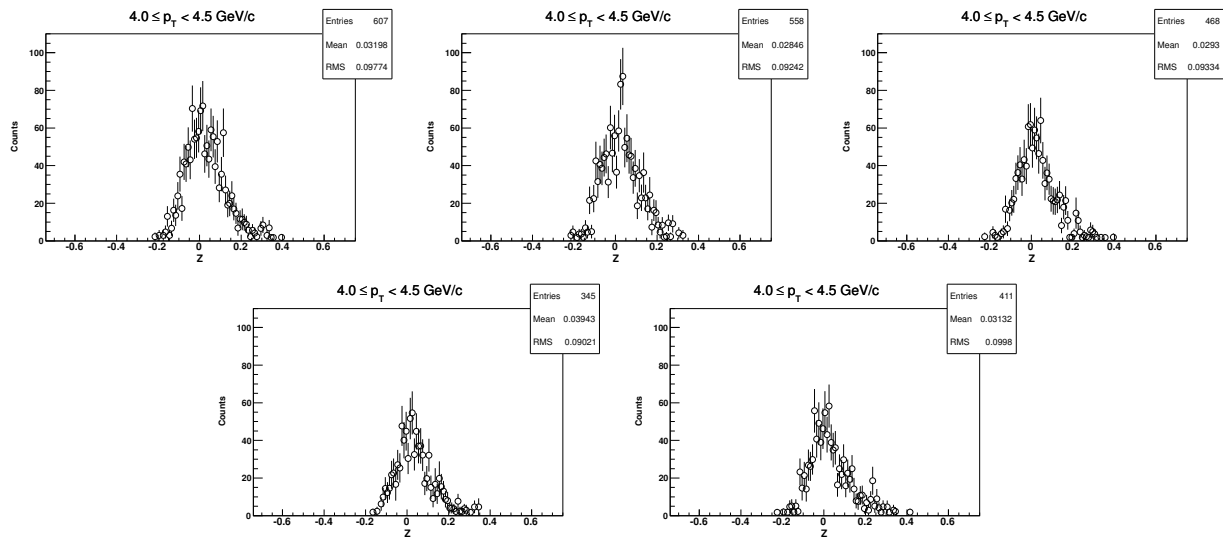
6.1.7 Z-distribution of d for $3.0 < p_T < 3.5 \text{ GeV}/c$ ($\sqrt{s_{NN}} = 62.4 \text{ GeV}$, 0-80%)



6.1.8 Z-distribution of d for $3.5 < p_T < 4.0 \text{ GeV}/c$ ($\sqrt{s_{NN}} = 62.4 \text{ GeV}$, 0-80%)

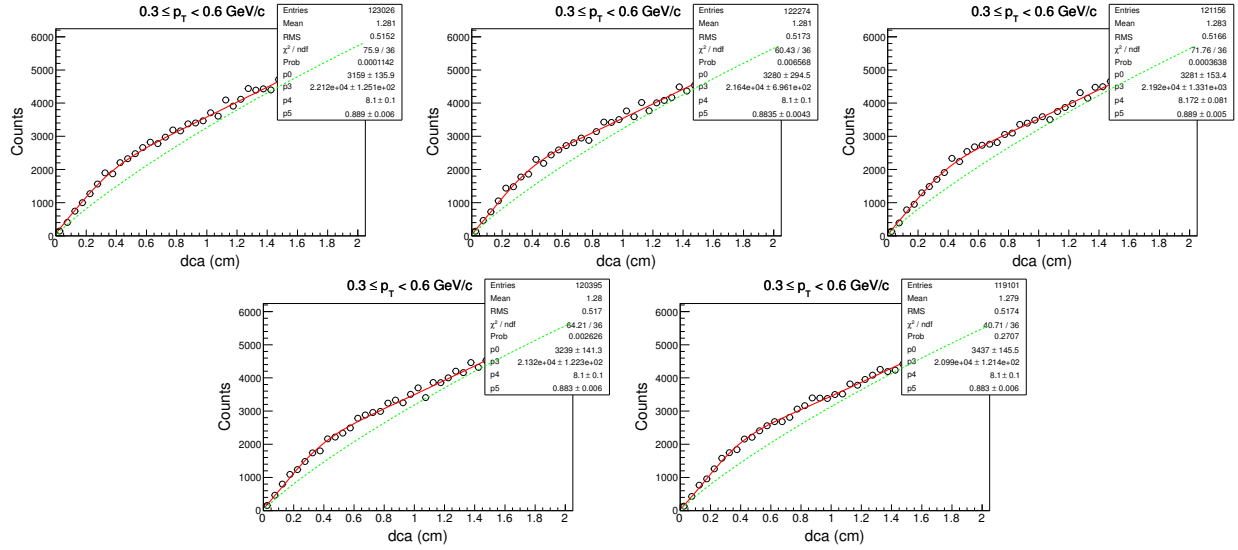


6.1.9 Z-distribution of d for $4.0 < p_T < 4.5 \text{ GeV}/c$ ($\sqrt{s_{NN}} = 62.4 \text{ GeV}$, 0-80%)

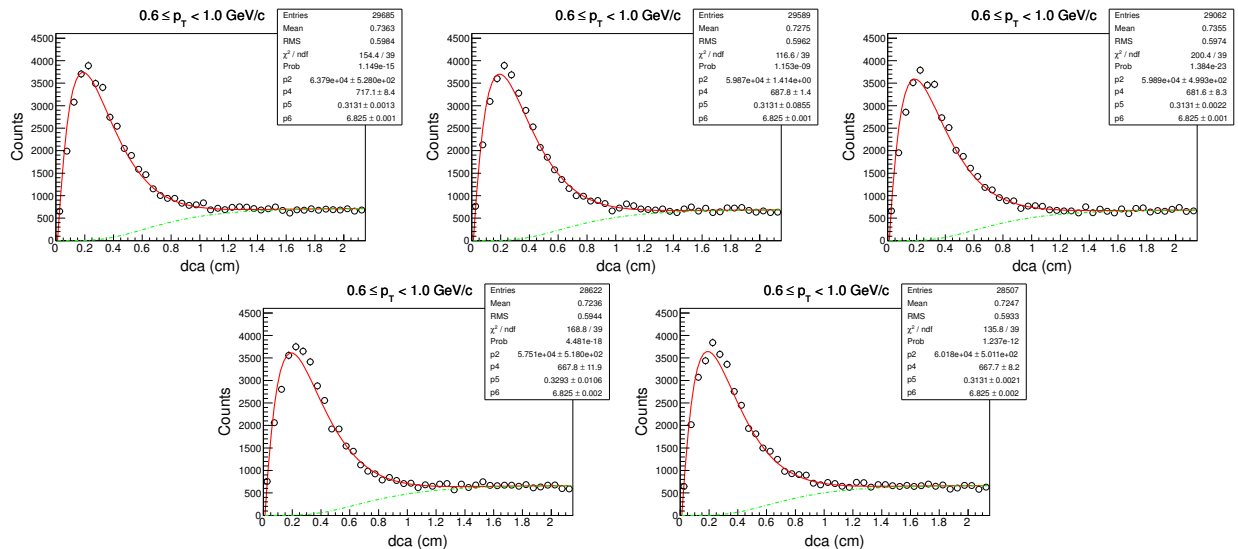


6.2 Centrality: 0-30%

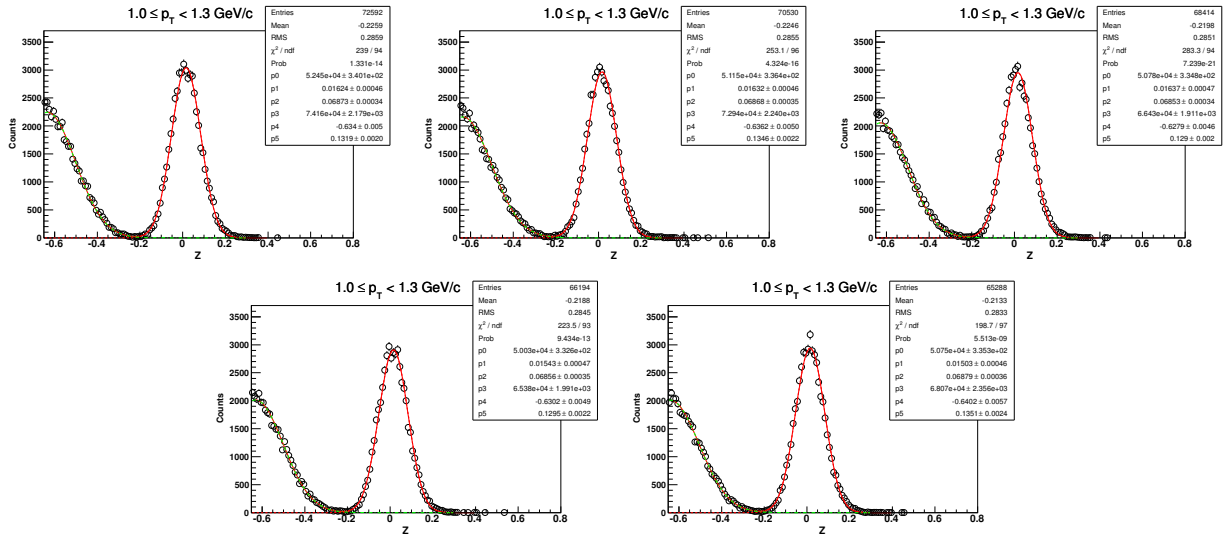
6.2.1 DCA-distribution of d for $0.3 < p_T < 0.6 \text{ GeV}/c$



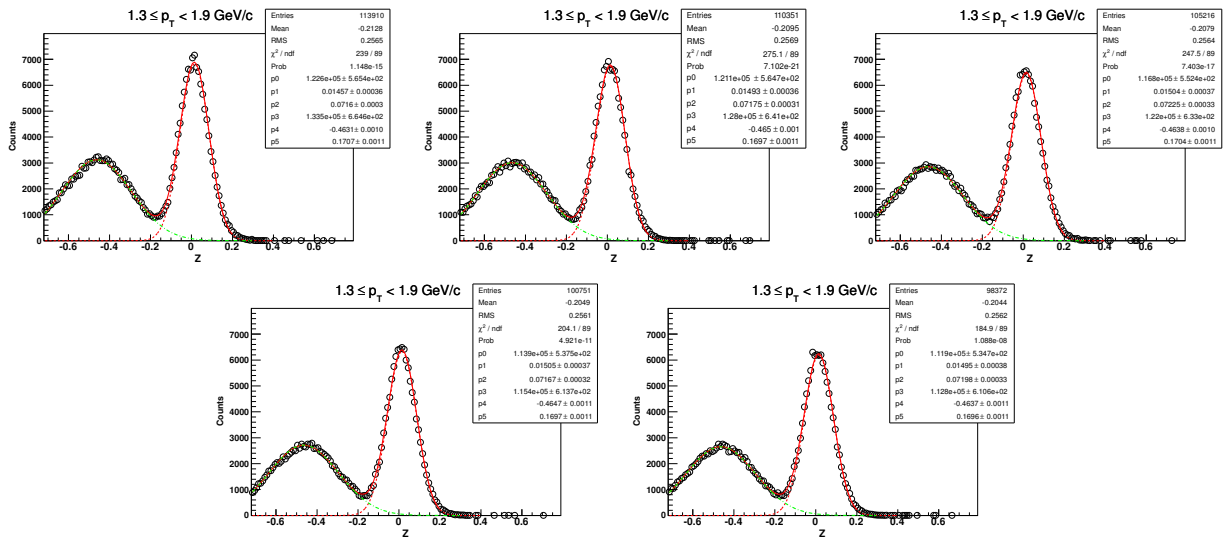
6.2.2 DCA-distribution of d for $0.6 < p_T < 1.0 \text{ GeV}/c$



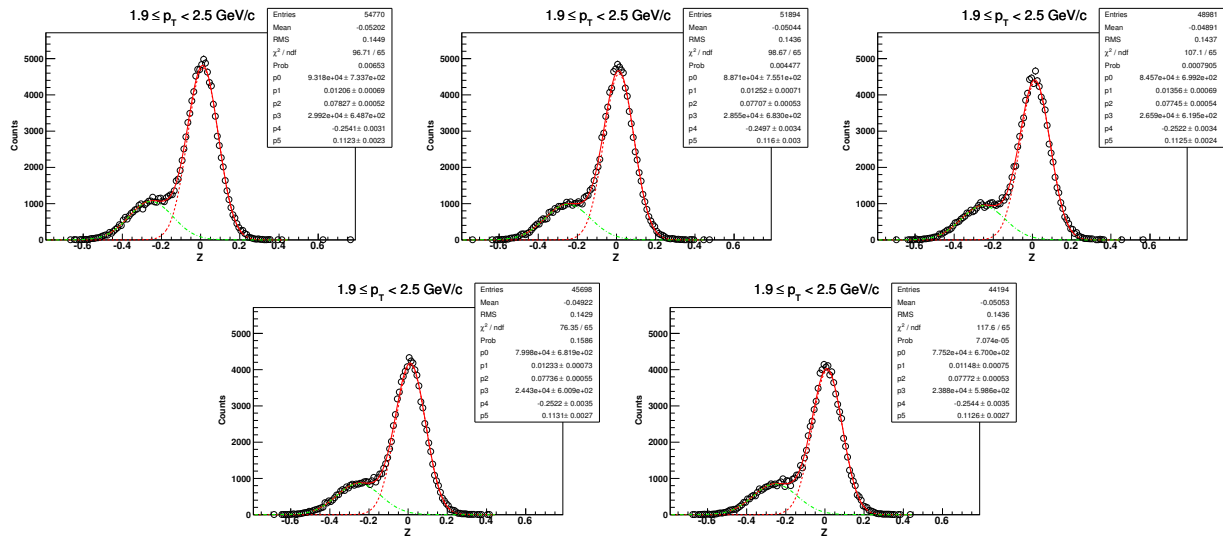
6.2.3 Z-distribution of d for $1.0 < p_T < 1.3 \text{ GeV}/c$ ($\sqrt{s_{NN}} = 62.4 \text{ GeV}$, 0-30%)



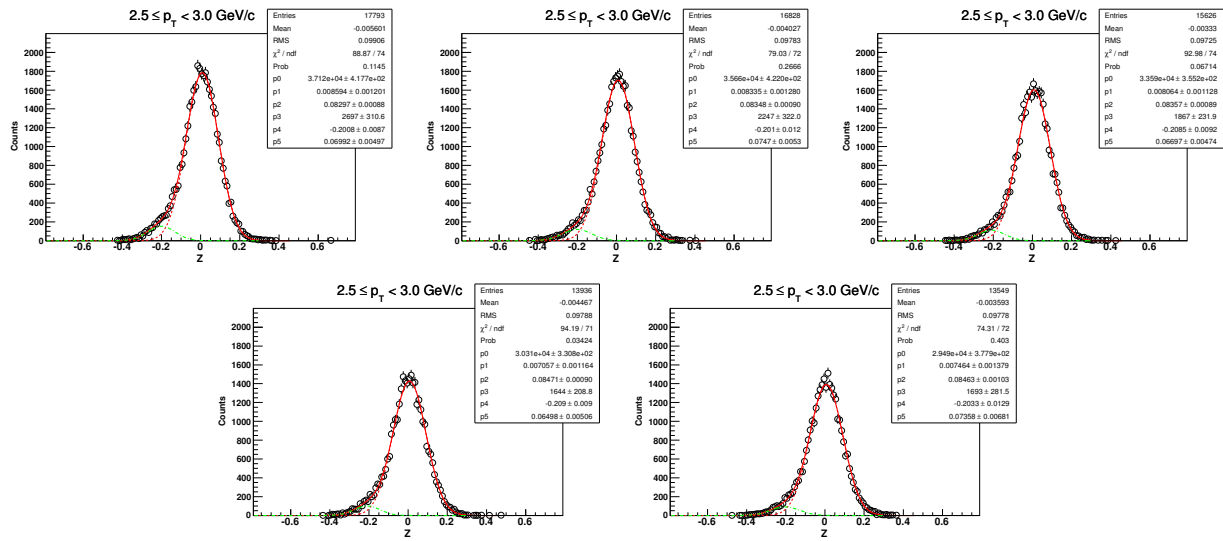
6.2.4 Z-distribution of d for $1.3 < p_T < 1.9 \text{ GeV}/c$ ($\sqrt{s_{NN}} = 62.4 \text{ GeV}$, 0-30%)



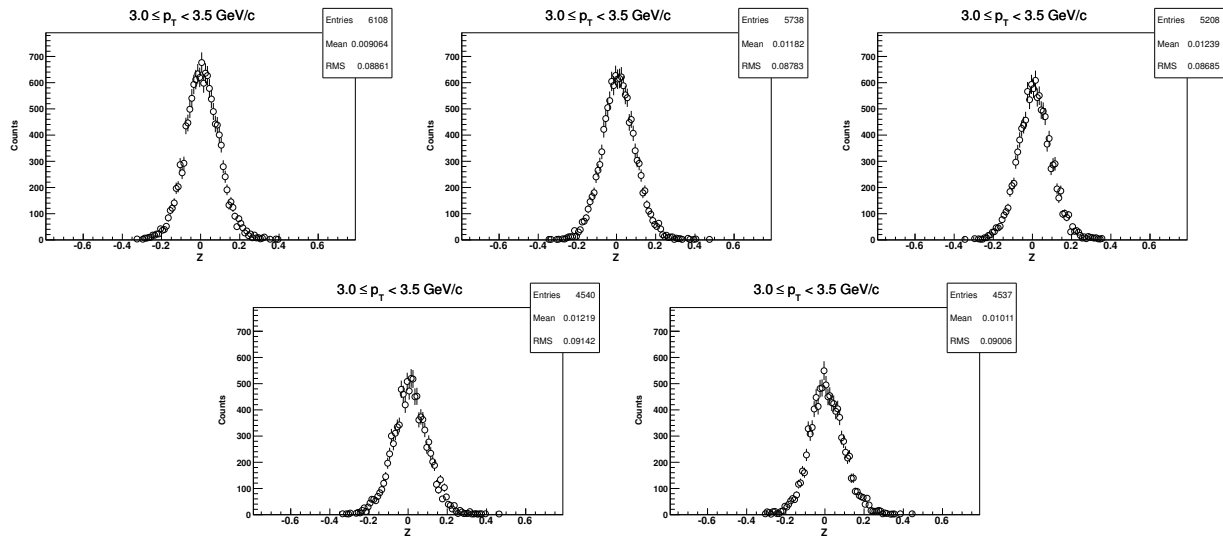
6.2.5 Z-distribution of d for $1.9 < p_T < 2.5 \text{ GeV}/c$ ($\sqrt{s_{NN}} = 62.4 \text{ GeV}$, 0-30%)



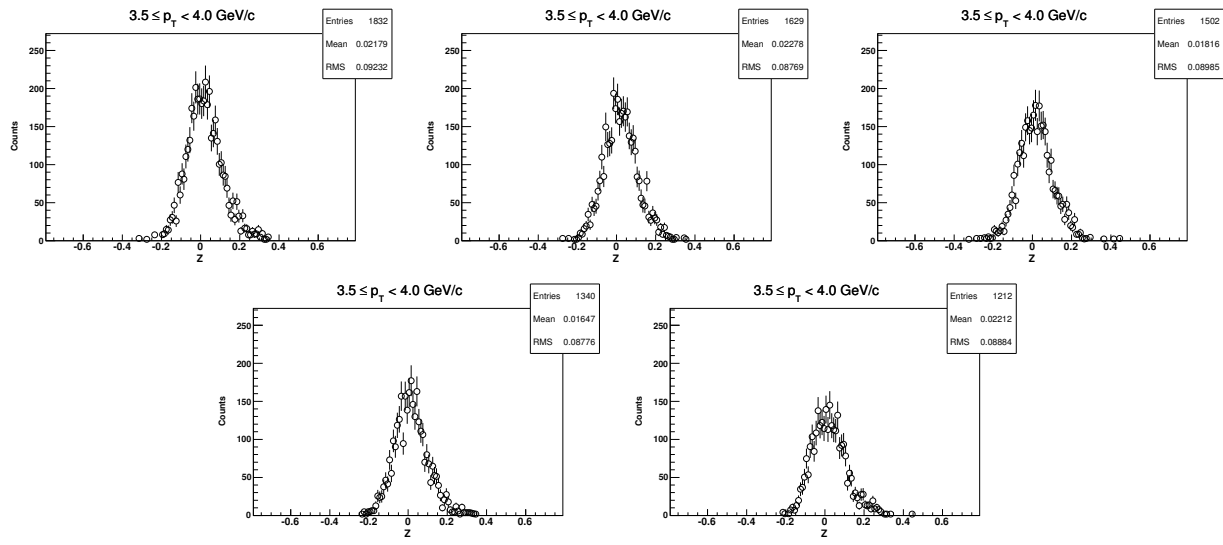
6.2.6 Z-distribution of d for $2.5 < p_T < 3.0 \text{ GeV}/c$ ($\sqrt{s_{NN}} = 62.4 \text{ GeV}$, 0-30%)



6.2.7 Z-distribution of d for $3.0 < p_T < 3.5 \text{ GeV}/c$ ($\sqrt{s_{NN}} = 62.4 \text{ GeV}$, 0-30%)

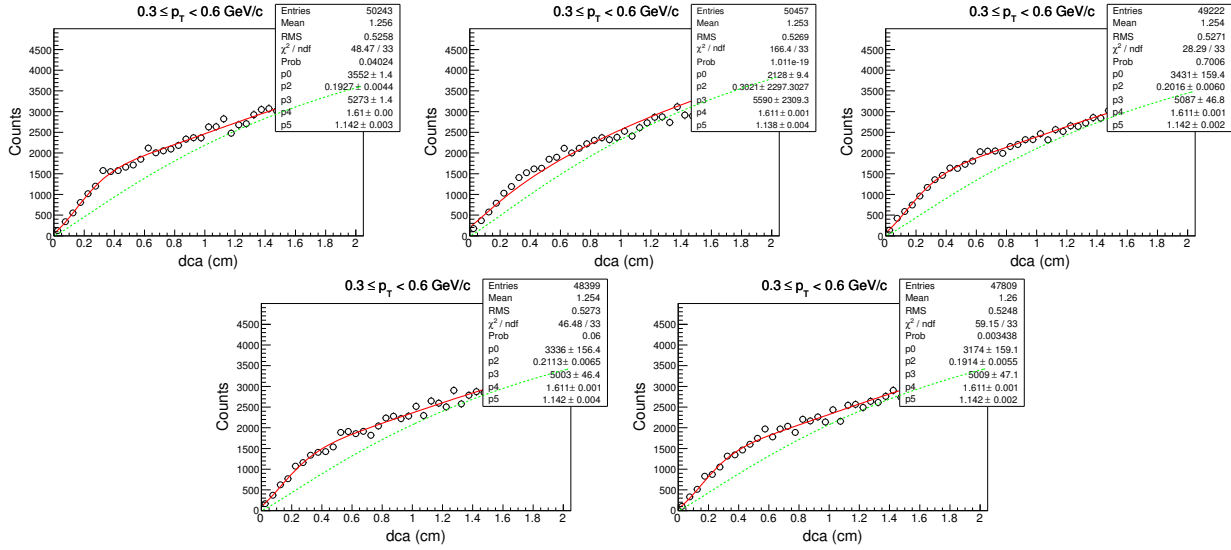


6.2.8 Z-distribution of d for $3.5 < p_T < 4.0 \text{ GeV}/c$ ($\sqrt{s_{NN}} = 62.4 \text{ GeV}$, 0-30%)

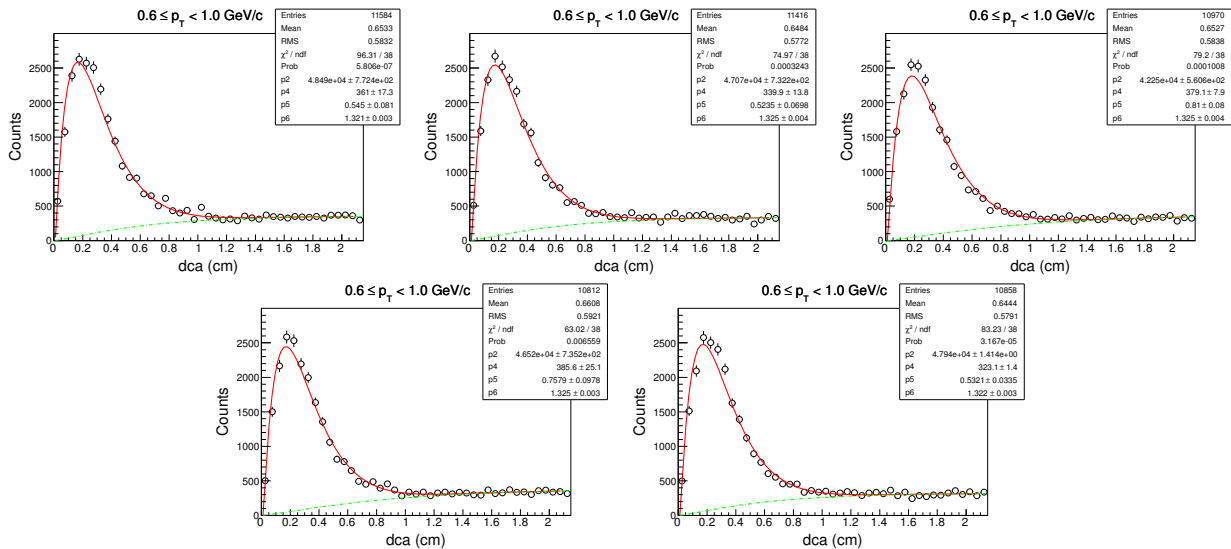


6.3 Centrality: 30-80%

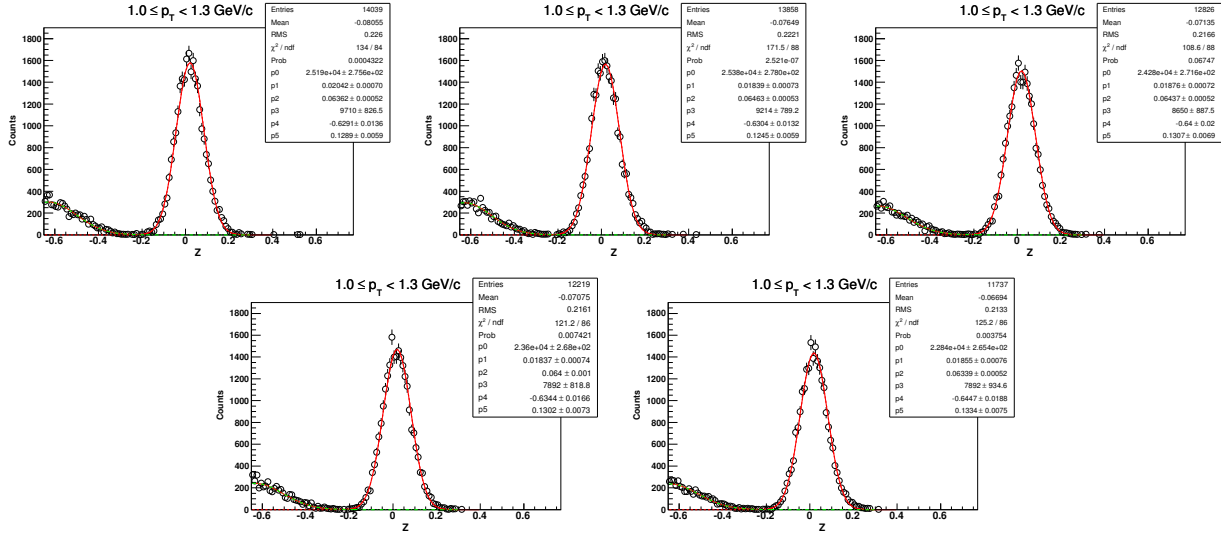
6.3.1 DCA-distribution of d for $0.3 < p_T < 0.6 \text{ GeV}/c$



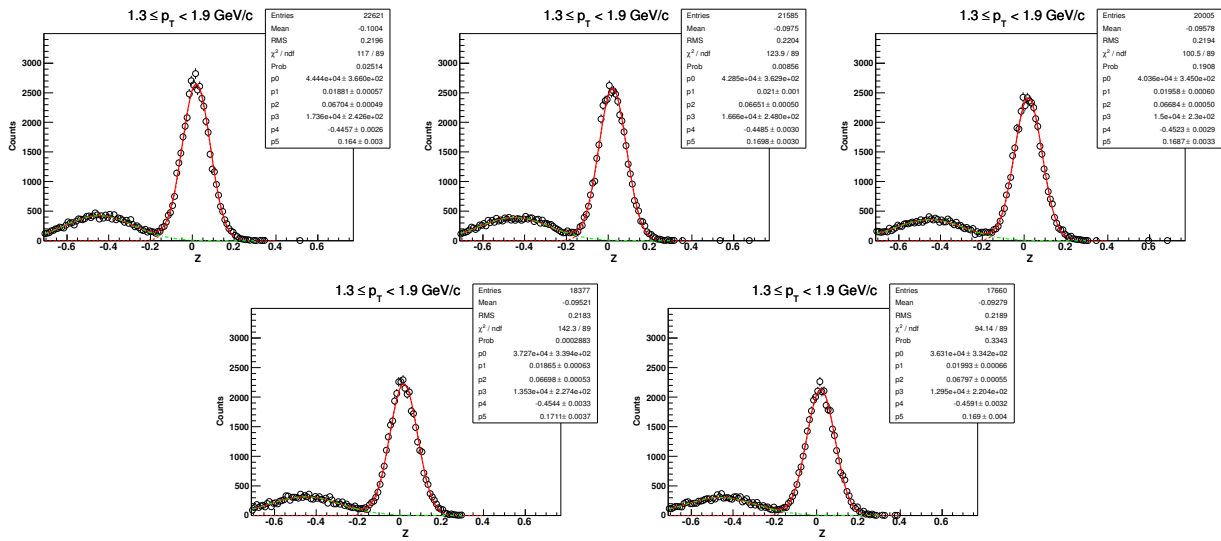
6.3.2 DCA-distribution of d for $0.6 < p_T < 1.0 \text{ GeV}/c$ ($\sqrt{s_{NN}} = 62.4 \text{ GeV}$, 30-80%)



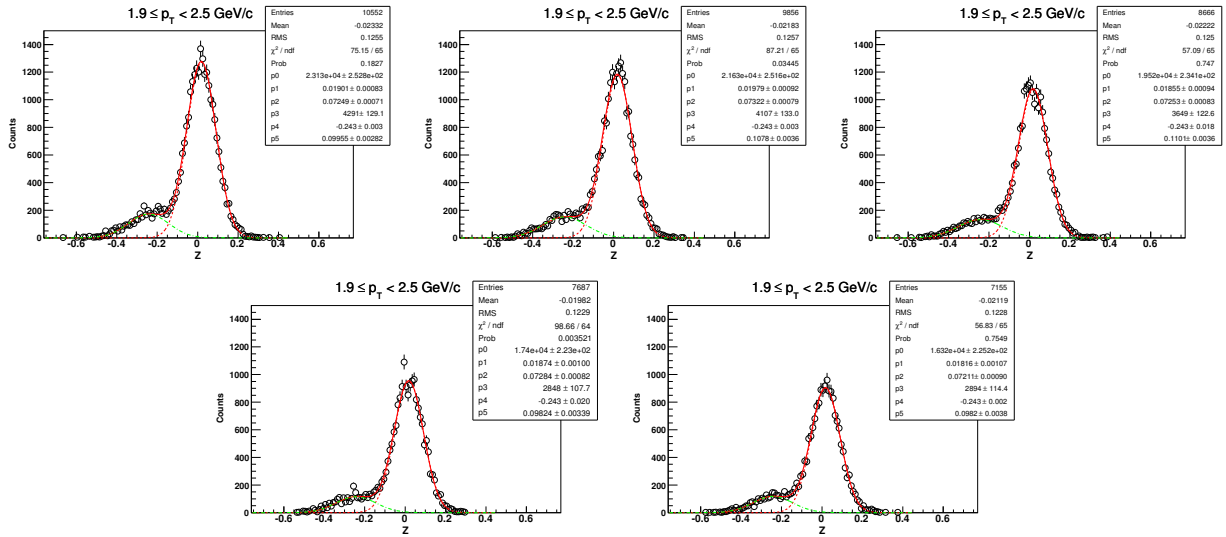
6.3.3 Z-distribution of d for $1.0 < p_T < 1.3 \text{ GeV}/c$ ($\sqrt{s_{NN}} = 62.4 \text{ GeV}$, 30-80%)



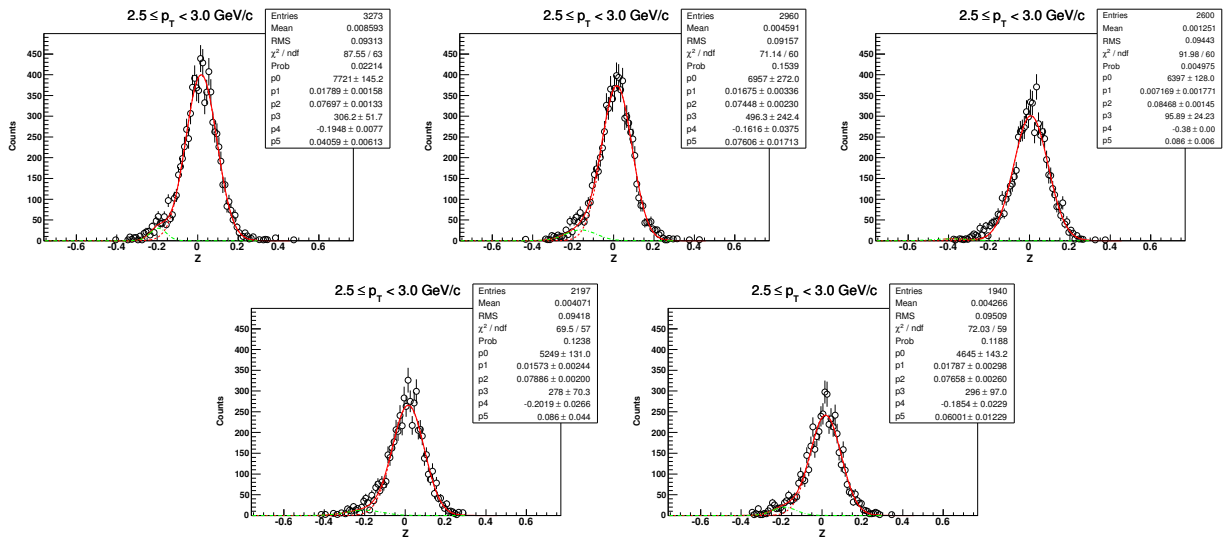
6.3.4 Z-distribution of d for $1.3 < p_T < 1.9 \text{ GeV}/c$ ($\sqrt{s_{NN}} = 62.4 \text{ GeV}$, 30-80%)



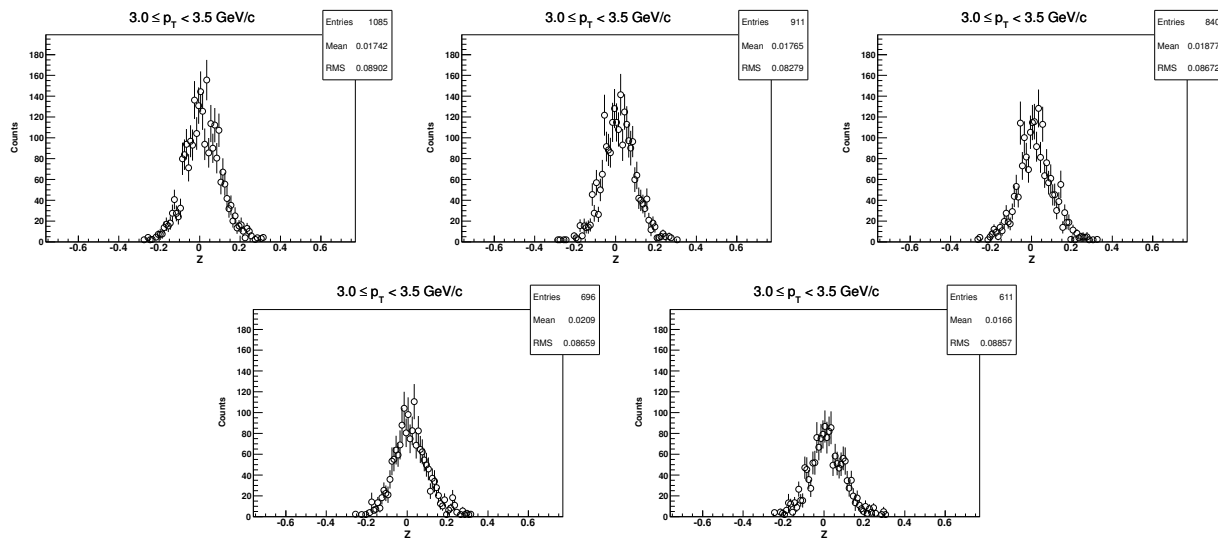
6.3.5 Z-distribution of d for $1.9 < p_T < 2.5 \text{ GeV}/c$ ($\sqrt{s_{NN}} = 62.4 \text{ GeV}$, 30-80%)



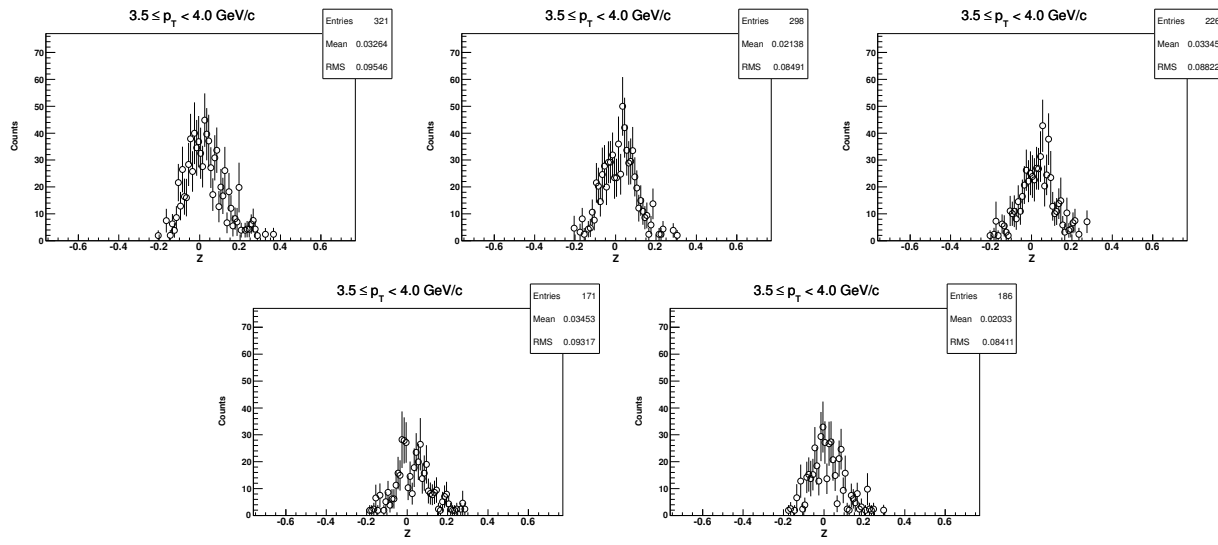
6.3.6 Z-distribution of d for $2.5 < p_T < 3.0 \text{ GeV}/c$ ($\sqrt{s_{NN}} = 62.4 \text{ GeV}$, 30-80%)



6.3.7 Z-distribution of d for $3.0 < p_T < 3.5 \text{ GeV}/c$ ($\sqrt{s_{NN}} = 62.4 \text{ GeV}$, 30-80%)

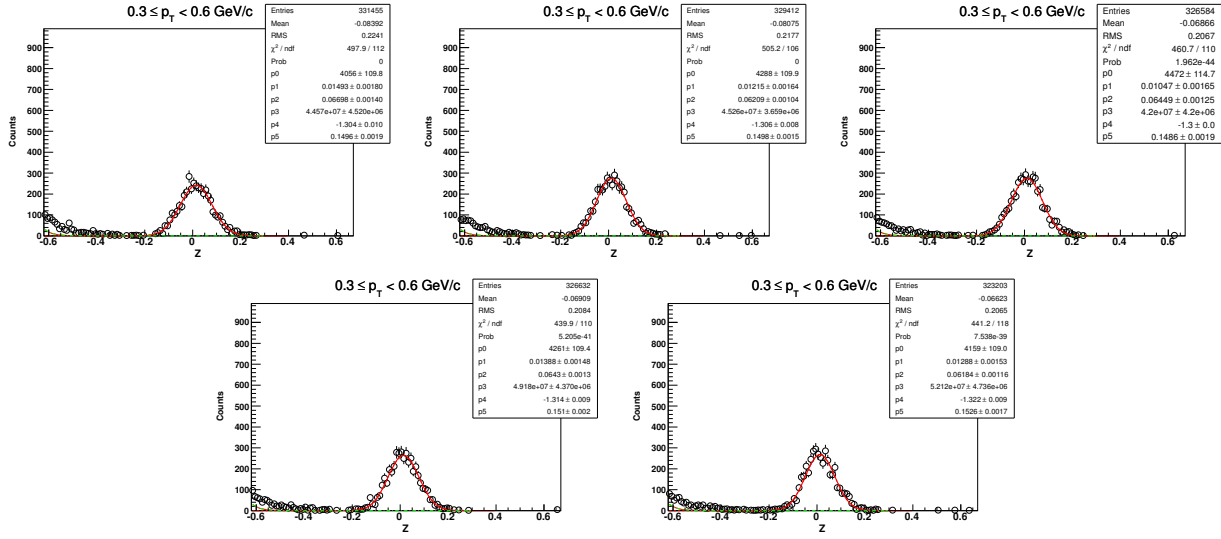


6.3.8 Z-distribution of d for $3.5 < p_T < 4.0 \text{ GeV}/c$ ($\sqrt{s_{NN}} = 62.4 \text{ GeV}$, 30-80%)

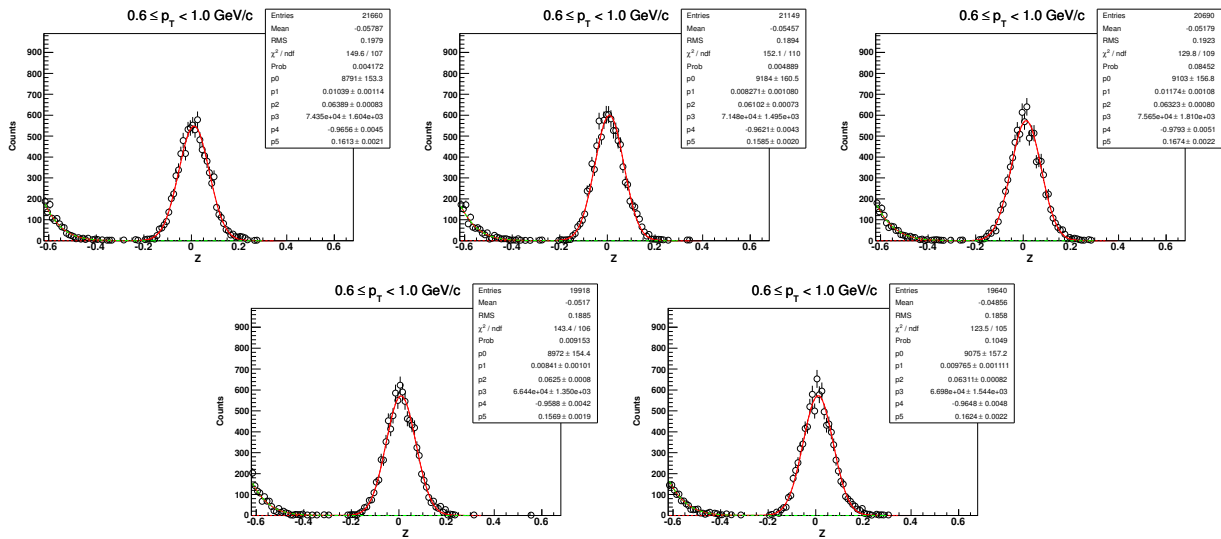


6.4 \bar{d} in $\sqrt{s_{NN}} = 62.4$ GeV for centrality: 0-80%

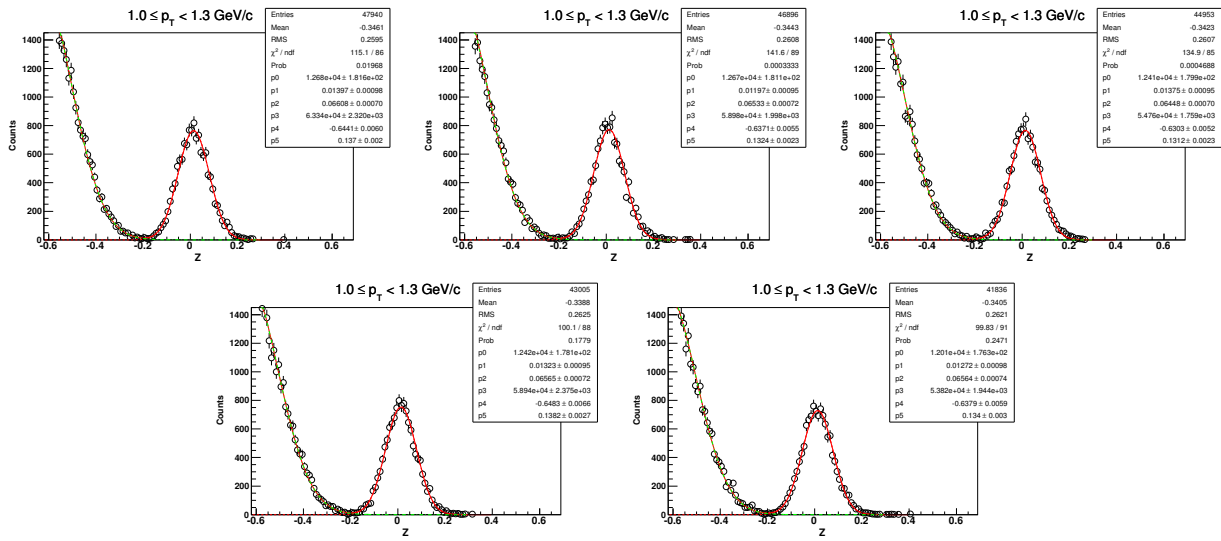
6.4.1 Z-distribution of \bar{d} for $0.3 < p_T < 0.6$ GeV/c



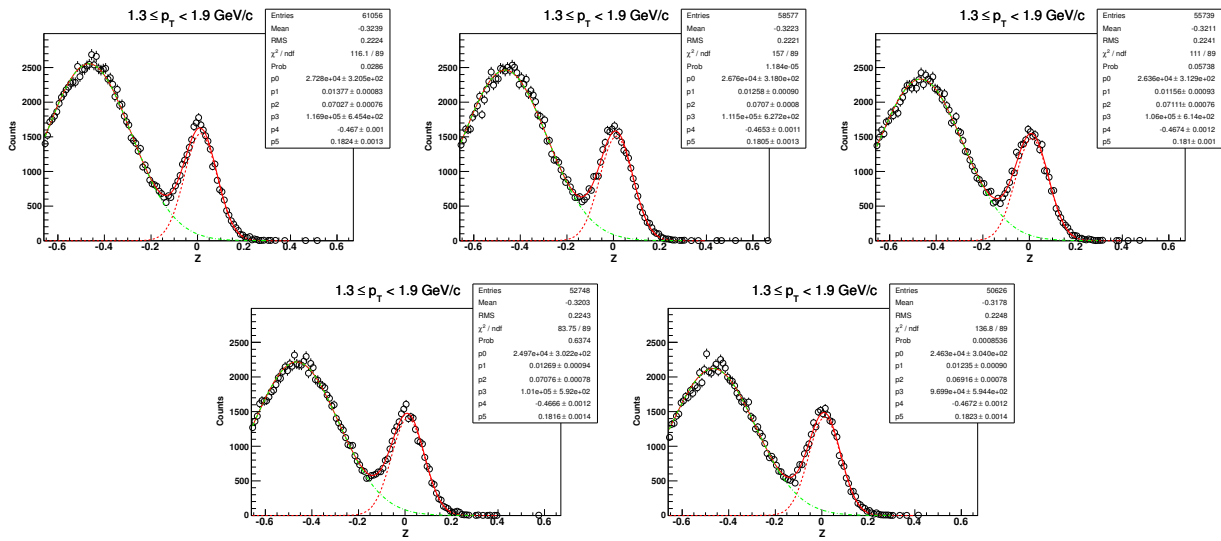
6.4.2 Z-distribution of \bar{d} for $0.6 < p_T < 1.0$ GeV/c



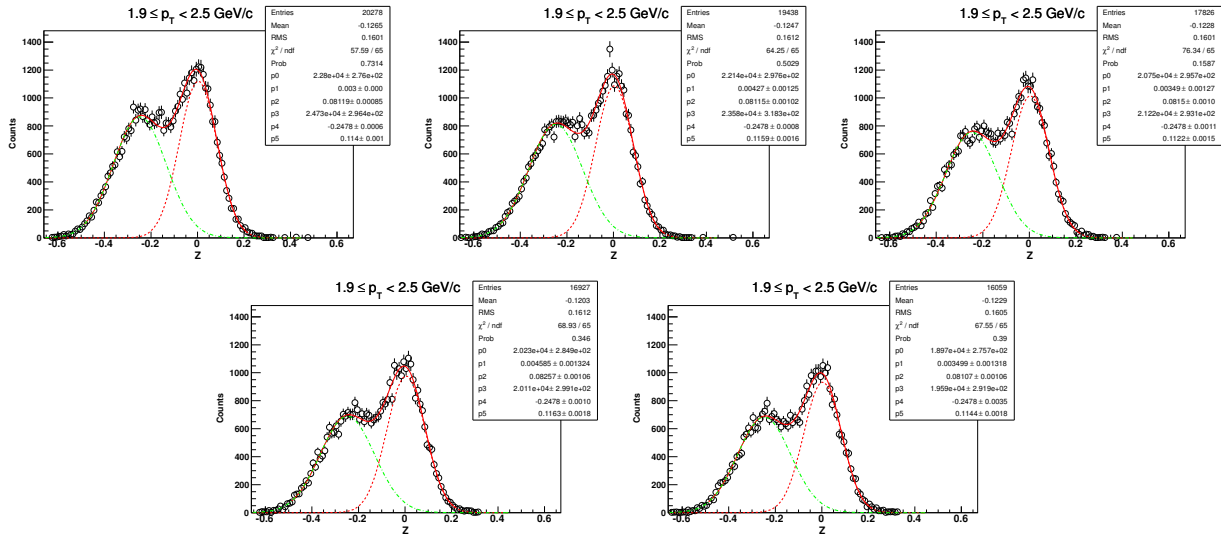
6.4.3 Z-distribution of \bar{d} for $1.0 < p_T < 1.3 \text{ GeV}/c$ ($\sqrt{s_{NN}} = 62.4 \text{ GeV}$, 0-80%)



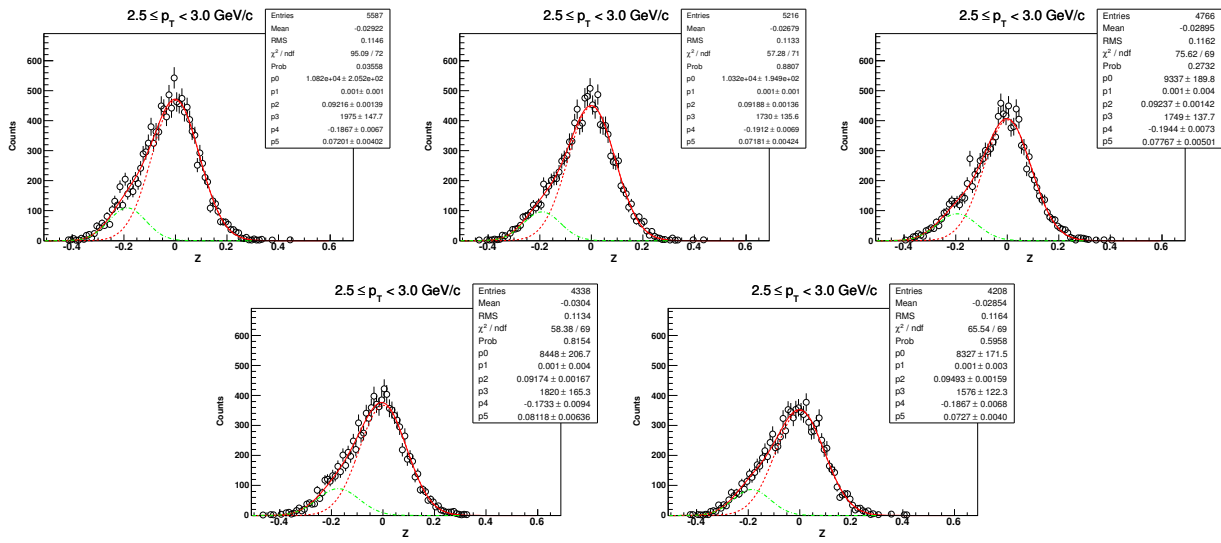
6.4.4 Z-distribution of \bar{d} for $1.3 < p_T < 1.9 \text{ GeV}/c$ ($\sqrt{s_{NN}} = 62.4 \text{ GeV}$, 0-80%)



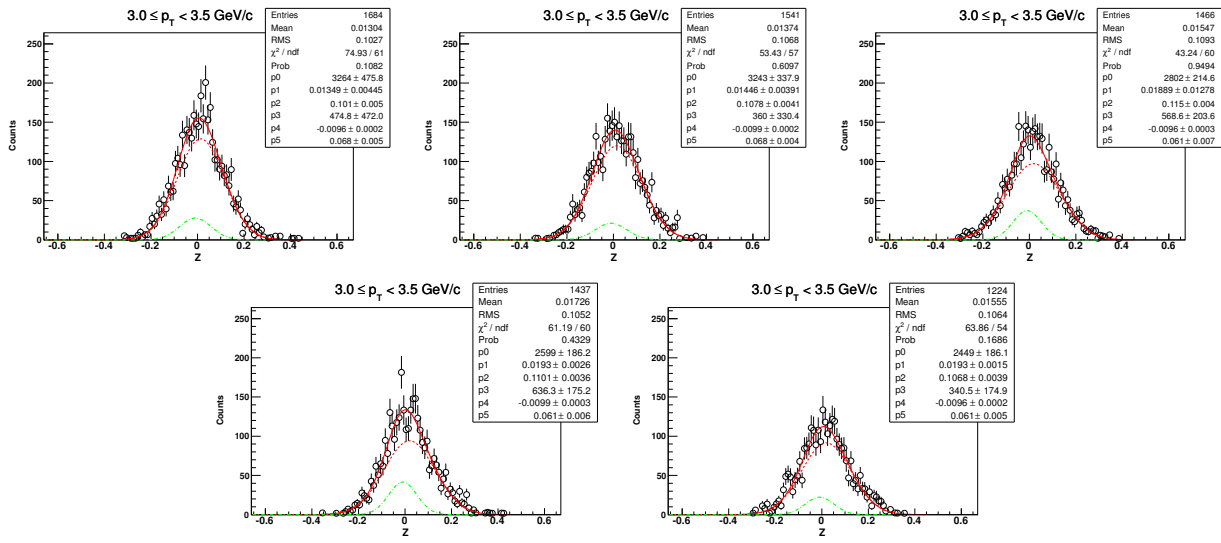
6.4.5 Z-distribution of \bar{d} for $1.9 < p_T < 2.5$ GeV/c ($\sqrt{s_{NN}} = 62.4$ GeV, 0-80%)



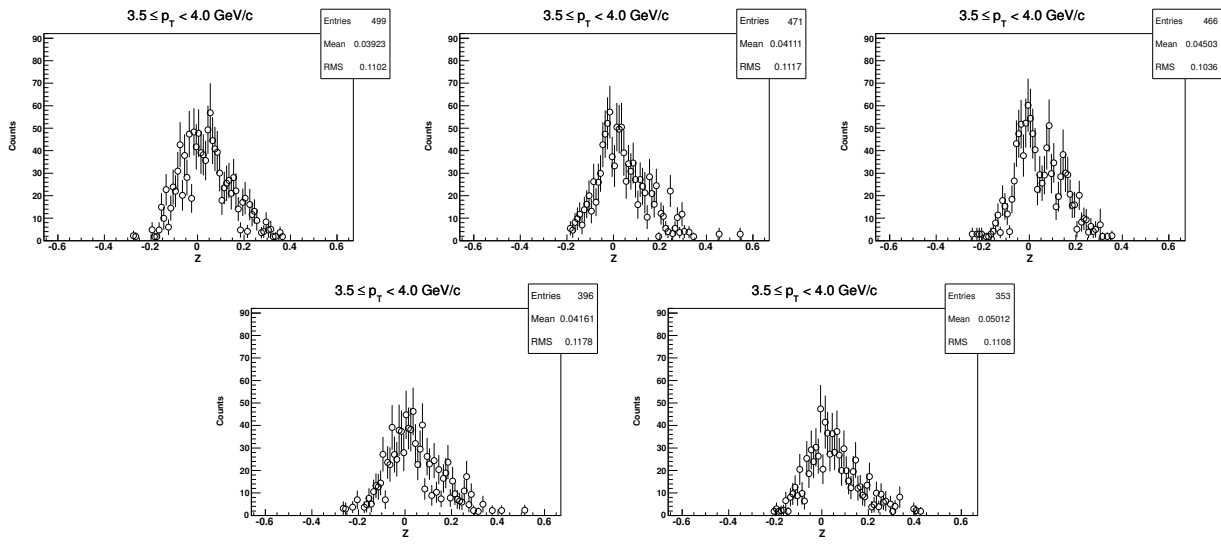
6.4.6 Z-distribution of \bar{d} for $2.5 < p_T < 3.0$ GeV/c ($\sqrt{s_{NN}} = 62.4$ GeV, 0-80%)



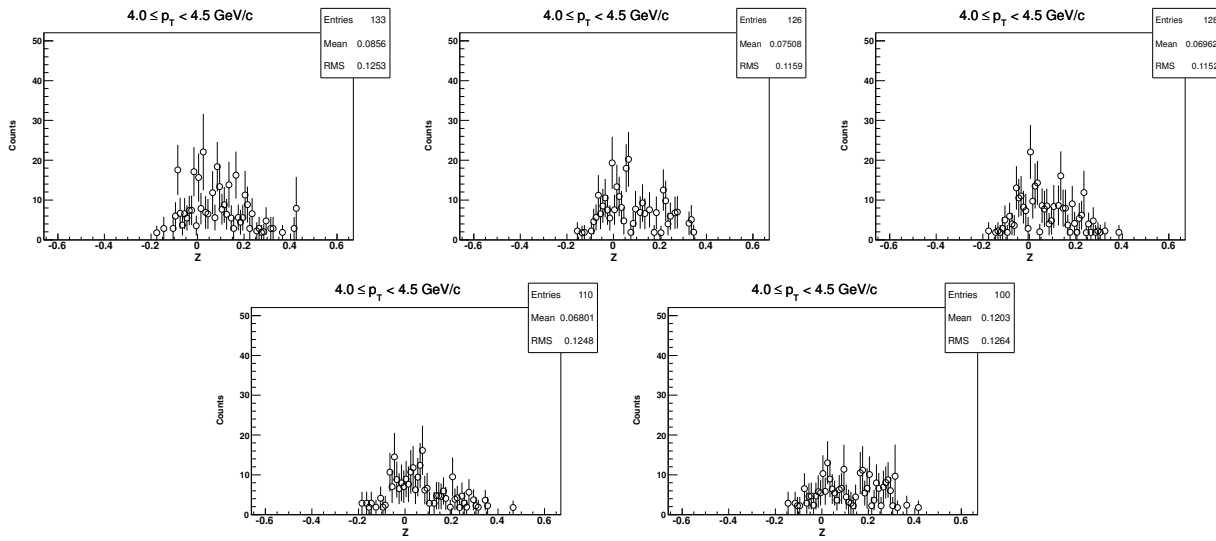
6.4.7 Z-distribution of \bar{d} for $3.0 < p_T < 3.5 \text{ GeV}/c$ ($\sqrt{s_{NN}} = 62.4 \text{ GeV}$, 0-80%)



6.4.8 Z-distribution of \bar{d} for $3.5 < p_T < 4.0 \text{ GeV}/c$ ($\sqrt{s_{NN}} = 62.4 \text{ GeV}$, 0-80%)

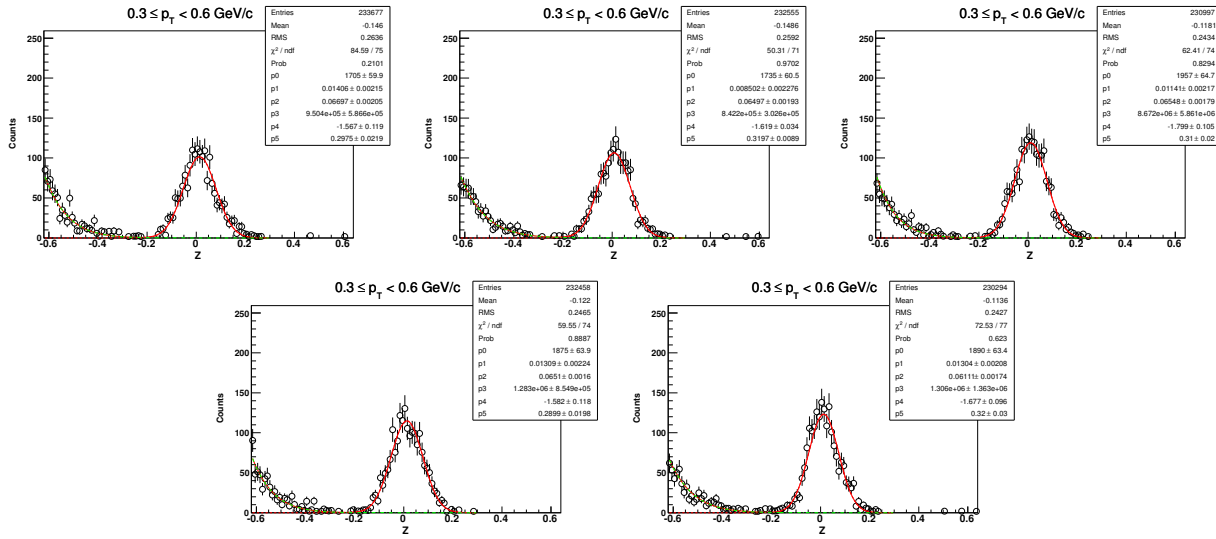


6.4.9 Z-distribution of \bar{d} for $4.0 < p_T < 4.5 \text{ GeV}/c$ ($\sqrt{s_{NN}} = 62.4 \text{ GeV}$, 0-80%)

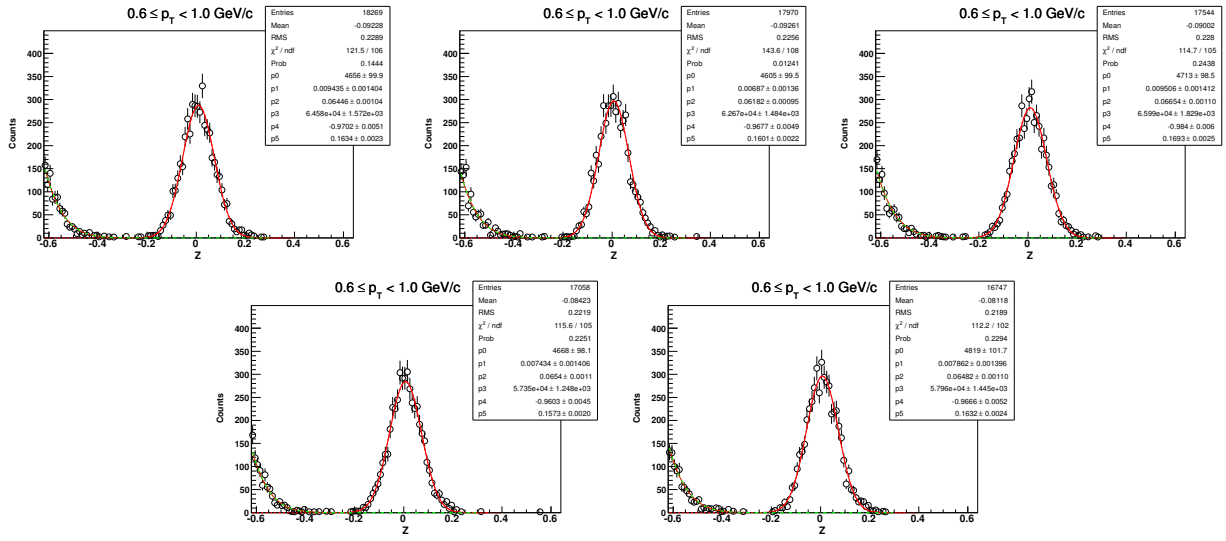


6.5 Centrality: 0-30%

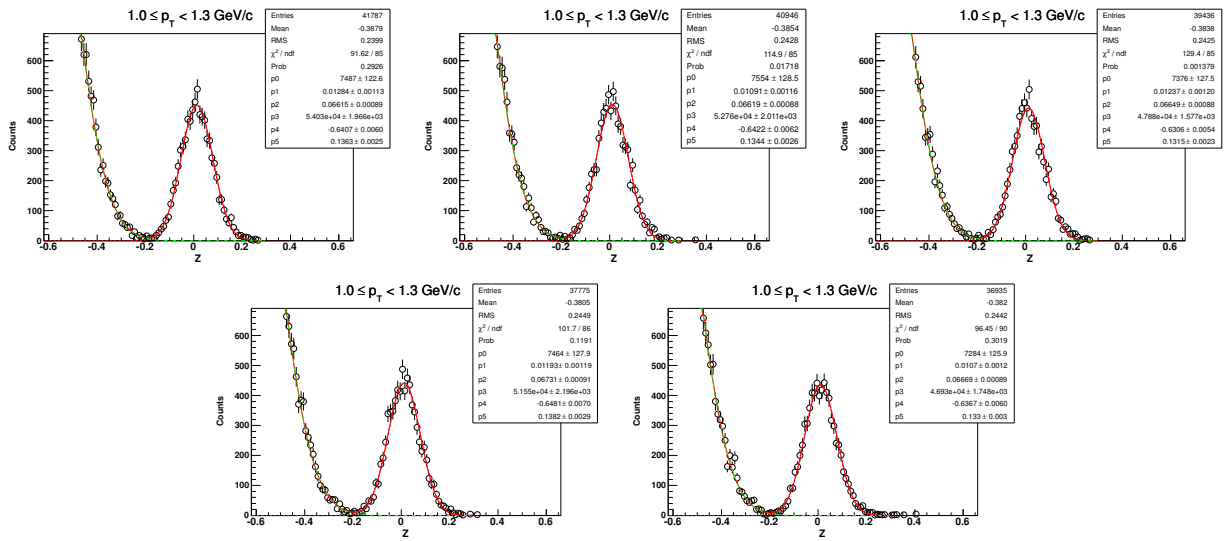
6.5.1 Z-distribution of \bar{d} for $0.3 < p_T < 0.6 \text{ GeV}/c$



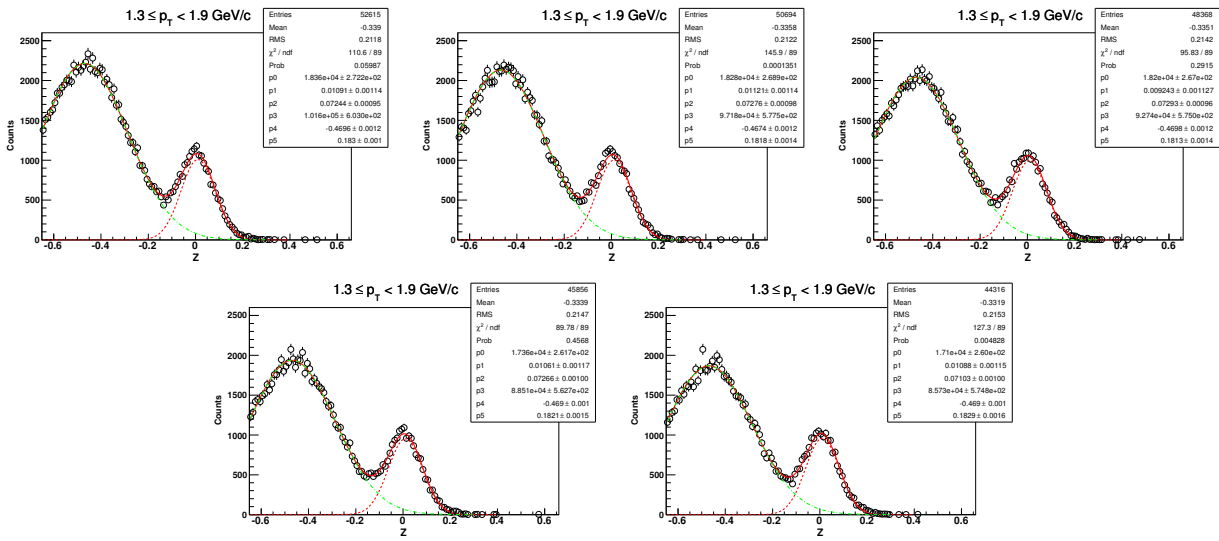
6.5.2 Z-distribution of \bar{d} for $0.6 < p_T < 1.0$ GeV/c ($\sqrt{s_{NN}} = 62.4$ GeV, 0-30%)



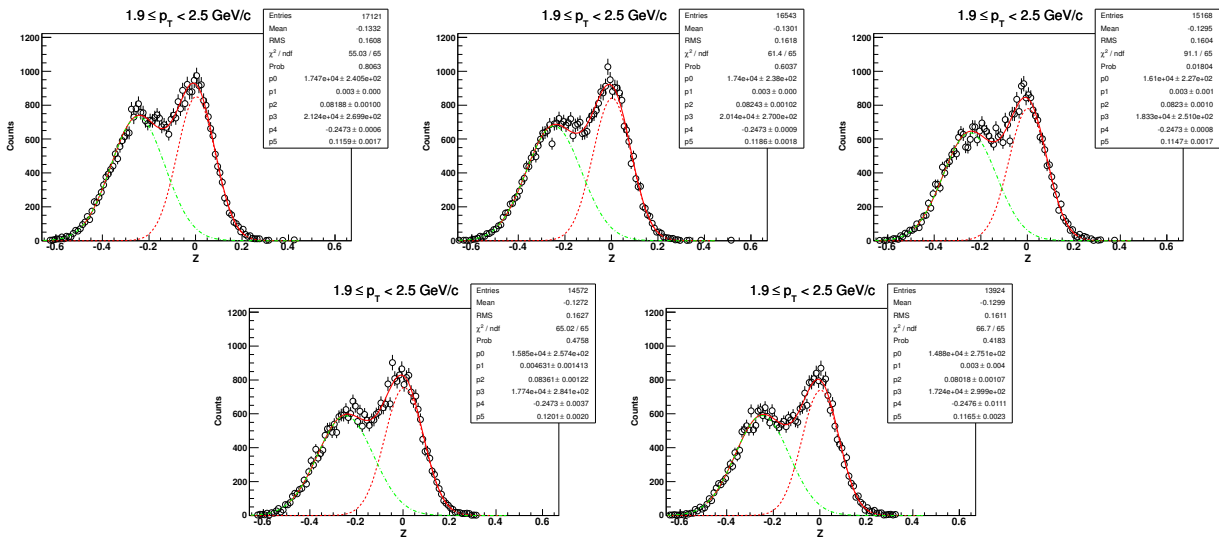
6.5.3 Z-distribution of \bar{d} for $1.0 < p_T < 1.3$ GeV/c ($\sqrt{s_{NN}} = 62.4$ GeV, 0-30%)



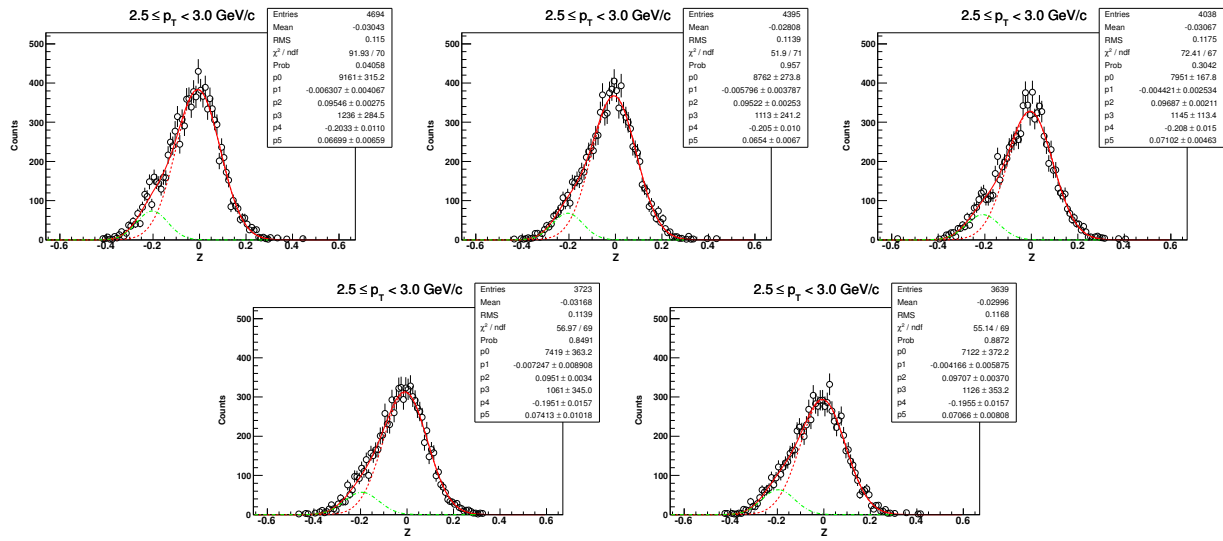
6.5.4 Z-distribution of \bar{d} for $1.3 < p_T < 1.9 \text{ GeV}/c$ ($\sqrt{s_{NN}} = 62.4 \text{ GeV}$, 0-30%)



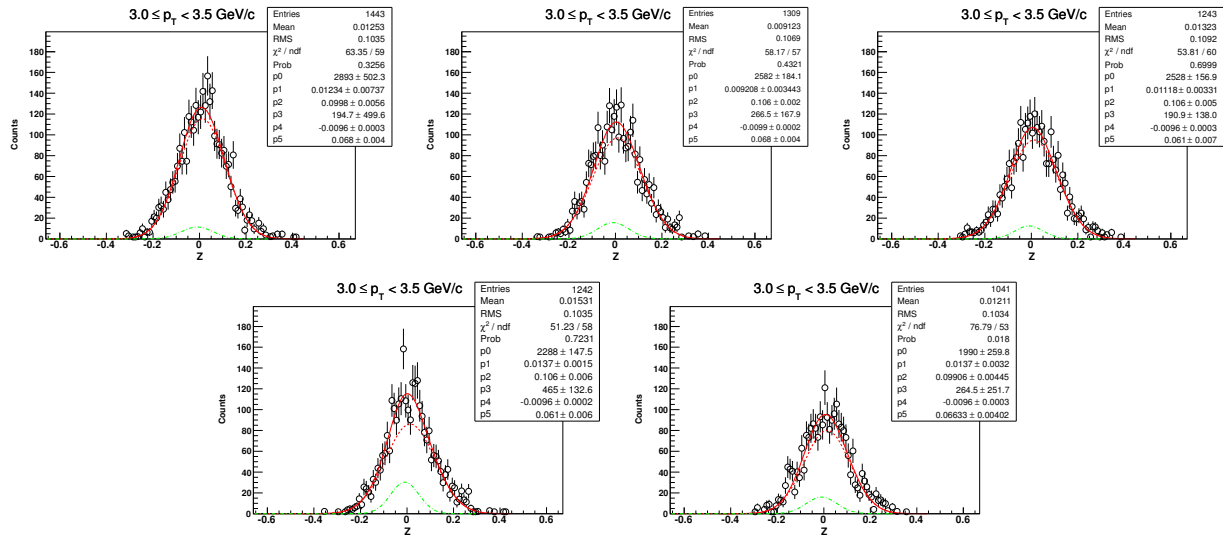
6.5.5 Z-distribution of \bar{d} for $1.9 < p_T < 2.5 \text{ GeV}/c$ ($\sqrt{s_{NN}} = 62.4 \text{ GeV}$, 0-30%)



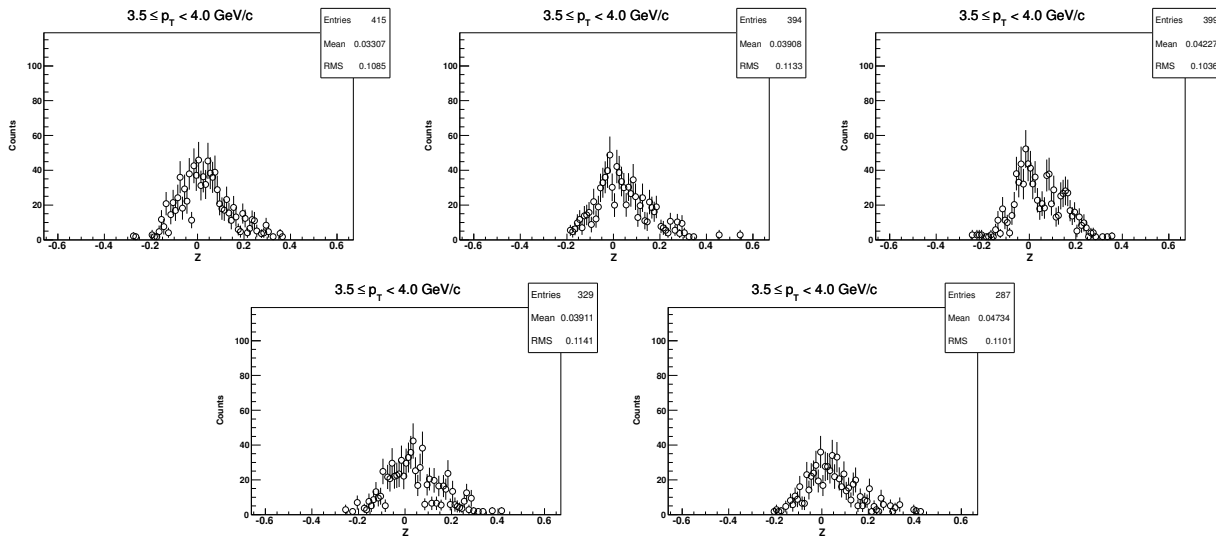
6.5.6 Z-distribution of \bar{d} for $2.5 < p_T < 3.0$ GeV/c ($\sqrt{s_{NN}} = 62.4$ GeV, 0-30%)



6.5.7 Z-distribution of \bar{d} for $3.0 < p_T < 3.5$ GeV/c ($\sqrt{s_{NN}} = 62.4$ GeV, 0-30%)

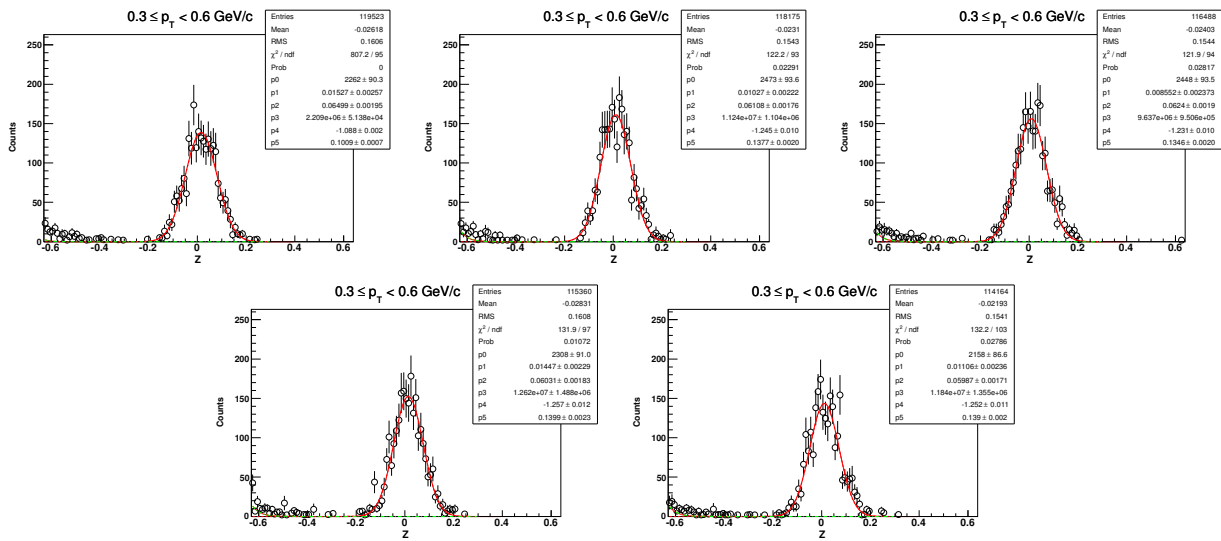


6.5.8 Z-distribution of \bar{d} for $3.5 < p_T < 4.0 \text{ GeV}/c$ ($\sqrt{s_{NN}} = 62.4 \text{ GeV}$, 0-30%)

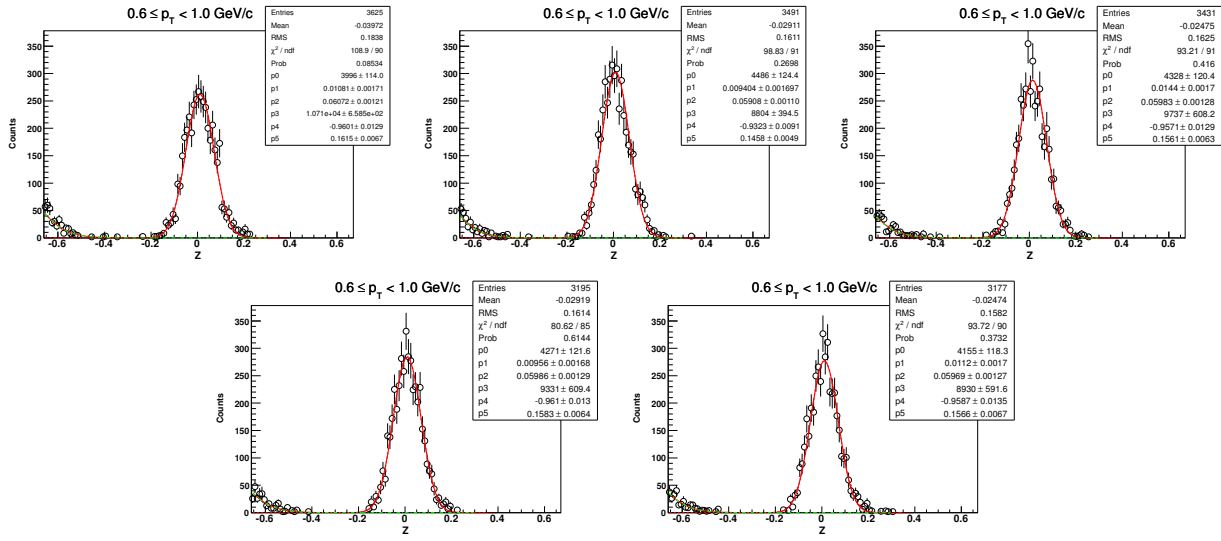


6.6 Centrality: 30-80%

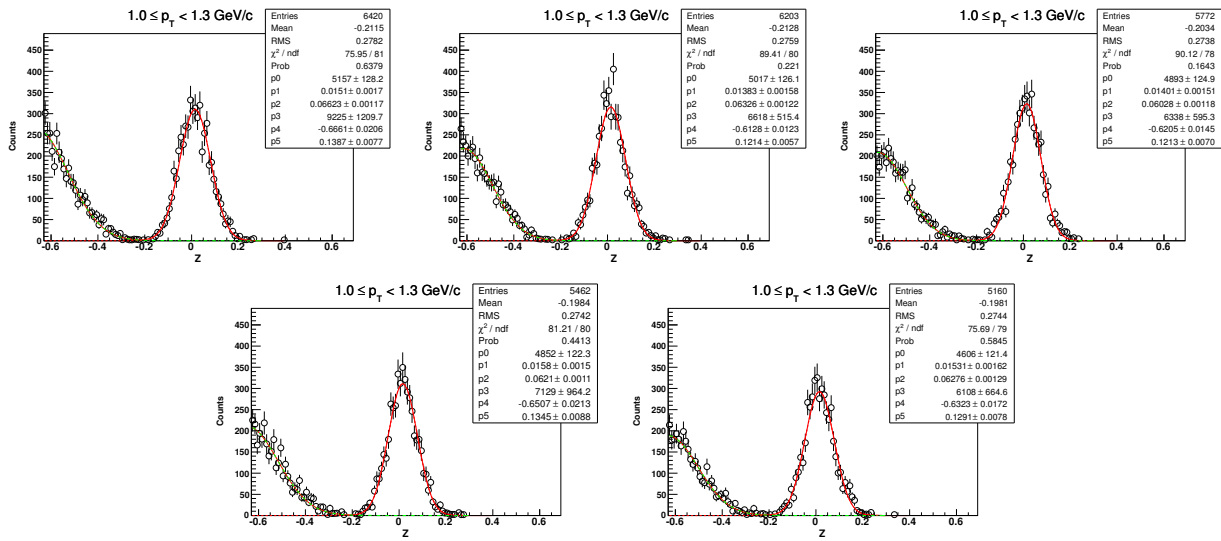
6.6.1 Z-distribution of \bar{d} for $0.3 < p_T < 0.6 \text{ GeV}/c$ ($\sqrt{s_{NN}} = 62.4 \text{ GeV}$, 30-80%)



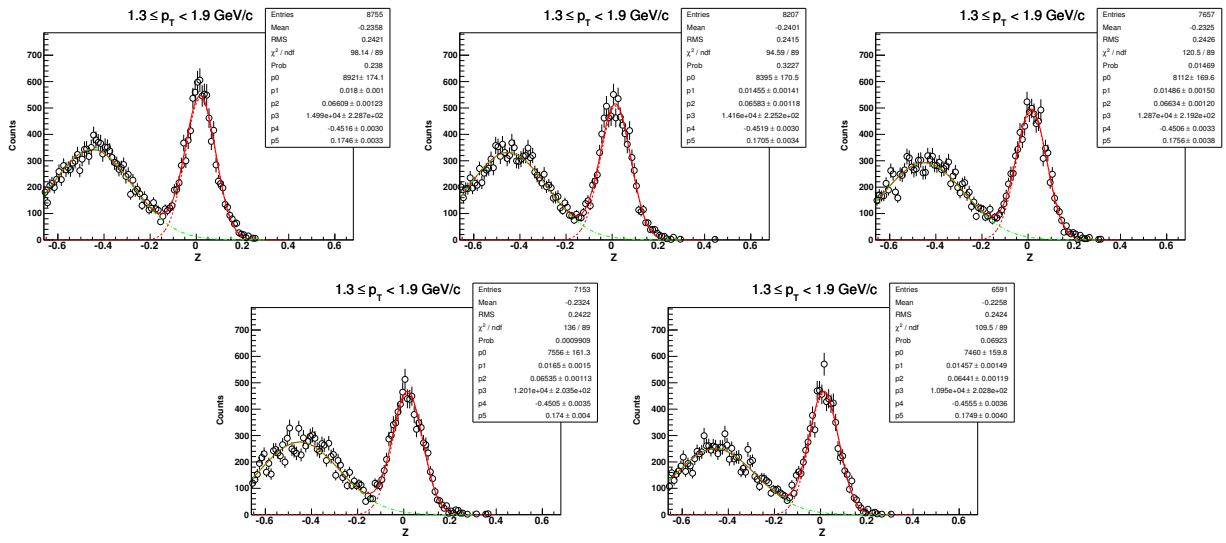
6.6.2 Z-distribution of \bar{d} for $0.6 < p_T < 1.0 \text{ GeV}/c$ ($\sqrt{s_{NN}} = 62.4 \text{ GeV}$, 30-80%)



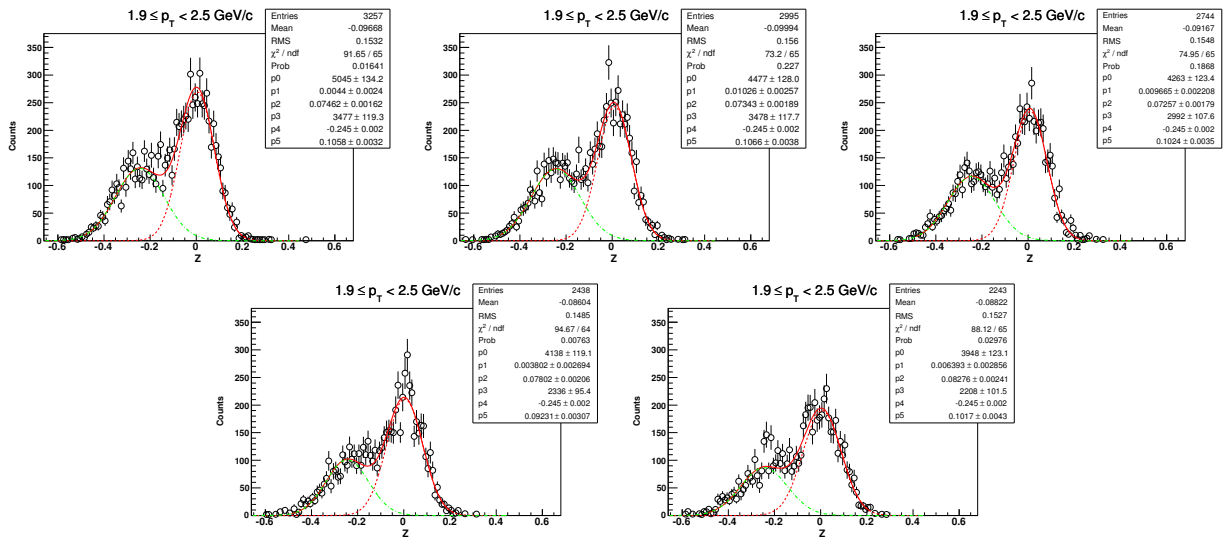
6.6.3 Z-distribution of \bar{d} for $1.0 < p_T < 1.3 \text{ GeV}/c$ ($\sqrt{s_{NN}} = 62.4 \text{ GeV}$, 30-80%)



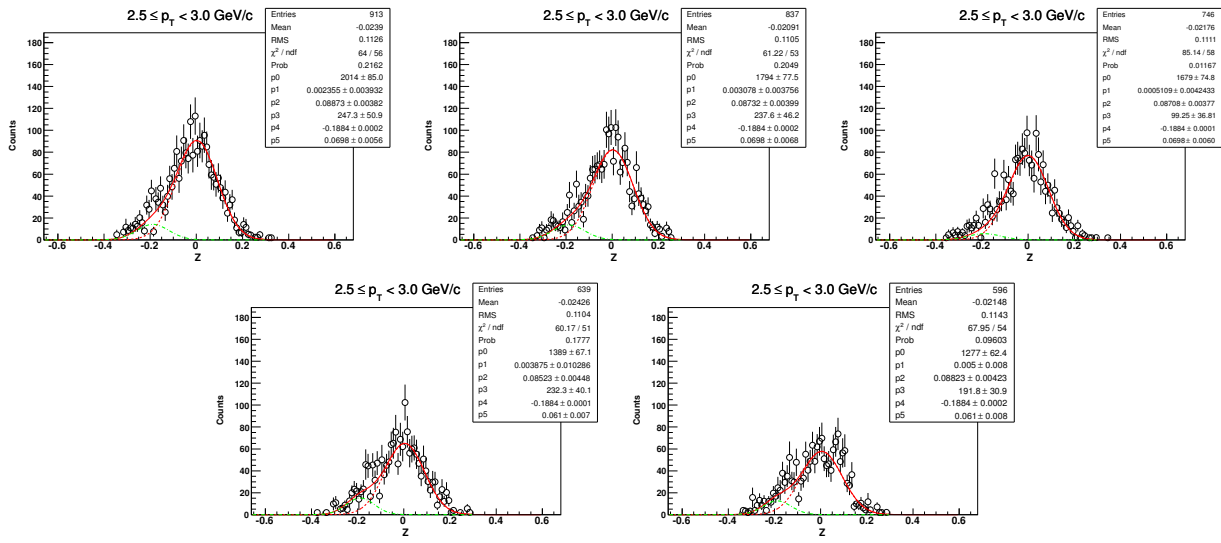
6.6.4 Z-distribution of \bar{d} for $1.3 < p_T < 1.9 \text{ GeV}/c$ ($\sqrt{s_{NN}} = 62.4 \text{ GeV}$, 30-80%)



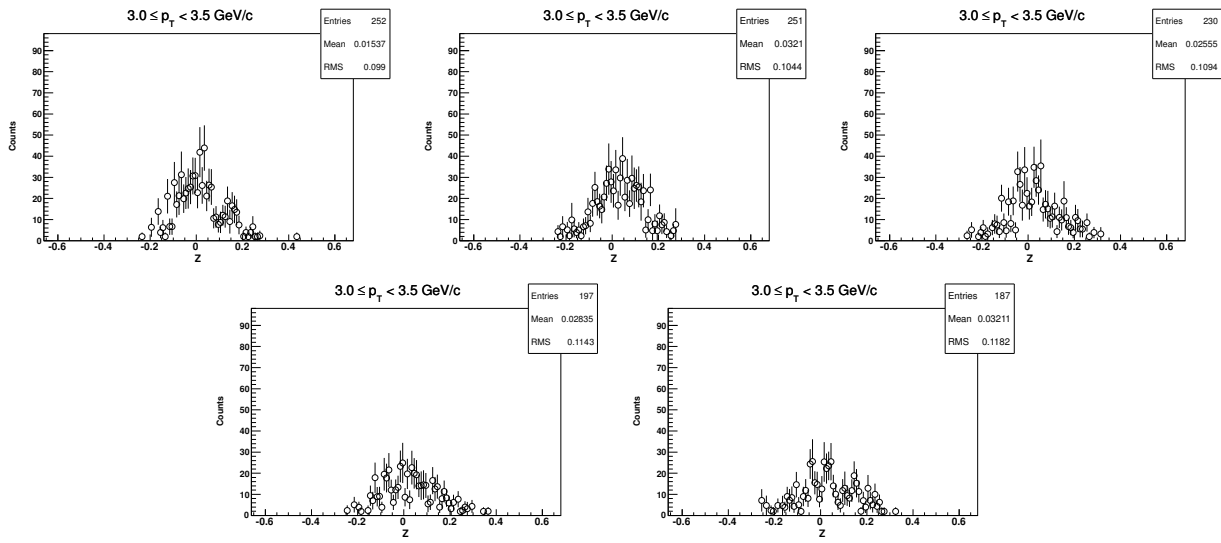
6.6.5 Z-distribution of \bar{d} for $1.9 < p_T < 2.5 \text{ GeV}/c$ ($\sqrt{s_{NN}} = 62.4 \text{ GeV}$, 30-80%)



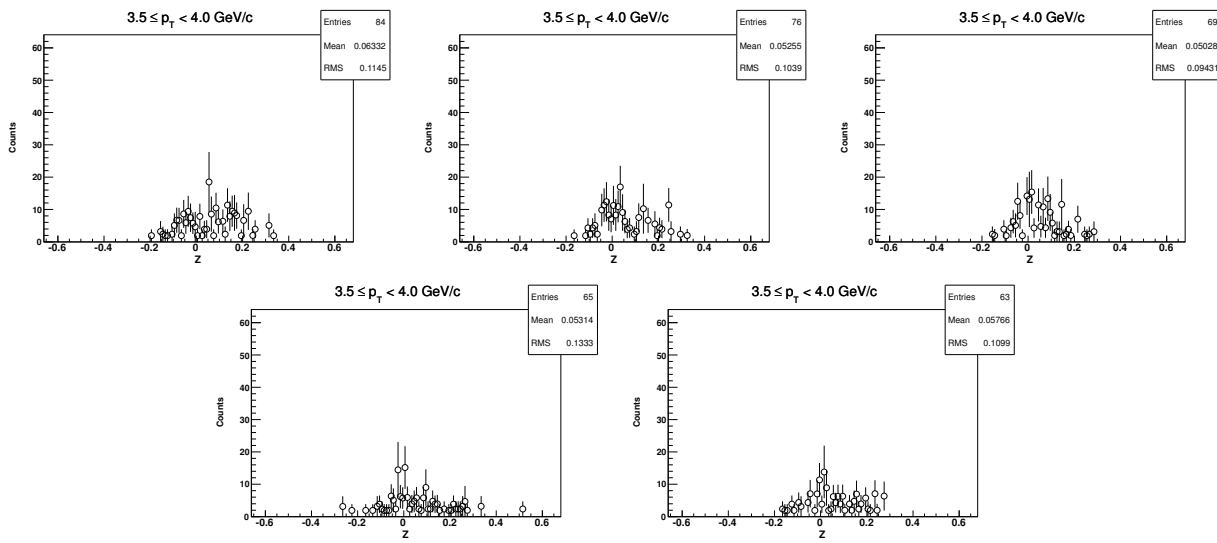
6.6.6 Z-distribution of \bar{d} for $2.5 < p_T < 3.0 \text{ GeV}/c$ ($\sqrt{s_{NN}} = 62.4 \text{ GeV}$, 30-80%)



6.6.7 Z-distribution of \bar{d} for $3.0 < p_T < 3.5 \text{ GeV}/c$ ($\sqrt{s_{NN}} = 62.4 \text{ GeV}$, 30-80%)

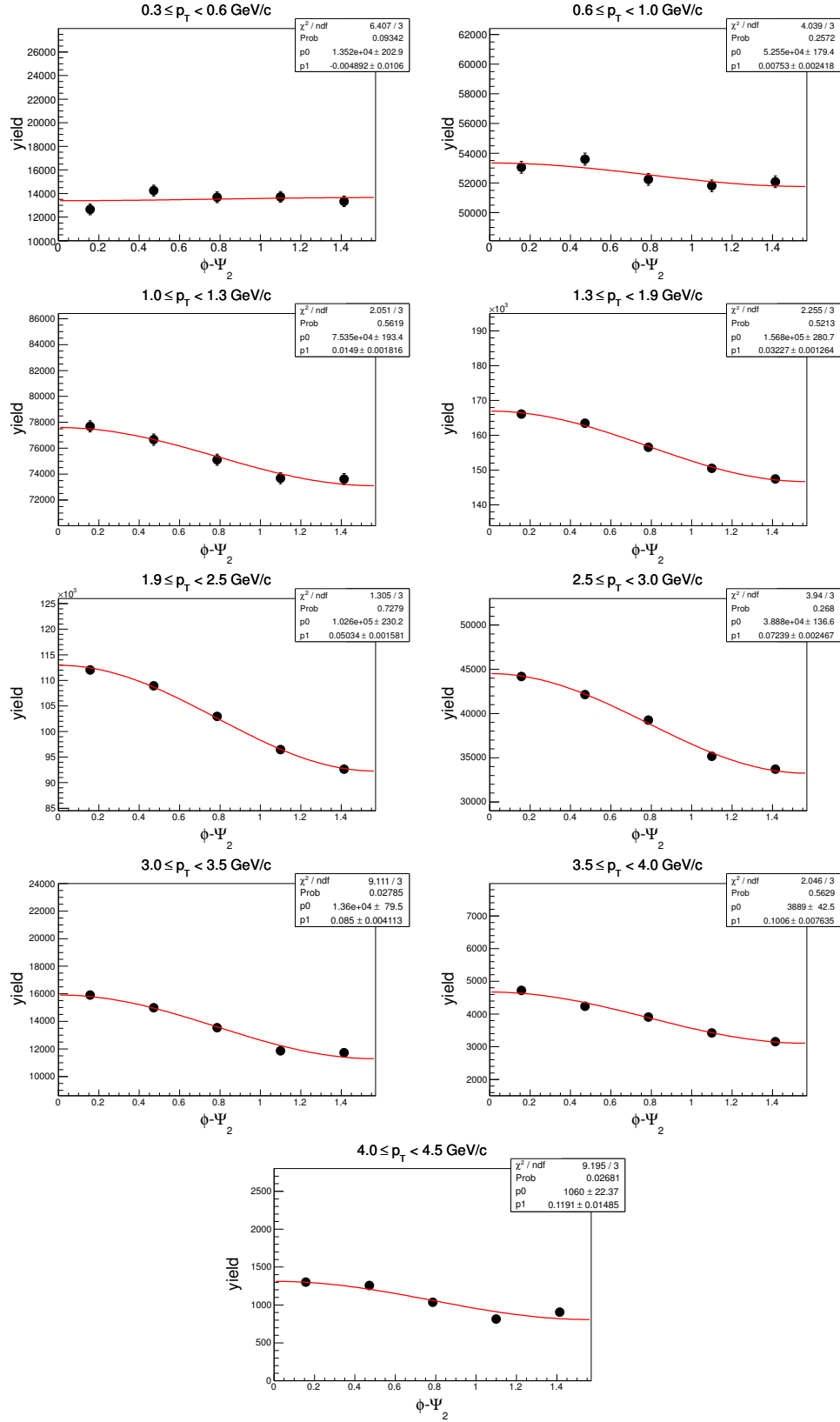


6.6.8 Z-distribution of \bar{d} for $3.5 < p_T < 4.0 \text{ GeV}/c$ ($\sqrt{s_{NN}} = 62.4 \text{ GeV}$, 30-80%)

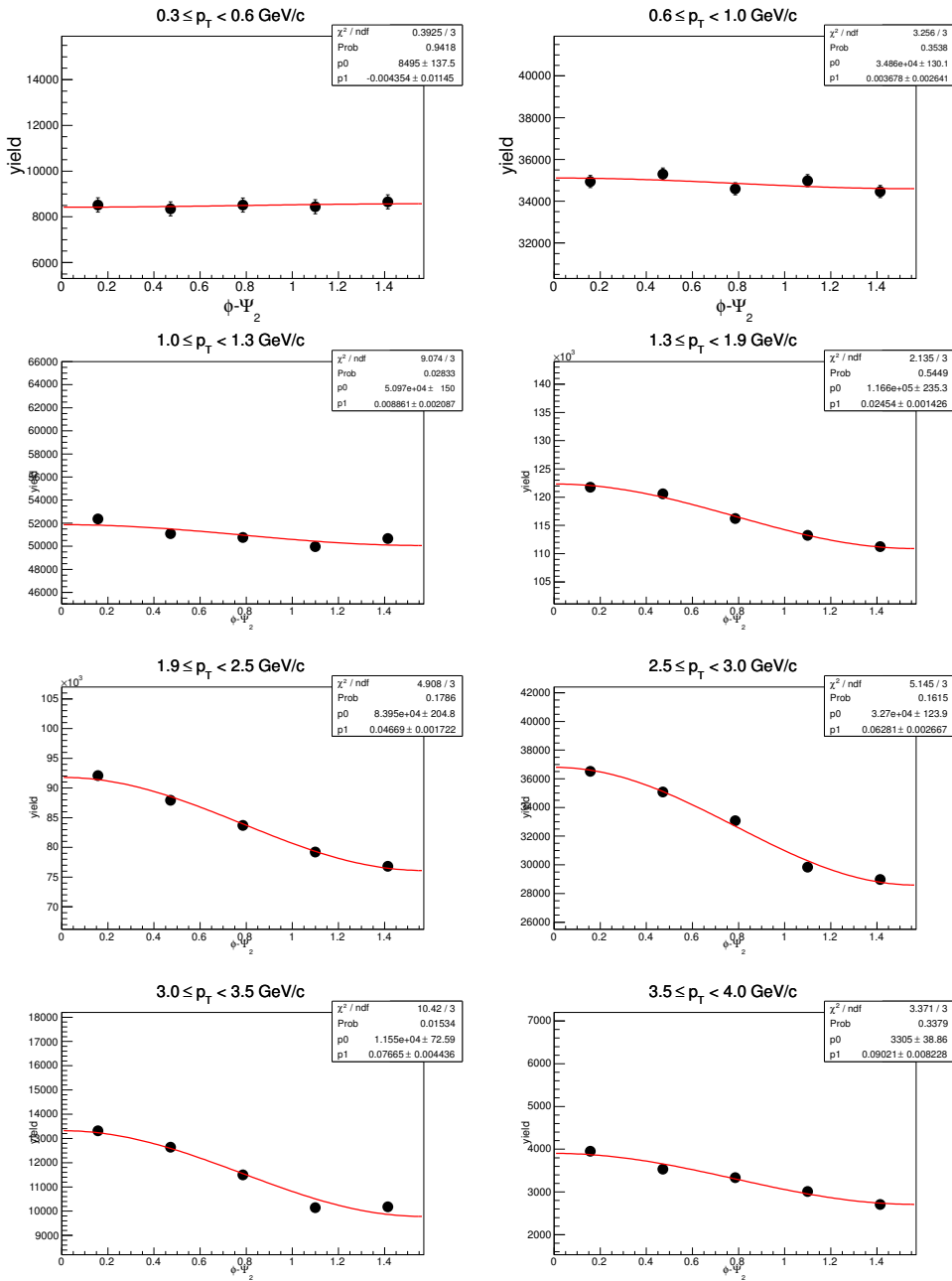


6.7 $\phi - \Psi_2$ distributions in Au+Au at $\sqrt{s_{NN}} = 62.4$ GeV

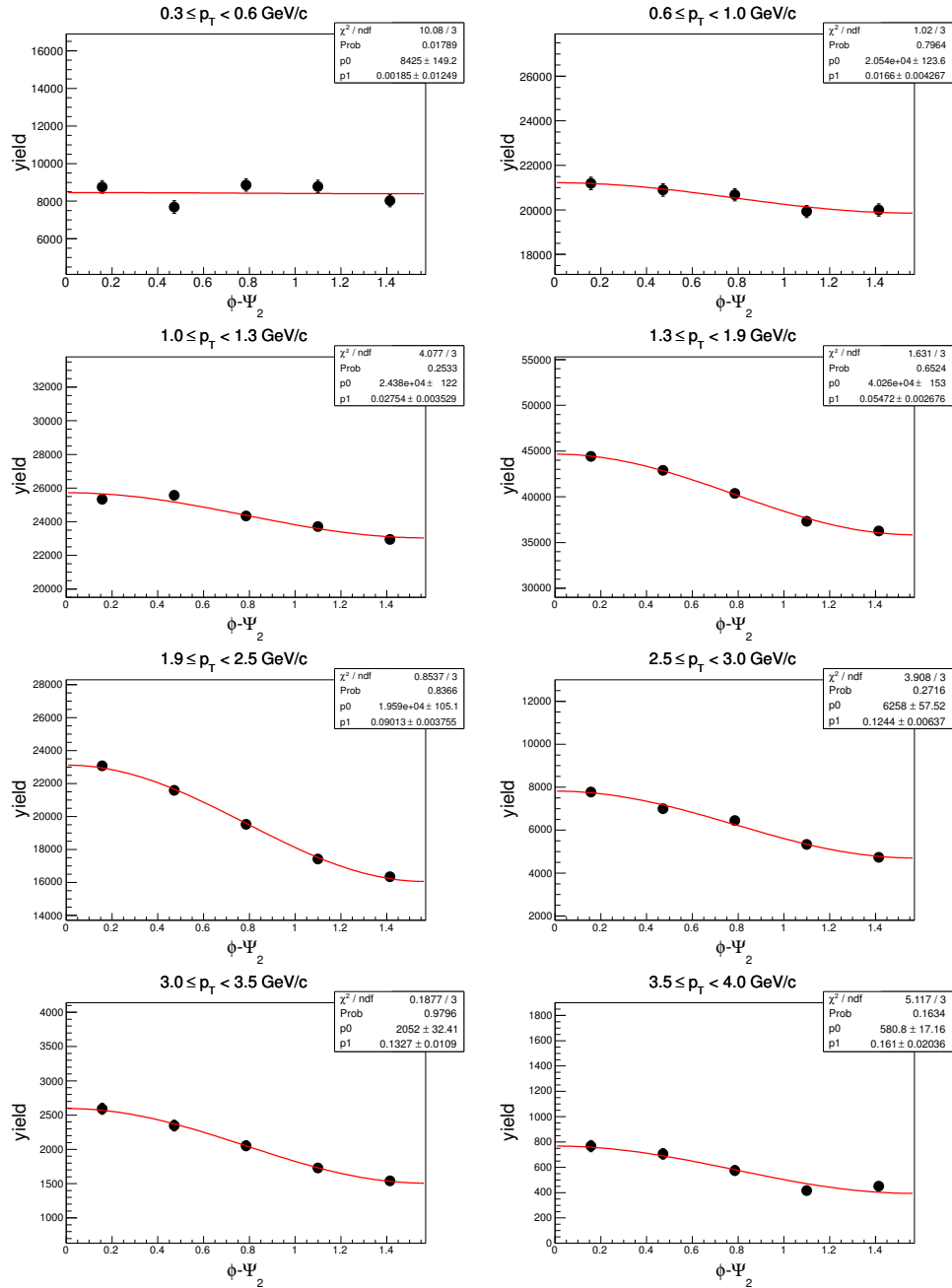
6.7.1 $\phi - \Psi_2$ of d in centrality: 0-80%



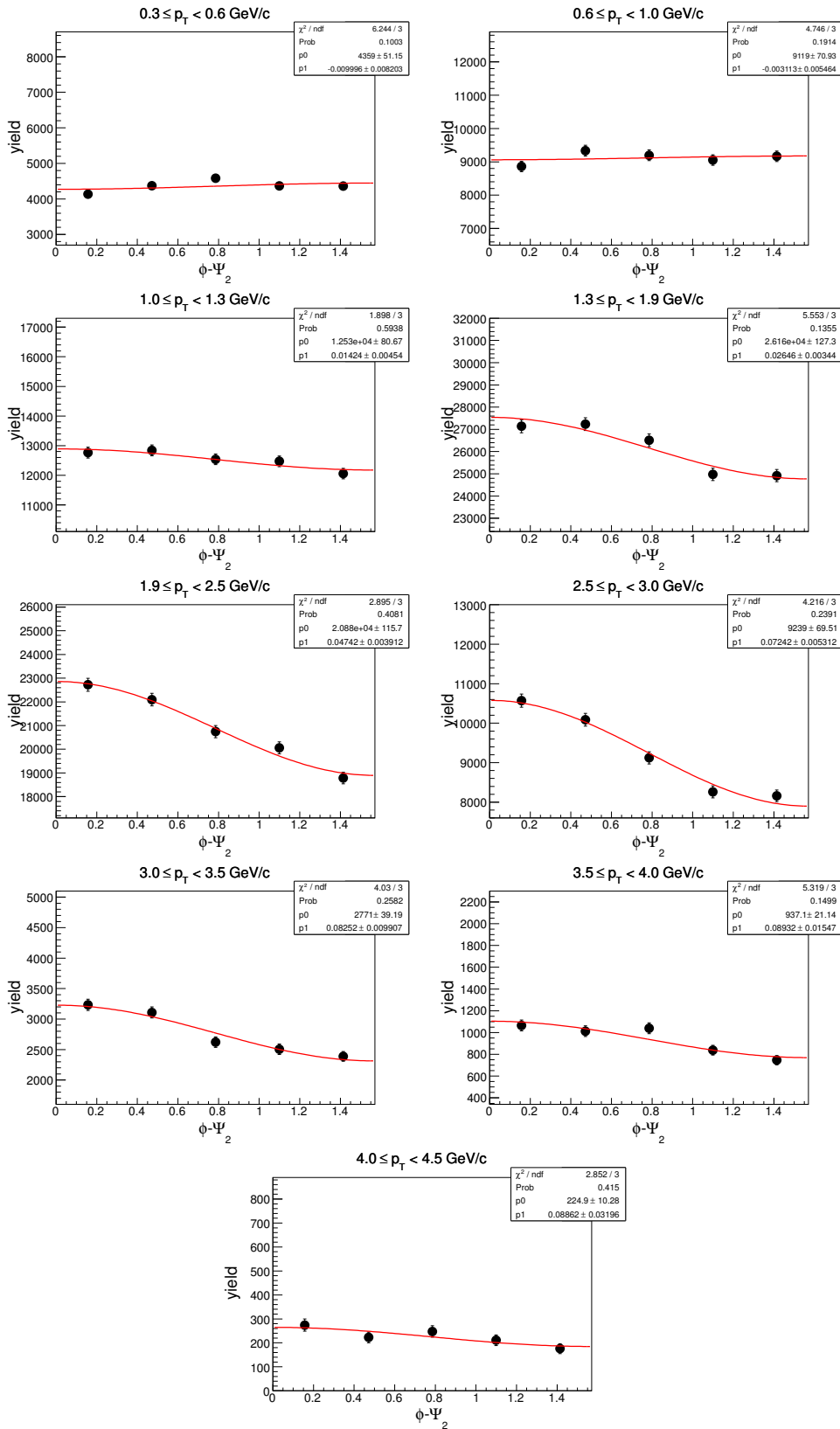
6.7.2 $\phi - \Psi_2$ of d in centrality: 0-30% ($\sqrt{s_{NN}} = 62.4$ GeV)



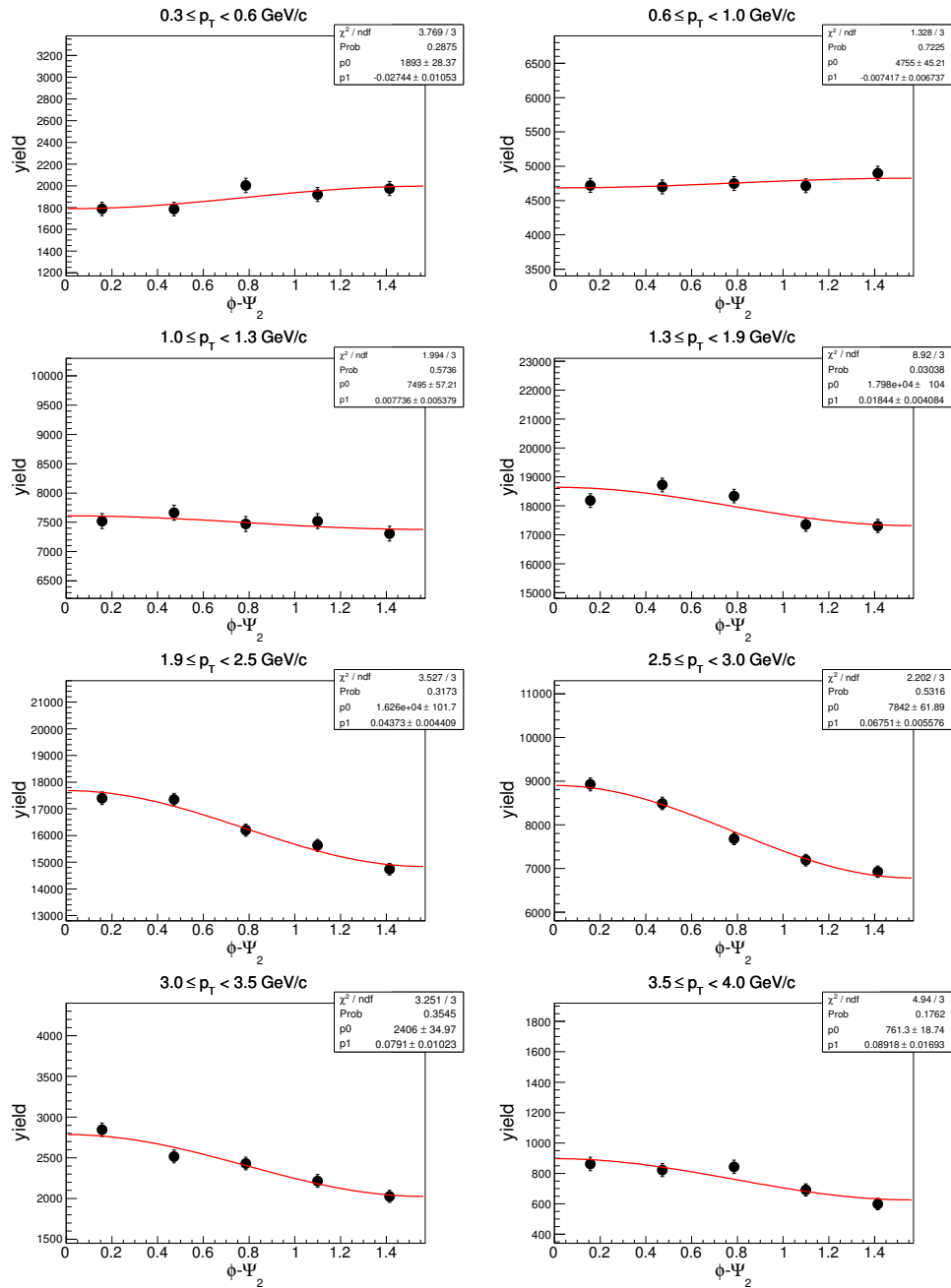
6.7.3 $\phi - \Psi_2$ of d in centrality: 30-80% ($\sqrt{s_{NN}} = 62.4$ GeV)



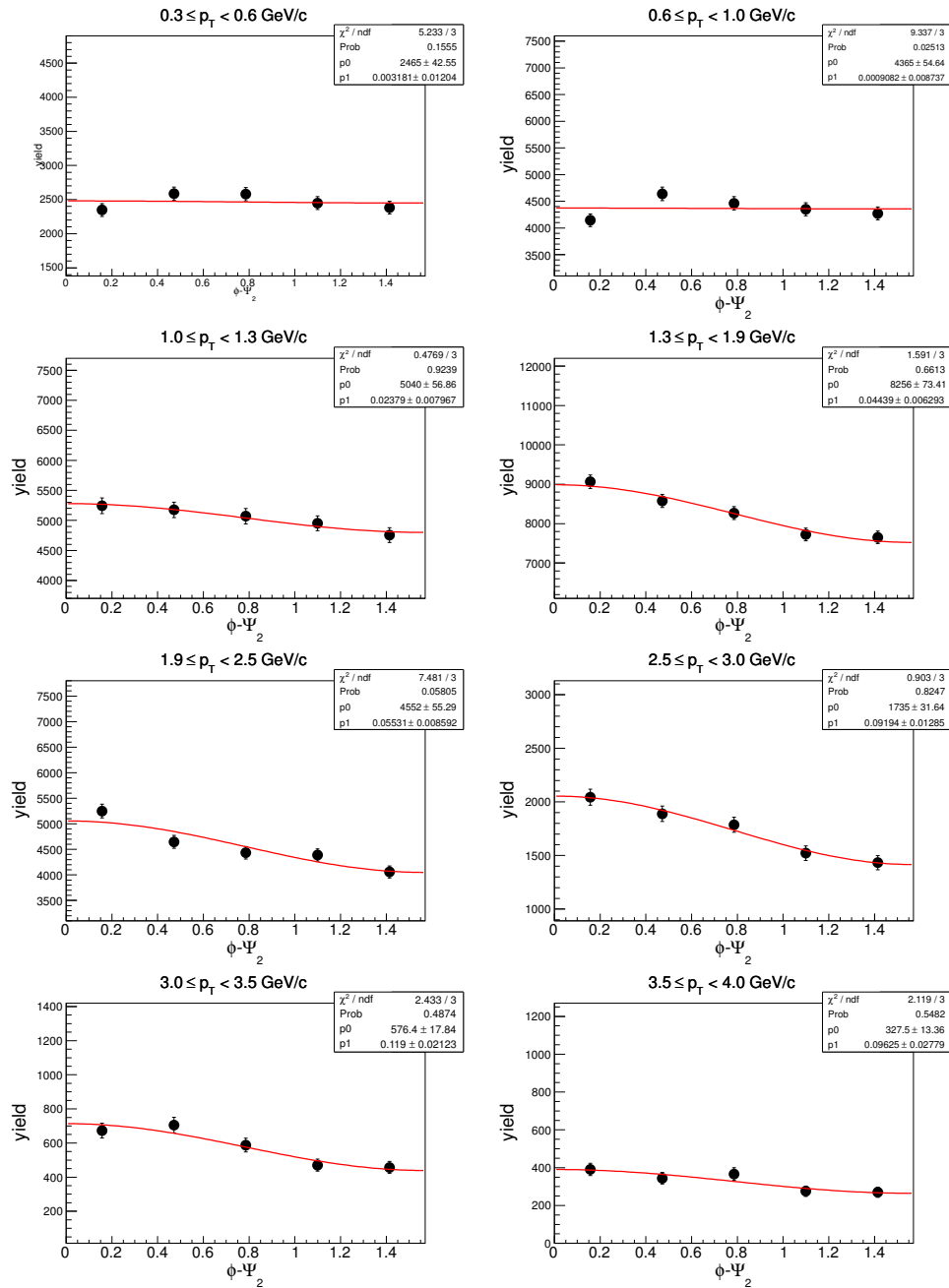
6.7.4 $\phi - \Psi_2$ of \bar{d} in centrality: 0-80% ($\sqrt{s_{NN}} = 62.4$ GeV)



6.7.5 $\phi - \Psi_2$ of \bar{d} in centrality: 0-30% ($\sqrt{s_{NN}} = 62.4$ GeV)

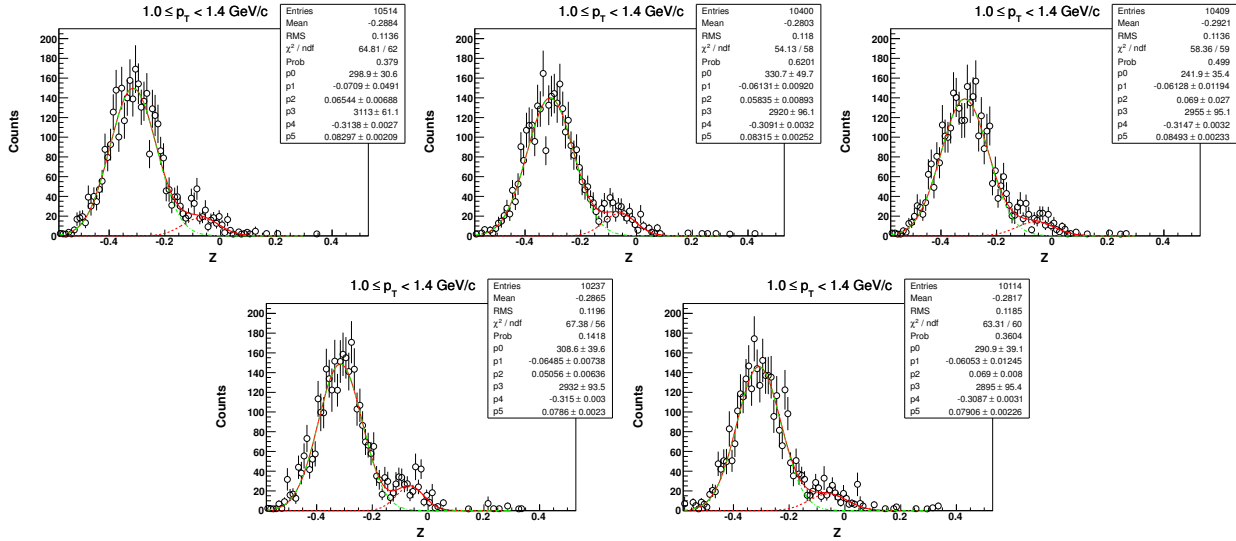


6.7.6 $\phi - \Psi_2$ of \bar{d} in centrality: 30-80% ($\sqrt{s_{NN}} = 62.4$ GeV)

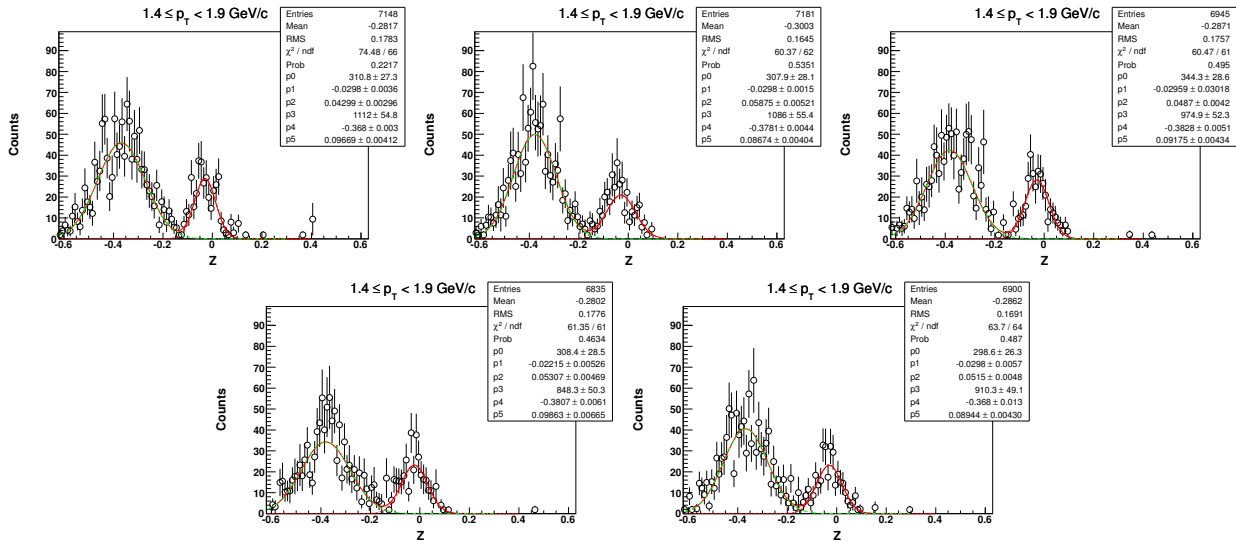


6.8 Z distribution of 3He in $\sqrt{s_{NN}} = 62.4$ GeV (centrality: 0-80%)

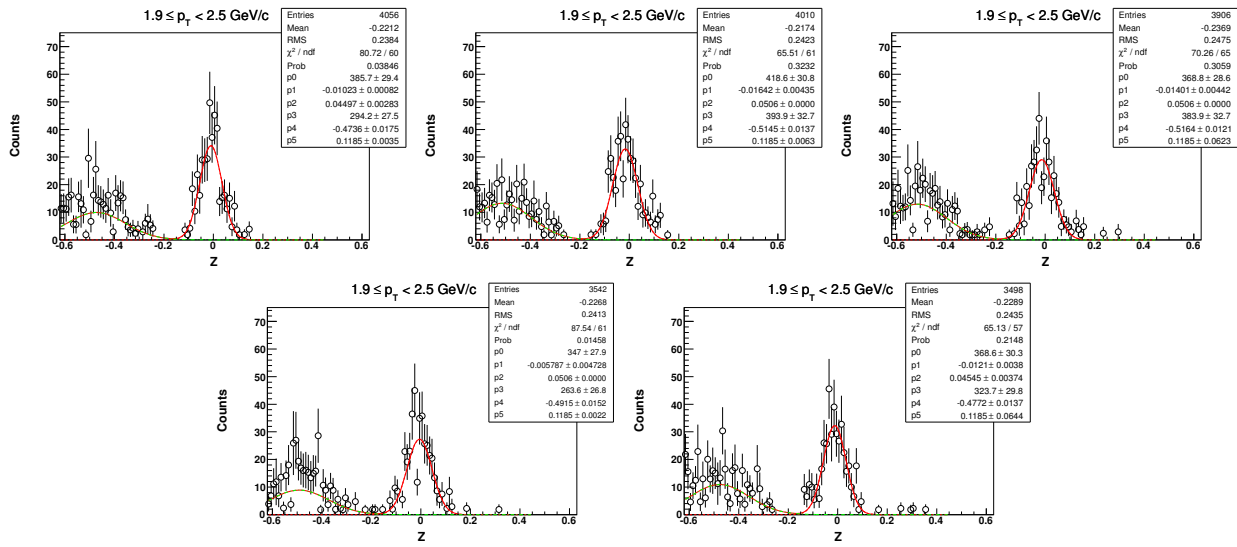
6.8.1 Z-distribution of 3He for $1.0 < p_T < 1.4$ GeV/c



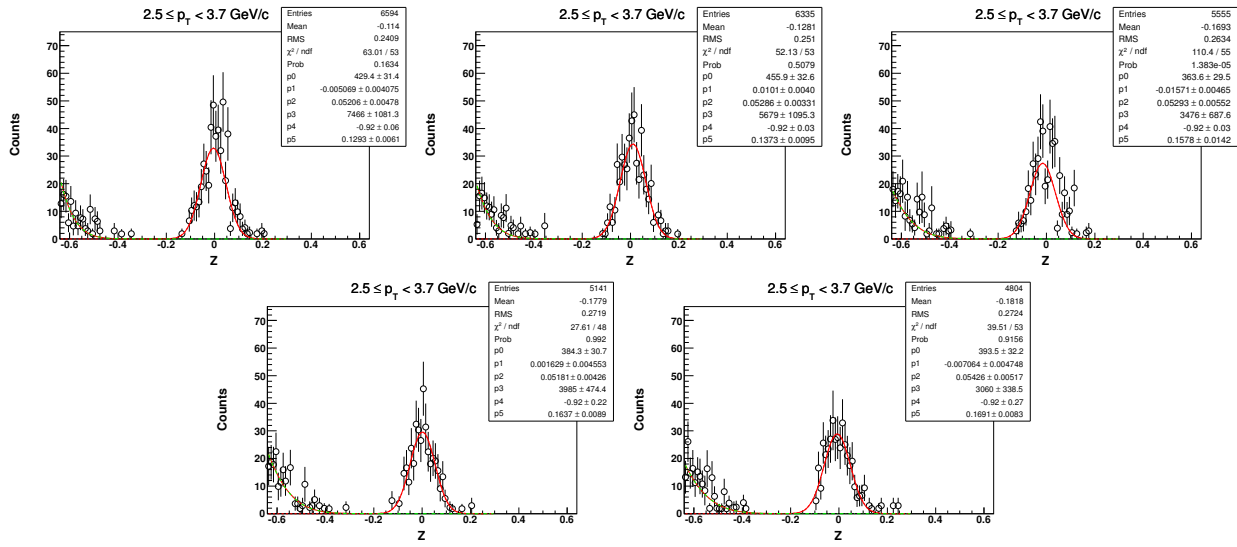
6.8.2 Z-distribution of 3He for $1.4 < p_T < 1.9$ GeV/c ($\sqrt{s_{NN}} = 62.4$ GeV, 0-80%)



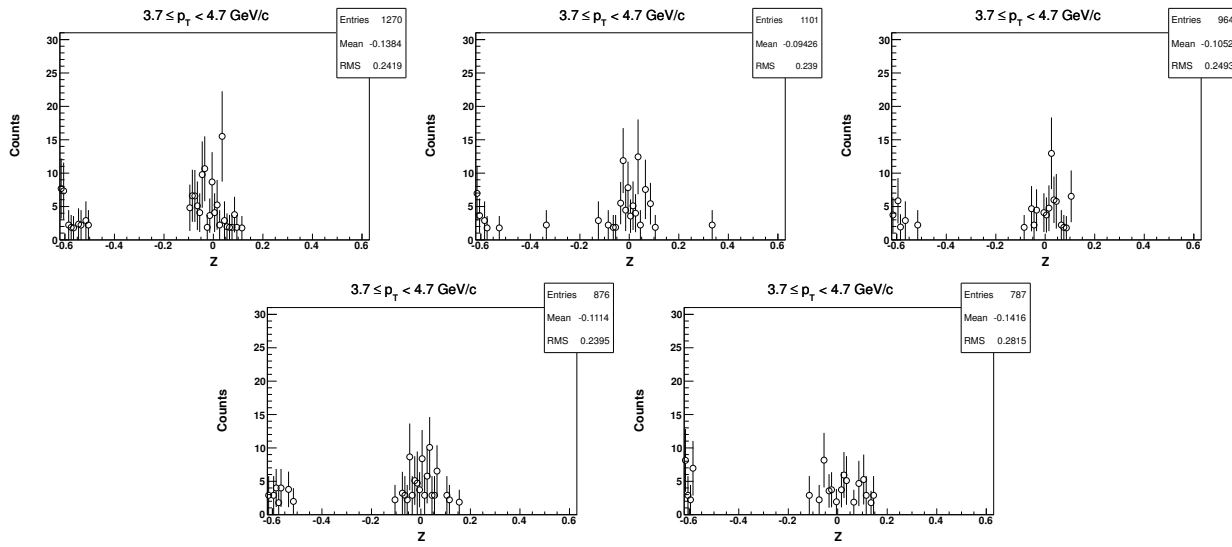
6.8.3 Z-distribution of ^3He for $1.9 < p_T < 2.5 \text{ GeV}/c$ ($\sqrt{s_{NN}} = 62.4 \text{ GeV}$, 0-80%)



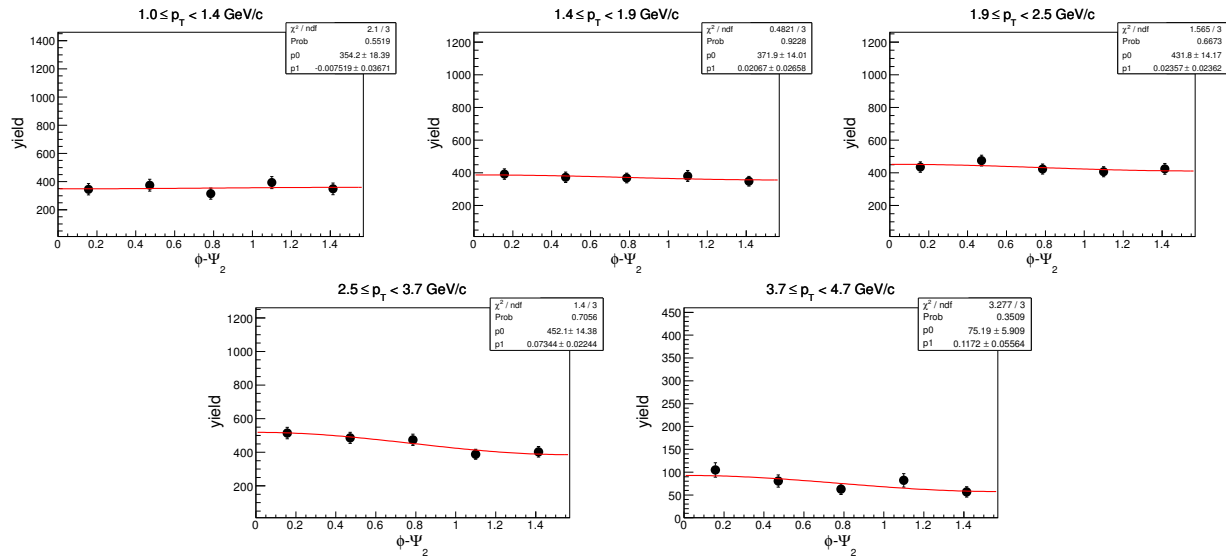
6.8.4 Z-distribution of ^3He for $2.5 < p_T < 3.7 \text{ GeV}/c$ ($\sqrt{s_{NN}} = 62.4 \text{ GeV}$, 0-80%)



6.8.5 Z-distribution of ^3He for $3.7 < p_T < 4.7 \text{ GeV}/c$ ($\sqrt{s_{NN}} = 62.4 \text{ GeV}$, 0-80%)

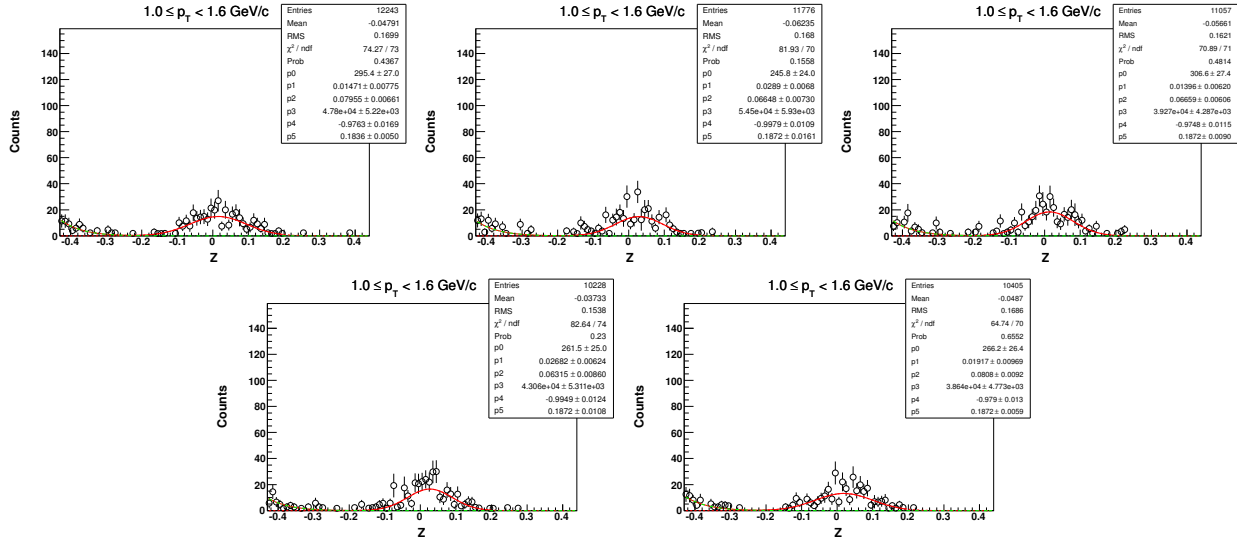


6.8.6 $\phi - \Psi_2$ of ^3He in centrality: 0-80% ($\sqrt{s_{NN}} = 62.4 \text{ GeV}$)

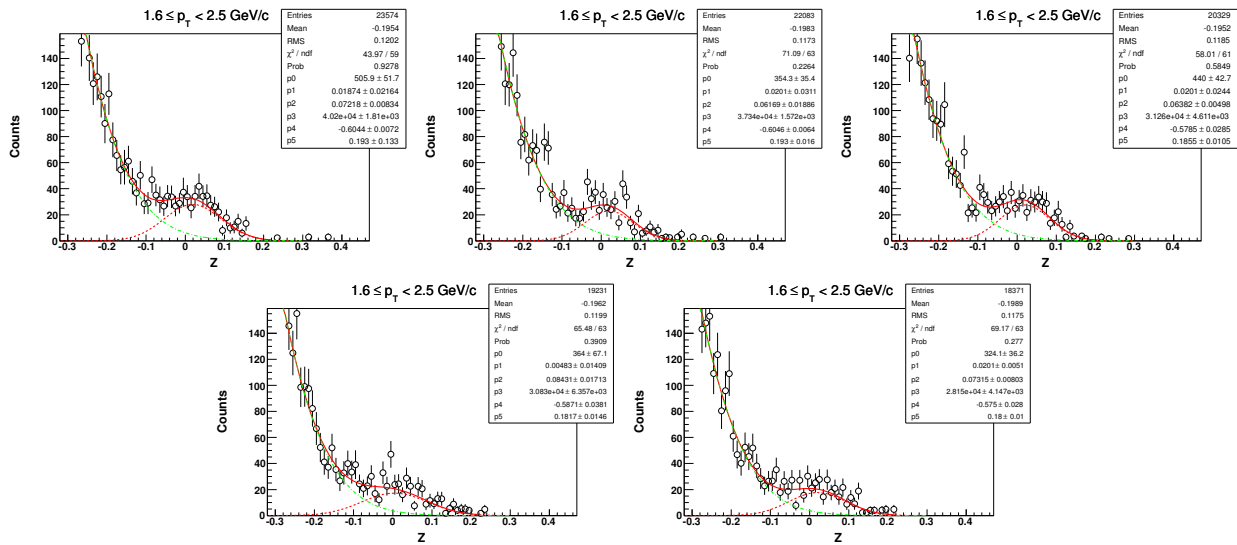


6.9 Z distribution of t in $\sqrt{s_{NN}} = 62.4 \text{ GeV}$ (centrality: 0-80%)

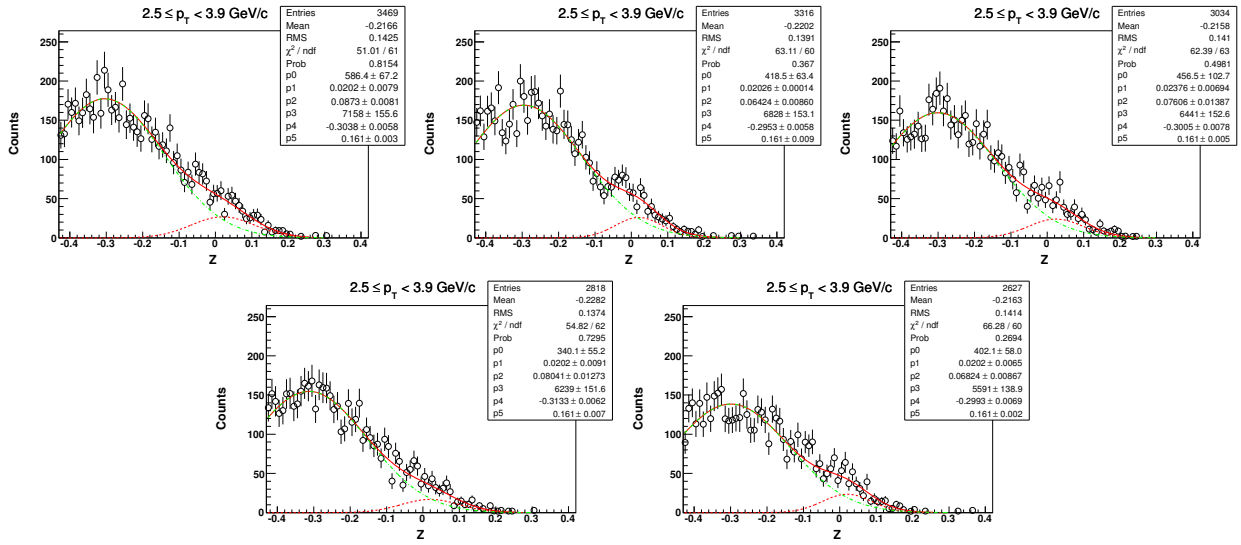
6.9.1 Z-distribution of t for $1.0 < p_T < 1.6 \text{ GeV}/c$



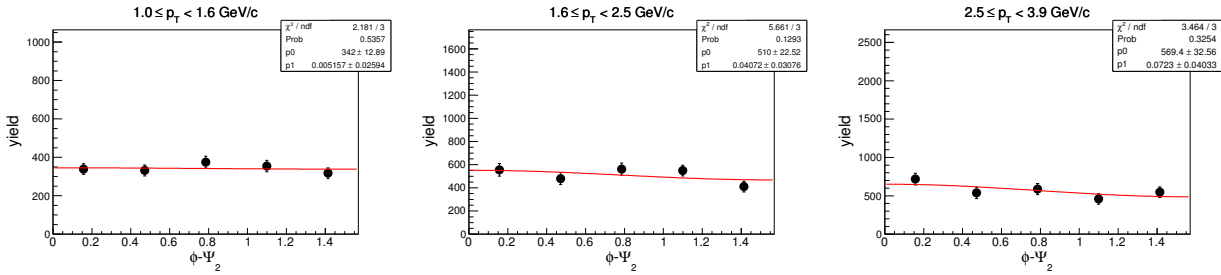
6.9.2 Z-distribution of t for $1.6 < p_T < 2.5 \text{ GeV}/c$ ($\sqrt{s_{NN}} = 62.4 \text{ GeV}$, 0-80%)



6.9.3 Z-distribution of t for $2.5 < p_T < 3.9 \text{ GeV}/c$ ($\sqrt{s_{NN}} = 62.4 \text{ GeV}$, 0-80%)



6.9.4 $\phi - \Psi_2$ of t in centrality: 0-80% ($\sqrt{s_{NN}} = 62.4 \text{ GeV}$)

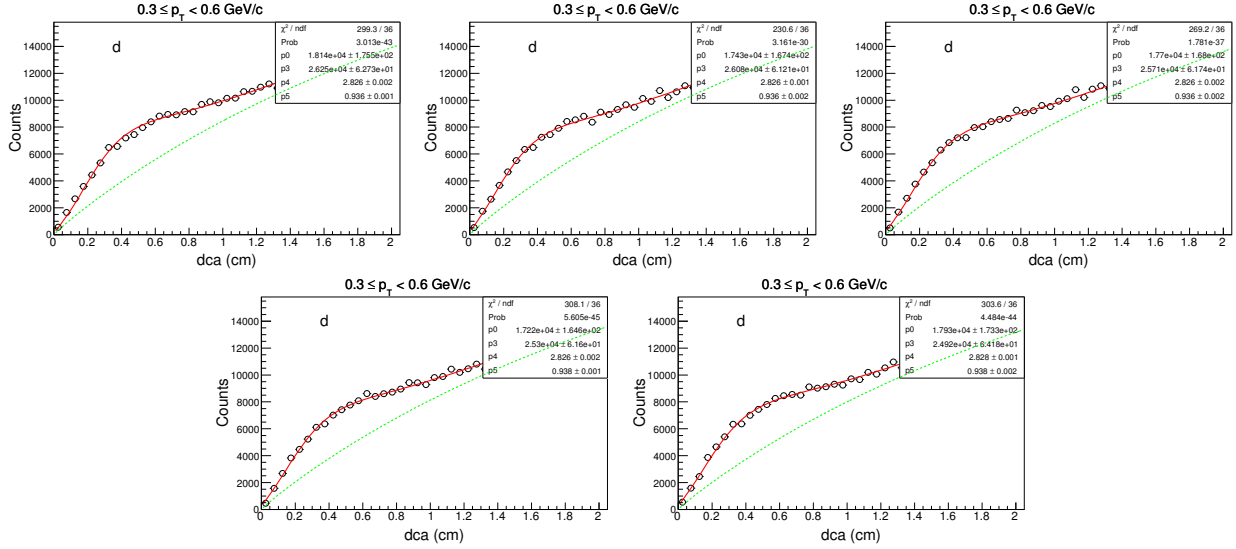


7 DCA and Z-distributions for Au+Au at $\sqrt{s_{NN}} = 39$ GeV

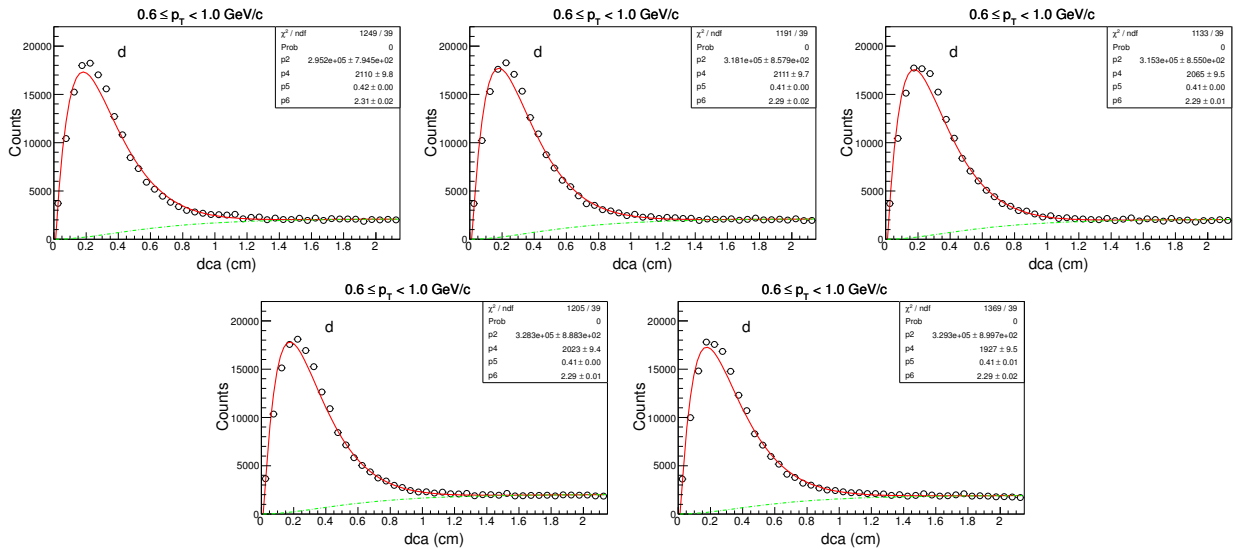
In this section we show the DCA and Z-distribution of deuteron and anti-deuteron for five different ($\phi - \Psi_2$) bins namely, $0 - \frac{\pi}{10}$, $\frac{\pi}{10} - \frac{2\pi}{10}$, $\frac{2\pi}{10} - \frac{3\pi}{10}$, $\frac{3\pi}{10} - \frac{4\pi}{10}$ and $\frac{4\pi}{10} - \frac{5\pi}{10}$. DCA and Z-distribution of d for all centrality and all p_T bins are shown in the later sub-sections.

7.1 Centrality: 0-80%

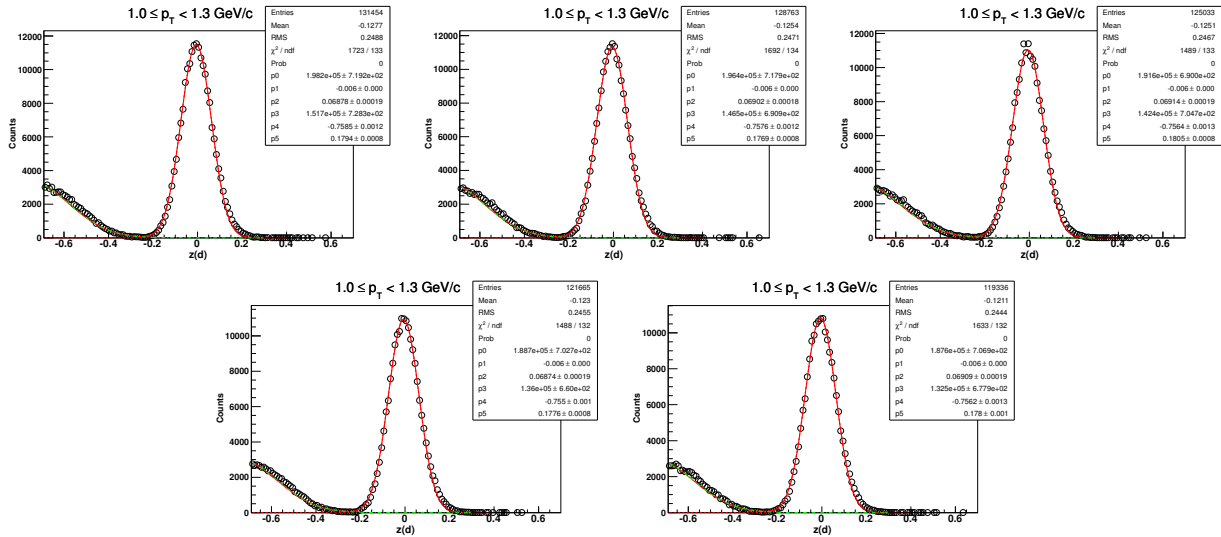
7.1.1 DCA-distribution of d for $0.3 < p_T < 0.6$ GeV/c



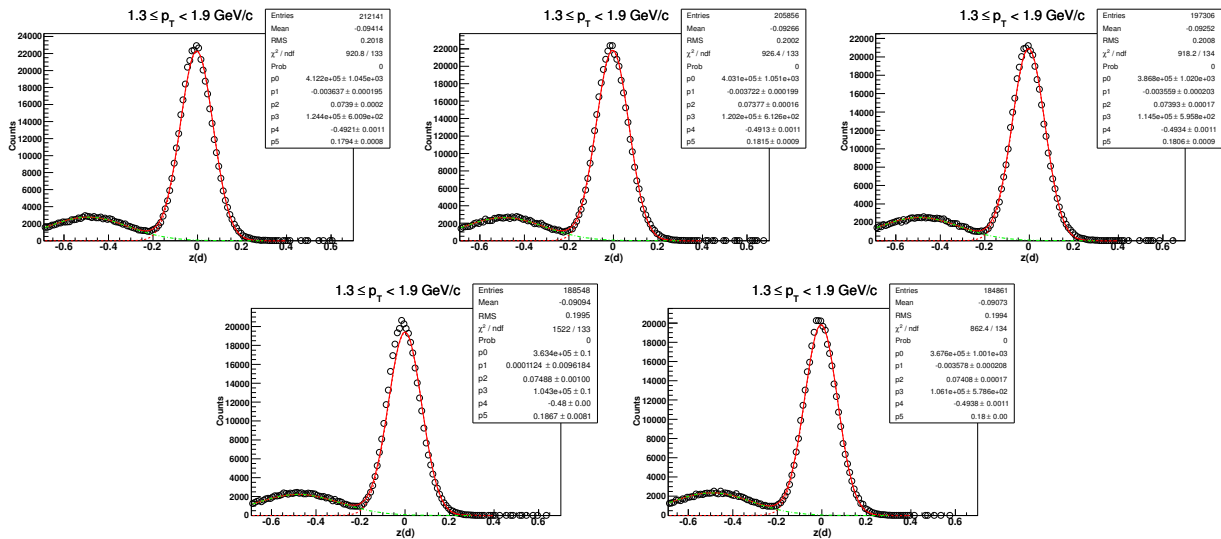
7.1.2 DCA-distribution of d for $0.6 < p_T < 1.0$ GeV/c ($\sqrt{s_{NN}} = 39$ GeV, 0-80%)



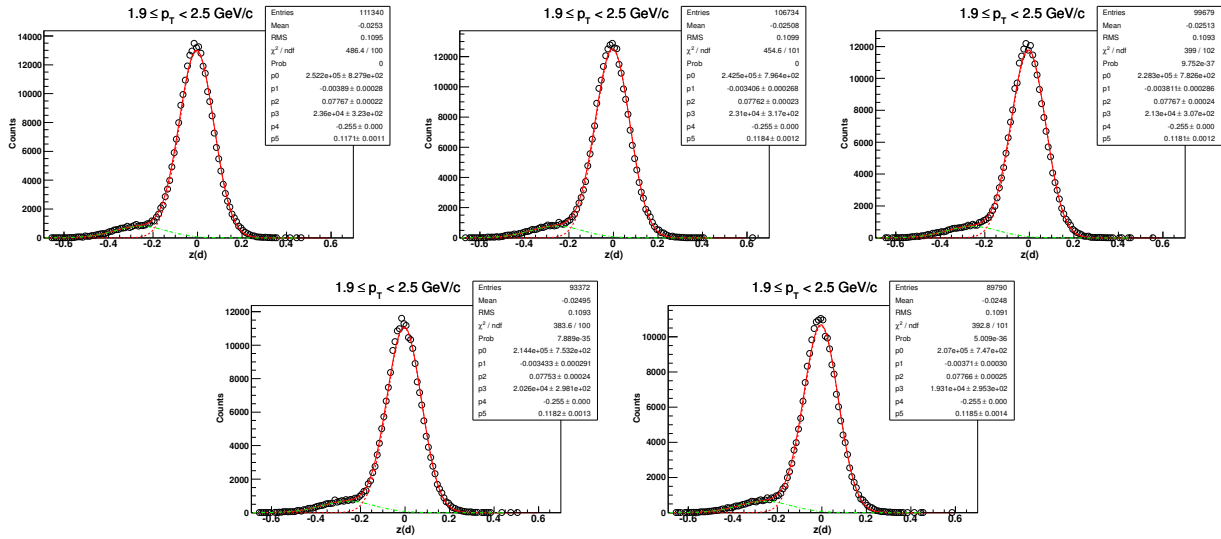
7.1.3 Z-distribution of d for $1.0 < p_T < 1.3 \text{ GeV}/c$ ($\sqrt{s_{NN}} = 39 \text{ GeV}$, 0-80%)



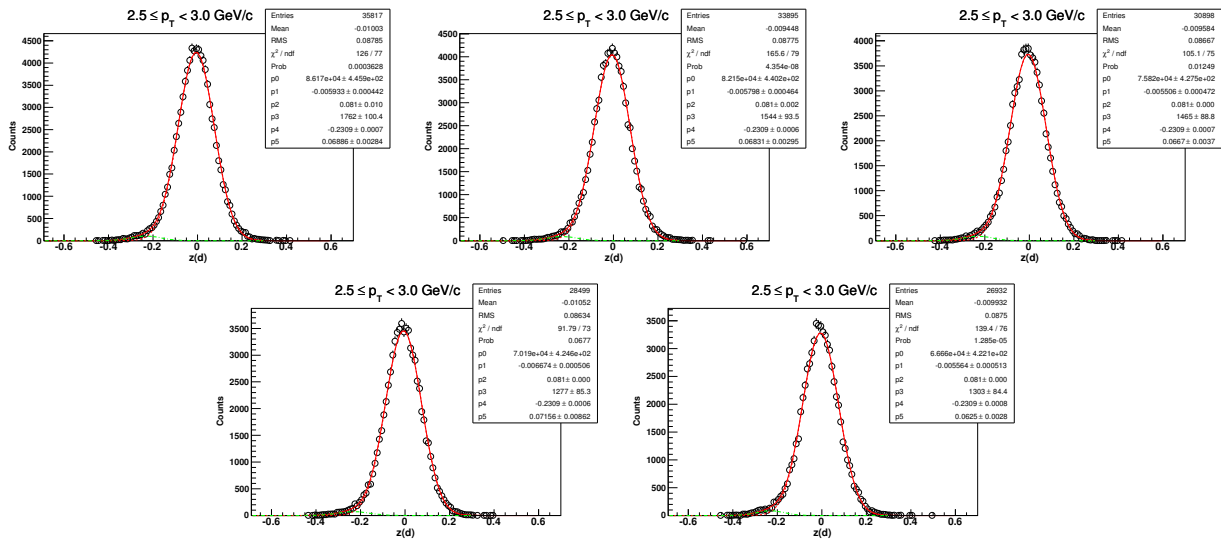
7.1.4 Z-distribution of d for $1.3 < p_T < 1.9 \text{ GeV}/c$ ($\sqrt{s_{NN}} = 39 \text{ GeV}$, 0-80%)



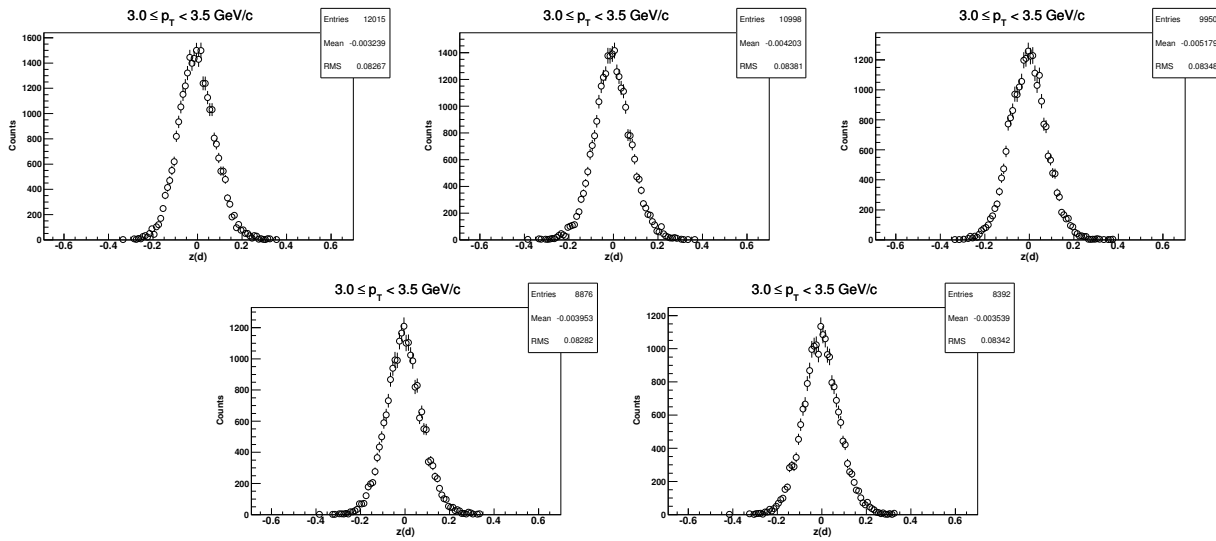
7.1.5 Z-distribution of d for $1.9 < p_T < 2.5 \text{ GeV}/c$ ($\sqrt{s_{NN}} = 39 \text{ GeV}$, 0-80%)



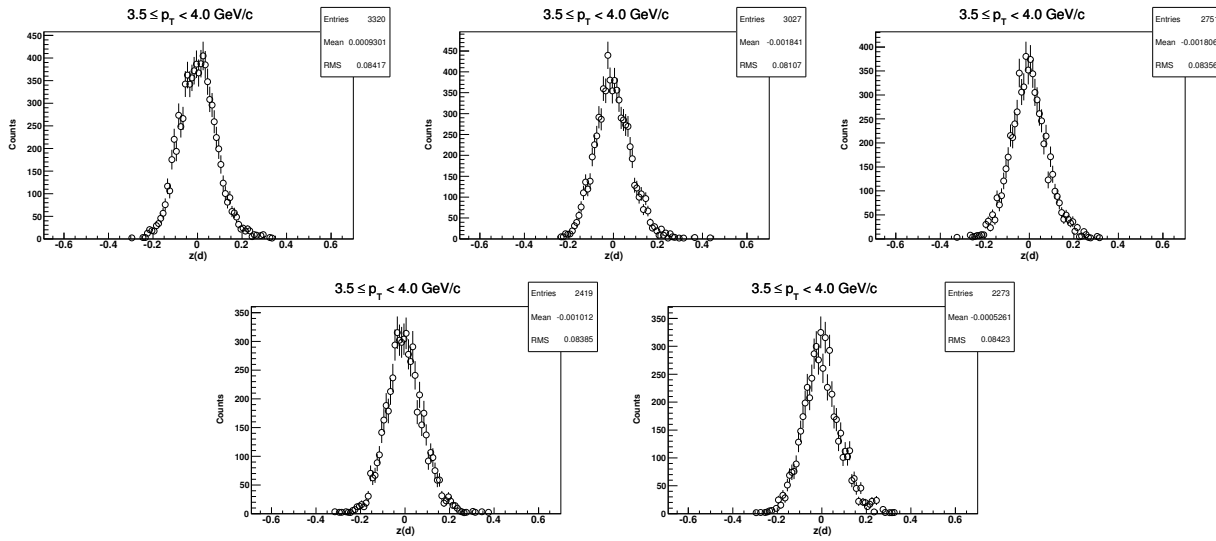
7.1.6 Z-distribution of d for $2.5 < p_T < 3.0 \text{ GeV}/c$ ($\sqrt{s_{NN}} = 39 \text{ GeV}$, 0-80%)



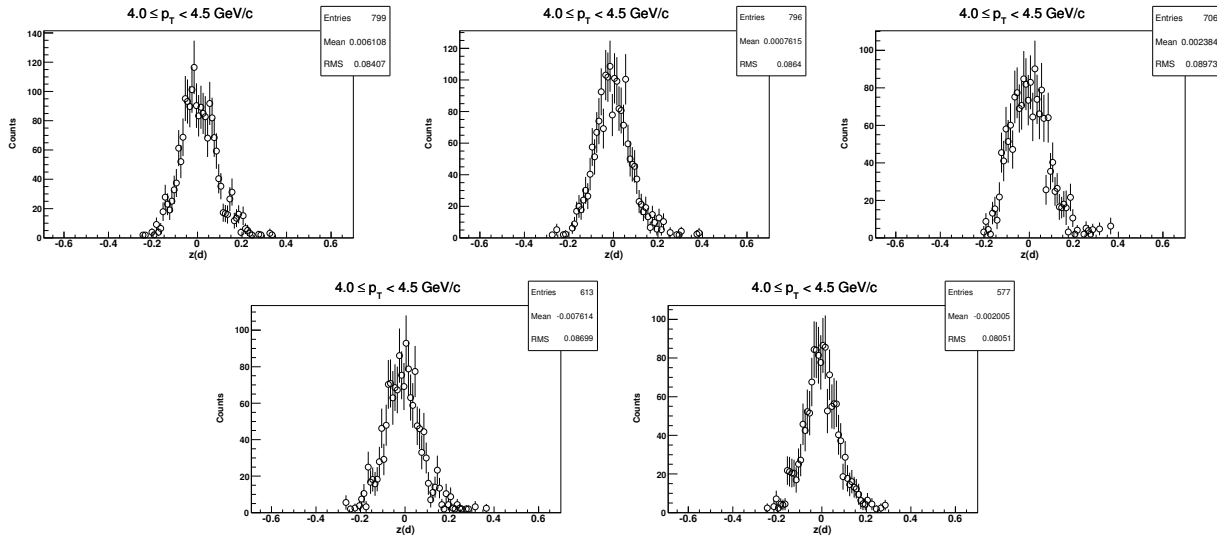
7.1.7 Z-distribution of d for $3.0 < p_T < 3.5 \text{ GeV}/c$ ($\sqrt{s_{NN}} = 39 \text{ GeV}$, 0-80%)



7.1.8 Z-distribution of d for $3.5 < p_T < 4.0 \text{ GeV}/c$ ($\sqrt{s_{NN}} = 39 \text{ GeV}$, 0-80%)

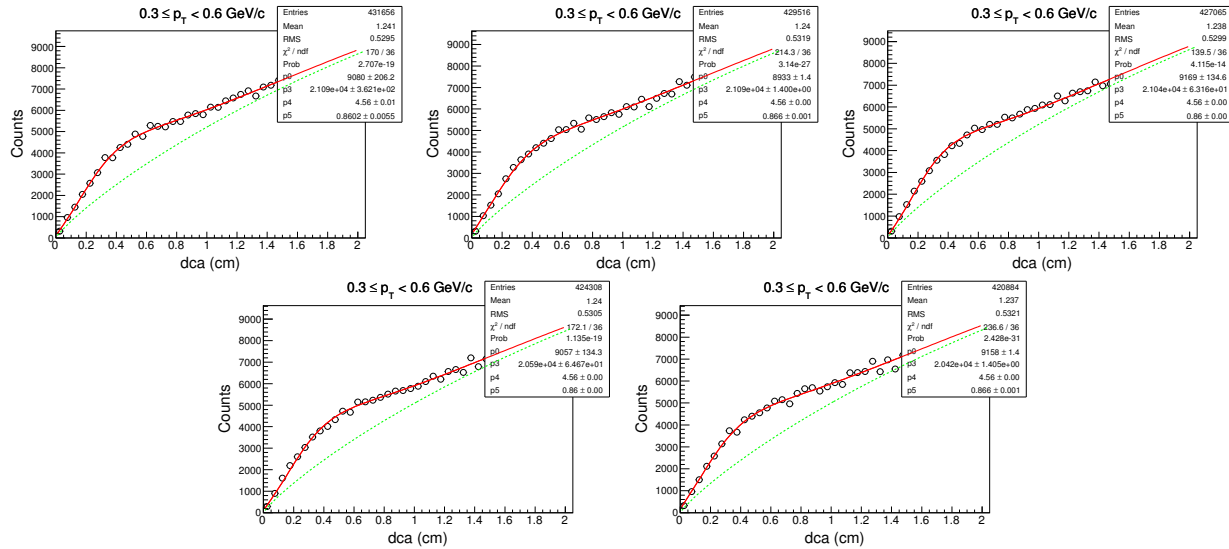


7.1.9 Z-distribution of d for $4.0 < p_T < 4.5 \text{ GeV}/c$ ($\sqrt{s_{NN}} = 39 \text{ GeV}$, 0-80%)

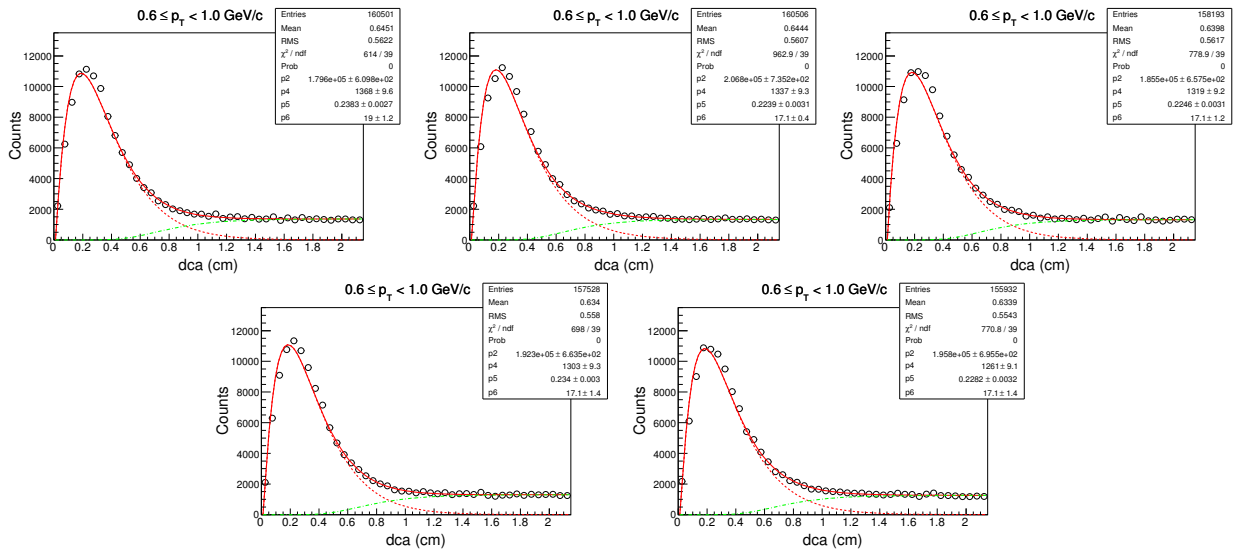


7.2 Centrality: 0-30%

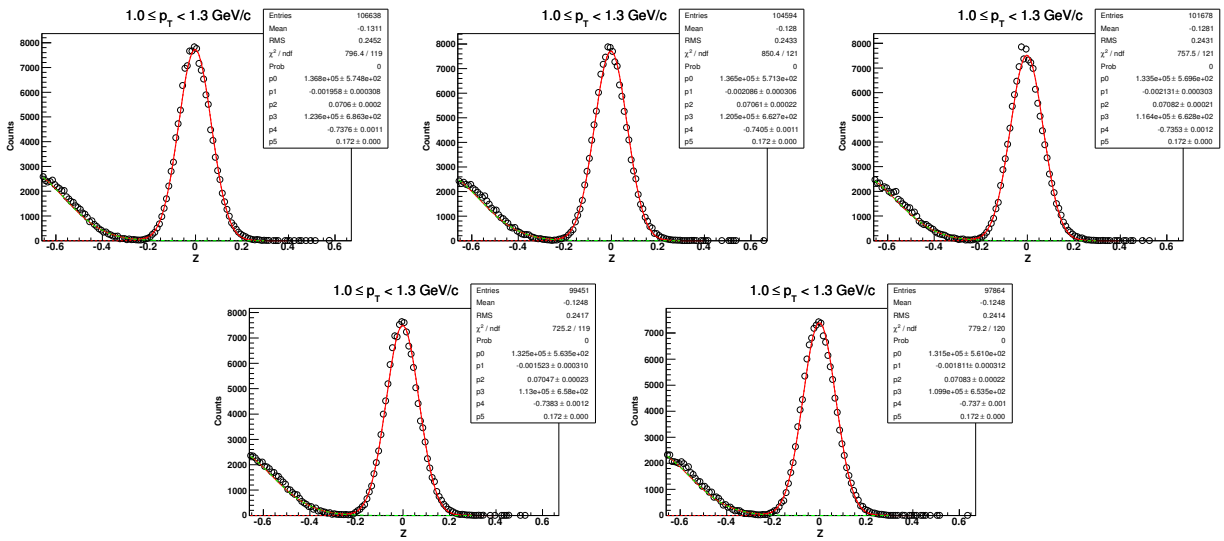
7.2.1 DCA-distribution of d for $0.3 < p_T < 0.6 \text{ GeV}/c$



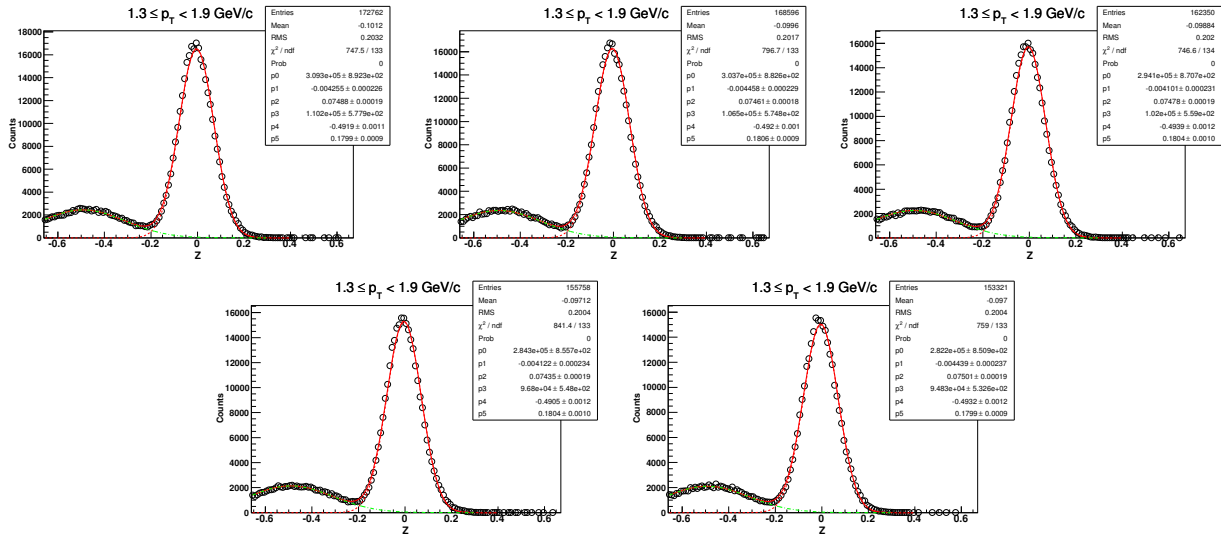
7.2.2 DCA-distribution of d for $0.6 < p_T < 1.0 \text{ GeV}/c$



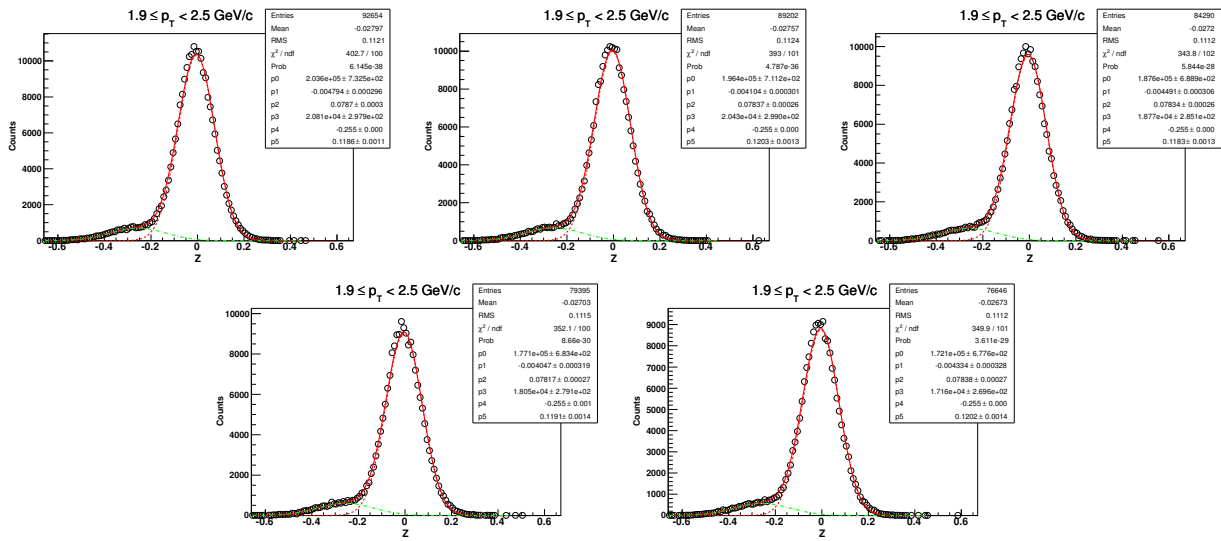
7.2.3 Z-distribution of d for $1.0 < p_T < 1.3 \text{ GeV}/c$ ($\sqrt{s_{NN}} = 39 \text{ GeV}$, 0-30%)



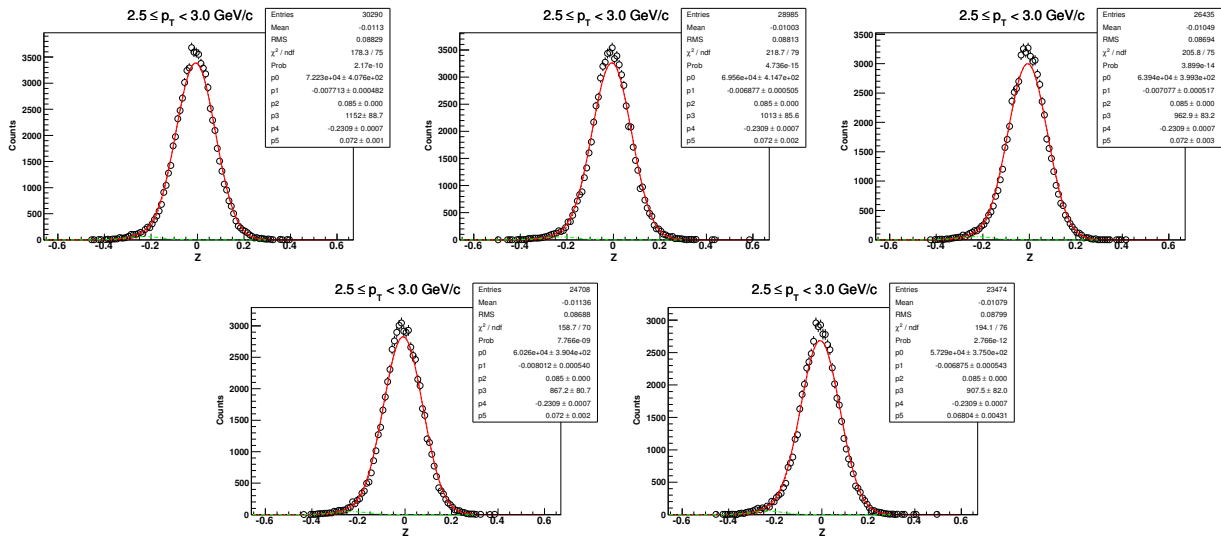
7.2.4 Z-distribution of d for $1.3 < p_T < 1.9 \text{ GeV}/c$ ($\sqrt{s_{NN}} = 39 \text{ GeV}$, 0-30%)



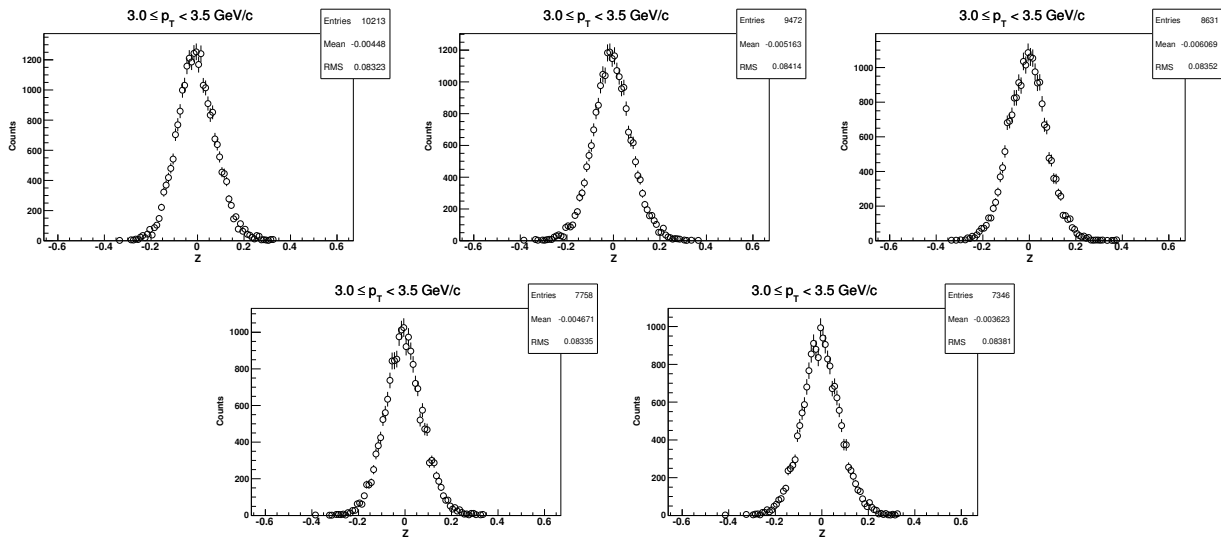
7.2.5 Z-distribution of d for $1.9 < p_T < 2.5 \text{ GeV}/c$ ($\sqrt{s_{NN}} = 39 \text{ GeV}$, 0-30%)



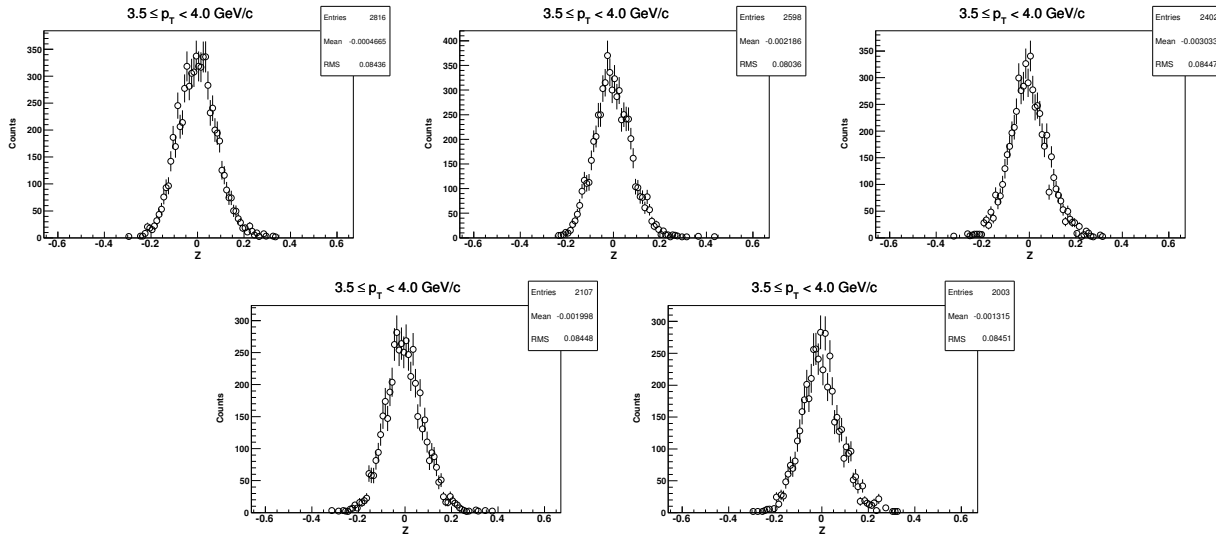
7.2.6 Z-distribution of d for $2.5 < p_T < 3.0 \text{ GeV}/c$ ($\sqrt{s_{NN}} = 39 \text{ GeV}$, 0-30%)



7.2.7 Z-distribution of d for $3.0 < p_T < 3.5 \text{ GeV}/c$ ($\sqrt{s_{NN}} = 39 \text{ GeV}$, 0-30%)

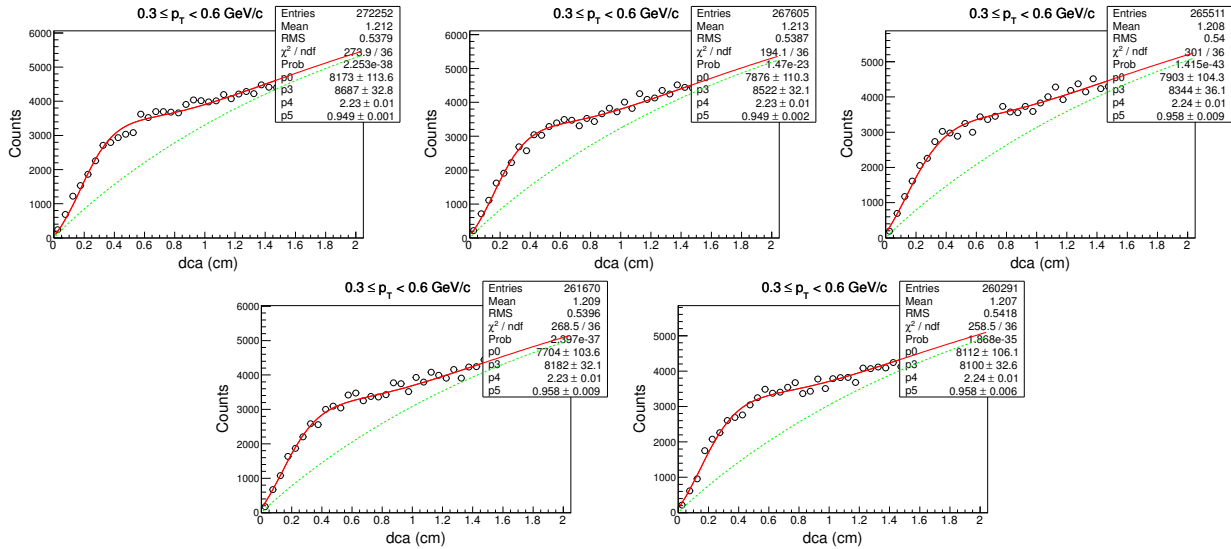


7.2.8 Z-distribution of d for $3.5 < p_T < 4.0 \text{ GeV}/c$ ($\sqrt{s_{NN}} = 39 \text{ GeV}$, 0-30%)

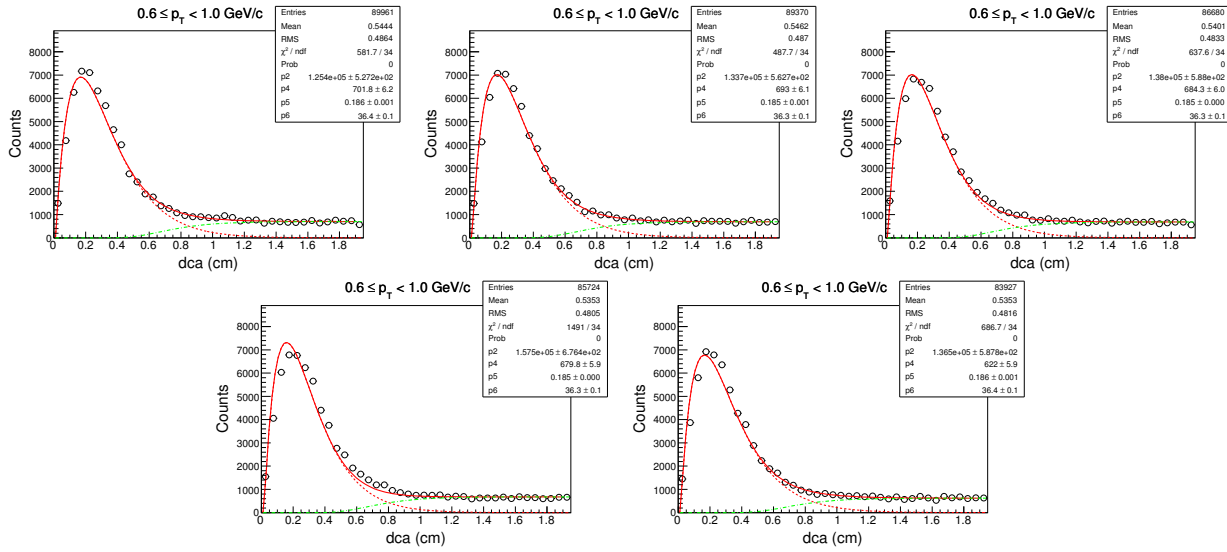


7.3 Centrality: 30-80%

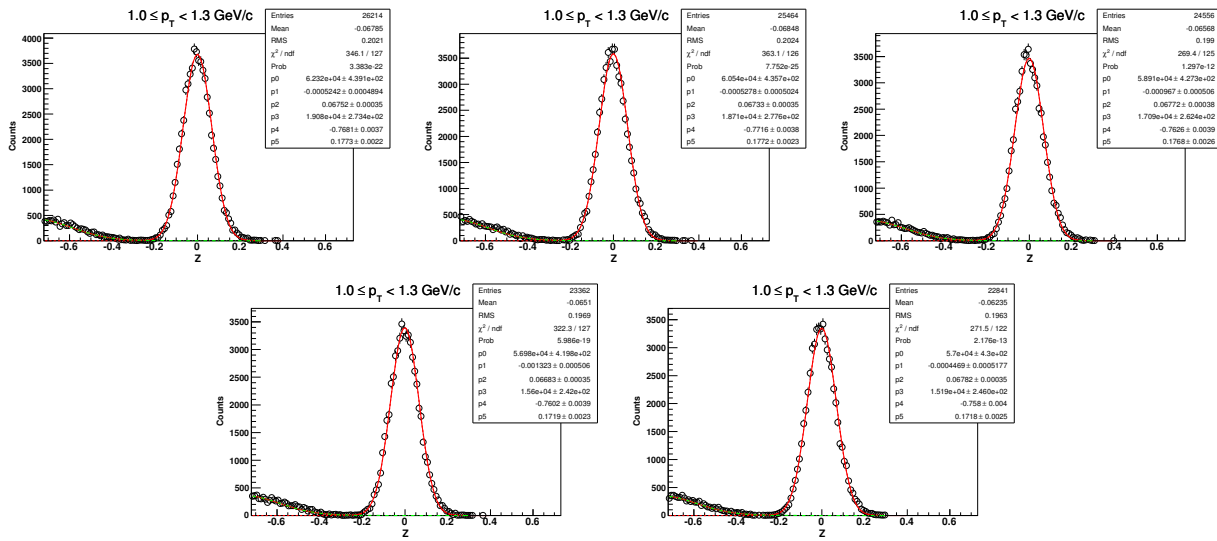
7.3.1 DCA-distribution of d for $0.3 < p_T < 0.6 \text{ GeV}/c$



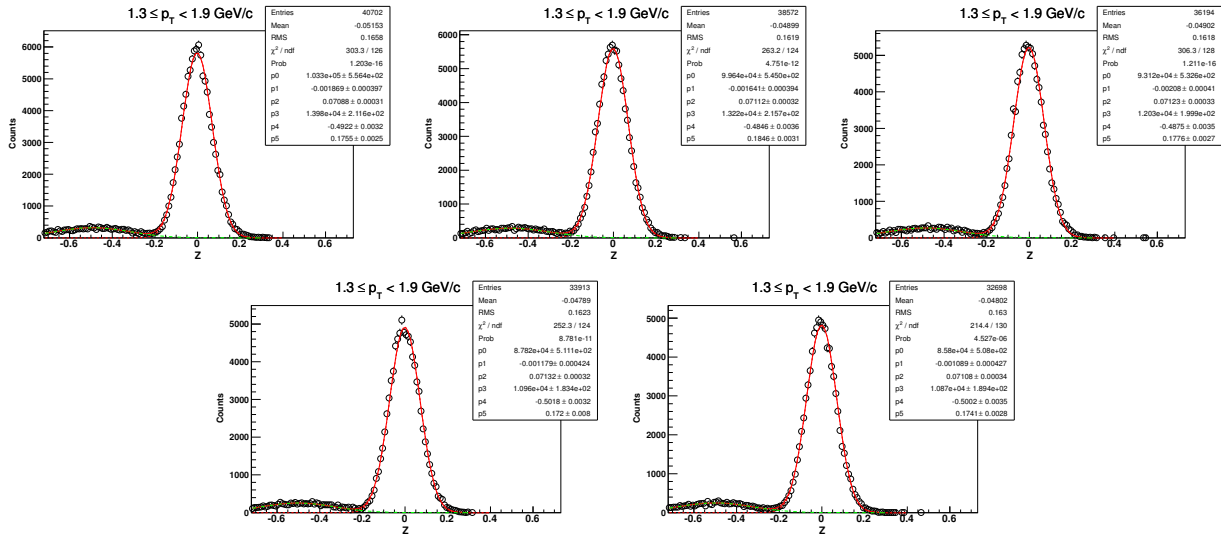
7.3.2 DCA-distribution of d for $0.6 < p_T < 1.0 \text{ GeV}/c$ ($\sqrt{s_{NN}} = 39 \text{ GeV}$, 30-80%)



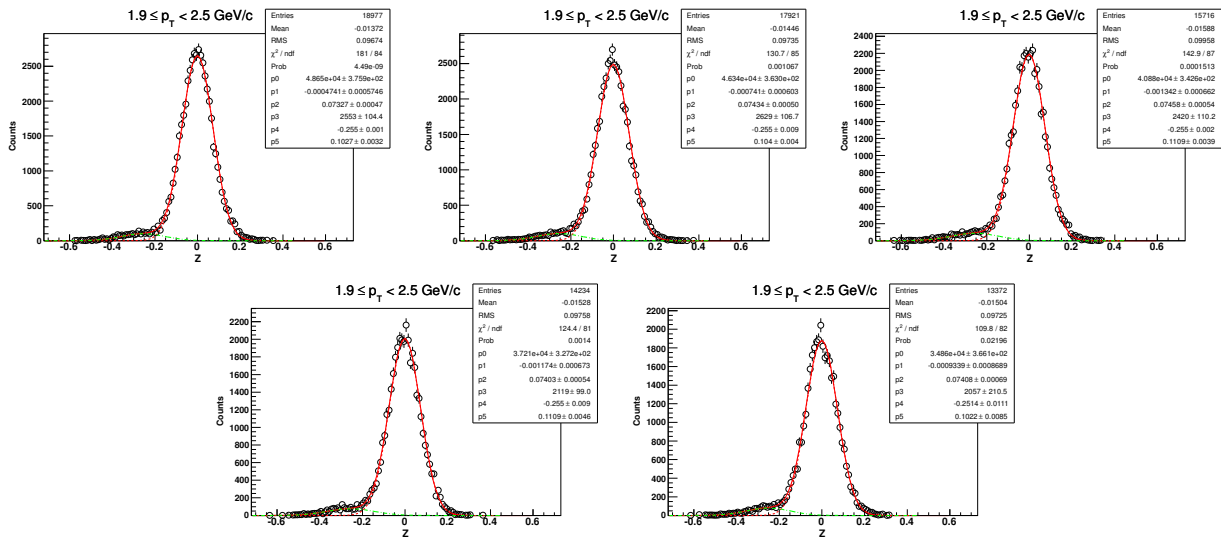
7.3.3 Z-distribution of d for $1.0 < p_T < 1.3 \text{ GeV}/c$ ($\sqrt{s_{NN}} = 39 \text{ GeV}$, 30-80%)



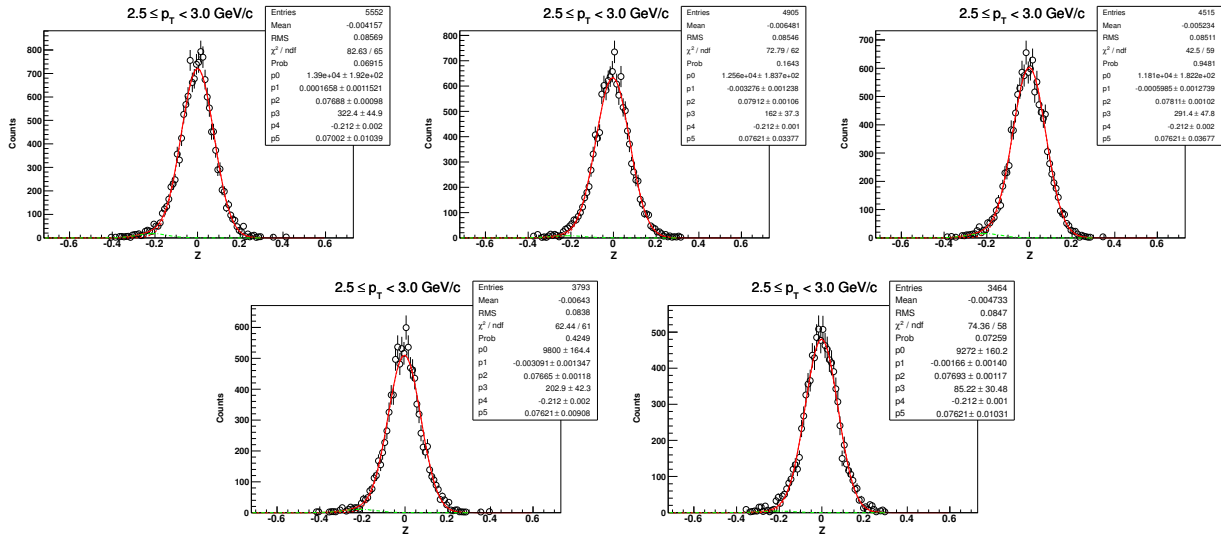
7.3.4 Z-distribution of d for $1.3 < p_T < 1.9 \text{ GeV}/c$ ($\sqrt{s_{NN}} = 39 \text{ GeV}$, 30-80%)



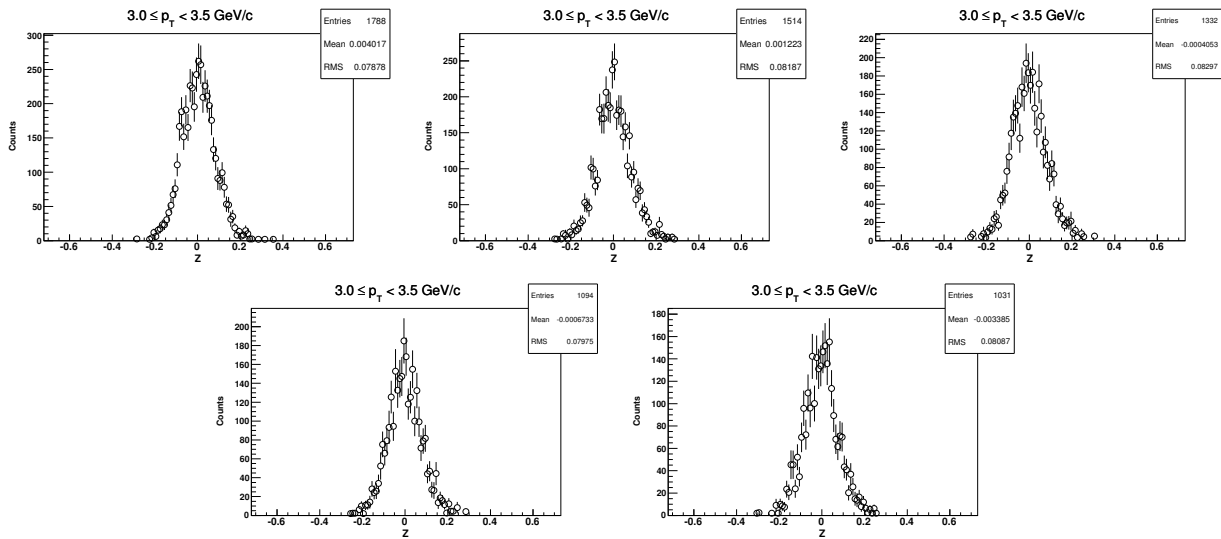
7.3.5 Z-distribution of d for $1.9 < p_T < 2.5 \text{ GeV}/c$ ($\sqrt{s_{NN}} = 39 \text{ GeV}$, 30-80%)



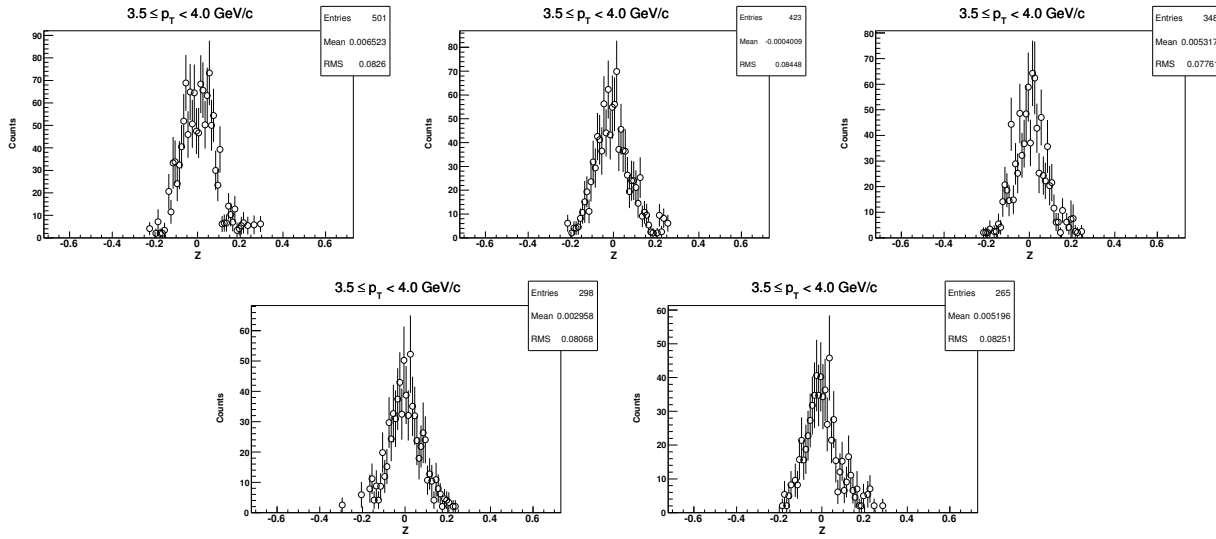
7.3.6 Z-distribution of d for $2.5 < p_T < 3.0 \text{ GeV}/c$ ($\sqrt{s_{NN}} = 39 \text{ GeV}$, 30-80%)



7.3.7 Z-distribution of d for $3.0 < p_T < 3.5 \text{ GeV}/c$ ($\sqrt{s_{NN}} = 39 \text{ GeV}$, 30-80%)

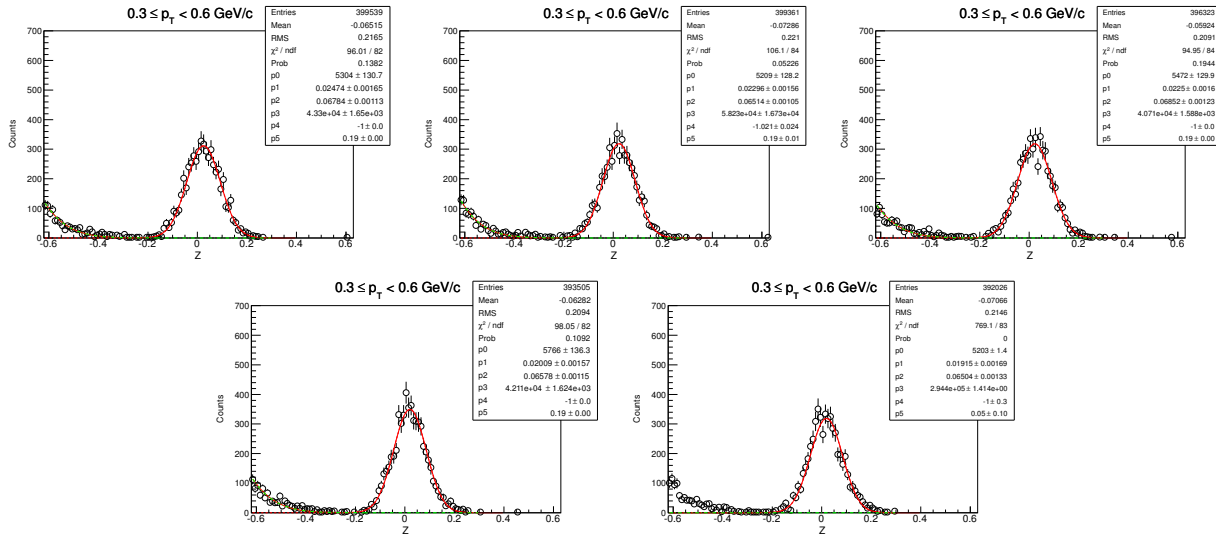


7.3.8 Z-distribution of d for $3.5 < p_T < 4.0 \text{ GeV}/c$ ($\sqrt{s_{NN}} = 39 \text{ GeV}$, 30-80%)

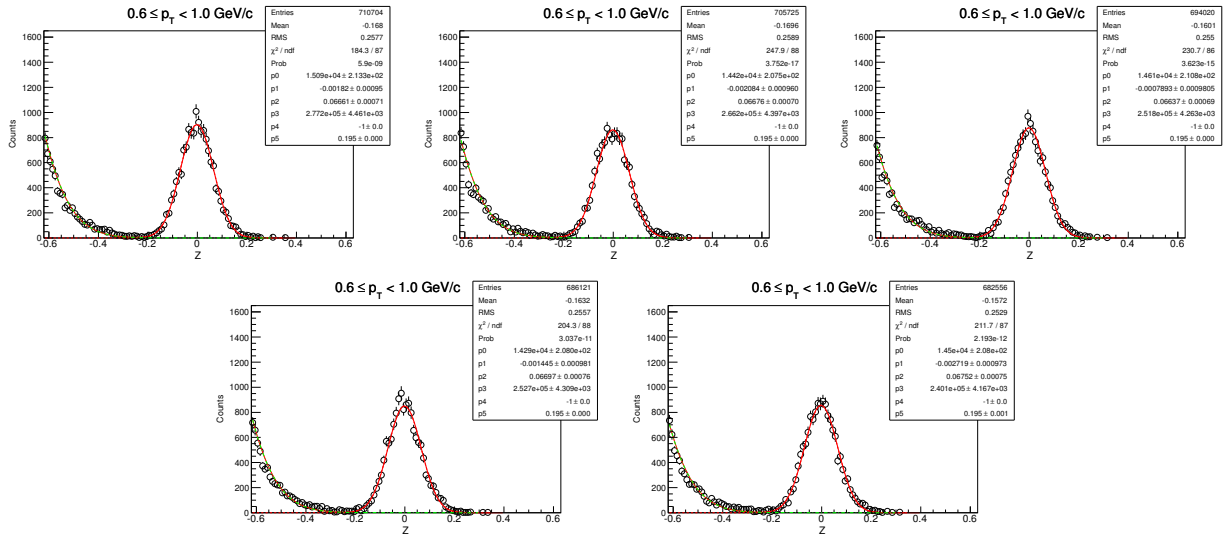


7.4 \bar{d} in $\sqrt{s_{NN}} = 39 \text{ GeV}$ for centrality: 0-80%

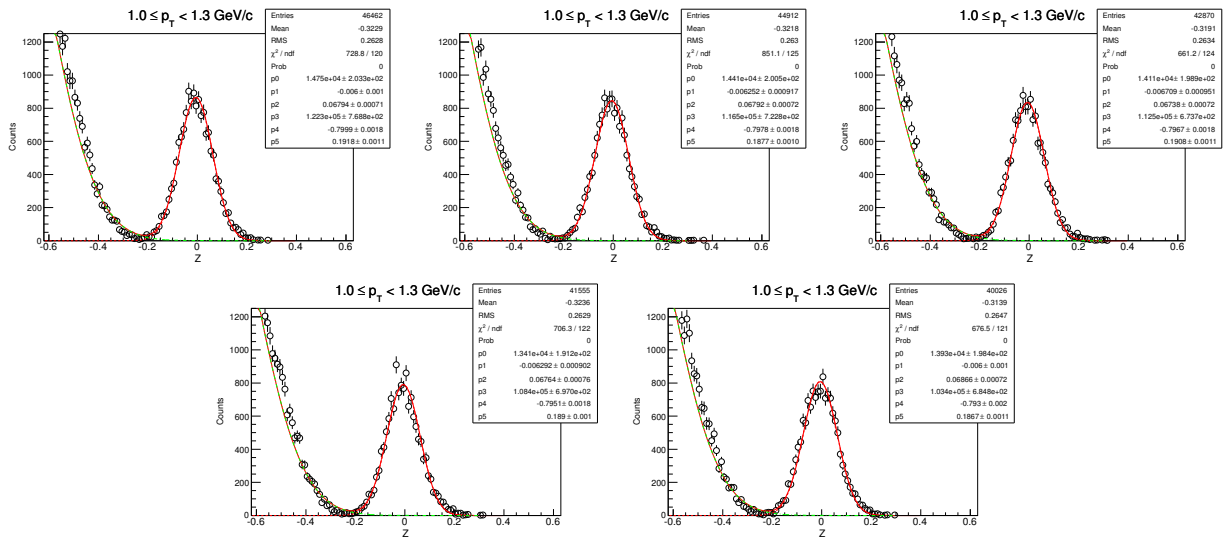
7.4.1 Z-distribution of \bar{d} for $0.3 < p_T < 0.6 \text{ GeV}/c$



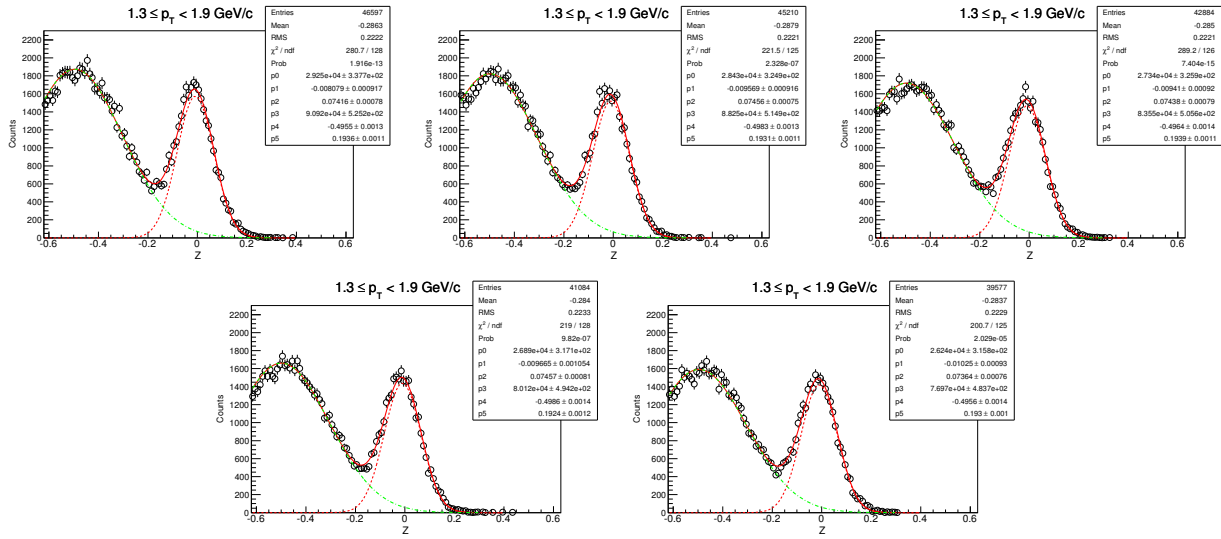
7.4.2 Z-distribution of \bar{d} for $0.6 < p_T < 1.0 \text{ GeV}/c$



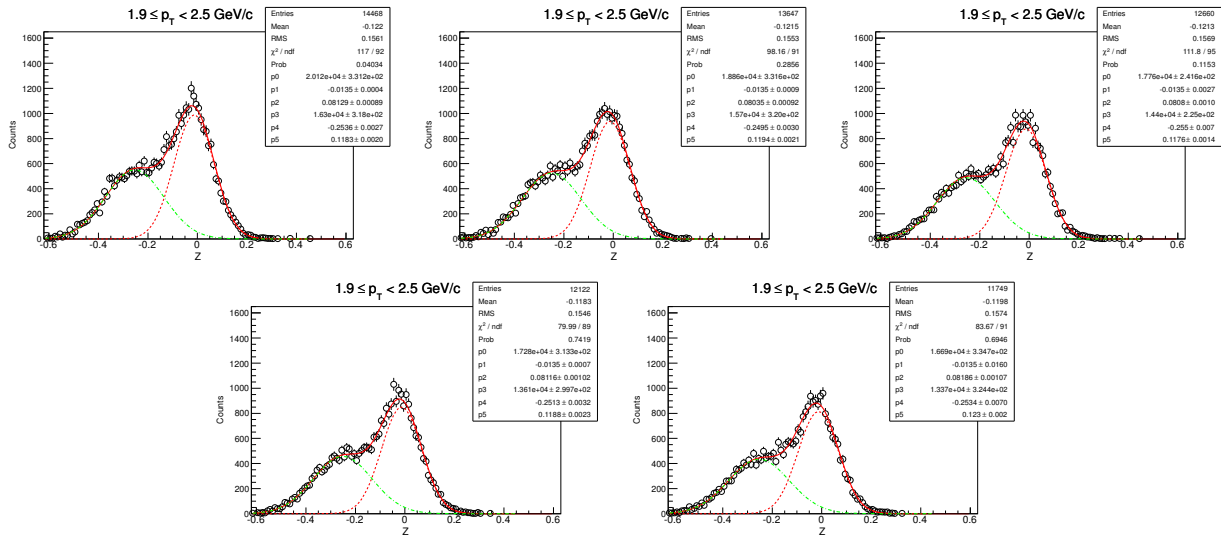
7.4.3 Z-distribution of \bar{d} for $1.0 < p_T < 1.3 \text{ GeV}/c$ ($\sqrt{s_{NN}} = 39 \text{ GeV}$, 0-80%)



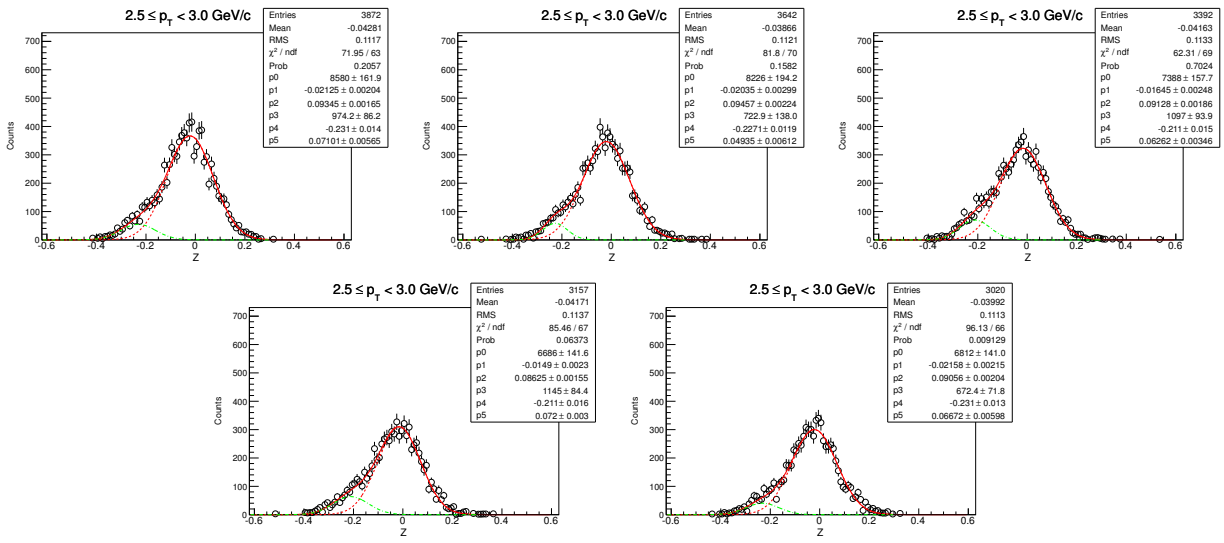
7.4.4 Z-distribution of \bar{d} for $1.3 < p_T < 1.9 \text{ GeV}/c$ ($\sqrt{s_{NN}} = 39 \text{ GeV}$, 0-80%)



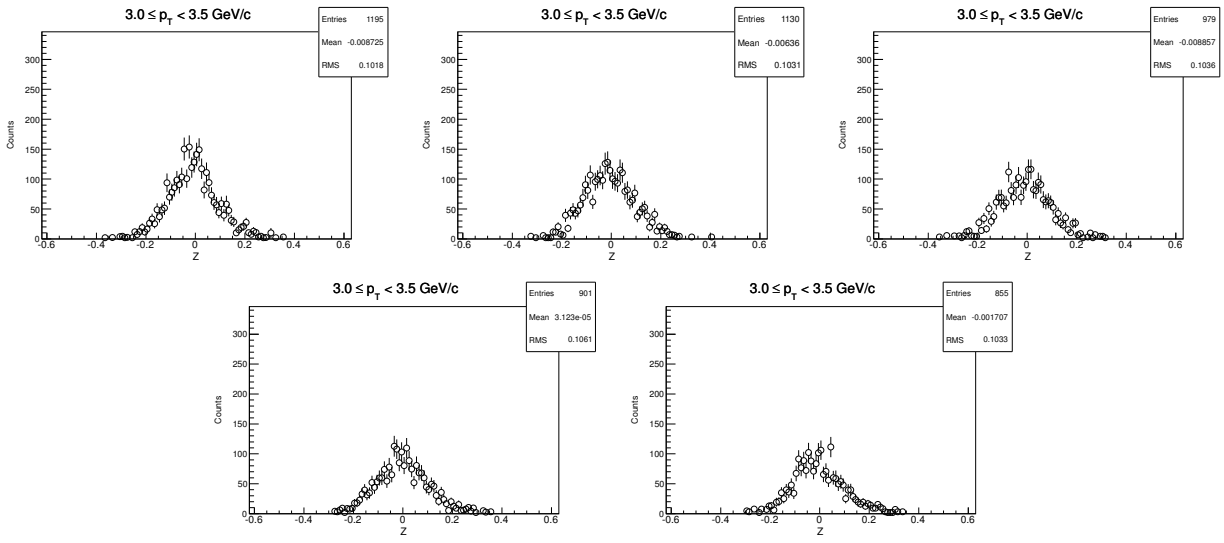
7.4.5 Z-distribution of \bar{d} for $1.9 < p_T < 2.5 \text{ GeV}/c$ ($\sqrt{s_{NN}} = 39 \text{ GeV}$, 0-80%)



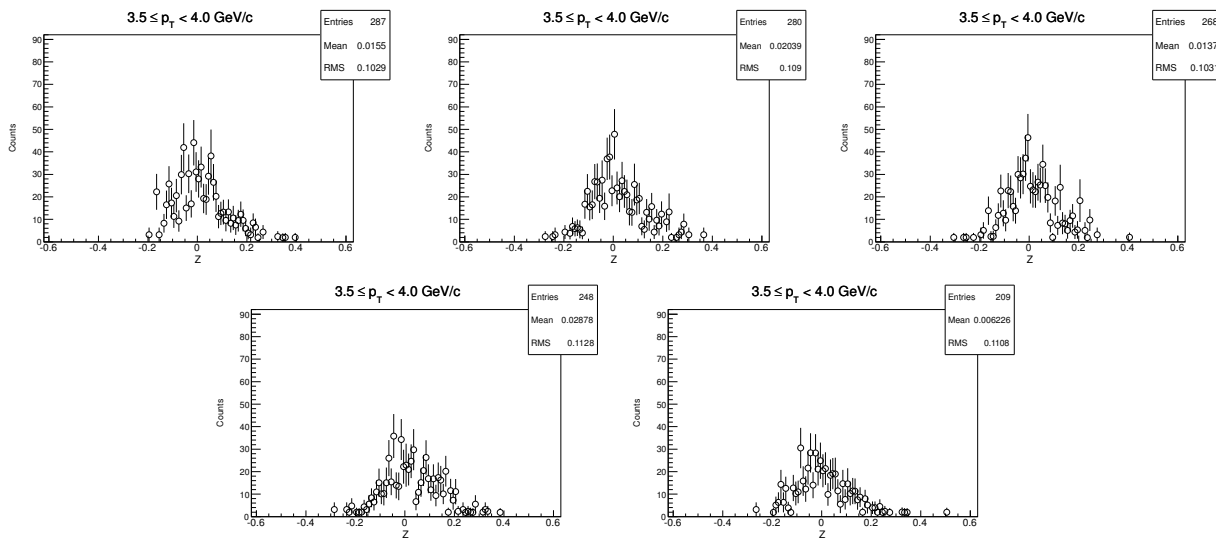
7.4.6 Z-distribution of \bar{d} for $2.5 < p_T < 3.0 \text{ GeV}/c$ ($\sqrt{s_{NN}} = 39 \text{ GeV}$, 0-80%)



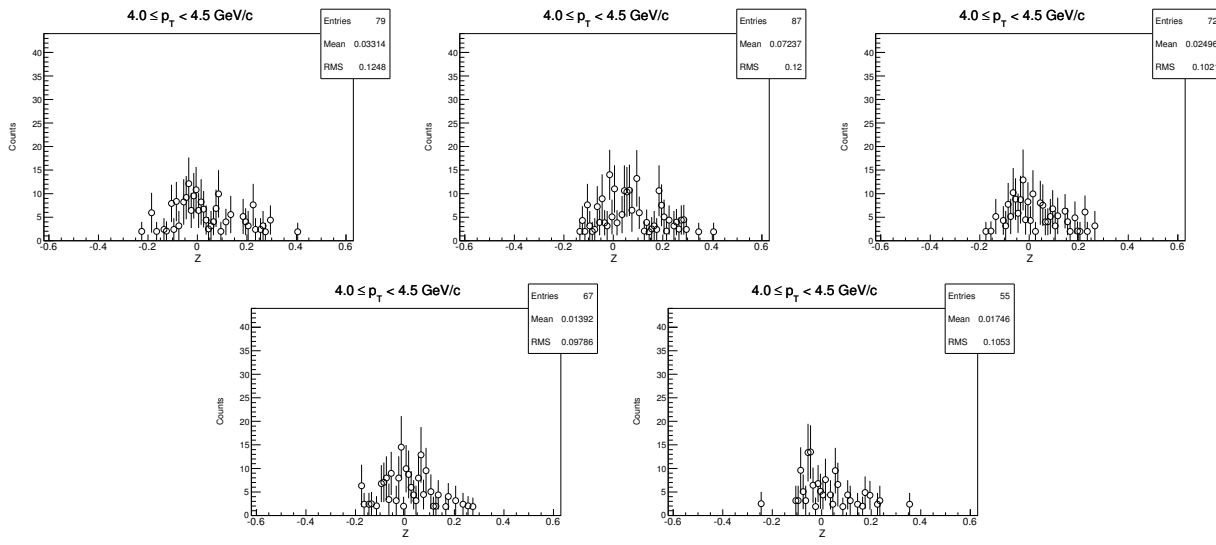
7.4.7 Z-distribution of \bar{d} for $3.0 < p_T < 3.5 \text{ GeV}/c$ ($\sqrt{s_{NN}} = 39 \text{ GeV}$, 0-80%)



7.4.8 Z-distribution of \bar{d} for $3.5 < p_T < 4.0 \text{ GeV}/c$ ($\sqrt{s_{NN}} = 39 \text{ GeV}$, 0-80%)

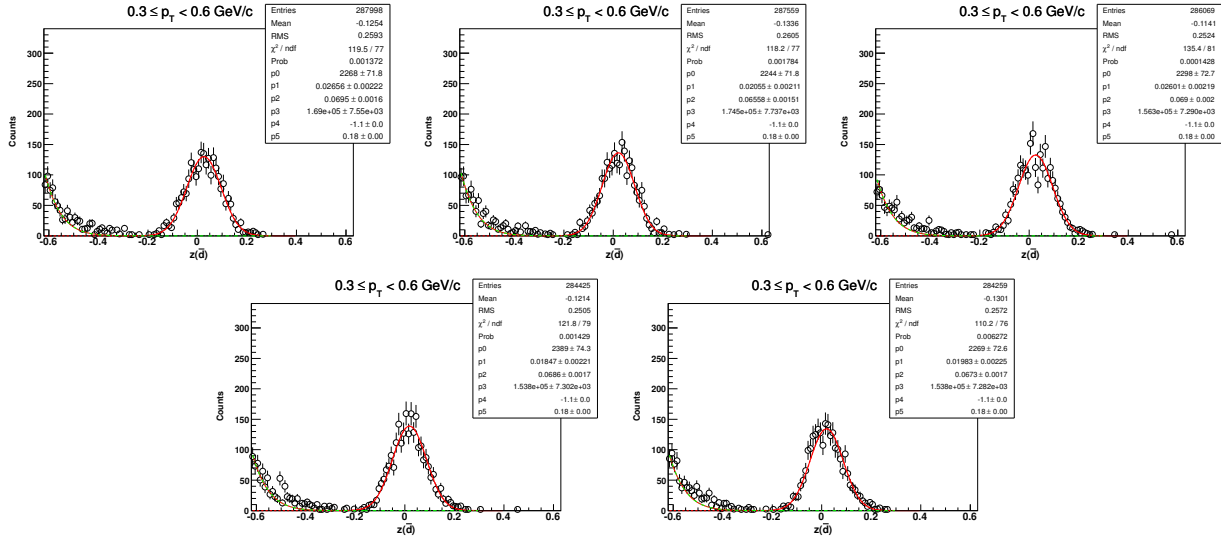


7.4.9 Z-distribution of \bar{d} for $4.0 < p_T < 4.5 \text{ GeV}/c$ ($\sqrt{s_{NN}} = 39 \text{ GeV}$, 0-80%)

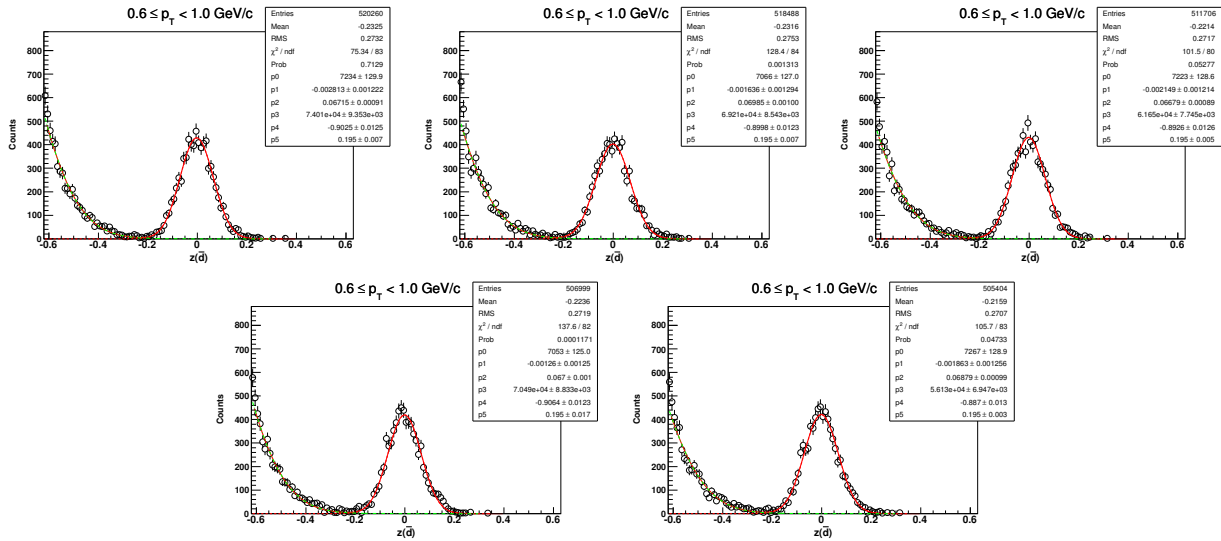


7.5 Centrality: 0-30%

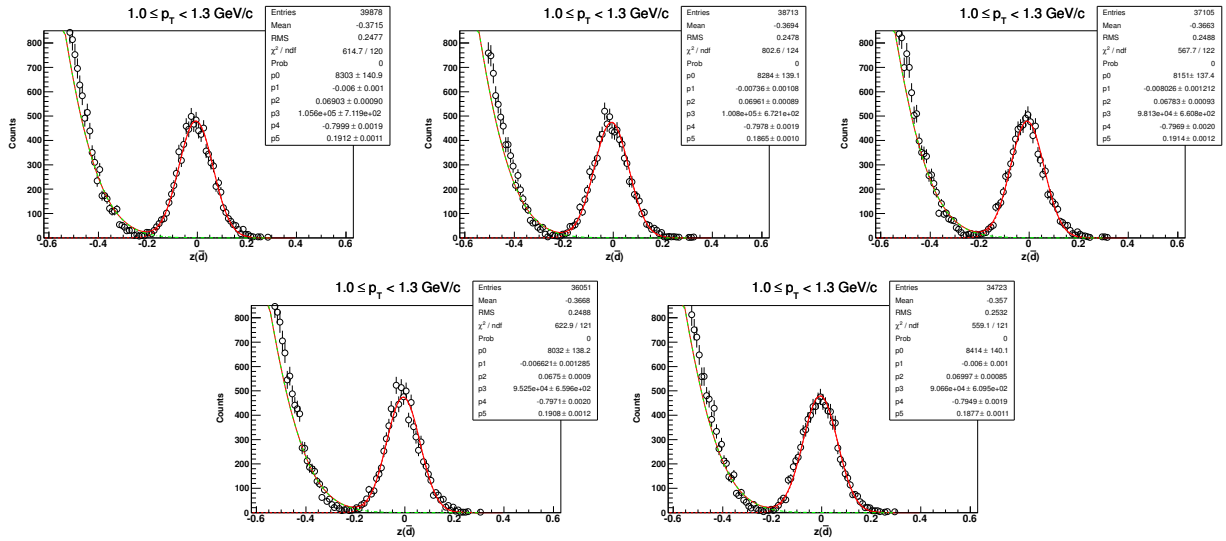
7.5.1 Z-distribution of \bar{d} for $0.3 < p_T < 0.6 \text{ GeV}/c$



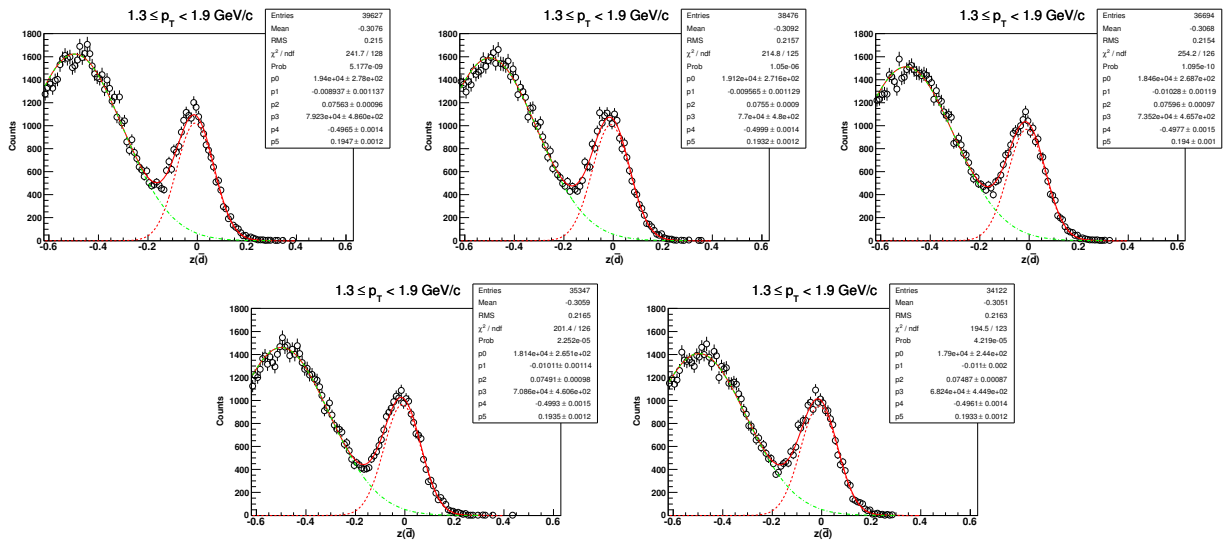
7.5.2 Z-distribution of \bar{d} for $0.6 < p_T < 1.0 \text{ GeV}/c$ ($\sqrt{s_{NN}} = 39 \text{ GeV}$, 0-30%)



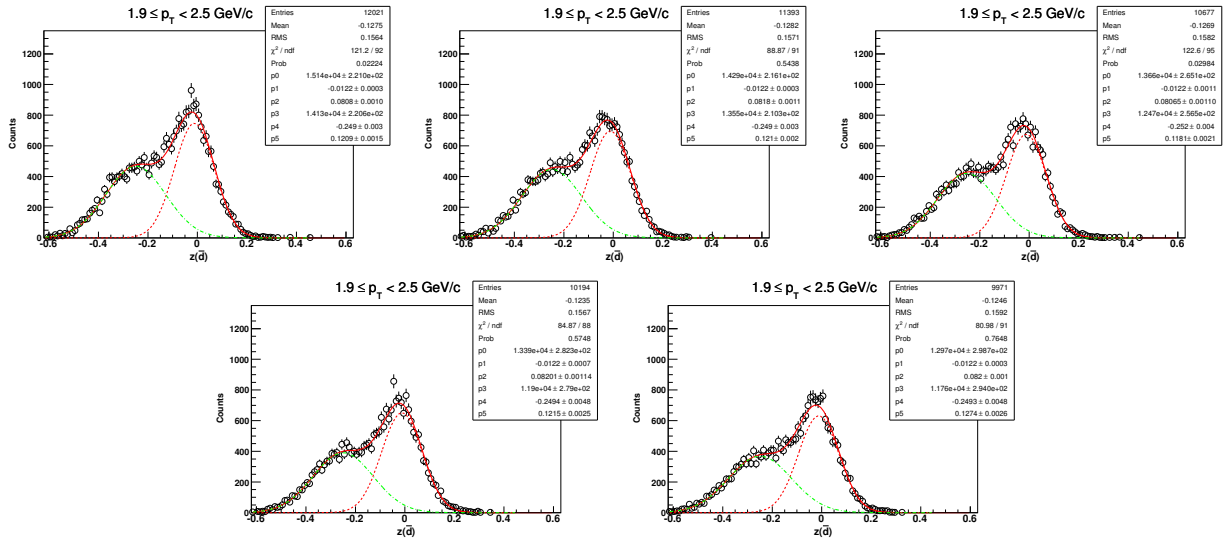
7.5.3 Z-distribution of \bar{d} for $1.0 < p_T < 1.3 \text{ GeV}/c$ ($\sqrt{s_{NN}} = 39 \text{ GeV}$, 0-30%)



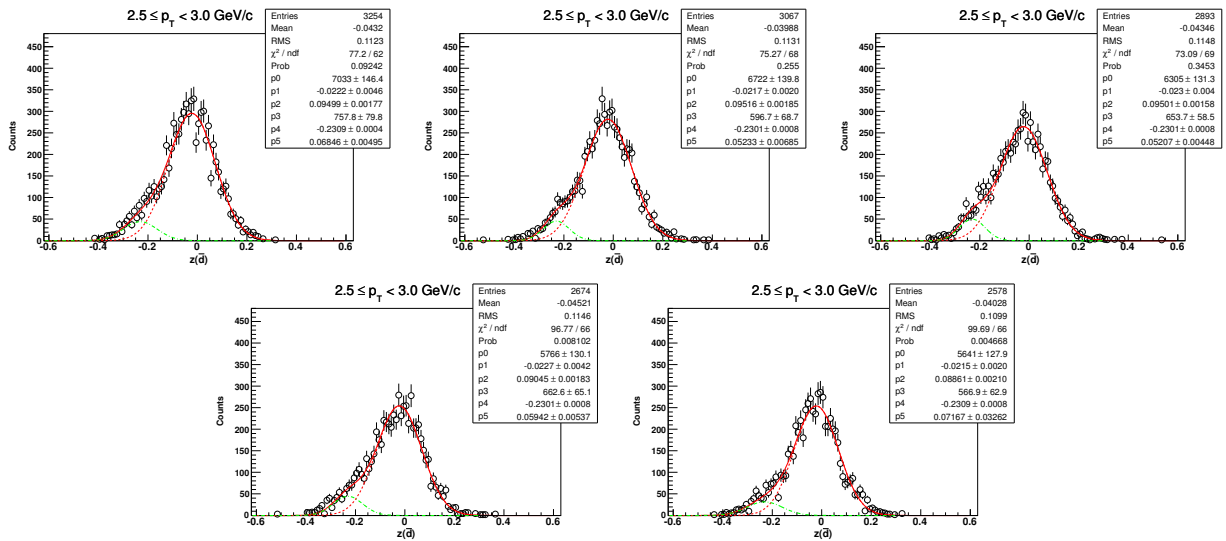
7.5.4 Z-distribution of \bar{d} for $1.3 < p_T < 1.9 \text{ GeV}/c$ ($\sqrt{s_{NN}} = 39 \text{ GeV}$, 0-30%)



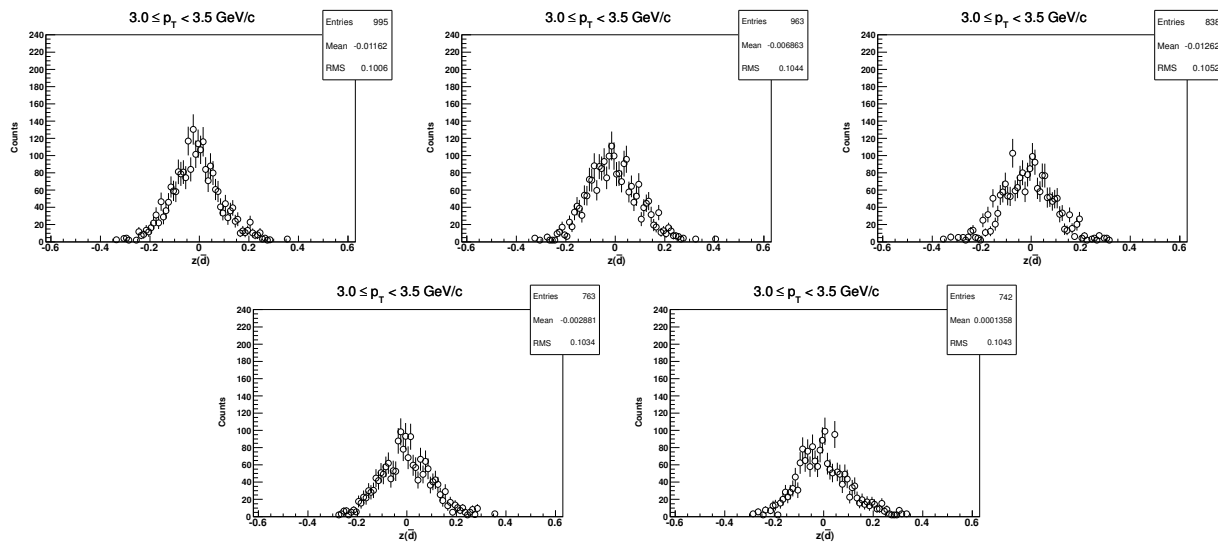
7.5.5 Z-distribution of \bar{d} for $1.9 < p_T < 2.5 \text{ GeV}/c$ ($\sqrt{s_{NN}} = 39 \text{ GeV}$, 0-30%)



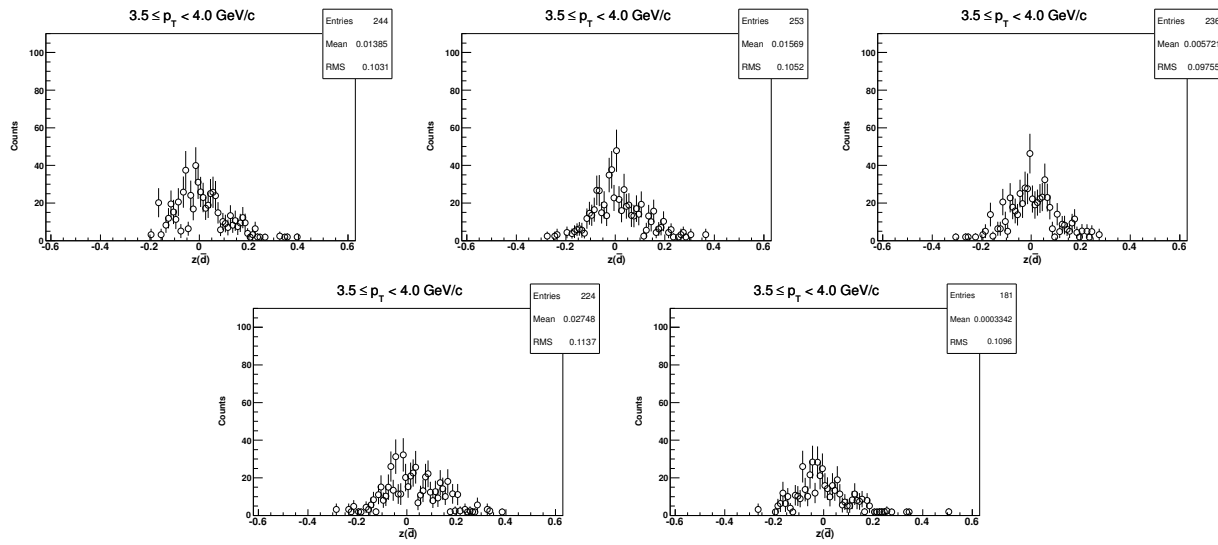
7.5.6 Z-distribution of \bar{d} for $2.5 < p_T < 3.0 \text{ GeV}/c$ ($\sqrt{s_{NN}} = 39 \text{ GeV}$, 0-30%)



7.5.7 Z-distribution of \bar{d} for $3.0 < p_T < 3.5 \text{ GeV}/c$ ($\sqrt{s_{NN}} = 39 \text{ GeV}$, 0-30%)

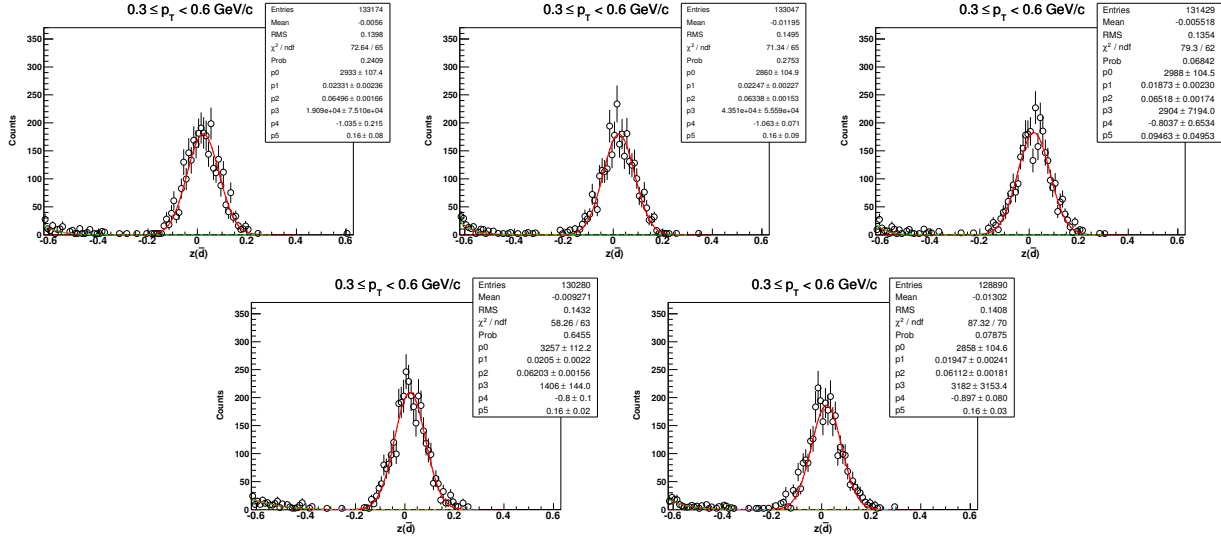


7.5.8 Z-distribution of \bar{d} for $3.5 < p_T < 4.0 \text{ GeV}/c$ ($\sqrt{s_{NN}} = 39 \text{ GeV}$, 0-30%)

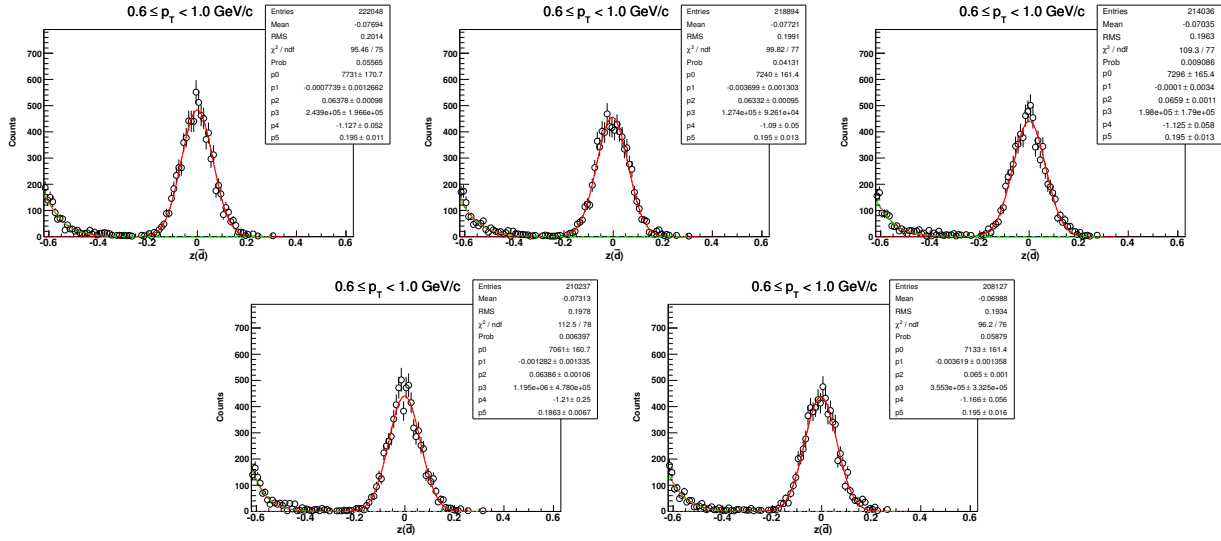


7.6 Centrality: 30-80%

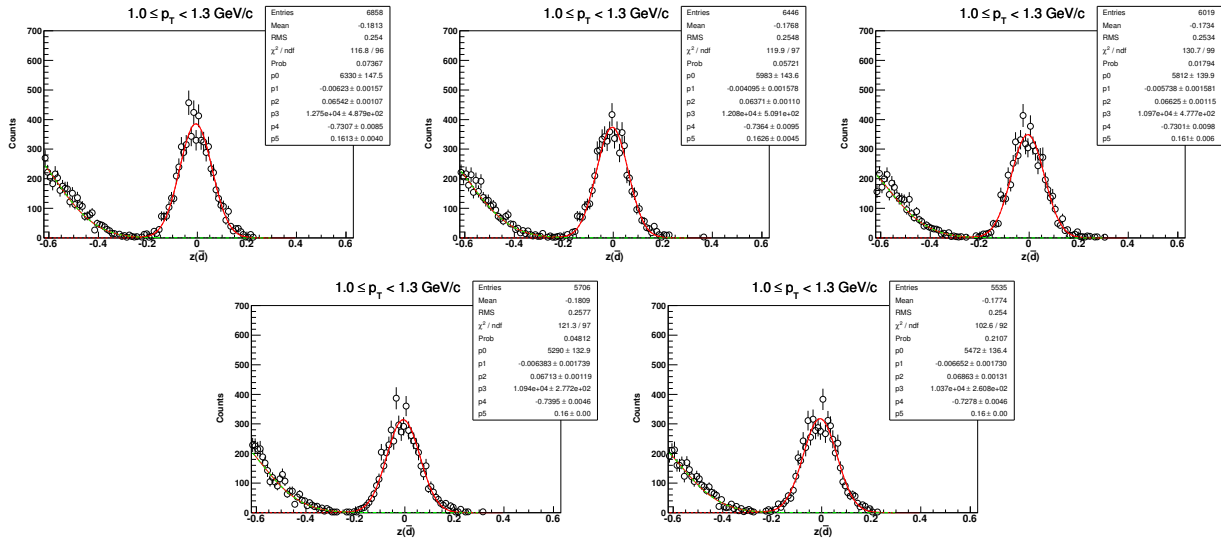
7.6.1 Z-distribution of \bar{d} for $0.3 < p_T < 0.6 \text{ GeV}/c$ ($\sqrt{s_{NN}} = 39 \text{ GeV}, 30\text{-}80\%$)



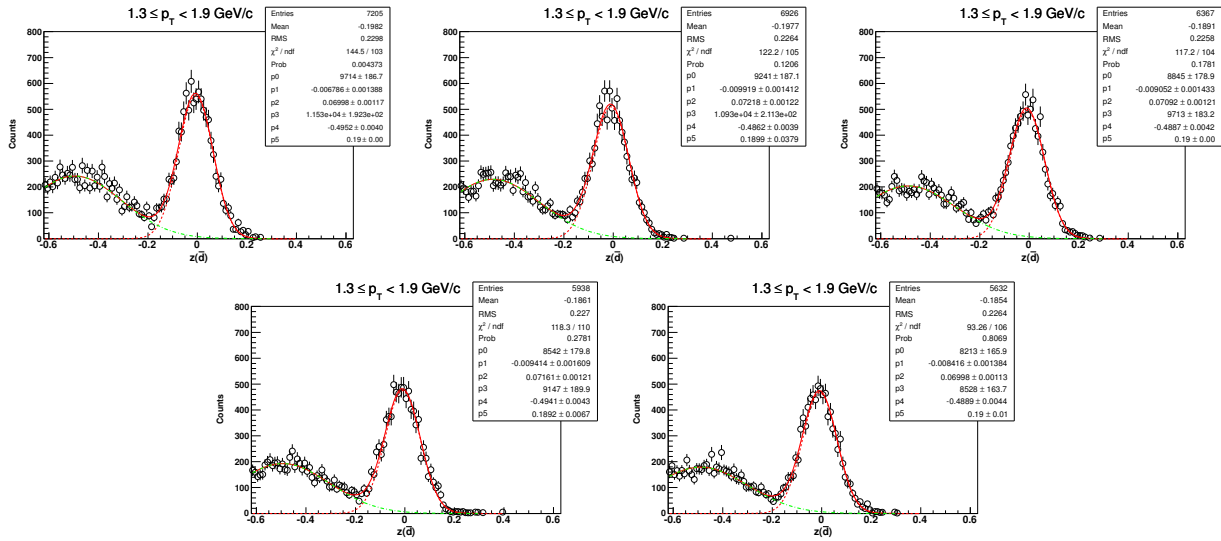
7.6.2 Z-distribution of \bar{d} for $0.6 < p_T < 1.0 \text{ GeV}/c$ ($\sqrt{s_{NN}} = 39 \text{ GeV}, 30\text{-}80\%$)



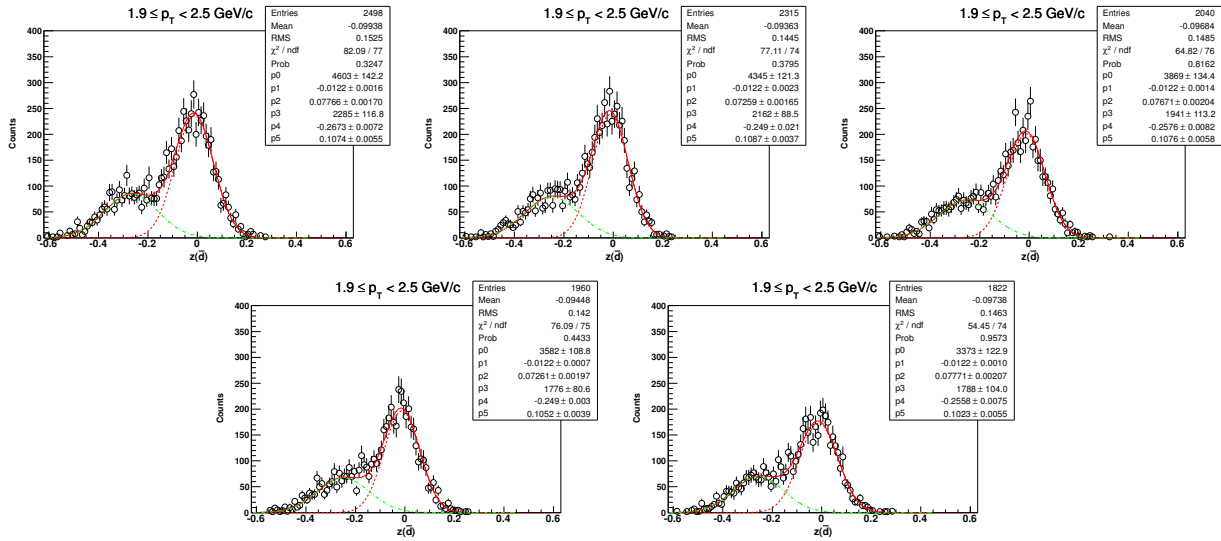
7.6.3 Z-distribution of \bar{d} for $1.0 < p_T < 1.3 \text{ GeV}/c$ ($\sqrt{s_{NN}} = 39 \text{ GeV}$, 30-80%)



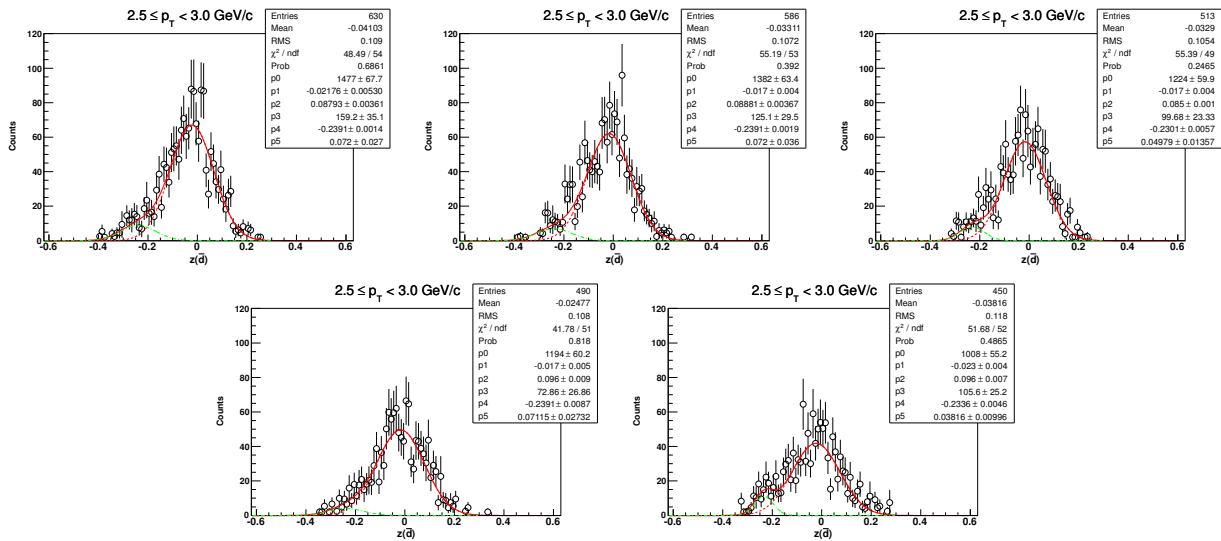
7.6.4 Z-distribution of \bar{d} for $1.3 < p_T < 1.9 \text{ GeV}/c$ ($\sqrt{s_{NN}} = 39 \text{ GeV}$, 30-80%)



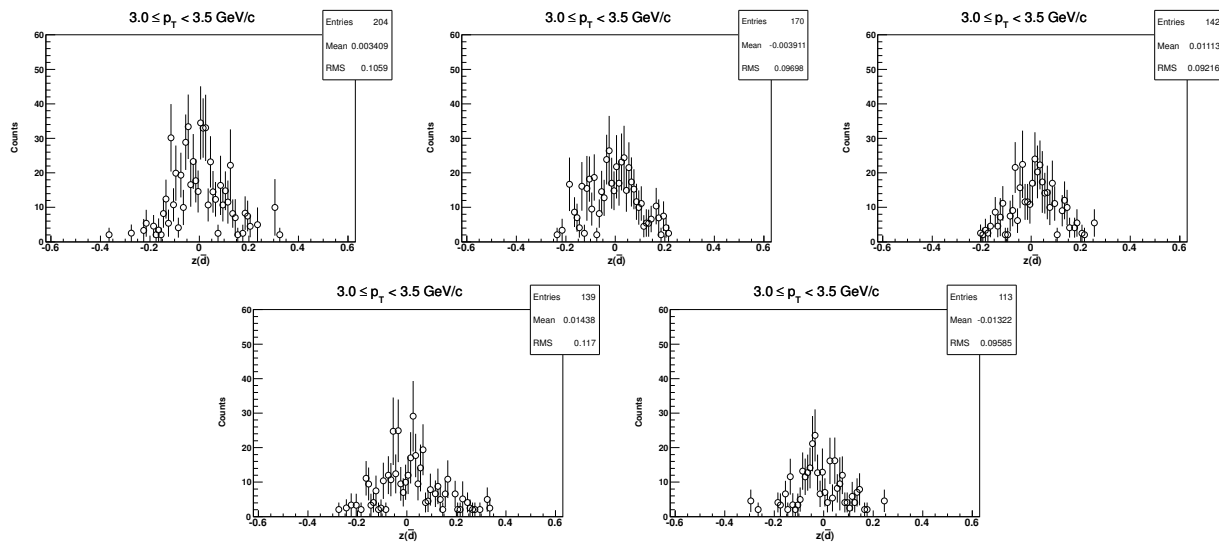
7.6.5 Z-distribution of \bar{d} for $1.9 < p_T < 2.5$ GeV/c ($\sqrt{s_{NN}} = 39$ GeV, 30-80%)



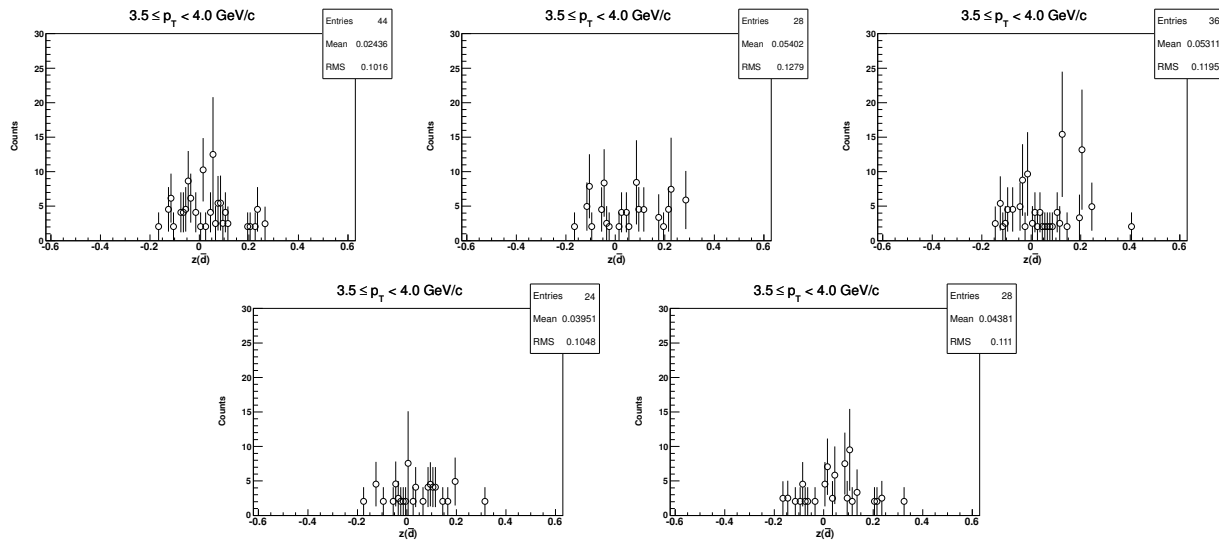
7.6.6 Z-distribution of \bar{d} for $2.5 < p_T < 3.0$ GeV/c ($\sqrt{s_{NN}} = 39$ GeV, 30-80%)



7.6.7 Z-distribution of \bar{d} for $3.0 < p_T < 3.5 \text{ GeV}/c$ ($\sqrt{s_{NN}} = 39 \text{ GeV}$, 30-80%)

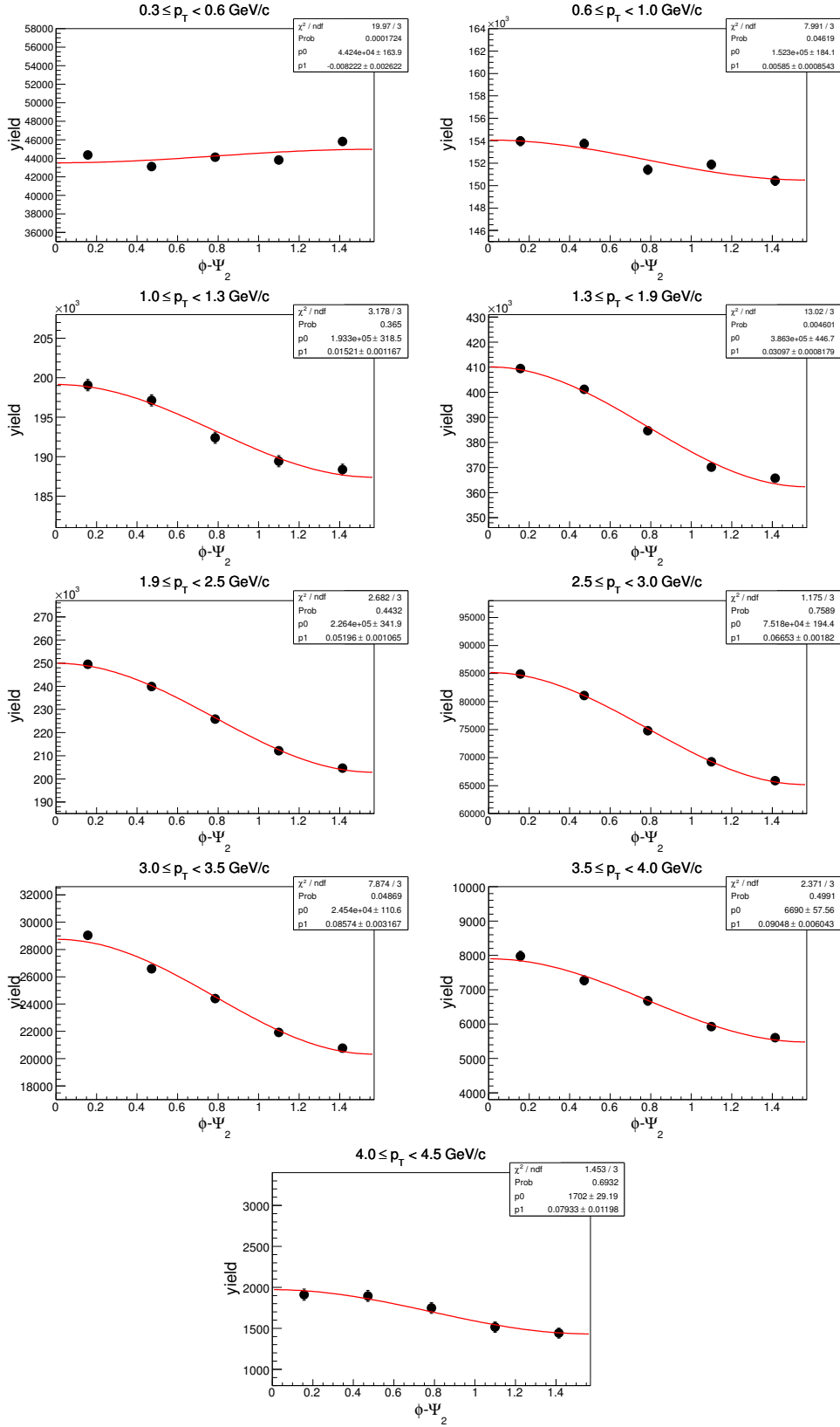


7.6.8 Z-distribution of \bar{d} for $3.5 < p_T < 4.0 \text{ GeV}/c$ ($\sqrt{s_{NN}} = 39 \text{ GeV}$, 30-80%)

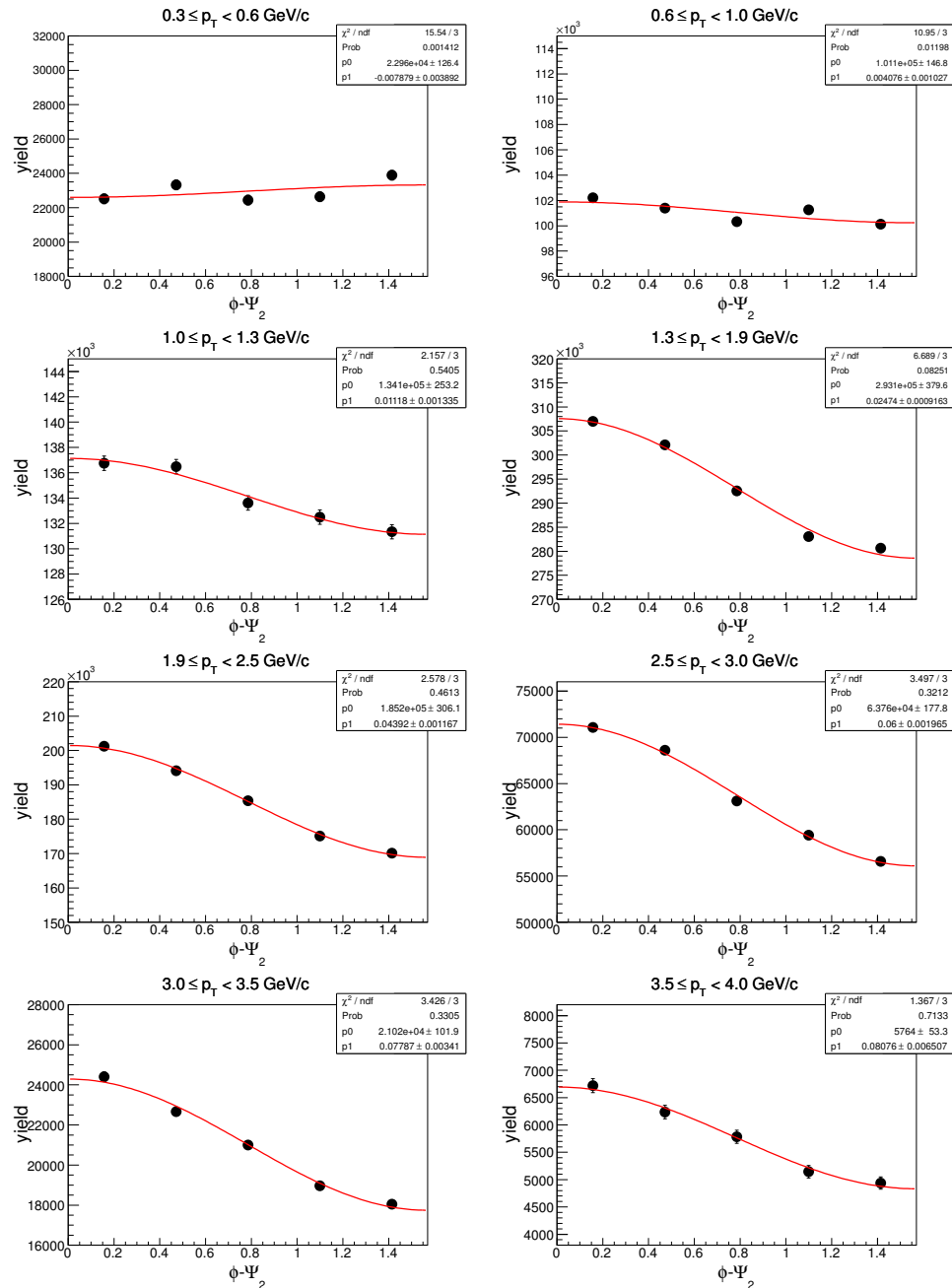


7.7 $\phi - \Psi_2$ distributions in Au+Au at $\sqrt{s_{NN}} = 39$ GeV

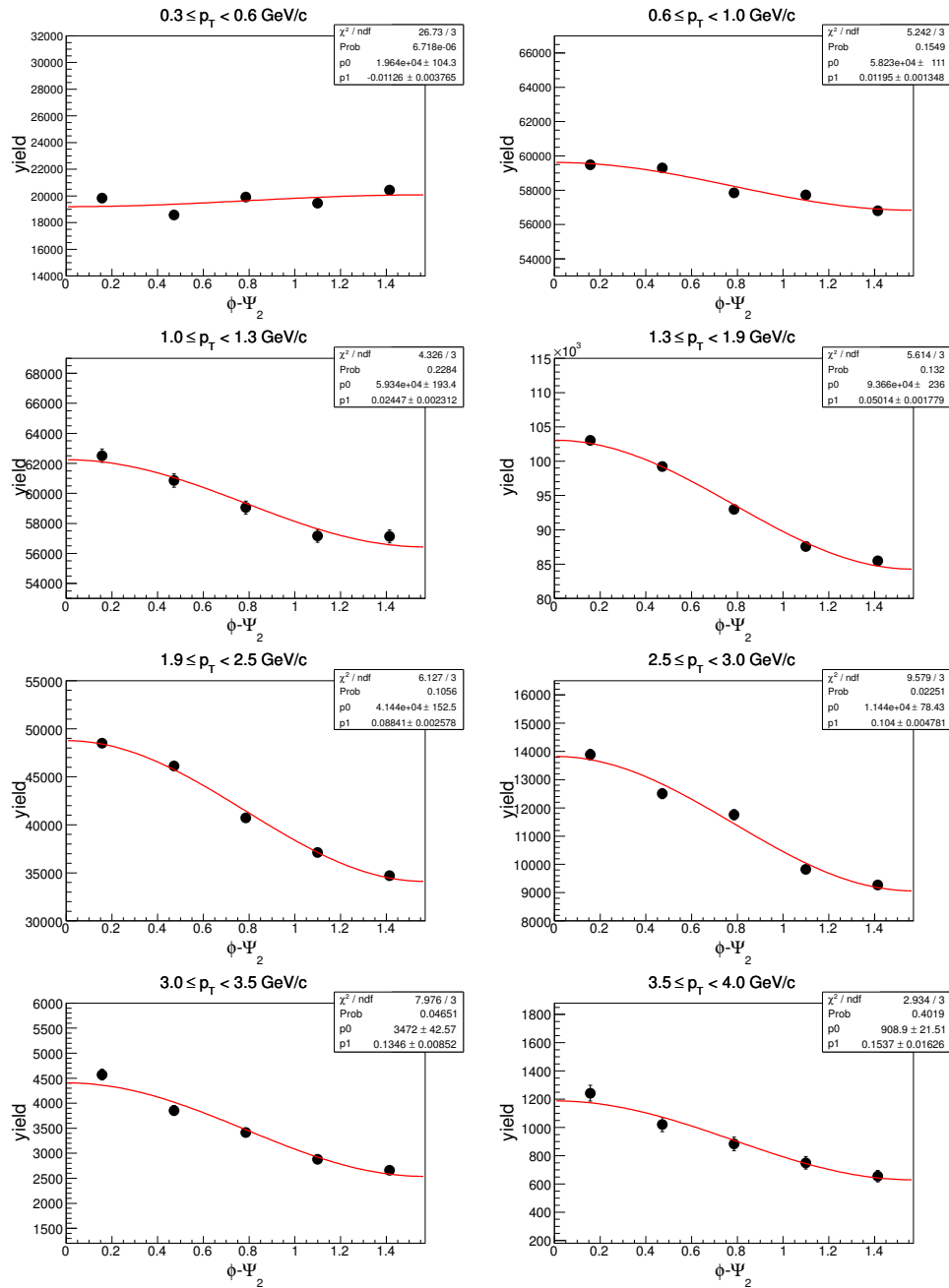
7.7.1 $\phi - \Psi_2$ of d in centrality: 0-80%



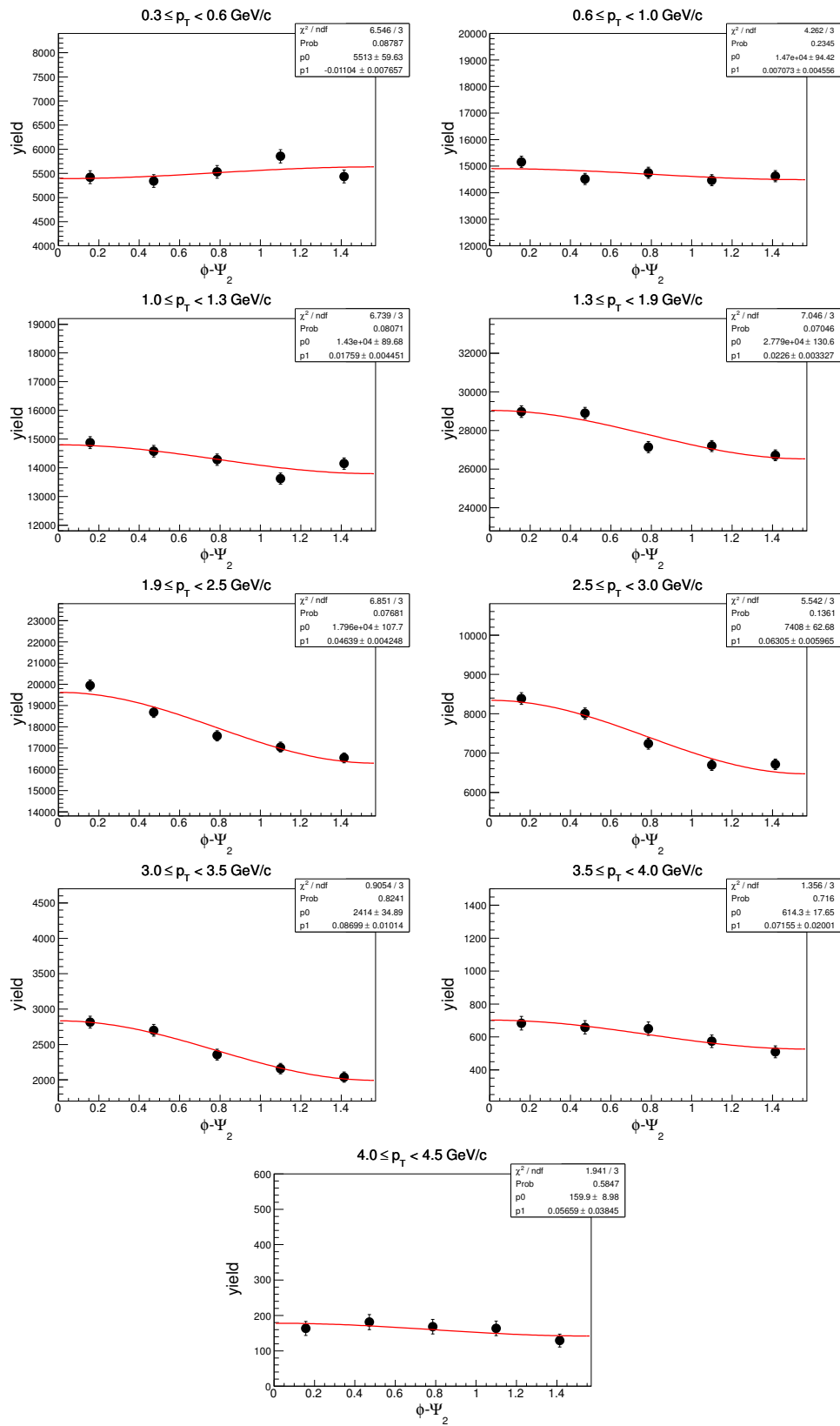
7.7.2 $\phi - \Psi_2$ of d in centrality: 0-30% ($\sqrt{s_{NN}} = 39$ GeV)



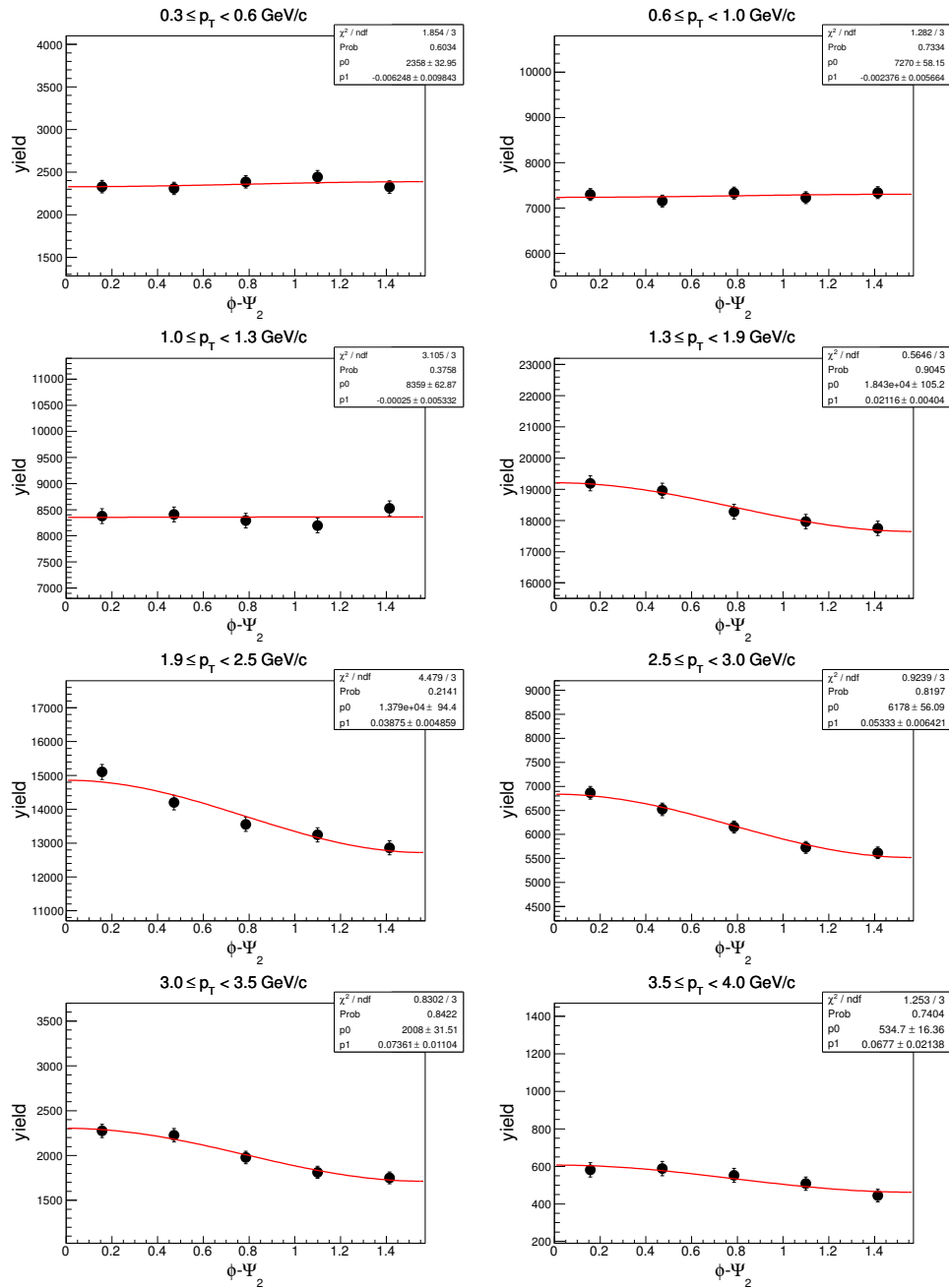
7.7.3 $\phi - \Psi_2$ of d in centrality: 30-80% ($\sqrt{s_{NN}} = 39$ GeV)



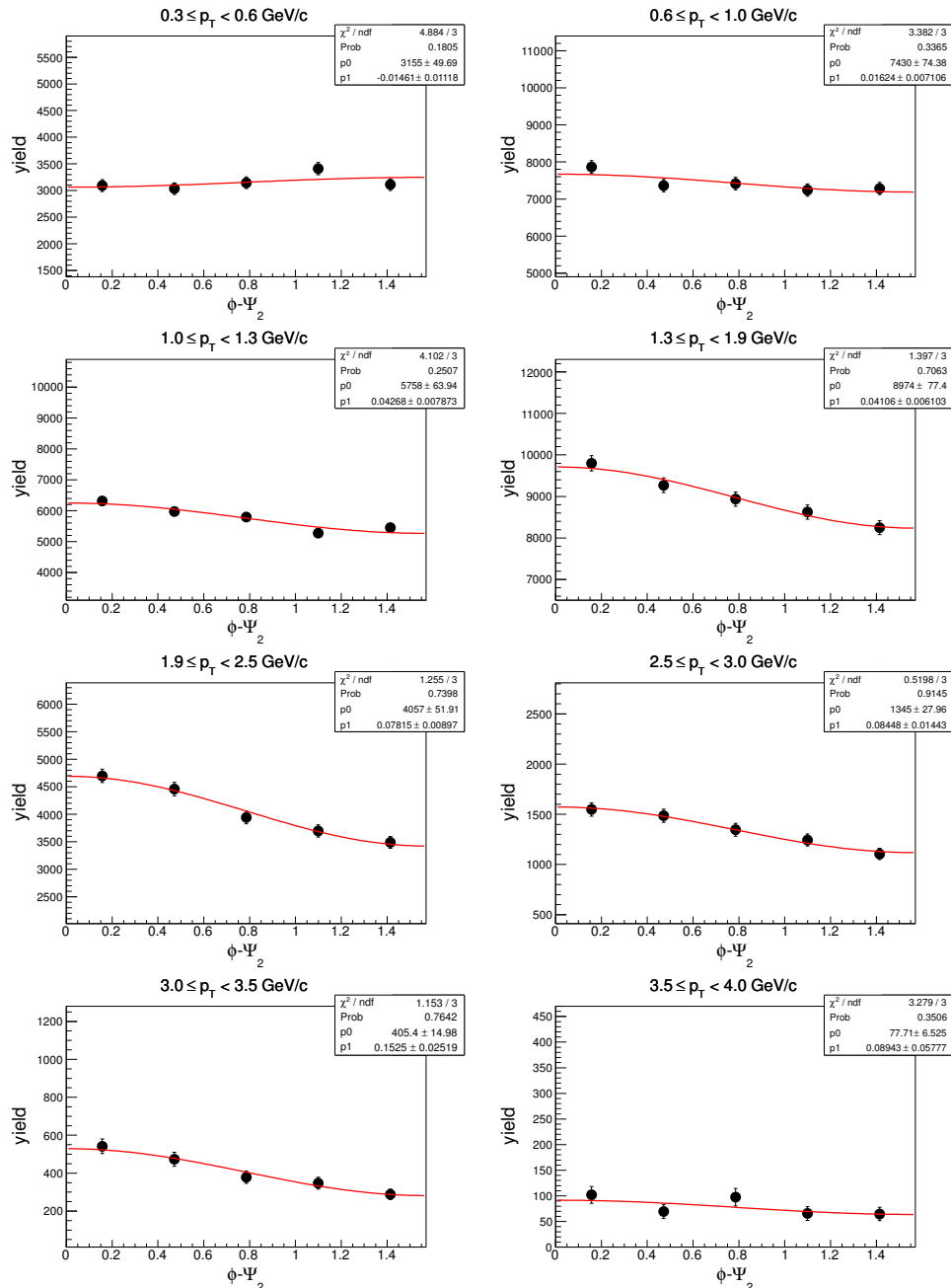
7.7.4 $\phi - \Psi_2$ of \bar{d} in centrality: 0-80% ($\sqrt{s_{NN}} = 39$ GeV)



7.7.5 $\phi - \Psi_2$ of \bar{d} in centrality: 0-30% ($\sqrt{s_{NN}} = 39$ GeV)

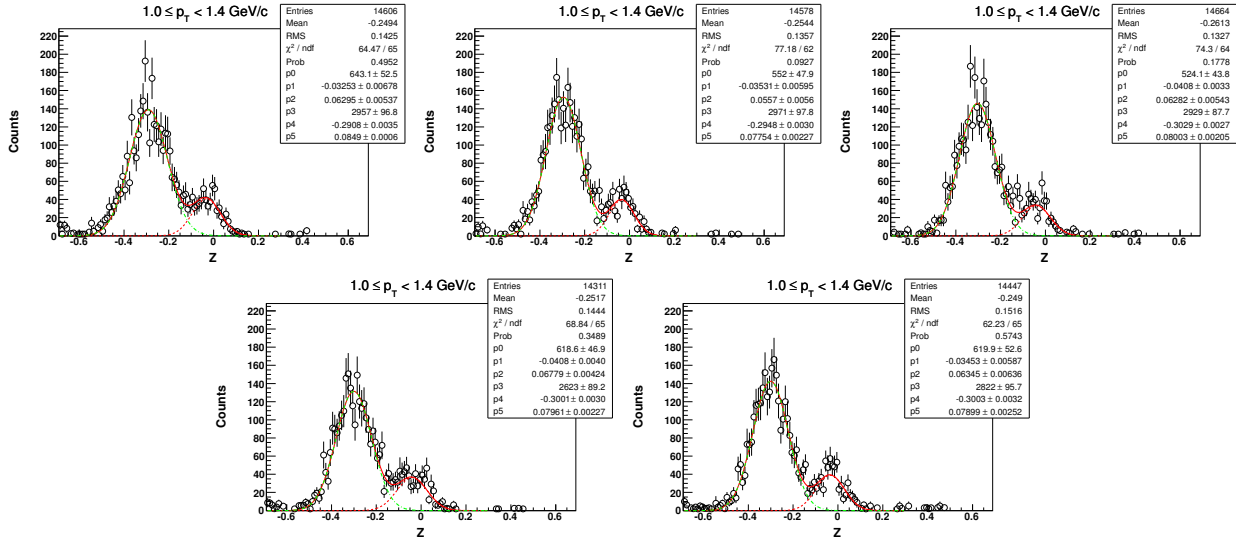


7.7.6 $\phi - \Psi_2$ of \bar{d} in centrality: 30-80% ($\sqrt{s_{NN}} = 39$ GeV)

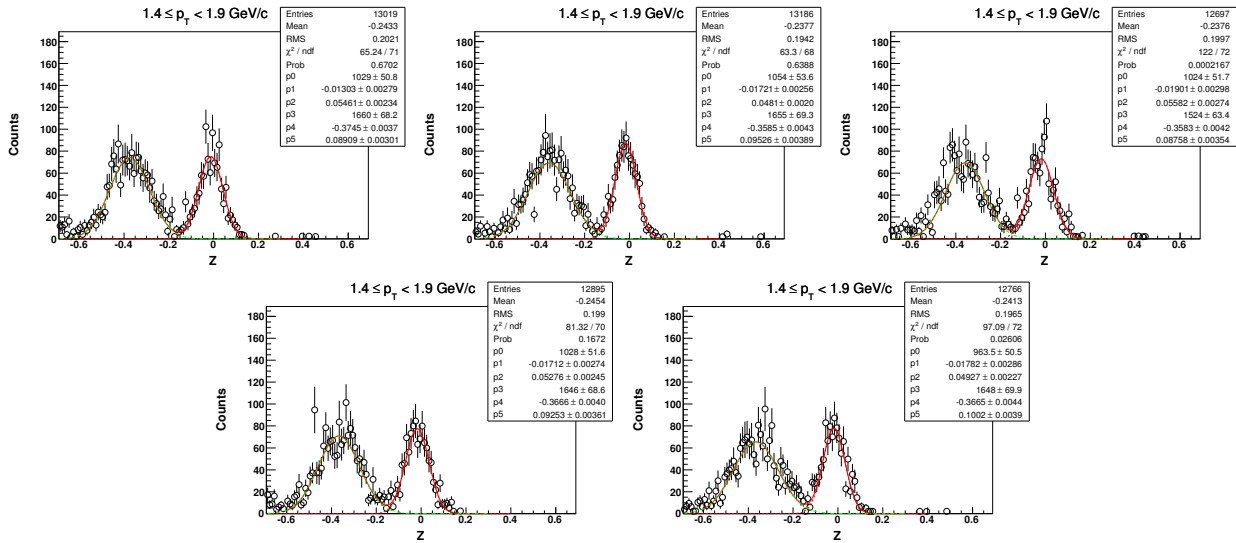


7.8 Z distribution of 3He in $\sqrt{s_{NN}} = 39$ GeV (centrality: 0-80%)

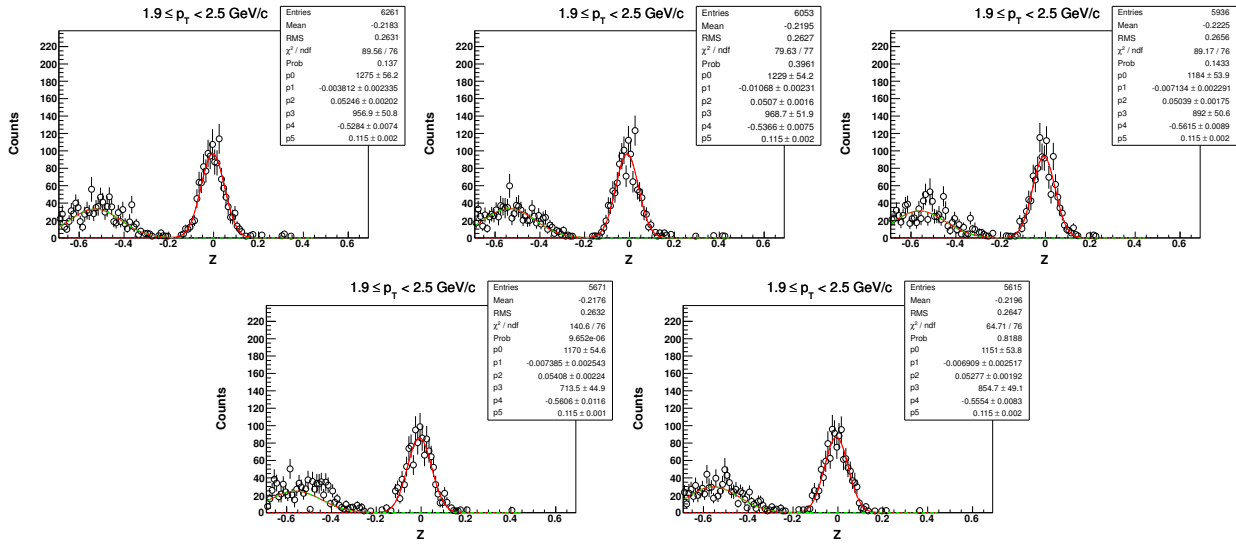
7.8.1 Z-distribution of 3He for $1.0 \leq p_T < 1.4$ GeV/c



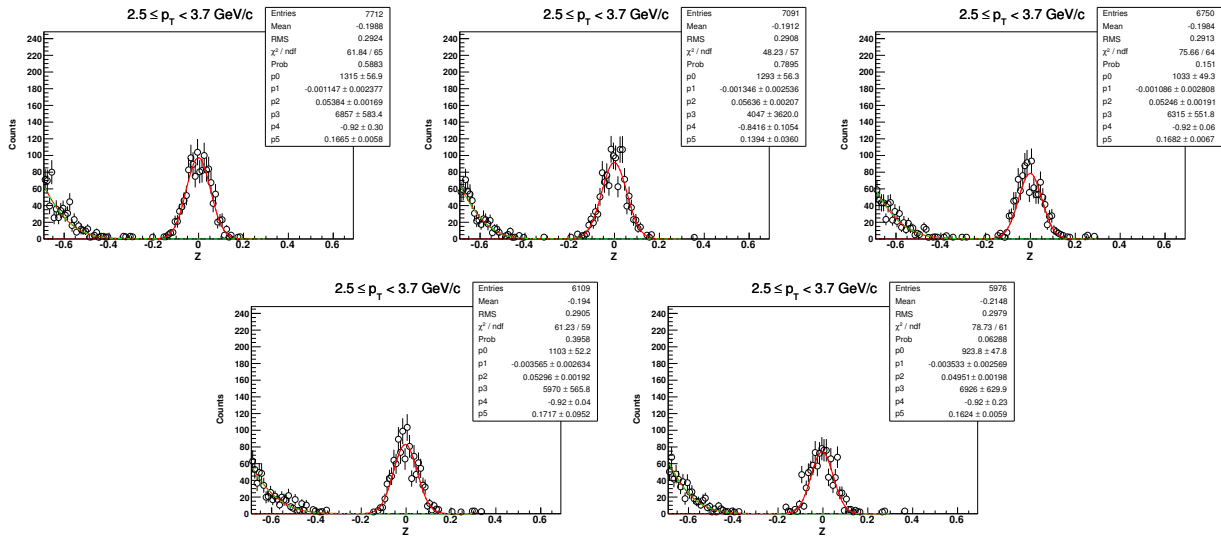
7.8.2 Z-distribution of 3He for $1.4 < p_T < 1.9$ GeV/c ($\sqrt{s_{NN}} = 39$ GeV, 0-80%)



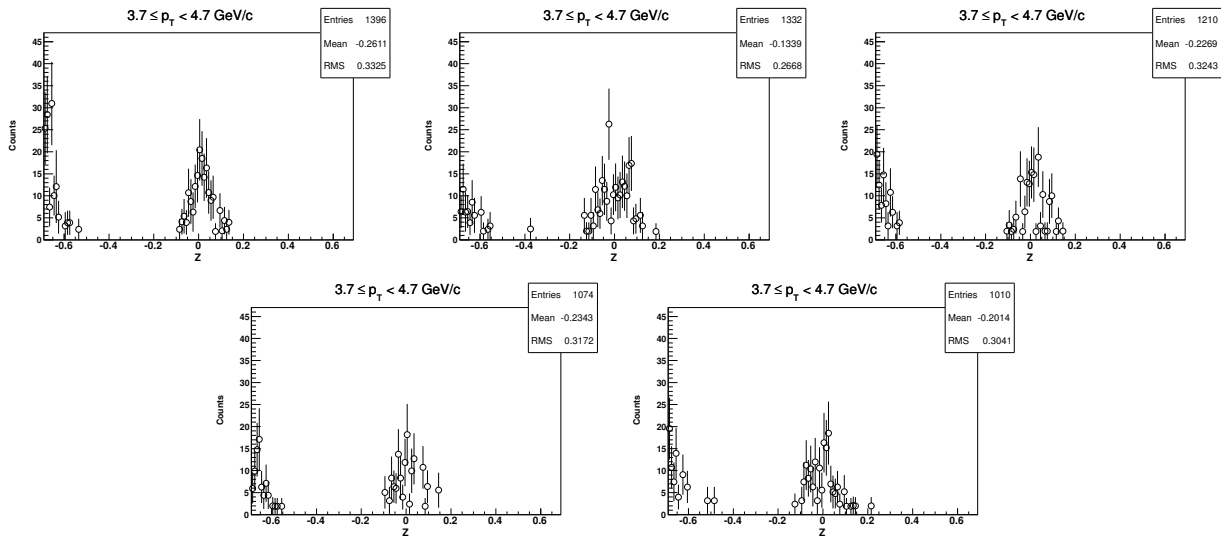
7.8.3 Z-distribution of 3He for $1.9 < p_T < 2.5 \text{ GeV}/c$ ($\sqrt{s_{NN}} = 39 \text{ GeV}$, 0-80%)



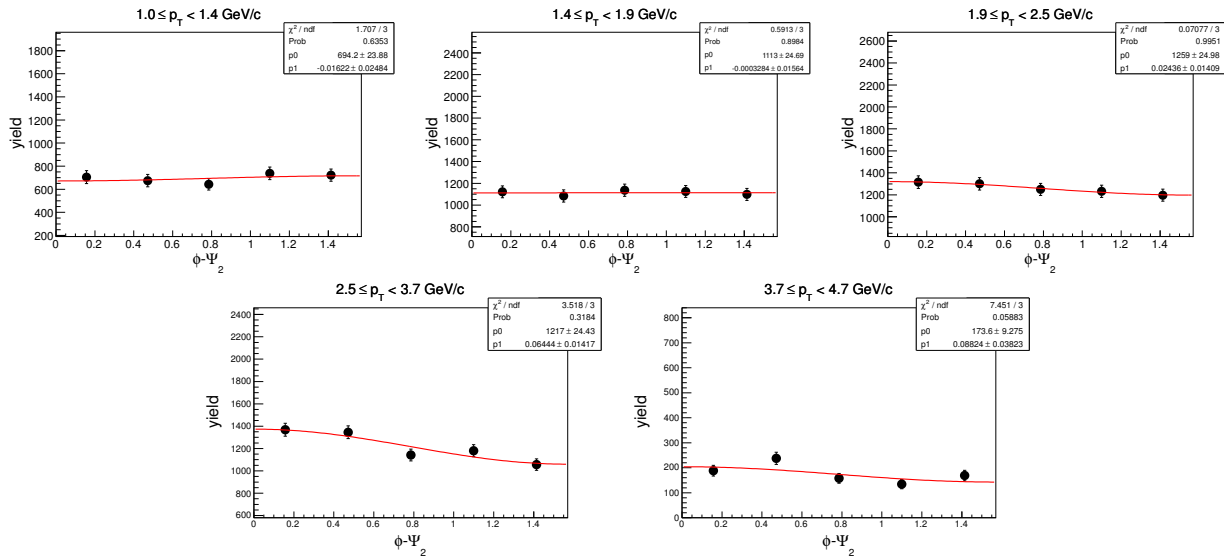
7.8.4 Z-distribution of 3He for $2.5 < p_T < 3.7 \text{ GeV}/c$ ($\sqrt{s_{NN}} = 39 \text{ GeV}$, 0-80%)



7.8.5 Z-distribution of ^3He for $3.7 < p_T < 4.7 \text{ GeV}/c$ ($\sqrt{s_{NN}} = 39 \text{ GeV}$, 0-80%)

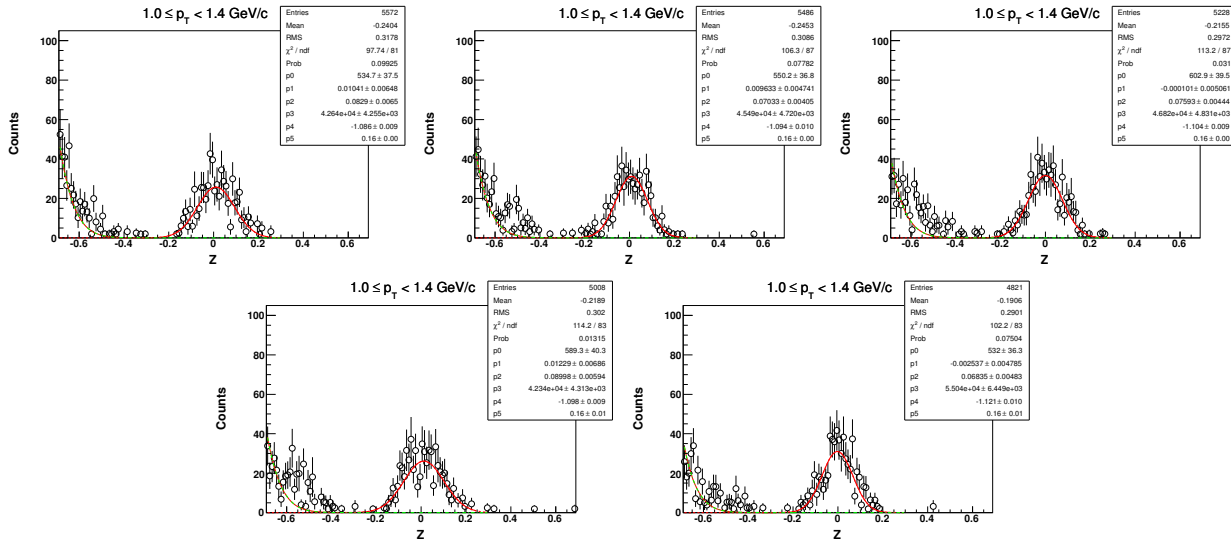


7.8.6 $\phi - \Psi_2$ of ^3He in centrality: 0-80% ($\sqrt{s_{NN}} = 39 \text{ GeV}$)

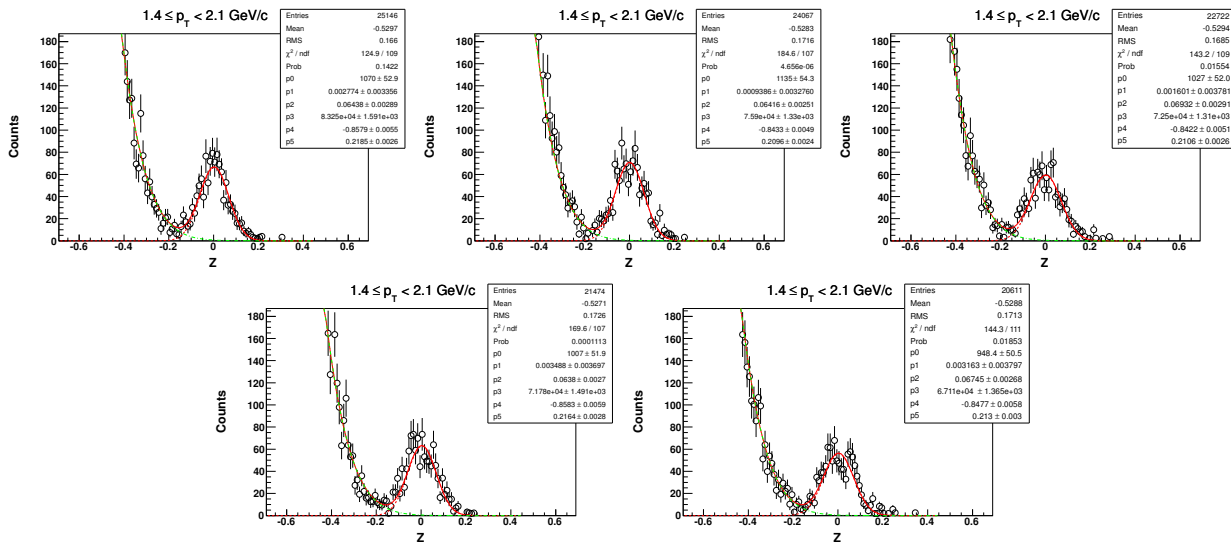


7.9 Z distribution of t in $\sqrt{s_{NN}} = 39 \text{ GeV}$ (centrality: 0-80%)

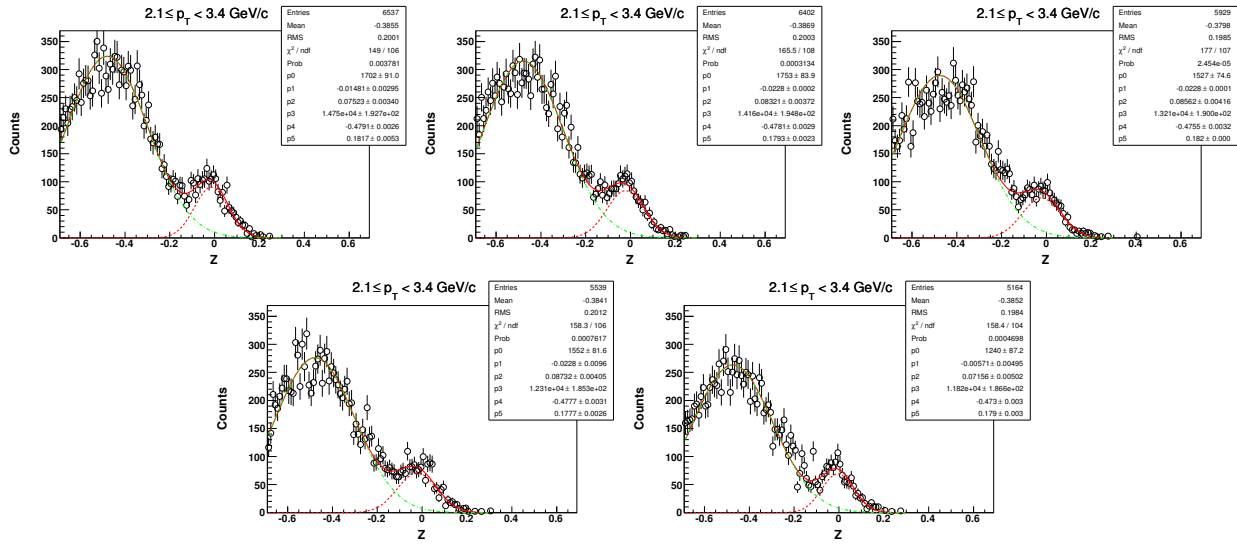
7.9.1 Z-distribution of t for $1.0 < p_T < 1.4 \text{ GeV}/c$



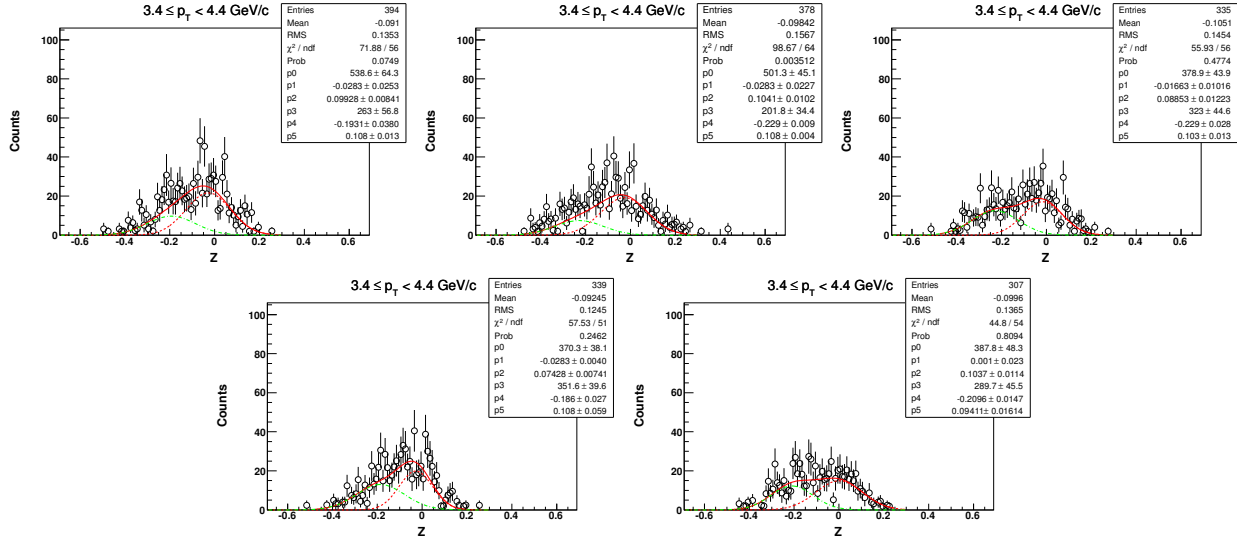
7.9.2 Z-distribution of t for $1.4 < p_T < 2.1 \text{ GeV}/c$ ($\sqrt{s_{NN}} = 39 \text{ GeV}$, 0-80%)



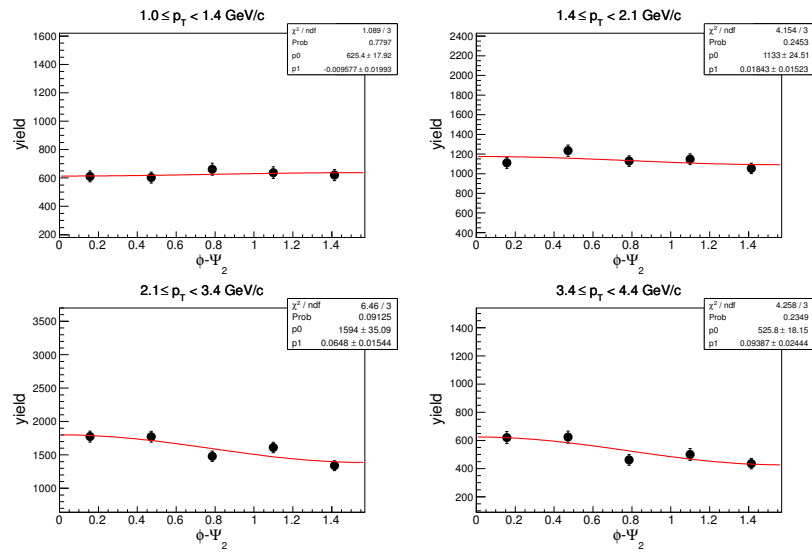
7.9.3 Z-distribution of t for $2.1 < p_T < 3.4 \text{ GeV}/c$ ($\sqrt{s_{NN}} = 39 \text{ GeV}$, 0-80%)



7.9.4 Z-distribution of t for $3.4 < p_T < 4.4 \text{ GeV}/c$ ($\sqrt{s_{NN}} = 39 \text{ GeV}$, 0-80%)



7.9.5 $\phi - \Psi_2$ of t in centrality: 0-80% ($\sqrt{s_{NN}} = 39$ GeV)

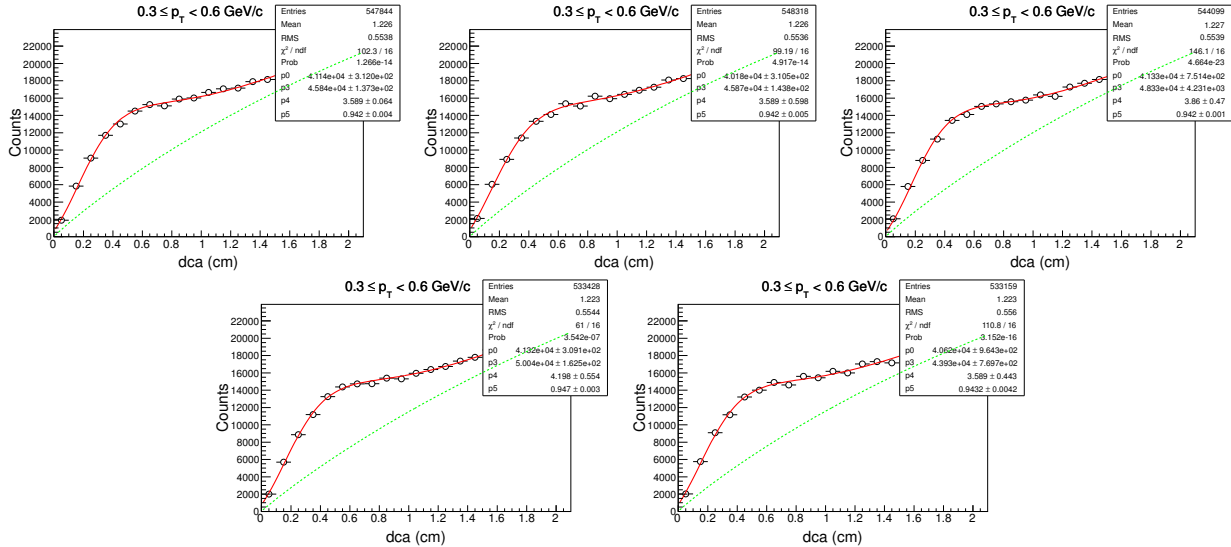


8 DCA and Z-distributions for Au+Au at $\sqrt{s_{NN}} = 27$ GeV

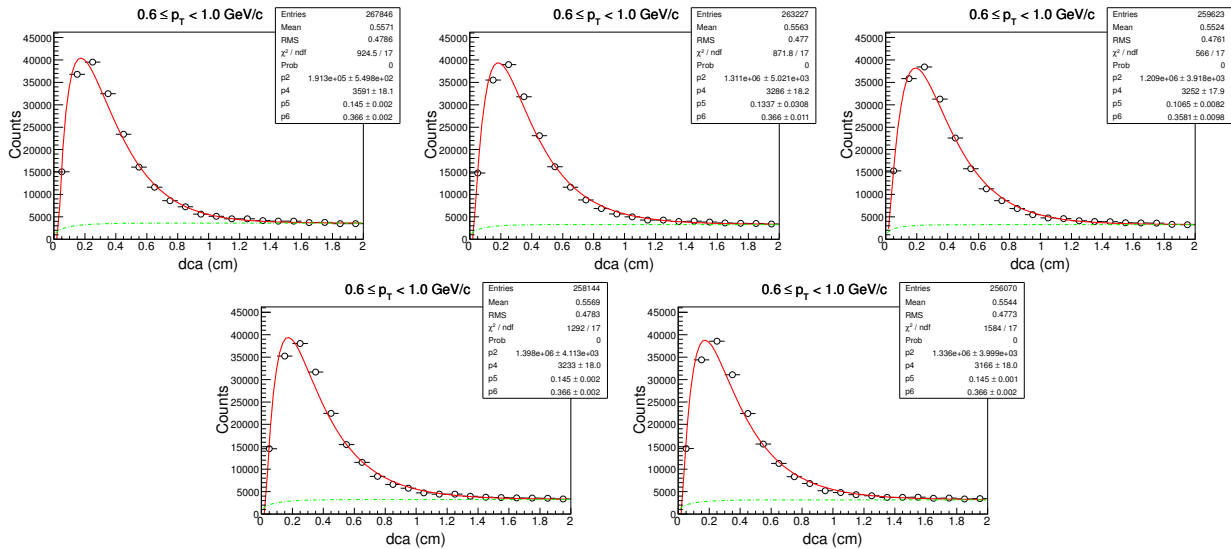
In this section we show the DCA and Z-distribution of deuteron and anti-deuteron for five different ($\phi - \Psi_2$) bins namely, $0 - \frac{\pi}{10}$, $\frac{\pi}{10} - \frac{2\pi}{10}$, $\frac{2\pi}{10} - \frac{3\pi}{10}$, $\frac{3\pi}{10} - \frac{4\pi}{10}$ and $\frac{4\pi}{10} - \frac{5\pi}{10}$. DCA and Z-distribution of d for all centrality and all p_T bins are shown in the later sub-sections.

8.1 Centrality: 0-80%

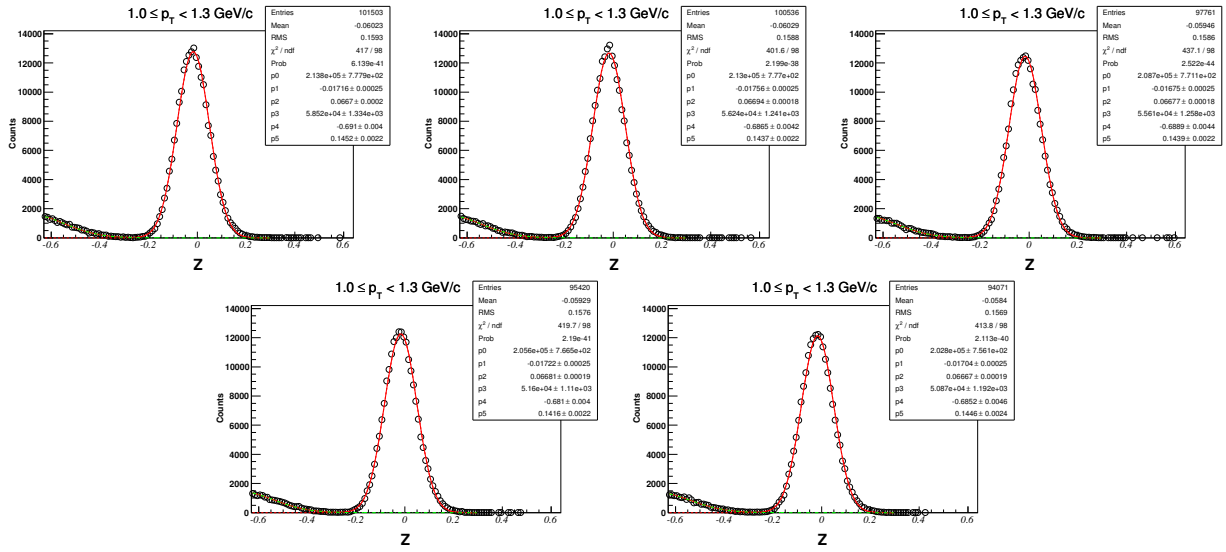
8.1.1 DCA-distribution of d for $0.3 < p_T < 0.6$ GeV/c



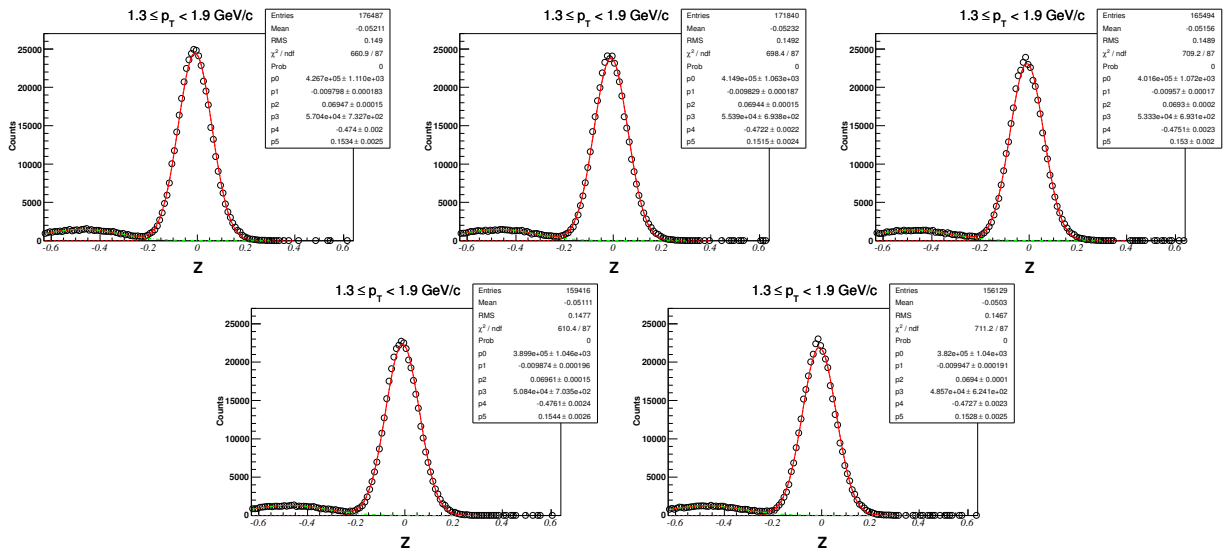
8.1.2 DCA-distribution of d for $0.6 < p_T < 1.0$ GeV/c ($\sqrt{s_{NN}} = 27$ GeV, 0-80%)



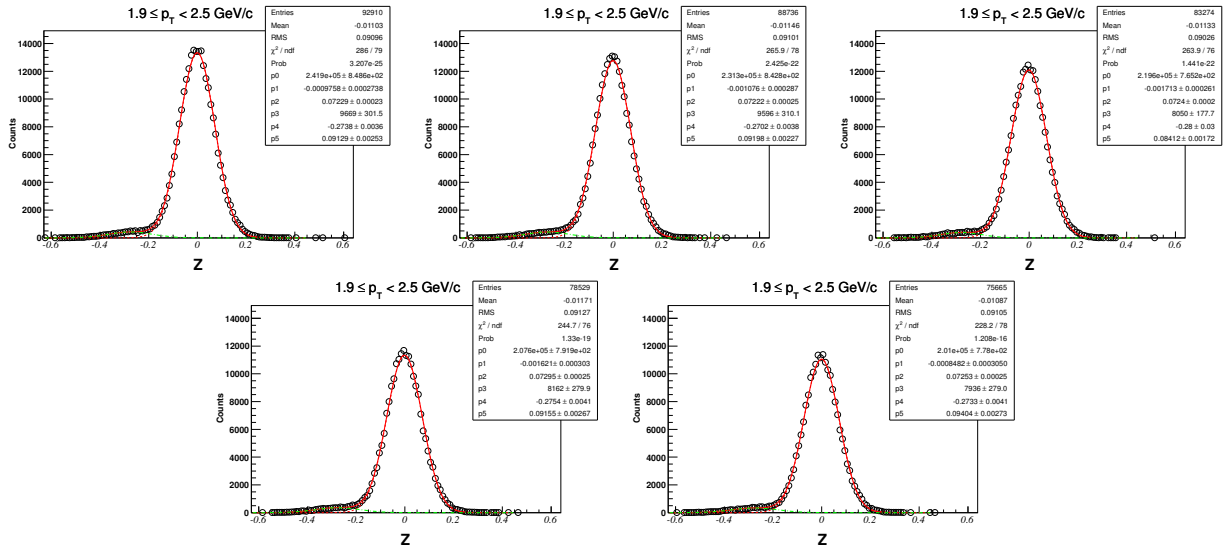
8.1.3 Z-distribution of d for $1.0 < p_T < 1.3 \text{ GeV}/c$ ($\sqrt{s_{NN}} = 27 \text{ GeV}$, 0-80%)



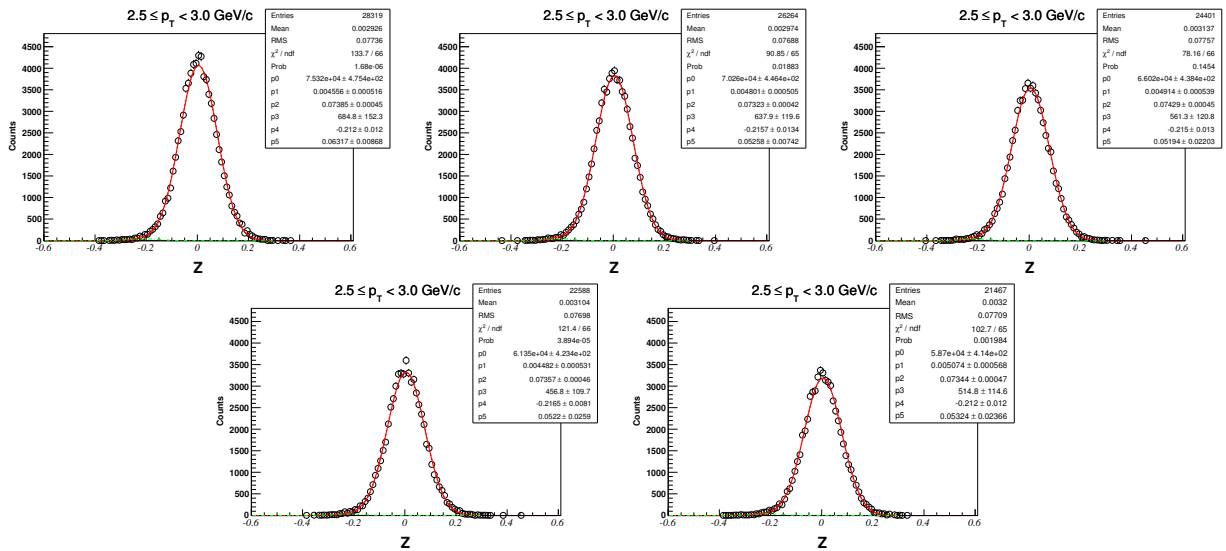
8.1.4 Z-distribution of d for $1.3 < p_T < 1.9 \text{ GeV}/c$ ($\sqrt{s_{NN}} = 27 \text{ GeV}$, 0-80%)



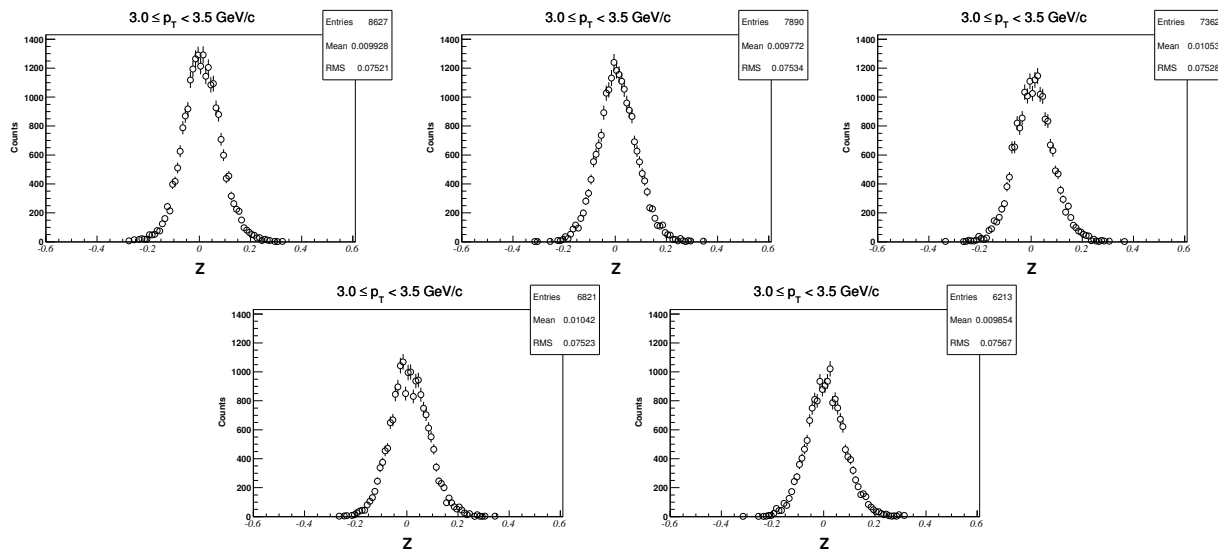
8.1.5 Z-distribution of d for $1.9 < p_T < 2.5 \text{ GeV}/c$ ($\sqrt{s_{NN}} = 27 \text{ GeV}$, 0-80%)



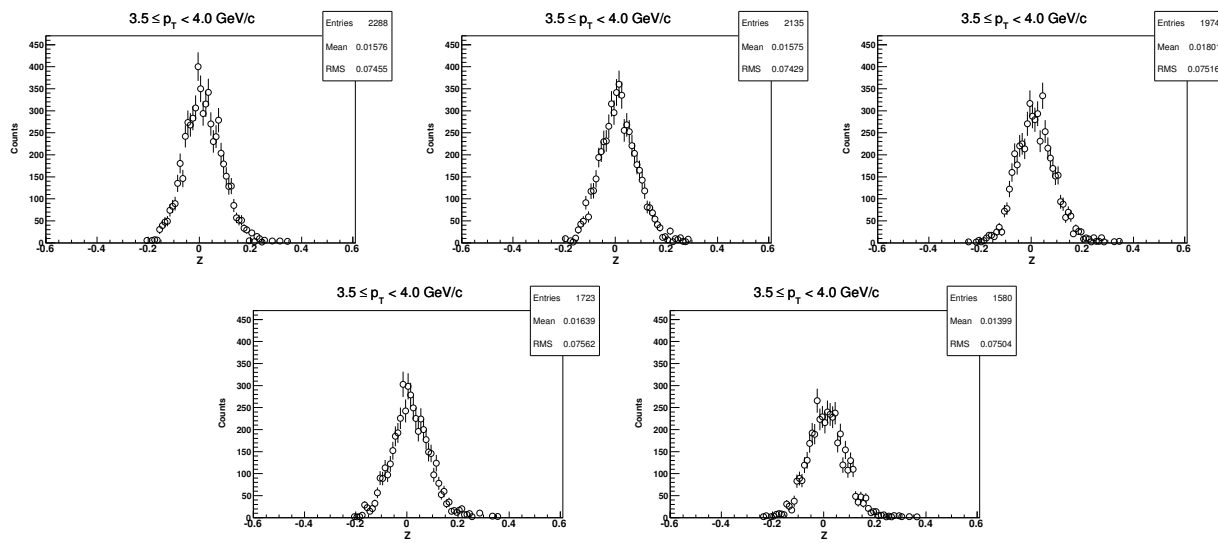
8.1.6 Z-distribution of d for $2.5 < p_T < 3.0 \text{ GeV}/c$ ($\sqrt{s_{NN}} = 27 \text{ GeV}$, 0-80%)



8.1.7 Z-distribution of d for $3.0 < p_T < 3.5 \text{ GeV}/c$ ($\sqrt{s_{NN}} = 27 \text{ GeV}$, 0-80%)

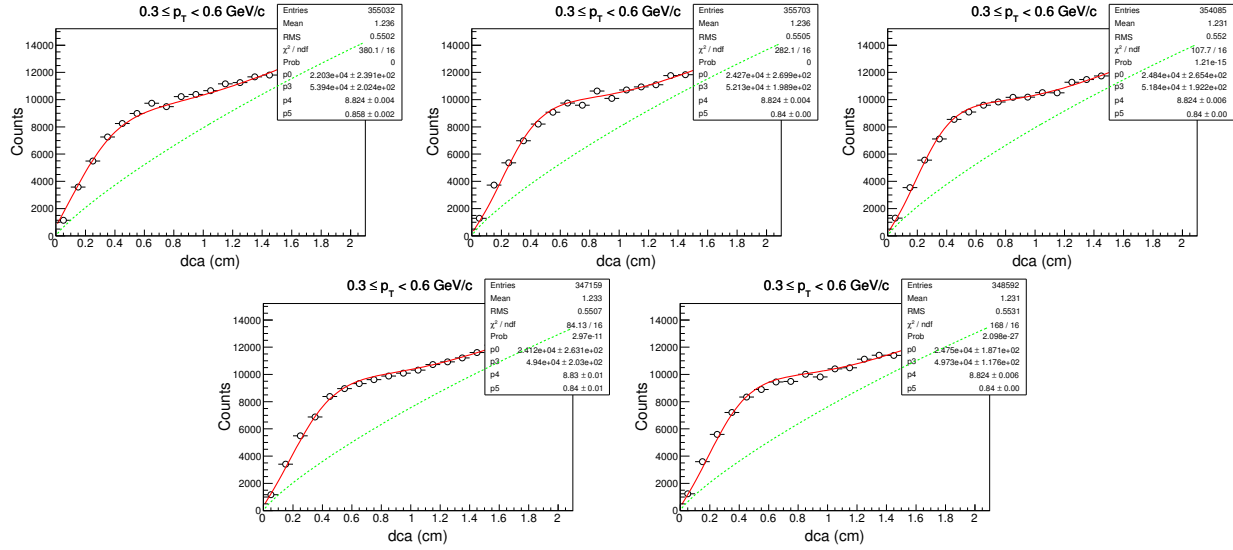


8.1.8 Z-distribution of d for $3.5 < p_T < 4.0 \text{ GeV}/c$ ($\sqrt{s_{NN}} = 27 \text{ GeV}$, 0-80%)

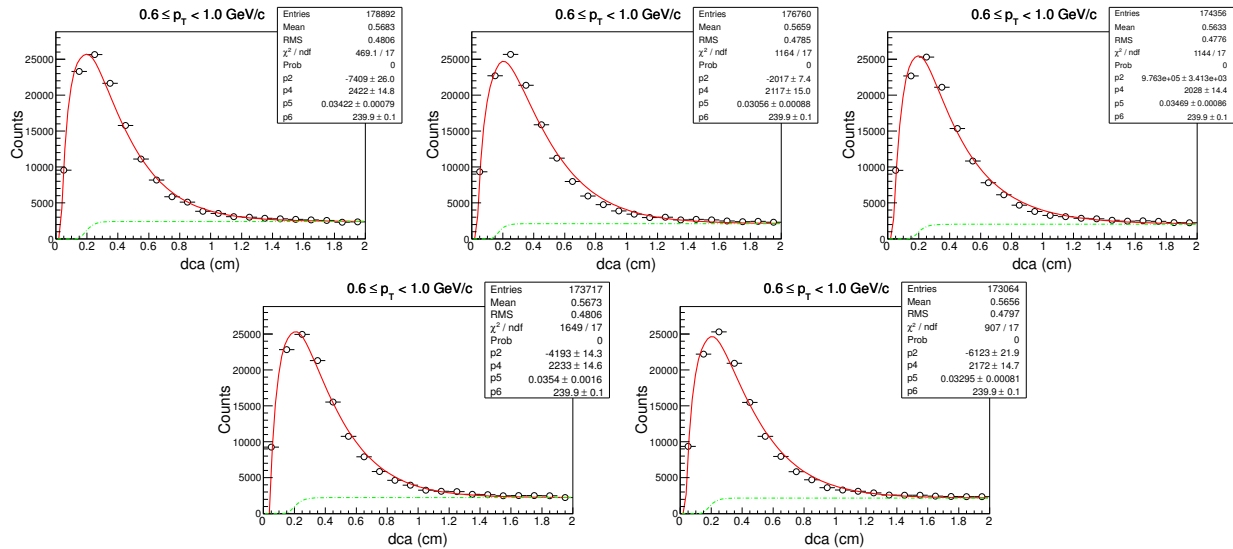


8.2 Centrality: 0-30%

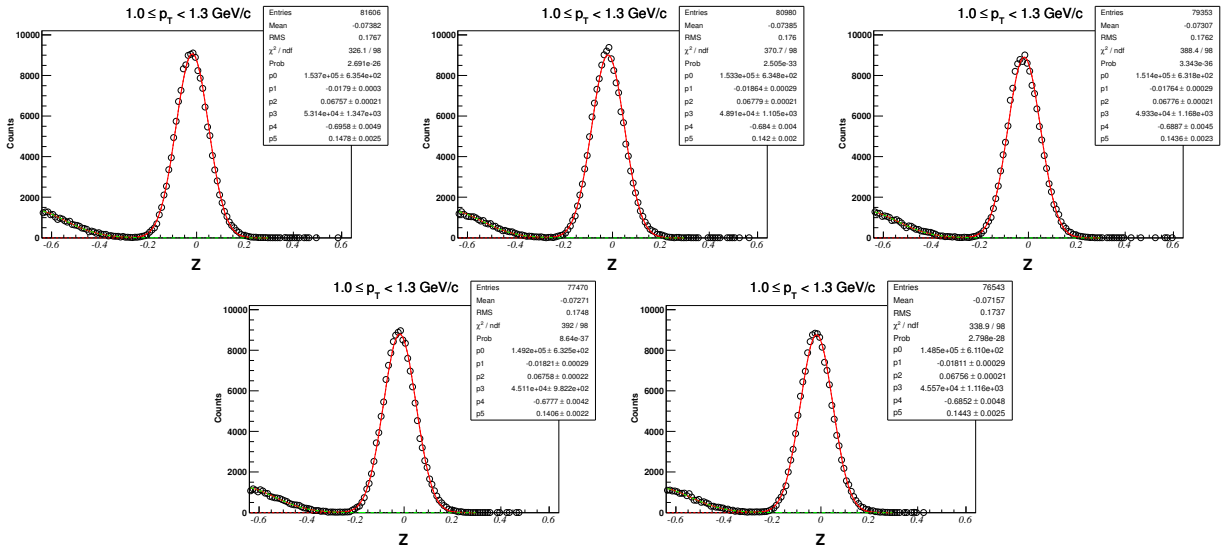
8.2.1 DCA-distribution of d for $0.3 < p_T < 0.6 \text{ GeV}/c$



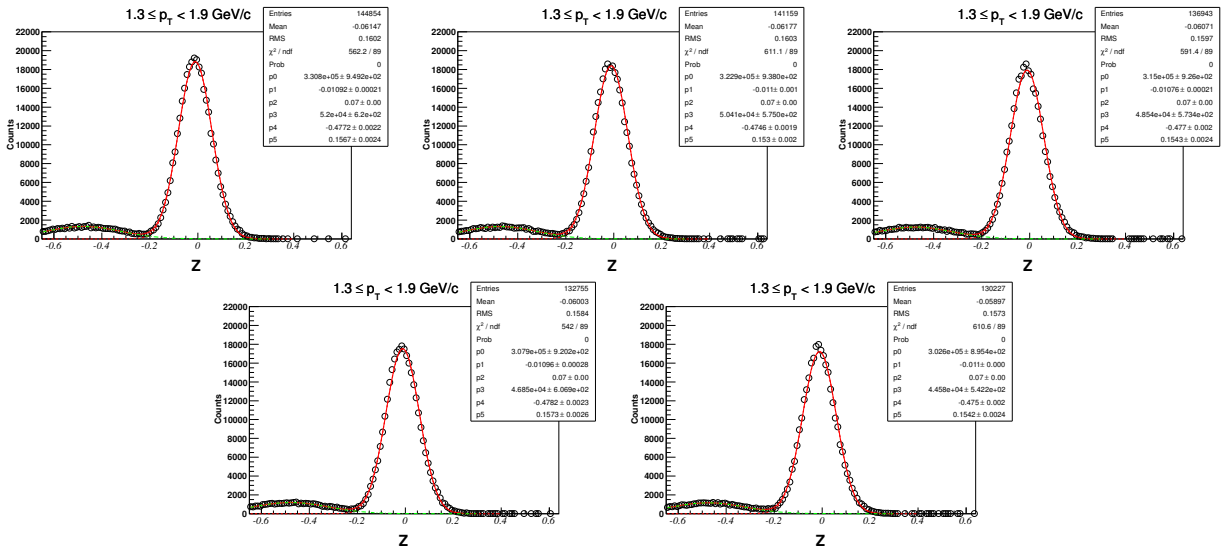
8.2.2 DCA-distribution of d for $0.6 < p_T < 1.0 \text{ GeV}/c$



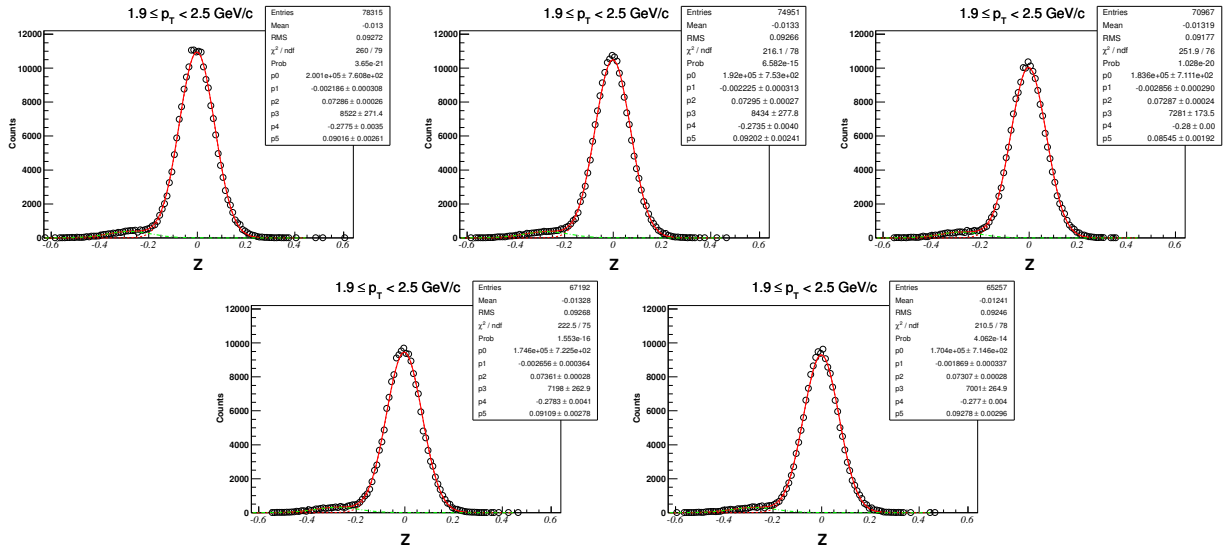
8.2.3 Z-distribution of d for $1.0 < p_T < 1.3 \text{ GeV}/c$ ($\sqrt{s_{NN}} = 27 \text{ GeV}$, 0-30%)



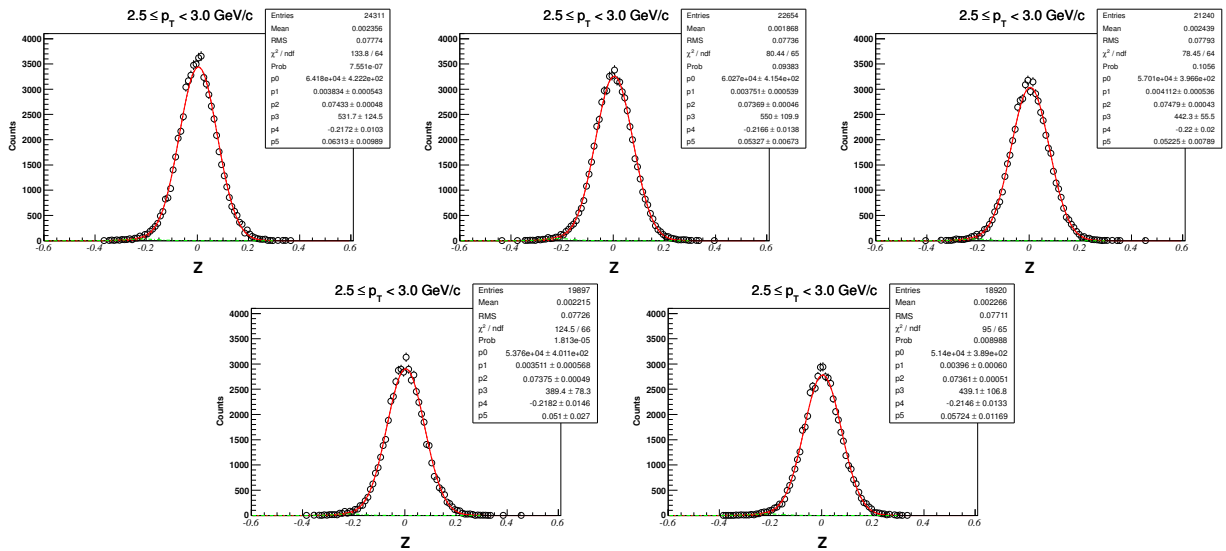
8.2.4 Z-distribution of d for $1.3 < p_T < 1.9 \text{ GeV}/c$ ($\sqrt{s_{NN}} = 27 \text{ GeV}$, 0-30%)



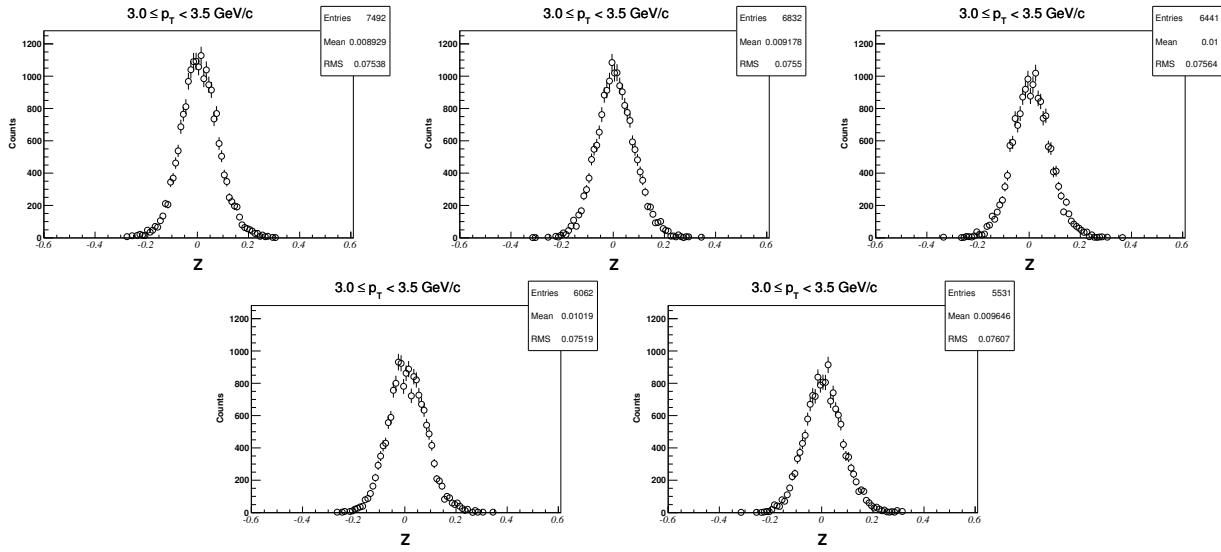
8.2.5 Z-distribution of d for $1.9 < p_T < 2.5 \text{ GeV}/c$ ($\sqrt{s_{NN}} = 27 \text{ GeV}$, 0-30%)



8.2.6 Z-distribution of d for $2.5 < p_T < 3.0 \text{ GeV}/c$ ($\sqrt{s_{NN}} = 27 \text{ GeV}$, 0-30%)

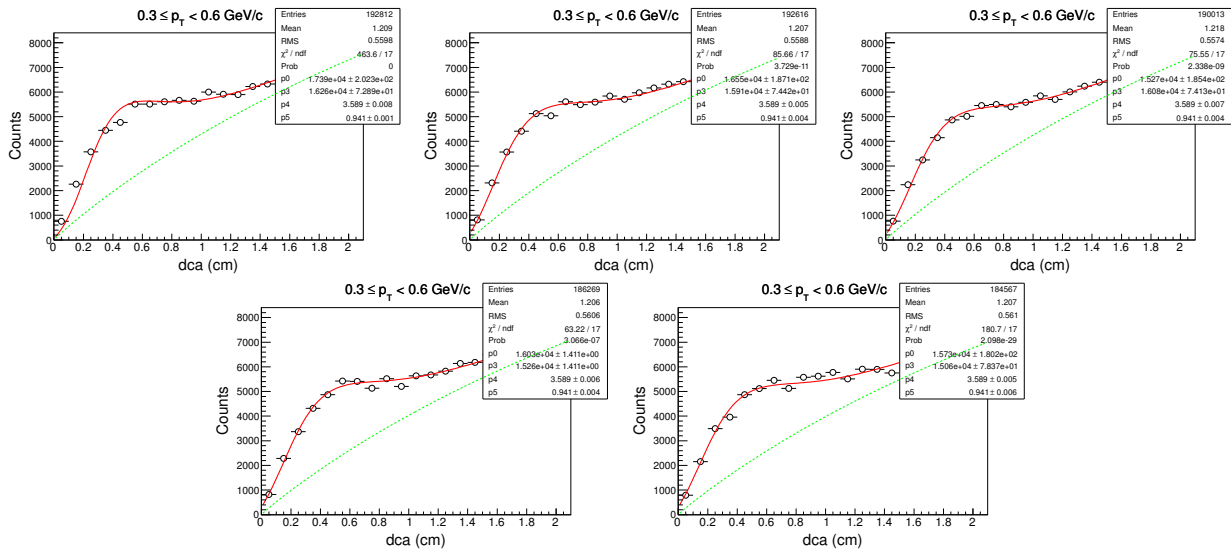


8.2.7 Z-distribution of d for $3.0 < p_T < 3.5 \text{ GeV}/c$ ($\sqrt{s_{NN}} = 27 \text{ GeV}$, 0-30%)

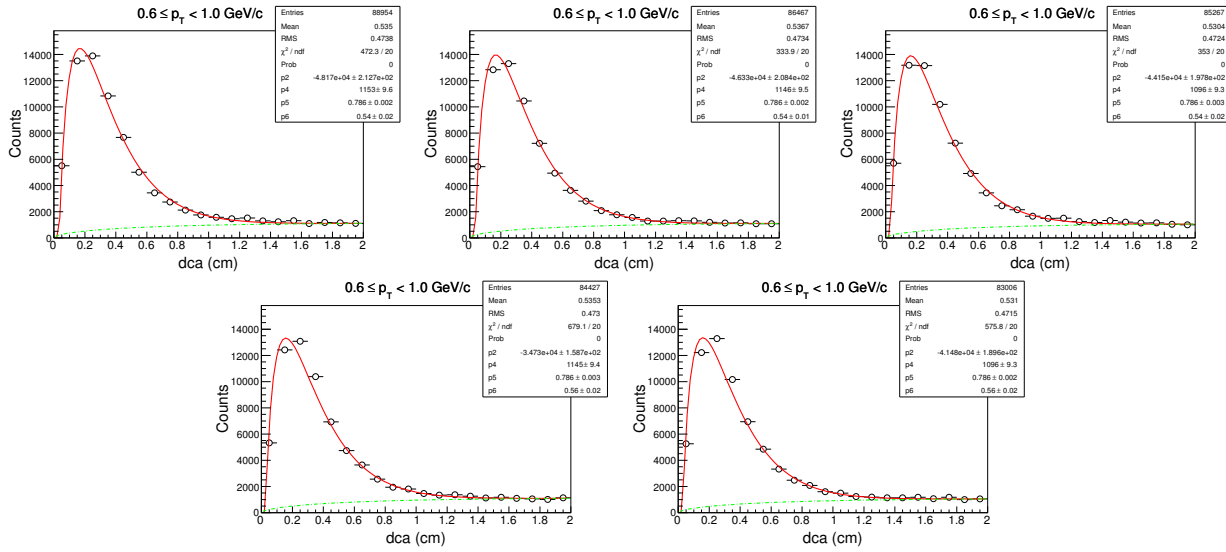


8.3 Centrality: 30-80%

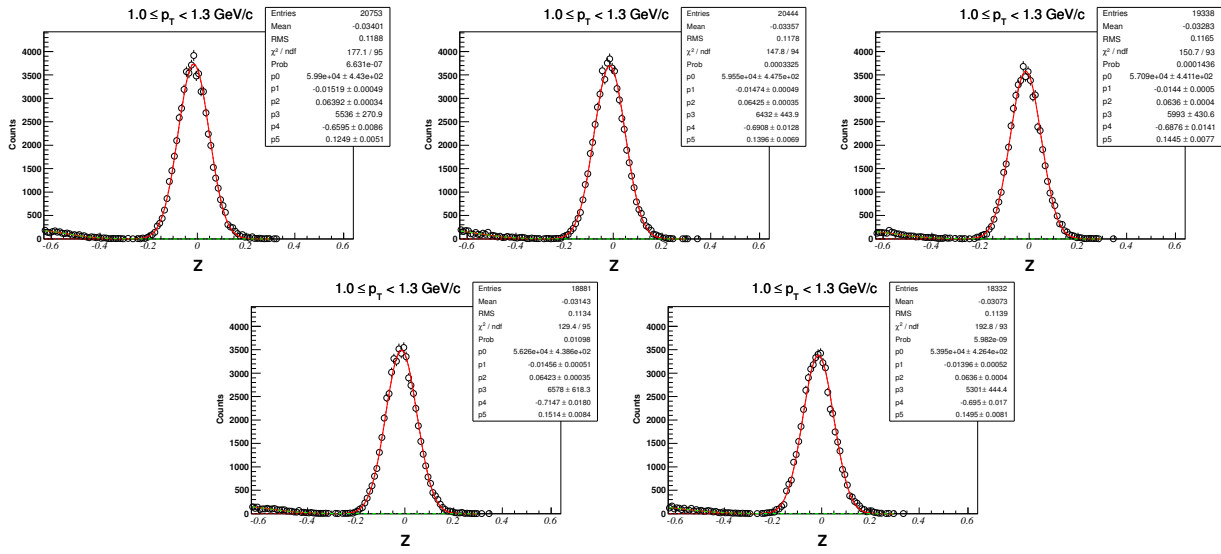
8.3.1 DCA-distribution of d for $0.3 < p_T < 0.6 \text{ GeV}/c$



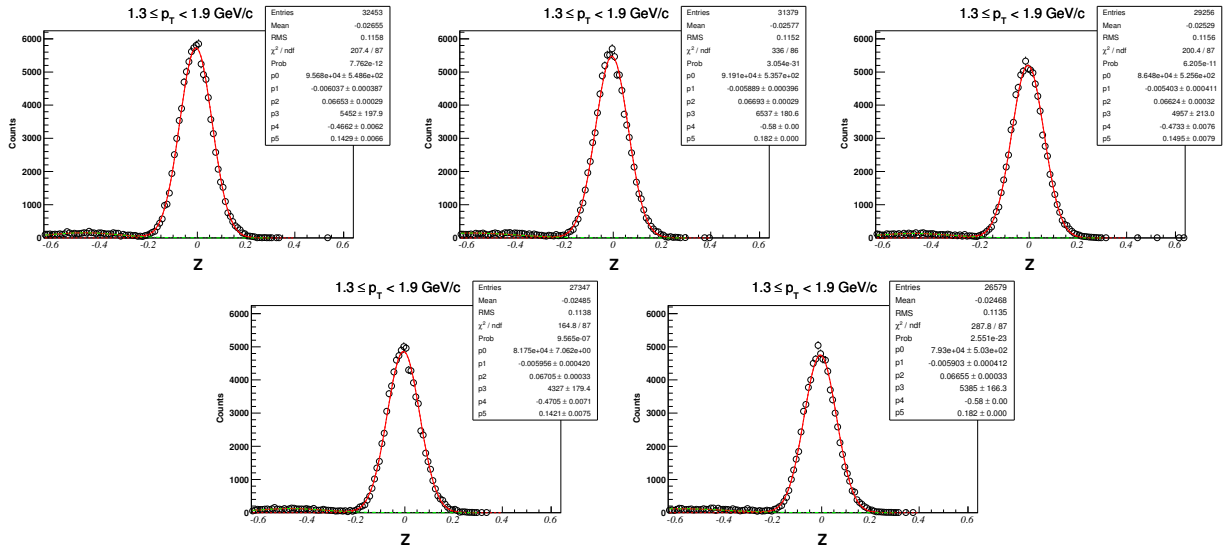
8.3.2 DCA-distribution of d for $0.6 < p_T < 1.0 \text{ GeV}/c$ ($\sqrt{s_{NN}} = 27 \text{ GeV}$, 30-80%)



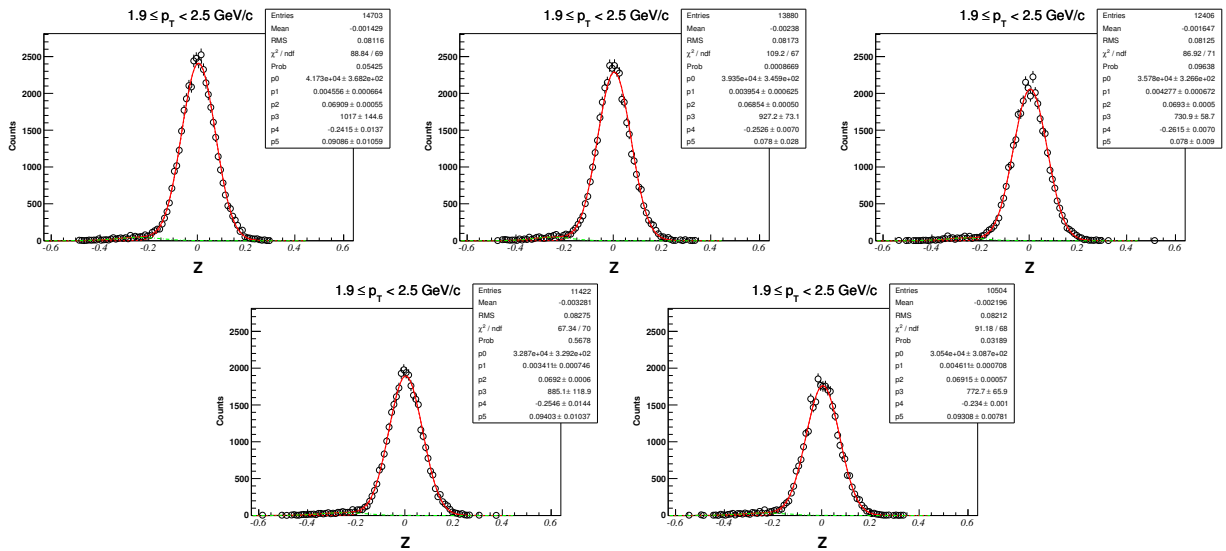
8.3.3 Z-distribution of d for $1.0 < p_T < 1.3 \text{ GeV}/c$ ($\sqrt{s_{NN}} = 27 \text{ GeV}$, 30-80%)



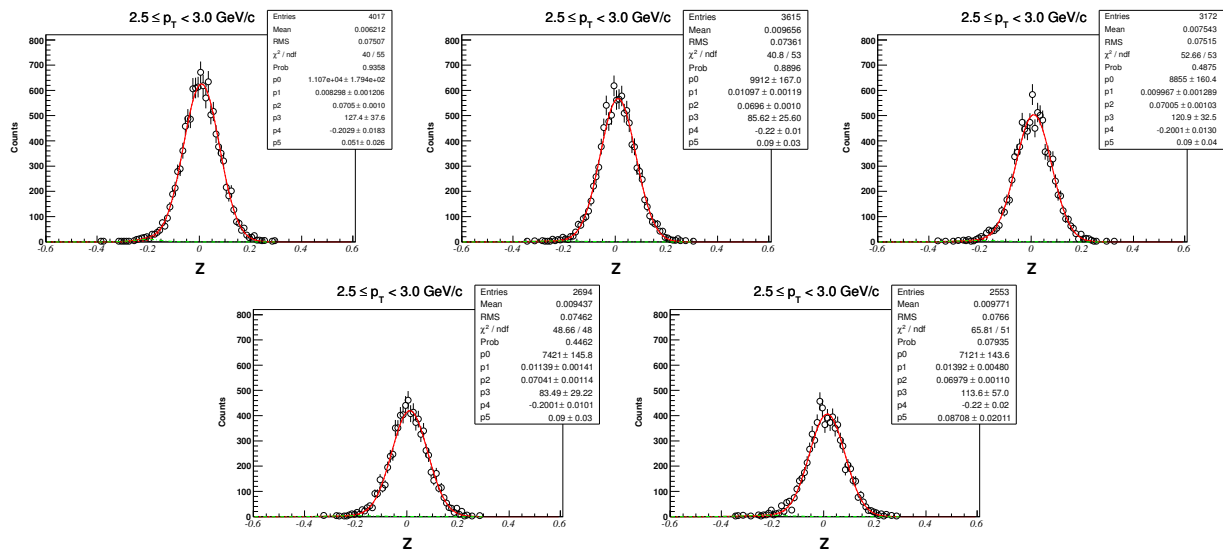
8.3.4 Z-distribution of d for $1.3 < p_T < 1.9 \text{ GeV}/c$ ($\sqrt{s_{NN}} = 27 \text{ GeV}$, 30-80%)



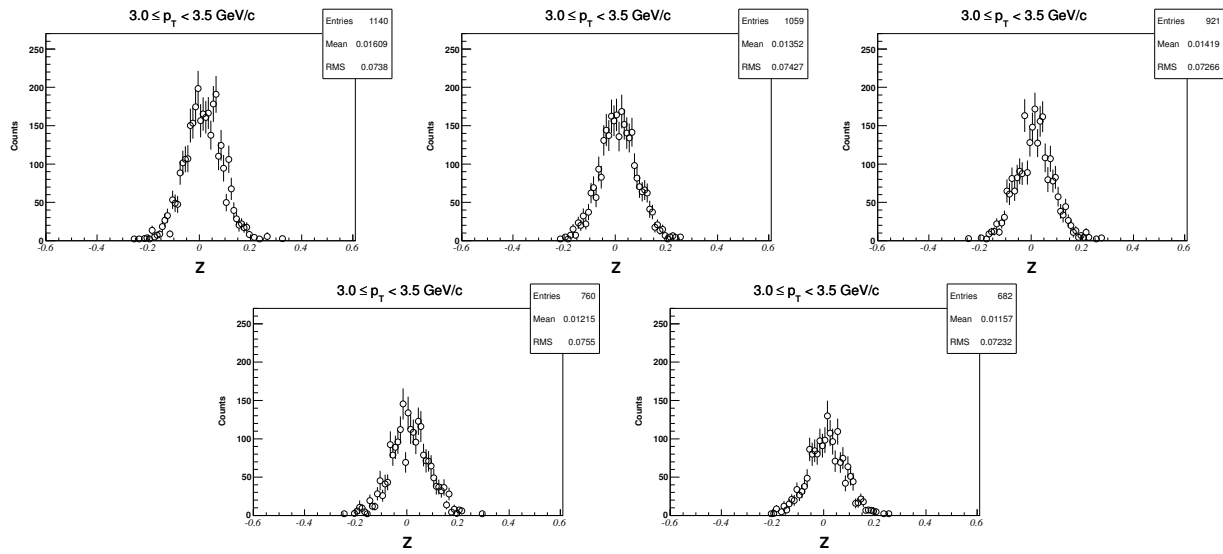
8.3.5 Z-distribution of d for $1.9 < p_T < 2.5 \text{ GeV}/c$ ($\sqrt{s_{NN}} = 27 \text{ GeV}$, 30-80%)



8.3.6 Z-distribution of d for $2.5 < p_T < 3.0 \text{ GeV}/c$ ($\sqrt{s_{NN}} = 27 \text{ GeV}$, 30-80%)

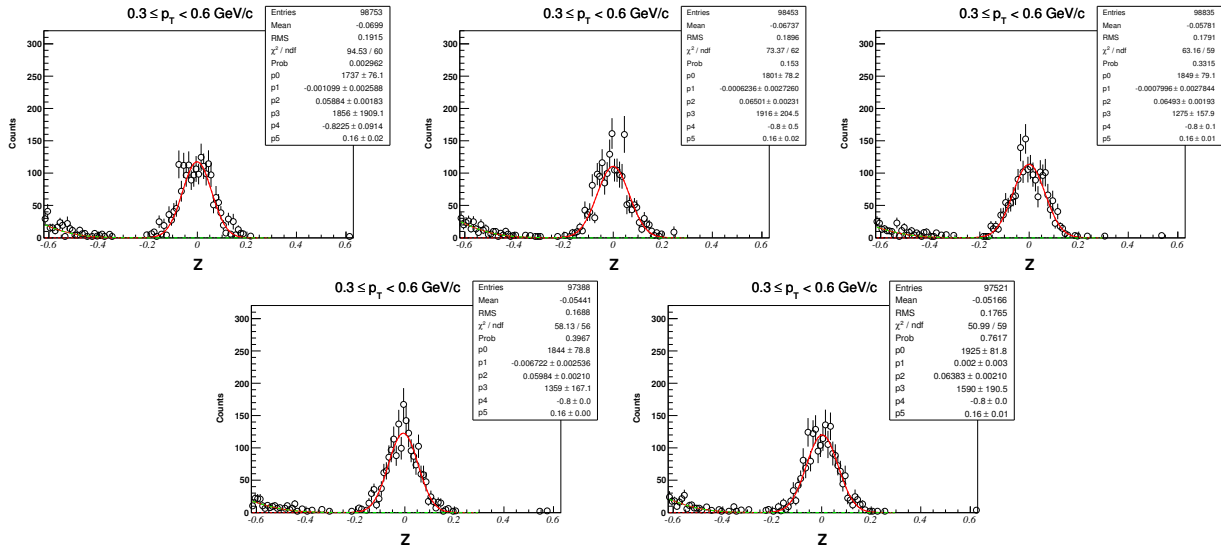


8.3.7 Z-distribution of d for $3.0 < p_T < 3.5 \text{ GeV}/c$ ($\sqrt{s_{NN}} = 27 \text{ GeV}$, 30-80%)

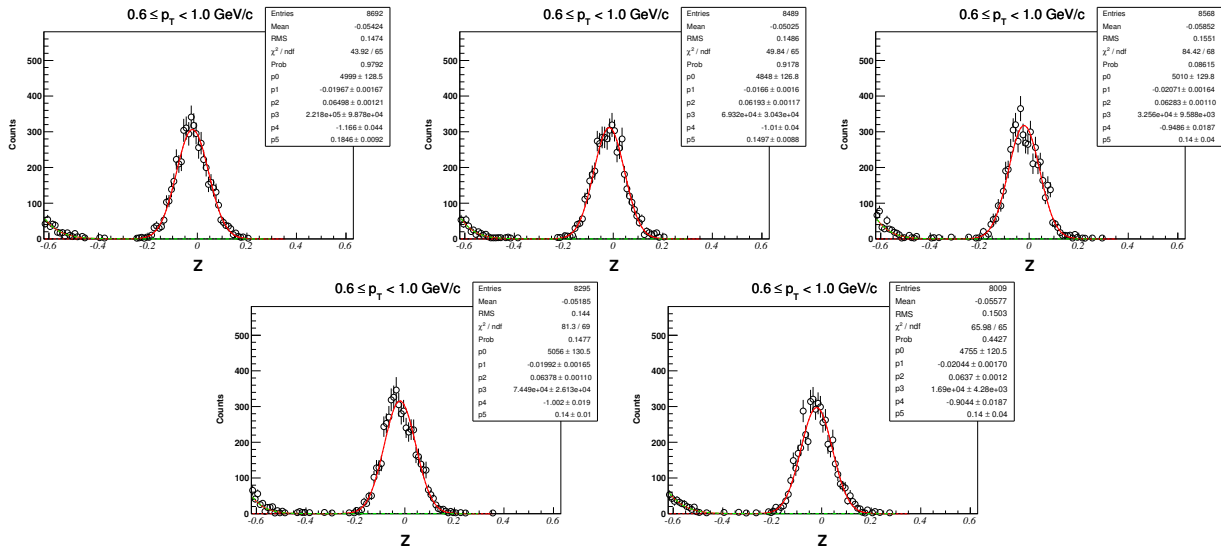


8.4 Z-distribution of \bar{d} in $\sqrt{s_{NN}} = 27$ GeV for centrality: 0-80%

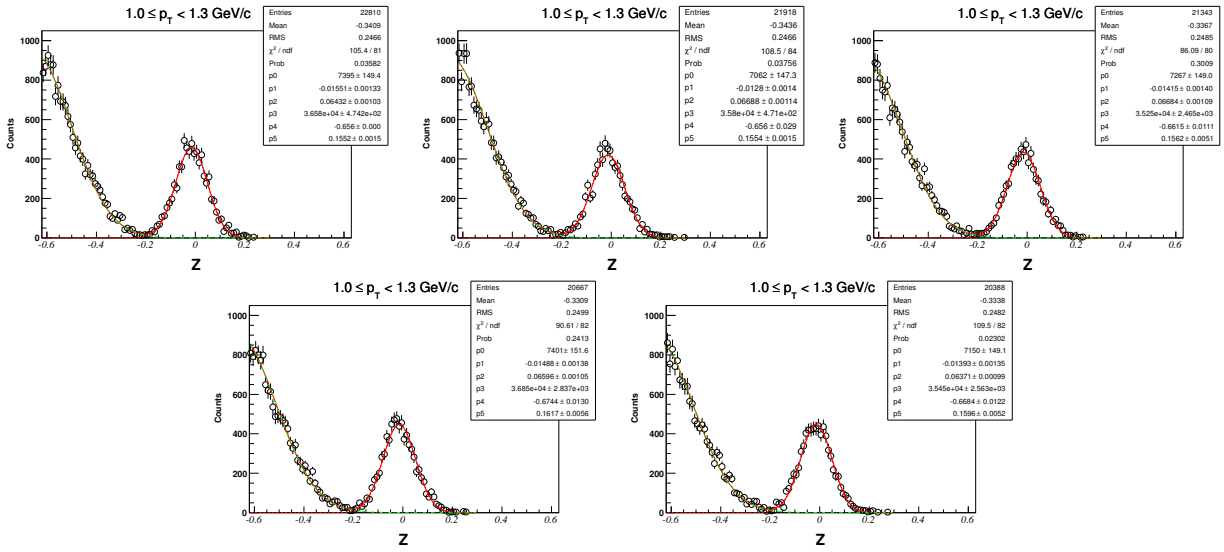
8.4.1 Z-distribution of \bar{d} for $0.3 < p_T < 0.6$ GeV/c



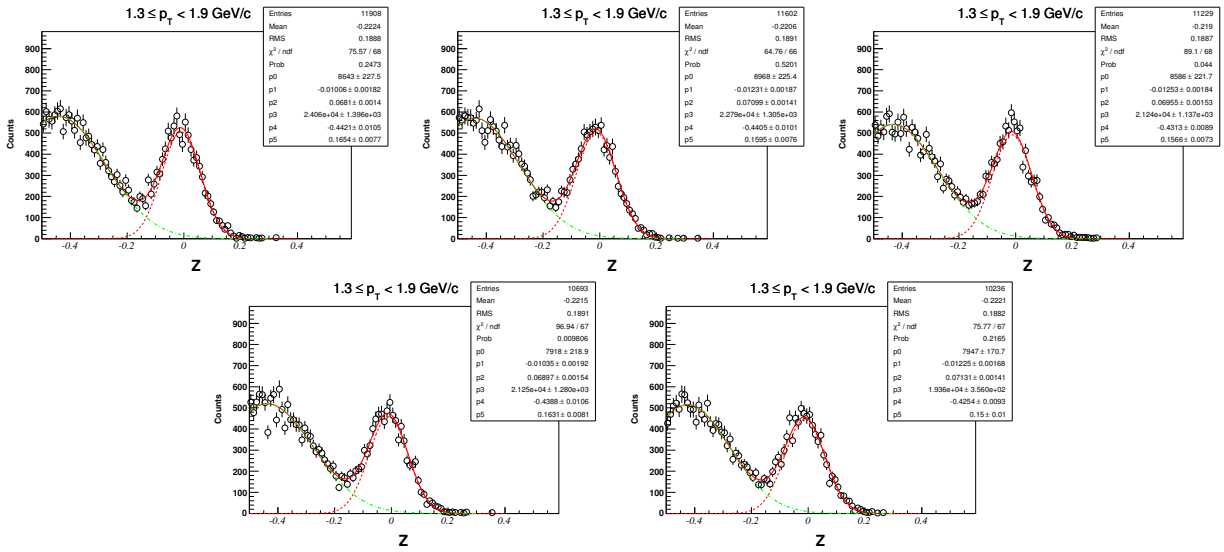
8.4.2 Z-distribution of \bar{d} for $0.6 < p_T < 1.0$ GeV/c



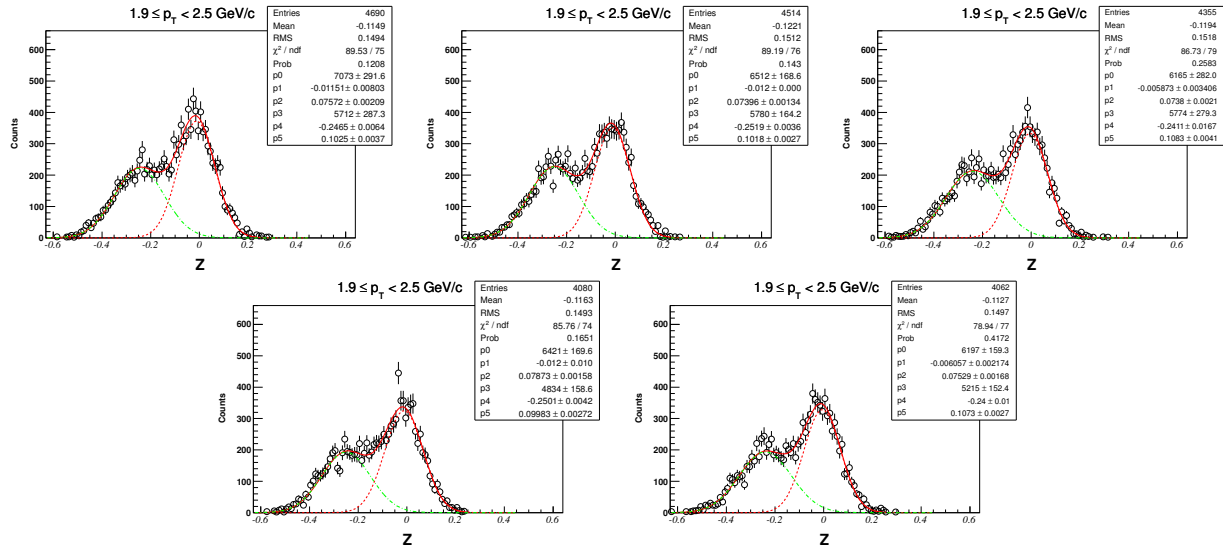
8.4.3 Z-distribution of \bar{d} for $1.0 < p_T < 1.3 \text{ GeV}/c$ ($\sqrt{s_{NN}} = 27 \text{ GeV}$, 0-80%)



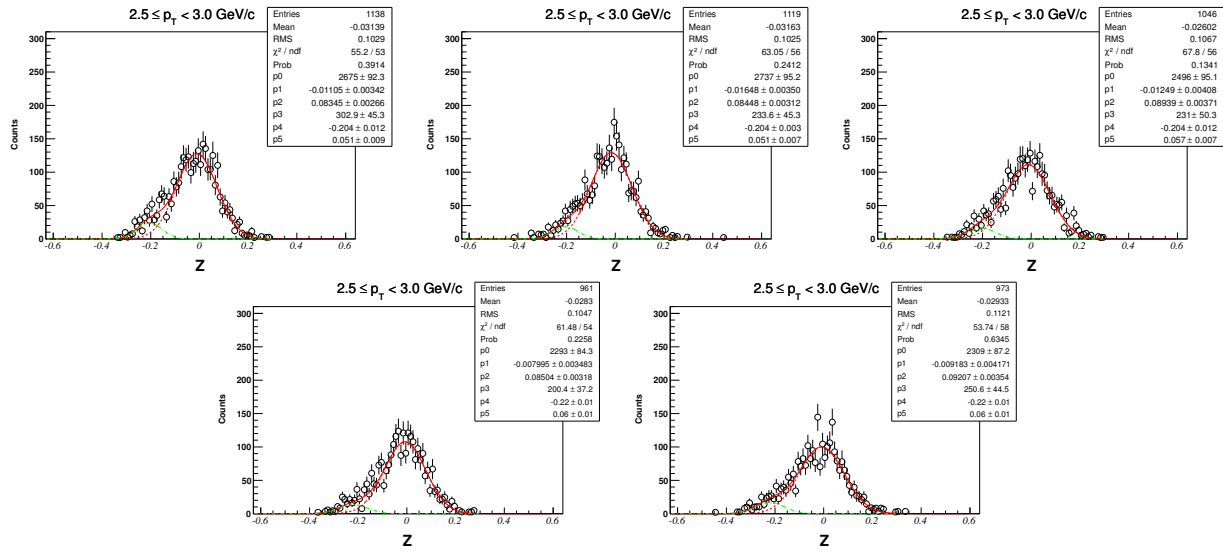
8.4.4 Z-distribution of \bar{d} for $1.3 < p_T < 1.9 \text{ GeV}/c$ ($\sqrt{s_{NN}} = 27 \text{ GeV}$, 0-80%)



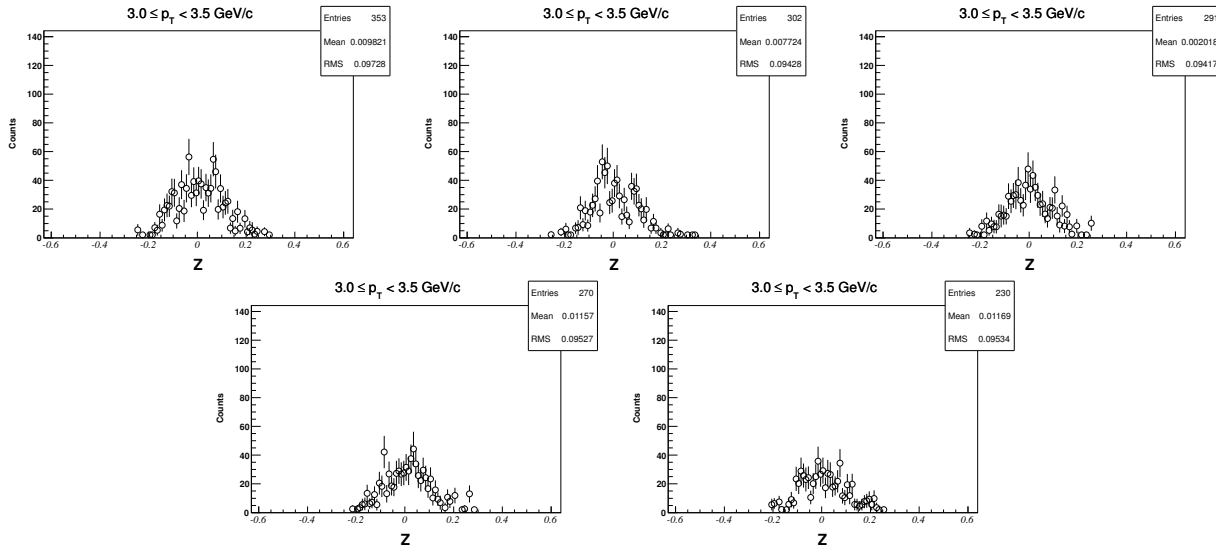
8.4.5 Z-distribution of \bar{d} for $1.9 < p_T < 2.5 \text{ GeV}/c$ ($\sqrt{s_{NN}} = 27 \text{ GeV}$, 0-80%)



8.4.6 Z-distribution of \bar{d} for $2.5 < p_T < 3.0 \text{ GeV}/c$ ($\sqrt{s_{NN}} = 27 \text{ GeV}$, 0-80%)

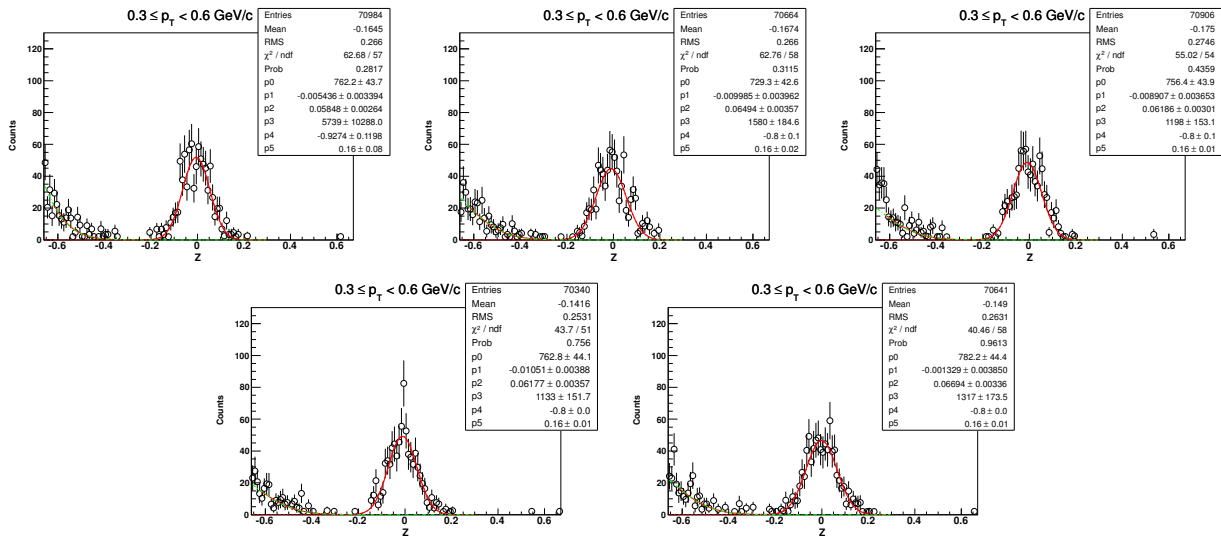


8.4.7 Z-distribution of \bar{d} for $3.0 < p_T < 3.5 \text{ GeV}/c$ ($\sqrt{s_{NN}} = 27 \text{ GeV}$, 0-80%)

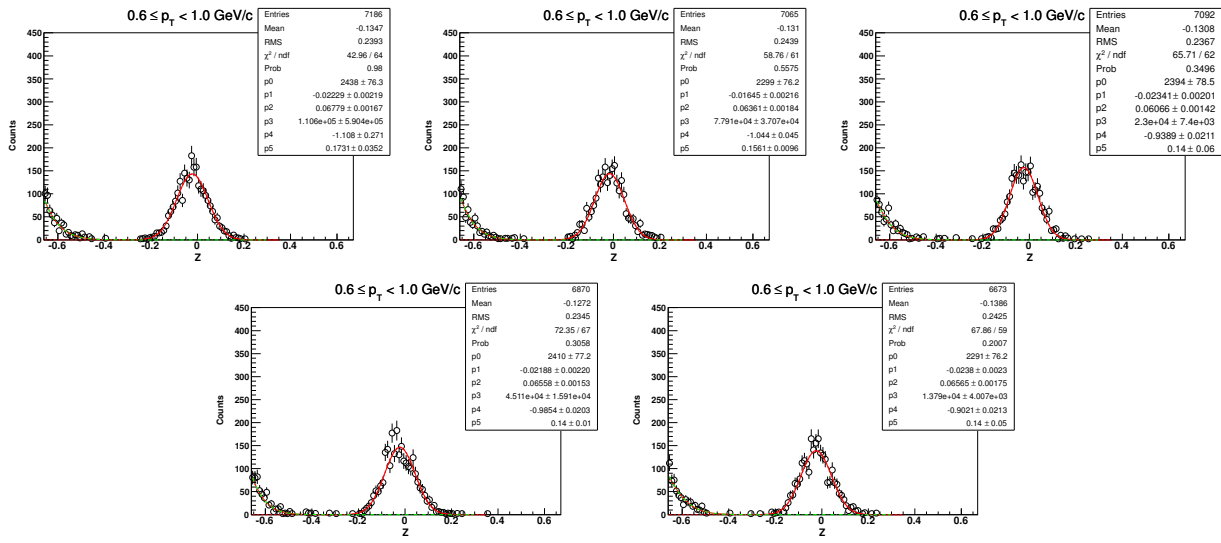


8.5 Centrality: 0-30%

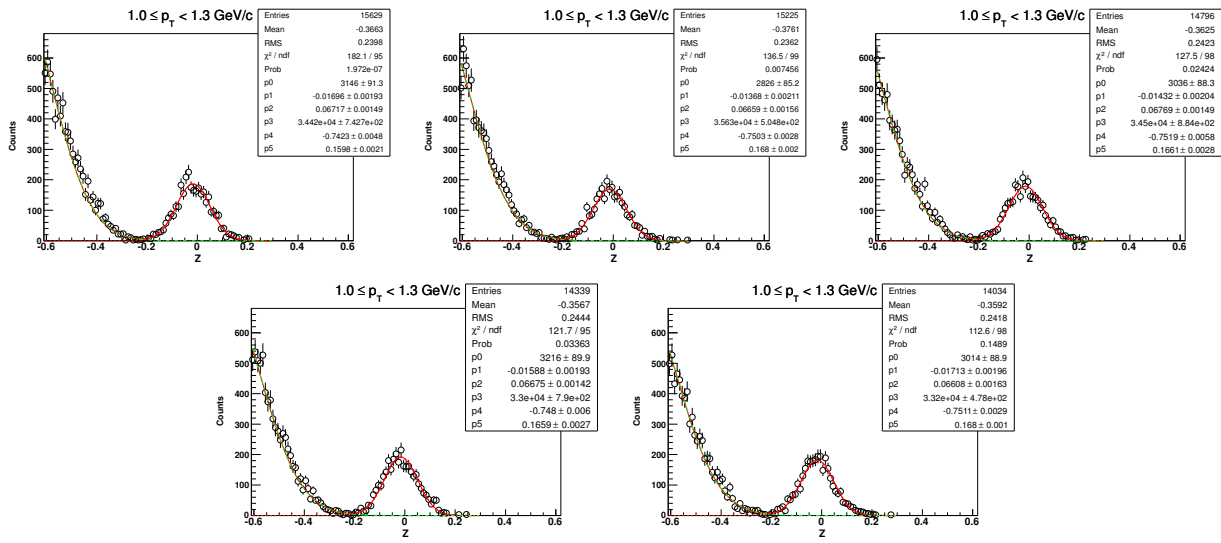
8.5.1 Z-distribution of \bar{d} for $0.3 < p_T < 0.6 \text{ GeV}/c$



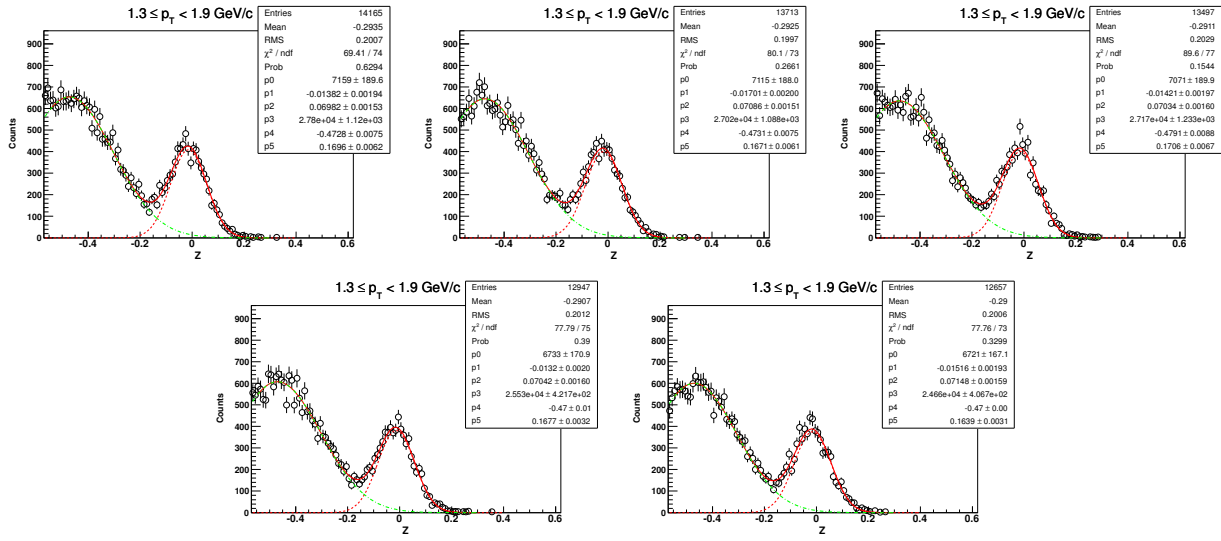
8.5.2 Z-distribution of \bar{d} for $0.6 < p_T < 1.0 \text{ GeV}/c$ ($\sqrt{s_{NN}} = 27 \text{ GeV}$, 0-30%)



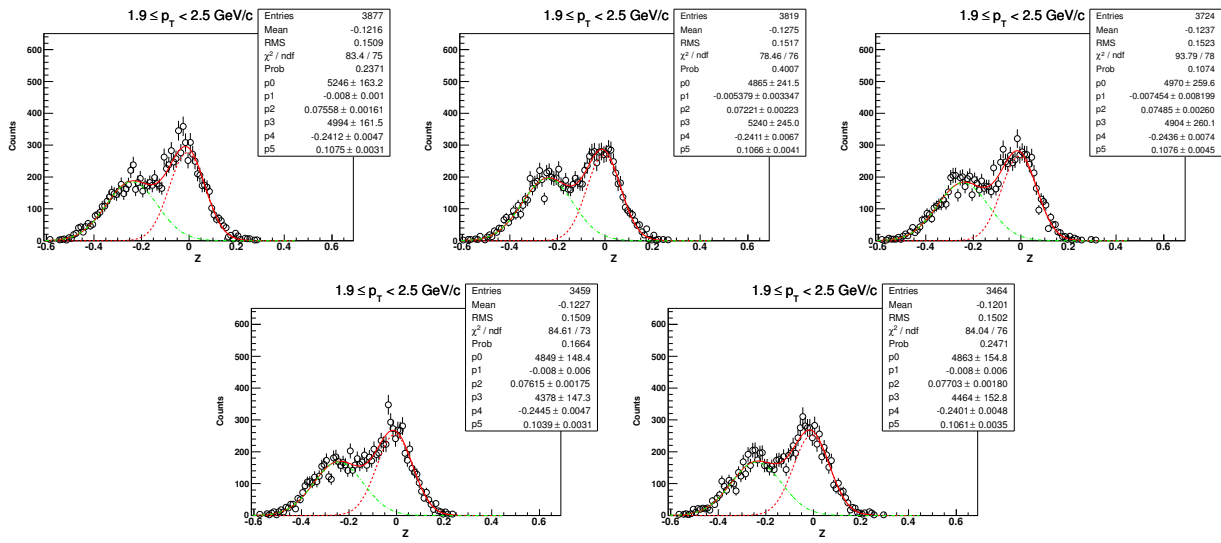
8.5.3 Z-distribution of \bar{d} for $1.0 < p_T < 1.3 \text{ GeV}/c$ ($\sqrt{s_{NN}} = 27 \text{ GeV}$, 0-30%)



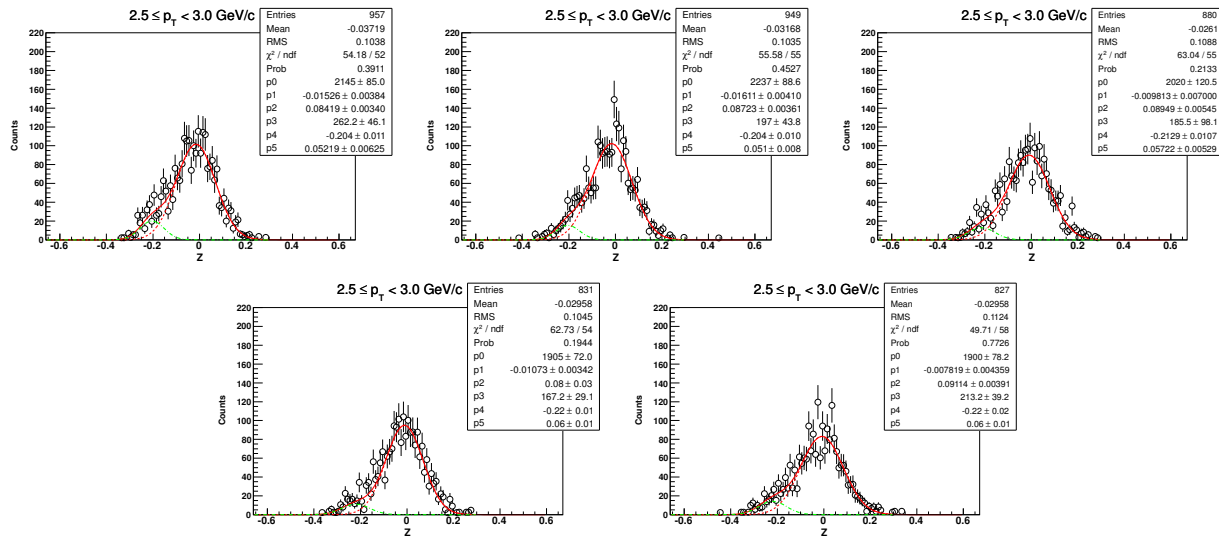
8.5.4 Z-distribution of \bar{d} for $1.3 < p_T < 1.9 \text{ GeV}/c$ ($\sqrt{s_{NN}} = 27 \text{ GeV}$, 0-30%)



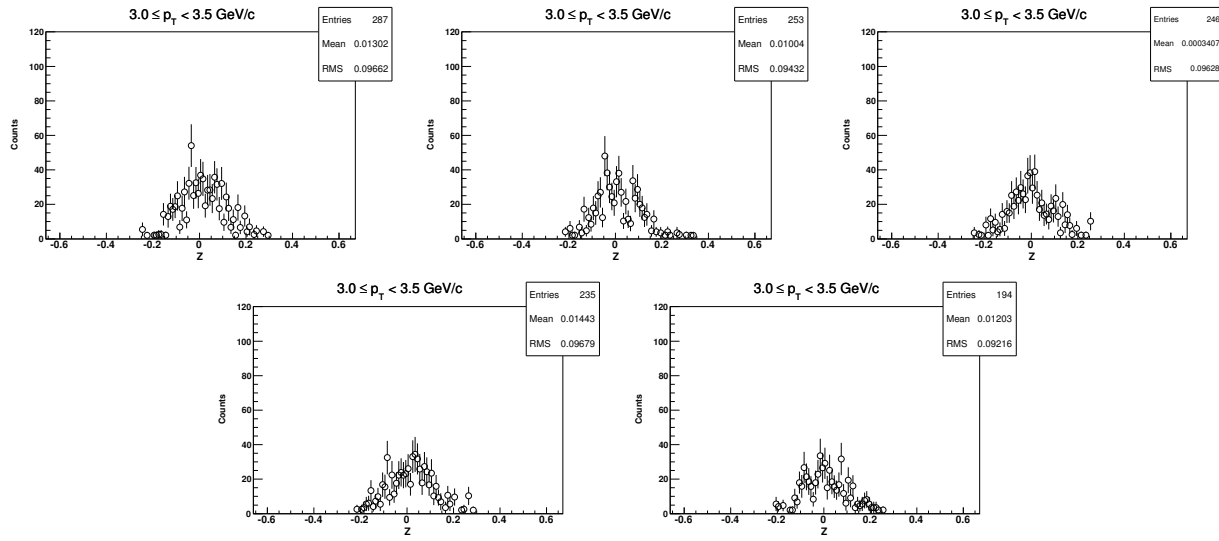
8.5.5 Z-distribution of \bar{d} for $1.9 < p_T < 2.5 \text{ GeV}/c$ ($\sqrt{s_{NN}} = 27 \text{ GeV}$, 0-30%)



8.5.6 Z-distribution of \bar{d} for $2.5 < p_T < 3.0 \text{ GeV}/c$ ($\sqrt{s_{NN}} = 27 \text{ GeV}$, 0-30%)

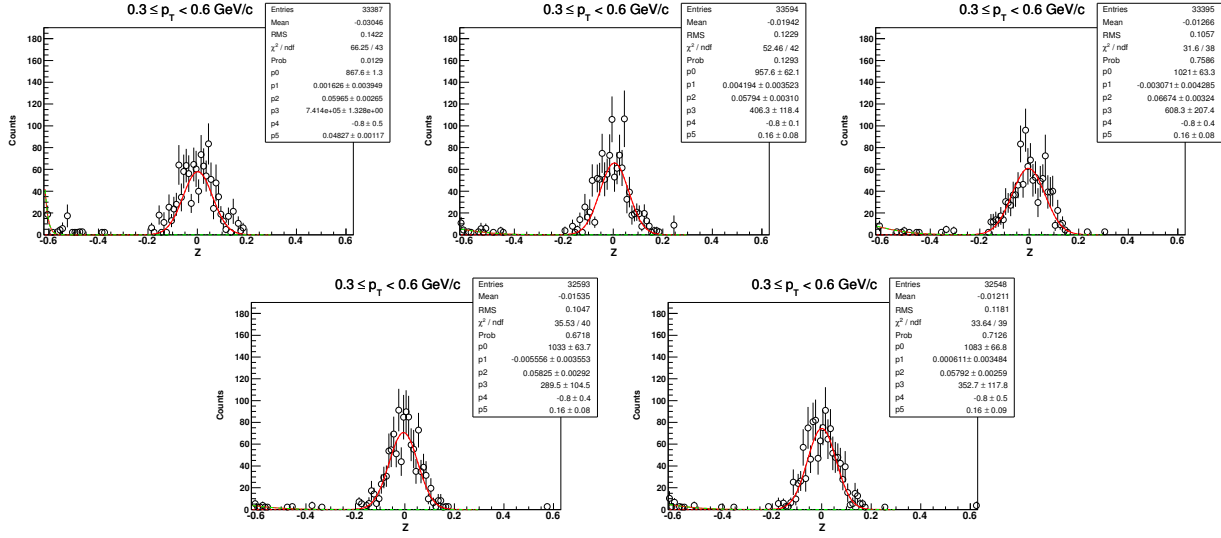


8.5.7 Z-distribution of \bar{d} for $3.0 < p_T < 3.5 \text{ GeV}/c$ ($\sqrt{s_{NN}} = 27 \text{ GeV}$, 0-30%)

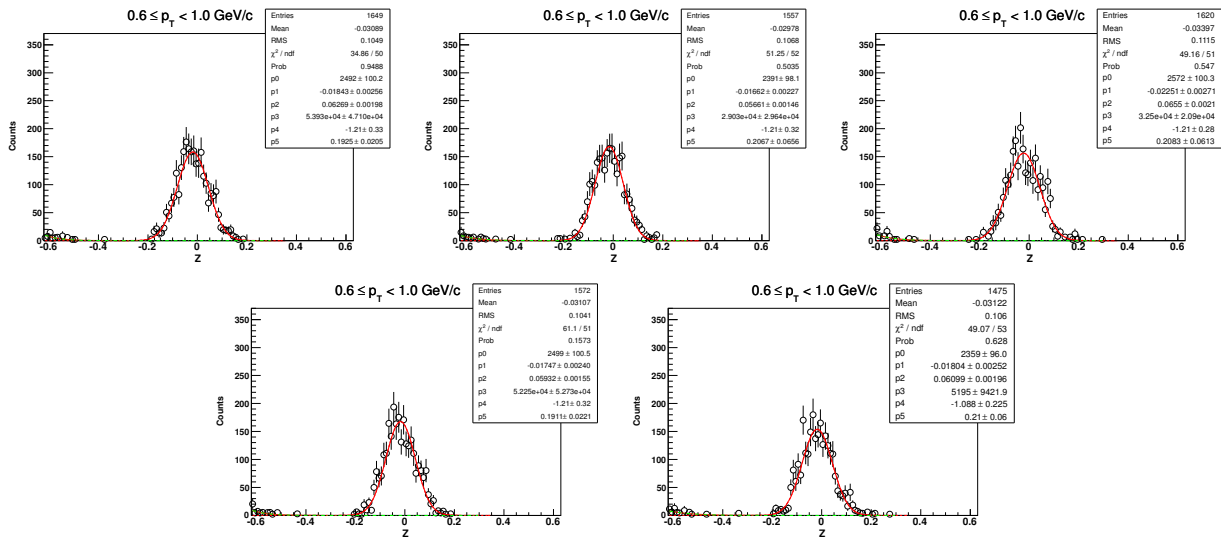


8.6 Centrality: 30-80%

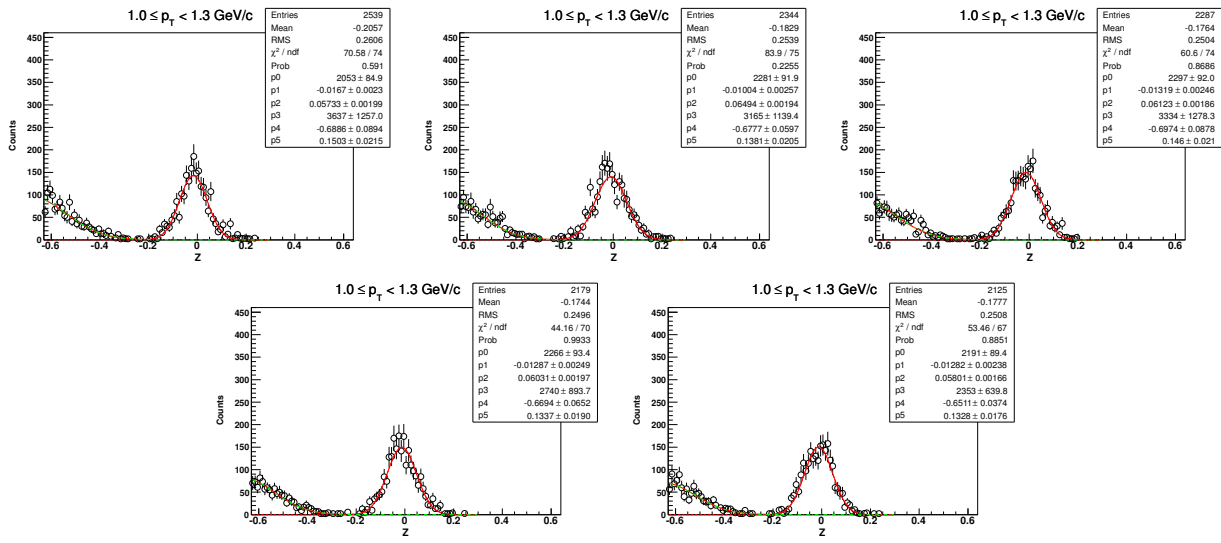
8.6.1 Z-distribution of \bar{d} for $0.3 < p_T < 0.6 \text{ GeV}/c$ ($\sqrt{s_{NN}} = 27 \text{ GeV}$, 30-80%)



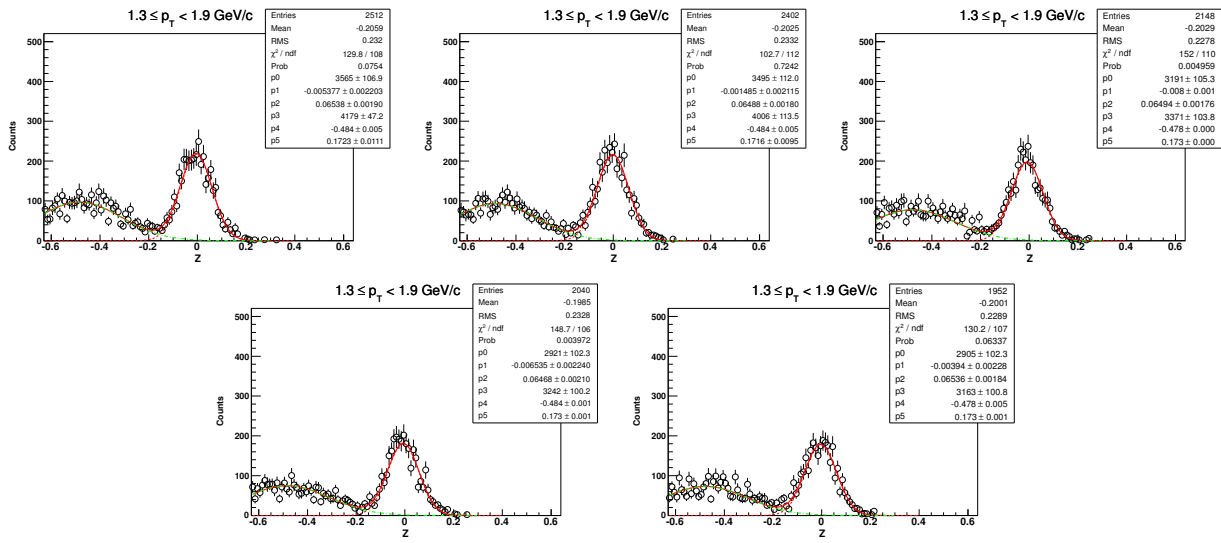
8.6.2 Z-distribution of \bar{d} for $0.6 < p_T < 1.0 \text{ GeV}/c$ ($\sqrt{s_{NN}} = 27 \text{ GeV}$, 30-80%)



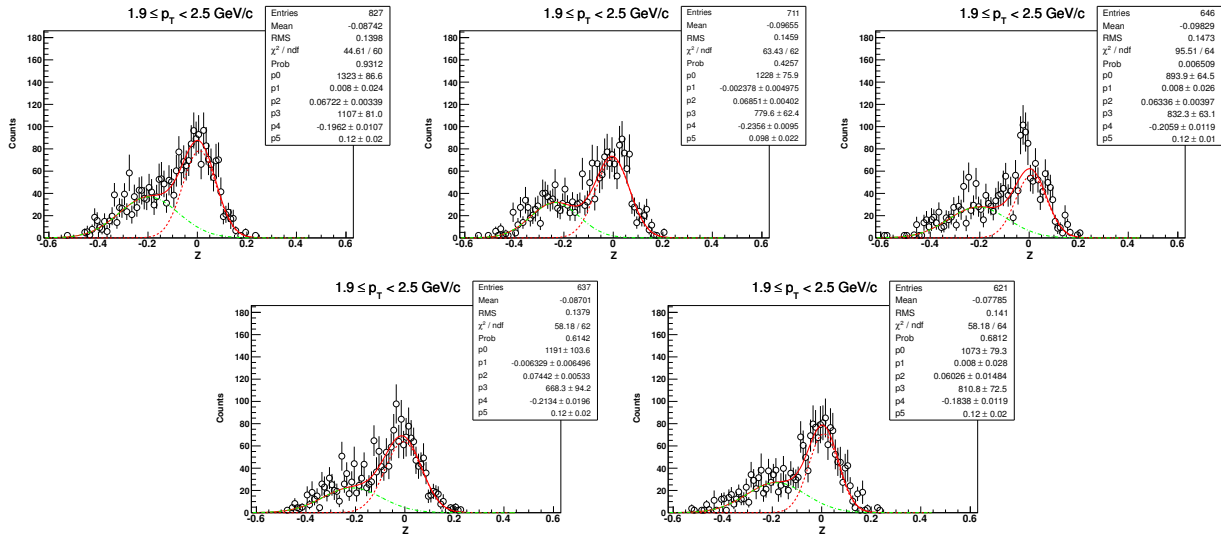
8.6.3 Z-distribution of \bar{d} for $1.0 < p_T < 1.3 \text{ GeV}/c$ ($\sqrt{s_{NN}} = 27 \text{ GeV}$, 30-80%)



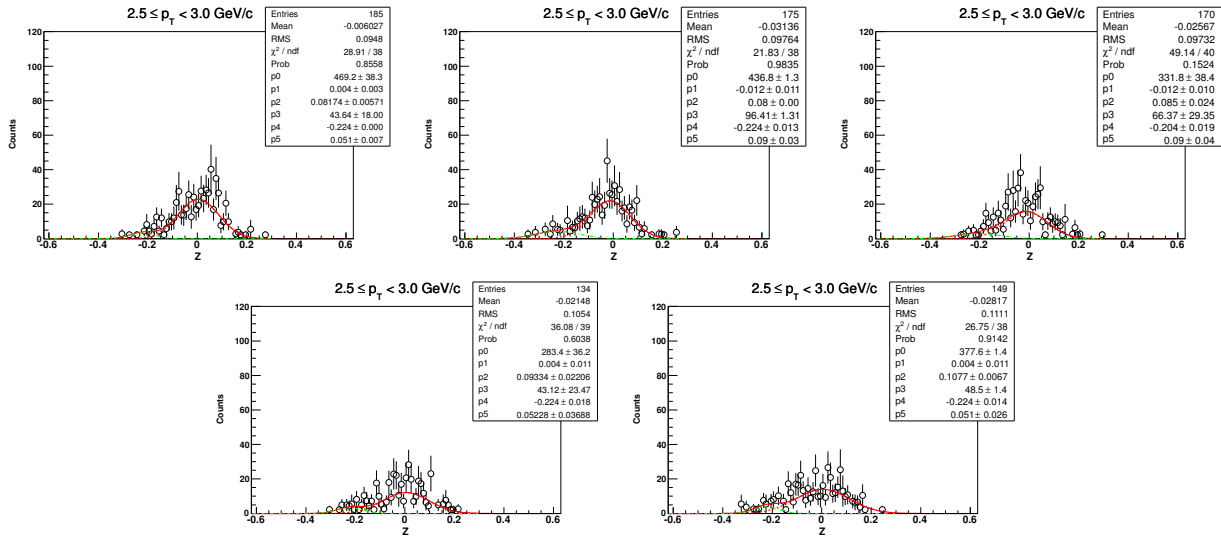
8.6.4 Z-distribution of \bar{d} for $1.3 < p_T < 1.9 \text{ GeV}/c$ ($\sqrt{s_{NN}} = 27 \text{ GeV}$, 30-80%)



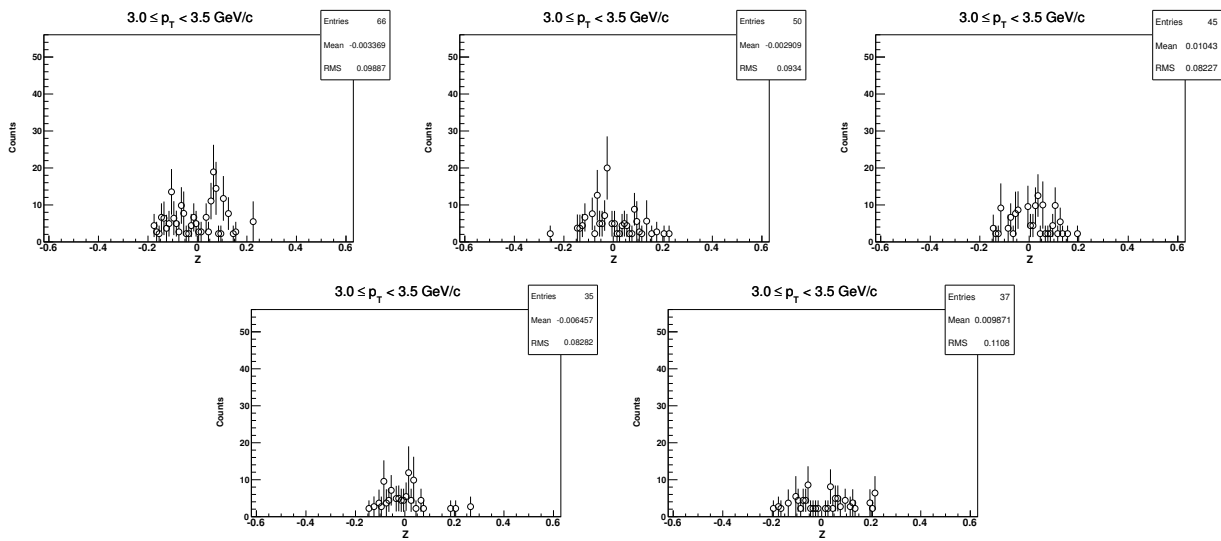
8.6.5 Z-distribution of \bar{d} for $1.9 < p_T < 2.5$ GeV/c ($\sqrt{s_{NN}} = 27$ GeV, 30-80%)



8.6.6 Z-distribution of \bar{d} for $2.5 < p_T < 3.0$ GeV/c ($\sqrt{s_{NN}} = 27$ GeV, 30-80%)

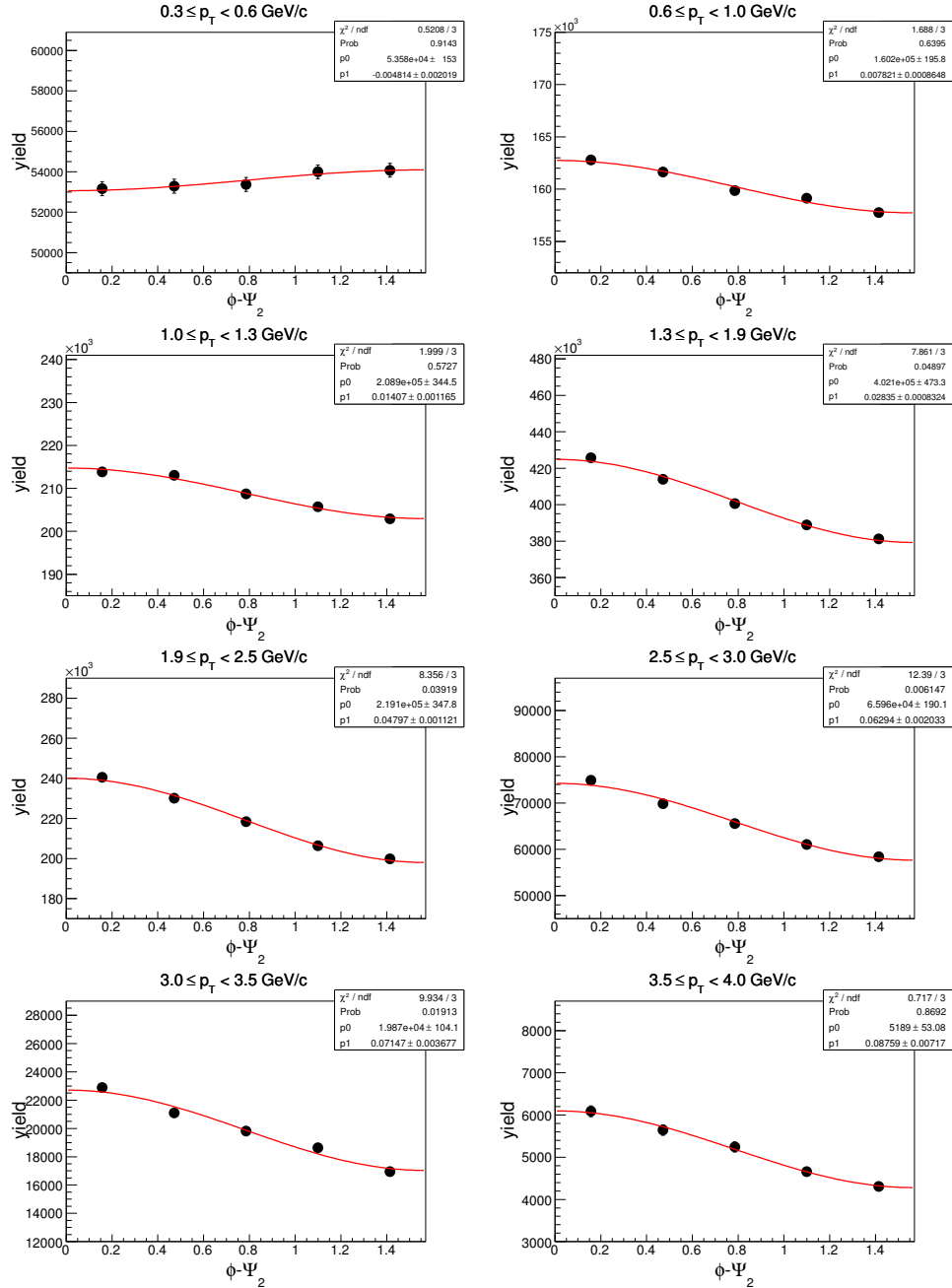


8.6.7 Z-distribution of \bar{d} for $3.0 < p_T < 3.5 \text{ GeV}/c$ ($\sqrt{s_{NN}} = 27 \text{ GeV}$, 30-80%)

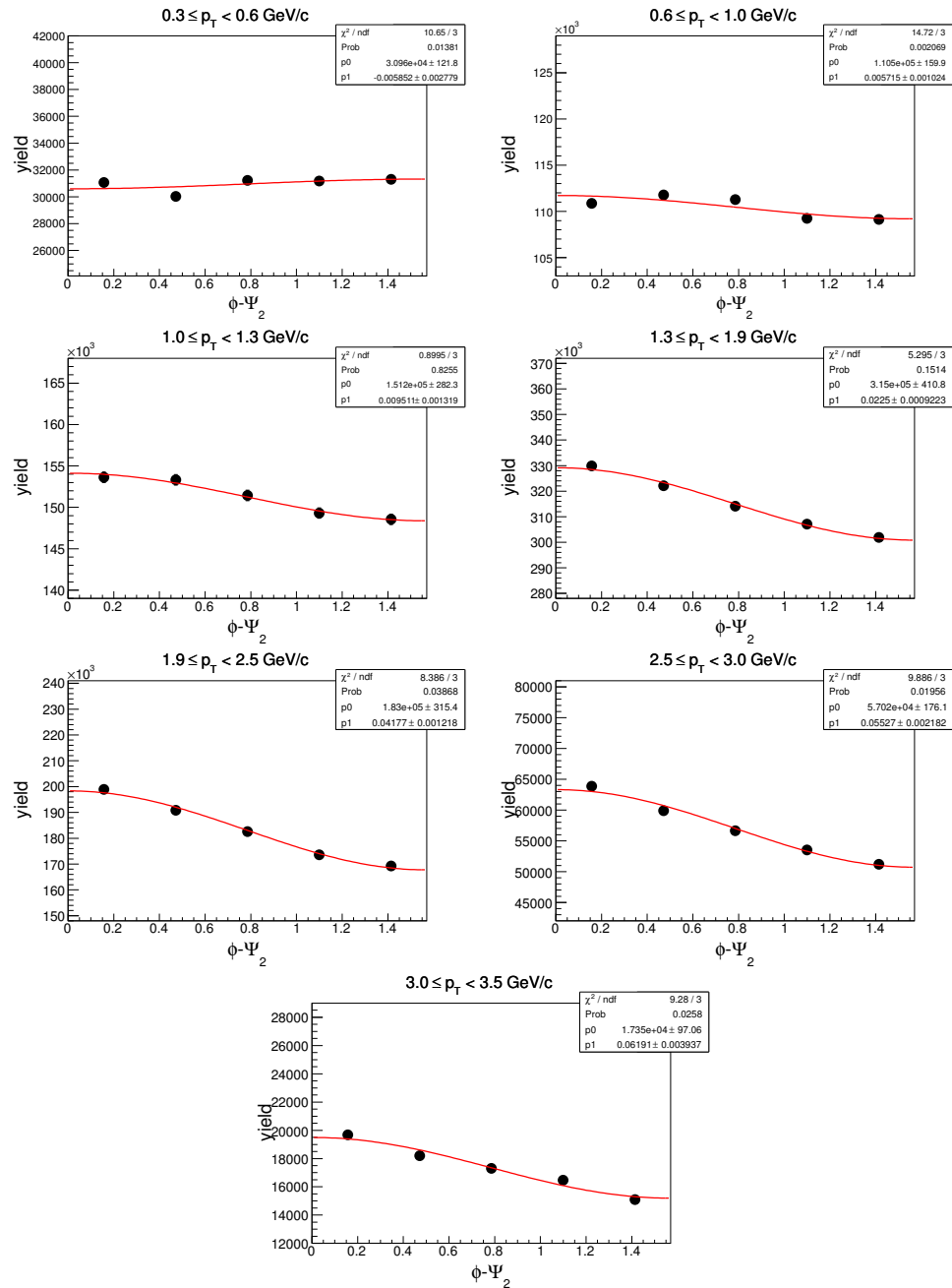


8.7 $\phi - \Psi_2$ distributions in Au+Au at $\sqrt{s_{NN}} = 27$ GeV

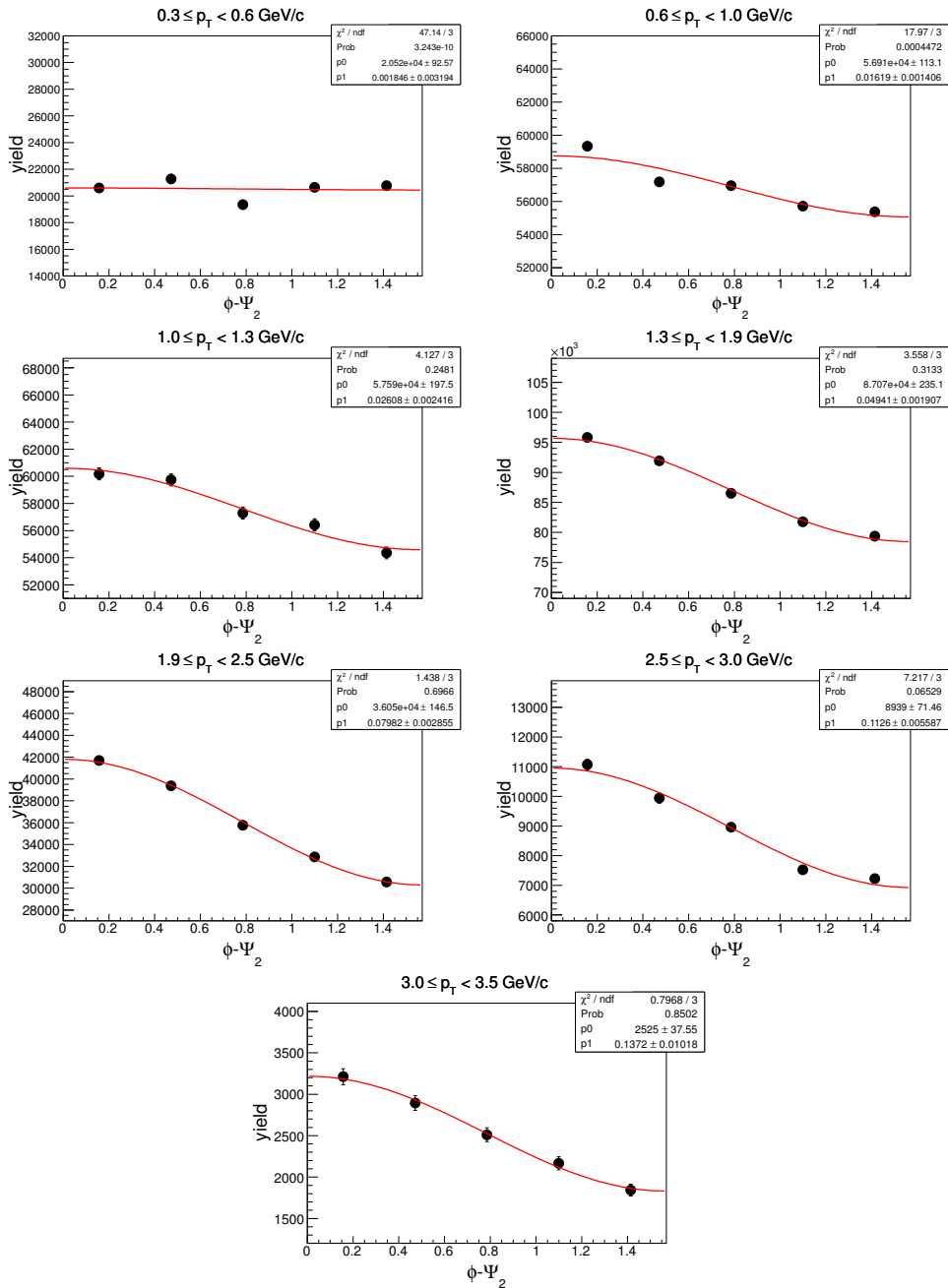
8.7.1 $\phi - \Psi_2$ of d in centrality: 0-80%



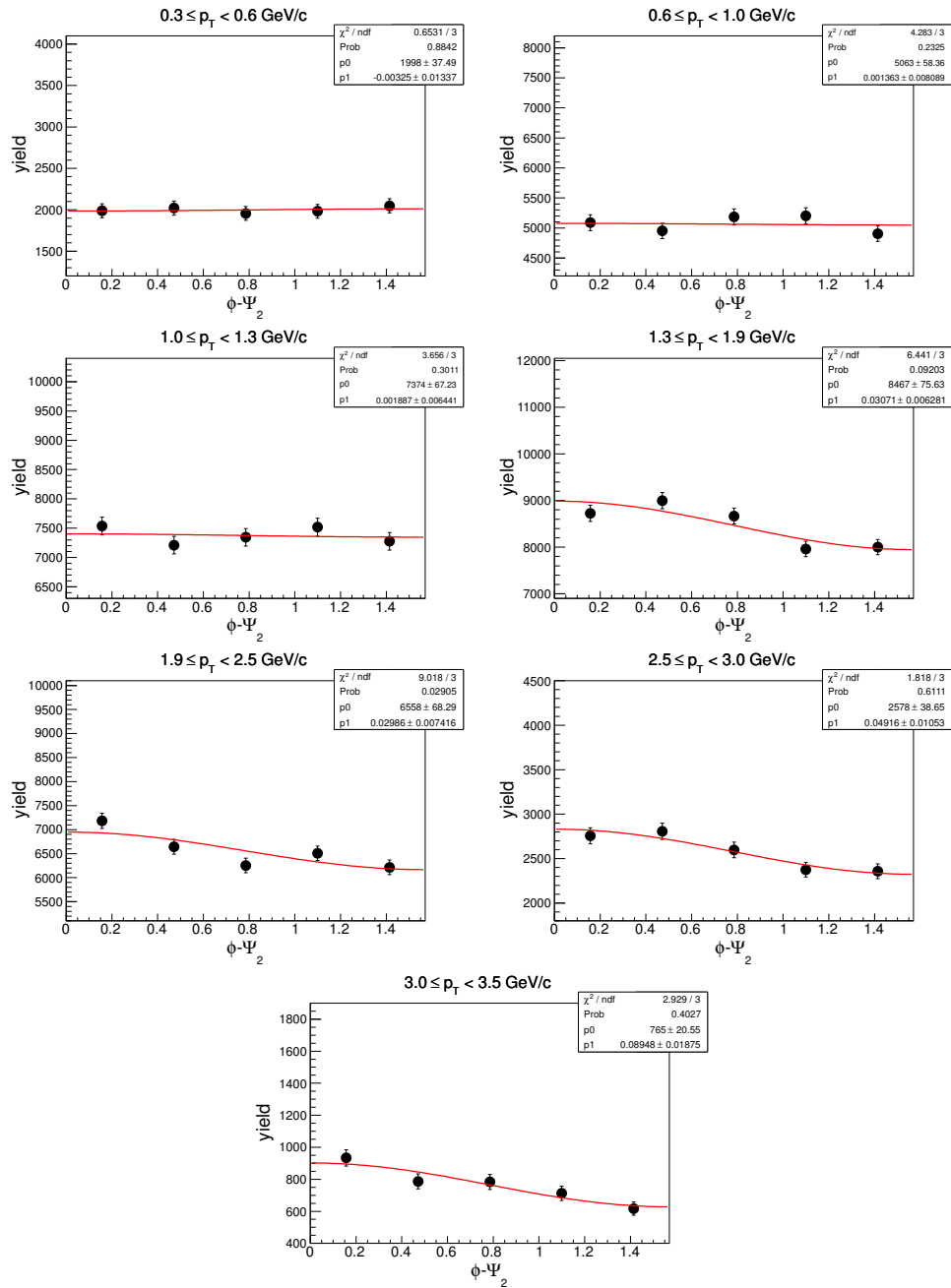
8.7.2 $\phi - \Psi_2$ of d in centrality: 0-30% ($\sqrt{s_{NN}} = 27$ GeV)



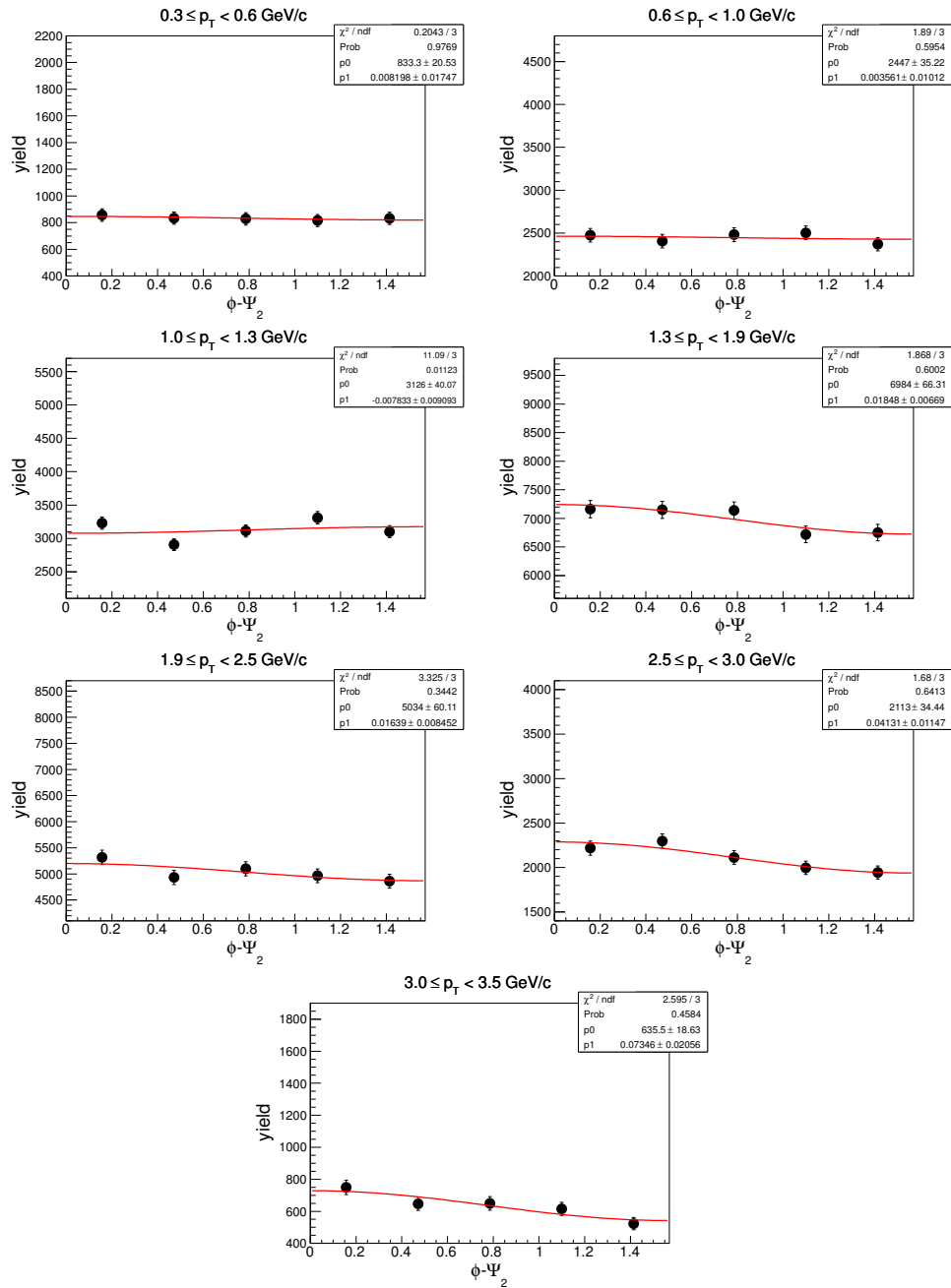
8.7.3 $\phi - \Psi_2$ of d in centrality: 30-80% ($\sqrt{s_{NN}} = 27$ GeV)



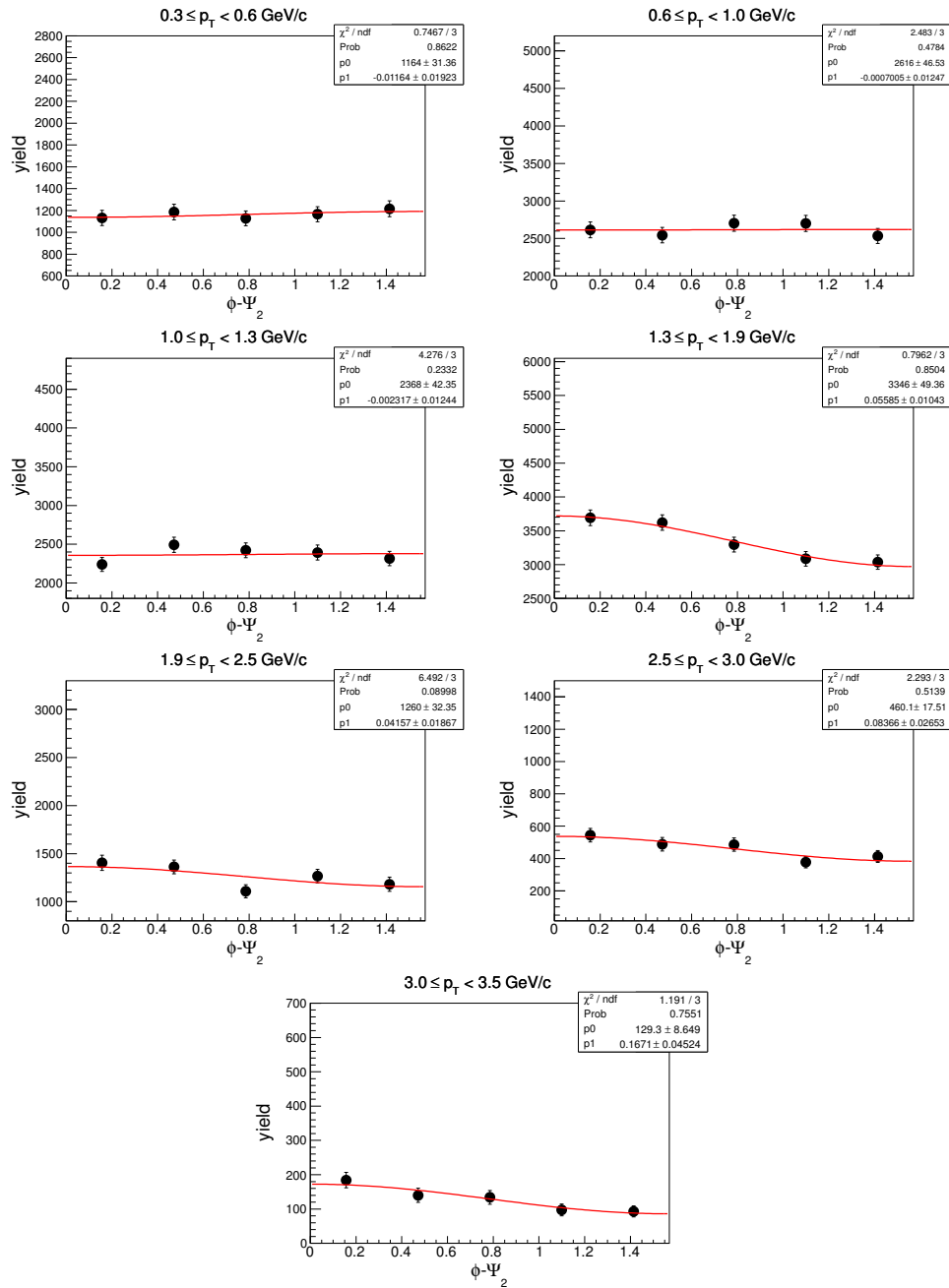
8.7.4 $\phi - \Psi_2$ of \bar{d} in centrality: 0-80% ($\sqrt{s_{NN}} = 27$ GeV)



8.7.5 $\phi - \Psi_2$ of \bar{d} in centrality: 0-30% ($\sqrt{s_{NN}} = 27$ GeV)

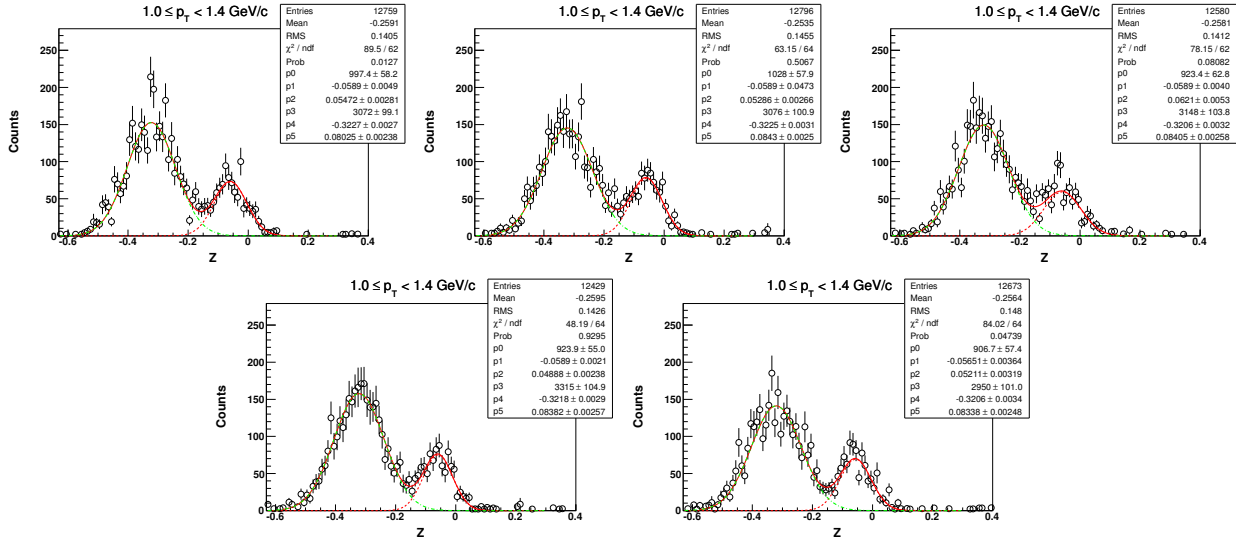


8.7.6 $\phi - \Psi_2$ of \bar{d} in centrality: 30-80% ($\sqrt{s_{NN}} = 27$ GeV)

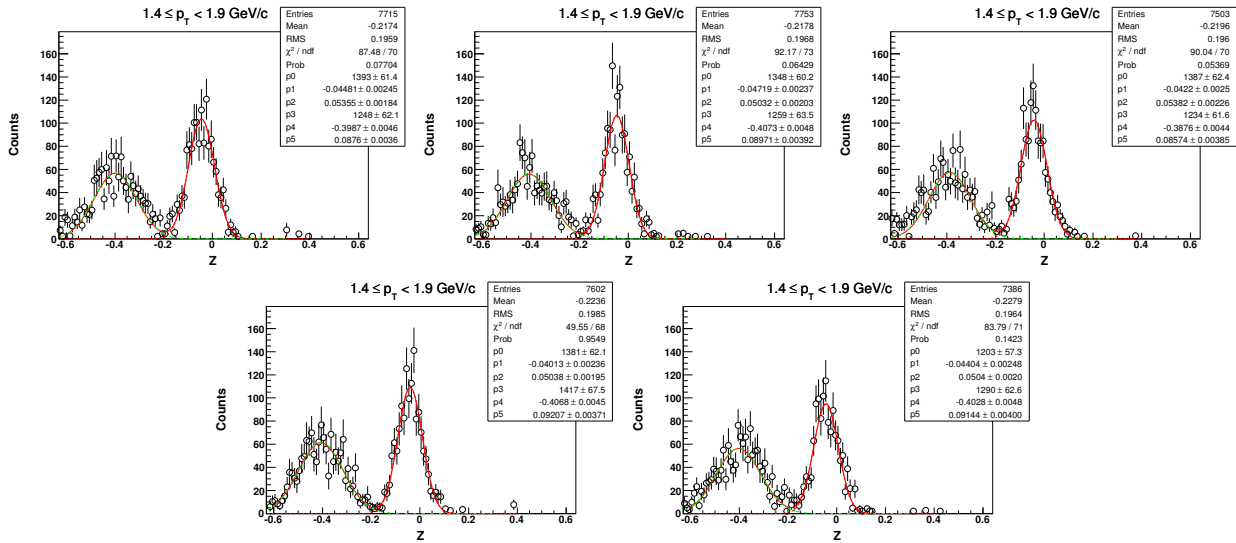


8.8 Z distribution of 3He in $\sqrt{s_{NN}} = 27$ GeV (centrality: 0-80%)

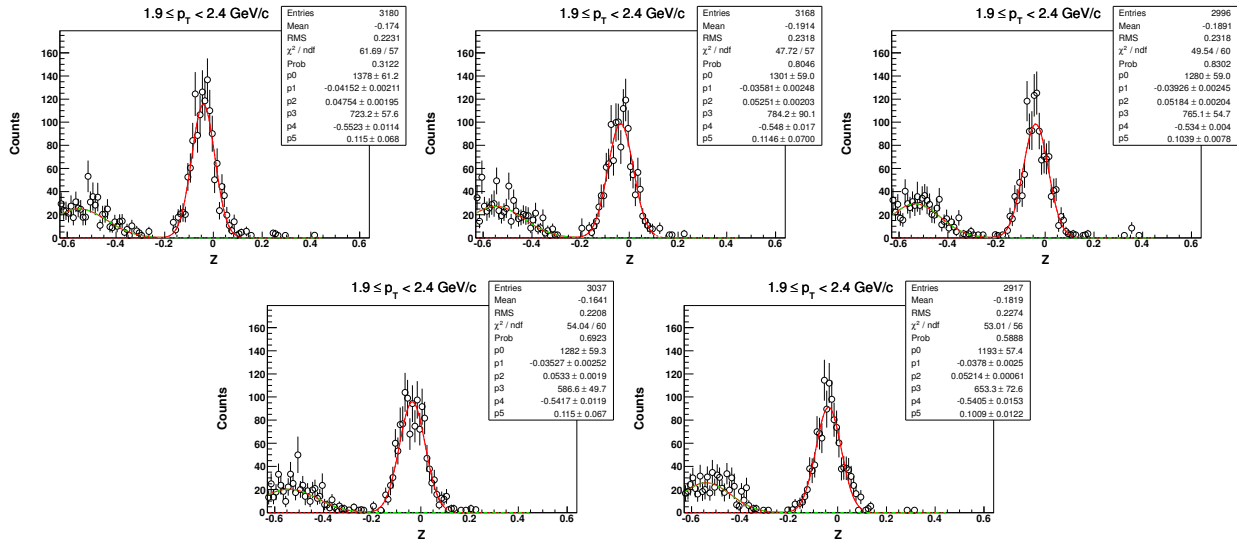
8.8.1 Z-distribution of 3He for $1.0 < p_T < 1.4$ GeV/c



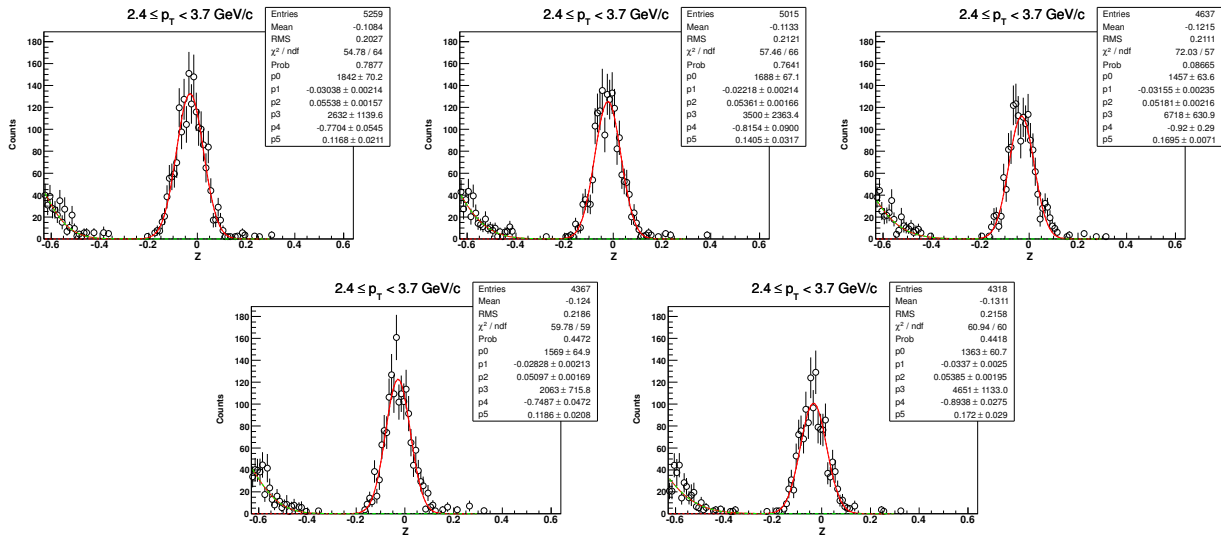
8.8.2 Z-distribution of 3He for $1.4 < p_T < 1.9$ GeV/c ($\sqrt{s_{NN}} = 27$ GeV, 0-80%)



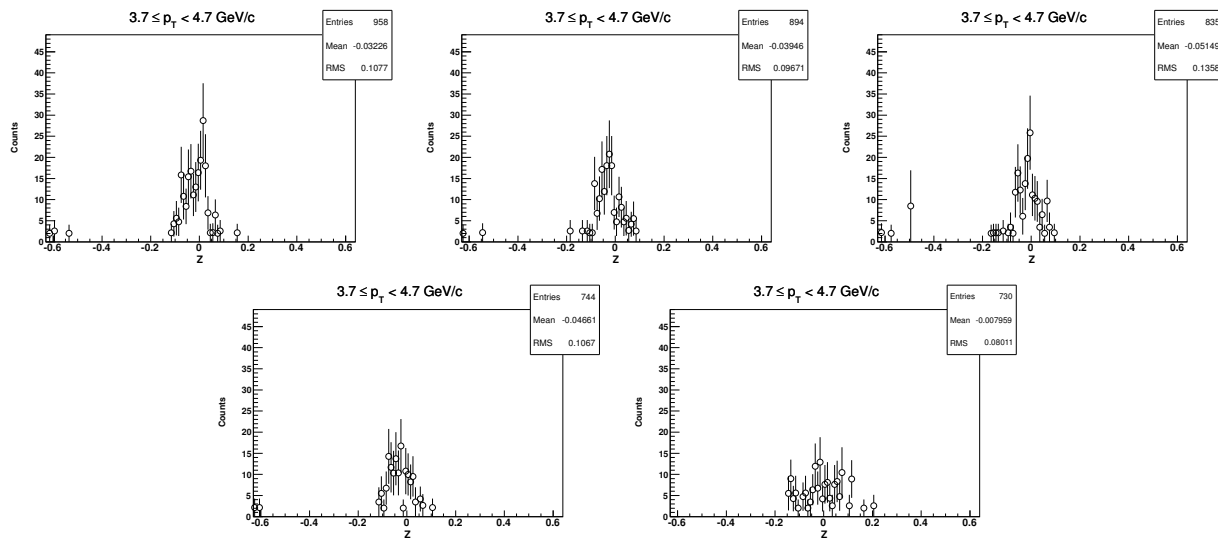
8.8.3 Z-distribution of 3He for $1.9 < p_T < 2.4 \text{ GeV}/c$ ($\sqrt{s_{NN}} = 27 \text{ GeV}$, 0-80%)



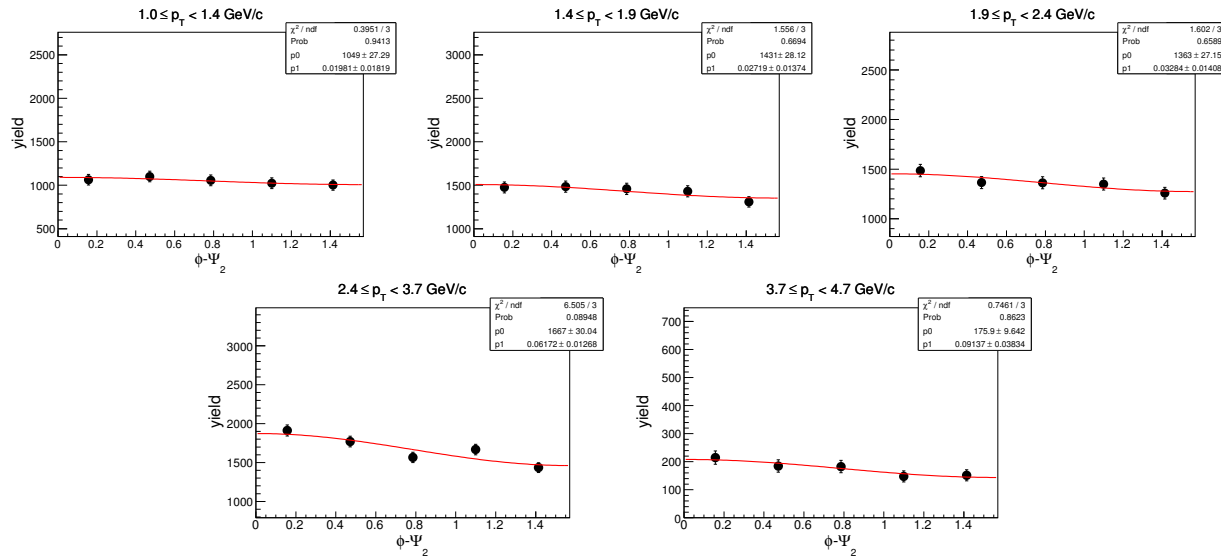
8.8.4 Z-distribution of 3He for $2.4 < p_T < 3.7 \text{ GeV}/c$ ($\sqrt{s_{NN}} = 27 \text{ GeV}$, 0-80%)



8.8.5 Z-distribution of ^3He for $3.7 < p_T < 4.7 \text{ GeV}/c$ ($\sqrt{s_{NN}} = 27 \text{ GeV}$, 0-80%)

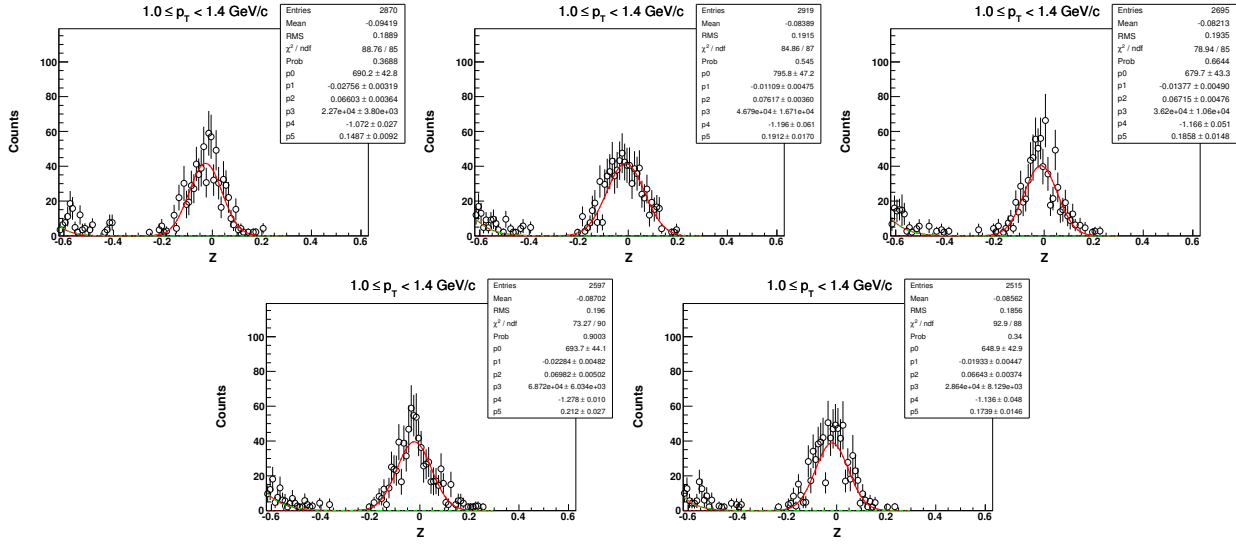


8.8.6 $\phi - \Psi_2$ of ^3He in centrality: 0-80% ($\sqrt{s_{NN}} = 27 \text{ GeV}$)

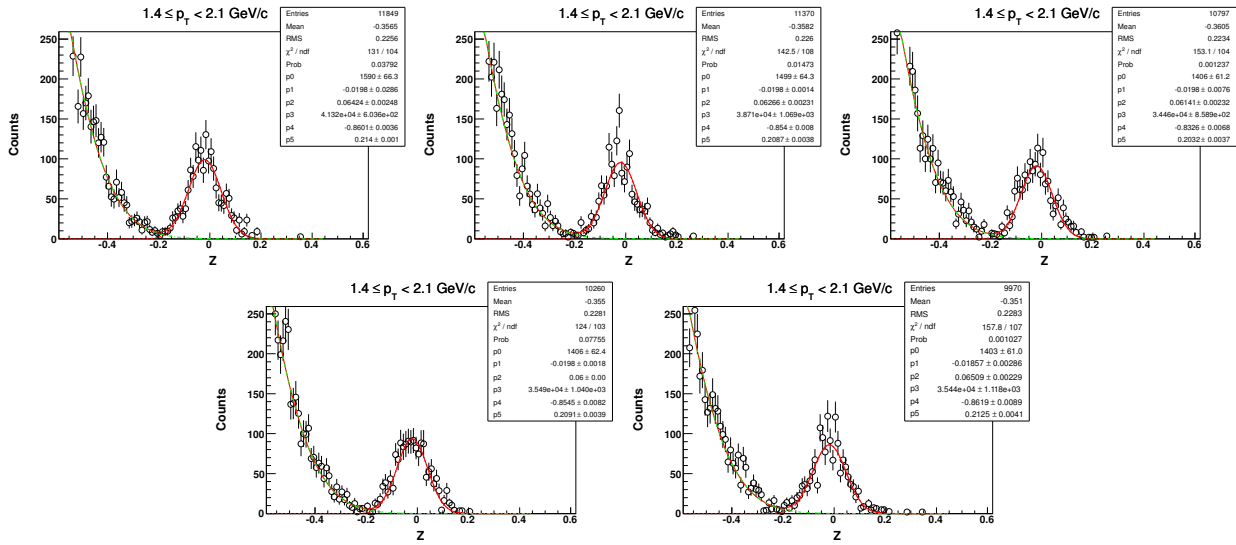


8.9 Z distribution of t in $\sqrt{s_{NN}} = 27 \text{ GeV}$ (centrality: 0-80%)

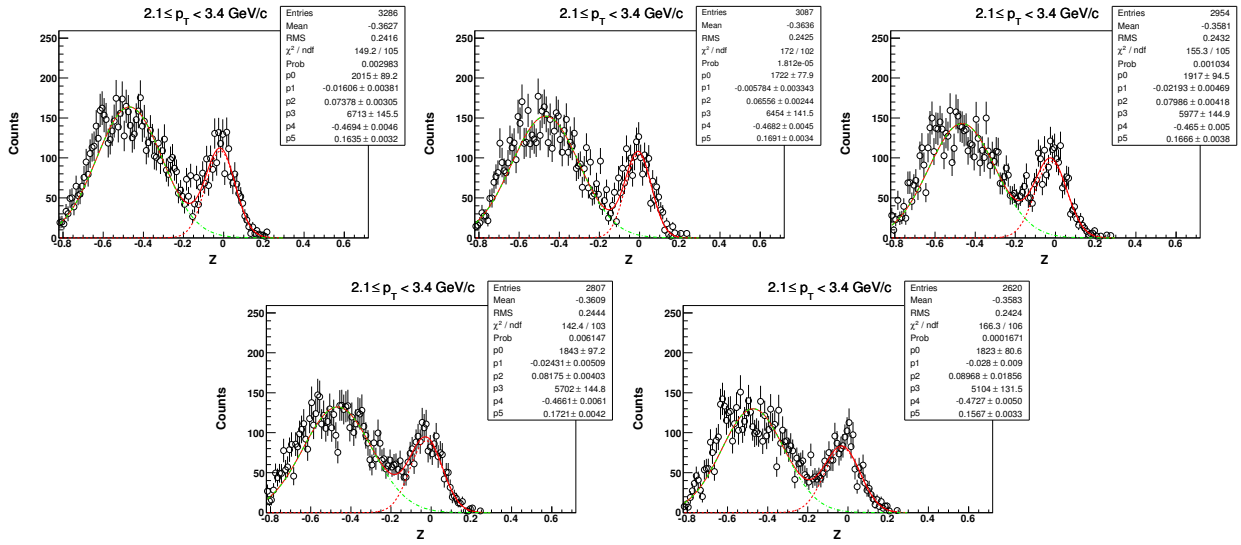
8.9.1 Z-distribution of t for $1.0 < p_T < 1.4 \text{ GeV}/c$



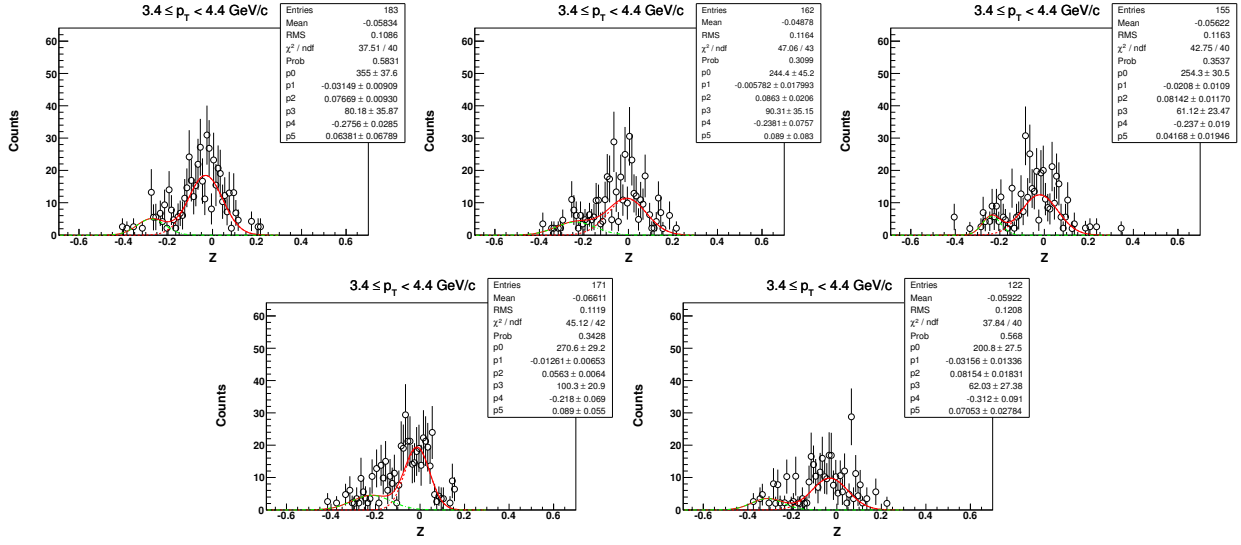
8.9.2 Z-distribution of t for $1.4 < p_T < 2.1 \text{ GeV}/c$ ($\sqrt{s_{NN}} = 27 \text{ GeV}$, 0-80%)



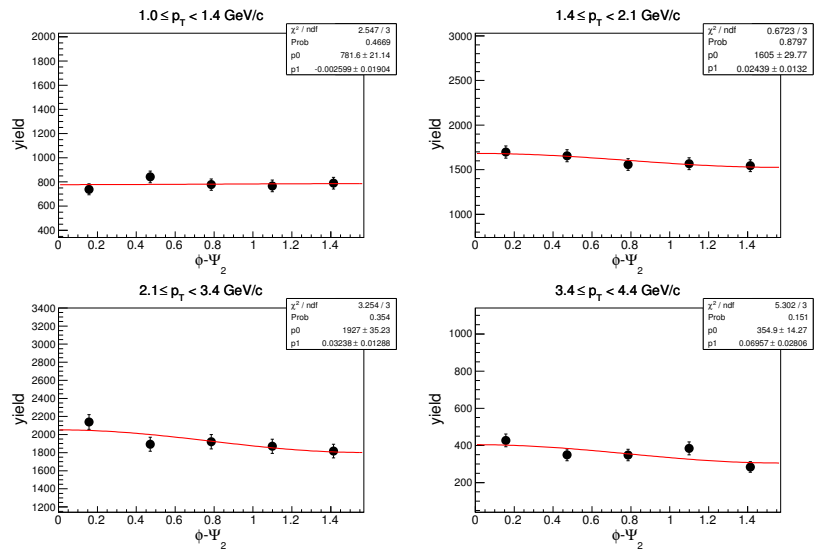
8.9.3 Z-distribution of t for $2.1 < p_T < 3.4 \text{ GeV}/c$ ($\sqrt{s_{NN}} = 27 \text{ GeV}$, 0-80%)



8.9.4 Z-distribution of t for $3.4 < p_T < 4.4 \text{ GeV}/c$ ($\sqrt{s_{NN}} = 27 \text{ GeV}$, 0-80%)



8.9.5 $\phi - \Psi_2$ of t in centrality: 0-80% ($\sqrt{s_{NN}} = 27$ GeV)

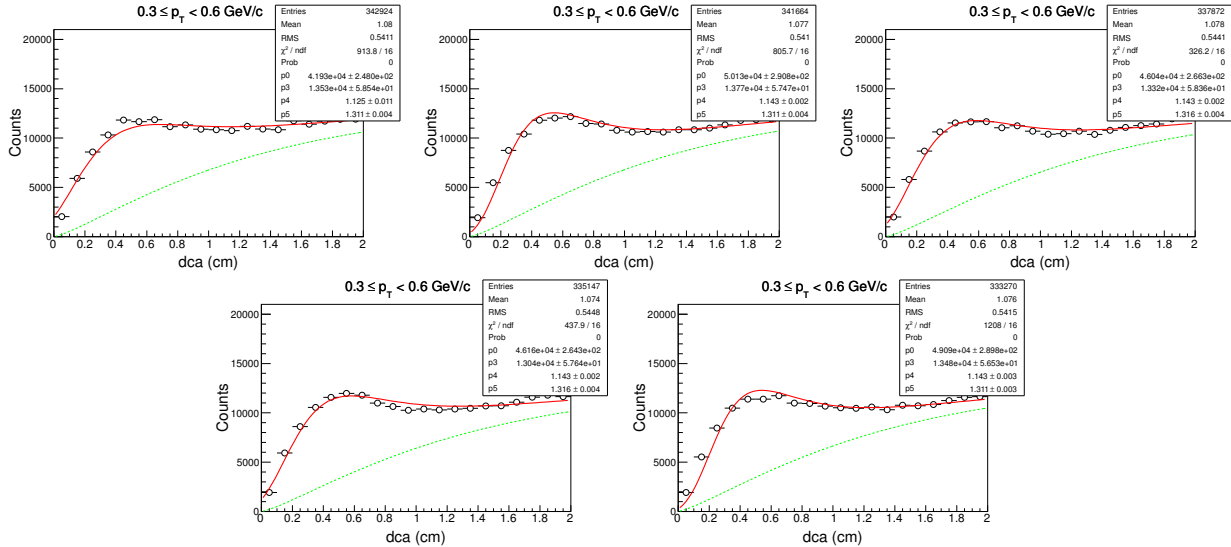


9 DCA and Z-distributions for Au+Au at $\sqrt{s_{NN}} = 19.6$ GeV

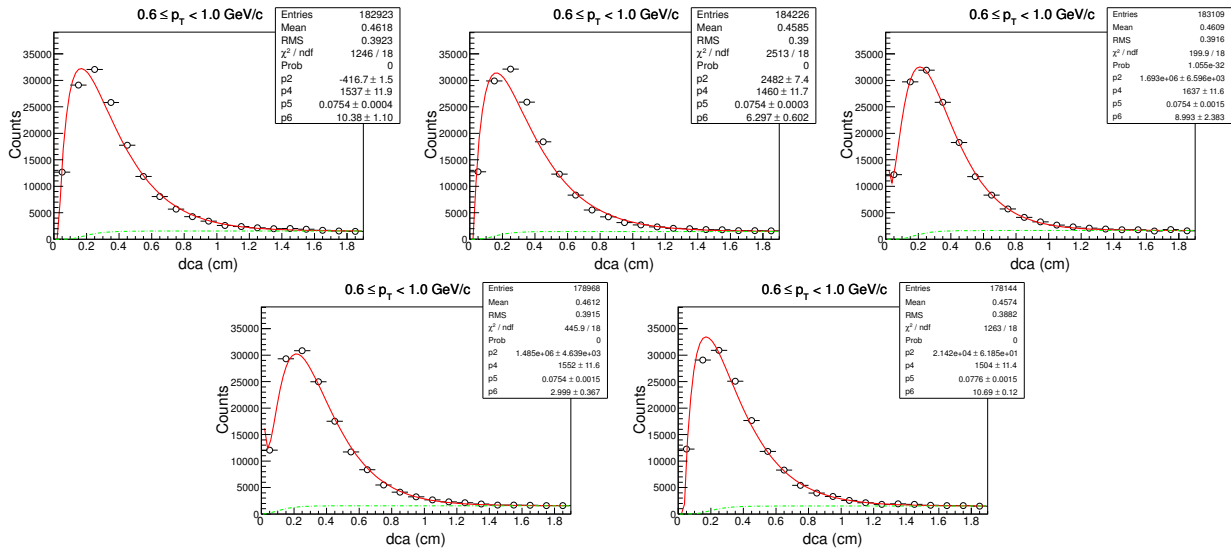
In this section we show the DCA and Z-distribution of deuteron and anti-deuteron for five different ($\phi - \Psi_2$) bins namely, $0 - \frac{\pi}{10}$, $\frac{\pi}{10} - \frac{2\pi}{10}$, $\frac{2\pi}{10} - \frac{3\pi}{10}$, $\frac{3\pi}{10} - \frac{4\pi}{10}$ and $\frac{4\pi}{10} - \frac{5\pi}{10}$. DCA and Z-distribution of d for all centrality and all p_T bins are shown in the later sub-sections.

9.1 Centrality: 0-80%

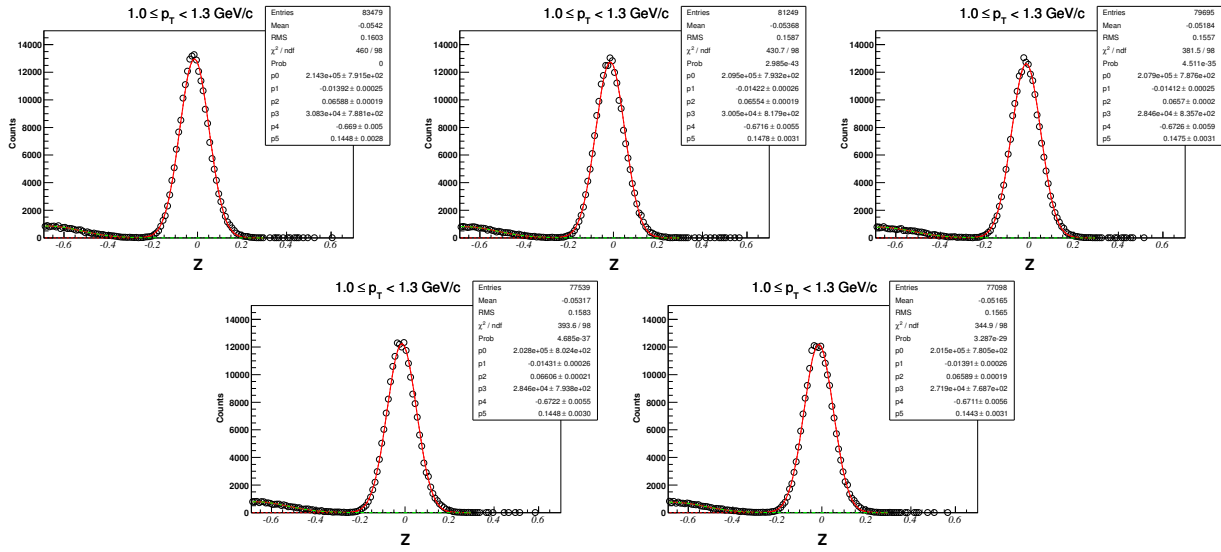
9.1.1 DCA-distribution of d for $0.3 < p_T < 0.6$ GeV/c



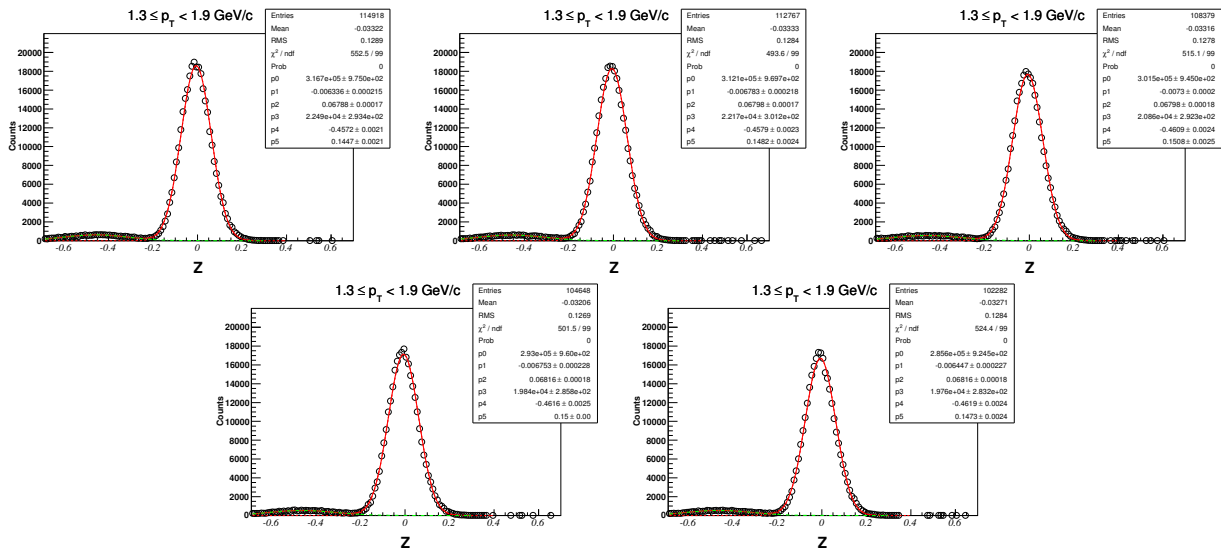
9.1.2 DCA-distribution of d for $0.6 < p_T < 1.0$ GeV/c ($\sqrt{s_{NN}} = 19.6$ GeV, 0-80%)



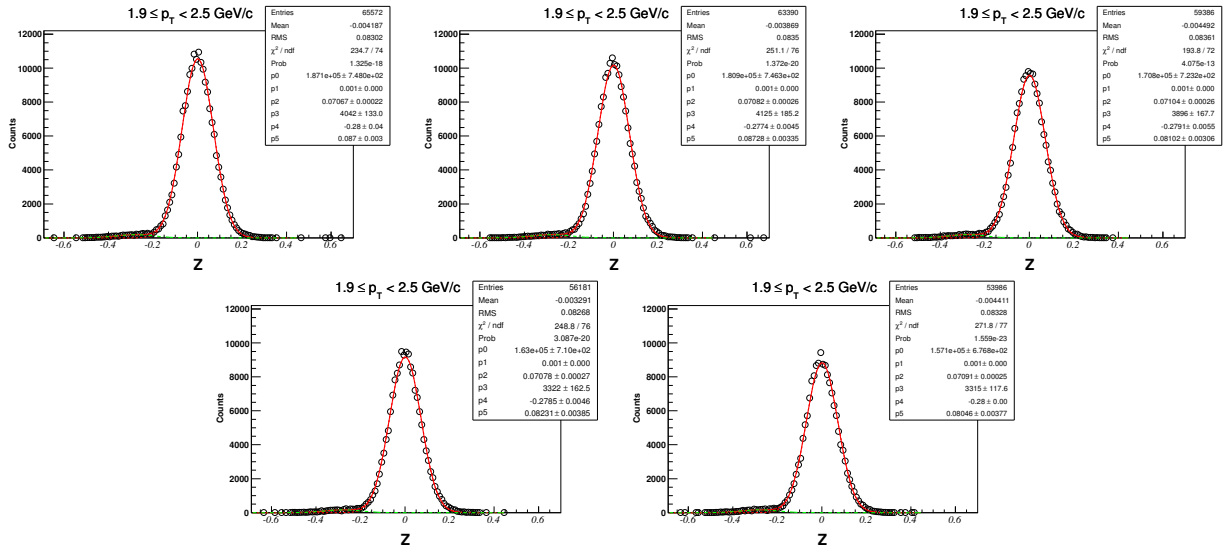
9.1.3 Z-distribution of d for $1.0 < p_T < 1.3 \text{ GeV}/c$ ($\sqrt{s_{NN}} = 19.6 \text{ GeV}$, 0-80%)



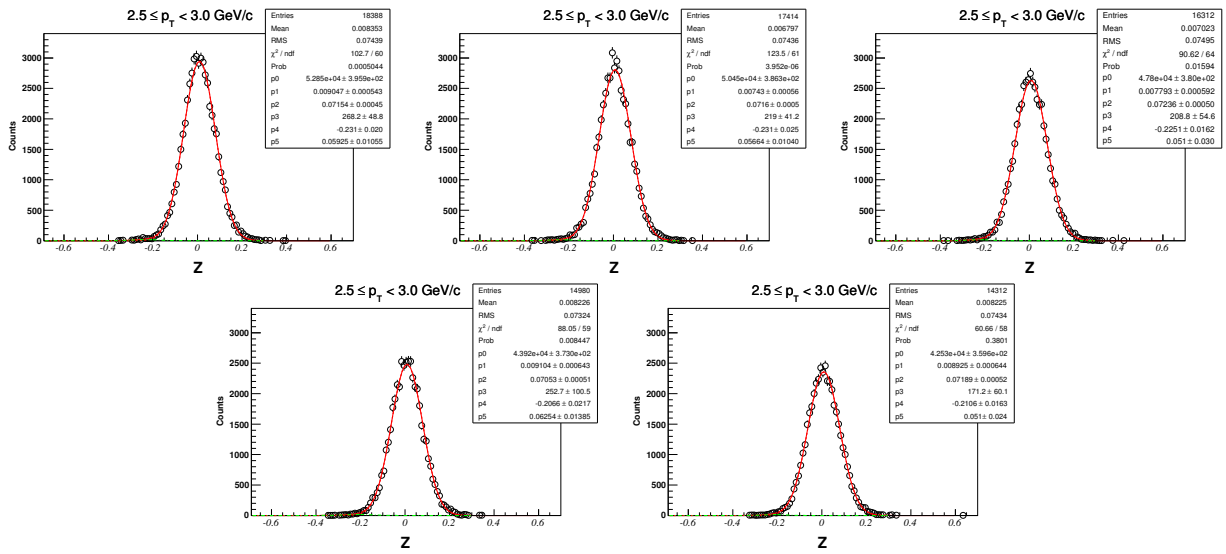
9.1.4 Z-distribution of d for $1.3 < p_T < 1.9 \text{ GeV}/c$ ($\sqrt{s_{NN}} = 19.6 \text{ GeV}$, 0-80%)



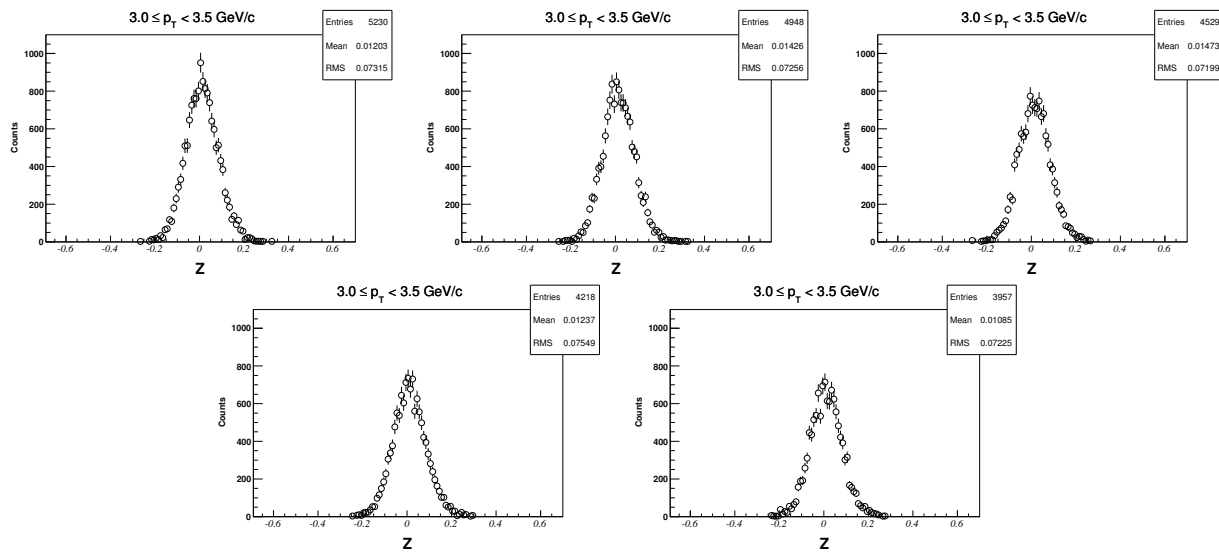
9.1.5 Z-distribution of d for $1.9 < p_T < 2.5 \text{ GeV}/c$ ($\sqrt{s_{NN}} = 19.6 \text{ GeV}$, 0-80%)



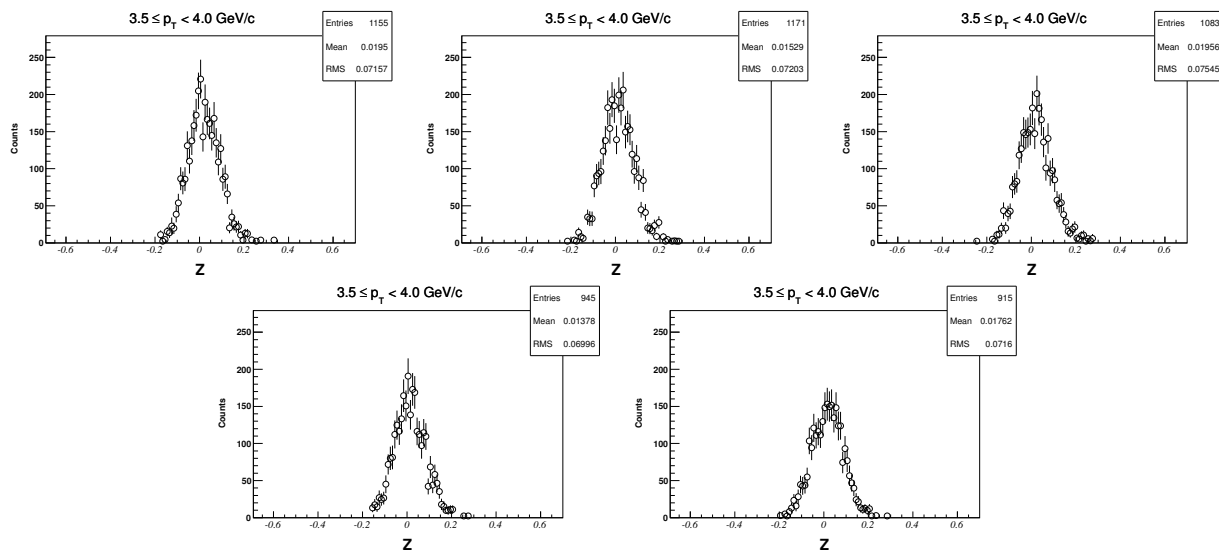
9.1.6 Z-distribution of d for $2.5 < p_T < 3.0 \text{ GeV}/c$ ($\sqrt{s_{NN}} = 19.6 \text{ GeV}$, 0-80%)



9.1.7 Z-distribution of d for $3.0 < p_T < 3.5 \text{ GeV}/c$ ($\sqrt{s_{NN}} = 19.6 \text{ GeV}$, 0-80%)

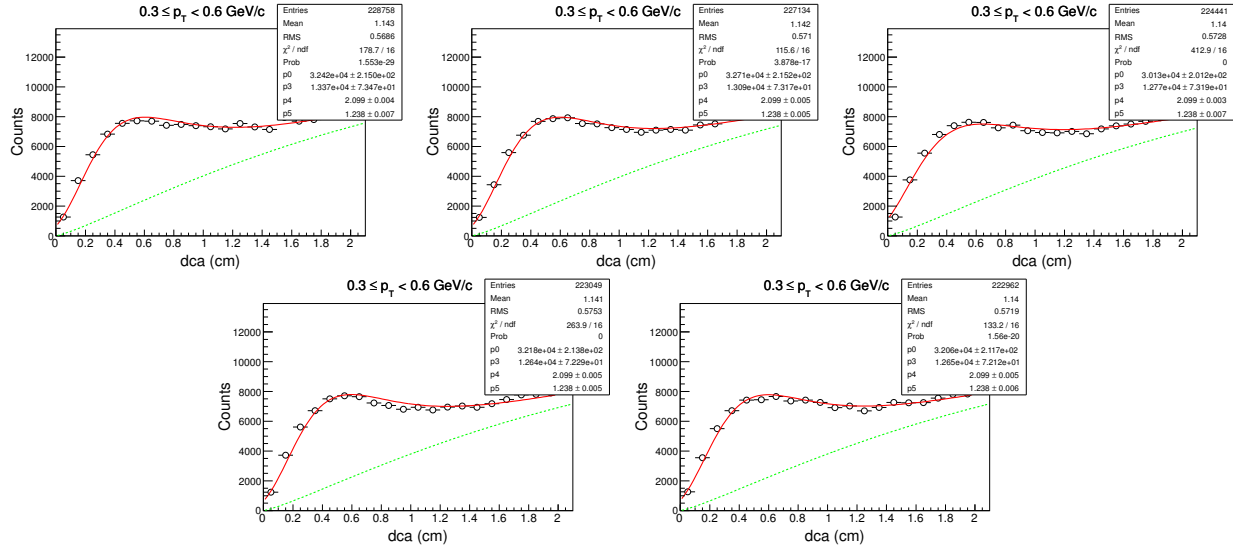


9.1.8 Z-distribution of d for $3.5 < p_T < 4.0 \text{ GeV}/c$ ($\sqrt{s_{NN}} = 19.6 \text{ GeV}$, 0-80%)

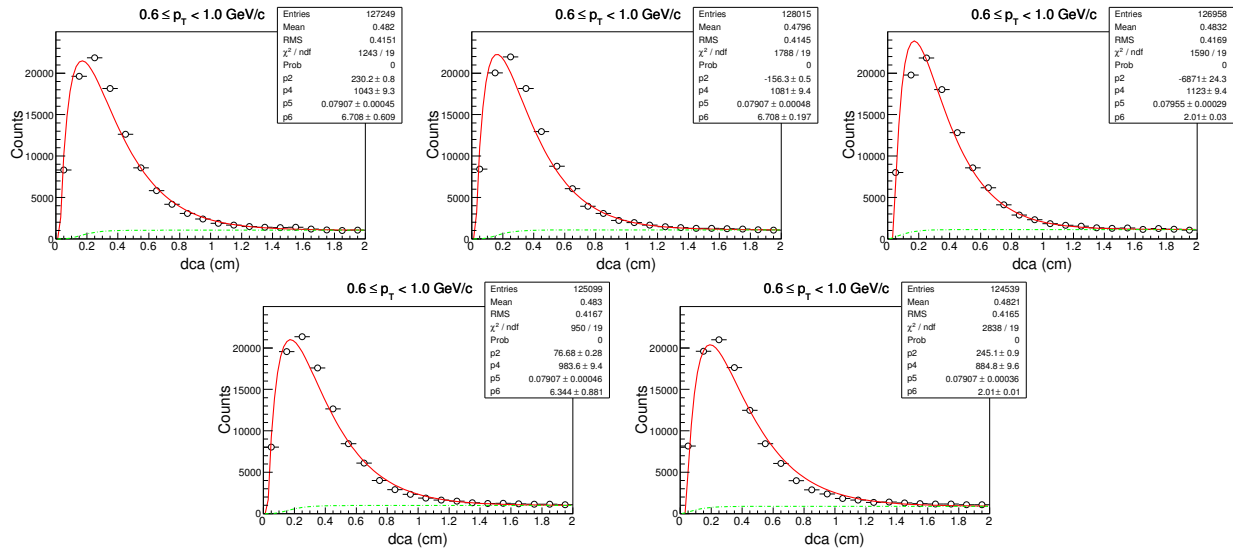


9.2 Centrality: 0-30%

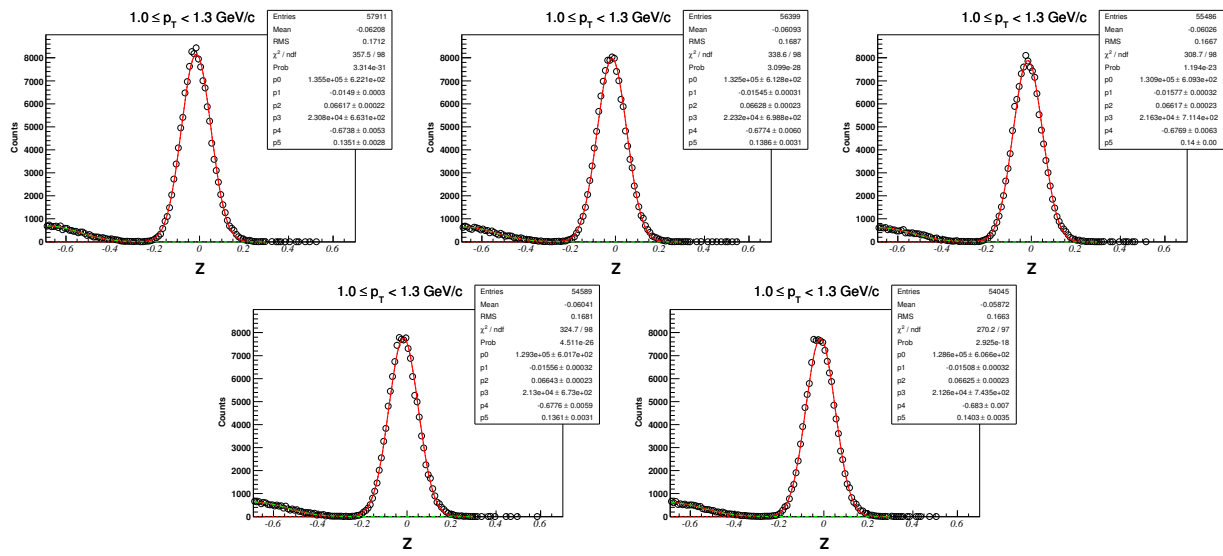
9.2.1 DCA-distribution of d for $0.3 < p_T < 0.6 \text{ GeV}/c$



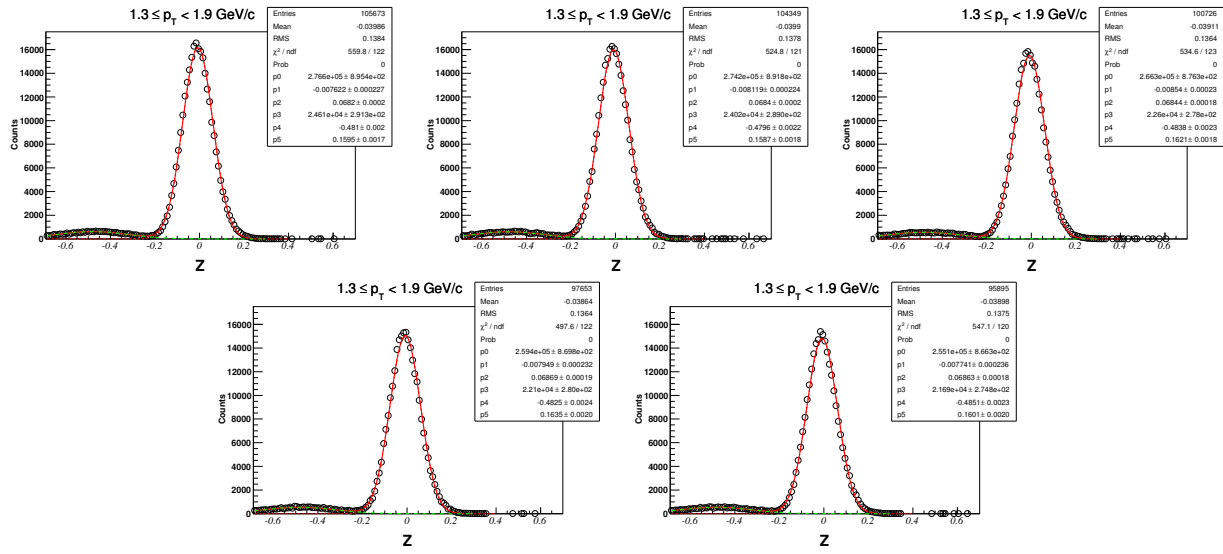
9.2.2 DCA-distribution of d for $0.6 < p_T < 1.0 \text{ GeV}/c$



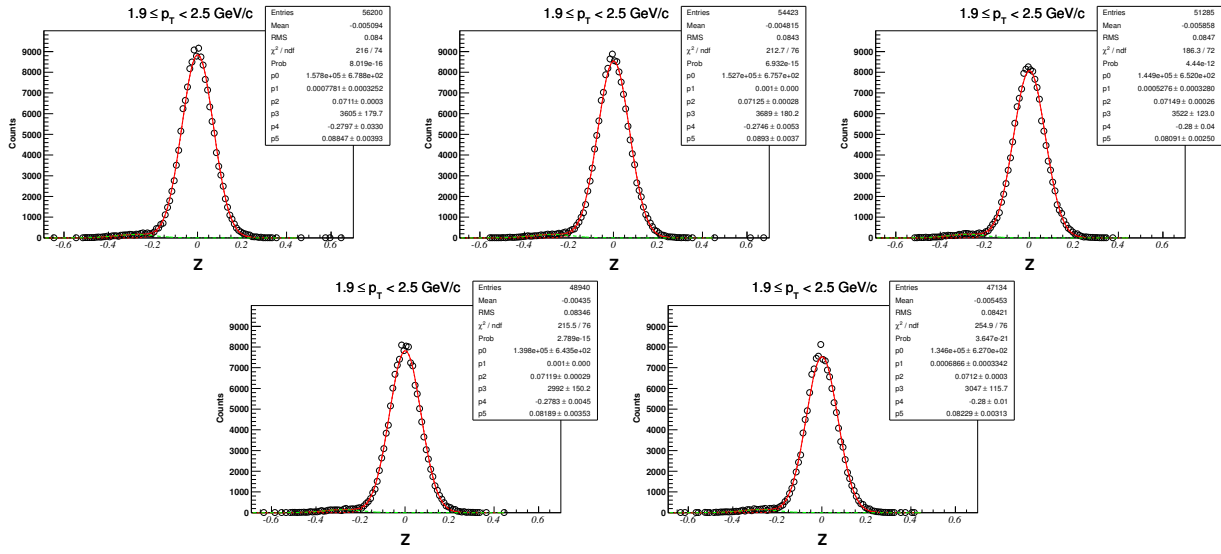
9.2.3 Z-distribution of d for $1.0 < p_T < 1.3 \text{ GeV}/c$ ($\sqrt{s_{NN}} = 19.6 \text{ GeV}$, 0-30%)



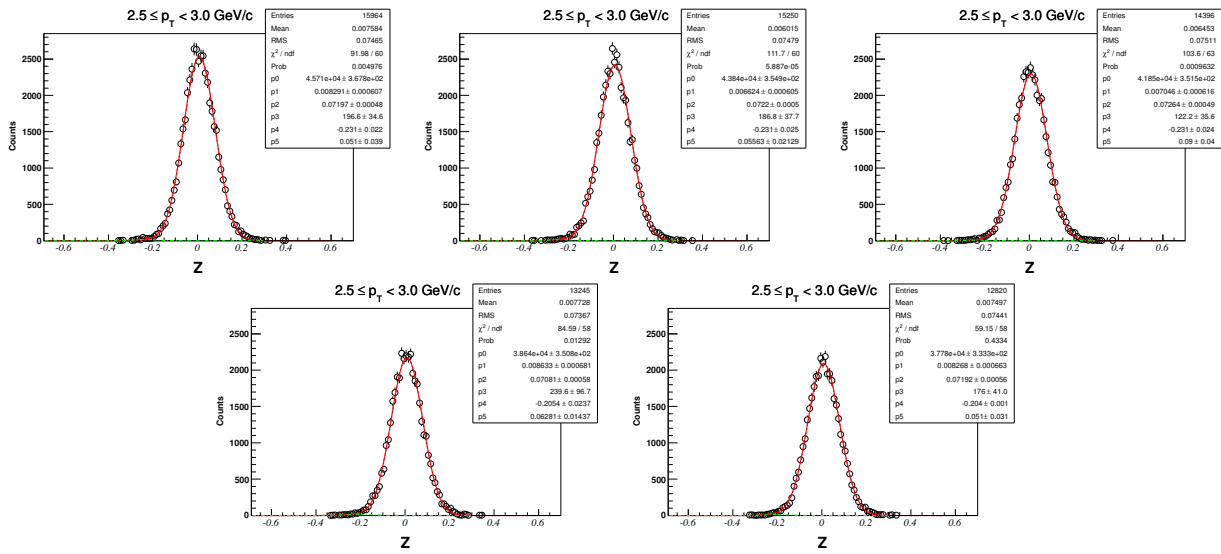
9.2.4 Z-distribution of d for $1.3 < p_T < 1.9 \text{ GeV}/c$ ($\sqrt{s_{NN}} = 19.6 \text{ GeV}$, 0-30%)



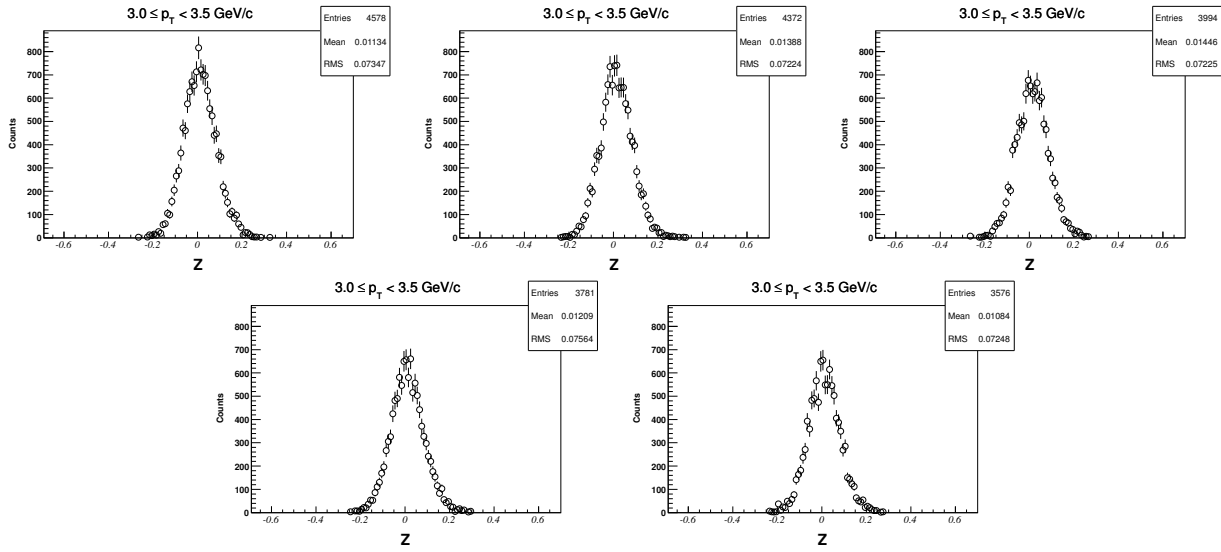
9.2.5 Z-distribution of d for $1.9 < p_T < 2.5 \text{ GeV}/c$ ($\sqrt{s_{NN}} = 19.6 \text{ GeV}$, 0-30%)



9.2.6 Z-distribution of d for $2.5 < p_T < 3.0 \text{ GeV}/c$ ($\sqrt{s_{NN}} = 19.6 \text{ GeV}$, 0-30%)

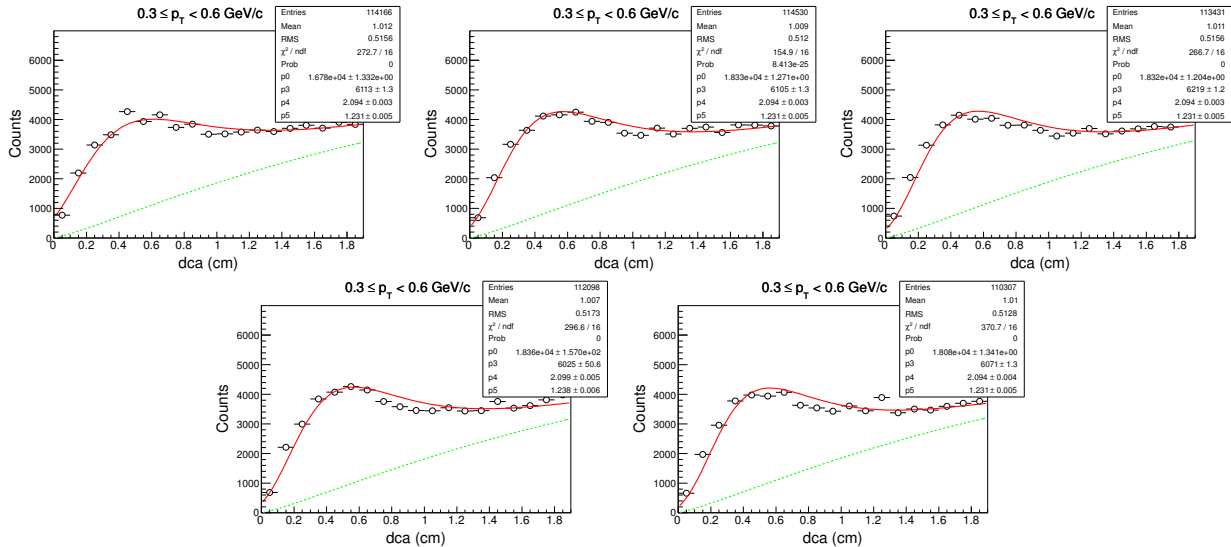


9.2.7 Z-distribution of d for $3.0 < p_T < 3.5 \text{ GeV}/c$ ($\sqrt{s_{NN}} = 19.6 \text{ GeV}$, 0-30%)

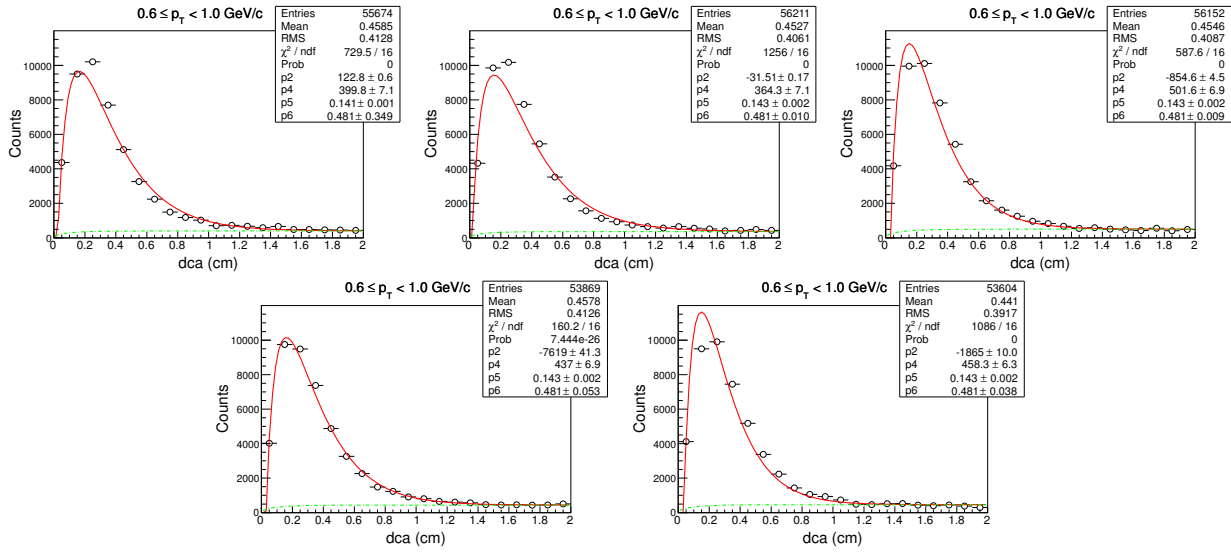


9.3 Centrality: 30-80%

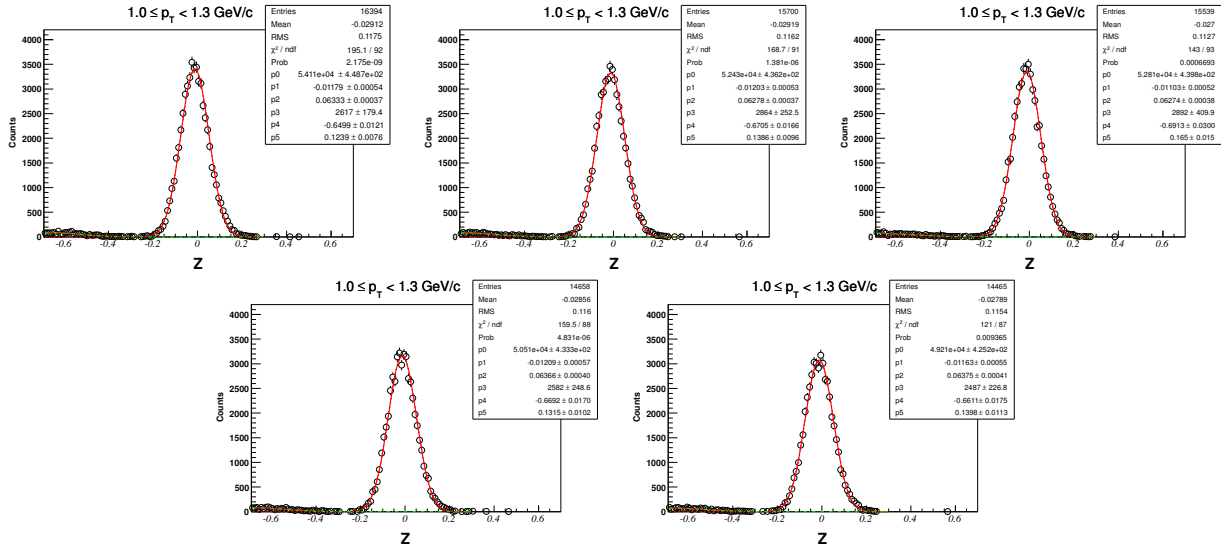
9.3.1 DCA-distribution of d for $0.3 < p_T < 0.6 \text{ GeV}/c$



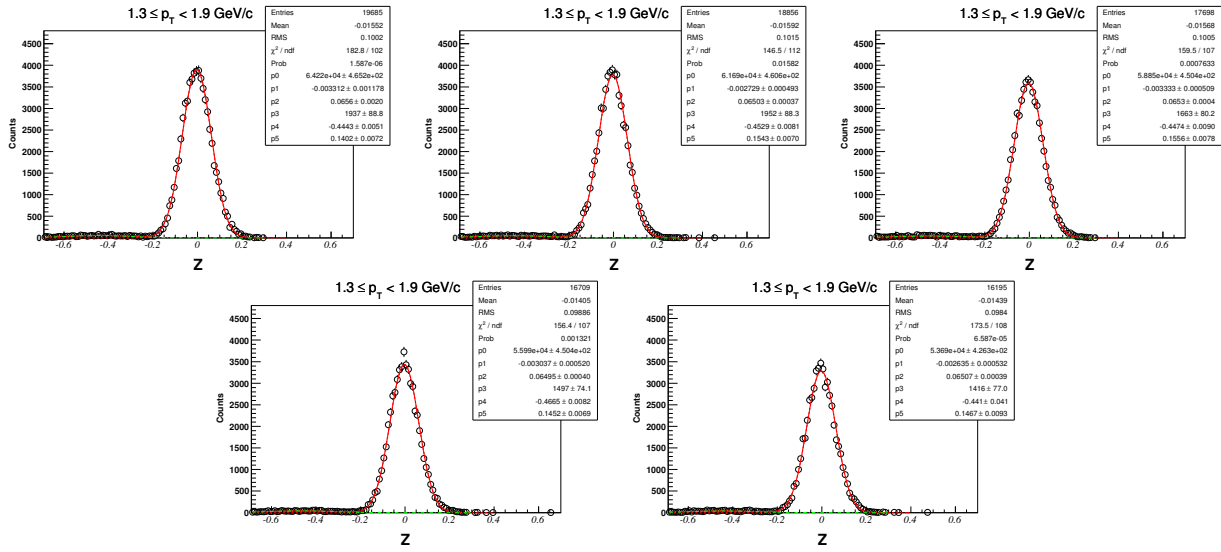
9.3.2 DCA-distribution of d for $0.6 < p_T < 1.0 \text{ GeV}/c$ ($\sqrt{s_{NN}} = 19.6 \text{ GeV}$, 30-80%)



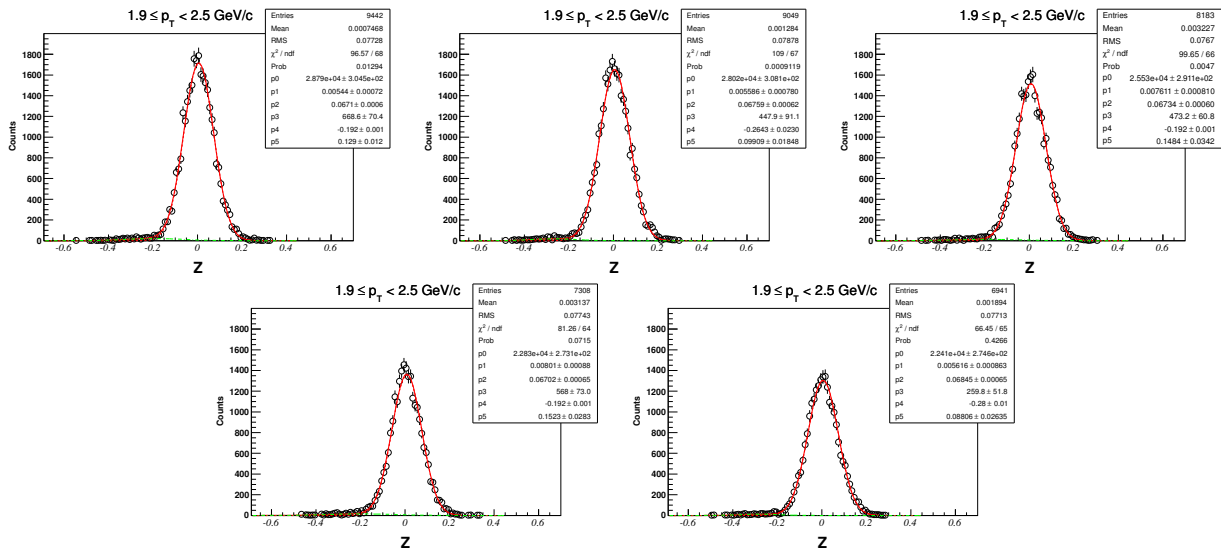
9.3.3 Z-distribution of d for $1.0 < p_T < 1.3 \text{ GeV}/c$ ($\sqrt{s_{NN}} = 19.6 \text{ GeV}$, 30-80%)



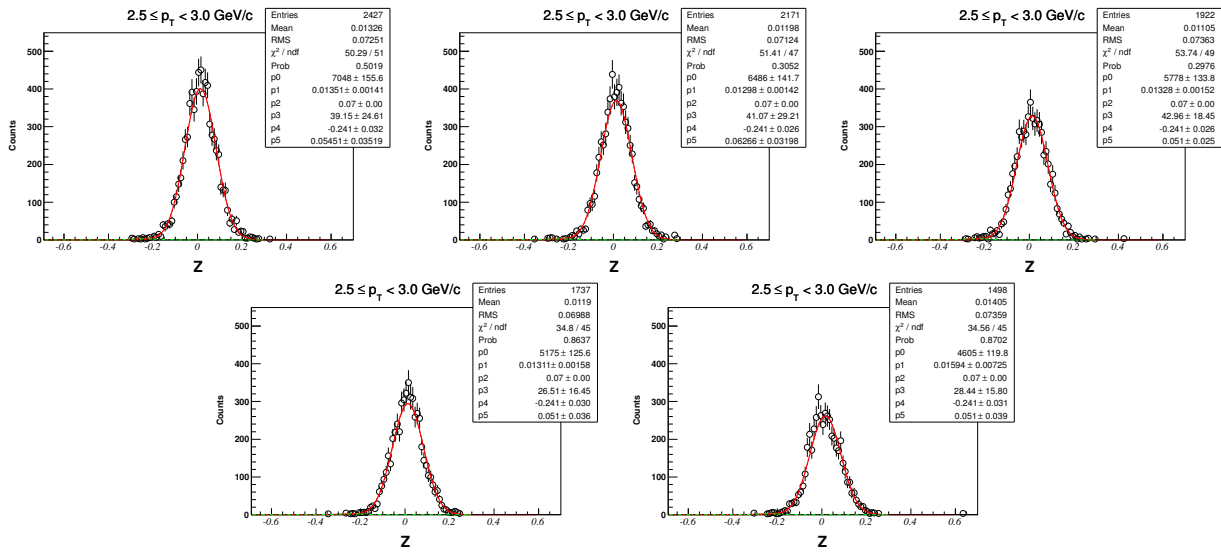
9.3.4 Z-distribution of d for $1.3 < p_T < 1.9 \text{ GeV}/c$ ($\sqrt{s_{NN}} = 19.6 \text{ GeV}$, 30-80%)



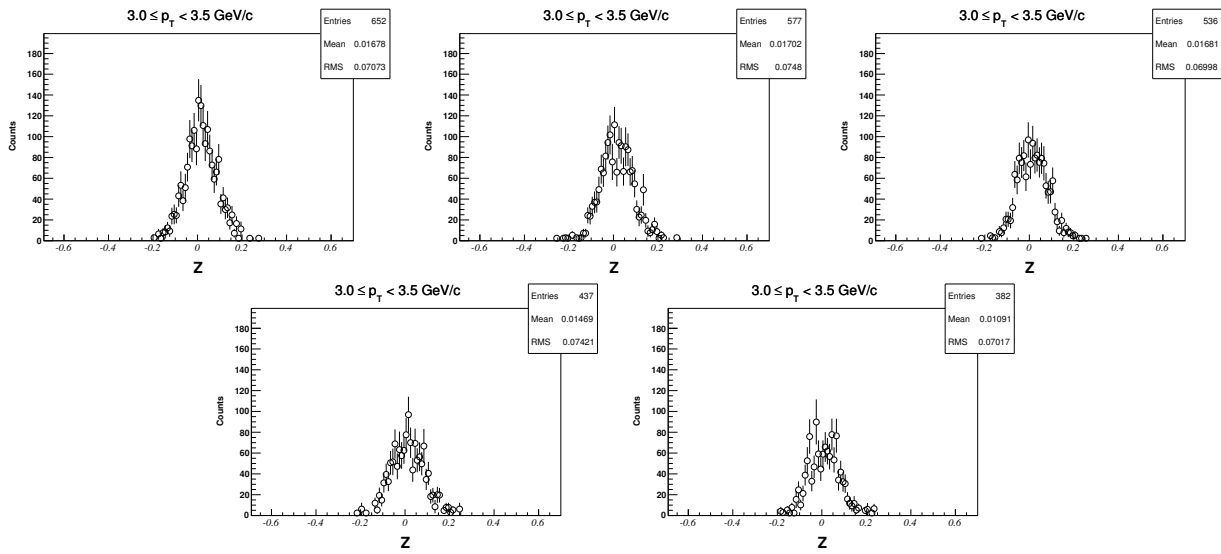
9.3.5 Z-distribution of d for $1.9 < p_T < 2.5 \text{ GeV}/c$ ($\sqrt{s_{NN}} = 19.6 \text{ GeV}$, 30-80%)



9.3.6 Z-distribution of d for $2.5 < p_T < 3.0 \text{ GeV}/c$ ($\sqrt{s_{NN}} = 19.6 \text{ GeV}$, 30-80%)

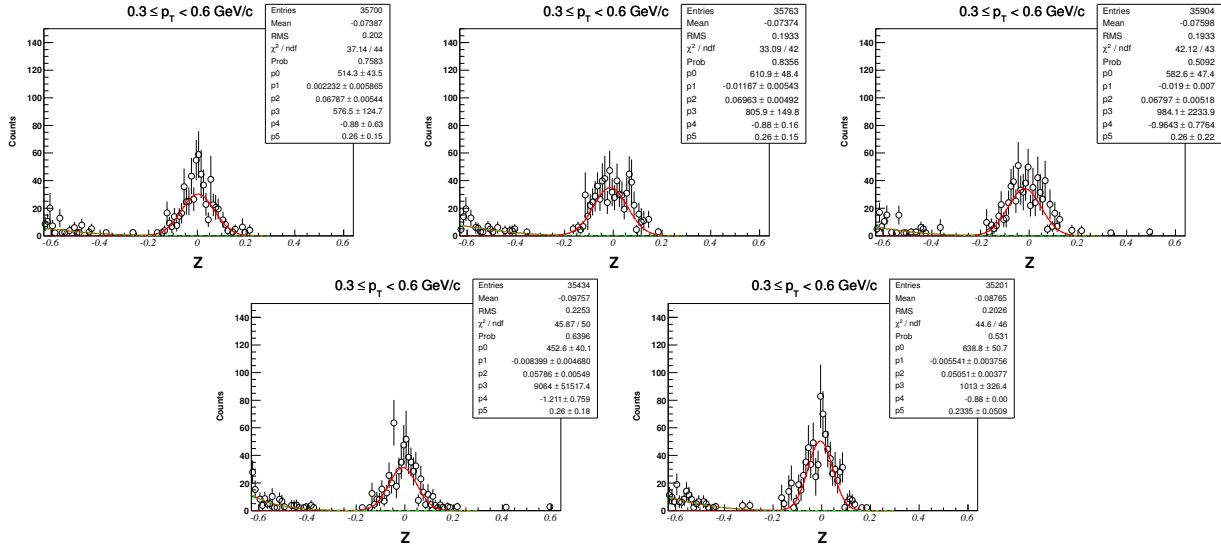


9.3.7 Z-distribution of d for $3.0 < p_T < 3.5 \text{ GeV}/c$ ($\sqrt{s_{NN}} = 19.6 \text{ GeV}$, 30-80%)

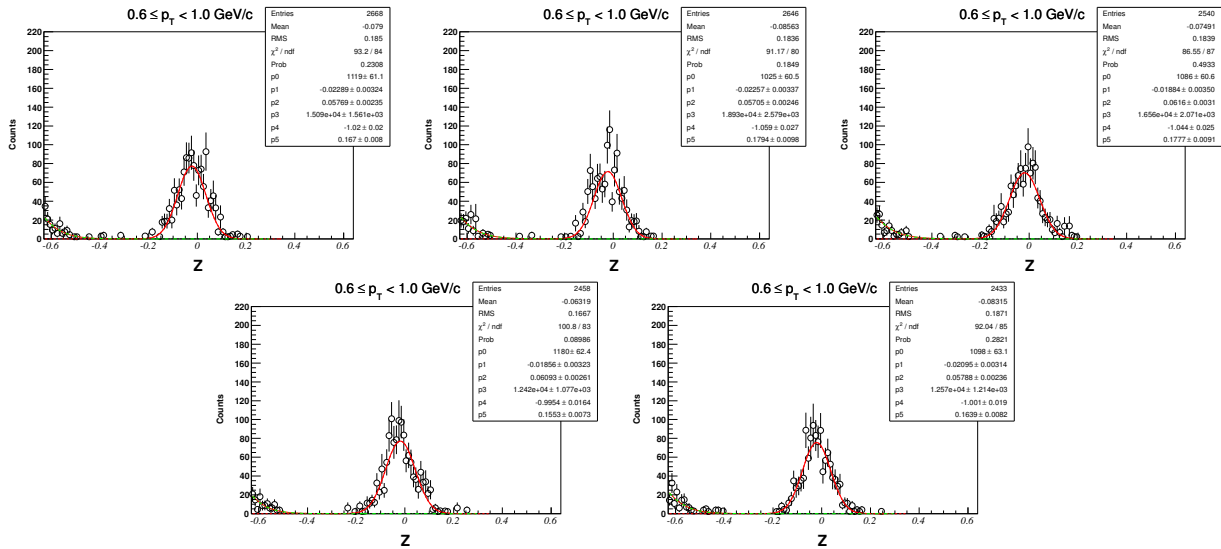


9.4 Z-distribution of \bar{d} in $\sqrt{s_{NN}} = 19.6$ GeV for centrality: 0-80%

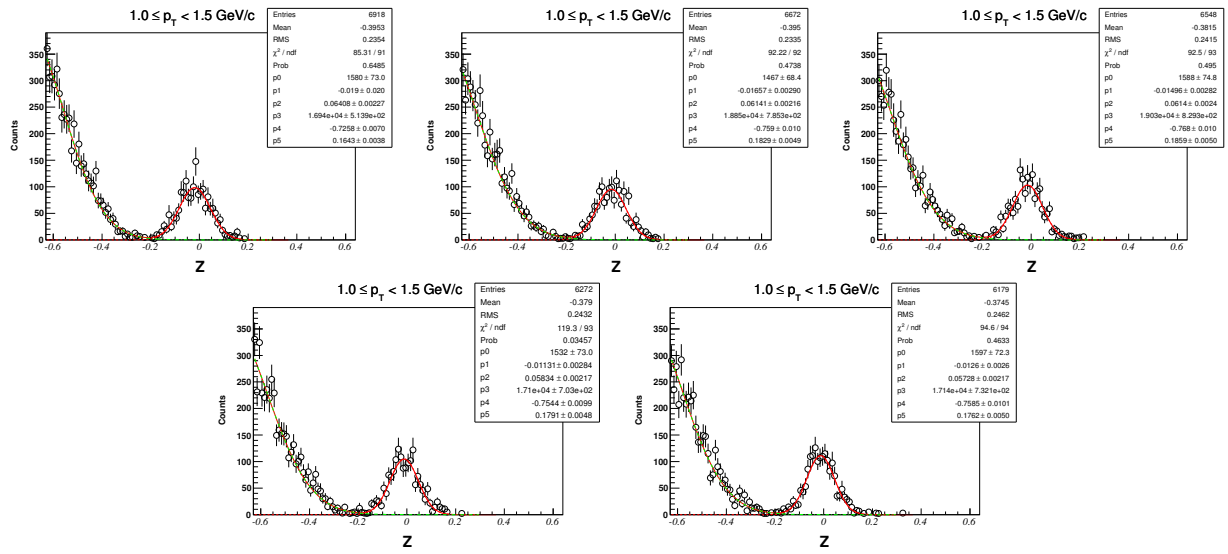
9.4.1 Z-distribution of \bar{d} for $0.3 < p_T < 0.6$ GeV/c



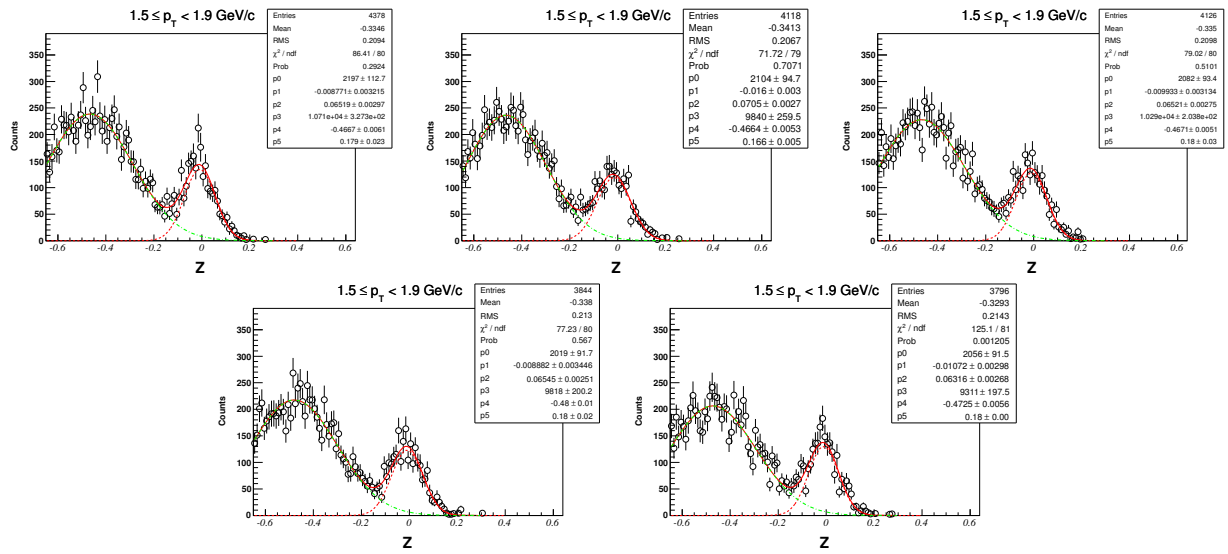
9.4.2 Z-distribution of \bar{d} for $0.6 < p_T < 1.0$ GeV/c



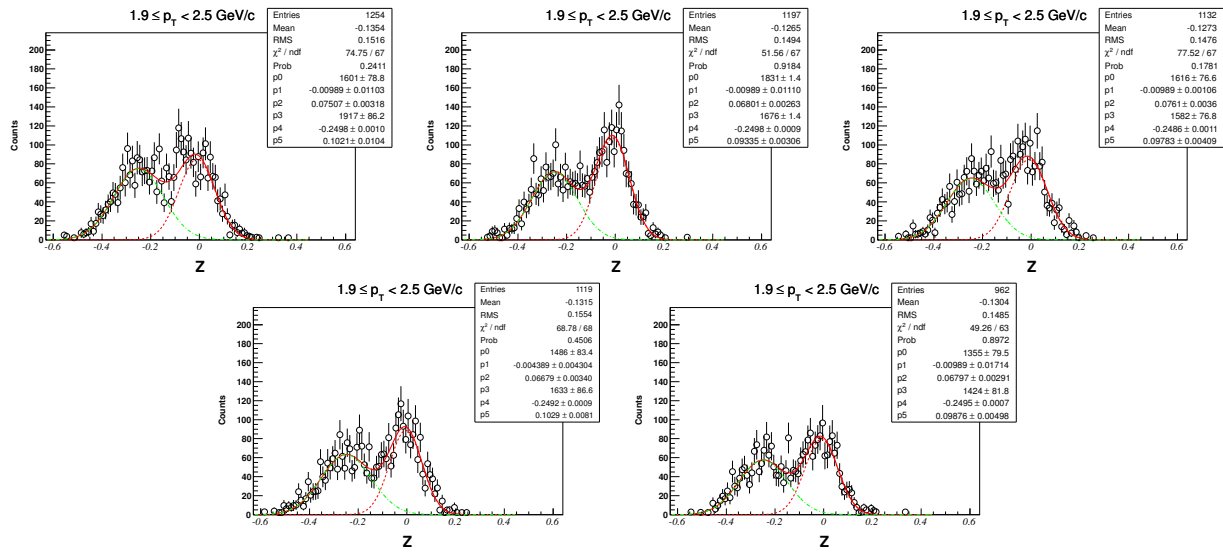
9.4.3 Z-distribution of \bar{d} for $1.0 < p_T < 1.3 \text{ GeV}/c$ ($\sqrt{s_{NN}} = 19.6 \text{ GeV}$, 0-80%)



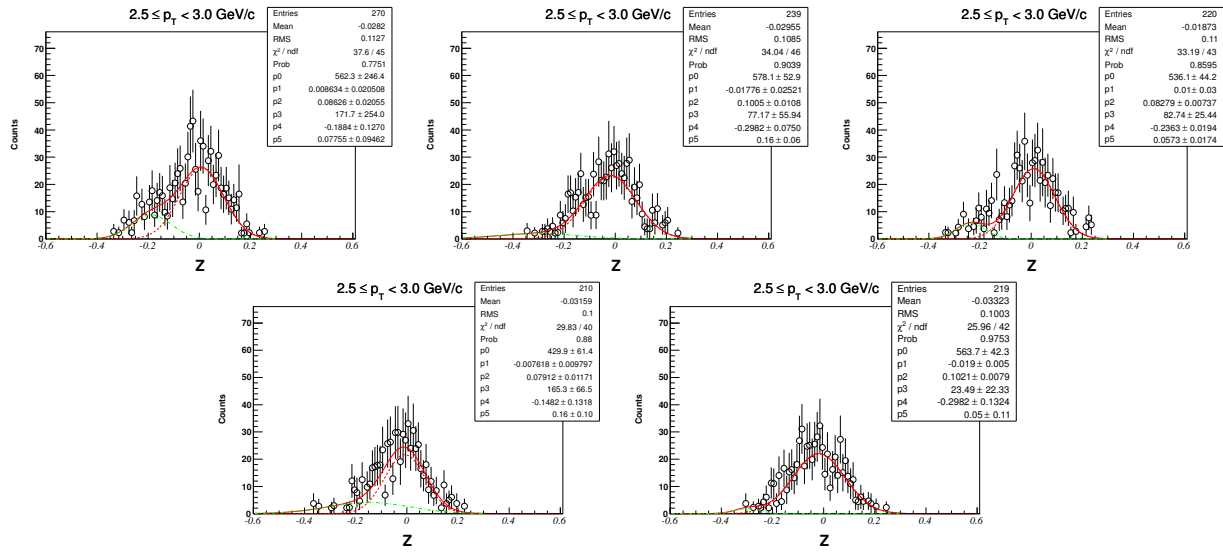
9.4.4 Z-distribution of \bar{d} for $1.3 < p_T < 1.9 \text{ GeV}/c$ ($\sqrt{s_{NN}} = 19.6 \text{ GeV}$, 0-80%)



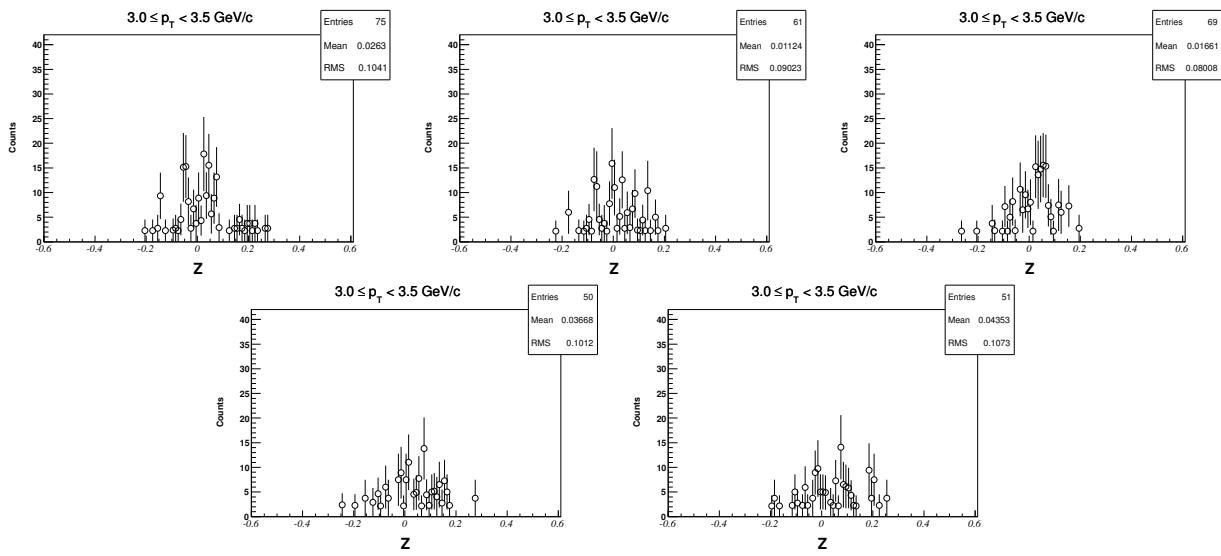
9.4.5 Z-distribution of \bar{d} for $1.9 < p_T < 2.5$ GeV/c ($\sqrt{s_{NN}} = 19.6$ GeV, 0-80%)



9.4.6 Z-distribution of \bar{d} for $2.5 < p_T < 3.0$ GeV/c ($\sqrt{s_{NN}} = 19.6$ GeV, 0-80%)

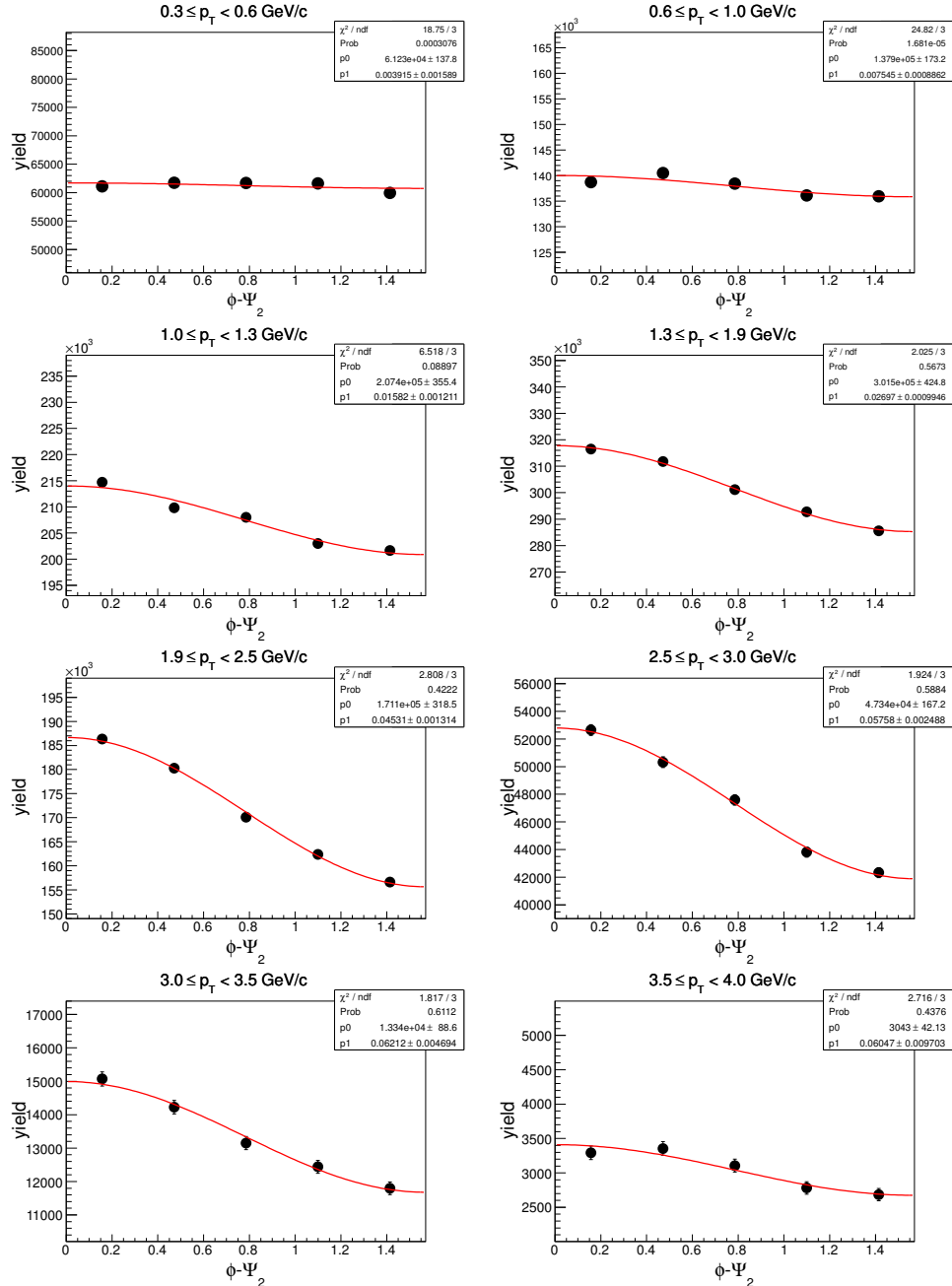


9.4.7 Z-distribution of \bar{d} for $3.0 < p_T < 3.5 \text{ GeV}/c$ ($\sqrt{s_{NN}} = 19.6 \text{ GeV}$, 0-80%)

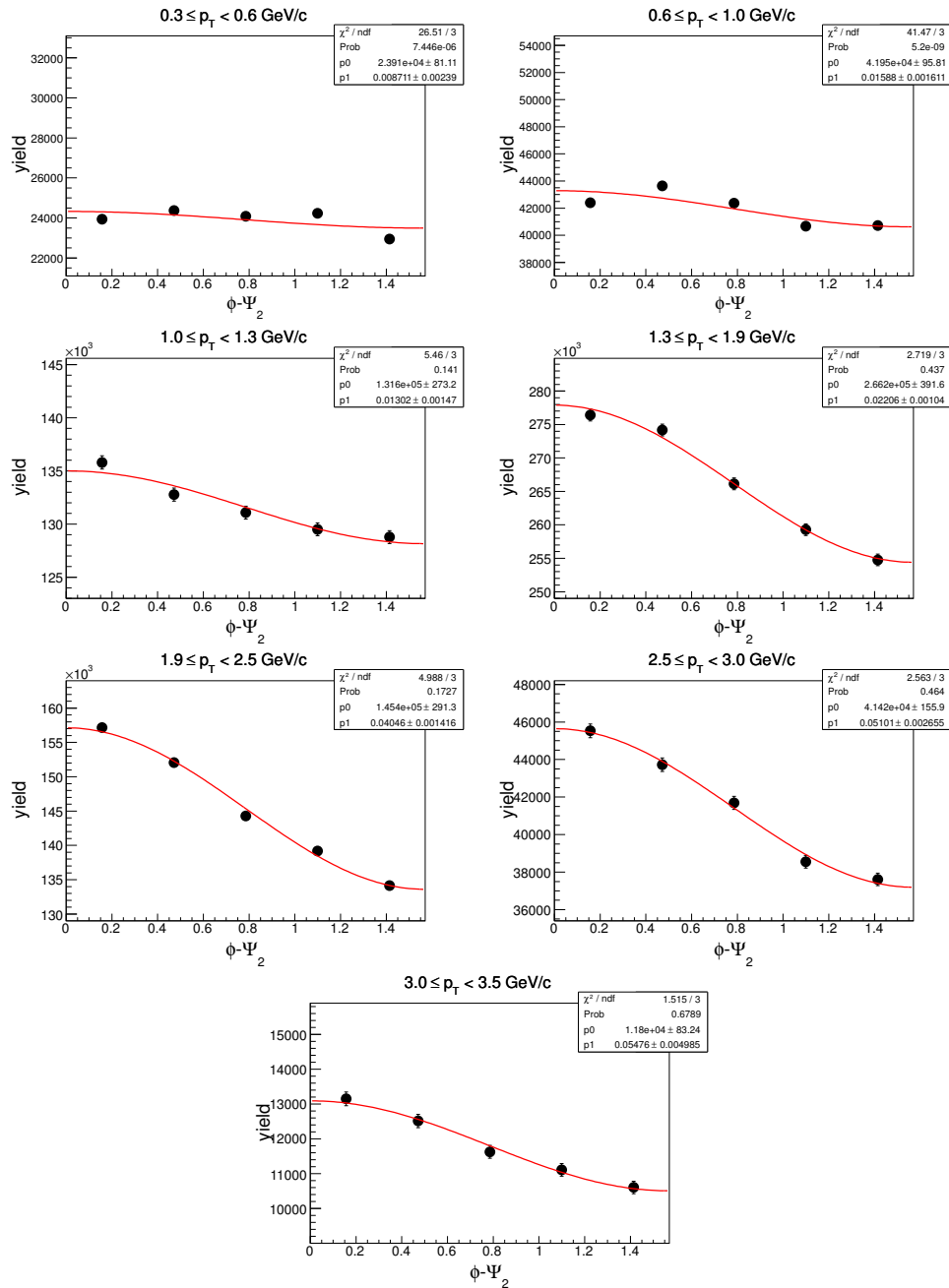


9.5 $\phi - \Psi_2$ distributions in Au+Au at $\sqrt{s_{NN}} = 19.6$ GeV

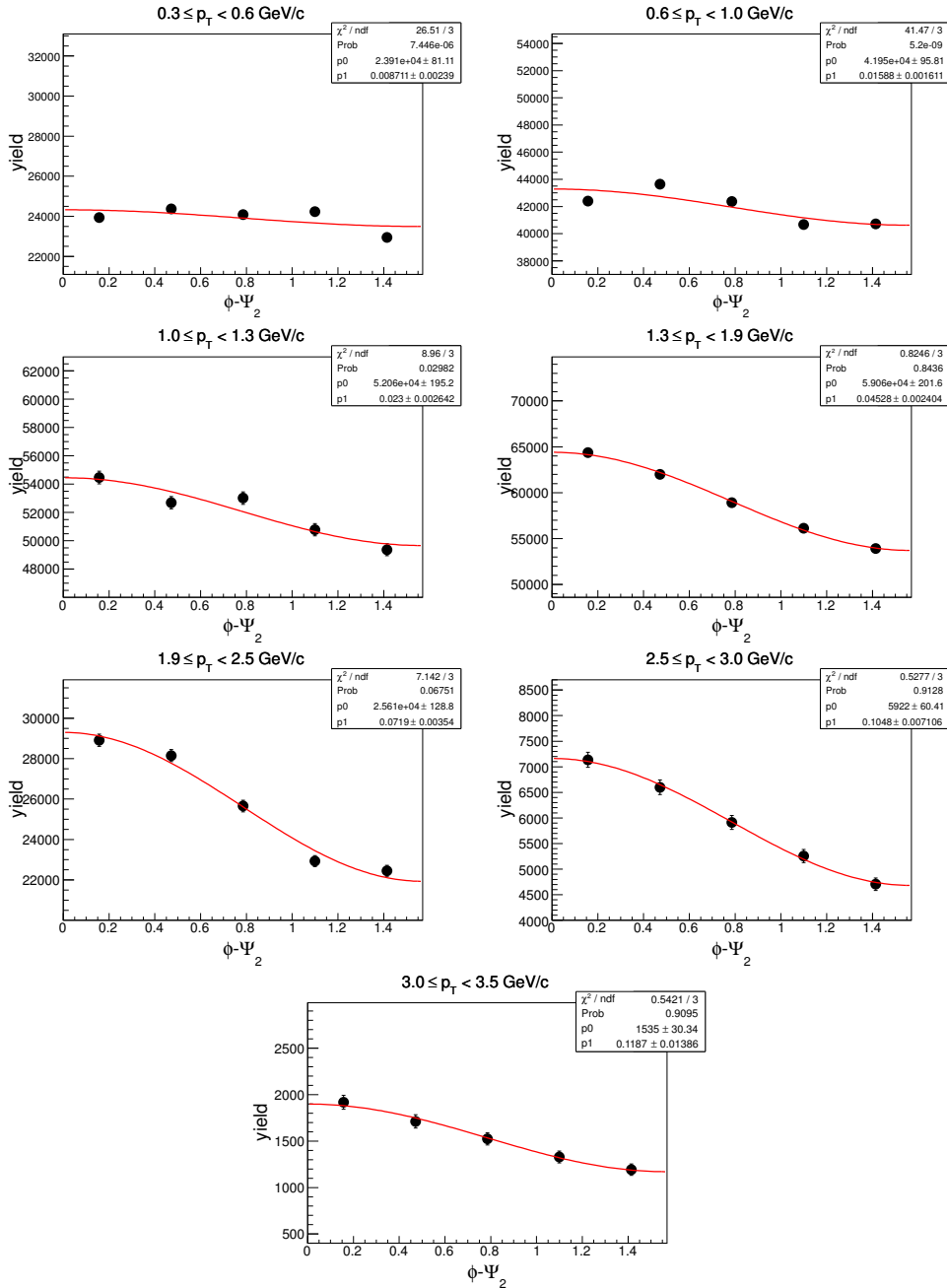
9.5.1 $\phi - \Psi_2$ of d in centrality: 0-80%



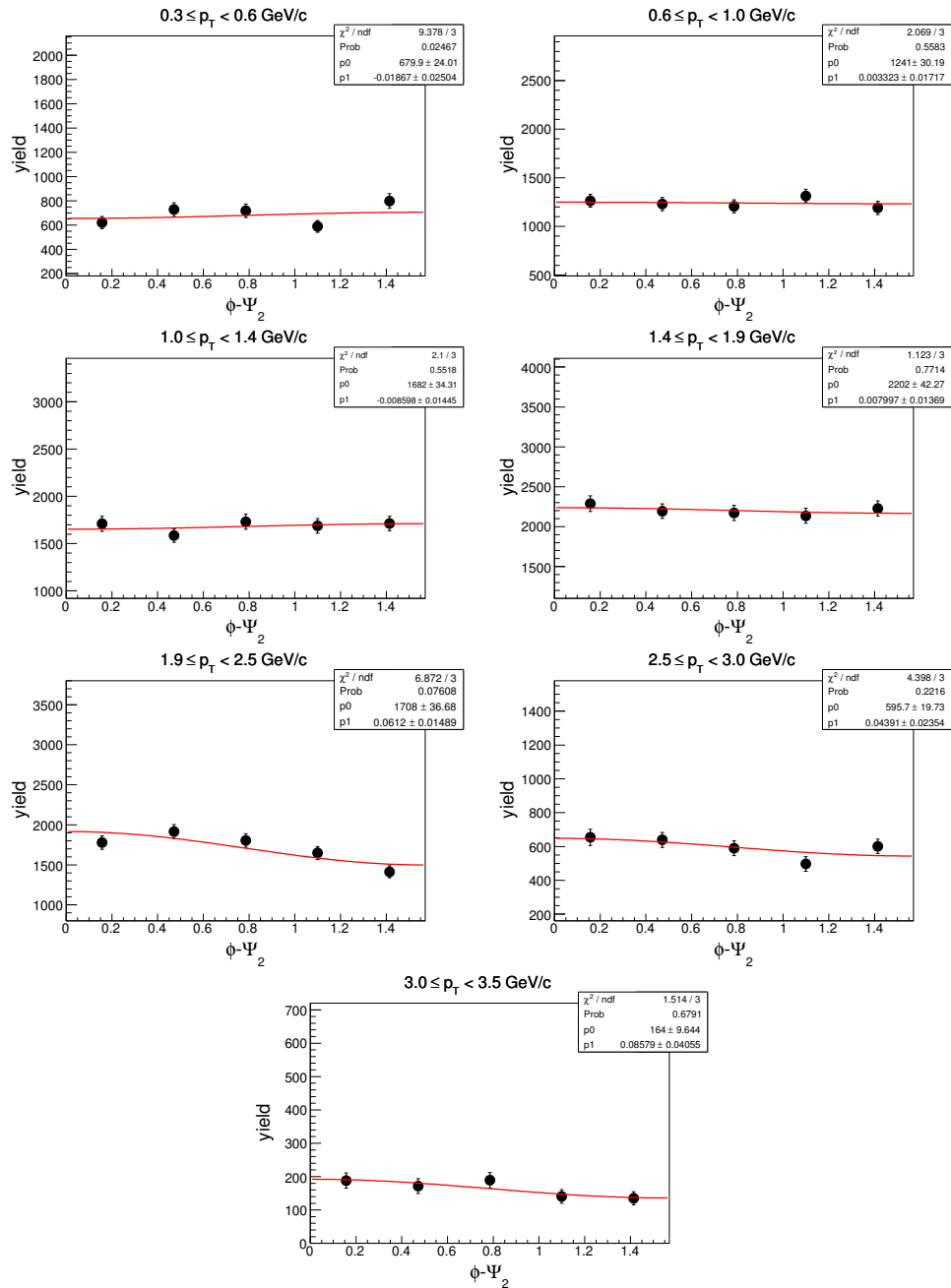
9.5.2 $\phi - \Psi_2$ of d in centrality: 0-30% ($\sqrt{s_{NN}} = 19.6$ GeV)



9.5.3 $\phi - \Psi_2$ of d in centrality: 30-80% ($\sqrt{s_{NN}} = 19.6$ GeV)

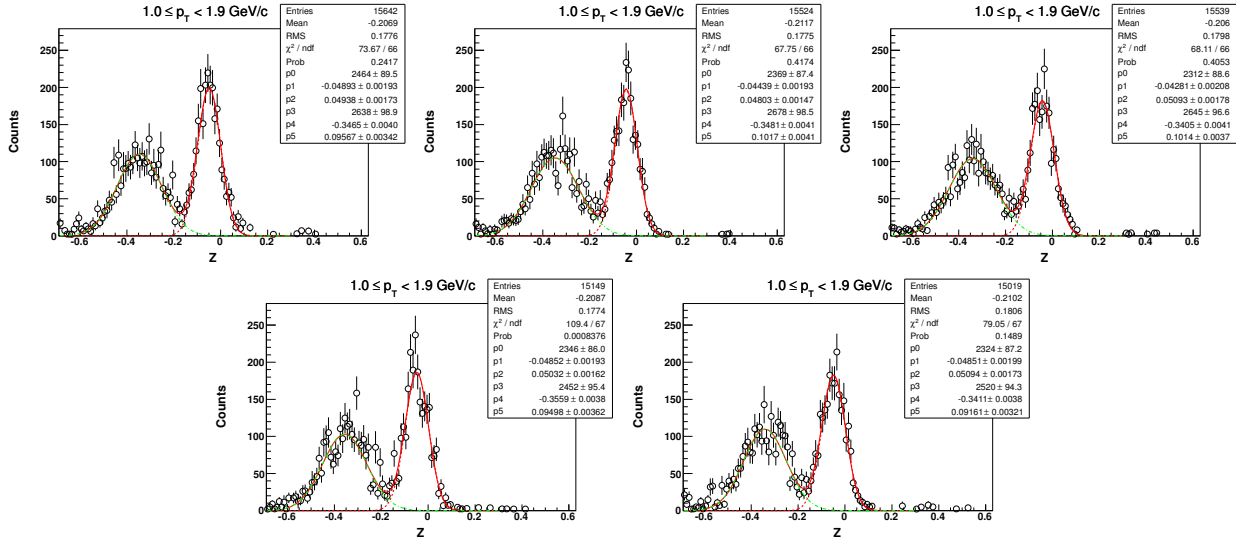


9.5.4 $\phi - \Psi_2$ of \bar{d} in centrality: 0-80% ($\sqrt{s_{NN}} = 19.6$ GeV)

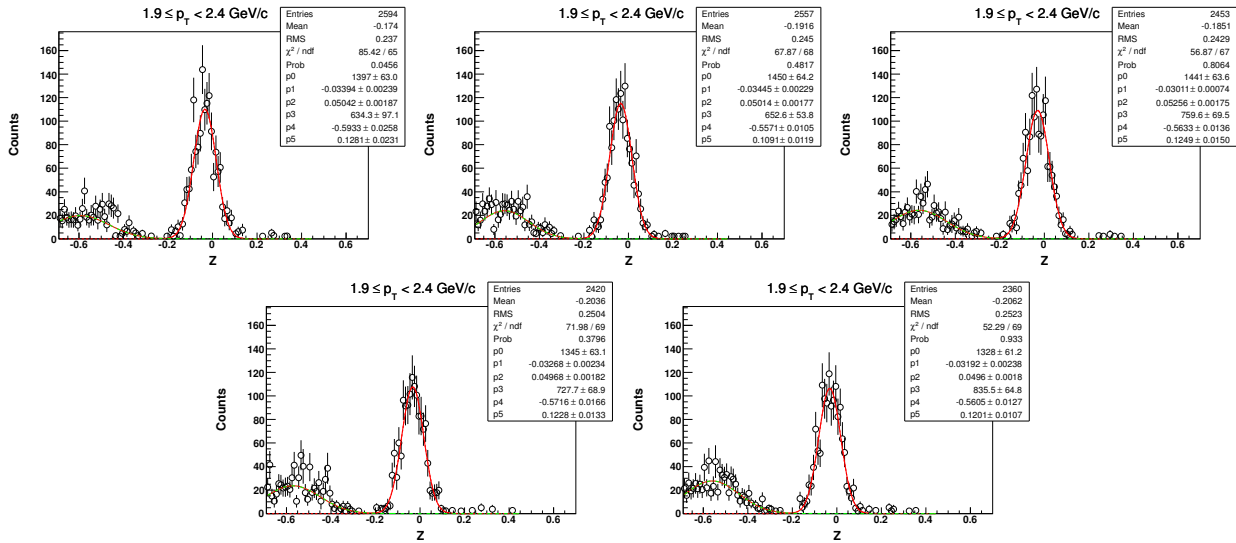


9.6 Z distribution of 3He in $\sqrt{s_{NN}} = 19.6$ GeV (centrality: 0-80%)

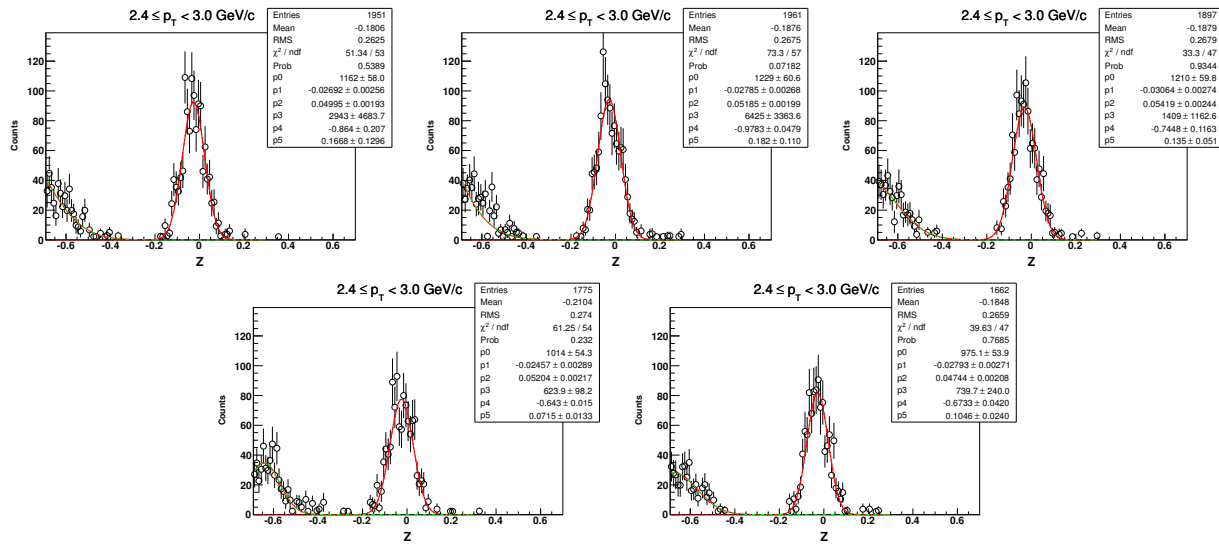
9.6.1 Z-distribution of 3He for $1.0 < p_T < 1.9$ GeV/c



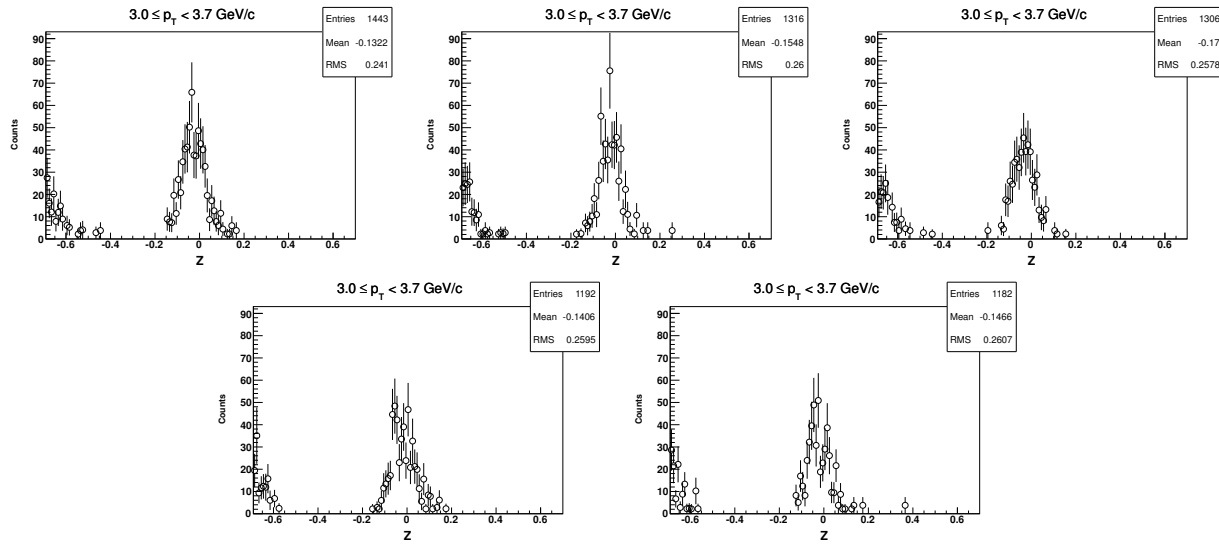
9.6.2 Z-distribution of 3He for $1.9 < p_T < 2.4$ GeV/c ($\sqrt{s_{NN}} = 19.6$ GeV, 0-80%)



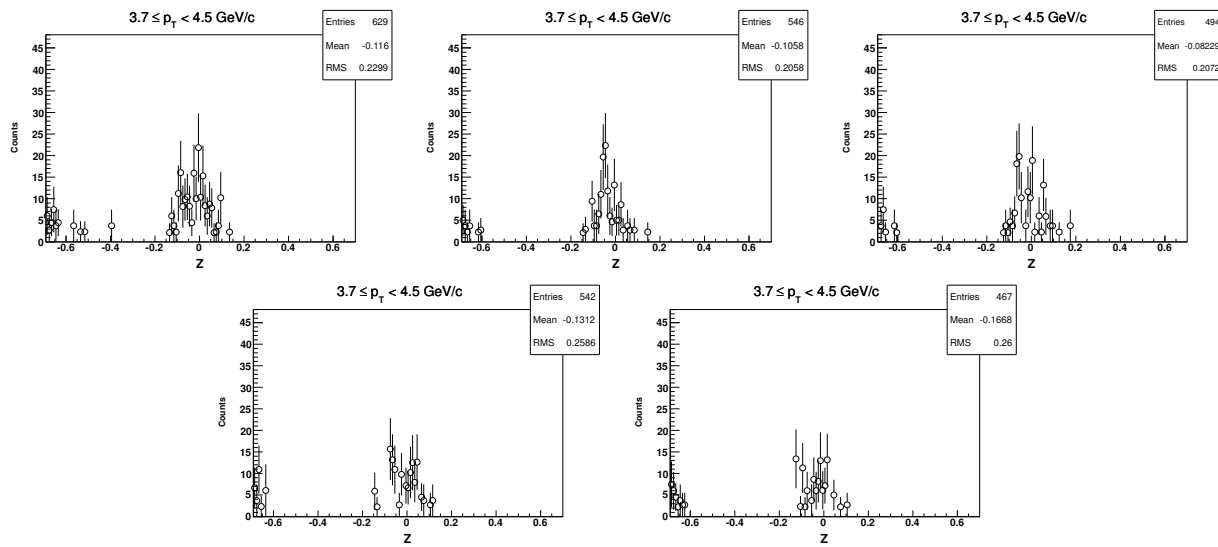
9.6.3 Z-distribution of 3He for $2.4 < p_T < 3.0 \text{ GeV}/c$ ($\sqrt{s_{NN}} = 19.6 \text{ GeV}$, 0-80%)



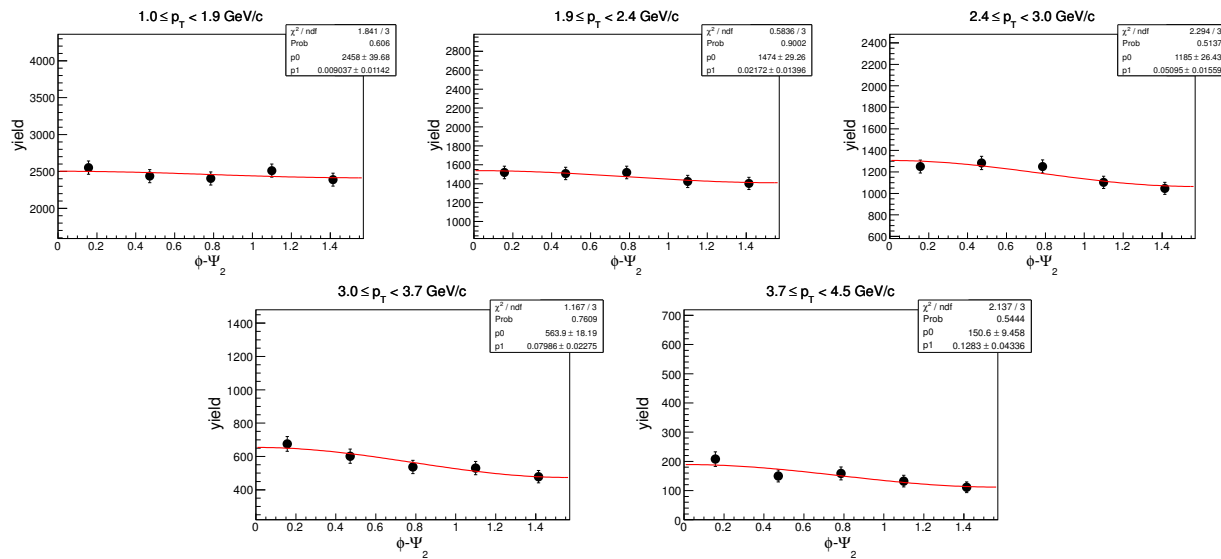
9.6.4 Z-distribution of 3He for $3.0 < p_T < 3.7 \text{ GeV}/c$ ($\sqrt{s_{NN}} = 19.6 \text{ GeV}$, 0-80%)



9.6.5 Z-distribution of ^3He for $3.7 < p_T < 4.5 \text{ GeV}/c$ ($\sqrt{s_{NN}} = 19.6 \text{ GeV}$, 0-80%)

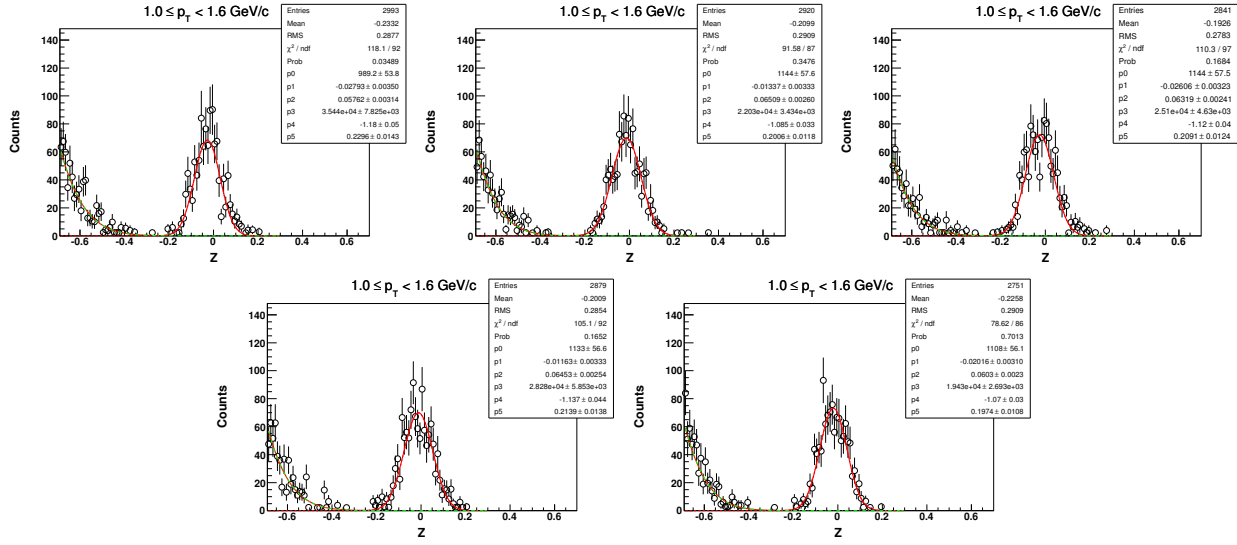


9.6.6 $\phi - \Psi_2$ of ^3He in centrality: 0-80% ($\sqrt{s_{NN}} = 19.6 \text{ GeV}$)

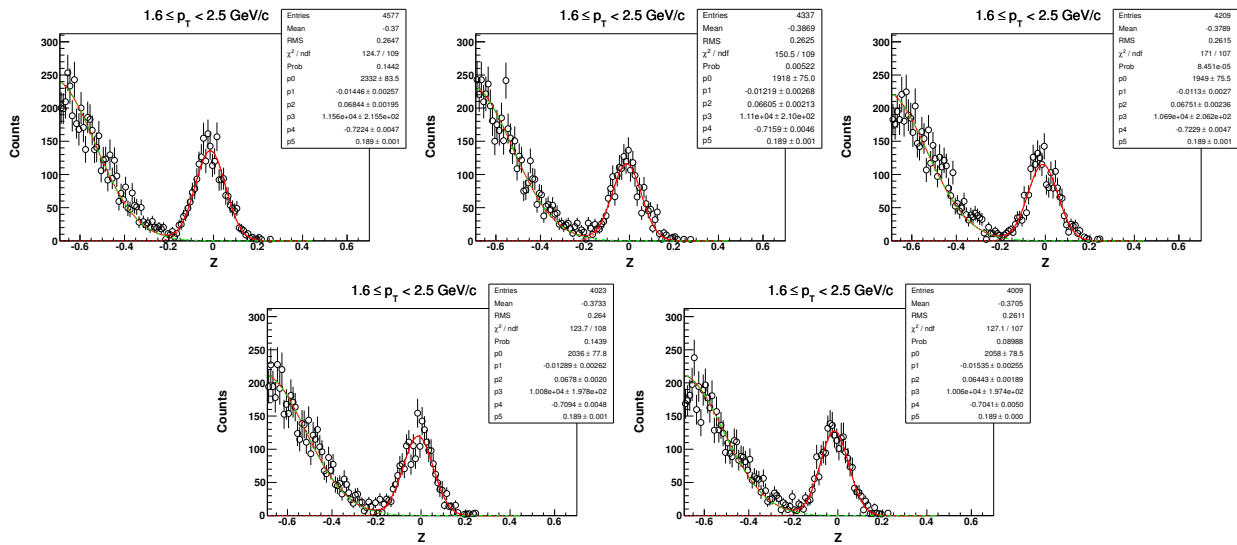


9.7 Z distribution of t in $\sqrt{s_{NN}} = 19.6$ GeV (centrality: 0-80%)

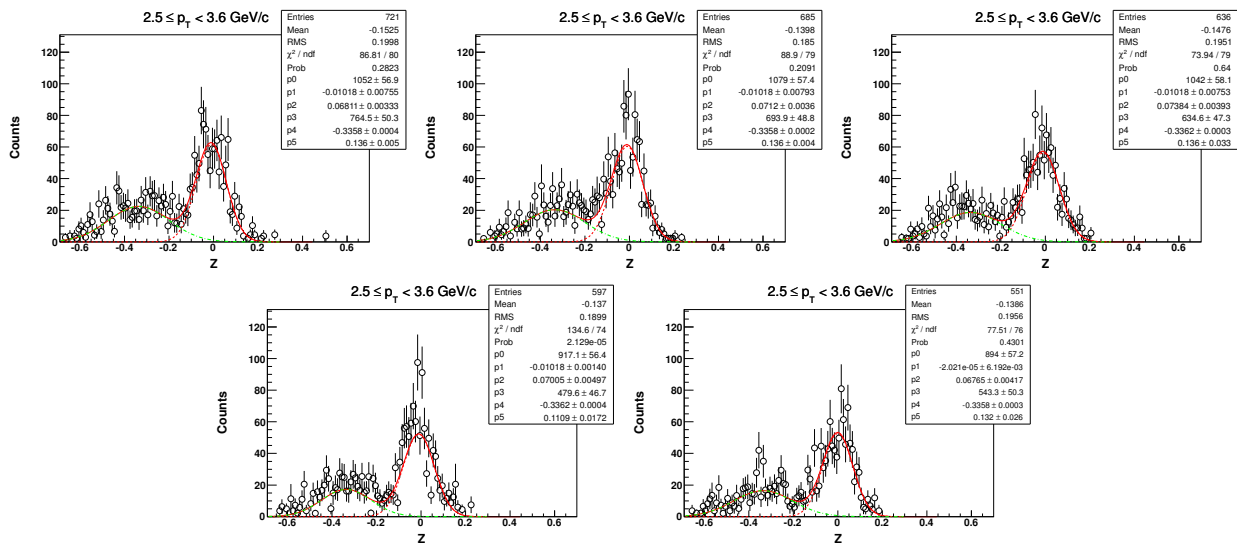
9.7.1 Z-distribution of t for $1.0 < p_T < 1.6$ GeV/c



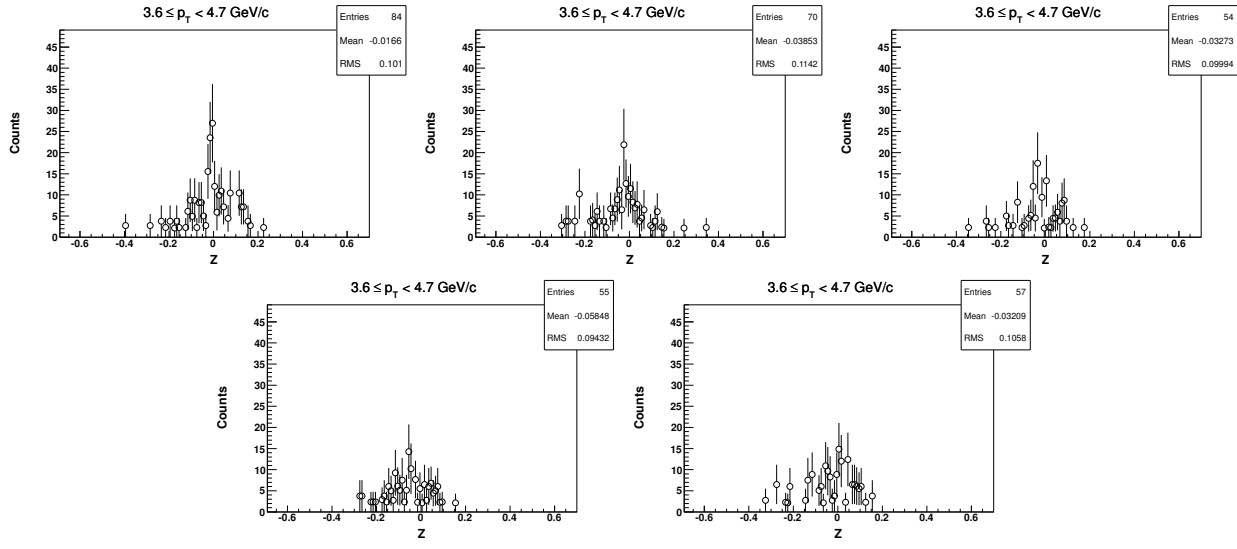
9.7.2 Z-distribution of t for $1.6 < p_T < 2.5$ GeV/c ($\sqrt{s_{NN}} = 19.6$ GeV, 0-80%)



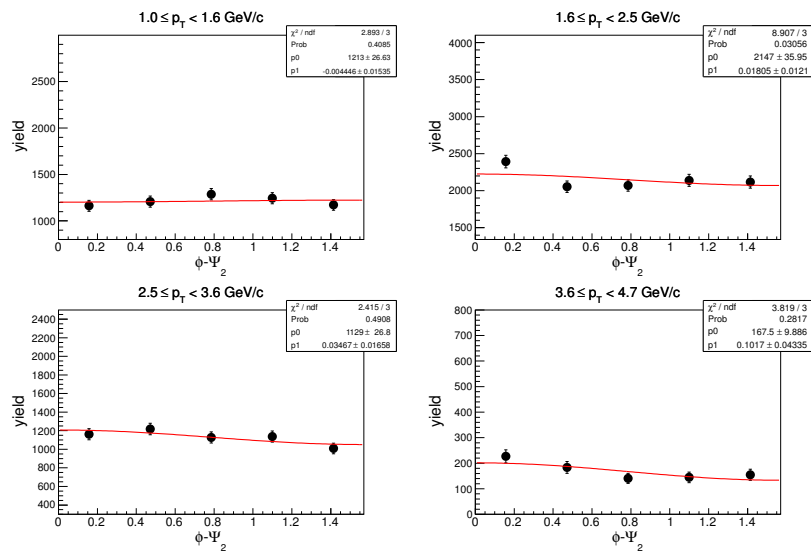
9.7.3 Z-distribution of t for $2.5 < p_T < 3.6 \text{ GeV}/c$ ($\sqrt{s_{NN}} = 19.6 \text{ GeV}$, 0-80%)



9.7.4 Z-distribution of t for $3.6 < p_T < 4.7 \text{ GeV}/c$ ($\sqrt{s_{NN}} = 19.6 \text{ GeV}$, 0-80%)



9.7.5 $\phi - \Psi_2$ of t in centrality: 0-80% ($\sqrt{s_{NN}} = 19.6$ GeV)

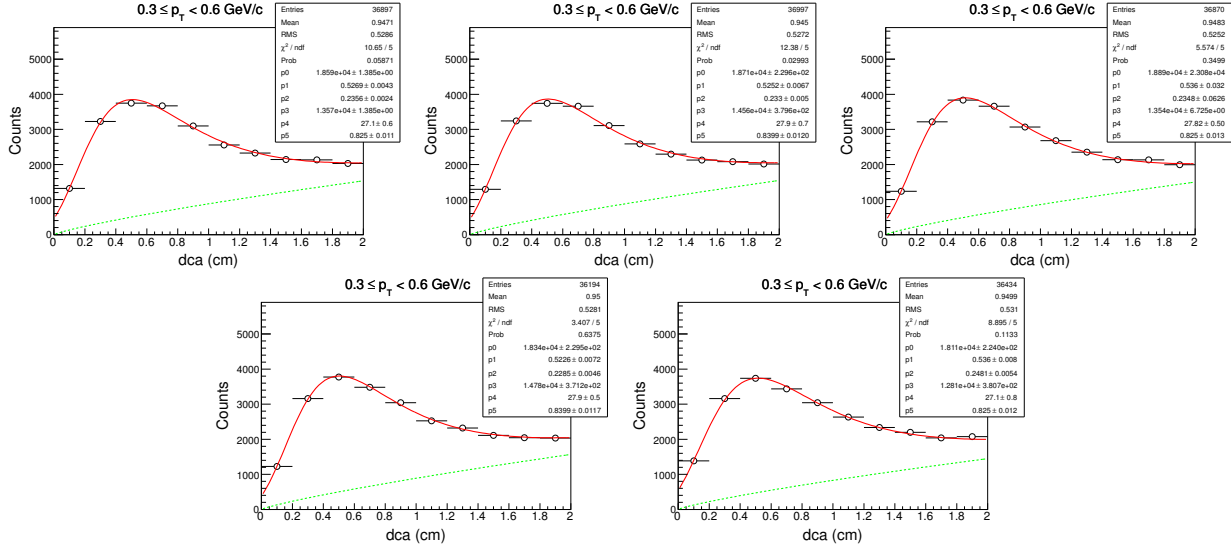


10 DCA and Z-distributions for Au+Au at $\sqrt{s_{NN}} = 11.5$ GeV

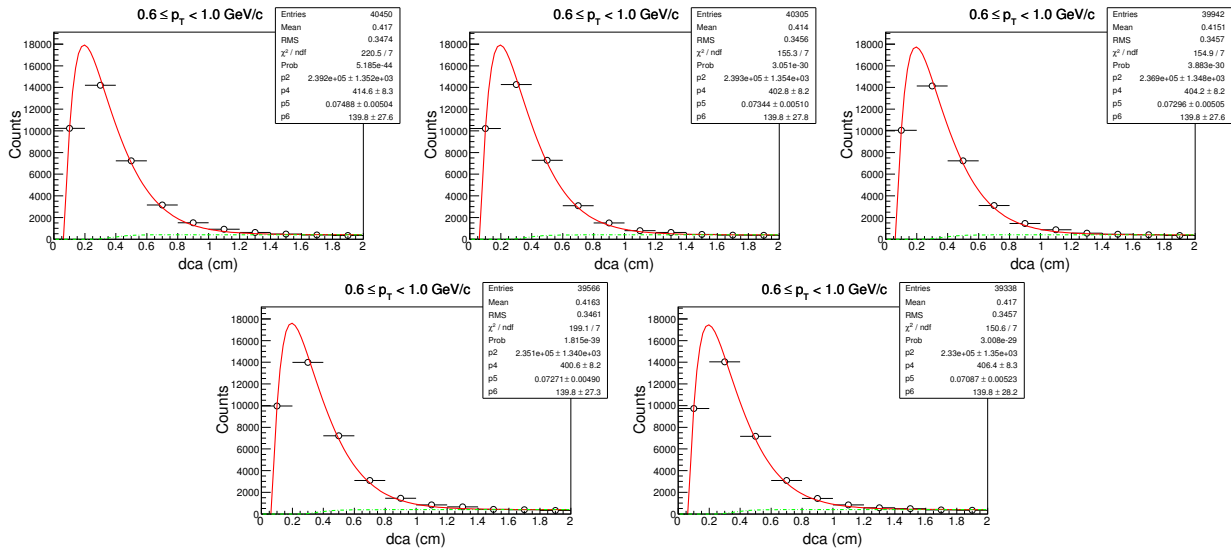
In this section we show the DCA and Z-distribution of deuteron and anti-deuteron for five different ($\phi - \Psi_2$) bins namely, $0 - \frac{\pi}{10}$, $\frac{\pi}{10} - \frac{2\pi}{10}$, $\frac{2\pi}{10} - \frac{3\pi}{10}$, $\frac{3\pi}{10} - \frac{4\pi}{10}$ and $\frac{4\pi}{10} - \frac{5\pi}{10}$. DCA and Z-distribution of d for all centrality and all p_T bins are shown in the later sub-sections.

10.1 Centrality: 0-80%

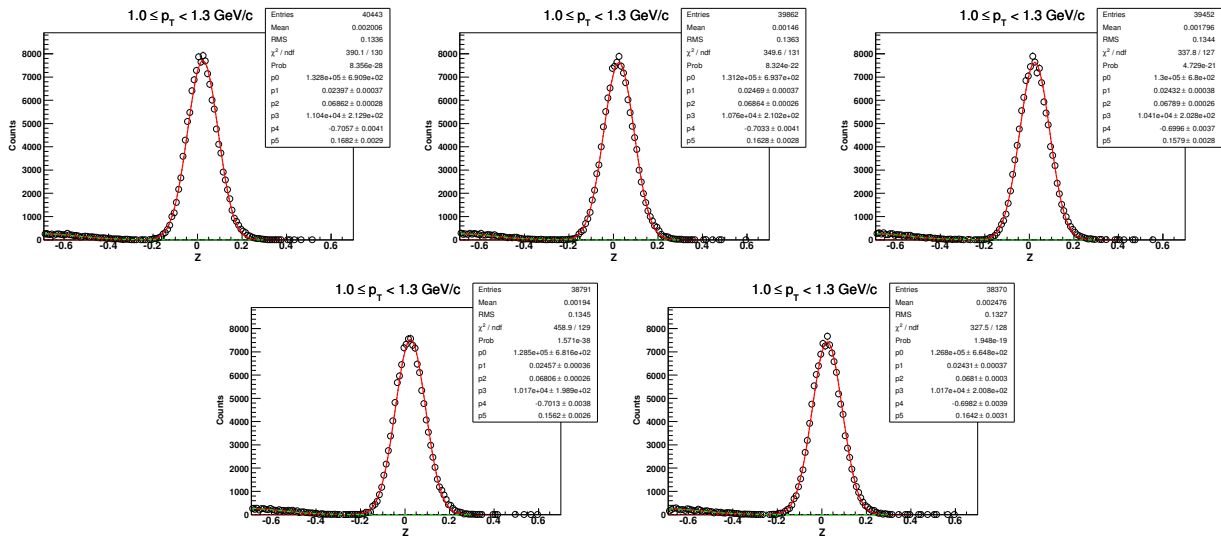
10.1.1 DCA-distribution of d for $0.3 < p_T < 0.6$ GeV/c



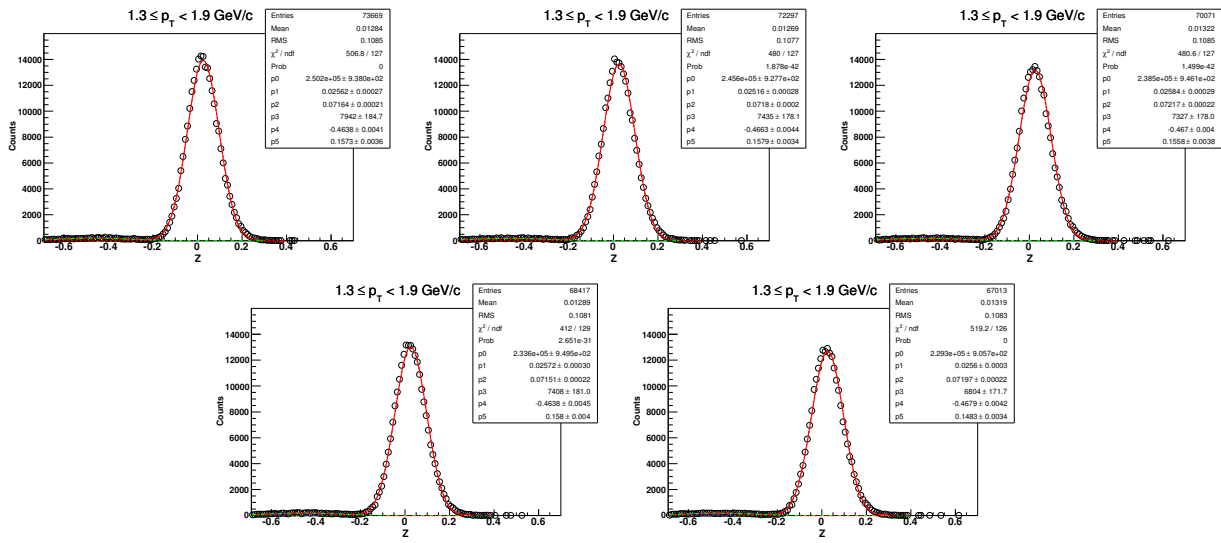
10.1.2 DCA-distribution of d for $0.6 < p_T < 1.0$ GeV/c ($\sqrt{s_{NN}} = 11.5$ GeV, 0-80%)



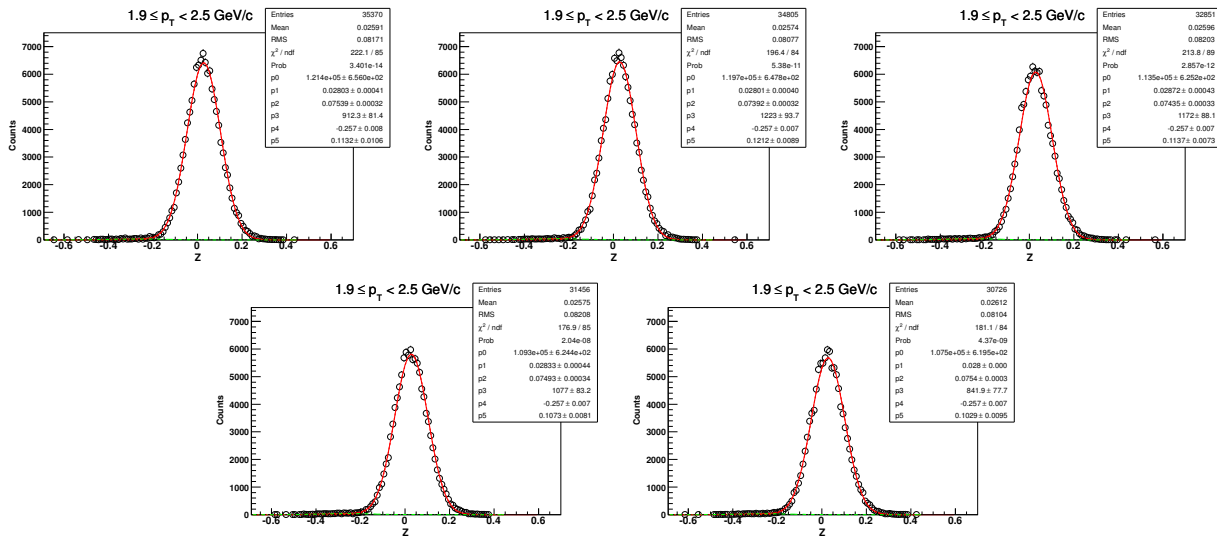
10.1.3 Z-distribution of d for $1.0 < p_T < 1.3 \text{ GeV}/c$ ($\sqrt{s_{NN}} = 11.5 \text{ GeV}$, 0-80%)



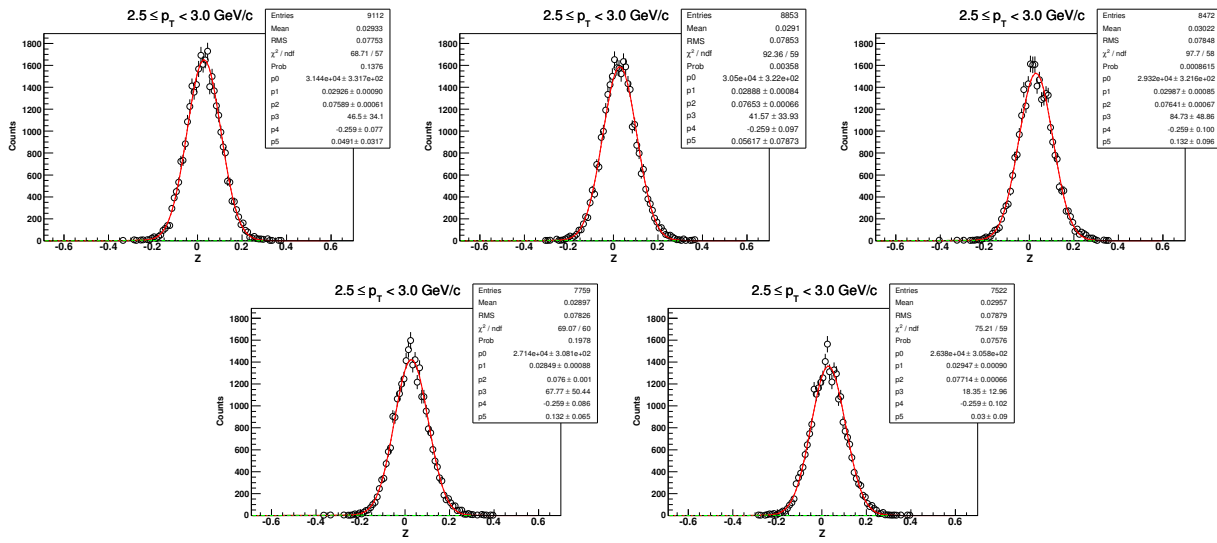
10.1.4 Z-distribution of d for $1.3 < p_T < 1.9 \text{ GeV}/c$ ($\sqrt{s_{NN}} = 11.5 \text{ GeV}$, 0-80%)



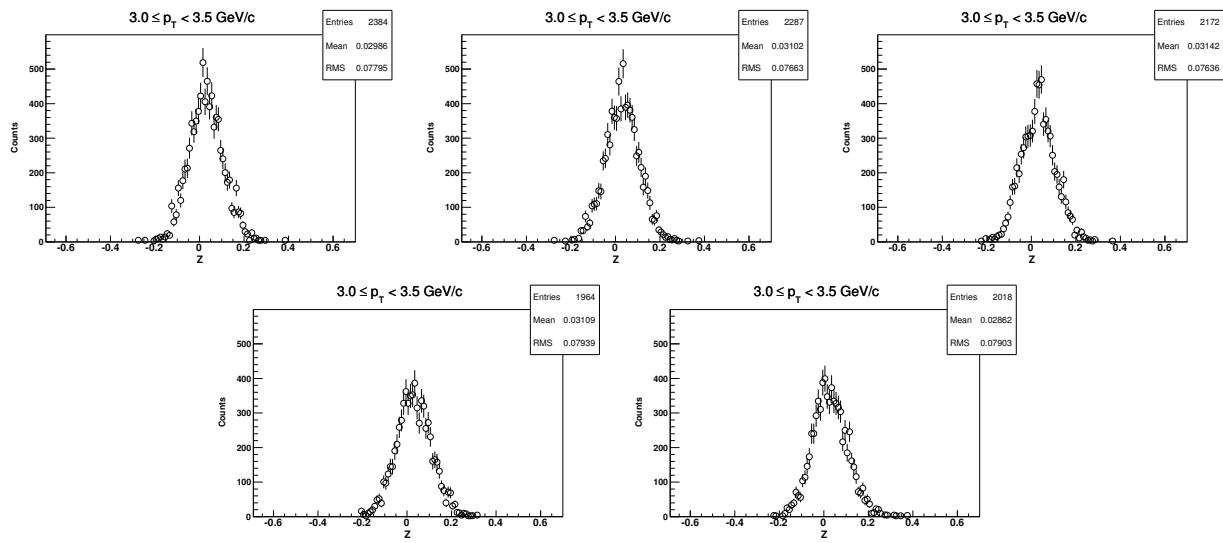
10.1.5 Z-distribution of d for $1.9 < p_T < 2.5 \text{ GeV}/c$ ($\sqrt{s_{NN}} = 11.5 \text{ GeV}$, 0-80%)



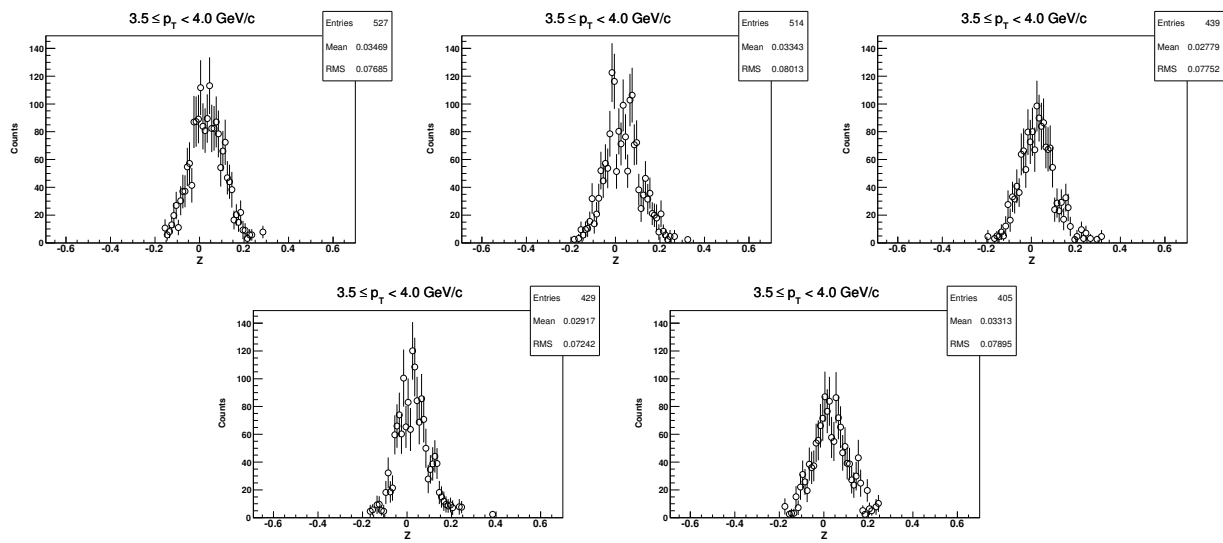
10.1.6 Z-distribution of d for $2.5 < p_T < 3.0 \text{ GeV}/c$ ($\sqrt{s_{NN}} = 11.5 \text{ GeV}$, 0-80%)



10.1.7 Z-distribution of d for $3.0 < p_T < 3.5 \text{ GeV}/c$ ($\sqrt{s_{NN}} = 11.5 \text{ GeV}$, 0-80%)

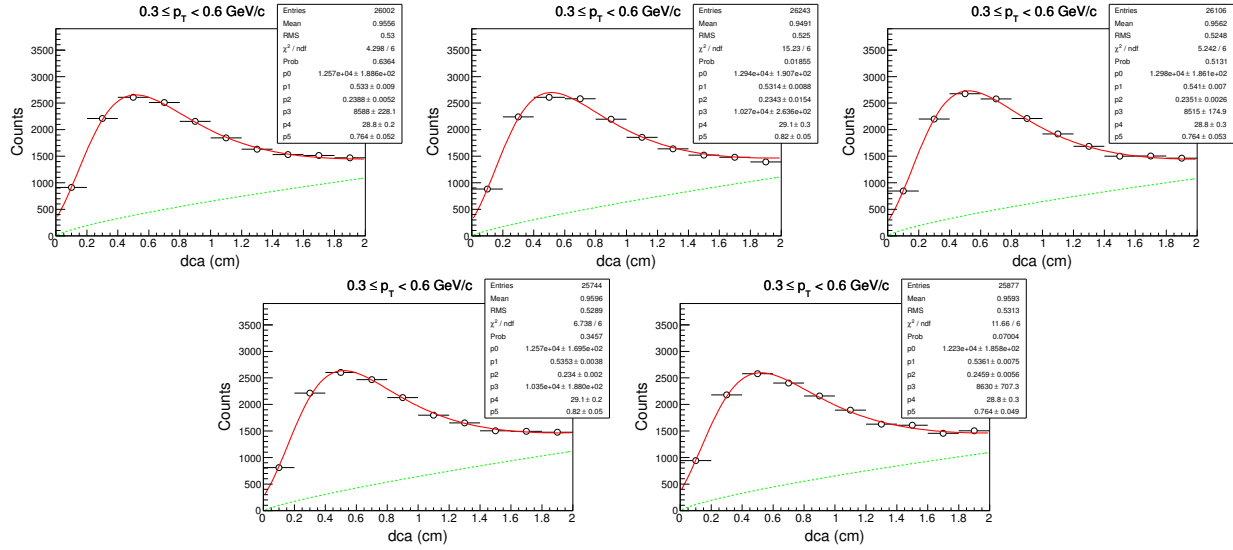


10.1.8 Z-distribution of d for $3.5 < p_T < 4.0 \text{ GeV}/c$ ($\sqrt{s_{NN}} = 11.5 \text{ GeV}$, 0-80%)

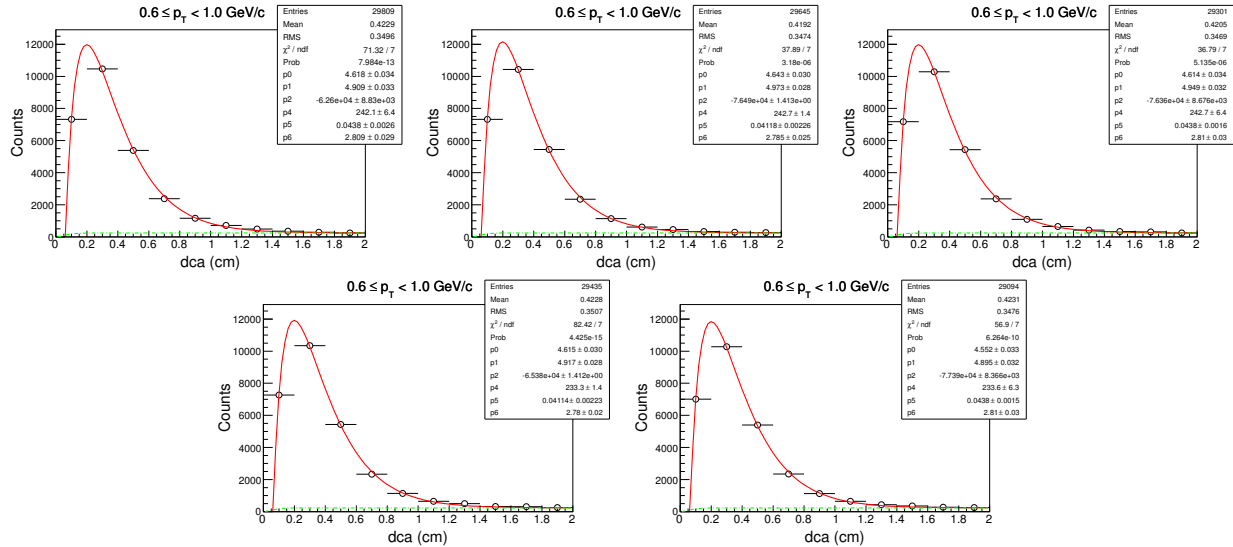


10.2 Centrality: 0-30%

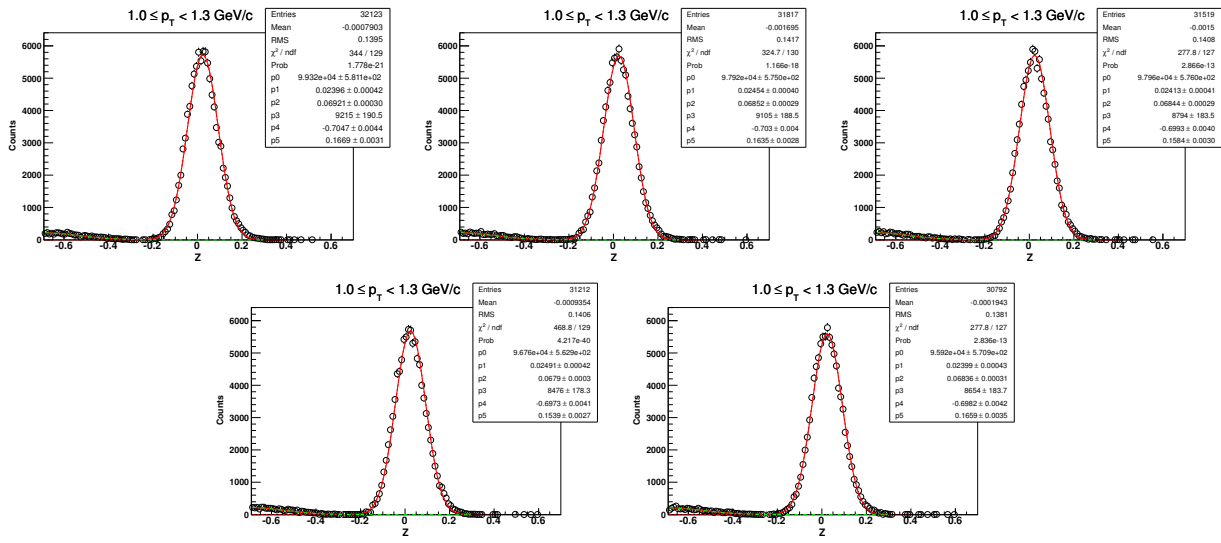
10.2.1 DCA-distribution of d for $0.3 < p_T < 0.6 \text{ GeV}/c$



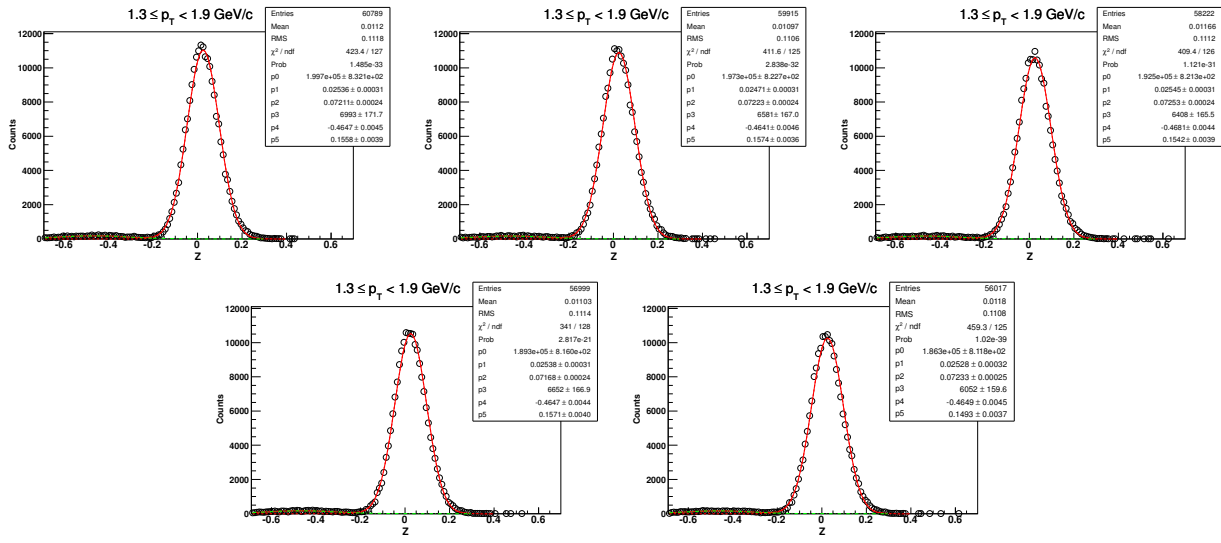
10.2.2 DCA-distribution of d for $0.6 < p_T < 1.0 \text{ GeV}/c$



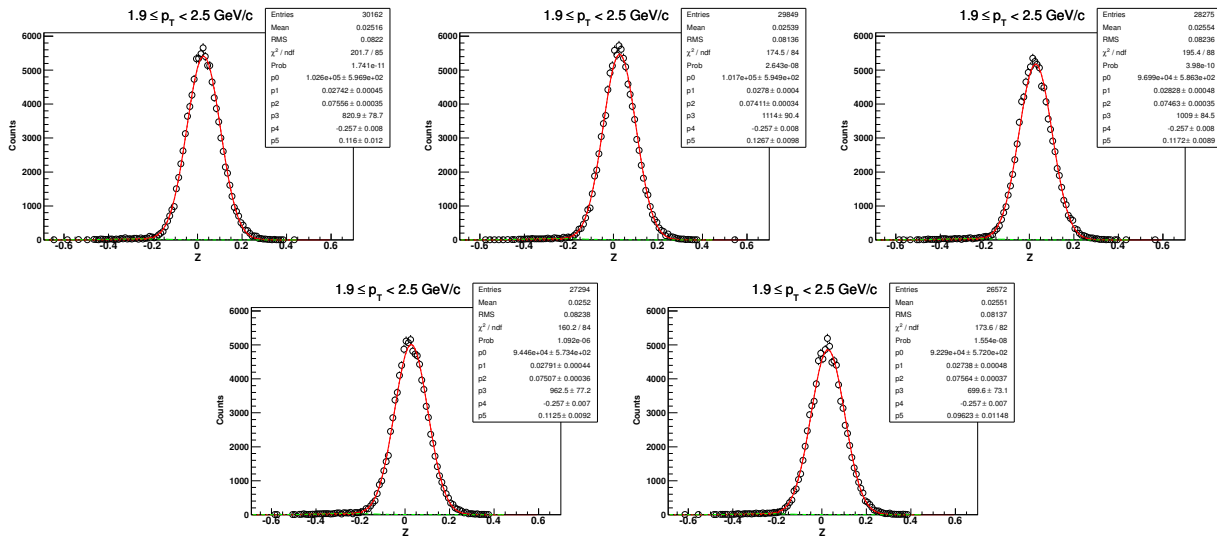
10.2.3 Z-distribution of d for $1.0 < p_T < 1.3 \text{ GeV}/c$ ($\sqrt{s_{NN}} = 11.5 \text{ GeV}$, 0-30%)



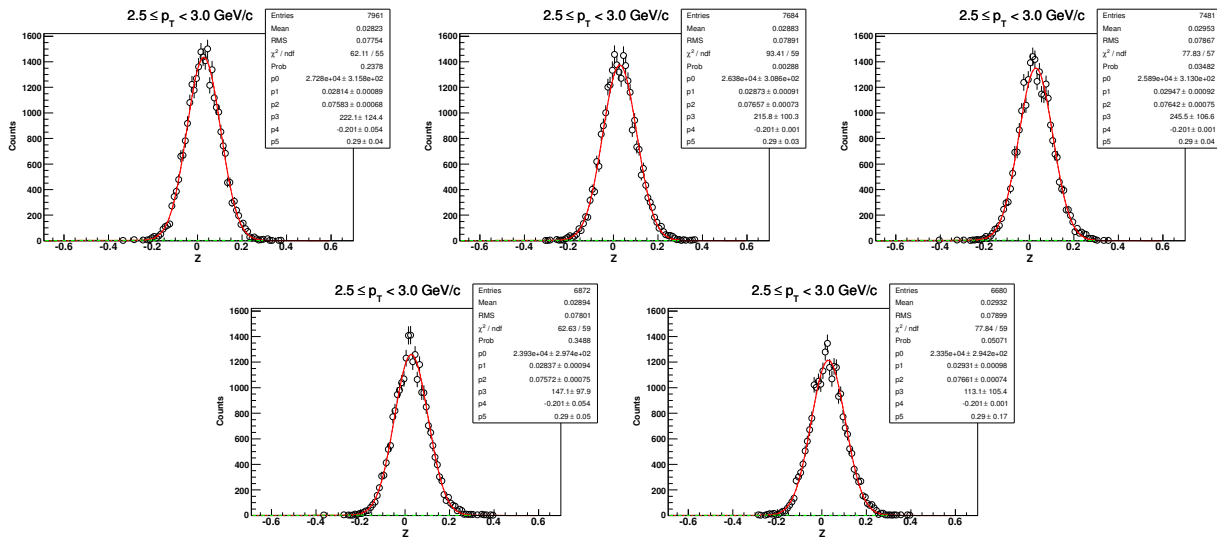
10.2.4 Z-distribution of d for $1.3 < p_T < 1.9 \text{ GeV}/c$ ($\sqrt{s_{NN}} = 11.5 \text{ GeV}$, 0-30%)



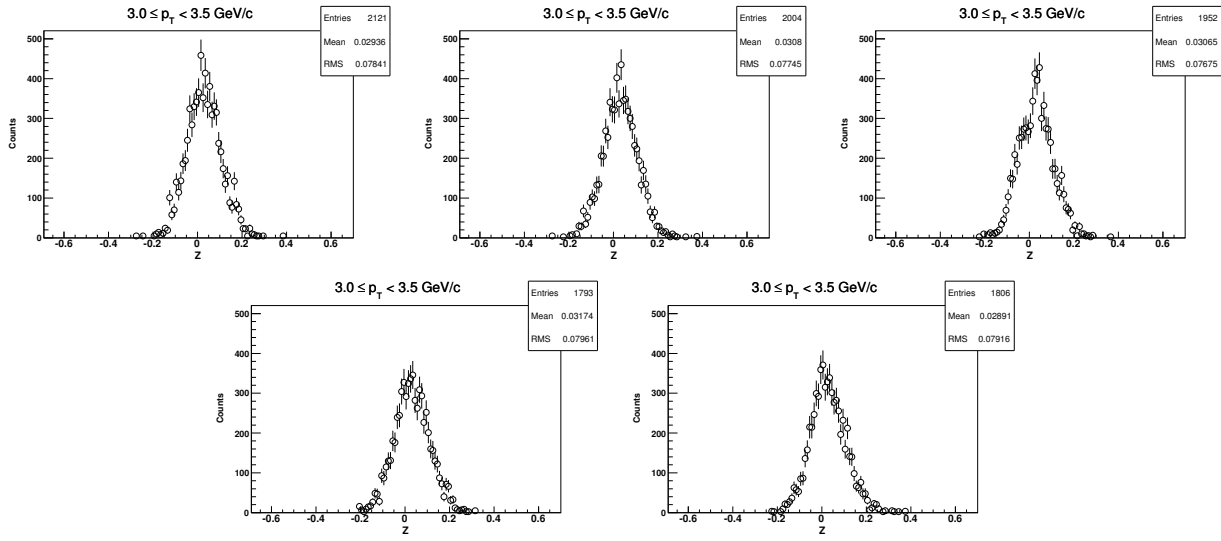
10.2.5 Z-distribution of d for $1.9 < p_T < 2.5 \text{ GeV}/c$ ($\sqrt{s_{NN}} = 11.5 \text{ GeV}$, 0-30%)



10.2.6 Z-distribution of d for $2.5 < p_T < 3.0 \text{ GeV}/c$ ($\sqrt{s_{NN}} = 11.5 \text{ GeV}$, 0-30%)

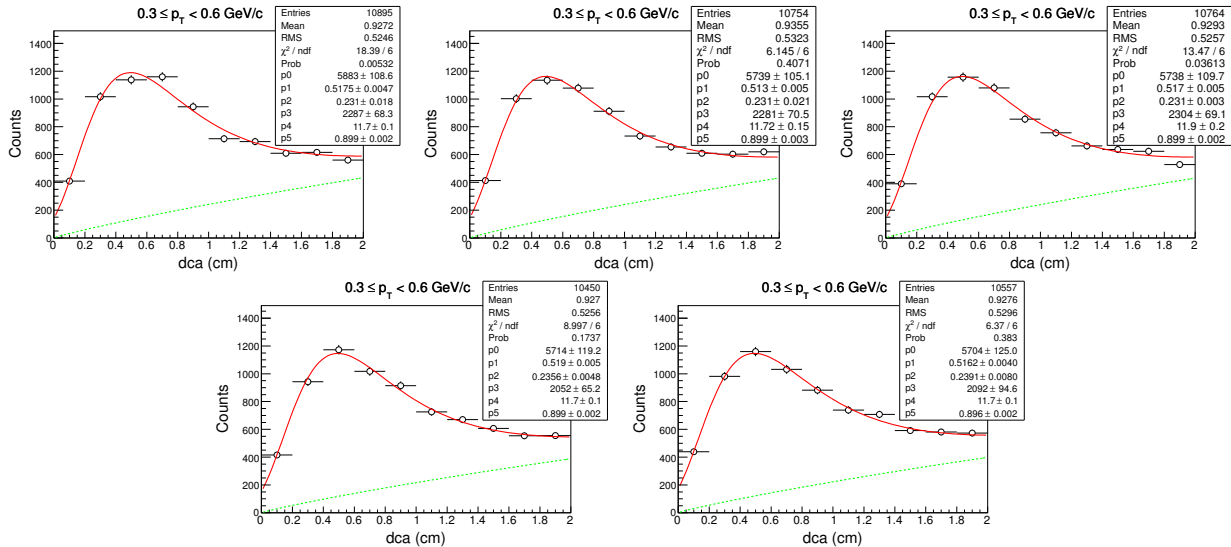


10.2.7 Z-distribution of d for $3.0 < p_T < 3.5 \text{ GeV}/c$ ($\sqrt{s_{NN}} = 11.5 \text{ GeV}$, 0-30%)

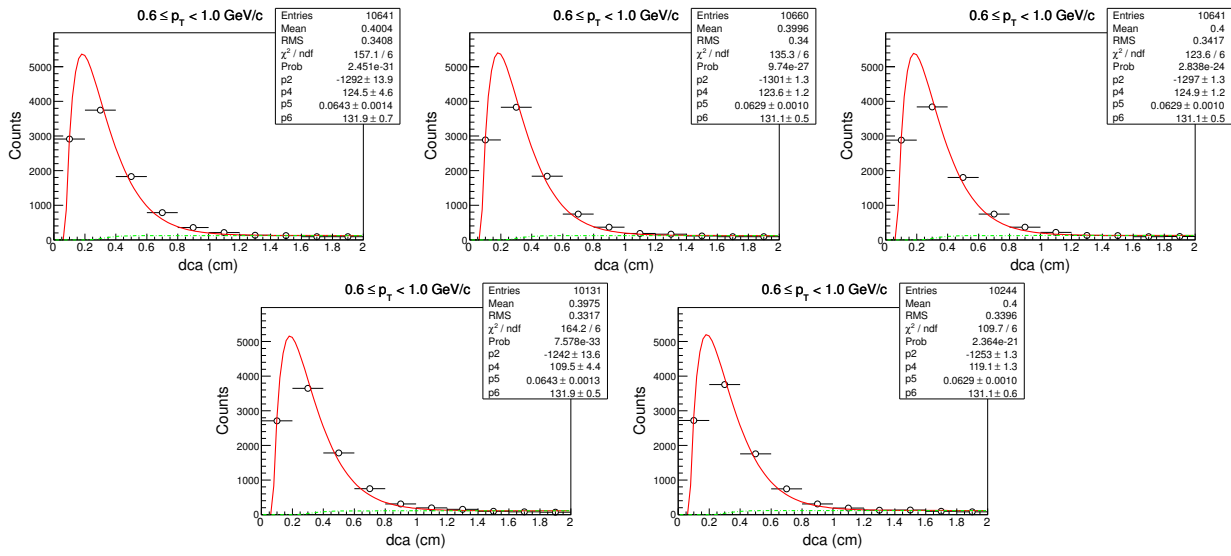


10.3 Centrality: 30-80%

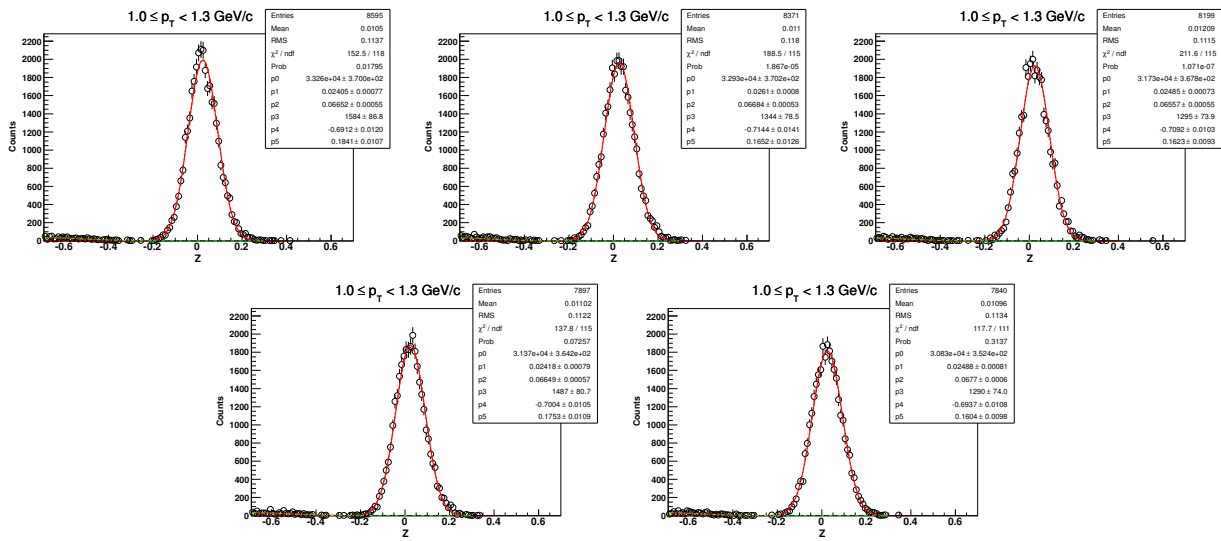
10.3.1 DCA-distribution of d for $0.3 < p_T < 0.6 \text{ GeV}/c$



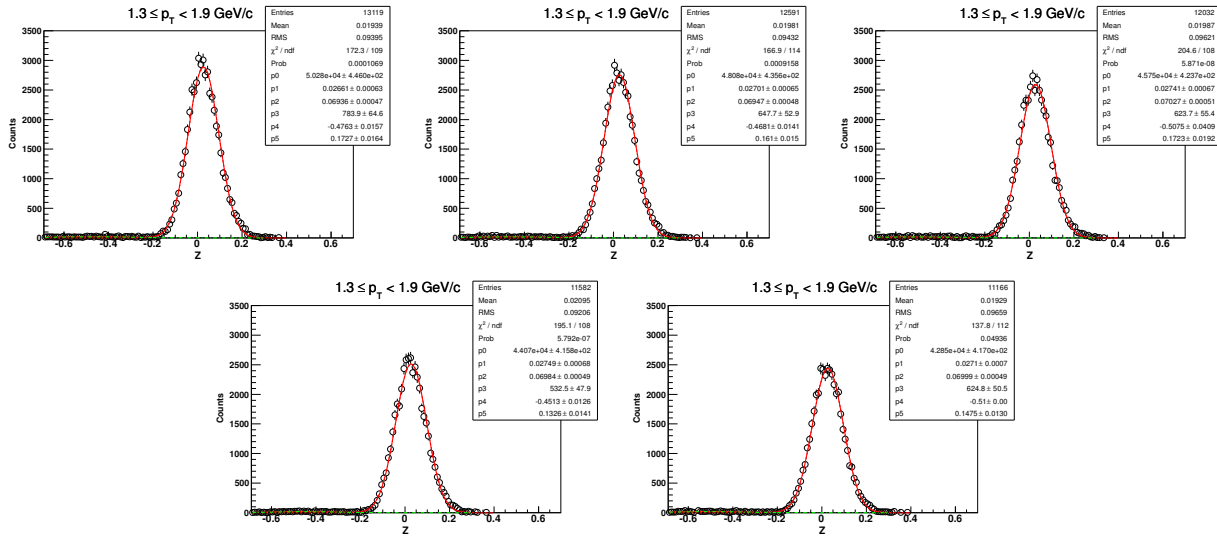
10.3.2 DCA-distribution of d for $0.6 < p_T < 1.0 \text{ GeV}/c$ ($\sqrt{s_{NN}} = 11.5 \text{ GeV}$, 30-80%)



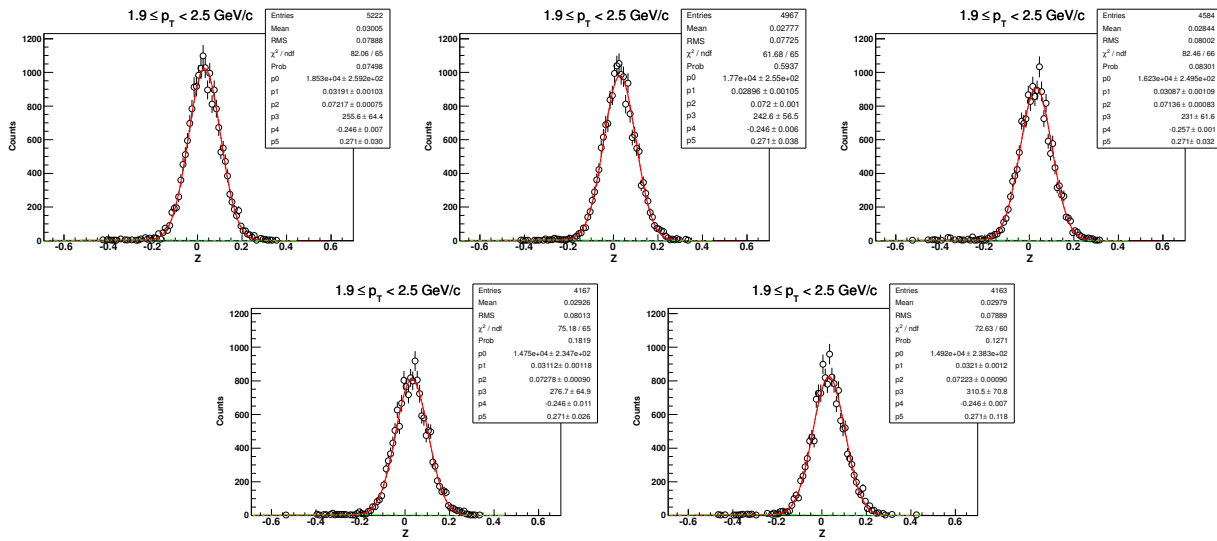
10.3.3 Z-distribution of d for $1.0 < p_T < 1.3 \text{ GeV}/c$ ($\sqrt{s_{NN}} = 11.5 \text{ GeV}$, 30-80%)



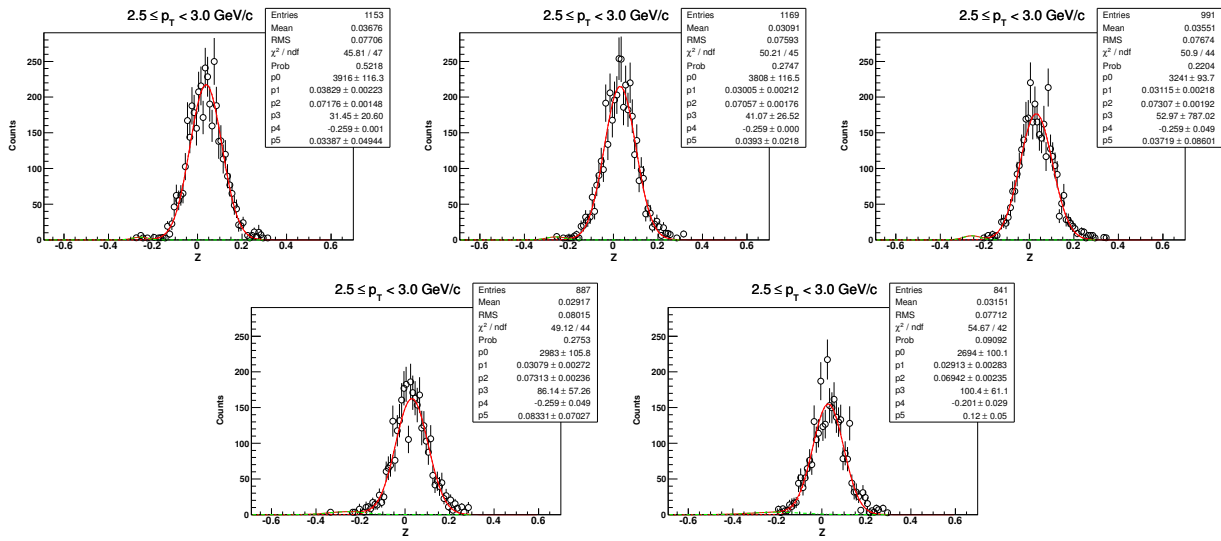
10.3.4 Z-distribution of d for $1.3 < p_T < 1.9 \text{ GeV}/c$ ($\sqrt{s_{NN}} = 11.5 \text{ GeV}$, 30-80%)



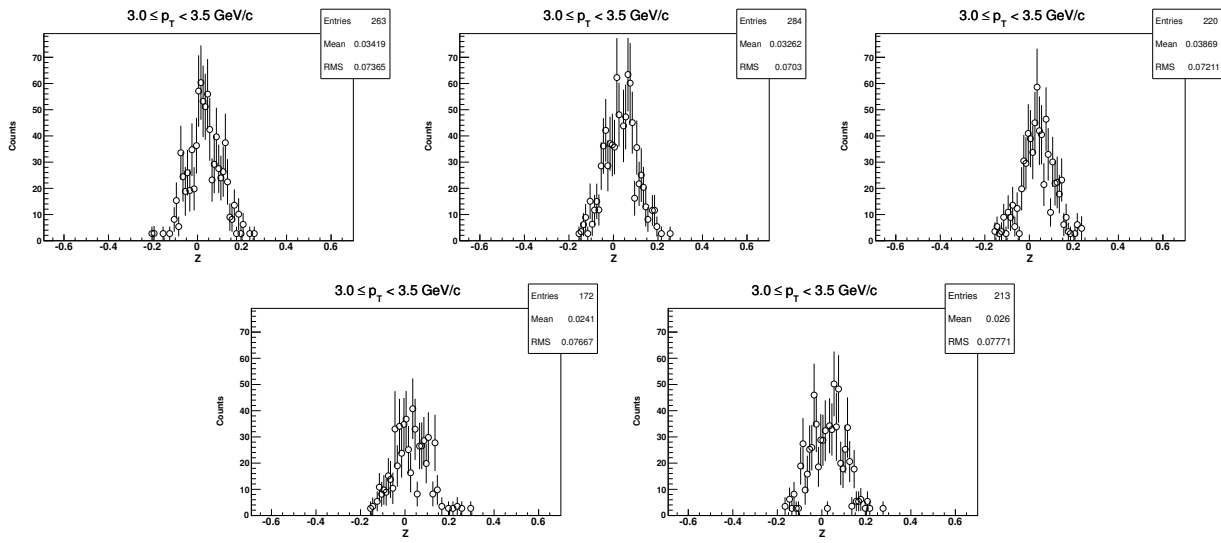
10.3.5 Z-distribution of d for $1.9 < p_T < 2.5 \text{ GeV}/c$ ($\sqrt{s_{NN}} = 11.5 \text{ GeV}$, 30-80%)



10.3.6 Z-distribution of d for $2.5 < p_T < 3.0 \text{ GeV}/c$ ($\sqrt{s_{NN}} = 11.5 \text{ GeV}$, 30-80%)

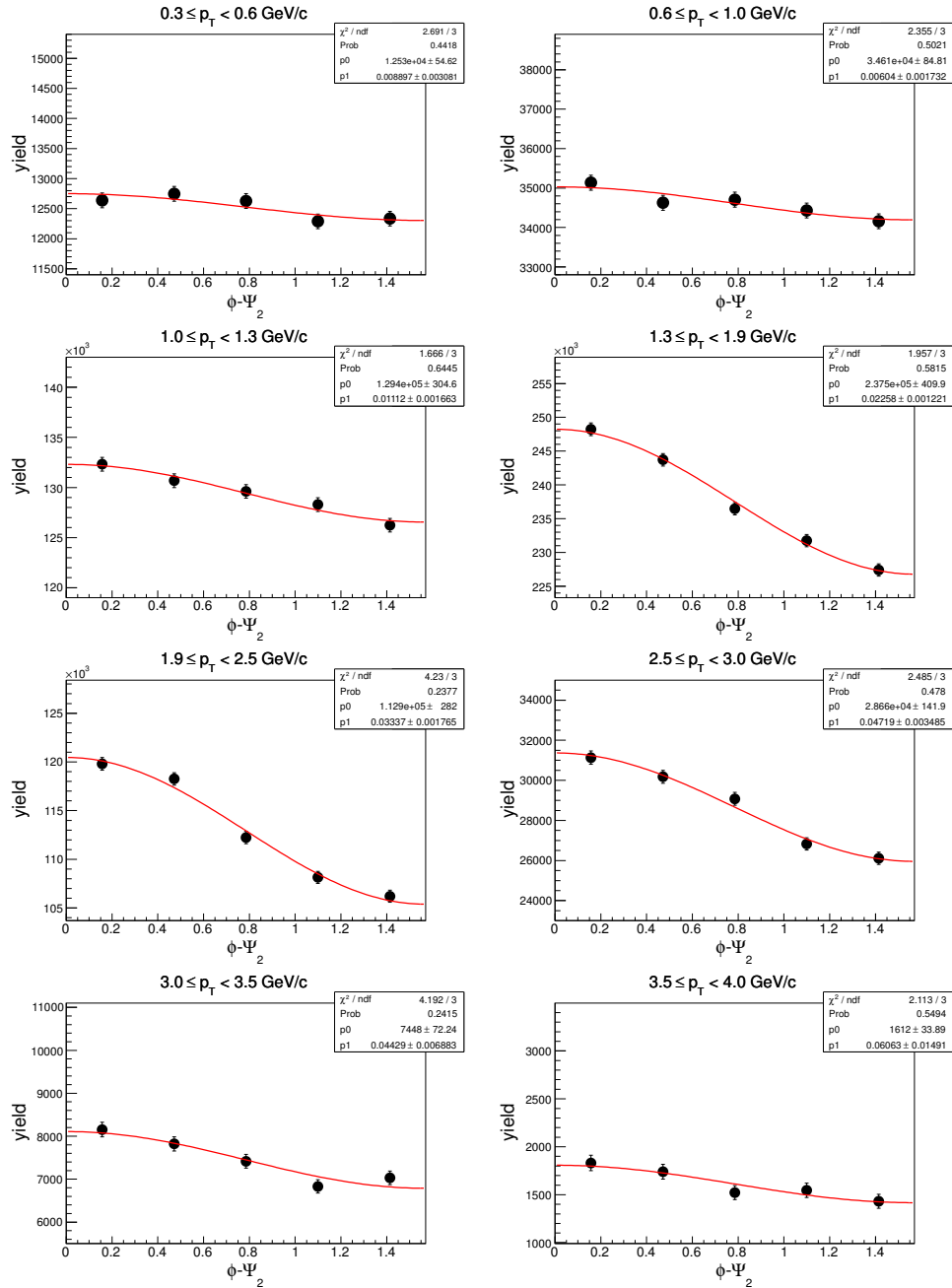


10.3.7 Z-distribution of d for $3.0 < p_T < 3.5 \text{ GeV}/c$ ($\sqrt{s_{NN}} = 11.5 \text{ GeV}$, 30-80%)

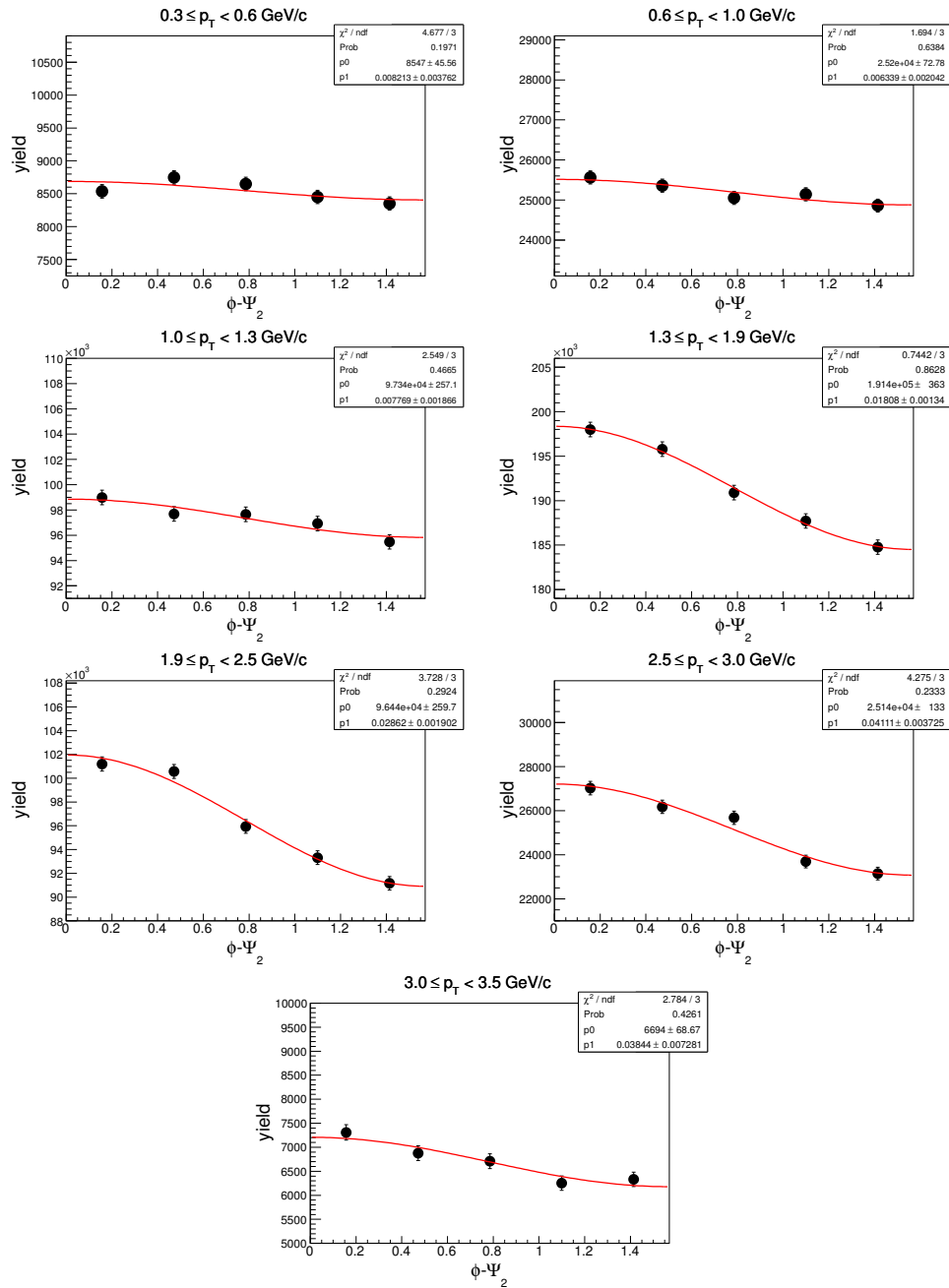


10.4 $\phi - \Psi_2$ distributions in Au+Au at $\sqrt{s_{NN}} = 11.5$ GeV

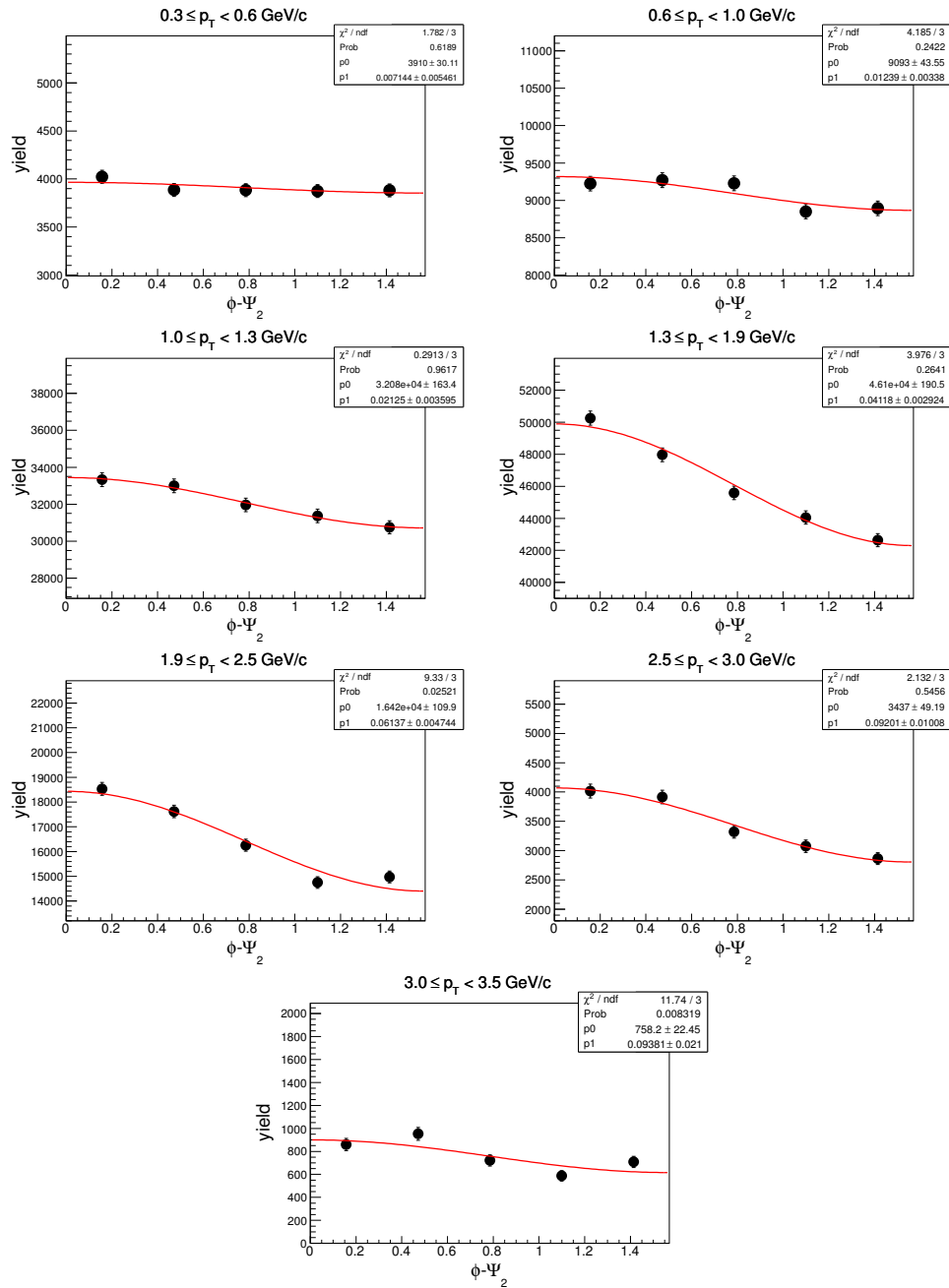
10.4.1 $\phi - \Psi_2$ of d in centrality: 0-80%



10.4.2 $\phi - \Psi_2$ of d in centrality: 0-30% ($\sqrt{s_{NN}} = 11.5$ GeV)

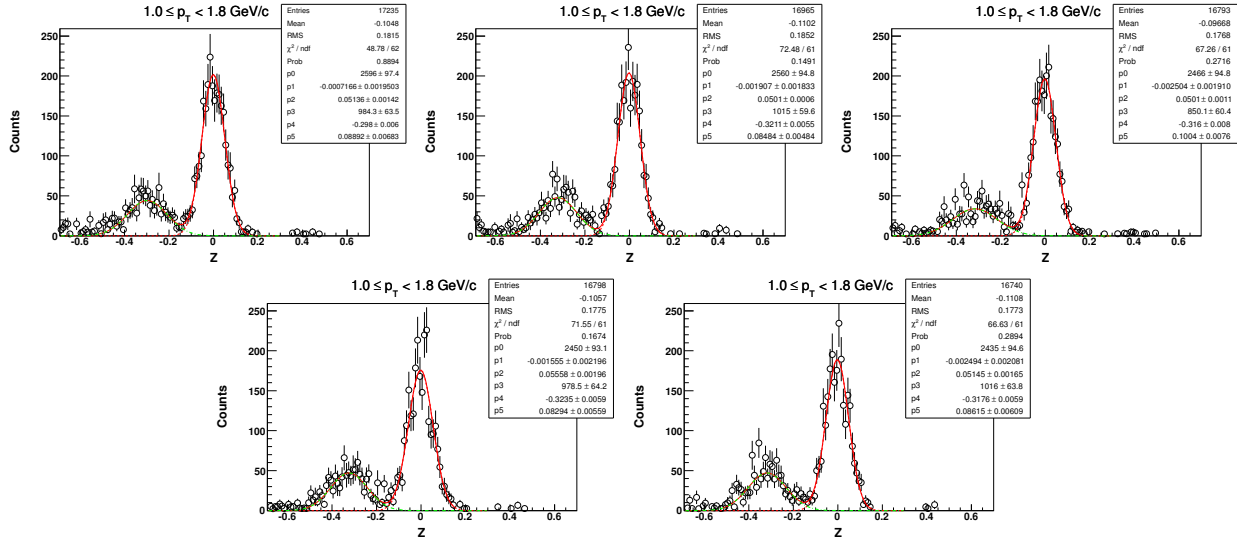


10.4.3 $\phi - \Psi_2$ of d in centrality: 30-80% ($\sqrt{s_{NN}} = 11.5$ GeV)

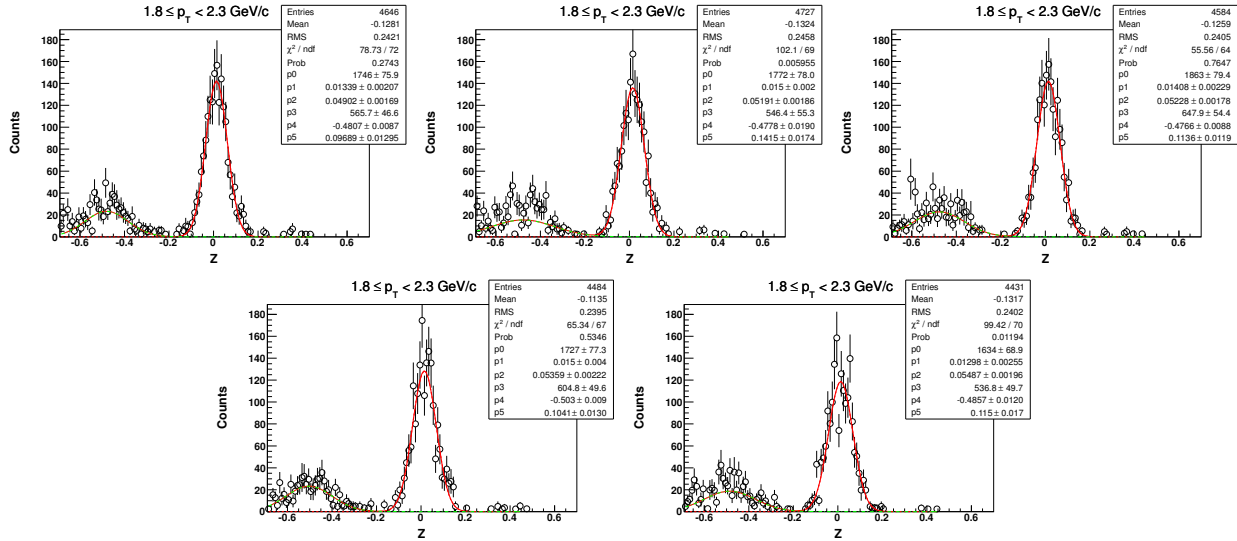


10.5 Z distribution of 3He in $\sqrt{s_{NN}} = 11.5$ GeV (centrality: 0-80%)

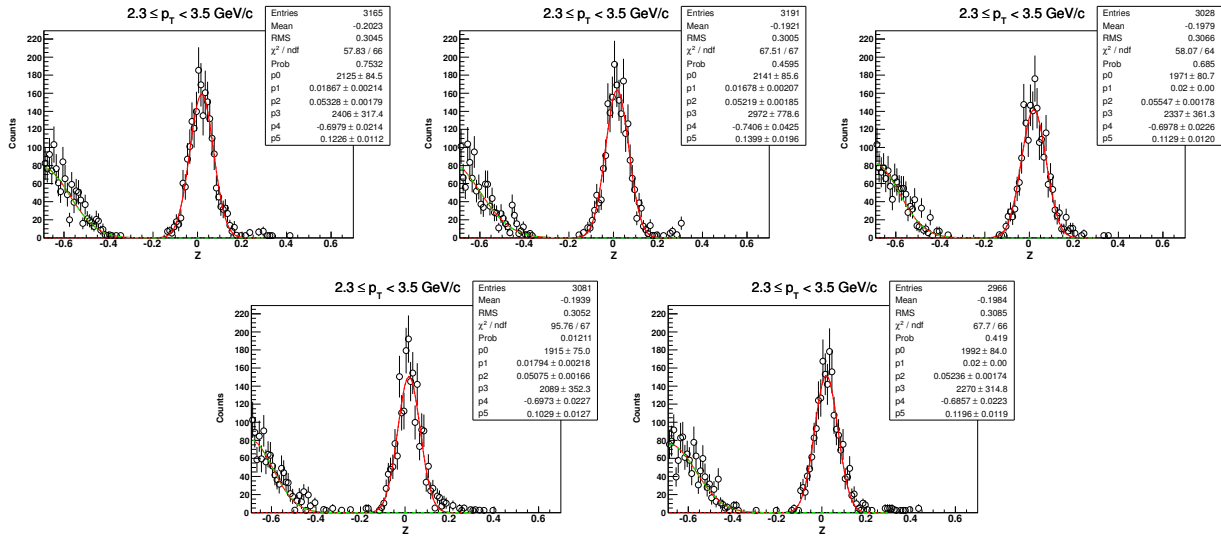
10.5.1 Z-distribution of 3He for $1.0 < p_T < 1.8$ GeV/c



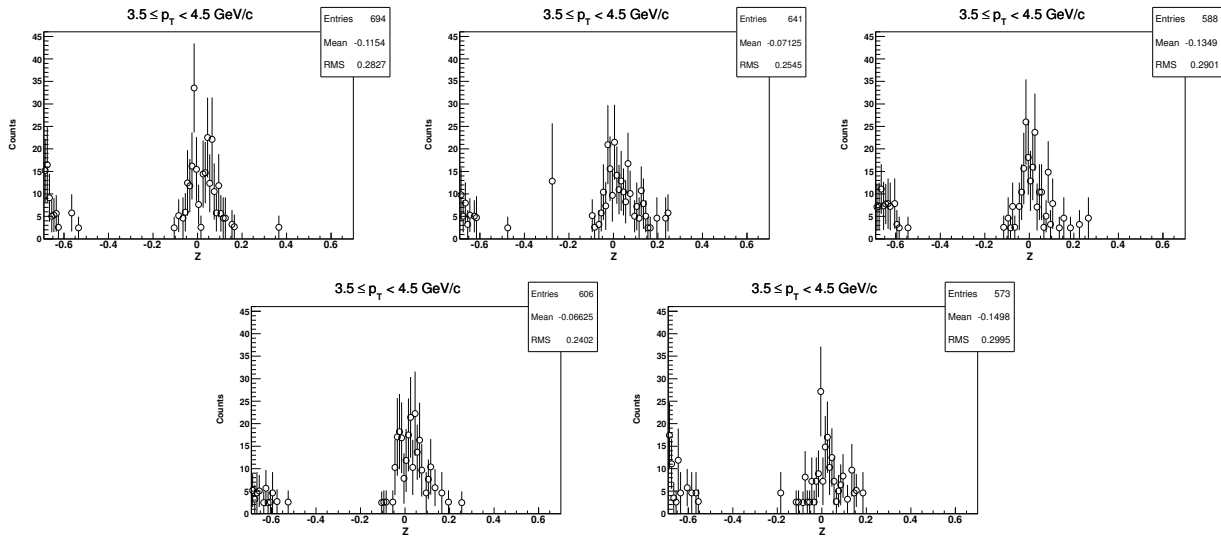
10.5.2 Z-distribution of 3He for $1.8 < p_T < 2.3$ GeV/c ($\sqrt{s_{NN}} = 11.5$ GeV, 0-80%)



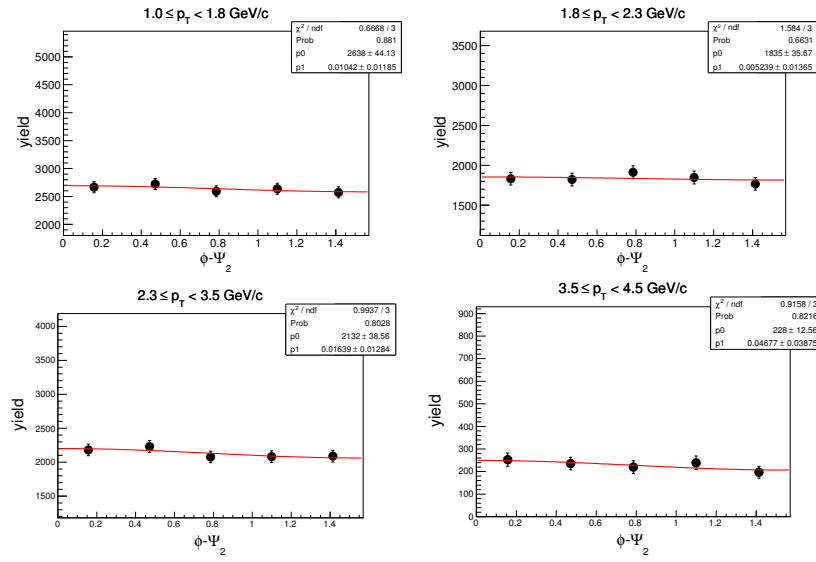
10.5.3 Z-distribution of 3He for $2.3 < p_T < 3.5 \text{ GeV}/c$ ($\sqrt{s_{NN}} = 11.5 \text{ GeV}$, 0-80%)



10.5.4 Z-distribution of 3He for $3.5 < p_T < 4.5 \text{ GeV}/c$ ($\sqrt{s_{NN}} = 11.5 \text{ GeV}$, 0-80%)

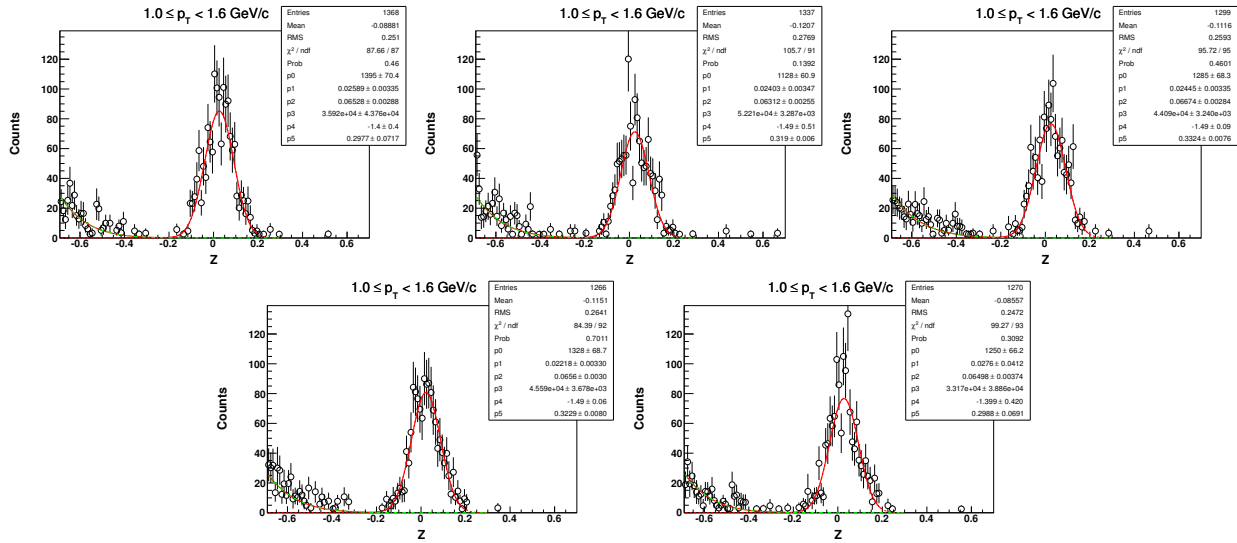


10.5.5 $\phi - \Psi_2$ of 3He in centrality: 0-80% ($\sqrt{s_{NN}} = 11.5$ GeV)

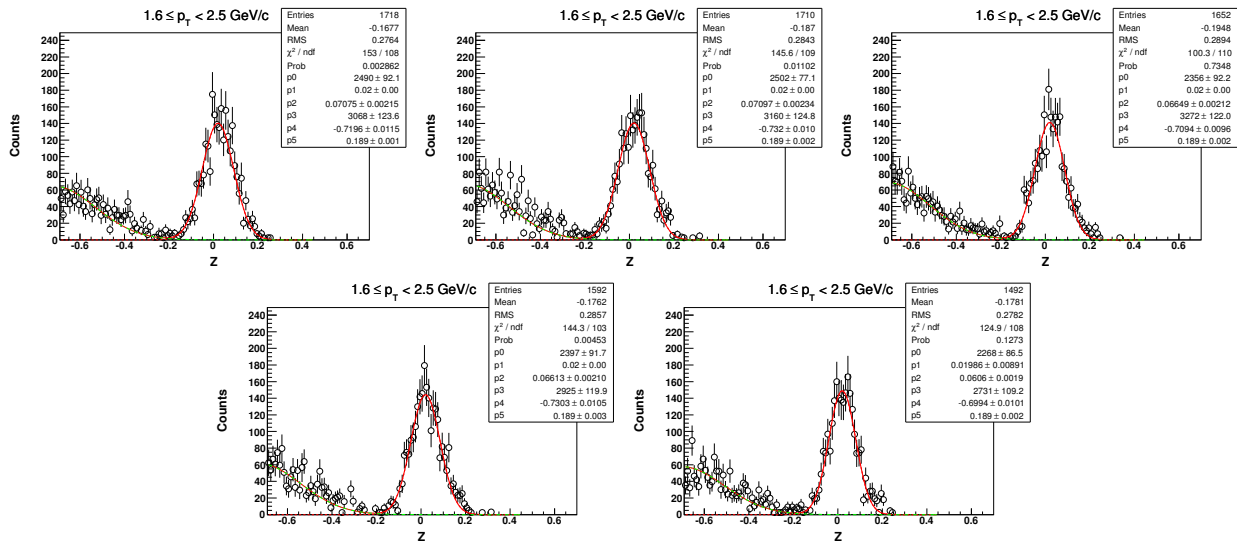


10.6 Z distribution of t in $\sqrt{s_{NN}} = 11.5$ GeV (centrality: 0-80%)

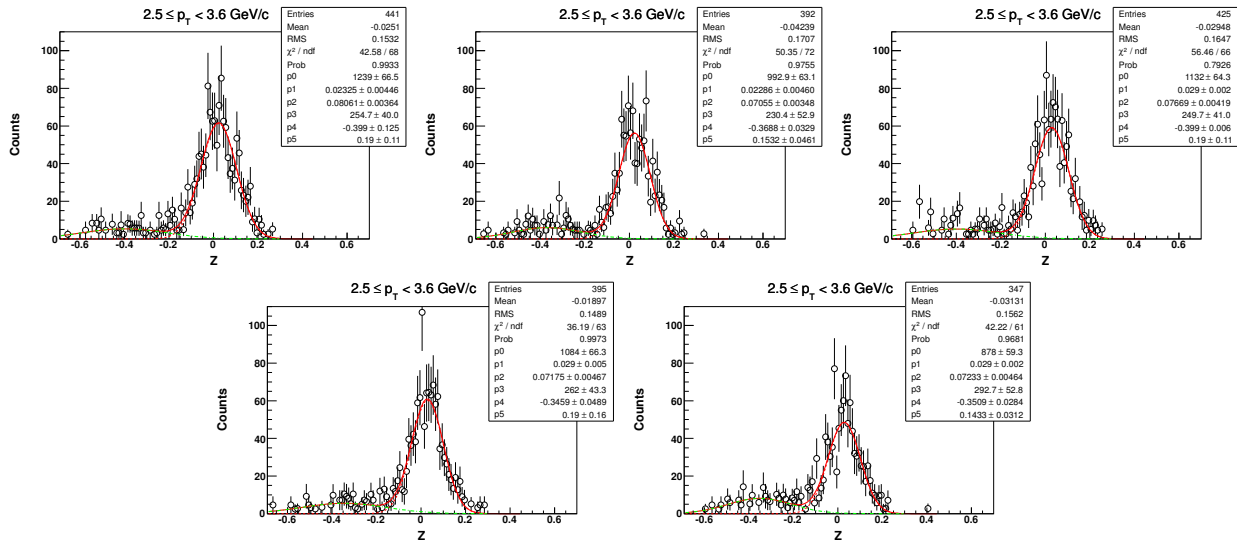
10.6.1 Z-distribution of t for $1.0 < p_T < 1.6$ GeV/c



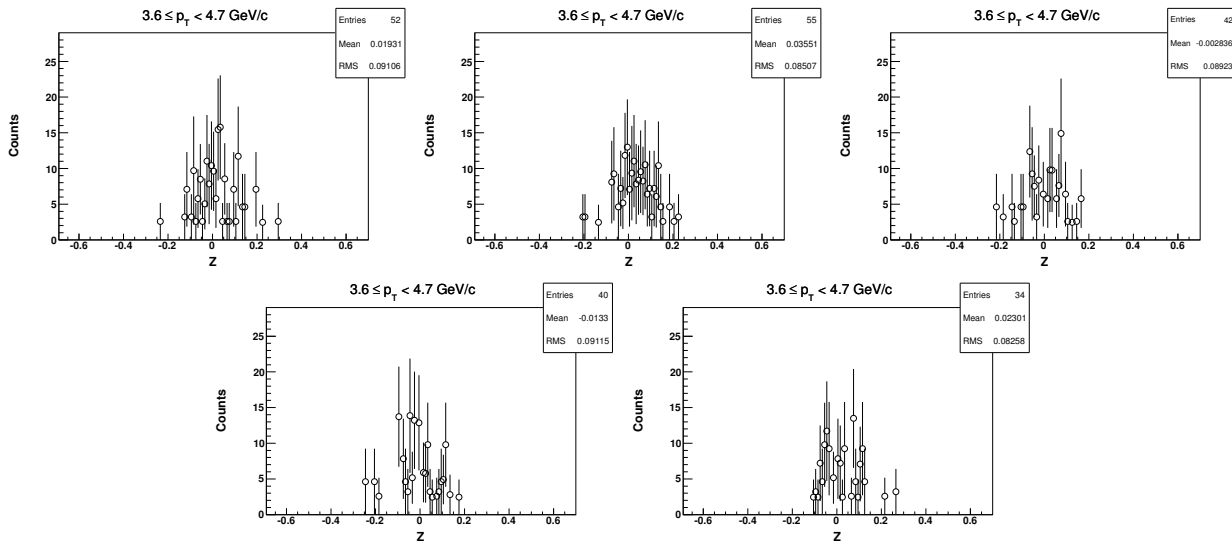
10.6.2 Z-distribution of t for $1.6 < p_T < 2.5 \text{ GeV}/c$ ($\sqrt{s_{NN}} = 11.5 \text{ GeV}$, 0-80%)



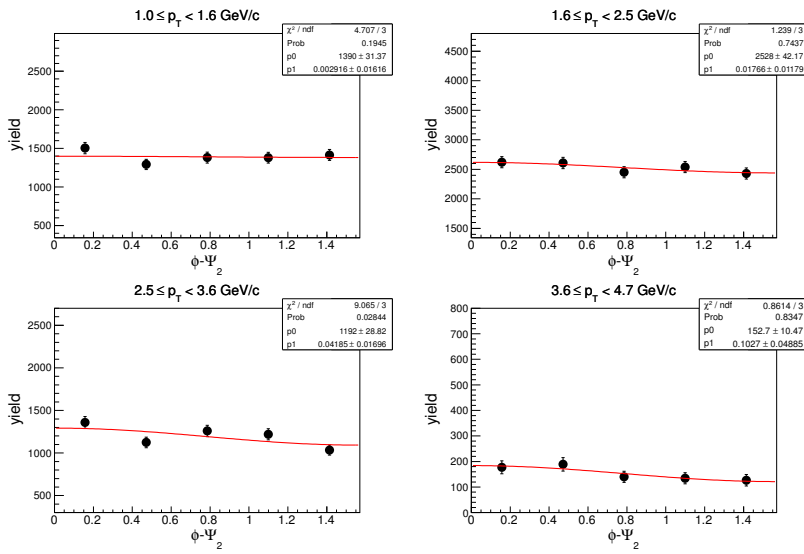
10.6.3 Z-distribution of t for $2.5 < p_T < 3.6 \text{ GeV}/c$ ($\sqrt{s_{NN}} = 11.5 \text{ GeV}$, 0-80%)



10.6.4 Z-distribution of t for $3.6 < p_T < 4.7 \text{ GeV}/c$ ($\sqrt{s_{NN}} = 11.5 \text{ GeV}$, 0-80%)



10.6.5 $\phi - \Psi_2$ of t in centrality: 0-80% ($\sqrt{s_{NN}} = 11.5 \text{ GeV}$)

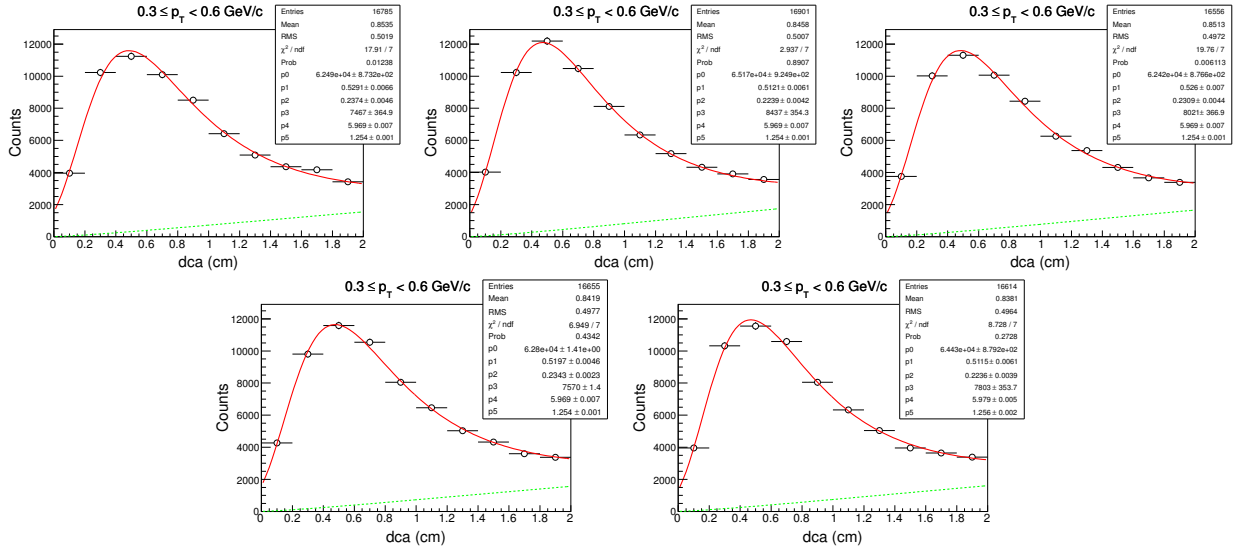


11 DCA and Z-distributions for Au+Au at $\sqrt{s_{NN}} = 7.7$ GeV

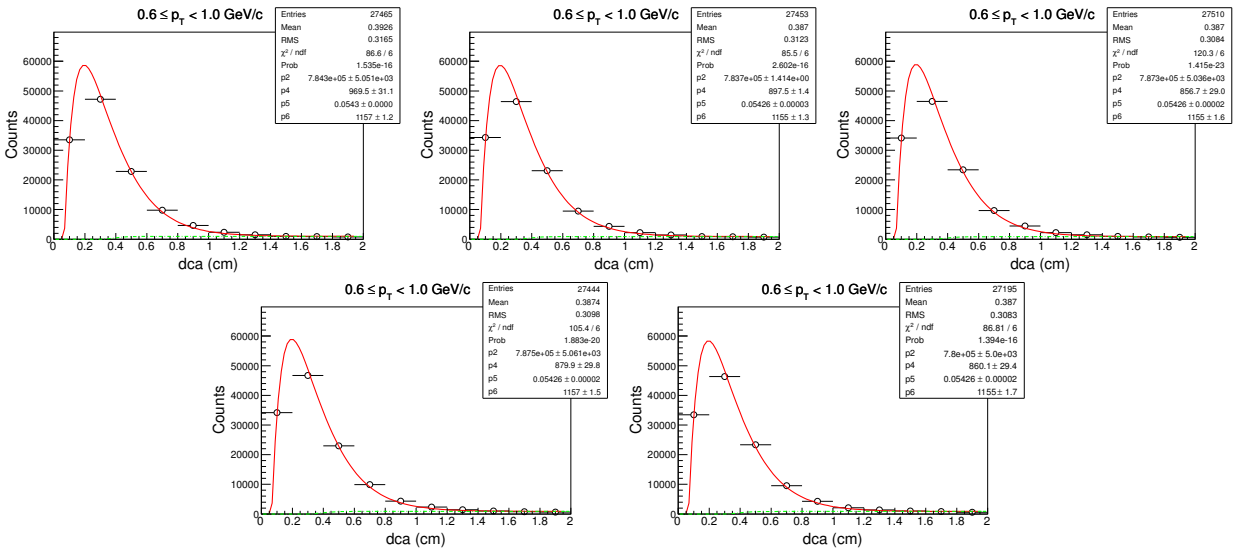
In this section we show the DCA and Z-distribution of deuteron and anti-deuteron for five different ($\phi - \Psi_2$) bins namely, $0 - \frac{\pi}{10}$, $\frac{\pi}{10} - \frac{2\pi}{10}$, $\frac{2\pi}{10} - \frac{3\pi}{10}$, $\frac{3\pi}{10} - \frac{4\pi}{10}$ and $\frac{4\pi}{10} - \frac{5\pi}{10}$. DCA and Z-distribution of d for all centrality and all p_T bins are shown in the later sub-sections.

11.1 Centrality: 0-80%

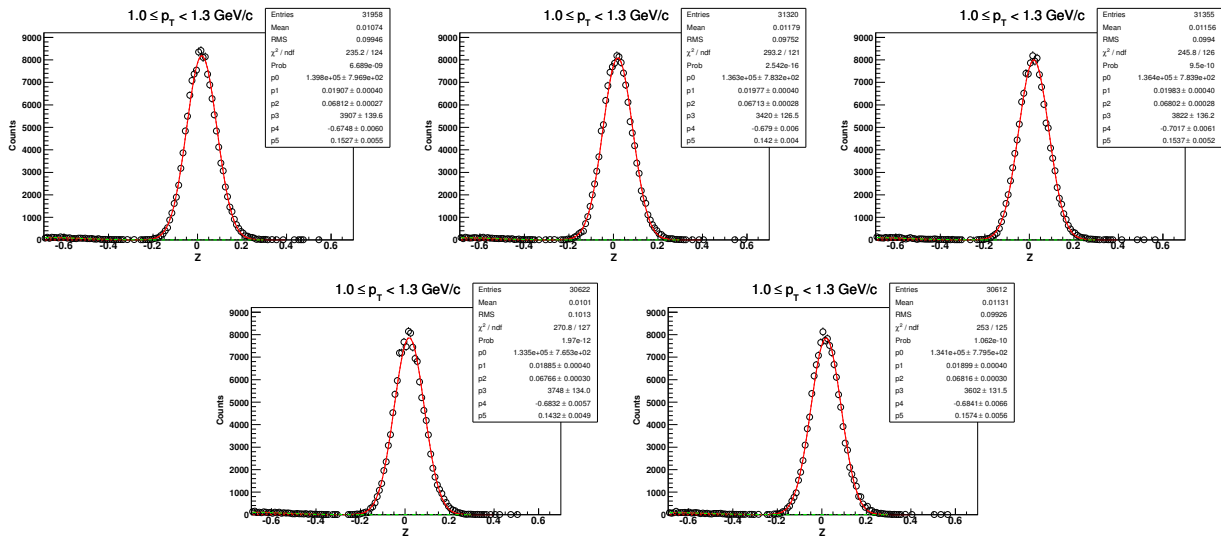
11.1.1 DCA-distribution of d for $0.3 < p_T < 0.6$ GeV/c



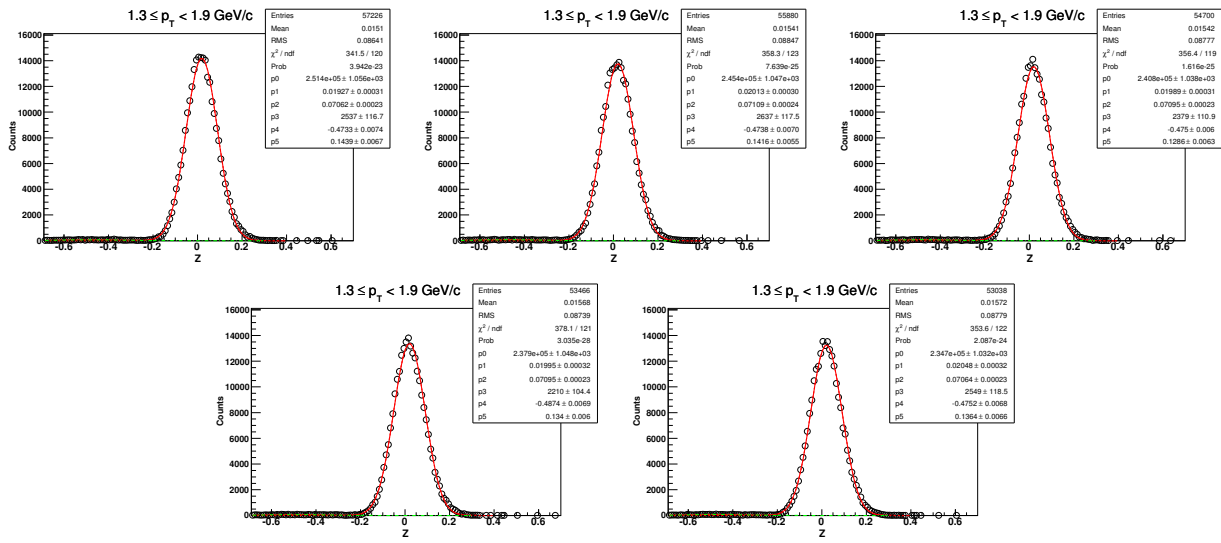
11.1.2 DCA-distribution of d for $0.6 < p_T < 1.0$ GeV/c ($\sqrt{s_{NN}} = 7.7$ GeV, 0-80%)



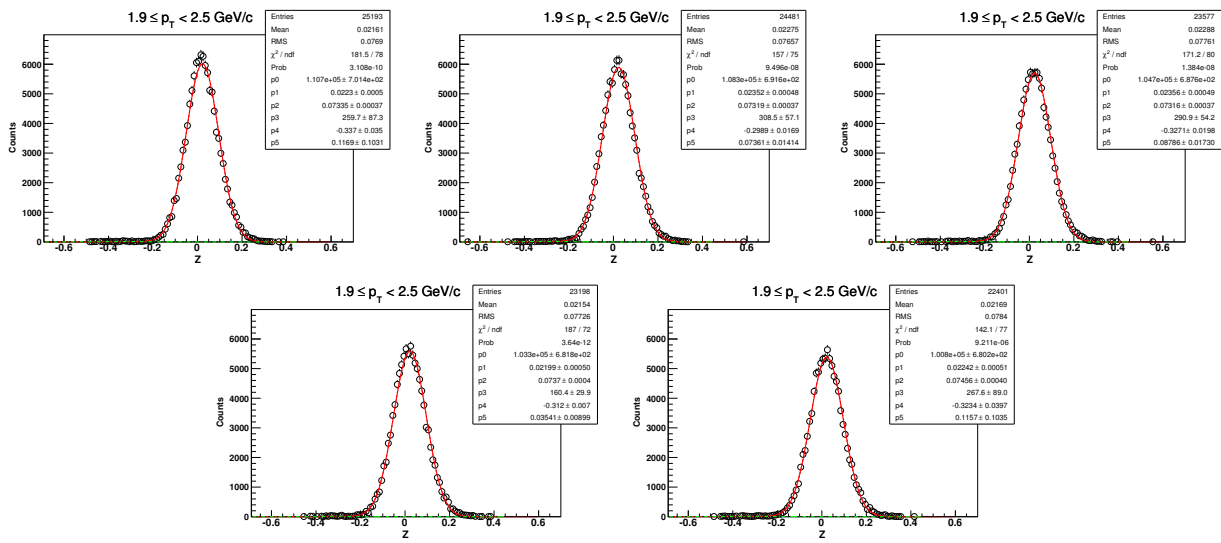
11.1.3 Z-distribution of d for $1.0 < p_T < 1.3 \text{ GeV}/c$ ($\sqrt{s_{NN}} = 7.7 \text{ GeV}$, 0-80%)



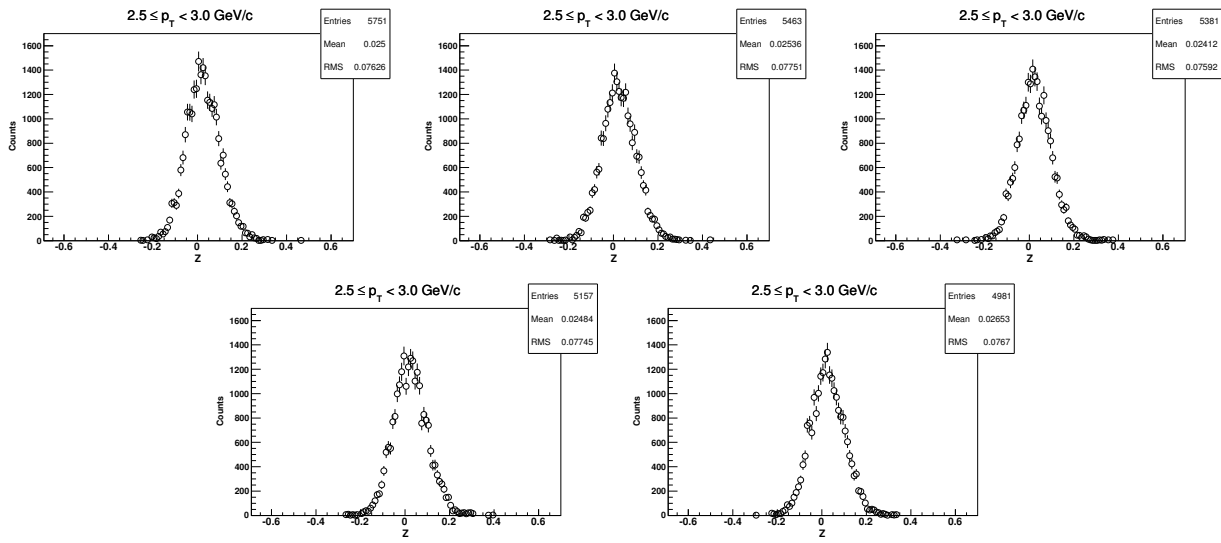
11.1.4 Z-distribution of d for $1.3 < p_T < 1.9 \text{ GeV}/c$ ($\sqrt{s_{NN}} = 7.7 \text{ GeV}$, 0-80%)



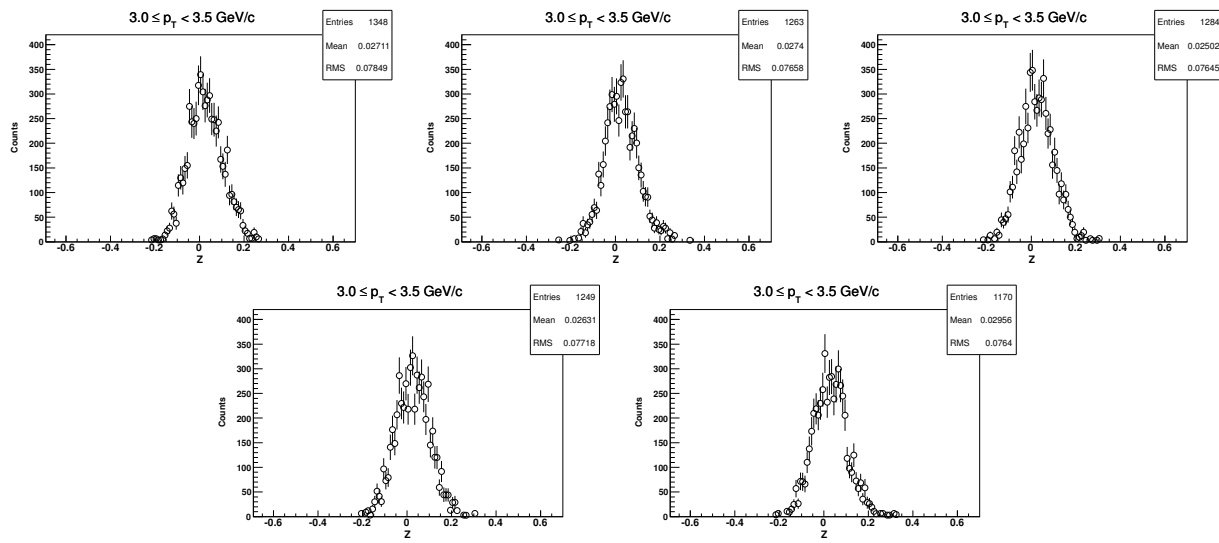
11.1.5 Z-distribution of d for $1.9 < p_T < 2.5 \text{ GeV}/c$ ($\sqrt{s_{NN}} = 7.7 \text{ GeV}$, 0-80%)



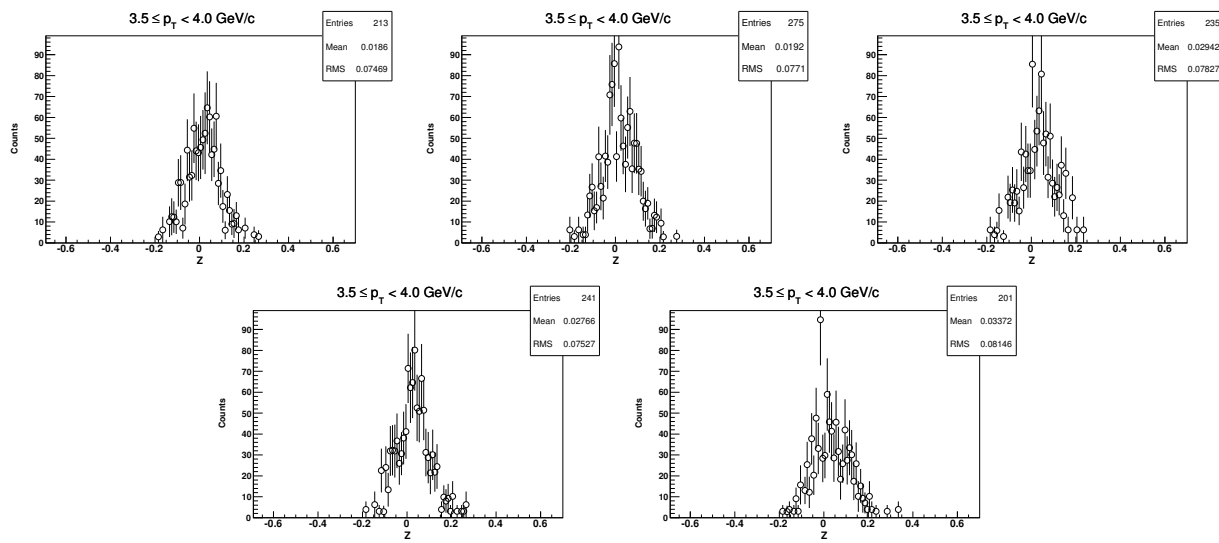
11.1.6 Z-distribution of d for $2.5 < p_T < 3.0 \text{ GeV}/c$ ($\sqrt{s_{NN}} = 7.7 \text{ GeV}$, 0-80%)



11.1.7 Z-distribution of d for $3.0 < p_T < 3.5 \text{ GeV}/c$ ($\sqrt{s_{NN}} = 7.7 \text{ GeV}$, 0-80%)

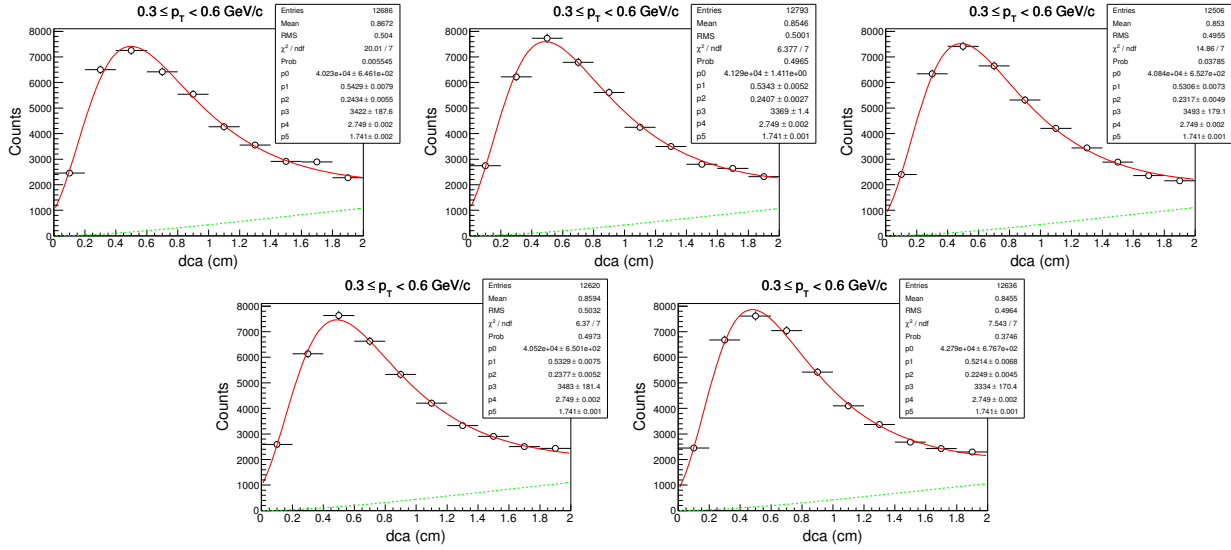


11.1.8 Z-distribution of d for $3.5 < p_T < 4.0 \text{ GeV}/c$ ($\sqrt{s_{NN}} = 7.7 \text{ GeV}$, 0-80%)

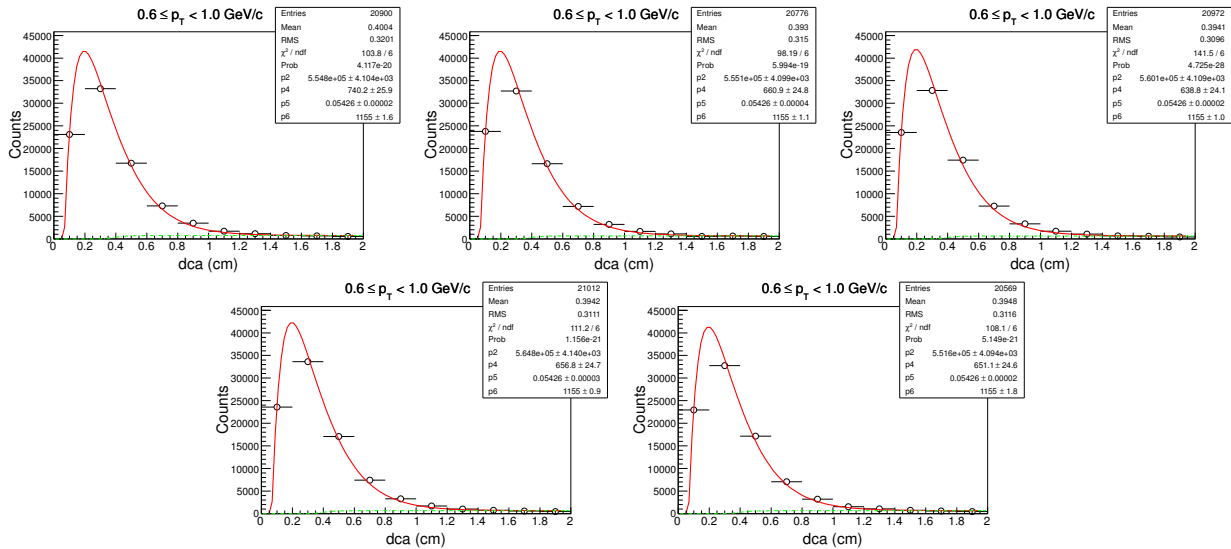


11.2 Centrality: 0-30%

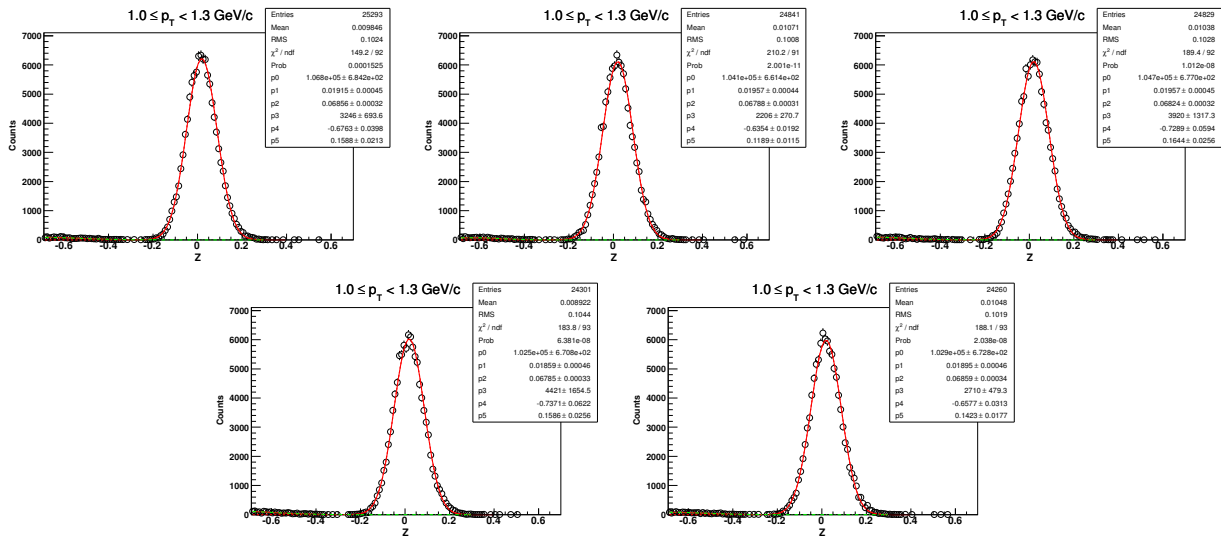
11.2.1 DCA-distribution of d for $0.3 < p_T < 0.6 \text{ GeV}/c$



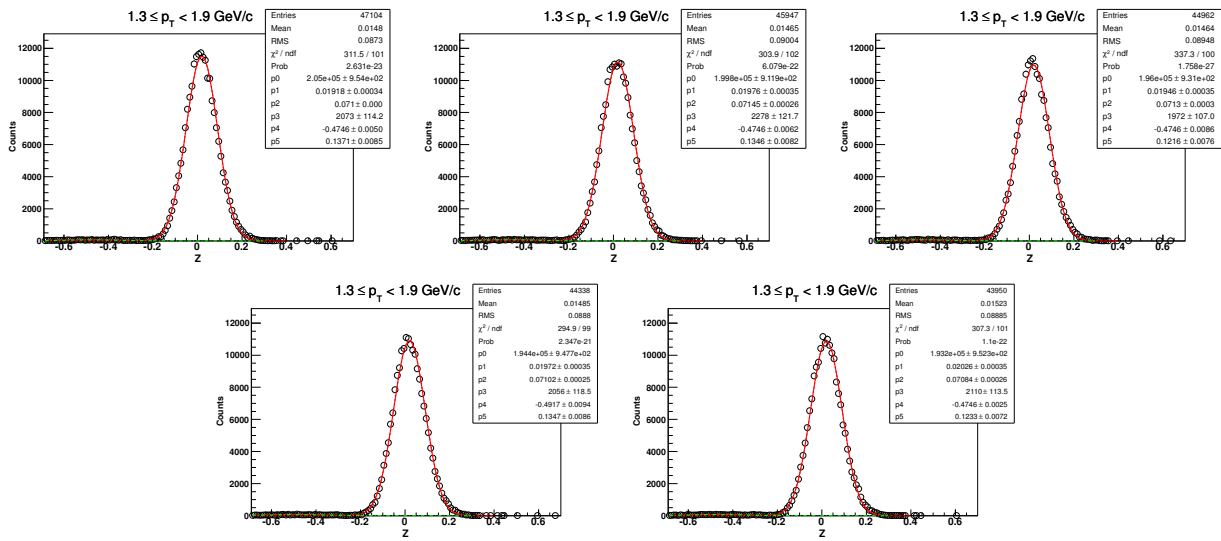
11.2.2 DCA-distribution of d for $0.6 < p_T < 1.0 \text{ GeV}/c$



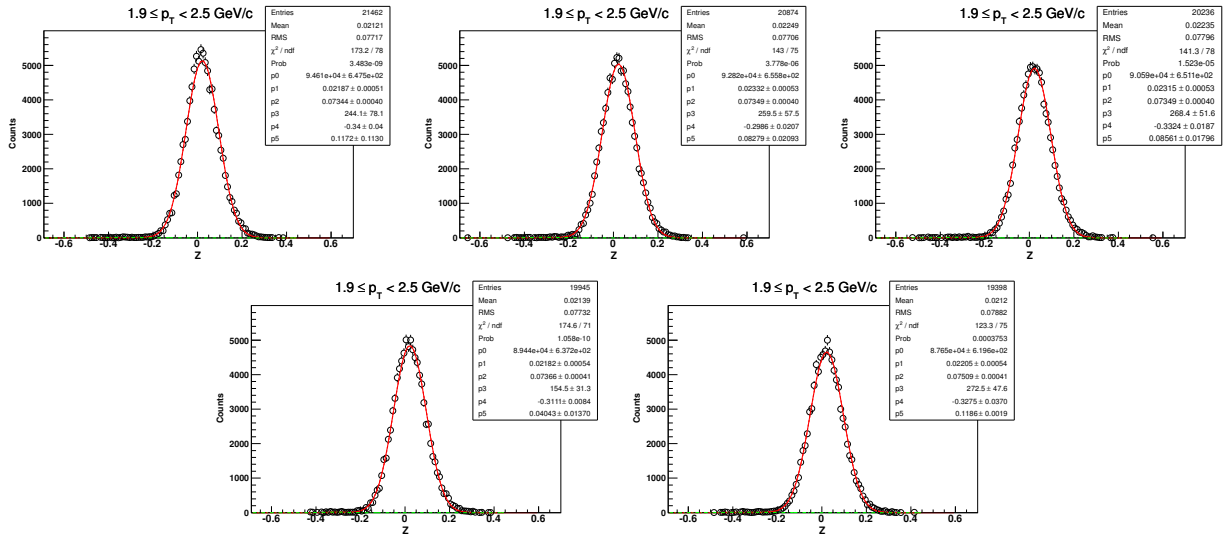
11.2.3 Z-distribution of d for $1.0 < p_T < 1.3 \text{ GeV}/c$ ($\sqrt{s_{NN}} = 7.7 \text{ GeV}$, 0-30%)



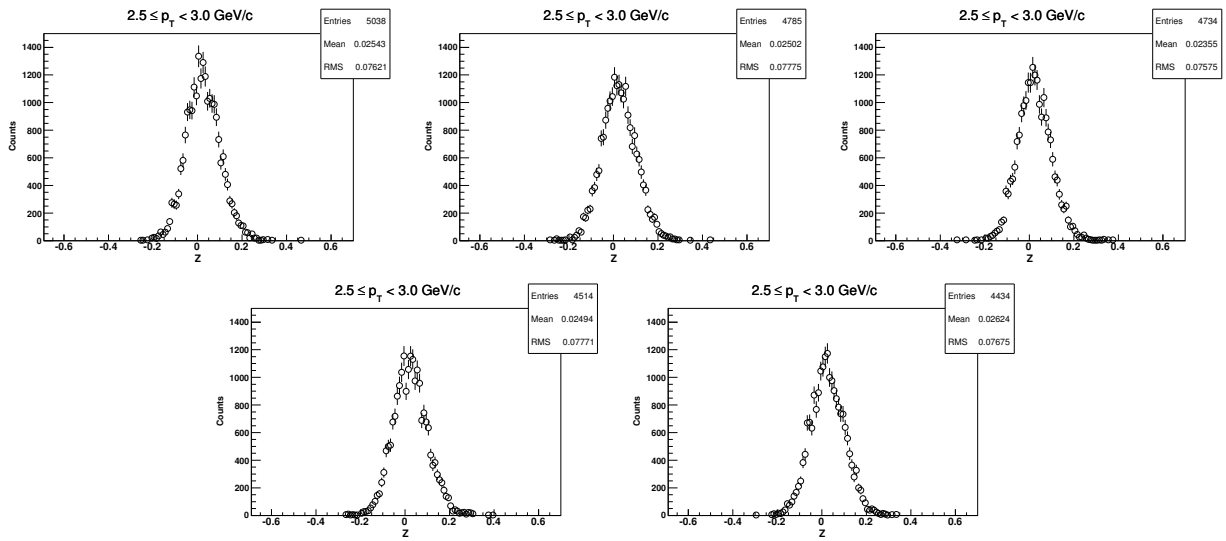
11.2.4 Z-distribution of d for $1.3 < p_T < 1.9 \text{ GeV}/c$ ($\sqrt{s_{NN}} = 7.7 \text{ GeV}$, 0-30%)



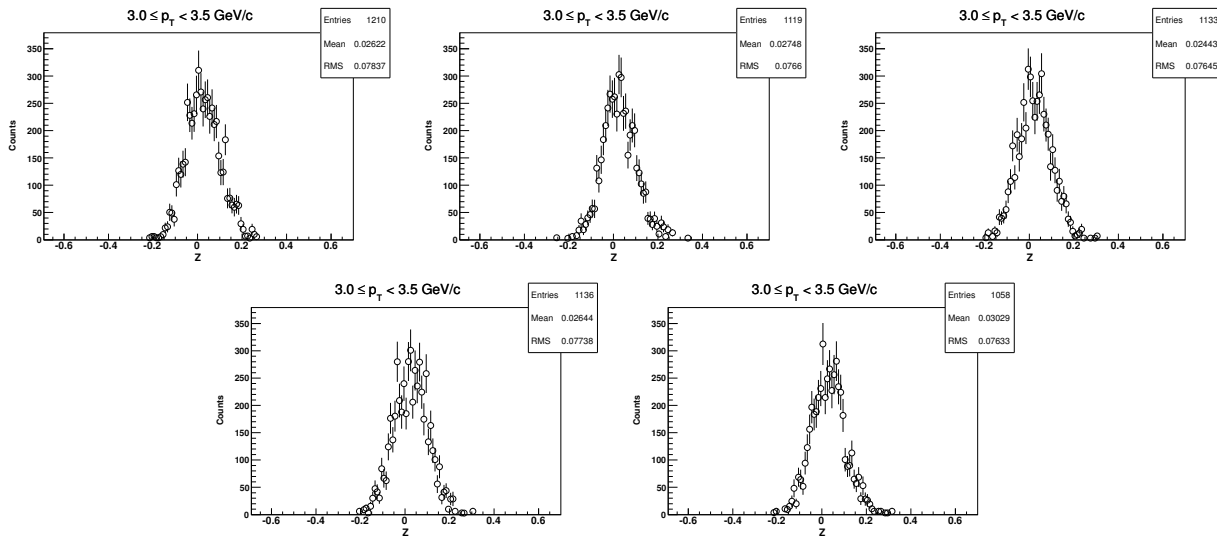
11.2.5 Z-distribution of d for $1.9 < p_T < 2.5 \text{ GeV}/c$ ($\sqrt{s_{NN}} = 7.7 \text{ GeV}$, 0-30%)



11.2.6 Z-distribution of d for $2.5 < p_T < 3.0 \text{ GeV}/c$ ($\sqrt{s_{NN}} = 7.7 \text{ GeV}$, 0-30%)

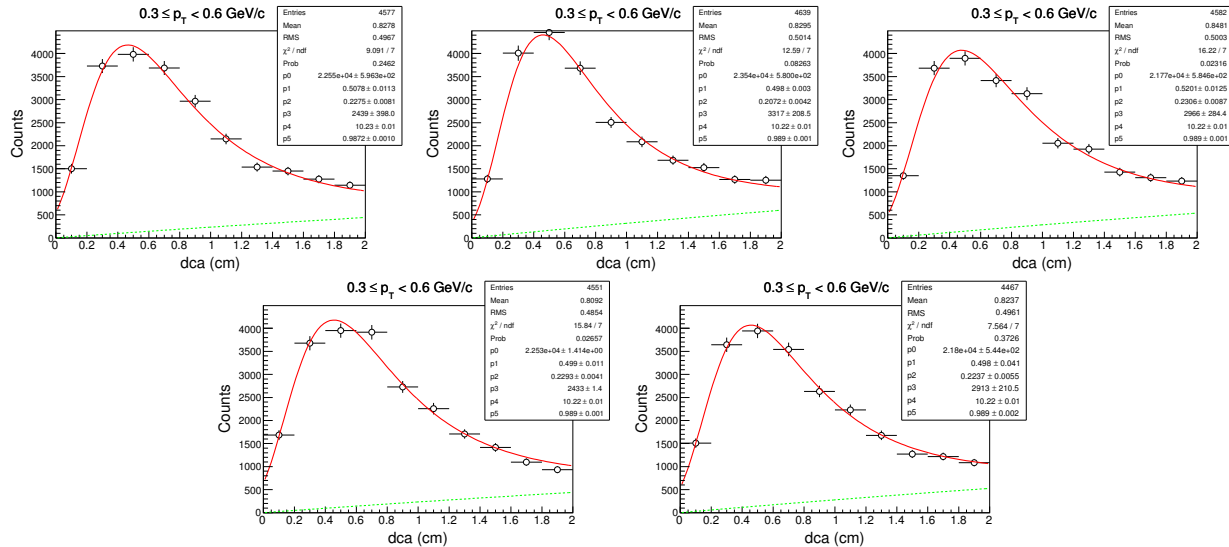


11.2.7 Z-distribution of d for $3.0 < p_T < 3.5 \text{ GeV}/c$ ($\sqrt{s_{NN}} = 7.7 \text{ GeV}$, 0-30%)

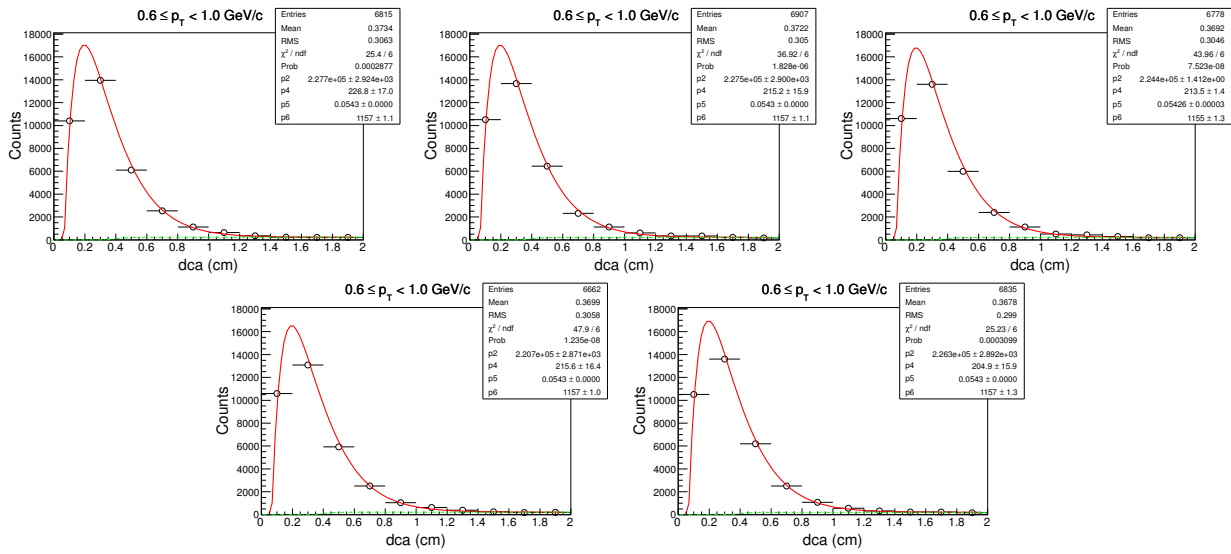


11.3 Centrality: 30-80%

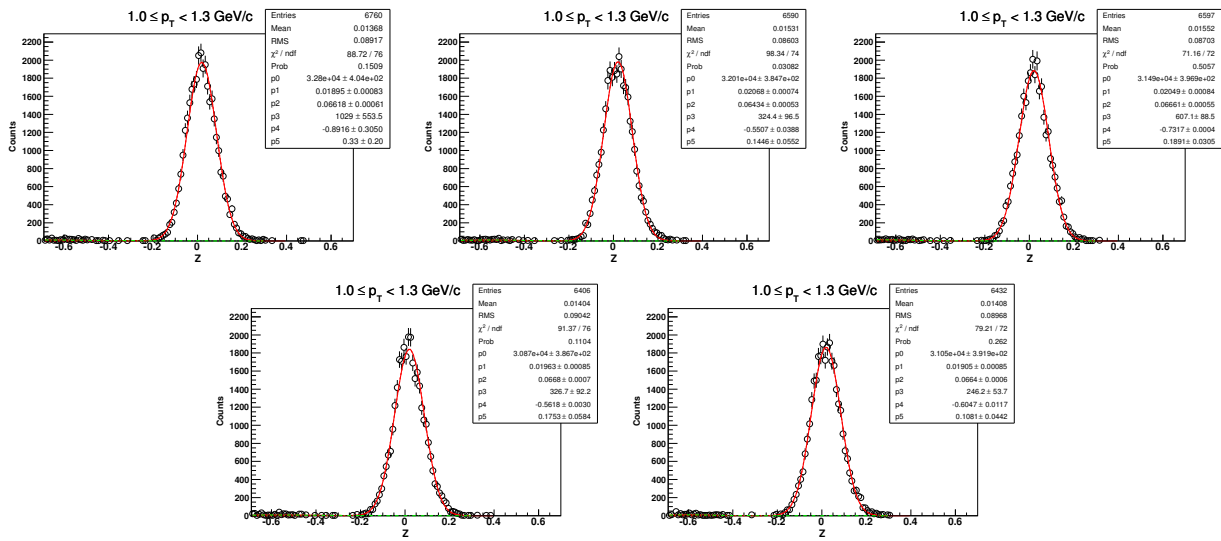
11.3.1 DCA-distribution of d for $0.3 < p_T < 0.6 \text{ GeV}/c$



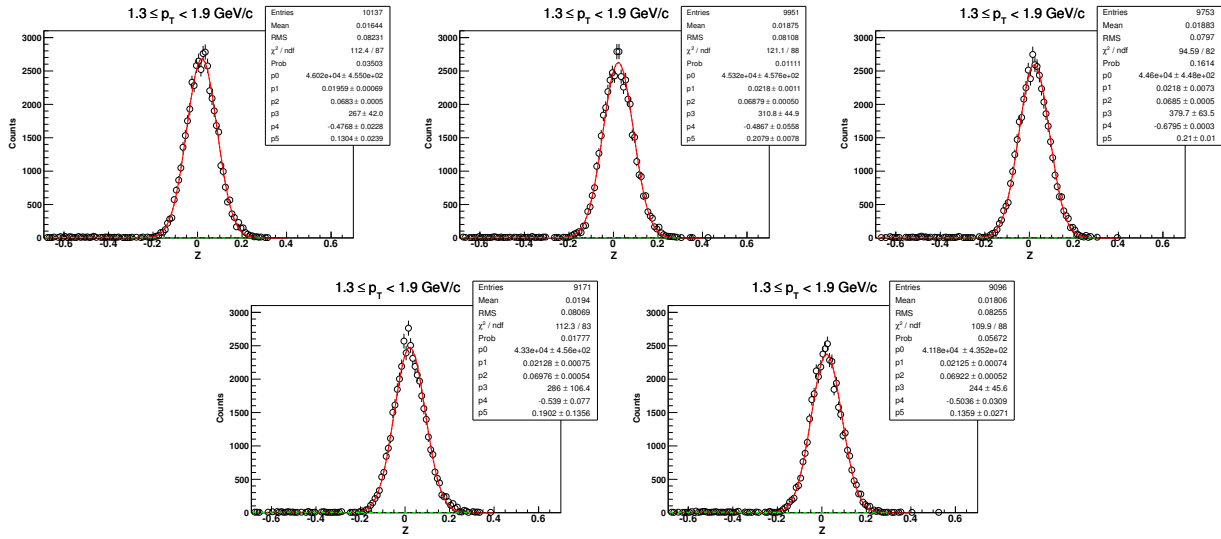
11.3.2 DCA-distribution of d for $0.6 < p_T < 1.0 \text{ GeV}/c$ ($\sqrt{s_{NN}} = 7.7 \text{ GeV}$, 30-80%)



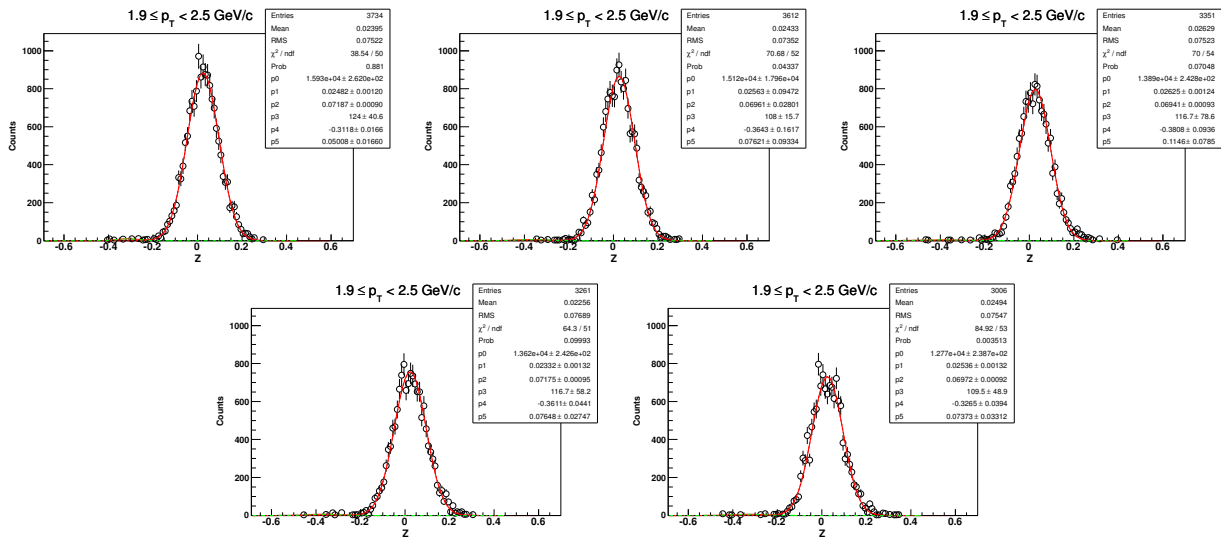
11.3.3 Z-distribution of d for $1.0 < p_T < 1.3 \text{ GeV}/c$ ($\sqrt{s_{NN}} = 7.7 \text{ GeV}$, 30-80%)



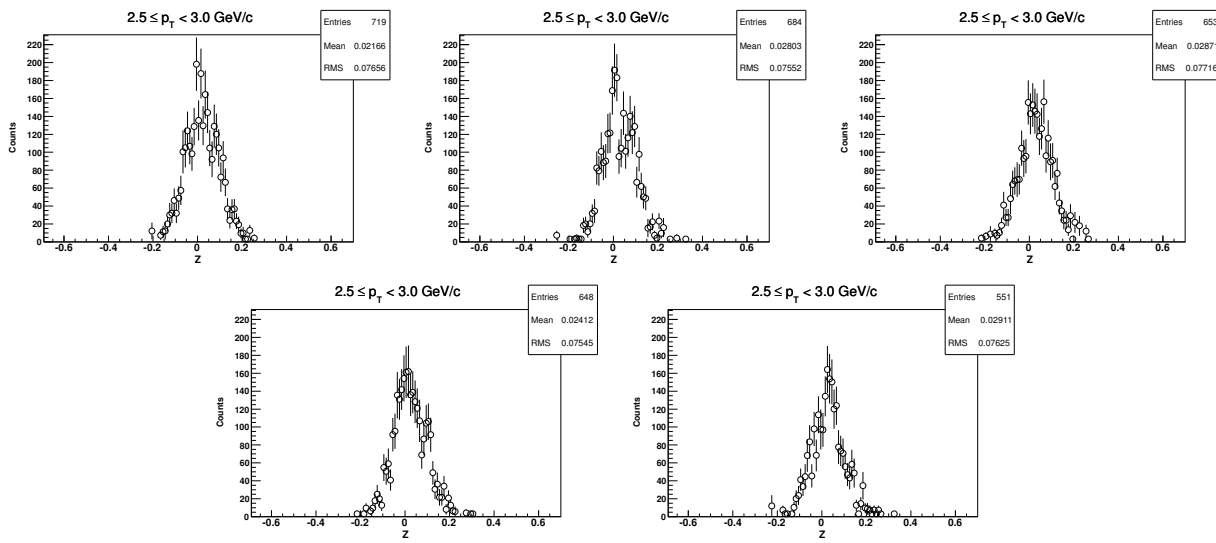
11.3.4 Z-distribution of d for $1.3 < p_T < 1.9 \text{ GeV}/c$ ($\sqrt{s_{NN}} = 7.7 \text{ GeV}$, 30-80%)



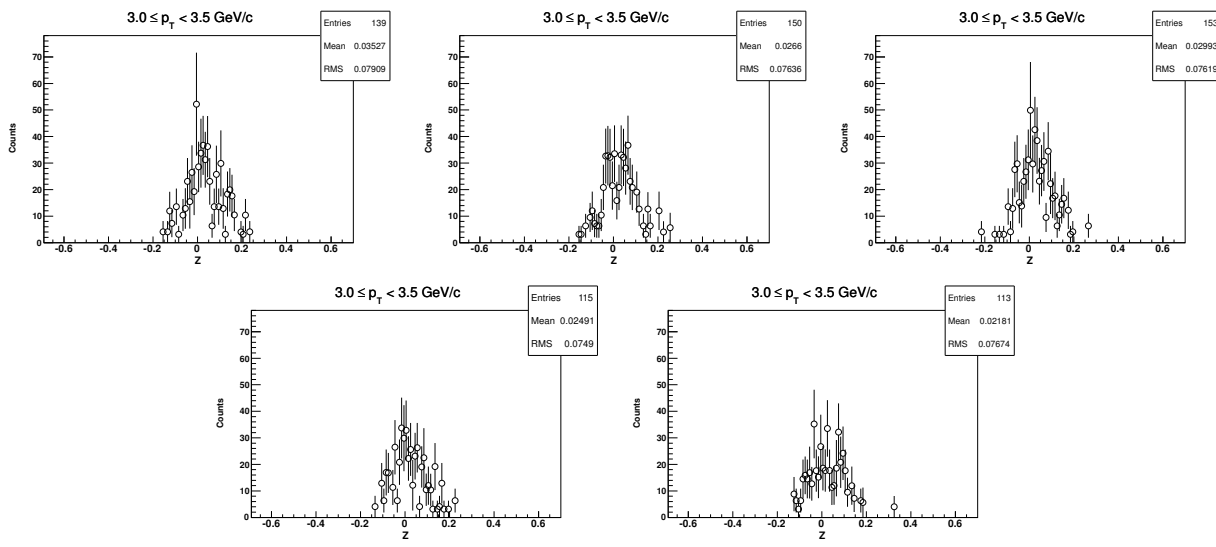
11.3.5 Z-distribution of d for $1.9 < p_T < 2.5 \text{ GeV}/c$ ($\sqrt{s_{NN}} = 7.7 \text{ GeV}$, 30-80%)



11.3.6 Z-distribution of d for $2.5 < p_T < 3.0 \text{ GeV}/c$ ($\sqrt{s_{NN}} = 7.7 \text{ GeV}$, 30-80%)

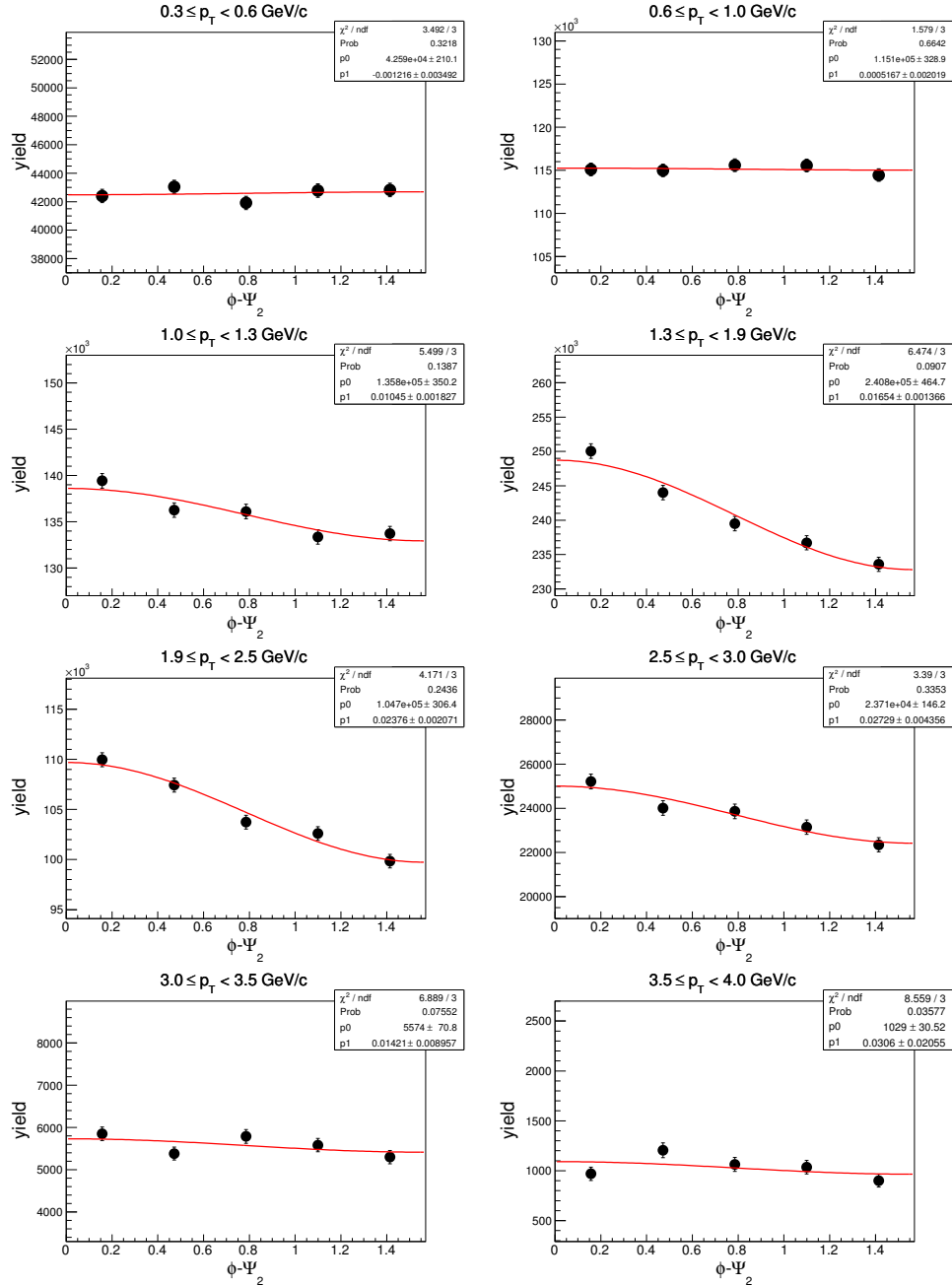


11.3.7 Z-distribution of d for $3.0 < p_T < 3.5 \text{ GeV}/c$ ($\sqrt{s_{NN}} = 7.7 \text{ GeV}$, 30-80%)

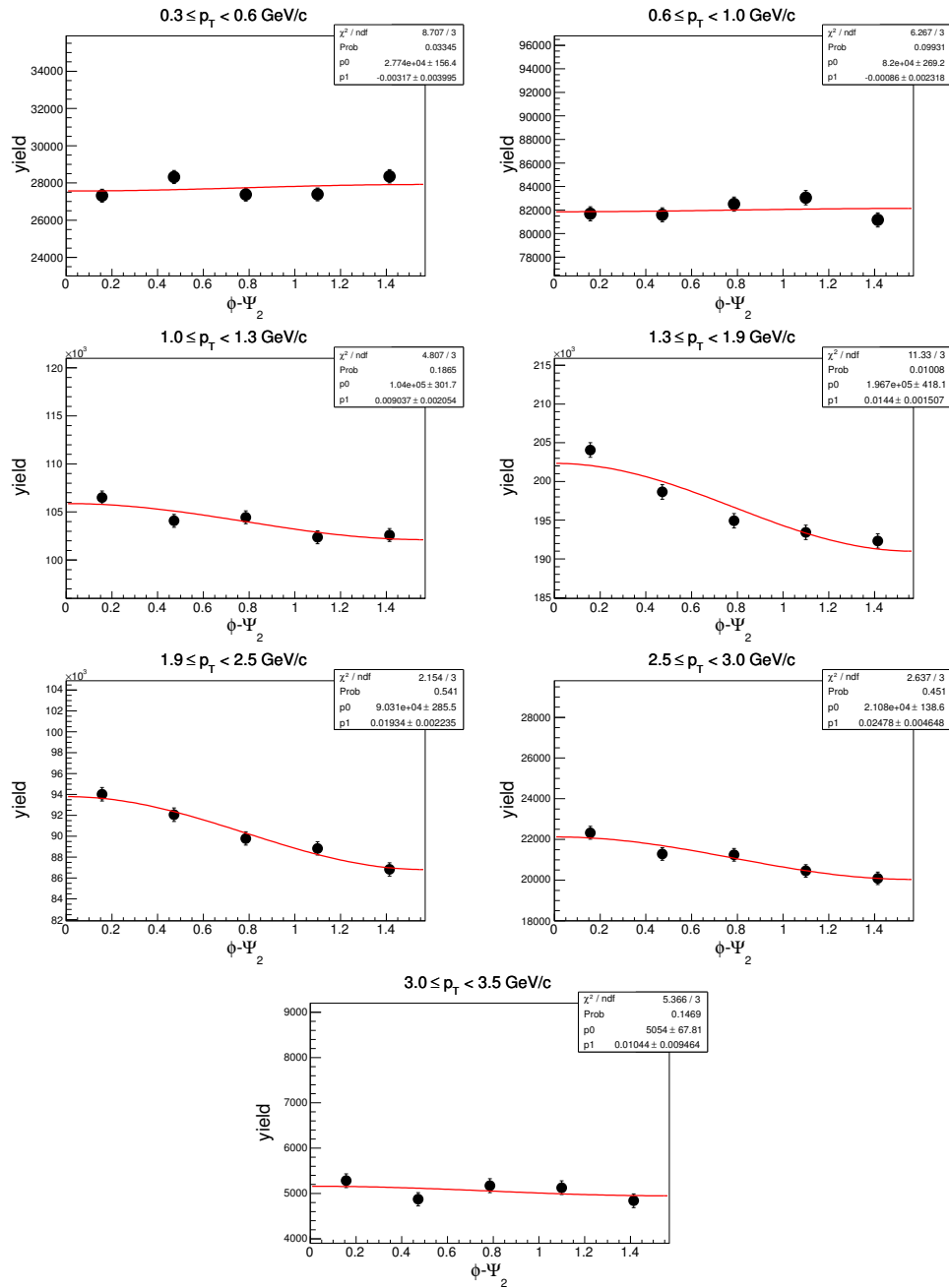


11.4 $\phi - \Psi_2$ distributions in Au+Au at $\sqrt{s_{NN}} = 7.7$ GeV

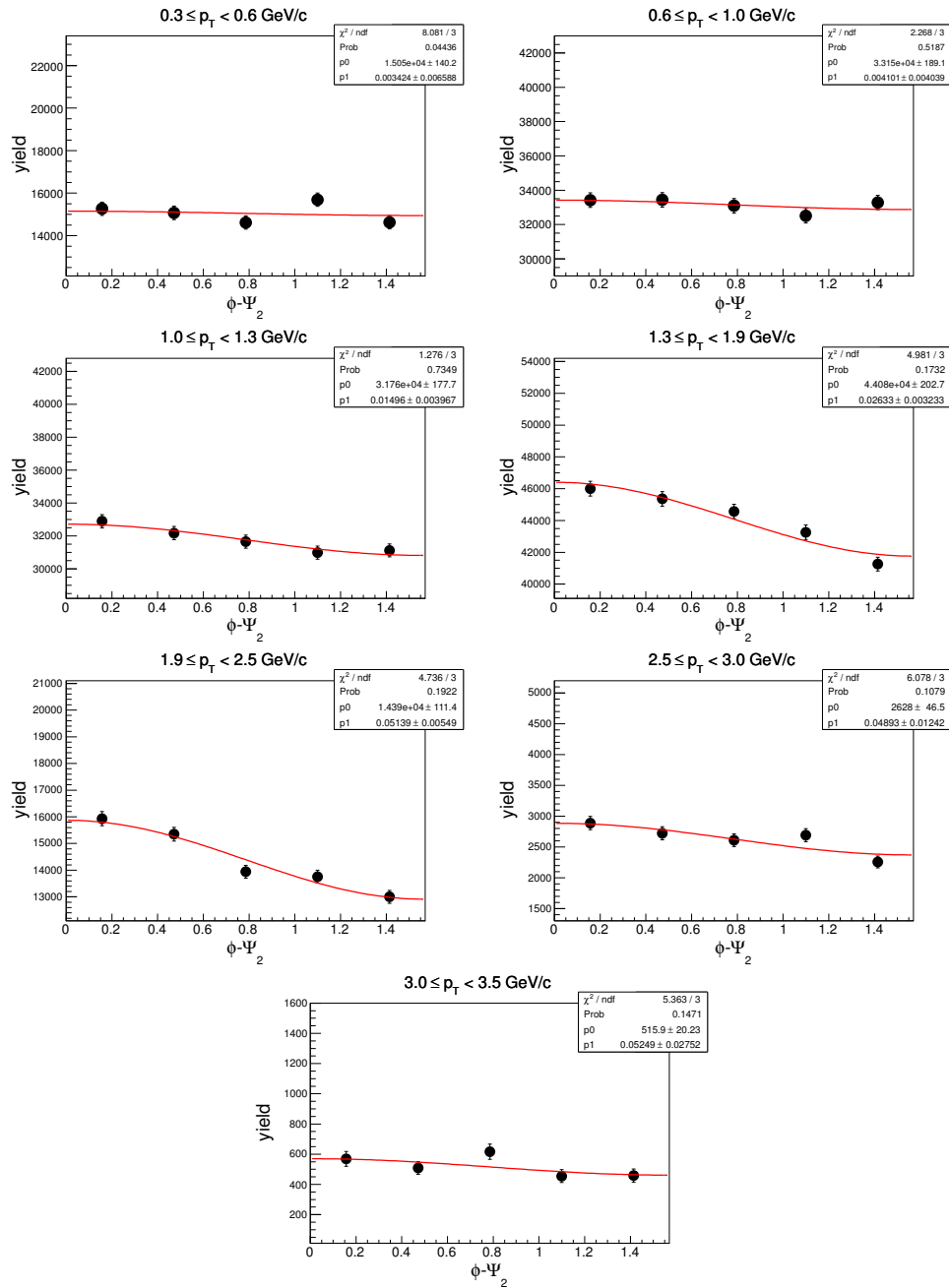
11.4.1 $\phi - \Psi_2$ of d in centrality: 0-80%



11.4.2 $\phi - \Psi_2$ of d in centrality: 0-30% ($\sqrt{s_{NN}} = 7.7$ GeV)

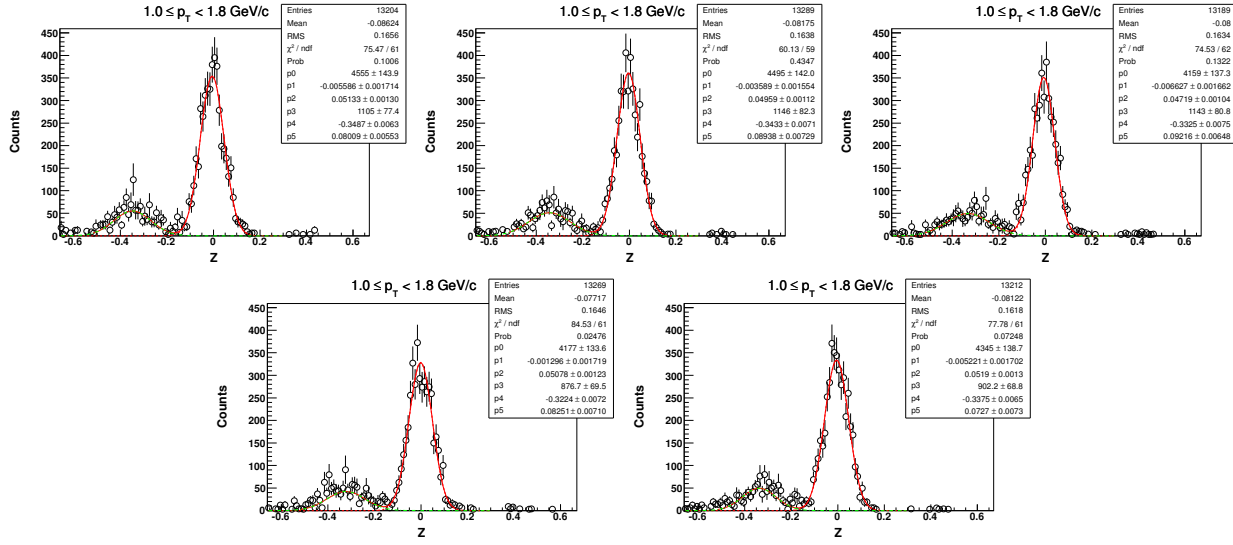


11.4.3 $\phi - \Psi_2$ of d in centrality: 30-80% ($\sqrt{s_{NN}} = 7.7$ GeV)

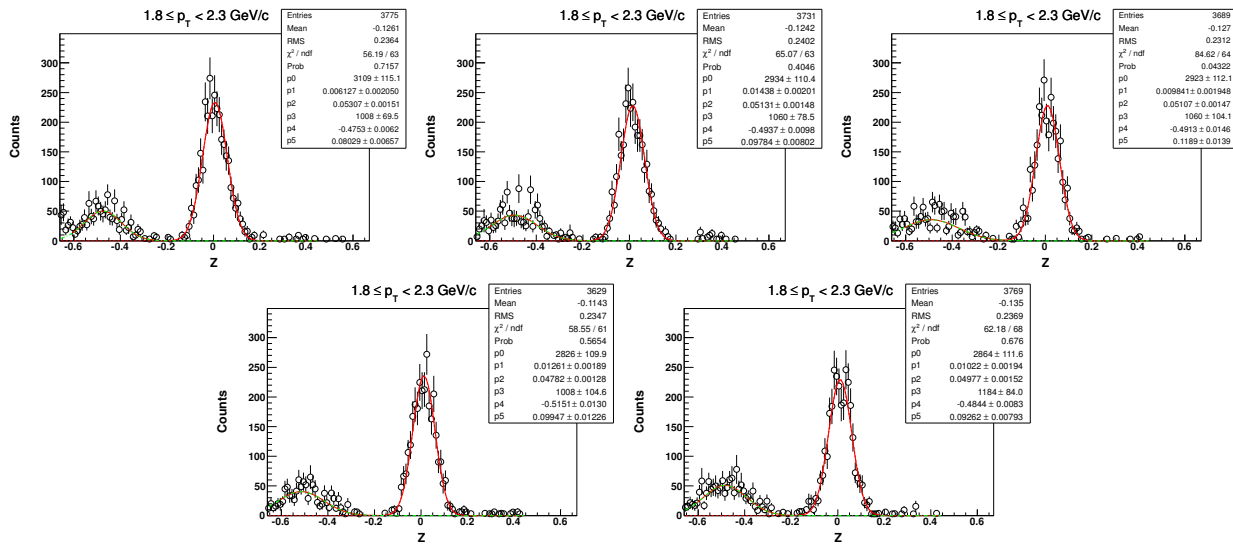


11.5 Z distribution of 3He in $\sqrt{s_{NN}} = 7.7$ GeV (centrality: 0-80%)

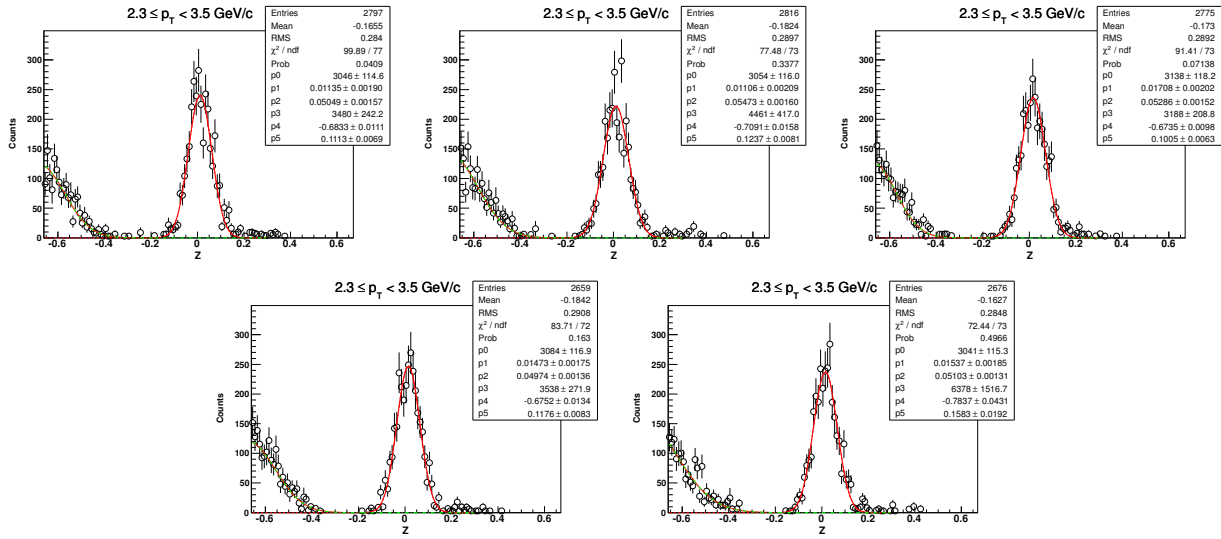
11.5.1 Z-distribution of 3He for $1.0 < p_T < 1.8$ GeV/c



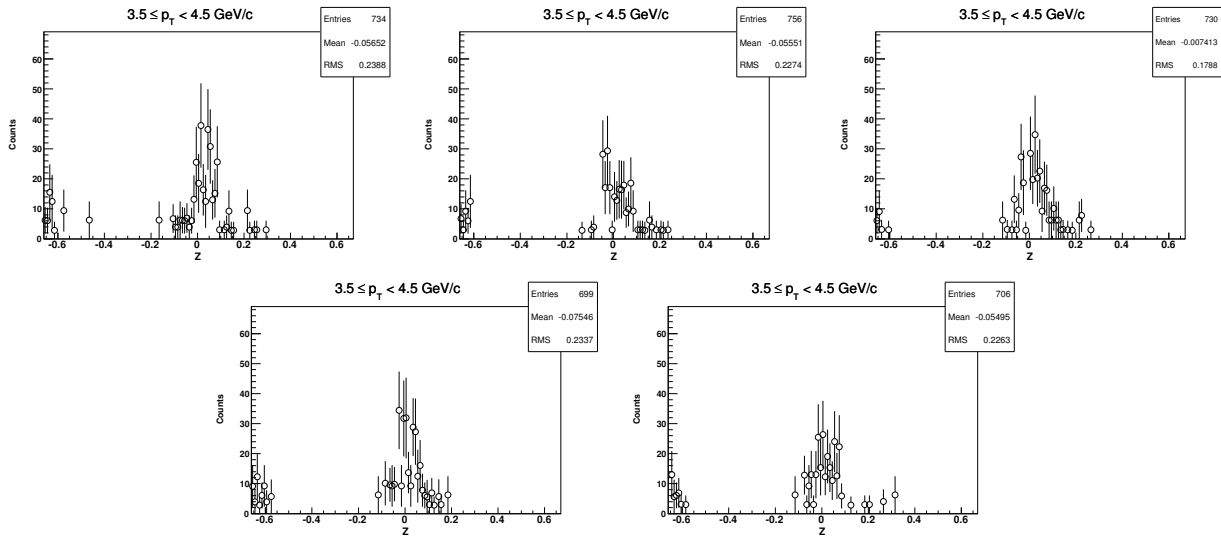
11.5.2 Z-distribution of 3He for $1.8 < p_T < 2.3$ GeV/c ($\sqrt{s_{NN}} = 7.7$ GeV, 0-80%)



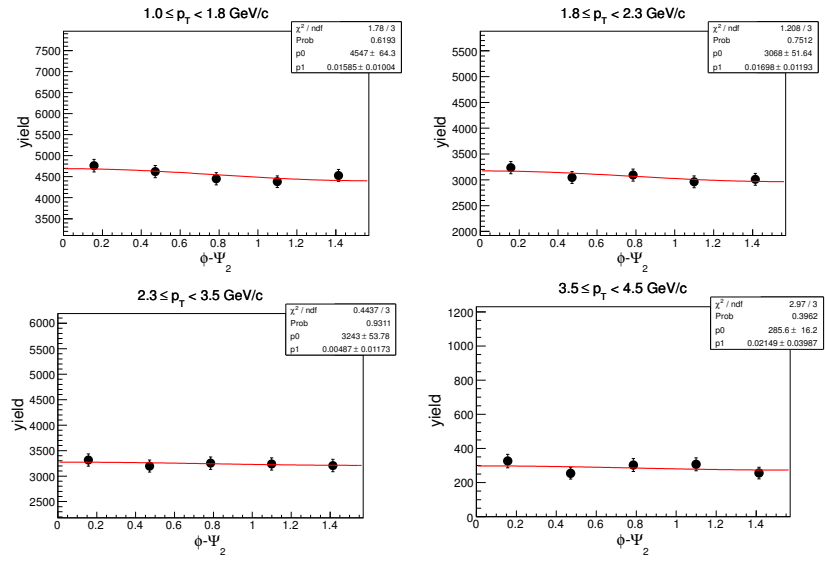
11.5.3 Z-distribution of 3He for $2.3 < p_T < 3.5 \text{ GeV}/c$ ($\sqrt{s_{NN}} = 7.7 \text{ GeV}$, 0-80%)



11.5.4 Z-distribution of 3He for $3.5 < p_T < 4.5 \text{ GeV}/c$ ($\sqrt{s_{NN}} = 7.7 \text{ GeV}$, 0-80%)

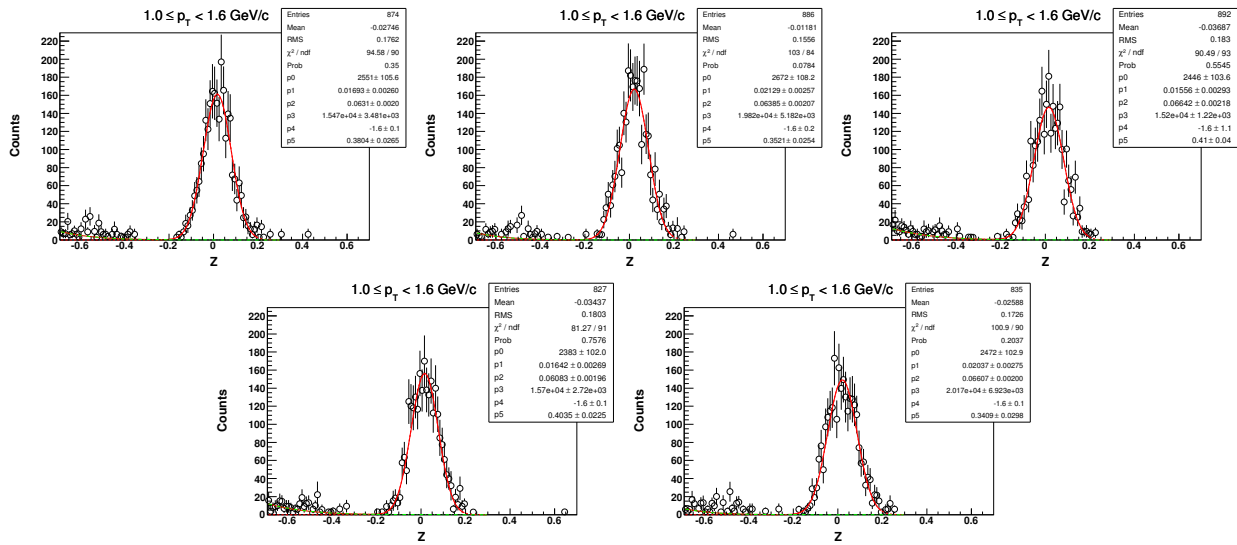


11.5.5 $\phi - \Psi_2$ of 3He in centrality: 0-80% ($\sqrt{s_{NN}} = 7.7$ GeV)

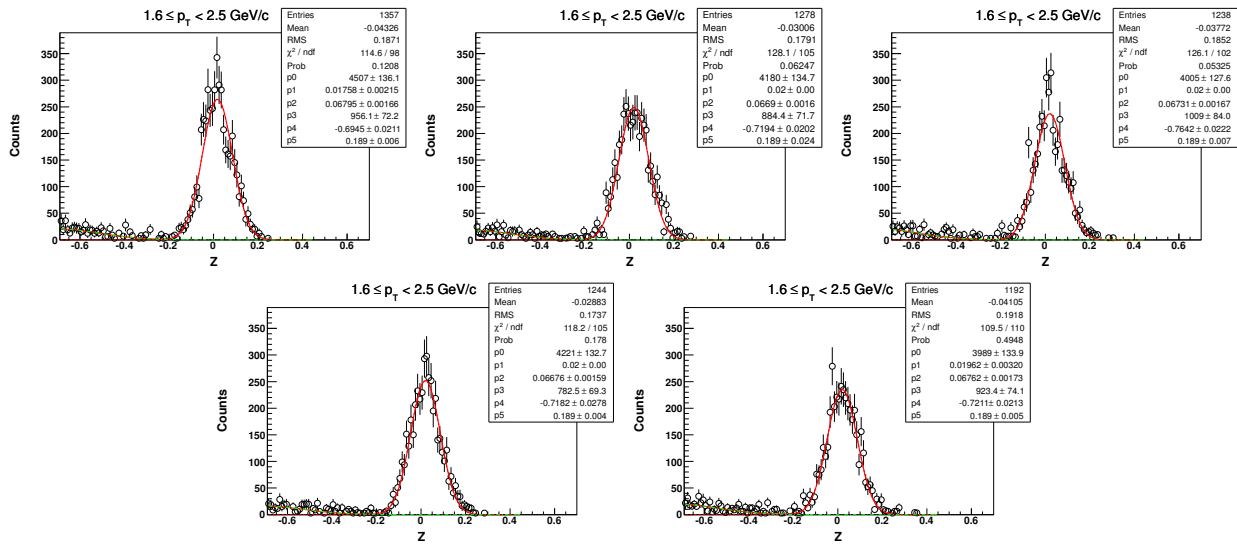


11.6 Z distribution of t in $\sqrt{s_{NN}} = 7.7$ GeV (centrality: 0-80%)

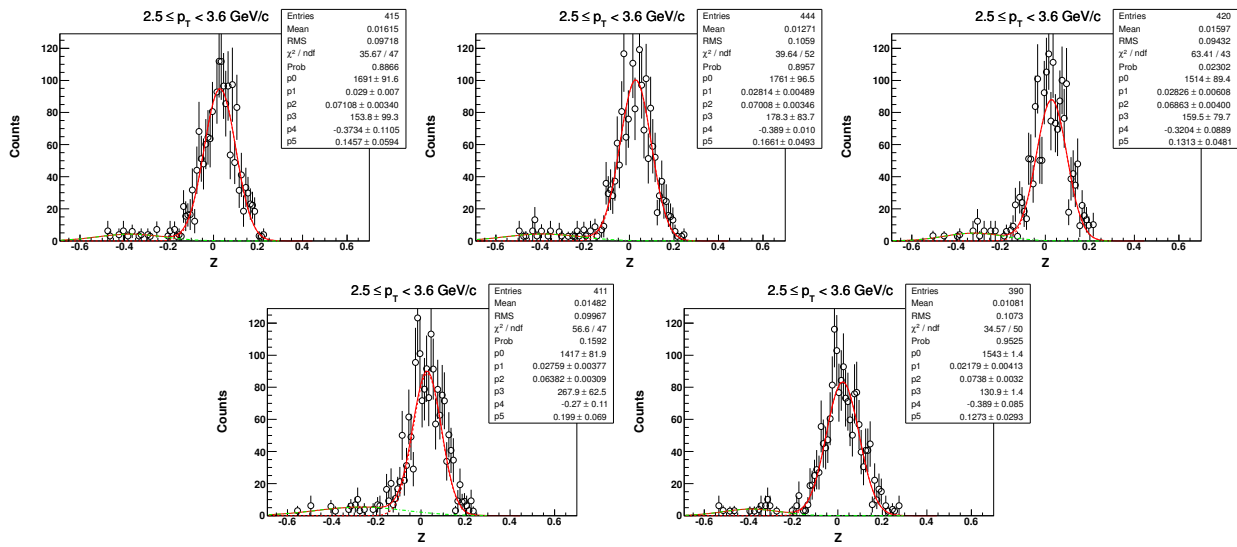
11.6.1 Z-distribution of t for $1.0 < p_T < 1.6$ GeV/c



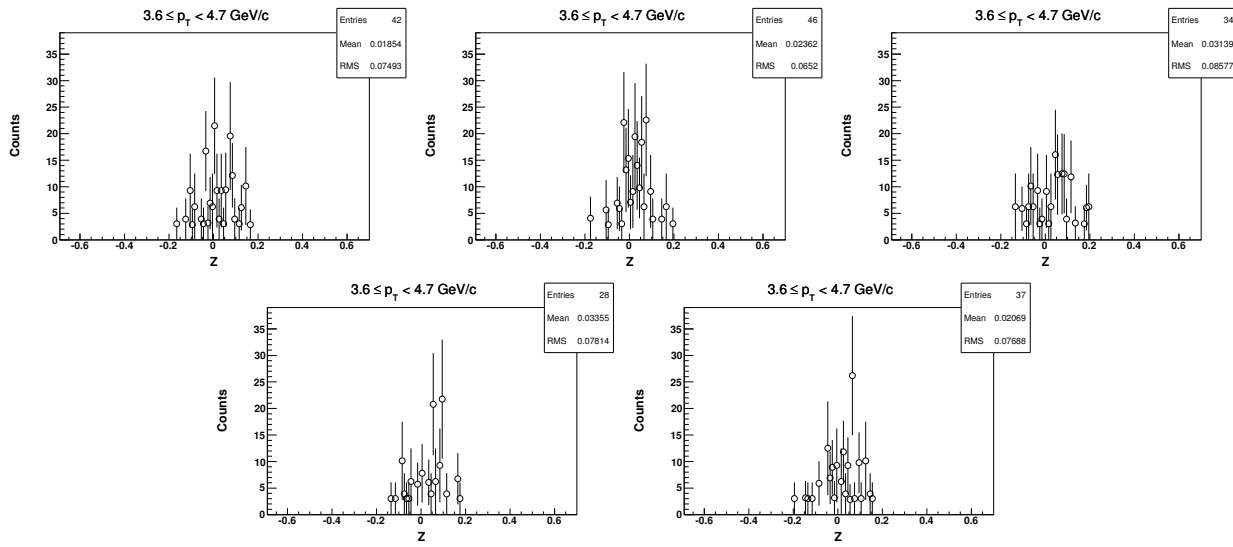
11.6.2 Z-distribution of t for $1.6 < p_T < 2.5 \text{ GeV}/c$ ($\sqrt{s_{NN}} = 7.7 \text{ GeV}$, 0-80%)



11.6.3 Z-distribution of t for $2.5 < p_T < 3.6 \text{ GeV}/c$ ($\sqrt{s_{NN}} = 7.7 \text{ GeV}$, 0-80%)



11.6.4 Z-distribution of t for $3.6 < p_T < 4.7 \text{ GeV}/c$ ($\sqrt{s_{NN}} = 7.7 \text{ GeV}$, 0-80%)



11.6.5 $\phi - \Psi_2$ of t in centrality: 0-80% ($\sqrt{s_{NN}} = 7.7 \text{ GeV}$)

